Engineering Materials

Islam Shyha
Dehong Huo *Editors*

Advances in Machining of Composite Materials

Conventional and Non-conventional Processes

Springer

Engineering Materials

This series provides topical information on innovative, structural and functional materials and composites with applications in optical, electrical, mechanical, civil, aeronautical, medical, bio- and nano-engineering. The individual volumes are complete, comprehensive monographs covering the structure, properties, manufacturing process and applications of these materials. This multidisciplinary series is devoted to professionals, students and all those interested in the latest developments in the Materials Science field, that look for a carefully selected collection of high quality review articles on their respective field of expertise.

Indexed at Compendex (2021)

More information about this series at http://www.springer.com/series/4288

Islam Shyha · Dehong Huo
Editors

Advances in Machining of Composite Materials

Conventional and Non-conventional Processes

Springer

Editors
Islam Shyha
School of Engineering
and the Built Environment
Edinburgh Napier University
Edinburgh, UK

Dehong Huo
School of Engineering
Newcastle University
Newcastle upon Tyne, UK

ISSN 1612-1317 ISSN 1868-1212 (electronic)
Engineering Materials
ISBN 978-3-030-71437-6 ISBN 978-3-030-71438-3 (eBook)
https://doi.org/10.1007/978-3-030-71438-3

This Springer imprint is published by the registered company Springer Nature Switzerland AG
The registered company address is: Gewerbestrasse 11, 6330 Cham, Switzerland

Contents

Introduction

Islam Shyha, Dehong Huo, and J. Paulo Davim

Abstract When two or more different materials are combined, the result is a composite. People think composite materials were discovered recently. However, surprisingly, composites were firstly used in around 1500 BC when ancient Egyptians and Mesopotamian settlers used a mixture of mud and straw to create healthy and durable buildings. Straw has also been used as reinforcement to ancient composite products including pottery and boats. Scientists successfully developed various types of plastics in the early 1900s. However, plastics alone cannot provide enough strength for some structural applications. Therefore, reinforcement was deemed essential to provide additional strength and rigidity; subsequently, composites entered a new era. In 1935, Owens Corning introduced the first glass fibre (fibreglass). Fibreglass, when combined with a plastic polymer, creates an incredibly strong structure that is also lightweight. This is believed to be the beginning of the fibre-reinforced polymer (FRP) composites industry.

1 Composite Materials

The Boeing 787 makes greater use of composite materials in its airframe and primary structure (Fig. 1) than any previous Boeing commercial aeroplanes, whereas the Airbus A380 uses composite materials in around 25% of its airframe weight. Research is ongoing to increase these numbers due to the noteworthy benefits composites provide compared to conventional metallic materials.

I. Shyha (✉)
School of Engineering and the Built Environment, Edinburgh Napier University, Edinburgh EH10 5DT, United Kingdom
e-mail: i.shyha@napier.ac.uk

D. Huo
Mechanical Engineering, School of Engineering, Newcastle University, Newcastle upon Tyne NE1 7RU, UK

J. P. Davim
Department of Mechanical Engineering, University of Aveiro, Campus Santiago, 3810-193 Aveiro, Portugal

I. Shyha and D. Huo (eds.), *Advances in Machining of Composite Materials*, Engineering Materials, https://doi.org/10.1007/978-3-030-71438-3_1

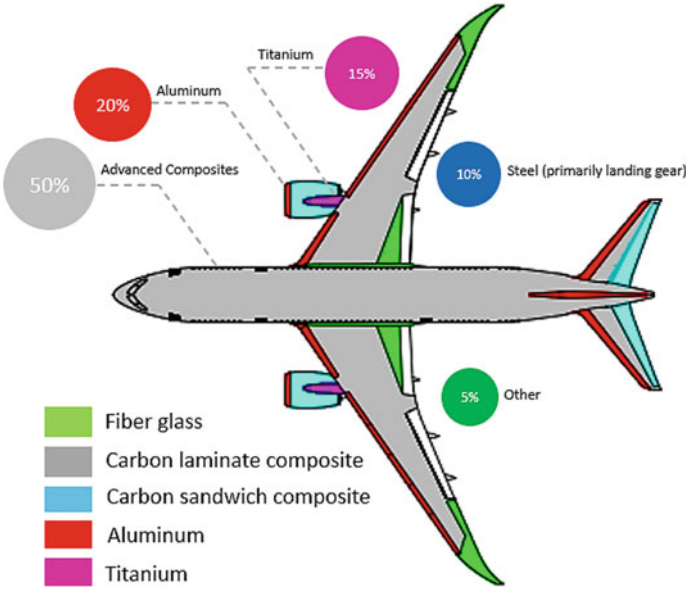

Fig. 1 The application of composites as a structural material in the Boeing 787 Dreamliner (adapted from [1])

The new Boeing 787 aircraft uses approximately 126.5 tons of composite material compared with its predecessor Boeing 777, saving around 98 tons of overall weight. It uses carbon fibre-reinforced plastic (CFRP) composites for half of its airframe, which contributes to almost 20% of weight savings compared to conventional aluminium design in the Boeing 777. This leads to a dramatic reduction in fuel consumption of such lightweight aircraft. Figure 2 shows the high fuel efficiency of the Boeing 787 compared to other aircraft as a function of maximum take-off mass. The aeroplane consumes around 20% less fuel for comparable load and flight distance than other similarly sized counterparts, which in turn reduces the equivalent amount of CO_2 emissions.

In addition to reducing weight, replacing metals by composites in primary aircraft structures can increase their life cycle, hence reducing maintenance costs. For example, less than 35% of the scheduled maintenance time is required for the composite tail of the Boeing 777 compared to the Boeing 767 aluminium tail. This is due to the significant enhancements of corrosion resistance and fatigue strength when using composites rather than metals. Similarly, the composite floor beam of the Boeing 777 can operate over 10 years without replacement.

Similar benefits can be seen in the automotive industry, where the use of composite materials is rapidly growing due to the ongoing desire for reduction in part weights. Carbon fibre composites are the most popular materials that have been applied in vehicle manufacturing. These materials have half the density of steel with around fourfold higher specific strength. The application of carbon fibre composites could

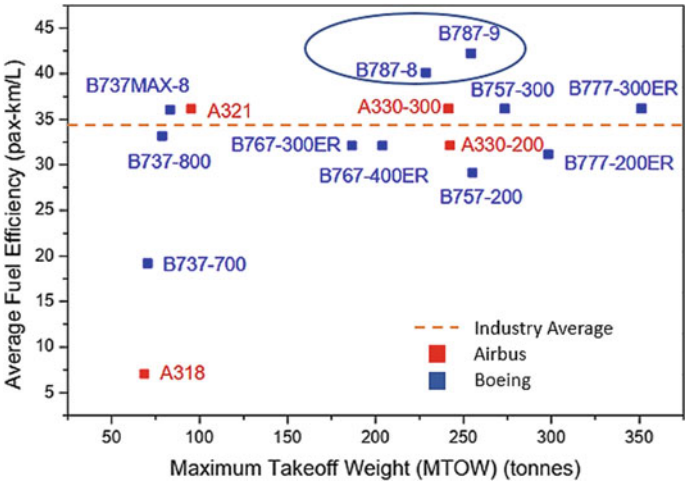

Fig. 2 Fuel efficiency of Boeing 787 in comparison with other similar aircraft (transatlantic route, 2017) (adapted from [2])

reduce vehicle weight by 50–70% compared metallic counterparts. Volkswagen has been trying to reduce vehicle weight by using more CFRP, and has succeeded in offering the XL1 model, which utilises around 21% polymer composites (including outer panels and monocoque). This results in a dramatic weight reduction which has consequently improved fuel efficiency to less than a litre diesel per 100 km.

The demand for weight reduction using composites can also be found in the medical sector. The light wheelchair frame is an example; see Fig. 3. The weight of a conventional foldable wheelchair made from metals is around 12–20 kg which is difficult for many disabled people to handle. Therefore, the use of polymer composites in wheelchair frame design is a solution to reduce its weight while still satisfying criteria for the strength required. A wheelchair frame made from carbon-based polymer composites also operates as a vibration absorber [3].

2 Classifications of Composite Materials

Composite materials are formed from two or more materials yielding properties that could not be obtained from a single material. One of the constituent materials acts as the matrix, and at least one other constituent material acts as the reinforcement in the composite. The matrix material is used to protect the reinforcement materials, distribute the stress to the reinforcement material(s), and provide the final shape of the composite part. The role of the reinforcement(s) is to give the composite superior mechanical properties. It also reinforces the matrix in preferential directions for fibre reinforced composites.

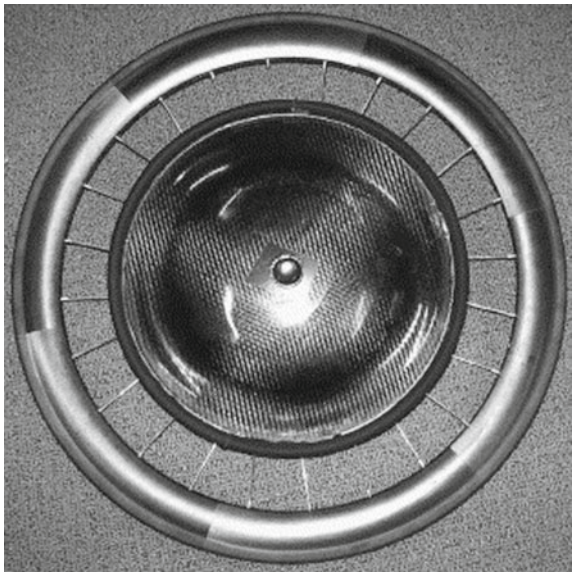

Fig. 3 Carbon fibre composite wheel providing 44% mass reduction and 27% stiffness increase (copyright permission from [4])

The properties of a composite material depend on the properties of the reinforcement and the matrix, the form of the reinforcement (particles, fibres) and the relative content of reinforcement and matrix expressed as volume fraction:

$$V_f = (\text{reinforcement volume})/(\text{composite volume});$$

$$V_m = (\text{matrix volume})/(\text{composite volume});$$

where $V_f + V_m = 1$.

Composite materials can be classified on the basis of matrix material, reinforcement structure and more recently, the size of the reinforcing material. According to the matrix material, the groups are:

- polymer matrix composites (PMCs);
- metal matrix composites (MMCs);
- ceramic matrix composites (CMCs).

2.1 Classification Based on the Matrix

This is the most common classification of composites since the matrix material plays a critical role in composite applications while the reinforcing phase improves the mechanical properties; in particular, for structural applications.

2.1.1 Polymer Matrix Composites (PMCs)

The most common form of reinforcing material used in PMCs is fibre, such as carbon fibre (CF), glass fibre (GF) or aramid fibre (AF), due to their high strength compared to particle reinforcement. Both CF- and GF-reinforced polymer composites provide high strength and stiffness-to-weight ratios. Still, AF reinforced polymer can only be used at low temperature, and stiffness is not a significant concern. However, glass fibre-reinforced plastic (GFRP) is the most commonly applied material due to its low cost and comparable mechanical strength. The fibres can also be classified based on their form, including continuous and discontinuous fibres. These are identified by the length-to-diameter ratio (l/d) or aspect ratio. Generally, a higher aspect ratio (higher length or smaller diameter) leads to higher strength in the fibre direction. However, it also entails higher production costs. Two typical examples of continuous-fibre composites are unidirectional and woven, with the reinforcing volume up to 60–70%. For discontinuous fibres, their distribution within the polymer matrix is mostly random. The unidirectional type provides the best mechanical properties in polymer composites [5].

The applications of PMC are mostly based on the type of matrix materials. The polymer includes two major types of thermoset and thermoplastic, as explained in more detail in Chapter "Fibre Reinforced Polymer Composites". Thermoset polymer composites are commercially used in industrial areas such as sporting goods (Fig. 4) and the aerospace and automotive industries. Despite the lower strength compared to epoxy, polyester composites are used to manufacture structural panels, pressure vessels and water tanks due to its low cost. In contrast to thermoset polymers, thermoplastic composites are mostly applied where high temperature is not considered. However, these composites can provide excellent mechanical properties and can be used in the aerospace and automotive sectors.

Fig. 4 Carbon fibre composite bicycle (copyright permission from [6])

2.1.2 Metal Matrix Composites (MMCs)

Industrial applications for MMCs are mostly for engine components that operate at high temperature. There is also fibre reinforcement in MMCs, but the most common fillers are ceramic particles. Following the general rule, fibre forms can provide a better strengthening effect. However, the high density of metal matrices and the high affinity of chemical reactions with the reinforcement are the main challenges in MMC fabrication and possibly use. Therefore, the incorporation of fibre reinforcement (with higher interface area than particle form) into a metal matrix usually fails. Meanwhile the fabrication of ceramic fibre is also more costly due to their high brittleness compared to the particle form. The addition of around 20 vol.% ceramic particles can significantly enhance tensile strength, stiffness and wear resistance of the composites, but also reduces their ductility. Therefore, low-cost particle-reinforced MMCs are mostly used to manufacture automobile components (Fig. 5) or sports equipment.

2.1.3 Ceramic Matrix Composites (CMCs)

In contrast to PMC and MMC, the main driver of reinforcement addition in a ceramic matrix is to improve its fracture toughness, as this material already possesses high stiffness and strength. Due to their high stability (mechanical and chemical properties), and corrosion resistance at high temperature (beyond the capability of metals), CMCs are mostly applied to manufacture heat shield for space vehicles, combustion chambers, turbine blades for high-temperature gas turbines, slide bearings and brake disks (Fig. 6). Alumina (Al_2O_3) and silicon carbide (SiC) are the most common reinforcements in MMCs. The addition of 30 vol.% of SiC whisker can double the fracture toughness of base alumina [8]. More details on MMCs are presented in Chapter "Metal Matrix Composites".

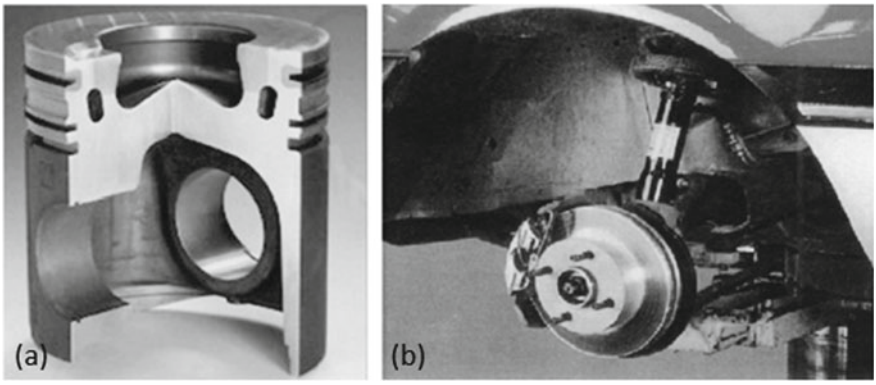

Fig. 5 Applications of MMC in the car industry: **a** short fibre-reinforced light metal diesel piston; **b** vented passenger car brake disc made of particle reinforced aluminium (Open Access from [7])

Fig. 6 A carbon fibre-reinforced ceramic braking system of the ZR1 Corvette, which is nearly 5 kg lighter than iron predecessors (*Source* New York Times)

2.2 Classification Based on Reinforcement Size

Composite classification based on reinforcement size considers that conventional composites are those with reinforcing material above a few micrometres in size in all dimensions, while nanocomposites with reinforcement size are at nanoscale in at least one dimension. The initial purpose of reducing filler size is to increase its aspect ratio (l/d), hence improving strengthening efficiency. Additionally, a better distribution due to reduction in filler size contributes to better mechanical properties due to less stress concentration and the larger surface area of nanofillers. However, this trends is not always followed when reducing filler size; for example, pristine carbon nanotubes (CNTs) tend to agglomerate when added into the matrix due to Van der Waals force, which could result in less efficient distribution. This can be overcome by using filler surface treatment. Furthermore, nanoscale reinforcements have exhibited high mechanical properties (e.g. tensile strength and stiffness) compared to conventional fillers. Therefore, nanofillers are expected to provide better strengthening efficiency in nanocomposites compared to conventional composites. One typical example of the evolution of composite by reducing filler size is carbon fibrous reinforcement, as shown in Fig. 7.

3 Machining of Composite Materials

Composite components, including those fabricated using laying-up techniques such as fibre-reinforced polymers (FRPs) and those fabricated using casting techniques such as metal matrix composites, are typically made to near-net-shapes. However, subsequent machining operations are indispensable, especially for precision composite components. Machining operations bring composite components into the required accuracy of dimensional form, surface finish, and complex shapes, and

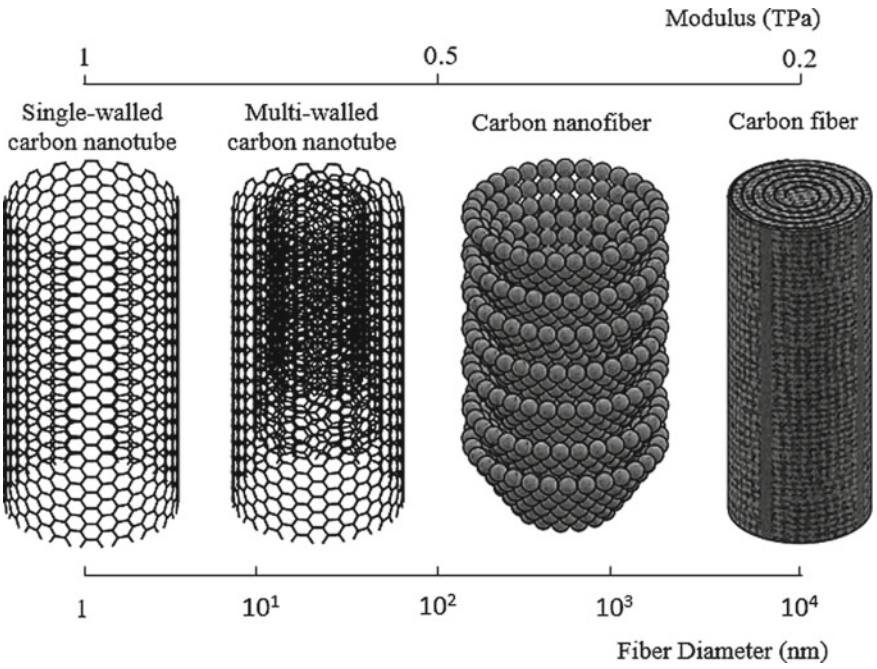

Fig. 7 Filler size reduction from micro- to nanoscale with carbon fibre reinforcement (adapted from [9])

prepare them for assembly. However, being heterogeneous materials that consist of distinctly different phases, which are usually anisotropic and reinforced by hard and abrasive materials, such as glass, granite, hard metal oxides, nitrides, and carbides, composite materials are difficult to machine.

The machining of composite materials is different when compared to metals in many respects. Composite materials generally have much lower machinability compared with their matrix materials. Excessive tool wear (Fig. 8), short tool life and high tooling costs, and hence associated relatively low surface finish and sub-surface damage, are the main issues when machining composite materials.

Various conventional machining operations, such as turning, milling, drilling and grinding, have been widely applied to cut both particulate and fibrous composite materials. The machinability of commonly used structural composites, such as CFRP and GFRP, Al/SiC MMCs, has been thoroughly investigated and optimal machining parameters and tooling are readily available. Figure 9 shows a few examples of composite damage due to machining. Meanwhile the machining of other types of composites such as ceramic matrix composites require continuous effort from the machining community. More details on machining PMCs, MMCs and CMCs are presented in Chapters "Conventional Machining Processes of Fibre Reinforced Polymer Composites", "Conventional Machining of Metal Matrix Composites" and "Machining of Ceramic Matrix Composites" respectively.

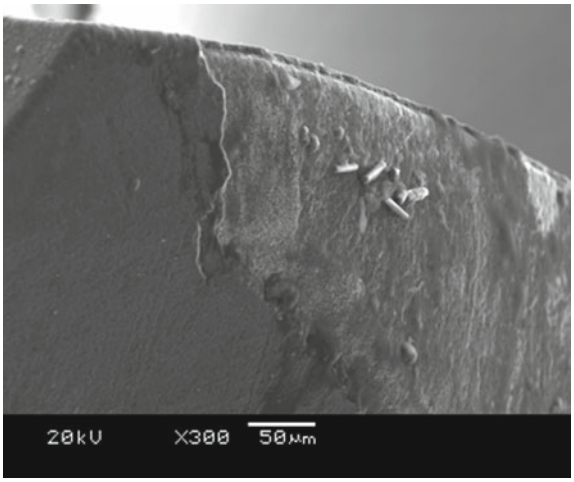

Fig. 8 Drilling tool used for cutting CFRP panels

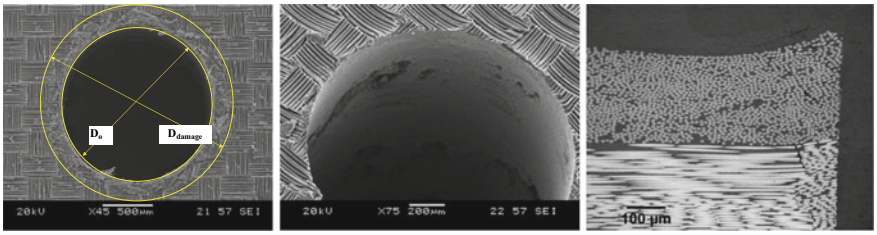

Fig. 9 Various damage types when drilling CFRP composites

Recent developments in composite materials have led to the fabrication of nanocomposite materials comprising nanoscale reinforcements, such as MMCs reinforced with nanoparticles and polymer-based nanocomposite. While the properties of these materials are being characterised, limited research on their machinability has been carried out. As the significant applications of these relatively new materials are expected to be at micro- or mesoscale, research effort focuses on micro-machinability through micromachining experiments [10]. This is challenging, because several critical issues arise in micromachining; namely, the cutting edge size effect and material size effect. These affect the generation of micro-machined surface characteristics [11]. More details on the micromachining of MMCs reinforced with nanoparticles are presented in Chapter "Conventional Machining of Metal Matrix Composites".

Nonconventional machining operations have been increasingly applied in processing composite materials. Some unique machining characteristics that cannot be found in conventional machining may be exhibited in nonconventional machining methods. For example, mechanical stresses, chatter and vibration problems can be eliminated using nonconventional machining methods. Electro discharge machining

(EDM), laser beam machining (LBM) and abrasive water jet machining (AWJM) have found applications in processing composite materials with some success, although in general nonconventional machining cannot achieve the same accuracy and surface finish when compared to conventional machining. More details on the nonconventional machining of composite materials are discussed in Chapters "Nonconventional Machining Processes of Fibre Reinforced Polymer Composites" and "Non-conventional Machining of Metal Matrix Composites".

Continuous efforts to enhance manufacturing performance have led to a combination of two or more processes to form a hybrid machining process which exploits the advantages of one process and overcomes the limitation of others. Over the last two decades, numerous hybrid machining processes have been proposed and developed. Among these methods, vibration-assisted machining has been successfully applied in processing composite materials. Vibration-assisted machining allow us to obtain good surface quality and extend tool life when machining both particulate and fibrous composite materials. This is attributed to the intermittent separation of workpiece and tool, where the temperature in the cutting zone is lower than that in conventional processes [12]. Another recently developed hybrid cutting-abrasive tool [13] has shown improved form accuracy and efficiency when machining fibre-reinforced polymer composites.

4 Structure of the Book

This comprehensive book details a range of conventional and nonconventional machining processes of different composite materials, including polymer matrix composites, metal matrix composites, ceramic matrix composites, green and natural composites, hybrid composites and new emerging nanostructured composites. The book distinctively clarifies how to machine different composite materials in terms of operating conditions, cutting tools, and the appropriate machines. It also presents typical damage patterns caused by machining operations and strategies to reduce induced damage. Current practices and requirements for producing high quality critical composite components (e.g. in the aerospace sector) are also presented. For each major composite group (fibre reinforced composites and metal matrix composites), a dedicated chapter is introduced to discuss mechanical and physical properties, applications, manufacturing techniques and classification followed by chapters discussing conventional and nonconventional processing respectively, with a further chapter on modelling techniques.

Each chapter begins with a concise introduction to a specific composite group, then presents physical, mechanical and thermal properties, applications and a classification of this group. Process-based chapters will begin with a critical review of the machining of the specific composite group followed by removal mechanisms. Consequently, the influence of composite properties/specifications and process operating conditions on productivity, surface quality/integrity, tool life and cutting forces are

considered. Finally, review questions will be added at the end of each chapter, aiming to recapitulate the knowledge gained by readers.

The book aims to critically discuss the available literature in the field of composite materials and composite machining and present it in an accessible format to researchers and engineers working in the field of composite manufacturing. The book contents can be classified into three main groups of chapters. Firstly, properties, applications and primary manufacturing technology to produce the near-net shape of a specific composite group are presented in Chapters "Fibre Reinforced Polymer Composites", "Metal Matrix Composites", "Ceramic Matrix Composites (CMCs)", "Nano-structured Polymer-Based Composites" and "Green, Natural Fibre and Hybrid Composites". These are followed by one chapter or more to provide comprehensive contents on different types of machining operation employed for this particular composite group, such as in Chapters "Conventional Machining Processes of Fibre Reinforced Polymer Composites", "Nonconventional Machining Processes of Fibre Reinforced Polymer Composites", "Conventional Machining of Metal Matrix Composites", "Non-conventional Machining of Metal Matrix Composites", "Drilling of Fibre Reinforced Polymers and Hybrid Stacked Materials", "Machining of Ceramic Matrix Composites", "Machining of Nano-structured Polymer Composites", "Machining of Bio-Composites" and "Grinding and Abrasive Machining of Composite Materials". The final group of chapters offers knowledge that covers various composite types, such as Chapters "Introduction", "Cutting Tools for Machining Composites", "Health and Safety Considerations in Machining of Composite Machining" and "Recycling of Composite Materials".

In addition to presenting the most recent research on machining different types of composite materials, the book includes chapters that are believed to be new compared to other available books which are anticipated to benefit readers. These include Chapter "Cutting Tools for Machining Composites" (cutting tools for machining composites), which focuses on tools with unique geometries and coatings that make them suitable for composite machining, Chapter "Health and Safety Considerations in Machining of Composite Machining" (health and safety when machining composites) which presents challenges, risk assessment, and health and safety considerations when cutting composites aiming to raise the awareness of readers in order for preventive action and responsible measures to be introduced so as minimise the risk to individuals and environment. Finally, it is difficult to talk about composite materials without touching on the life cycle of composites since initial composite products are coming to the end of their life and methods for recycling must be discussed. This will be covered in Chapter "Recycling of Composite Materials". Figure 10 shows a detailed structure of the book.

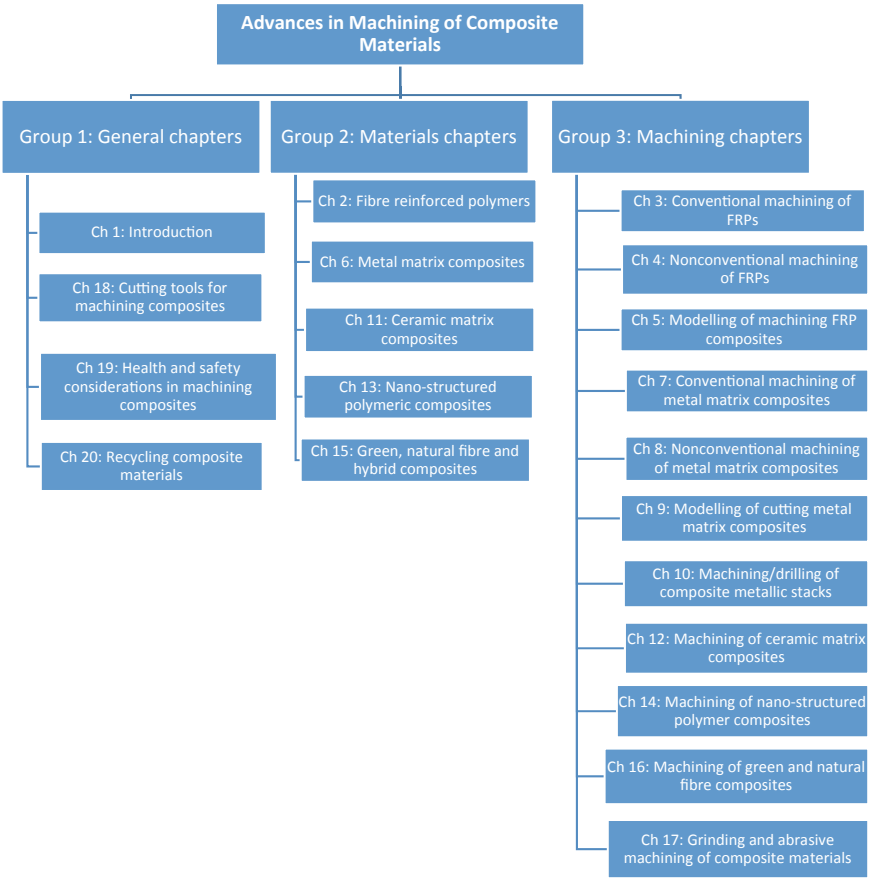

Fig. 10 Structure of the book

References

1. Burridge, E.: Boeing's 787 Dreamliner has some impressive environmental credentials. Available: https://www.icis.com/explore/resources/news/2009/12/14/9318715/boeing-s-787-dreamliner-has-some-impressive-environmental-credentials/ (2009). Accessed 4 Nov 2020
2. Graver, B., Rutherford, D.: Transatlantic airline fuel efficiency ranking, 2017. In: International Council on Clean Transportation (2018)
3. Chénier, F., Aissaoui, R.: Effect of wheelchair frame material on users' mechanical work and transmitted vibration. BioMed Res. Int. **2014** (2014)
4. Kalyanasundaram, S., Lowe, A., Watters, A.: Finite element analysis and optimization of composite wheelchair wheels. Compos. Struct. **75**, 393–399 (2006)
5. Tanwer, A.K.: Mechanical properties testing of uni-directional and bi-directional glass fibre reinforced epoxy based composites. Int. J. Res. Adv. Technol. **2**, 34–39 (2014)
6. Mathijsen, D.: The Novus bike. Reinf. Plast. **63**, 206–212 (2019)
7. Mavhungu, S., Akinlabi, E., Onitiri, M., Varachia, F.: Aluminum matrix composites for industrial use: advances and trends. Procedia Manuf. **7**, 178–182 (2017)

8. Homeny, J., Vaughn, W.L., Ferber, M.K.: Silicon carbide whisker/alumina matrix composites: effect of whisker surface treatment on fracture toughness. J. Am. Ceram. Soc. **73**, 394–402 (1990)
9. Vajtai, R.: Springer Handbook of Nanomaterials. Springer Science & Business Media (2013)
10. Kumar, M.N., Mahmoodi, M., TabkhPaz, M., Park, S., Jin, X.: Characterization and micro end milling of graphene nano platelet and carbon nanotube filled nanocomposites. J. Mater. Process. Technol. **249**, 96–107 (2017)
11. Teng, X., Chen, W., Huo, D., Shyha, I., Lin, C.: Comparison of cutting mechanism when machining micro and nano-particles reinforced SiC/Al metal matrix composites. Compos. Struct. **203**, 636–647 (2018)
12. Chen, W., Huo, D., Shi, Y., Hale, J.: State-of-the-art review on vibration-assisted milling: principle, system design, and application. Int. J. Adv. Manuf. Technol. **97**, 2033–2049 (2018)
13. Shyha, D.H.I., Hesamikojidi, P.: Performance of a new hybrid cutting-abrasive tool for the machining of fibre reinforced polymer composites. Int. J. Adv. Manuf. Technol. **112**, 1101-1113 (2021)

Fibre Reinforced Polymer Composites

Ben Wang and Hang Gao

Abstract Fibre reinforced polymer (FRP) composites are attractive engineering materials because they have excellent properties, such as high strength-to-weight, modulus-to-weight, magnetic and corrosion resistance. FRPs are formed by combining the fibres and polymer matrix, providing properties that could not be obtained from a single material component alone. Categories of fibre include carbon fibre, glass fibre, boron fibre, aramid fibre and others. The resin matrixes used are mainly thermosetting resin and thermoplastic resin. Besides, laminated and cylindrical FRPs are two common forms used in structural applications. Due to their excellent usability, FRPs have seen extensive applications in a wide range of industries including aerospace, aircraft, military, mobile phone, automobiles, infrastructure and sporting goods. Additionally, FRPs will be essential materials in many fields in the future.

1 Introduction

Fibre reinforced polymer composites (FRPs) are formed by a combination of the fibres and polymer matrix. In the FRPs, both fibres and matrix retain their physical and chemical identities. Still, they produce an excellent performance that cannot be achieved with either of the constituents acting alone. FRPs have many advantages, such as strength-to-weight (longitudinal tensile strength/density), high modulus-to-weight (longitudinal tensile modulus/density), fatigue strength, as well as fatigue damage tolerance. Categories of fibre mainly include carbon fibre, glass fibre, boron

B. Wang (✉)
Key Laboratory of Fundamental Science for National Defence of Aeronautical Digital Manufacturing Process, School of Mechanical and Electrical Engineering, Shenyang Aerospace University, Shenyang, Liaoning, China
e-mail: wangben211@163.com

H. Gao
Key Laboratory for Precision and Non-Traditional Machining Technology of Ministry of Education, School of Mechanical Engineering, Dalian University of Technology, Dalian, Liaoning, China

I. Shyha and D. Huo (eds.), *Advances in Machining of Composite Materials*, Engineering Materials, https://doi.org/10.1007/978-3-030-71438-3_2

fibre and aramid fibre. The resin matrixes used are mainly thermosetting resin (e.g. epoxy resin) and thermoplastic resin (e.g. PE-polyethylene). Since most of FRPs are laminated by prepregs through interweaving or layered pavement. FRPs are being applied in an increasing range of fields, especially in aerospace applications. The number of composite applications has become an important index used to measure the aerospace industry's advancement. Due to their excellent usability, polymeric composites have also been increasingly applied to automobiles, infrastructure and sporting good. FRPs will be an essential material in many fields in the future.

The prime components of fibre reinforced composites (FPRs) are long and thin fibres possessing high strength and stiffness. The fibres are bound with a matrix material whose volume fraction in a composite is usually less than 50%. FRPs have high strength-to-weight, high modulus-to-weight, strong fatigue-cracking resistance, good designability, corrosion resistance and are convenient for large-scale shaping. They also have unique electromagnetic and wave-absorbing stealth characteristics [1]. FRPs have an evident characteristic of integrating structural bearing and function and have been widely applied in various fields, including in aerospace and automotive. They are vital to the creation of lightweight and high-performance components.

The performance of composites is closely related to the type of fibre and resin matrix used. Fibres are the principal load-carrying members. The matrix plays a minor role in the tensile load-carrying capacity of a composite structure. However, the resin matrix keeps fibres in the desired location and orientation, acts as a load transfer medium between fibres, and protect fibres from environmental damages. Therefore, even though the fibres reinforce the matrix, both of them serve essential functions in FRPs.

New fibre and resin matrixes are continuously being developed. Currently, carbon fibre, glass fibre and aramid fibre are the widely used fibre types. This chapter discusses the types and characteristics of commonly used reinforced fibres, resin matrixes and composites. Their fields of application are also explored.

2 Classification of Polymer Matrix Composites

Fibres have significantly higher strength and stiffness in the length direction than in the other directions. This limits their use in a stand-alone form and underscores the need for a rigid matrix in the composite structure. The main fibre types are glass, carbon, aramid, boron, silicon carbide and alumina. The fibres also can be classified according to the shape and size into continuous, short and chopped fibres. According to the equivalent inclusion theory, the length-to-diameter ratio and volume content of fibre significantly influence the matrix reinforcement effect: the higher volume content and larger fibre length-to-diameter ratio strengthening effect to the matrix was more significantly [2]. Therefore, continuous fibres are mainly discussed in the following sections.

The matrix binds together the reinforcing fibres. The microstructure of a polymer matrix composite is shown in Fig. 1. The matrix resin protects the fibres from premature failure as a result of abrasion or environmental corrosion. More importantly, the matrix distributes an applied load and acts as a stress transfer medium so that when an individual fibre fails, the composite structure does not lose its load-carrying capability. Classification of FRPs is shown in Fig. 2. Typical mechanical and physical properties of fibres are shown in Table 1.

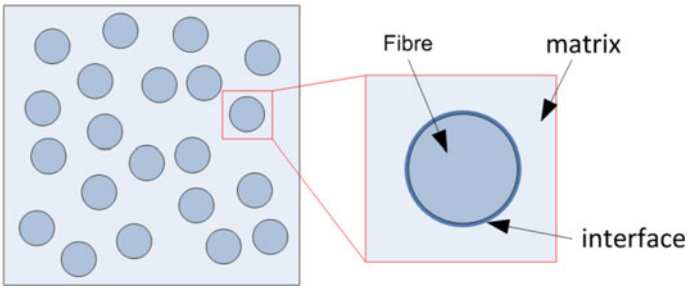

Fig. 1 The microstructure of a polymer matrix composite

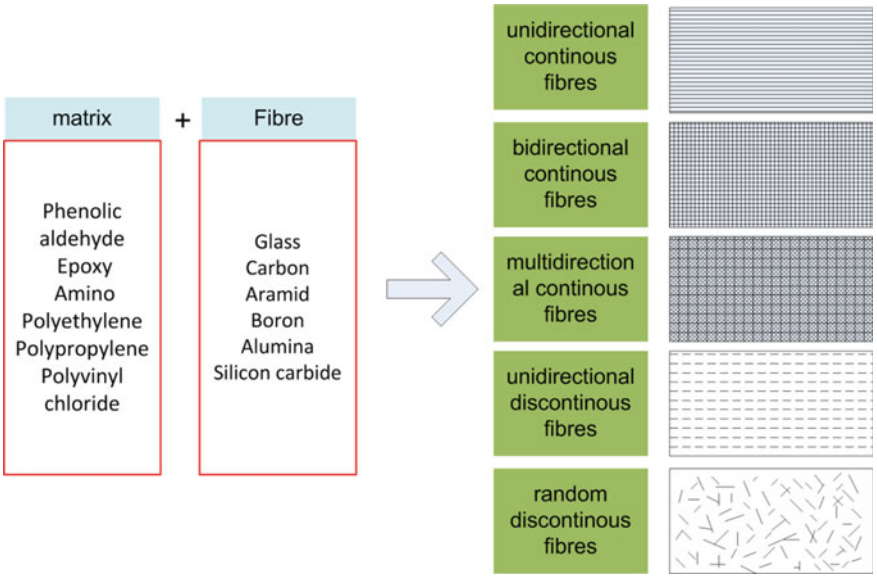

Fig. 2 Classification of FRPs

Table 1 Properties of different fibres [3]

	Density (g/cm^3)	Tensile strength (GPa)	Tensile modulus (GPa)
E-type glass fibre	2.54	3.45	72.4
Carbon fibre (T300)	1.76	3.65	231
Aramid fibre (Kevlar 49)	1.45	3.62	131
Boron fibre	2.7	3.1	393

2.1 Glass Fibre

Glass fibres are the most common of all reinforcing fibres for polymeric matrix composites, as shown in Fig. 3. Glass fibre provides good insulation, strong thermal endurance, high corrosion resistance, relatively low stiffness, high chemical and biological resistance and mechanical strength. However, it is brittle, sensitive to surface damage and has low abrasion resistance. Essential properties of glass as a reinforced fibre are their high strength which is maintained in humid environments but degrades under elevated temperatures [4].

Glass fibres are made from pyrophyllite, quartz sand, limestone, dolomite, borocalcite and camsellite using high-temperature melting. A molten mixture of silica (SiO_2) and other oxides is drawn through small holes in a platinum-alloy bushing. The fibres emerging from the bushing are drawn to size a constant speed and then quenched by air or water spray. A protective coating, or size, is applied to the

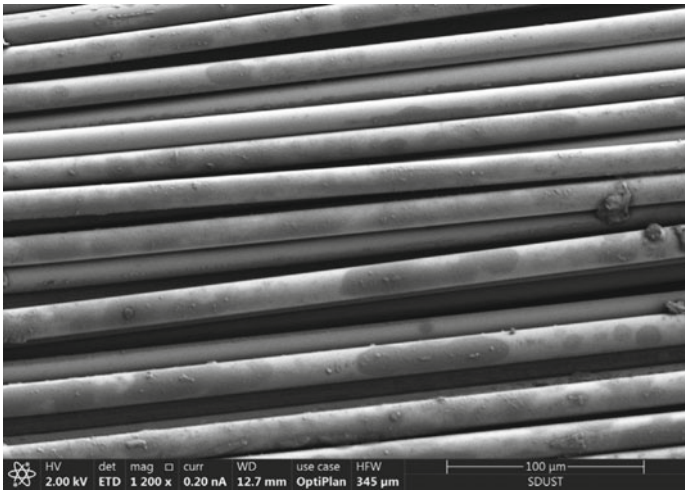

Fig. 3 Morphology of glass fibres [5]

fibres to protect their surface and enhance their binding to the polymer matrix. Glass is an amorphous material. Thus, it does not develop a preferred orientation in microstructure when drawn. It is, therefore considered isotropic. The diameter of glass fibre monofilament ranges from several to more than 20 μm. Fibre diameters for composites applications are in the range from 10 to 20 μm [6].

Glass is also highly abrasive, which poses a significant challenge when machining GFRPs. Commonly used fibres include E-type glass fibre and S-shaped glass fibre. E-type glass fibre has the lowest cost of all commercially available reinforcing fibres, which is why its widespread use in the FRPs. S-shaped glass fibre has a higher tensile strength than that of E-type glass fibre. However, the compositional difference and higher manufacturing cost make it more expensive than E-type glass fibre [7].

2.2 Carbon Fibre

Development of carbon fibre was a natural step aiming at a rise of fibre stiffness which was not exhibited by glass fibre. Modern carbon fibre demonstrates much higher modulus than that of glass fibre.

Carbon fibre has many outstanding properties, including high axial strength and modulus, low density, high-temperature resistance in oxidizing environments, good fatigue durability, specific heat and conductivity between those of non-metals and metals, low coefficient of thermal expansion (which provides dimensional stability over a wide range of temperatures), excellent corrosion resistance, good X-ray permeability, high heat conductivity, and adequate electromagnetic shielding. Their cons include the low strain-to-failure, low impact resistance and electrical conductivity. Their electrical conductivity is harmful during machining, as fibre chips may penetrate machine tool controls and cause short circuit electrical equipment.

Carbon fibre is a microlite graphite material created by the carbonization and graphitizing of piled organic fibres, like flake graphite, along the fibres' axial direction. They are anisotropic (transversely isotropic), and their properties are mainly affected by the degree of orientation of the graphite layers concerning the fibre axis. Carbon fibre is an inorganic polymer fibre with a carbon content of more than 90%. With more than 99% carbon content, the fibre is called graphite fibre. The diameter of carbon fibre monofilament ranges is about 5–7 μm. Carbon fibre in a CFRP after machining is shown in Fig. 4.

Carbon fibres can be divided into polyacrylonitrile (PAN)-based carbon fibre and pitch-based, depending on the raw material type. The pitch-based fibres have a higher modulus, but lower strength than the PAN-based fibres. For PAN-based fibre, the process consists of three stages: stabilization, carbonization and graphitization.

The tensile modulus values of carbon fibre vary in a large area, ranging from 207 GPa on the low side to 1035 GPa on the high side [3]. Carbon fibres can also be divided into universal, high-strength, middle-modulus, high-modulus and ultra-modulus carbon fibres according to performance. The middle-modulus and high-strength grades are almost universally PAN-based. Higher-modulus fibres with much

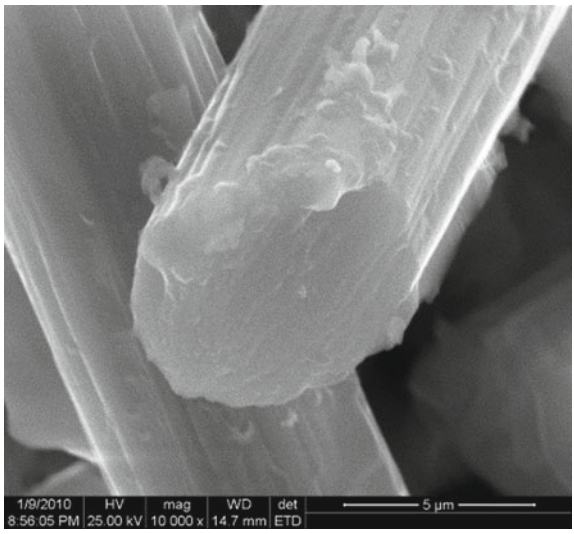

Fig. 4 Carbon fibre in a CFRP after machining

lower strength are most pitch-based produced at a lower cost. Generally, the low-modulus fibres have low density, low cost, higher tensile and compressive strength and higher tensile strains-to-failure than the high-modulus fibres.

The high stiffness and strength combined with low density and intermediate cost have made carbon fibres the second to glass fibre in use. However, their high cost has so far excluded them from widespread commercial applications. They are widely used mainly in the aerospace industry in the last century, where weight saving is considered more critical than the cost. Today, the cost of carbon fibre has decreased a lot. Decreased costs will allow penetration into more cost-sensitive markets such as automotive and sports goods.

2.3 Aramid Fibre

Aramid fibres are highly crystalline aromatic polyamide fibres with the lowest density and the highest tensile strength-to-weight ratio among the current reinforcing fibres [8]. Aramid fibres are organic fibres manufactured from aromatic polyamides (Aramids) by solution spinning. Polymer solution in sulfuric acid is extruded by spinning through small holes into fibres in which the molecules are aligned with the direction of shear. Further alignment of the fibres can be achieved by washing in a cold-water bath and stretching under heating.

Aramid fibres offer higher strength and stiffness relative to glass coupled with lightweight, high tensile strength, but lower compressive strength. As components of advanced composites for engineering applications, aramid fibres are characterized by low density providing strength-to-weight and stiffness, low thermal conductivity

resulting in high heat insulation. Like carbon fibres, they also have a negative coefficient of thermal expansion in the longitudinal direction, which is used to design low thermal expansion composite panels and construct hybrid composite elements that do not change their dimensions under heating. It consists of very thin filaments (fibrils) for a system, and aramid fibres have very high damage tolerance. It tends to respond under impact in a ductile manner instead of carbon fibre, which tends to fail in a more brittle manner. Their high strength in a longitudinal direction is accompanied with relatively low strength under tension in a transverse direction. Aramid fibres are characterized by pronounced temperature and time dependence for stiffness and strength [9]. The main disadvantages of AFRPs are their low compressive strengths. The outstanding toughness of aramid fibres also creates a problem during machining. The fibres are difficult to cut, and special tooling and techniques are required. Aramid fibre in an AFRP after machining is shown in Fig. 5.

Due to variations in the polymer structure, the aramid fibre family covers many categories. Meta-position aramid fibre and para-position aramid fibre are the most representative aramid fibres and have the highest practical value. Generally, para-position aramid fibre is used as a reinforcing material in composites. Para-position aramid fibre has a range of excellent characteristics, including lightweight, high strength, high modulus, high robustness, high-temperature resistance, good insulation and anti-ageing performance. Currently, aramid fibre is mainly produced in America and Japan. Manufacturers and brands of para-position aramid fibre mainly include Kevlar® fibre (DuPont, USA), Twaron® fibre and Technora® fibre (Teijin, Japan), Heracron® fibre (Kolon, Korea) and Armos® fibre (Tver, Russia).

Kevlar 49 is the trade name of one of the aramid fibres available in the market, most widely used in AFRP composites. It is a kind of para-position aramid fibre. During the filament drawing process, Kevlar 49 molecules become highly oriented in the filament axis direction. Weak hydrogen bonds between hydrogen and oxygen

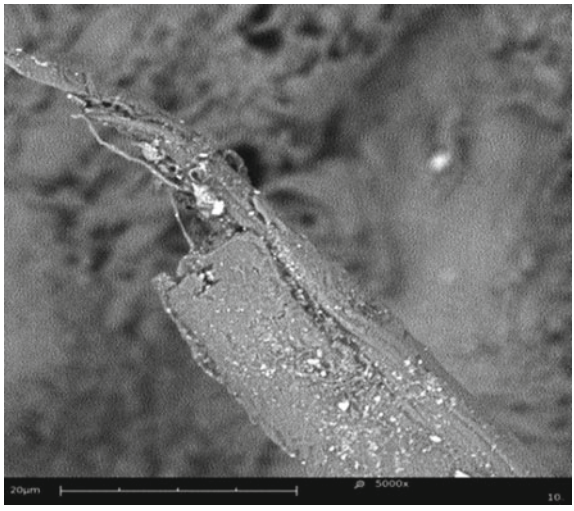

Fig. 5 Aramid fibre in an AFRP after machining

atoms in adjacent molecules hold them together in the transverse direction. As a result, the filament is highly anisotropic, with much better physical and mechanical properties in the longitudinal direction than in the radial direction. Especially, Kevlar 49 fibres exhibit a high degree of yielding on the compression side during bending. One application of this characteristic is found in soft, lightweight body armours and helmets [3].

2.4 Boron Fibre

Boron fibres are manufactured by chemical vapour deposition (CVD) of boron onto about 12 μm diameter a heated substrate (either a tungsten wire or a carbon monofilament). When the substrate is a tungsten wire, hydrogen and boron trichloride reacts on a hot tungsten filament to replace the amorphous boron deposition on the tungsten surface. Boron fibres have a relatively large diameter, 100–200 μm, shown in Fig. 6. According to this, boron fibres offer excellent resistance to buckling, which contributes to high compressive strength for the BFRP composites. Boron fibre has good high-temperature resistance in inert gas. However, its tensile and compressive strength decreases significantly at air temperatures above 500 °C. To prevent this degradation, chemical vapour deposition covers the fibre surface with about 5 μm thick layer of silicon carbide or boron carbide. Comparing to carbon fibre, glass and aramid fibres, boron fibres have now somewhat limited applications [10].

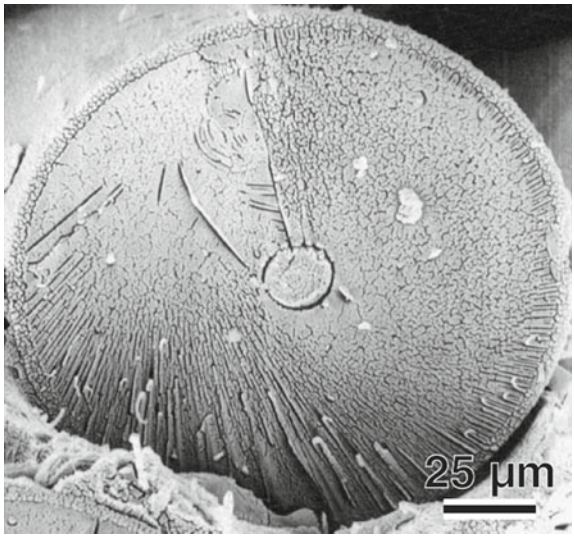

Fig. 6 Morphology of a boron fibre (with B4C coating) [11]

2.5 Resin Matrix

Matrix materials provide the final shape of the composite structure and govern the parameters of the manufacturing process. The resin matrix fulfils a variety of critical functions and merely maintains the shape of the composite structure and aligns the reinforcing fibres. Resin matrixes can be divided into thermoplastic and thermosetting resins. Optimal combination of fibre and matrix properties should satisfy a set of operational and manufacturing requirements. Fibre reinforced composites mainly use thermosetting resin, while the use of thermoplastic is in a gradual increase.

Thermosetting resin undergoes a chemical reaction under heating and pressurization, or a curing agent and ultraviolet light. The components further react into a single type of insoluble and in-fusible synthesized resin through cross-linking curing. Such resin is generally a solid or viscous liquid with low molecular weight before curing and can be softened or flowed in the forming process. It is plastic and can be shaped, accompanied by chemical reaction and cross-linking curing. Cured resin cannot be softened or flowed even upon pressurization and heating. Instead, the resin is decomposed or carbonized under excessive temperature. After thermosetting the resin, it forms a reticulate structure due to intermolecular cross-linking. Therefore, the thermosetting resin has the characteristics of high rigidity, high hardness, inflammability, but has the disadvantages of high brittleness and low mechanical properties. Thermosetting resins include phenolic aldehyde, epoxy, amino, unsaturated polyester and silicon ether resins.

The thermoplastic resin is a high-molecular-weight solid at room temperature. It is a linear polymer with a few branched chains and without intermolecular cross-linking. The thermosetting resin is only mutually attracted by Van Der Waals forces or hydrogen bonds. The resin is softened or flowed under pressure and heating (as shown in Fig. 7). As it makes no chemical cross-links, it can be shaped in a mould,

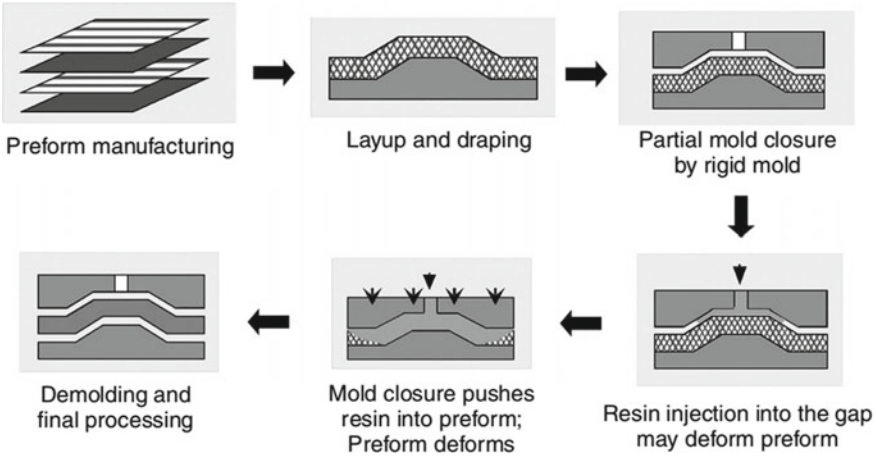

Fig. 7 The moulding process of resin [12]

Table 2 Maximum service temperature for some polymeric matrices [3]

Polymer	Tg (°C)	Maximum service temperature (°C)
DGEBA epoxy	180	125
TGDDM epoxy	240–260	190
PMR-15	340	316
Polyether ether ketone (PEEK)	143	250
Polyphenylene sulfide (PPS)	85	240
Polysulfone	185	160

with the finished product obtained after cooling. In a repeated heating process, the molecular structures remain constant. Thermoplastic resin can be degraded or decomposed under high temperatures for long durations; it has the characteristics of simple shaping and high mechanical energy but has low heat resistance and rigidity. Thermoplastic resins include polyethene (PE), polypropylene (PP), polyvinyl chloride (PVC), polystyrene (PS), polyamide (PA), polyformaldehyde (POM), polycarbonate (PC), polyphenyl ether, polysulfone and rubber.

For laminated composites, the mechanical properties of the interfaces between layers can be described by interlaminar shear strength or interlaminar fracture toughness. The interlaminar shear strength is an important design consideration for structures under bending loads, whereas the in-plane shear strength is essential under torsional loads. Matrix has a significant influence on the interlaminar shear strength, compressive strength, and in-plane shear strength of the FRPs. Besides, the interaction between fibres and matrix is essential in designing damage-tolerant structures. Therefore, the selection of a resin matrix has a significant influence on the properties of FRPs. Additionally, the manufacturing and machining of FRPs depend strongly on the processing characteristics of the matrix. Maximum service temperature for some polymeric matrices is shown in Table 2.

3 Properties of FRP Composites

Compared with traditional materials, composites have many advantages, including high strength-to-weight, high modulus-to-weight, anti-fatigue performance and good vibration damping performance. The components of the composites develop synergistic performance. In other words, the composite material properties are better than the property of each component, where the composite has new properties. Hence, the composite performs significantly better than the components alone.

Composite performance is related to many factors, including fibre direction, fibre content, resin type and curing technique. Compared with conventional metal materials, composites have outstanding mechanical properties. Composites composed of

different fibres and matrix materials have different performances. Generally, strength-to-weight and modulus-to-weight are used to compare the significant mechanical properties, mainly expressed as the materials' bearing capacity and rigidity under equal weights. High strength-to-weight and high modulus-to-weight imply high performance. Strength-to-weight and modulus-to-weight are determined according to the strength and elongation measured at a single stretching test. The structural bearing conditions and failure modes are diverse. Under this circumstance, mechanical properties cannot be measured entirely by strength-to-weight and modulus-to-weight. Therefore, strength-to-weight and modulus-to-weight are only two coarse qualitative performance indexes. Properties of different FRP composites are shown in Table 3.

GFRPs have high strength-to-weight, corrosion resistance, electric insulation, easy manufacturing and low cost. They have a long history of application and are extensively used nowadays. However, glass fibre reinforced composites have the characteristics of high modulus-to-weight.

CFRPs have relatively high strength-to-weight and high modulus-to-weight, high-temperature resistance, anti-fatigue performance and good thermostability. They are high cost and have been increasingly used [7].

AFRPs are a type of composite with high strength-to-weight and high modulus-to-weight. Although they have a higher cost than GFRPs, they have a lower cost than CFRPs. AFRPs are becoming a popular material.

Generally, FRPs have advantages shown as following:

(1) High strength-to-weight: especially high-strength carbon fibre and aramid fibre reinforced composites.
(2) High modulus-to-weight: except for GFRPs, composites have significantly higher modulus-to-weight than metals, especially high-modulus carbon fibre reinforced composites.
(3) Designability of materials: composites have significant differences compared with metallic materials. Composite performance is determined by fibre content and pavement and the performance of the fibre and matrix. Hence, fibres in composites can be designed in appropriate amounts and good pavements according to the loading conditions and structural shape. This aims to meet the design requirements with the least material used and maximum material performance.

Table 3 Properties of different FRP composites [3]

	Density (g/cm^3)	Tensile strength (GPa)	Tensile modulus (GPa)
CFRP (unidirectional)	1.55	1550	137.8
GFRP (unidirectional)	1.85	965	39.3
AFRP (unidirectional)	1.38	1378	75.8

(4) Simple manufacturing techniques and low cost: composite components generally do not require complicated machining equipment and require few production procedures. Thin-walled components with complicated shapes can be manufactured with low consumption of materials and processes.
(5) Some composites have good thermostability. For example, carbon fibre and aramid fibre have a negative coefficient of thermal expansion. Composites with a minimal thermal expansion coefficient can be prepared by combining carbon fibre or aramid fibre with a matrix material with a positive coefficient of thermal expansion. Structures only have minimal thermal stresses and thermal deformation upon changes in the environmental temperature.

Besides, various composites have many different useful characteristics, such as fatigue resistance, impact resistance, electromagnetic permeability, damping properties and corrosion resistance.

Generally, FRPs have disadvantages shown as following:

(1) Serious anisotropy. Although composites have good performance along the fibre direction, their performance perpendicular to it is mainly determined by the performance of the matrix material as well as the bonding strength between the matrix and fibres. Generally, the mechanical properties perpendicular to the fibre direction is lacking. In particular, the interlayer shearing strength is deficient in laminated composites.
(2) Composites have a great range of properties, making it challenging to realize quality control and detection. However, material quality can be improved by improving processing and detection technologies, which will also reduce performance disparities.
(3) Composites have high costs. At present, boron fibre reinforced composites are the most expensive. Carbon fibre reinforced composites are more expensive than metals, while glass fibre reinforced composite is low-cost.
(4) Some composites have low robustness and difficult mechanical jointing.

Based on the above disadvantages, some disadvantages can be mitigated through the design of the material. This is why composites are extensively used in many fields and have promising development prospects.

The interface is the region with a certain thickness (several angstroms to hundreds of angstroms) formed by physical and chemical interactions between fibres and the resin matrix [13]. The structural, chemical and physical properties of the interface are different from those of the fibres and resin. The interface is also called the interface phase or interface layer. However, the notion of interface or interphase remains relatively vague, as the interfacial zone does not exist in itself but is created during the implementation of the composite.

Properties affected by the interface include strength, modulus, and toughness. A weak interface also reduces fatigue endurance of aligned fibre composites. High adhesion between fibres and resin providing is a necessary condition for high-performance composites. The properties of the interface layer are affected by the reinforcement materials, matrix material, curing technique (e.g. pressure, temperature and density)

and service conditions [14, 15]. Proper adhesion can be reached for properly selected combinations of fibre and matrix materials under some additional conditions. Based on this, the fibre-matrix interface can transfer the stresses efficiently so that these excellent properties are maintained, and are not degraded by the environmental and other factors encountered in use.

Currently, various mixed fibre reinforced composites have been manufactured, which have better mechanical properties than single fibre reinforced composites. Hybrid composites, a class of composite material, have two or more high-performance reinforcements combined at the micrometres or molecular level [16]. When hybrid composites contain two types of reinforcing fibres, it is called hybrid fibre composites. The three most basic configurations are shown in Fig. 8 [17].

The purpose of bringing two fibre types in a single composite is to maintain both fibres' advantages and alleviate some disadvantages. In other words, it is considered that some of the individual components are a more favourable balance between the inherent advantages and disadvantages. Therefore, the hybrid composite containing two or more fibre types will beneficially complement what is deficient in the other. The hybrid composite strength depends on the fibre content's properties, length of distinct fibres, fibres orientation, fibre to matrix bonding and fibres sequence arrangement of both the fibres.

The hybrid structure is a mixture of each material's required properties, such as the ratio of strength-to-weight, modulus-to-weight, fatigue strength, and fatigue damage tolerance. The goal is to increase the failure strain, ductility, and toughness. The failure strain of individual fibres will justify the strength of the hybrid composite and highly strain compatible fibres will determine the maximum hybrid results. For example, replacing carbon fibres in the middle of a laminate by cheaper glass fibres can significantly reduce the cost, while the flexural properties remain almost unaffected [17]. If a hybrid composite is loaded in the fibre direction in tension, then the more brittle fibres will fail before the more ductile fibres.

Composites can improve material properties, prolong service life and strengthen functionality. Figure 9 shows the product life cycle of FRPs, beginning with fibres and polymers and ending with recycling the material [18]. To obtain an automated high

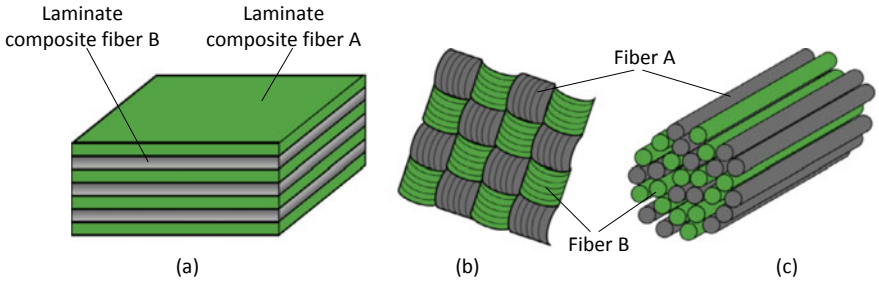

Fig. 8 The three main hybrid configurations **a** interlayer or layer-by-layer, **b** intralayer or yarn-by-yarn, **c** intrayarn or fibre-by-fibre [17]

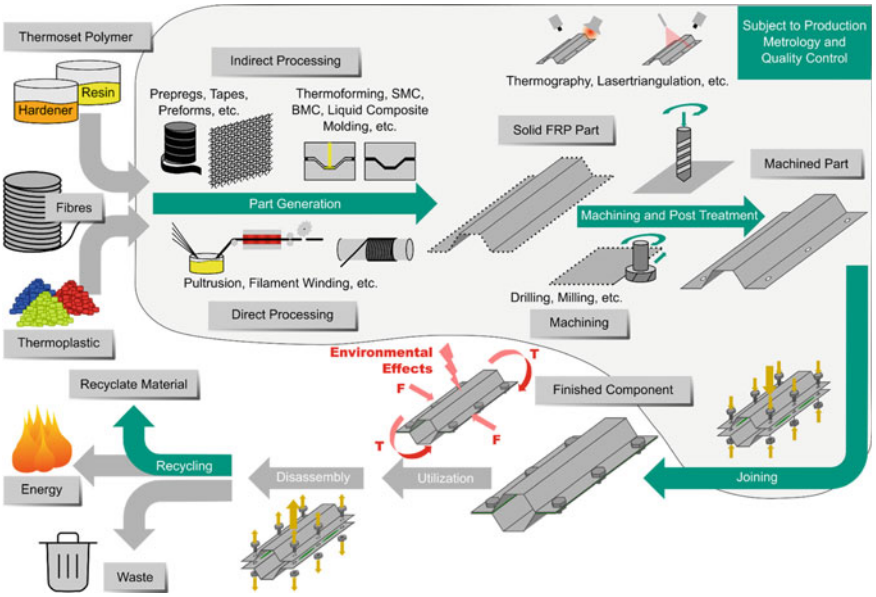

Fig. 9 The product life cycle for composite materials parts manufacturing [18]

volume FRPs in the future, considerable challenges in production technology still need to be mastered. Much attention is focused on conventional and unconventional machining technologies of FRP composites.

Recycling of FRPs has a significant impact on production processes. The resin will produce plastic flow, and the resin matrix size will be reduced when FRP is recycled, decomposed and reproduced. It will lead the FRP properties decreased on reprocessing. Hence, attention should be paid to the recyclability of composite parts. The use of FRPs has created an immediate legacy problem and business opportunity regarding the waste produced from manufacturing and end of life products.

The recycling of composite parts is complicated, and they can cause adverse impacts on the environment. Polymer-based composites are mainly inflammable substances and may release abundant toxic gases during combustion that pollutes the environment. Moreover, volatile components such as matrix solvents may be diffused into the air during moulding. Composites are composed of multiple components and are multi-phase materials. Composite parts should be degraded into single-material parts, but it is difficult to grind, thin, melt and degrades. As a result, such decomposition techniques have high costs, and the regeneration cost is relatively high. It is challenging to recover the original properties.

Different recycling processes are needed for thermoset and thermoplastic. Mostly, thermosetting resin composites cannot be melted and remoulded due to three-dimensional cross-linking structure. Recycling of thermosetting resin composites is more complicated than that of thermoplastic resin composites. Because thermosetting composites are widely used, unique high-efficient recycling technology is required.

Easy disassembly of parts is one of the major requirements for recycling. Recycling requires single materials as much as possible. Composites should be comprised of as few material categories as possible.

Considering the above principles, the usage rate of thermoplastic polyolefin and polypropylene foam material may be increased significantly. On the contrary, the usage rate of thermosetting resins is restricted. Currently, significant progress is achieved in regeneration and degradation under thermoset and thermoplastic of thermosetting resin composites.

4 Manufacturing Techniques of FRP Composites

Transformation of uncured or partially cured fibre-reinforced matrix into composite parts or structures involves curing the material at elevated temperatures and pressures for a period. High cure temperatures are required to initiate and sustain the chemical reaction that transforms the uncured or partially cured material into a fully cured solid. High pressures are used to provide the force needed for the flow of the highly viscous resin or fibre–resin mixture in the mould, as well as to remove volatiles and excess air, to facilitate the consolidation of the laminate, and to apply temperature and pressure to ensure good bonding during cure. For example, the most critical processing characteristics include the liquid viscosity, the curing temperature, and the curing time for epoxy resin polymers.

There are numerous methods for fabricating composite components. The selection of the fabrication method for a particular part is the most crucial before the part design and end-use or application. The first manufacturing method for FRPs structural parts used a hand lay-up technique. Recently, there is more emphasis on the development of manufacturing methods that can support mass production. Modern techniques of fabrication are developed such as vacuum bagging, autoclaves, Resin Transfer Moulding (RTM), Vacuum-Assisted Resin Transfer Moulding (VARTM), Resin Film Infusion (RFI), injection moulding, filament winding, pultrusion, and many other to produce a reliable and robust composite structure or component in primary composite fibres [19–21].

Different techniques can manufacture composites according to the structural shape required. Rotating components, such as pressure vessels and shells, can be prepared by fibre interweaving techniques. However, large plane structures can use the autoclave moulding technique.

4.1 Laminated Composites

Composites formed by the layered pavement of prepregs are called laminated composites. The laminate composite is produced by stacking several thin layers of fibres and matrix (called prepreg) and laying them into the desired thickness. The

ply consists of several fibres through the thickness that is aligned and continuous. Typical volume fractions of fibre are on the order of 60% [4]. In the preparation of composites, an epoxy resin matrix is infiltrated into the fibre and then dried into prepregs used to manufacture various products with a variety of specific manufacturing techniques. The structure of continuous fibre reinforced resin composites is shown in Fig. 10.

Unidirectional fibre prepregs are paved according to the designed angle and number of layers to manufacture plate or large-curvature components. Next, the material is put between platforms or moulds for pressurization and curing shaping with heat. Consequently, laminated-structured composites are formed. Thermosetting prepreg must be kept refrigerated until they are assembled and placed in the curing process. Thermoplastic prepreg, on the other hand, does not have to be stored under refrigeration. They tend to be stiff and are usually softened before assembly. The final manufacture could involve heating and form in matched moulds. The unidirectional prepreg can be cut and stacked to form the final product. Because the individual fibres are relatively straight, the use of a unidirectional prepreg provides a method, along with filament winding, of achieving finished products with excellent mechanical properties.

Laminating moulding is done to pave prepregs in different layers and then mould them at a specific temperature and pressure. After chemical curing, no plastic formability remains for thermosetting matrix FRPs. However, a subsequent plastic deformation is possible for thermoplastic matrix FRPs by reheating after cooling down. The modulus and strength of the thermoplastic matrix FRPs are lower compared to the thermosetting matrix FRPs. Besides, creeping is easily generated on thermoplastic matrix FRPs caused by long-term loads. Furthermore, the curing temperatures of thermoplastic polymers are higher than those of thermoset polymers.

Fibre direction in each layer and the stacking sequence of different layers in a laminate can be designed to produce a wide range of physical and mechanical properties for the laminated composite. The characteristics of the manufactured FRPs can be quasi-isotropic or anisotropic depending on the fibre orientation inside the composite. With fibre reinforcements, quasi-isotropic semi-structural FRPs can be produced by highly automated production processes. If fibres in the laminated composites are

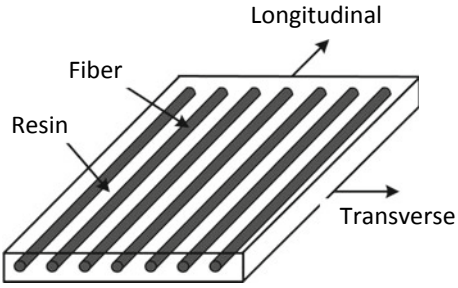

Fig. 10 Structure of monolayer fibre reinforced composites [22]

paved in the same direction, they are called a unidirectional composite. If fibres are paved in different directions, it is called a multidirectional composite.

Due to the fibre lay-up direction, unidirectional composites generally have high strength and modulus along with the fibre directions, but low mechanical properties perpendicular to them. In the preparation of FRPs, the fibre's lay-up direction can be chosen according to the stresses expected in the components, thus improving the usability of components.

Also, a relatively sizeable residual stress is generated in the curing process due to the significant difference in the coefficients of thermal expansion of fibre and resin. To reduce material deformation caused by stress, laminated prepregs are generally set symmetrically. A typical lay-up mode of laminated FRPs is shown in Fig. 11a. The cross-section microstructure of a multidirectional CFRP profile is shown in Fig. 11b.

According to the properties expected for FPRs, sometimes fibres are weaved in two orthogonal directions, in which the weft alternatingly crosses over and under the warp. This creates the highest crimp with the tightest fabric and poorest drape ability and the most resistant to in-plane shear movement. A typical lay-up mode of FRPs is shown in Fig. 12a. Furthermore, the cross-section microstructure of a multidirectional AFRP profile is shown in Fig. 12b.

4.2 Cylindrical Structures

The typical method for fabricating cylindrical composite structures is filament winding. Filament winding is an efficient automated process of placing resin-impregnated roving or monofilaments onto a rotating mandrel removed after curing the composite part. The matrix may be added to the fibre by running the fibre tow

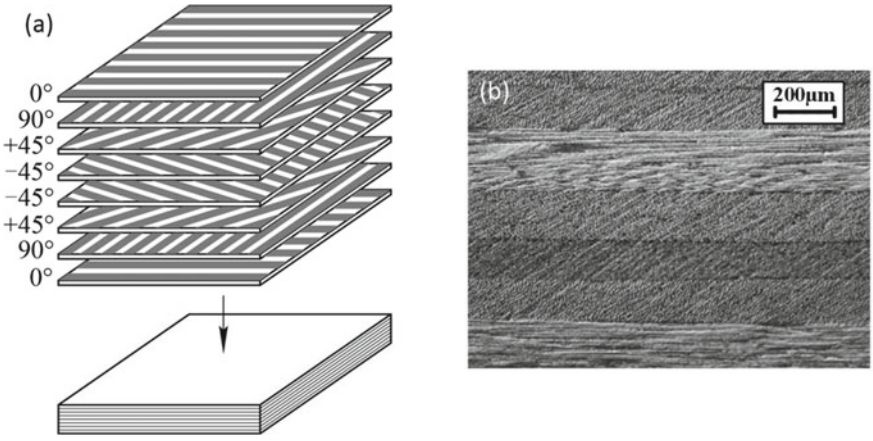

Fig. 11 Structure of a CFRP composite **a** stacking sequence, **b** cross-section

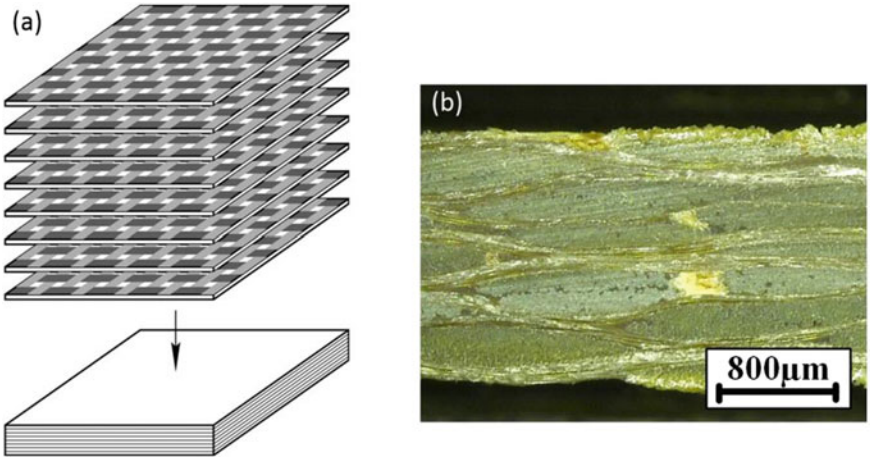

Fig. 12 Structure of an AFRP composite **a** stacking sequence, **b** cross-section

through a matrix bath at the time of placement, or else the roving may be prepregged before winding. The filament winding process consists of winding continuous-fibre tow, yarn, or tape around a form or mandrel to form the structure. Usually, the component's cure is done at room temperature or by applying heat without vacuum bagging or autoclave consolidation. Filament winding is typically a low-cost method because of the use of fibres and resins in their lowest-cost form, as well as highly automated and repeatable.

Preliminary tension applied to the roving in winding induces pressure between the layers providing compaction of the material. Varying the winding angle, it is possible to control material strength and stiffness within the layer and through the laminate thickness.

Filament winding processes can be subdivided into two groups regarding the basic design and the machine kinematics. On the one hand, the mandrel itself rotates. Simultaneously, the fibre placement is controlled to move longitudinally in a prescribed way to generate the required fibre inclination angle to the axis of rotation. The motion may be synchronized using CNC machines or by conventional machines similar to the lathe. On the other hand, there is a flexible robot winding.

Filament winding is a continuous fabrication method which has emerged as the primary process for composite cylindrical structures and axisymmetric hollow parts. Filament winding has been widely used for making automotive drive shafts, helicopter blades, oxygen tanks, pipelines, spherical pressure vessels, conical rocket motor cases, glass-fibre pipe, rocket motor cases, golf shafts, drilling risers, energy absorption tube, large underground gasoline storage tanks and other similar products.

The filament-winding process is also used to manufacture prepreg sheets or continuous fibre-reinforced sheet-moulding compounds. The most advantageous of filament winding is manufacturing thin-walled shells of revolution, though it can be

Fig. 13 Filament winding setup [23]

Fig. 14 GFRP cylindrical shells [23]

used in building composite structures with more complicated shapes. Besides, several specialized techniques are being considered for more complicated shapes. Filament winding setup and GFRP cylindrical shells are shown as in Figs. 13 and 14.

5 Applications of FRP Composites

Material selection is one of the most important and critical steps in the structural or mechanical design process. The properties of FRPs (especially strength and modulus) should be considered in the selection process depending on the performance requirements and possible mode of failure.

FRP composites have proven to be flexible and adaptable engineering material for many applications, including aerospace, aircraft, automotive, construction, marine, commodity, and sports. Commercial and industrial applications of FRP composites are so varied that it is impossible to list them all. Here, several application areas are given, including aircraft and military, automotive, infrastructure, and sporting goods. FRP composites are also used in electronics, building construction, furniture, power industry, oil industry, medical industry, and many industrial products, such as oxygen tanks, and power transmission shafts. The potential use of FRPs exists in many engineering fields, based on their unique mechanical, physical, and thermal characteristics.

Large-scale research projects undertaken in 1993 in the USA and Canada involving CFRP/GFRP composites confirmed the decision to use such materials in construction [24]. The USA is the largest producer and user of FRP composites and leads the world's composite technology development and implementation. The US composite industry is expanding despite the overall slow-down in the US economy in the past couple of years. FRP manufacturing is predicted to rise at a yearly rate of 4–5% over the next five years [25].

5.1 Aircraft and Aerospace Applications

Composites are the most typical materials used in the aerospace field. Using advanced composites in aerospace structures can reduce weight by 20–30%, which is beyond other advanced technologies. Advanced composites have become one of four structural materials used in the aerospace field after aluminium alloy, titanium alloy and high-strength steel. The increasing amount of advanced composites used has become an essential symbol of aircraft advancement. Composites for aircraft commenced with non-load-bearing components (e.g. cabin doors and antenna housings). Then they were used for secondary and principal load-bearing components (e.g., empennages and wing boxes) over the last 50 years [26].

The number of composite applications has become an important index used to measure the aerospace industry's advancement. Two iconic enterprises in the aerospace field, Boeing and Airbus, have given much attention to composites' use. In 1985, Airbus first used composites in aircraft manufacturing for the empennage of the A310 passenger plane. Subsequently, Airbus used composites in the wings of the A350 passenger plane. The Boeing 787 aircraft includes many technological innovations. The most attractive is that the main body structure (including wings and fuselage) uses about 50% composites [27, 28]. It is the first jetliner for civil use that uses composite in the main structure. To maintain competitiveness with Boeing, the Airbus A350 is also extensively comprised of composites. About 25% of the primary members of the A380 are made of advanced lightweight materials, and the mass of composites is about 32 tons, accounting for 22% of the total weight [26]. The components made of CFRPs used in Airbus 350 aircraft is shown in Fig. 15 [29]. It

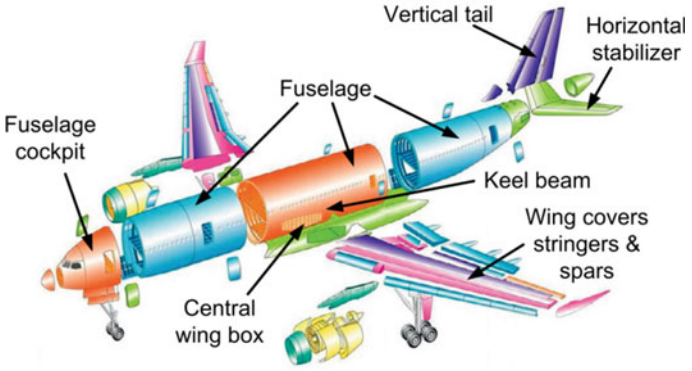

Fig. 15 Large-size CFRP composite components used in Airbus 350 [30]

is a fact that, rather than metals, composites have become the primary material used in aircraft structures.

Advanced composites have made outstanding contributions to the aerospace technological field and will occupy a vital role in aerospace technologies' future development. Since a satellite launch may cost tens of millions of dollars, it is important to use light structural materials with high performance. Therefore, composites play an irreplaceable role in launchers, missiles, satellites and aircraft.

5.2 Military Applications

Advanced composites have promising application prospects in weapon equipment. Increasing the use of composites is crucial to reduce weight and improve performance. For instance, the range of a strategic missile can be increased by 16 km for each 1 kg reduction in weight, and the range of a warhead can be increased by 20 km for each 1 kg reduction. The weight of a missile launcher can be reduced by more than 20% by using advanced composites, which increases its manoeuvrability and improves its fatigue and corrosion resistance.

With their outstanding impact resistance, aramid fibre reinforced composites have been highly useful in bulletproof equipment. After long-term perfection and development, the successful application of aramid fibre reinforced materials has become an important milestone in the strengthening and lightweight, protective armour design.

The traditional homogeneous armour used in tanks cannot resist attack by advanced antitank weapons, whose destructive power gradually increases. Although thickening armour can enhance the protection of tanks, it also may restrict their manoeuvrability. Composite armour is a kind of heterogeneous armour composed of multiple layers of protective materials with different properties. AFRP is an essential component of the multilayer structure of composite armour. Composite armour is

widely used in the third generation of main battle tanks to improve protection. For instance, Kevlar fibre reinforced composites are used in the interlayered composite armour structure in the M1A1 (as shown in Fig. 16) main battle tank (United States).

AFRP composites have replaced traditional massive metals in the physical armour field and become the primary material used in bulletproof helmets and personnel armour. In the 1970s, Natick Research Lab first produced a type of soft personnel armour using Kevlar fibre reinforced composites to replace steel materials and named it the Personnel Armour System for Ground Troops (PASGT). With ongoing development, PASGT has been improved and perfected continuously. Currently, the Advanced Combat Helmet (ACH), shown in Fig. 17, and Improved Outer Tactical Vest (IOTV), issued to US ground forces, as well as the Lightweight Helmet (LWH) and Modular Tactical Vest (MTV) used by the US Marine Corps, are all updated versions of PASGT. They all use Kevlar fibre reinforced composites as the primary bulletproof materials.

Aramid fibre reinforced materials have been widely used in the aerospace field as an advanced composite. In the 1970s, the L-1011 TriStar wide-body passenger plane developed by Lockheed Corporation (USA) used 1135 kg of Kevlar fibre reinforced composite. In 1977, the main body of the S-76 Spirit civil helicopter manufactured by Sikorsky Aircraft Corporation (USA) applied Kevlar fibre reinforced composites for as much as 50% of the aircraft's' area. In 1980, the An-124 heavy transport machine designed by Antonov Design Bureau of the Soviet Union mainly used aramid fibre reinforced materials in the main body, and the total weight was 3000 kg.

To manufacture high-pressure vessel structures similar to solid rocket engine casts, aramid fibre composite has become the first choice for replacing glass fibre reinforced composites. The three-stage solid rocket engine casts of the Trident submarine-based ballistic missiles and Peacekeeper ground-to-ground ballistic missiles, made in the USA in 1970, were all manufactured with interwoven Kevlar fibre reinforced

Fig. 16 Aramid composite armour [31]

Fig. 17 Aramid composite helmet [32]

composites. These casts were 50% lighter than the same size of glass fibre reinforced composite cast. Besides, aramid fibre reinforced materials are widely used in antenna structures for their excellent heat-insulating properties and electromagnetic wave permeability.

5.3 Mobile Phone Applications

Aramid fibre composites were viewed as strategic materials in the armour, aerospace and military industries. With the end of the cold war and rapid technological development, the market for aramid fibre reinforced composites in civil services opened and expanded quickly. In the competitive mobile phone industry, some mobile phones' rear shells use aramid fibre reinforced composites. Due to their strong robustness and friction resistance, aramid fibre gives mobile phones an excellent appearance and outstanding user experiences. The application of aramid fibre in the mobile phone is shown in Fig. 18.

5.4 Automotive Applications

Currently, there is increasing concern about the relationship between humans and nature. Environmental and energy challenges have become the key to each country's survival and development in the world. With the increasing consciousness of environmental protection and increasing environmental protection laws, green cars have become an essential trend in automobile development. Therefore, making cars that

Fig. 18 Mobile phone case of aramid fibre [33]

meet environmental protection requirements is on the agenda of automobile manufacturers. As the mainstream material used in cars, composites will play a vital role in future automobile development.

Composites can meet the requirements of lightweight car bodies. In the automobile field, composites are used in auto-body panels, interior trim parts, structural components and functional components. Replacing steel components with composites can reduce the structural weight by 40–60%, thus improving energy efficiency significantly.

Manufacturing and design of fibre-reinforced composite materials for automotive applications are significantly different from those for aircraft applications. One noticeable difference is in the production volume, which may range from 100 to 200 pieces per hour for automotive components compared with a few hundred pieces per year for aircraft components [3].

Composites can also lower fuel consumption and improve safety. Traditional car bodies mainly use thin steel plates alone, which cannot adapt to high speed and lightweight pursuit. Many automobile manufacturers have been researching and using new materials to reduce the weight of car bodies and fuel consumption and improve wind resistance coefficients. The driving distance attained with 1 L of fuel can be increased by 2 km if the car's weight is decreased by 50 kg. Fuel economy can be improved by about 5.5% if the car weight is decreased by only 10%. Many types of composites have been used successfully to achieve lightweight car bodies.

Moreover, racing cars made of CFRP maintain good stability even under high wind resistance, attributed to composites' higher rigidity than steel. Energy-saving, environmental-friendly and safe electric vehicles are a global development trend in the automobile industry. The main structure and energy storage flywheel can also be made of composites. A composite component is shown in Fig. 19.

Fig. 19 The surface geometry of a composite component is checked [34]

Boat structures and hulls incorporate composites to a large extent. GFRPs dominate in pleasure boat building because of its lightweight and resistance to corrosion. CFRP composites are also used in high-performance race boats.

5.5 Infrastructure Applications

In the industrial field, composites can be applied in various infrastructure fields, including roofs, bridges, tunnels and relevant concrete projects. Several reinforced concrete specimens are shown in Fig. 20. Replacing ordinary steel rebars with fibre reinforced polymer rebars increases the strength and fatigue resistance of the structure and can also offset ordinary rebars' ready corrosion. Also, composites are extensively used in the fences of drilling platforms, tunnels, drill collars and drilling tubes due to their strong corrosion and friction resistance.

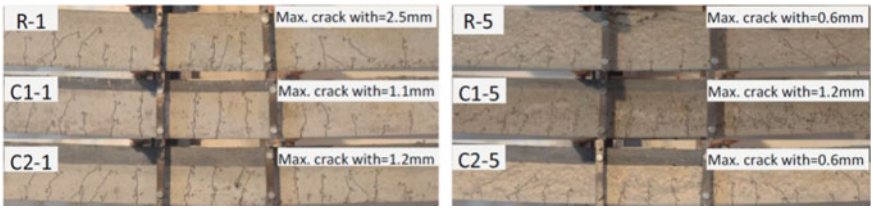

Fig. 20 Crack patterns and the measured maximum crack width of different reinforced concrete specimens [35]

Development of new energy resources and energy-saving and energy-storage technologies is an essential part of the current high-tech field. Energy technologies also need lightweight materials with high strength and resistance to high temperature and corrosion. For example, a single generator capacity has to be increased continuously (reaching about 1.5–2.5 MW) to lower wind power generation costs. The blade length can reach 50 m, which requires blades to have lightweight, high strength and high modulus. CFRP are the ideal material for this. Moreover, composites have promising application prospects in solar energy, atomic energy, ocean energy and super-conduction equipment [36–38].

5.6 Sporting Goods Applications

Composites have also been widely applied in the sports and leisure fields, after the aerospace and aircraft industries. Brassies, tennis rackets and fishing poles are three main composite products. Besides, composites have been used in bicycles, automobile racing, speed boats, skis and stay bars. Composite softball and baseball bats are shown in Fig. 21. CFRP composites dominate in sports applications because of its extraordinary strength and stiffness.

The lightweight, high strength and damping performance of composites can significantly improve the usability of sports products and help athletes achieve good performance. The advantages of using fibre-reinforced polymers are weight reduction, vibration damping, and design flexibility. Weight reduction achieved by substituting carbon fibre-reinforced epoxies for metals leads to higher speeds and quick manoeuvrings in competitive sports, such as bicycle races and canoe races. Some applications, such as tennis rackets or snow skis, sandwich constructions of carbon or boron fibre-reinforced epoxies as the skin material and a soft, lighter weight urethane

Fig. 21 Composite softball and baseball bats [39]

foam as the core material produces a higher weight reduction without sacrificing stiffness. Faster damping of vibrations provided by fibre-reinforced polymers reduces the shock transmitted to the player's arm in tennis or racketball games and provides a better feel for the ball. In archery bows and pole-vault poles, the high stiffness–weight ratio of fibre-reinforced composites is used to store high elastic energy per unit weight, which propels the arrow over a longer distance or the pole-vaulter to jump a greater height. It is an ongoing trend to apply fibre reinforced composites to sports products in the future.

6 Review Questions

(1) How do you select the appropriate preparation technique for composite components with different structures?
(2) In addition to carbon fibre, glass fibre and aramid fibre, what are some other new reinforced fibres and their mechanical properties and applications?
(3) What are the advantages and disadvantages of different types of composites?
(4) What are the major problems in the development of resin-based composites?
(5) Discuss the design and material selection consideration for drive shaft of an automobile, and why FRPs can be a good candidate material.
(6) Design a composite beam that is 30% lighter than the steel beam but has the same tensile strength.
(7) Discuss the use of FRP material components in human health in the future.
(8) Discuss the influence of fibre direction on the tensile strength of CFRP.
(9) What are the major impediments to widespread adoption of AFRP in the aircraft industry?
(10) Describe the major differences between thermosets and thermoplastics in the processing methods.
(11) Discuss the major differences between two composite material manufacturing with the same method, but the matrices are different (thermosets and thermoplastics).
(12) Discuss the terms isotropic and anisotropic as it applies to the matrix and fibres.
(13) Discuss the microstructure of the interface between carbon fibre and thermoset.
(14) Discuss the influence of FRP on the environment during manufacturing and machining.
(15) Discuss the development of environmentally friendly composite products.
(16) Indicate the general-purpose fulfilled by the matrix in fibre reinforced polymer composites.

Acknowledgements The editors would like to thank all the contributors, who participated out of scholarship and a desire to help in their busy schedules. Besides, this research is supported by the National Natural Science Foundation of China (Grant No. 51875367).

References

1. Munalli, D., Dimitrakis, G., Chronopoulos, D., et al.: Electromagnetic shielding effectiveness of carbon fibre reinforced composites. Compos. Part B Eng. **173**, 106906 (2019)
2. Eshelby, J.-D.: The determination of the elastic field of an ellipsoidal inclusion, and related problems. Proc. R. Soc. Lond. A **241**(1226) (1957)
3. Mallick, P.-K.: Fiber-Reinforced Composites: Materials, Manufacturing, and Design. CRC Press (1993)
4. Gardiner, G.: The Making of Glass Fiber [EB/OL]. https://www.compositesworld.com/articles/the-making-of-glass-fiber, 2020-06-01
5. Wang, D., Wang, Q., Wang, Z., et al.: Study on the long-term behaviour of glass fibre in the tensile stress field. Ceram. Int. **45**(9), 11578–11583 (2019)
6. Ahmad, J.: Machining of Polymer Composites. Springer-Verlag, DE (2009)
7. Dong, P.-A.V., Azzaro-Pantel, C., Cadene, A.-L.: Economic and environmental assessment of recovery and disposal pathways for CFRP waste management. Resour. Conserv. Recycl. **133**, 63–75 (2018)
8. Dixit, D., Pal, R., Kapoor, G., et al.: Lightweight composite materials processing. In: Lightweight Ballistic Composites, pp. 158–245 (2016)
9. Vasiliev, V.-V., Morozov, E.-V.: Mechanics and Analysis of Composite Materials. Elsevier (2001)
10. Vasiliev, V.-V., Morozov, E.-V.: Advanced Mechanics of Composite Materials and Structures (2018)
11. Luo, Z.-P., Sun, C.-Y.: Effect of the interfacial bonding status on the tensile fracture characteristics of a boron–fiber-reinforced aluminum composite. Mater. Charact. **50**(1), 51–58 (2003)
12. Advani, S.-G., Hsiao, K.-T.: Manufacturing Techniques for Polymer Matrix Composites (PMCs). Woodhead Publishing (2012)
13. Teklal, F., Djebbar, A., Allaoui, S., et al.: A review of analytical models to describe pull-out behavior—fiber/matrix adhesion. Compos. Struct. **201**, 791–815 (2018)
14. Karger-Kocsis, J., Mahmood, H., Pegoretti, A.: Recent advances in fiber/matrix interphase engineering for polymer composites. Progr. Mater. Sci. **73**, 1–43 (2015)
15. Sharma, M., Gao, S., Mäder, E., et al.: Carbon fiber surfaces and composite interphases. Compos. Sci. Technol. **102**, 35–50 (2014)
16. Supian, A.-B.-M., Sapuan, S.-M., Zuhri, M.-Y.-M., et al.: Hybrid reinforced thermoset polymer composite in energy absorption tube application: a review. Def. Technol. **14**(4), 291–305 (2018)
17. Swolfs, Y., Gorbatikh, L., Verpoest, I.: Fibre hybridization in polymer composites: a review. Compos. Part A Appl. Sci. Manuf. **67**, 181–200 (2014)
18. Fleischer, J., Teti, R., Lanza, G., et al.: Composite materials parts manufacturing. CIRP Ann. **67**(2), 603–626 (2018)
19. Abdewi, E.-F., Sulaiman, S., Hamouda, A.-M.-S., et al.: Effect of geometry on the crushing behaviour of laminated corrugated composite tubes. J. Mater. Process. Technol. **172**(3), 394–399 (2006)
20. Nirmal, U., Hashim, J., Megat Ahmad, M.-M.-H.: A review on tribological performance of natural fibre polymeric composites. Tribol. Int. **83**, 77–104 (2015)
21. Mamalis, A.-G., Manolakos, D.-E., Ioannidis, M.-B., et al.: On the crashworthiness of composite rectangular thin-walled tubes internally reinforced with aluminium or polymeric foams: experimental and numerical simulation. Compos. Struct. **89**(3), 416–423 (2009)
22. Liu, D., Tang, Y., Cong, W.-L.: A review of mechanical drilling for composite laminates. Compos. Struct. **94**(4), 1265–1279 (2012)
23. Panchagnula, K.-K., Panchagnula, J.-S.: Fabrication of hoop-wound glass fiber reinforced plastic cylindrical shells using filament winding machine. Mater. Today Proc. **27**, 1315–1318 (2020)
24. Mugahed Amran, Y.-H., Alyousef, R., Rashid, R.-S.-M., et al.: Properties and applications of FRP in strengthening RC structures: a review. Structures **16**, 208–238 (2018)

25. Hassan, W.-M., Hodhod, O.-A., Hilal, M.-S., et al.: Behavior of eccentrically loaded high strength concrete columns jacketed with FRP laminates. Constr. Build. Mater. **138**, 508–527 (2017)
26. Marsh, G.: Airbus A350 XWB update. Reinf. Plast. **54**(6), 20–24 (2010)
27. Boeing opts for composites for 7E7. Reinf. Plast. **47**(7), 10 (2003)
28. Marsh, G.: Boeing's 787: trials, tribulations, and restoring the dream. Reinf. Plast. **53**(8), 16–21 (2009)
29. M'Saoubi, R., Axinte, D., Soo, S.-L., et al.: High performance cutting of advanced aerospace alloys and composite materials. CIRP Ann. **64**(2), 557–580 (2015)
30. Hexcel Ready to Fly on the A350 XWB, pp. 25–26. Elsevier B.V. (2013)
31. Baidu: M1A1 Abrams [EB/OL]. https://baike.baidu.com/item/M1A1%E4%B8%BB%E6%88%98%E5%9D%A6%E5%85%8B/3721798?fr=aladdin, 2020-11-14
32. Kumalagov, S.: Aramid Composite Helmet 6B7-1M Russian Armed Forces [EB/OL]. https://www.worldmilitary.org/en/russia/ballistic_protection_russia/shlemy_kaski/RU-HE-00003 (2020)
33. Alibaba: High Quality Slim Mobile Cover Carbon Aramid Fiber Phone Case Cover Shell Black/Grey Twill Color for iPhone 12 iPhone12 Pro [EB/OL]. https://www.alibaba.com/product-detail/2020-High-quality-slim-mobile-cover_1600135591413.html?spm=a2700.galleryofferlist.topad_classic.d_image.54b13b9bFklQCF (2020)
34. Marsh, G.: Carbon composite car body panels gain traction with Gurit Automotive. Reinf. Plast. 24–27 (2011)
35. Turker, K., Torun, I.-B.: Flexural performance of highly reinforced composite beams with ultra-high performance fiber reinforced concrete layer. Eng. Struct. **219**, 110722 (2020)
36. Boisseau, A., Davies, P., Thiebaud, F.: Sea water ageing of composites for ocean energy conversion systems: influence of glass fibre type on static behaviour. Appl. Compos. Mater. **19**(3–4), 459–473 (2012)
37. Ferguson, A.-J., Blackburn, J.-L., Holt, J.-M., et al.: Photoinduced energy and charge transfer in P3HT:SWNT composites. J. Phys. Chem. Lett. **1**(15), 2406–2411 (2010)
38. Mao, S., Lu, G., Chen, J.: Three-dimensional graphene-based composites for energy applications. Nanoscale (2014)
39. Grande, D.-H., Greist, S., Jessie, T., et al.: 3.18 Composites in Sports Applications, 469–526. Elsevier (2018)

Conventional Machining Processes of Fibre Reinforced Polymer Composites

Ben Wang and Hang Gao

Abstract Although FRPs are usually fabricated to near net shapes after curing, post-machining operations are necessary to assure that the composite parts meet dimensional tolerance, surface quality and other functional requirements. Owing to the material's unique anisotropic characteristics, it is a challenge to machine FRPs without machining damage. Machining damages can arise in each phase of the material, including matrix cracking, fibre fracture, fibre pull-out, fibre-matrix debonding and delamination. Orthogonal cutting is a common machining process for better understanding of the mechanisms of common processing methods. Traditional machining operations, such as turning, milling and drilling, are still the primary processing mode of FRPs. With considerations to processing demands and material performance of different composite materials, developing the corresponding special cutter is the key technology to prolong the cutter's service life and improve processing quality.

1 Introduction

Performances of composite materials are significantly different from those of traditional metal materials as there are a series of difficulties in processing composite materials. Considering the processing demands of composite materials, the material removal processes are explored deeply based on analyzing the characteristics and performance of the materials during machining. It is the premise to study high-quality and high-efficiency processing technology of composite materials. Currently,

B. Wang (✉)
Key Laboratory of Fundamental Science for National Defense of Aeronautical Digital Manufacturing Process, School of Mechanical and Electrical Engineering, Shenyang Aerospace University, Shenyang, Liaoning, China
e-mail: wangben211@163.com

H. Gao
Key Laboratory for Precision and Non-Traditional Machining Technology of Ministry of Education, School of Mechanical Engineering, Dalian University of Technology, Dalian, Liaoning, China

I. Shyha and D. Huo (eds.), *Advances in Machining of Composite Materials*, Engineering Materials, https://doi.org/10.1007/978-3-030-71438-3_3

traditional processing technologies are still extensively used to process composite materials, mainly including turning, drilling and milling. In particular, the cutting tools' abrasion problem becomes very prominent due to the high strength of the fibre and low heat conductivity coefficient of the resin matrix.

During the past decades, fibre reinforced polymer (FRP) composites are increasingly demanded in various industries (such as aircraft, spacecraft, automobile, marine, and sporting goods) for high-performance. Although composite materials, especially the FRPs based on long fibre-reinforced resin, could be fabricated in a near-net shape via prepreg lay-up and autoclave processes, the prepared composite materials have to be machined, thus achieving the needed geometric and dimensional accuracy. At present, traditional machining is still the primary processing mode of composite materials. Since properties of FRPs are significantly different from metal materials, material removal mode, generation of machining damage, processing conditions and cutter specification in traditional machining of metal materials are challenging to be used in machining composite materials. Hence, problems in material removal of composite materials are significantly different. For instance, for the composite formed by prepregs' layered pavement, delamination is often generated during drilling of laminated composites. Otherwise, the angle between fibre direction and cutting direction has a significant influence on the machining quality. The properties of the composite are different along fibre direction, perpendicular to fibre direction or other directions. Additionally, as fibres' properties vary significantly, cutting parameters and cutting tools should be changed accordingly to the machined material (CFRP, GFPR and AFRP).

Many reliable and effective machining techniques have been developed for metal materials. However, it is not an appropriate decision to machine FRPs by directly applying those techniques. Although turning, drilling and milling are widely used in machining processes to shape FRPs, the machining parameters and machining tools for shaping FRP have been developed by considering the machining characteristics of FRPs.

2 Characteristics of Conventional Machining of FRPs

FRP is a type of heterogeneous material that is bonded and solidified using fibre and resin matrix according to specific design requirements. During traditional machining of composite materials, several properties of FRPs should be concerned as follows:

(1) Low interlayer strength. Composite materials are mainly paved by prepreg layer by layer. The properties of the resin matrix mainly decide the interlayer strength of materials. However, composite materials' interlayer strength is low due to the relatively poor mechanical properties of the resin, which can easily cause delamination during processing [1].
(2) Anisotropy. Since the fibres are paved toward a particular direction, fibre reinforces the composite materials' mechanical properties along the longitudinal

direction of the fibre. However, composite materials' horizontal mechanical properties remain poor, resulting in the strong anisotropy of the properties of composite materials.

(3) Difficult to machine the reinforcing fibres. Reinforced fibres generally have some processing difficulties due to their high strength and low heat conductivity coefficient. For example, the hardness of carbon fibre is about 648 HV [2], which is marginally higher than the ordinary high-speed steel (about 602 HV). Therefore, cutters are quickly worn during machining, thus shortening the tool life. When machining of CFPR by high-speed steel twist drill, each drill must be re-sharpened or changed after drilling 2–3 holes.

(4) High cutting temperature. Since heat conductivity coefficients of carbon fibre, aramid fibre and epoxy resin are low, the heat conductivity coefficient of composite materials, especially the interlayer heat conductivity coefficient is significantly low (<1.04 W/m K [3]) than that of ordinary metal materials (heat conductivity coefficient of 45# steel is 50.2 W/m K). It is easy to cause accumulation of heat in the cutting zone, resulting in the excessive temperature.

(5) Heat sensitivity of the resin matrix. High temperature can influence the performance of carbon fibre, but it may significantly affect the resin. The glass transition temperature of standard epoxy resin is about 150–200 °C. Softening temperature and curing temperature of epoxy resin are the same. If the cutting temperature is higher than the resin's glass transition temperature, the resin will be softened, chemical decomposition and degradation occurs even at moderate temperatures. The resin degradation could cause debonding of the fibre/matrix interface, leading to severe defects and deterioration of the overall performance of composite materials [4].

(6) Dry cutting. Since epoxy resin matrix is a macromolecular chain structure with abundant spaces inside, water molecules enter into composite materials through resin spaces or along with the carbon fibre/resin interface when the composite is in a liquid environment. The hydrolysis breakage of the chemical bond between fibre and resin might occur. The fibre/matrix interface is damaged due to resin expansion once water molecules accumulate on the carbon fibre/resin interface, thus reducing the composite's overall performance [5]. Hence, the cooling liquid is often not allowed in the processing of composite.

At present, the main technical difficulties when machining composite components include:

(1) Difficulty to obtain the required quality. The preparation of composite components determines the anisotropy of mechanical properties and low interlayer strength. High strength and low heat conductivity, reinforced fibres are elementary to produce fuzzing, tearing and other damages in machining, and even cause a scrap of expensive parts [6].

(2) Serious tool wear. Due to the high hardness of fibre and low heat conductivity of FPRs, tool wear is rapid during machining. The cutting zone temperature is high and concentrated at a narrow region close to the tool cutting edge. Therefore, the flank surface of the cutter is usually seriously worn during the

short cutting time. This influences the shape, size accuracy of products, and surface quality and claims a high production cost [7].

(3) High processing cost and risks. Most of FRPs are expensive, and their manufacturing cost is always high. However, these composite components can be hardly repaired upon unsatisfying holes or machining accuracy and quality in subsequent processing. It was reported that, in the aircraft industry, the rejection of parts made of composite laminates due to drilling-induced delamination damages during final assembly was as high as 60% [8].

(4) Dust pollution in the operating environment and damages to the equipment. Clouds of dust produced by machining composite materials are extremely harmful to workers health as well as equipment. Notably, carbon fibre has high electrical conductivity and can cause short-circuit of the peripheral electronic control system or a power grid in addition to the understandable environmental pollution.

3 Removal Mechanisms

The damage forms and failure modes of FRPs are deeply affected by their microstructures' changes and the interfacial properties, including fibre orientation, volume fraction, voids and cracks. It might generate new damages during the cutting process at the week points in the FRPs due to the high cutting force. Since composite is composed of the reinforced phase (fibre) and continuous phase (epoxy resin), composites' removal process is more complicated than that of homogeneous materials. Moreover, geometry and cutting angle of the cutter is adjustable in a practical cutting process. For example, cutting angle at different positions of the cutting edge varies during the drilling of FRPs using a standard twist drill. Thus, an uneven cutting force is applied to the FRPs, which can cause a complex stress state in the FRPs. The anisotropy of FRPs can be affected much by the complex stress state to form new damages.

Fibres are paved according to a specific direction and thereby form composite reinforced by long fibres. In other words, axial and transverse performances of fibre differ significantly. Unidirectional composite in which fibres are paved toward a consistent direction has strong anisotropy. In cutting mode analysis, the anisotropy of materials can be simplified into two models: cutting perpendicular to the axis of fibre in multi-layers (orthogonal machining [9]) and cutting in a layer (parallel cutting), as shown in Fig. 1 [10].

Orthogonal machining is mainly used to study anisotropy in composite processing. However, stress on materials during turning and drilling is significantly different from orthogonal machining. Material removal is not dominated by orthogonal machining but is dominated by cutting in a layer. Especially, multi-layer materials were cut in the same time by the main cutting edge in drilling. Cutting in a material layer is indeed the consequence of one section of the main cutting edge. Therefore, the drilling can be defined as cutting the corresponding fibre layer by a multi-stage main cutting edge. It can be decomposed into several cutting processes of cutting in a

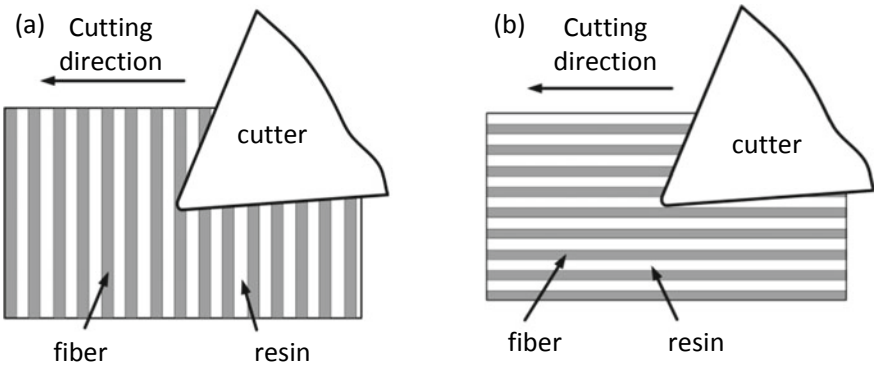

Fig. 1 Two cutting models during machining of unidirectional composites **a** orthogonal machining, **b** cutting in a layer

layer. Since the cutting speed used in drilling a composite is generally high, and the feeding rate is relatively low, the axial feeding rate when the cutter rotates by one cycle (feeding rate per turn) is relatively small [11]. Although drilling has both orthogonal machining and cutting in a layer, cutting in a layer may take the dominant role in drilling composites. The cutting mode of the main cutting edge of an ordinary twist drill can be simplified into orthogonal machining similar to turning.

3.1 Influence of Fibre Direction

The mechanical behaviours between composite and cutter mainly are influenced by material anisotropy and angle of the cutter. In composites, fibres are the main component that bears the cutting force and resin is mainly to transmit forces among fibres. Hence, material failure modes can be analyzed mainly from the perspective of stress on fibres.

3.1.1 Fibre Direction: 0°

Fibre direction is 0° which indicates cutting direction parallel to the fibre direction. When the tool cuts fibres at a certain speed, the principal cutting force is generated. The principal cutting force is generated by the interaction between the rake face of the cutter and materials. Therefore, the principal cutting force is perpendicular to the rake face of the tool.

The principal cutting force further generates the cutting force perpendicular to the fibre direction and parallel to the fibre direction. The stress state inside the uncut layer's material is the compressive stress σ^0 along with the fibre orientation and the in-plane shear stress (τ^p). The cutting force perpendicular to the fibre direction is

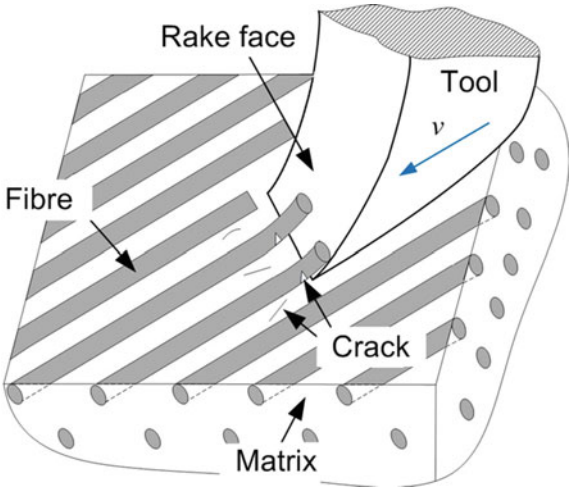

Fig. 2 Material removal mechanism of FRP when fibre direction is 0°

perpendicular to the direction of the fibre layer and points to the material surface, while the cutting force parallel to the fibre direction imposes compressive stresses on the fibre.

When the fibre direction is 0°, fibres bend by the cutting force of the tool. The carbon fibre is broken by extrusion or bending, forming powdery chips. However, directions of the bending deformation and position of cracks are influenced by the cutter's angle significantly. Material removal mechanism of CFRP when fibre direction is 0° is shown in Fig. 2.

3.1.2 Fibre Direction: 45°

The fibre direction 45° indicates the angle between cutting direction and fibre direction is 45°. When the fibre direction is 45°, the principal cutting force can be decomposed to cutting force perpendicular to the fibre direction and cutting force parallel to the fibre direction. The angle between fibres and tool movement direction is viewed as a blunt angle (Part I), while the angle between the other part of fibres and movement direction of the cutter is viewed as a sharp angle (Part II). Material removal mechanism of FRP when fibre direction is 45° is shown in Fig. 3.

The cutting force parallel to fibre direction induces Part I's material into compressive stress and Part II material into tensile stress. Meanwhile, the cutting force perpendicular to the fibre direction can be decomposed to the plane's force along with the fibre direction layer and the force perpendicular to the fibre direction layer. Therefore, deformation of Part II is significantly larger than that of Part I.

When the reinforced fibre is carbon fibre, a brittle material, small deformation can cause fibre cracks. Moreover, cracks are mainly generated at the position where it has the highest curvature. Hence, in Part II, fibres are easy to produce cracks, whereas

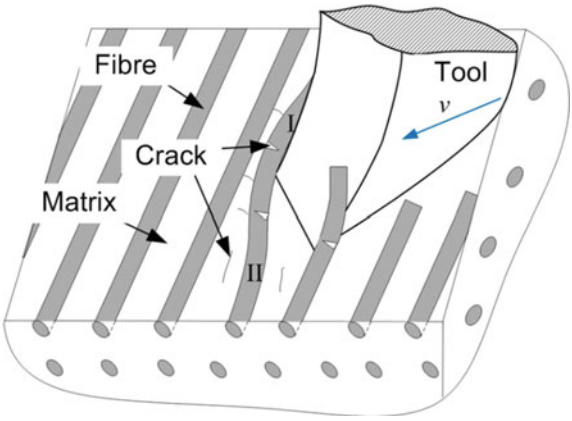

Fig. 3 Material removal mechanism of FRP when fibre direction is 45°

fibres in Part I are challenging to be cracked. Stresses at two sides of carbon fibre are different at the highest curvature ratio position. It is compressive stress on one side and tensile stress on the other side. The cracks produced on one side of tensile stress are easy to be propagated, while cracks on the side of compressive stress are challenging to be propagated. Hence, the failure of carbon fibre is mainly caused by generation and propagation of cracks induced by fibres' bending stress.

The cutting force between fibres and the tool can cause the failure of the resin base simultaneously. Bending of Part I makes resin matrix bear compressive stress and thereby produces compressive deformation. Consequently, cracks produced and propagated perpendicular to fibre directions at the fibre-resin interface area. Bending Part II makes the resin matrix develop tensile deformation due to tensile stress in the cutting zone. As a result, the debonding phenomenon between fibre and resin is produced, as well as cracks parallel to fibre in the resin.

3.1.3 Fibre Direction: 90°

Fibre direction is 90° which indicates a cutting direction perpendicular to the fibre direction. When the fibre direction is 90°, the principal cutting force is perpendicular to fibres' axis. The principal cutting force can be decomposed to the cutting force on the plane of the fibre layer and perpendicular to the fibre layer's plane. Stresses and deformations of fibres at two sides of the cutter are the same. Fibres might produce cracks at the contact position with the cutter on both sides. The resin matrix in front of the cutter bears compressive stress, thus producing cracks perpendicular to fibres. On the contrary, both sides of resin bear a tensile force produced by fibre deformation, thereby generating cracks parallel to the fibre direction. Material removal mechanism of CFRP when fibre direction is 90° is shown in Fig. 4.

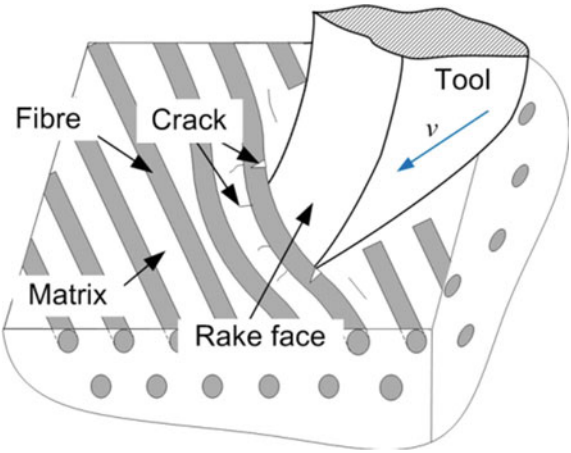

Fig. 4 Material removal mechanism of FRP when fibre direction is 90°

3.1.4 Material Removal Modes Along with Different Fibre Directions

The relationship between cutter and material is very complicated in the cutting process, and many factors influence it. Experimental observation and results analysis is complicated. The single-particle scratch is the most basic unit in complicated actual cutting. Studying the cutting mechanism based on single-point cutting tools' cutting behaviour is an effective means of understanding the complicated cutting effect.

Scratch test is to scratch along the testing material surface at a certain speed by using a single-point cutting tool. It is a kind of simulation test, and it is close to practical processing. Scratch test is an intuitive and useful mean to study the rupture failure law of materials in the cutting process.

To study the removal mechanism of FRPs, a scratch test was carried out. A unidirectional CFRP of T300/5208 was used in the scratch test. The volume fraction and diameter of carbon fibre are about 60% ± 5% and 7 μm, respectively. The resolution of both positive pressure and scratching force are 3 mN. The pressure head is a diamond Rockwell head with a diameter of 200 μm. Firstly, the pressure head prescans the profile of the workpiece surface at a positive pressure of 0.9 N. Secondly, the scratch test was carried out using a linear loading. The positive load is applied linearly at a rate of 0.9 ~ 50 N. The length of the scratch is 20 mm, and the scratching speed is 10 mm/min.

The scratch test was carried out in different angles layer to study the material damage and removal process during scratching along different fibre directions. The angle between the fibre direction and scratching direction was set 0°, 30°, 45°, 60° and 90°. In the scratching process, the scratch instrument recorded positive vertical pressure, horizontal scratching force, scratch depth and changing of acoustic emission signals.

The variation of scratching force along different fibre directions during the linear loading of 0.9 ~ 50 N of pressure head is shown in Fig. 5. With the increase of

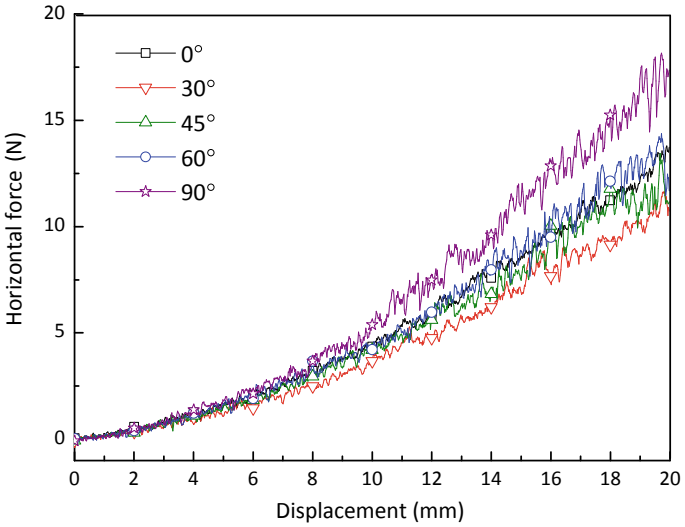

Fig. 5 Variations of the horizontal scratching force with the scratching displacement under different fibre directions

scratch depth and an abundant fibre bundle breakage, the scratching force along different fibre directions changed considerably. When the included angle between fibre direction and the scratching direction was 90°, the fibre stresses at two sides of the pressure head were same and could not yield to the left or right of the pressure head. Hence, the fibre can only be deformed along the perpendicular direction of the fibre. When the deformation reached a certain degree, the fibre bundle developed tensile failure. The scratching force's force was used for deformation of fibre bundle and resin, and the scratching force was the maximum under all angles. The fibre deformations at two sides of pressure head were different when the angle was 30°, 45° and 60°. The fibre bundle tended to be yielded from the pressure head, as the included angle between fibre and scratching direction was an obtuse angle. Firstly, the fibre bundle was bent because of the considerable normal stress, as the included angle between fibre and scratching direction was an acute angle. Therefore, it can be concluded from difficulties for fibre bundle yielding that when the fibre direction was 30°, the scratching force was the lowest, followed by 45° and 60° successively. The deformation of 0° fibre bundle was different from those under other angles. When the fibre direction was 0°, the fibre bundle was bent and finally broken to respond to the axial compressive force.

The scratching force under the same scratching depth can reflect difficulties for fibre cutting along different directions. It can be seen from Fig. 6 that scratching force is similar along different fibre directions given a small scratching depth, given a large scratching depth, the scratching force along 60° of the fibre direction was the highest, and the fibre bundle was the most difficult to be cut. The scratching force along 30° was the second-highest, and the fibre bundle was the second most difficult

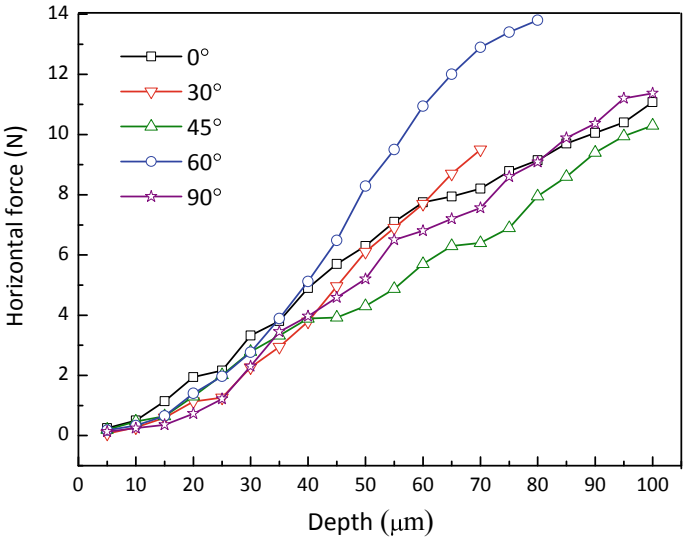

Fig. 6 Variations of the horizontal scratching force with the scratching depth under different fibre directions

to be cut. The scratching force changed consistent with the scratching depth when the fibre direction was 0° and 90°, but the scratching force reached the minimum when the fibre direction was 45°.

Scratching depth can reflect the difficulty for pressure head to press in materials under different fibre directions. In Fig. 7, the scratching depth changes significantly when the positive pressure varies within 0.9 ~ 50 N under different fibre directions. When the fibre direction was 90°, the scratching depth achieved the highest growth rate. This was mainly because with the increase of positive pressure, the scratching force bent the fibre bundle, and it was torn along the fibre direction, which was easier for pressing in of the pressure head. Similarly, when the fibre direction was 0°, the bottom fibre was easy to crack after long-term pressing of the pressure head against the same fibre bundle, and the scratch depth increased quickly in the late stage of scratching. When the fibre direction was 30°, 45° and 60°, the fibre bundle at the bottom of the pressure head was changing randomly, and it was challenging to be fractured. Therefore, the scratching depth was relatively small. Specifically, the fibre bundle suffered similar normal and tangential forces when the fibre direction was 45°. Consequently, the fibre bundle was easily deformed and cut, resulting in the relatively high scratching depth.

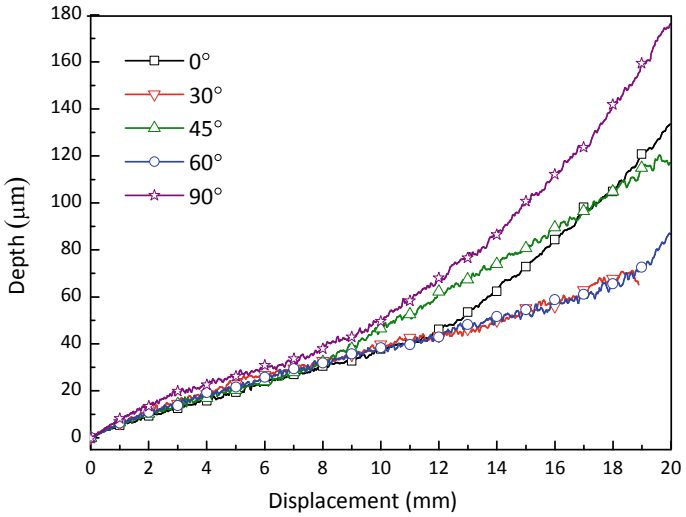

Fig. 7 Variations of the scratching depth with the scratching displacement under different fibre directions

3.2 Influence of Cutting Angle of the Cutter

Stresses on materials are different under different cutting angles of the cutter, resulting in different materials' mechanical behaviours. Mechanical behaviours of materials under different cutting angles of the cutter were studied. Cutting angle of the cutter includes a positive rake, zero rake and negative rake.

3.2.1 Positive Rake

During the cutting process under positive rake, materials accumulate on the cutter's rake face under the effect of cutting force. Moreover, the cutting force peels the fibre from the matrix. When the fibre deformation reaches a certain extent, fibres might be broken and removed. The rigidity of peeled fibre beam is relatively low, so some fibre beams are difficult to be eliminated and retained on the cutting surface, finally forming fuzzing (as shown in Fig. 8).

3.2.2 Negative Rake

During the cutting process under negative rake, cutting force points to the inside of the materials under the cutter's rake face. Fibres are squeezed by the cutting force and thereby produce bending deformation. Cracks might be produced and propagated on fibres when the deformation reaches a certain extent. Fibres are removed from the

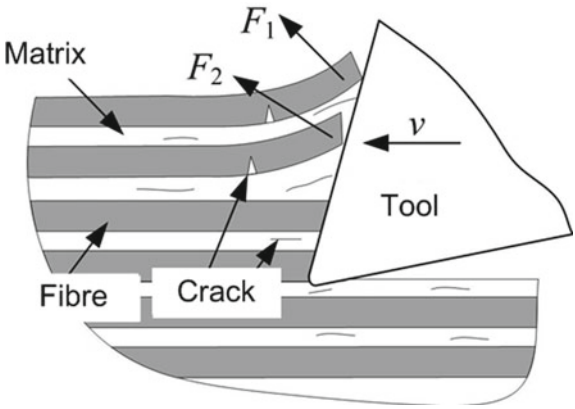

Fig. 8 Material removal mechanism of FRP when cutting angle of the cutter is positive

cutting zone as chips after breakage. In the cutting process, fibres are crushed down and challenging to form fuzzing and cutting surface quality is relatively good (as shown in Fig. 9).

Cracks are easily produced at the resin-fibre interface under different cutting angles. Cracks are formed at the fibre-resin interface under the effect of cutting force. With the increase of cutting force, cracks begin to propagate from the interface. Moreover, cracks at different fibre interfaces are connected into a large crack. Under negative rake, the cutting force points to the inside of the base. Cracks in brittle materials are easy to propagate toward the free surface, that is, material surface. Therefore, materials can be eliminated effectively.

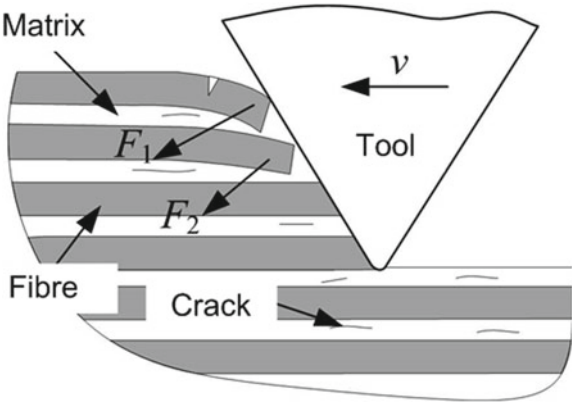

Fig. 9 Material removal mechanism of FRP when cutting angle of the cutter is negative

4 Classification of Conventional Machining Processes of FRPs

The geometric size of the composite component based on FRPs is close to the desired size. They may require machining to facilitate dimensional control for easy assembly and so on. Traditional machining of composite materials mainly includes turning, milling, and drilling. Moreover, some new processing techniques based on traditional processing means like helical milling and ultrasonic-assisted cutting have been developed to address existing problems based on traditional processing techniques.

4.1 Turning Processes

Cylinder or tubular workpieces made of FRPs need turning to gain high surface quality and the desired geometric size. A high-quality turning surface can improve strength properties, such as fatigue strength, corrosion resistance, assembly tolerance, wear rate and coefficient of friction etc. [12].

Some FRP components are tubular workpieces with low rigidity, thin-walled tubular workpiece, and cylinder workpiece with low rigidity, which has to be supported by certain rigidity during machining [13].

Tool angle and fibre direction are two essential factors that influence the turning quality of composite materials. Henerichs et al. [14] carried out a turning test of CFRP by using carbide cutter with different rake and relief angles. At the same time, processing quality and cutting force under different fibre directions were studied. They found that the cutter's relief angle influenced the cutting force more than the rake angle. Moreover, the cutting force was negatively correlated with the relief angle. The angle between cutting direction and fibre direction affects the tool wore significantly. The tool wear was light when the fibre direction was less than 90°.

Workpiece quality is influenced by fibre direction, as shown in Fig. 10. For the fibre direction is 0° ($\theta = 0°$), the machining surface shows only few fibre breakages and low roughness. Delamination does not occur. Fibre directions of $\theta = 30°$, 60° and 90° show less spring-back and hence less wash out of matrix material. However, fibre directions of $\theta = 30°$, 60° and 90° appear to be the most critical orientations as they cause the highest process forces, the most intensive wear and workpiece damage. Machining fibre direction $\theta = 135°$ results in a saw tooth-shaped profile.

The cutter life is generally short during turning using traditional uncoated carbide cutter. To increase the service life of the cutting tool, coated carbide cutter, CBN (Cubic Boron Nitride) cutter [15] and PCD (Polycrystalline Diamond) cutter [16] have been developed. Although the service life of CBN cutter and PCD cutter is long, they claim high cost. At present, the coated carbide cutter is most widely used.

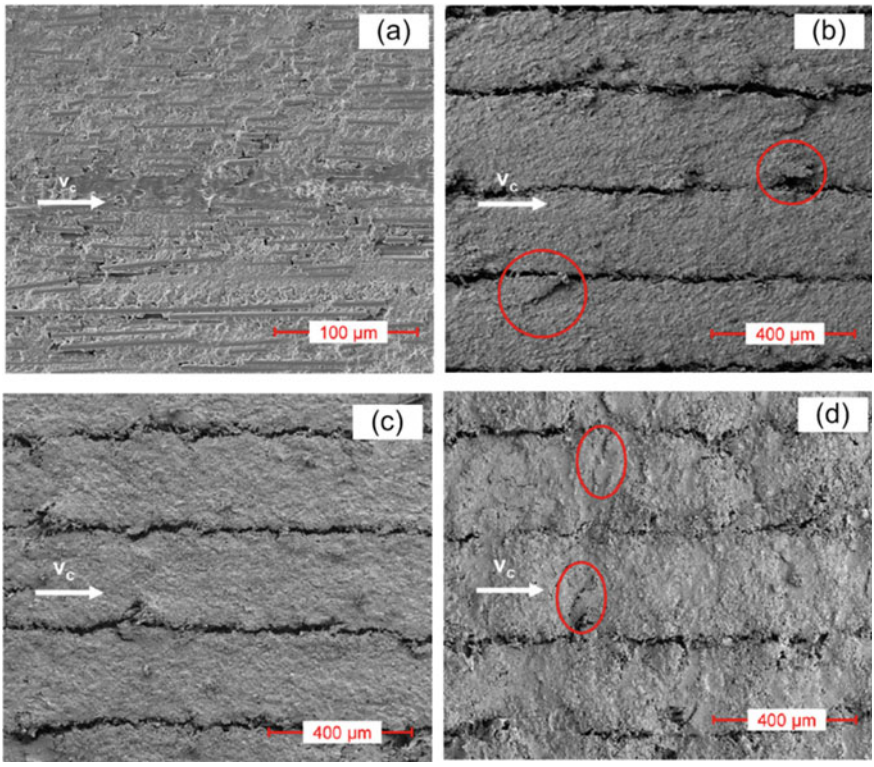

Fig. 10 Machined surface using a tool (10°, 7°) with different fibre direction **a** $\theta = 0°$, **b** $\theta = 30°$, **c** $\theta = 60°$, **d** $\theta = 90°$ [14]

4.2 Drilling Processes

4.2.1 Observations When Drilling FRPs

Composite laminates are usually used as structural materials and need to be connected to other metal or composite structures by a mechanical connection. As an essential final manufacturing process for composite laminates, the drilling process is extensively used for producing riveted and bolted joints for fastening the composite structure with other components. For rivets and bolted connections, damaged-free and precise holes must be drilled in the components to ensure high connection strength and precision.

For composite laminates, elasticity modulus and tensile strength along the horizontal direction (the fibre direction) are high. In contrast, the elasticity modulus and tensile strength along the thickness direction of the laminate are low. The laminate is easy to produce bending deflection under the drill top, pressing the chisel edge during drilling. The exit morphology during the CFRP drilling (Fig. 11) reflects that

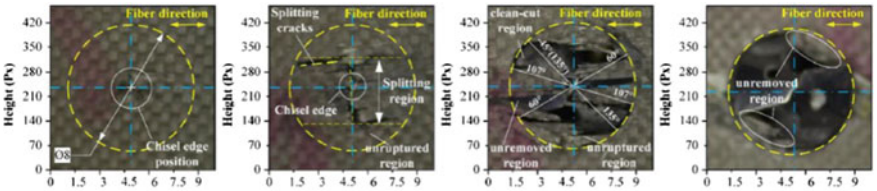

Fig. 11 The interaction between drill and workpiece during drilling out (diameter: 8 mm, cutting parameters: S = 3000 rpm, f = 150 mm/min) [17]

the laminate of composite material suffers the top pressing effect of the chisel edge and develops bending deformation first. The fibre is pulled. Subsequently, the main cutting edge is cut. In this process, the chisel edge provides a substantial top pressing effect with almost no cutting action.

4.2.2 Variations of Cutting Force and Cutting Temperature During the Drilling

Since delamination is easy to be generated in drilling and influences the usability of materials, cutting force is believed the main cause of delamination. Therefore, cutting force during the drilling has been focused on by many researchers [1].

The typical thrust force curve during the drilling is shown in Fig. 12 (the feeding rate, rotating speed and diameter of the drill were 150 mm/min, 3000 r/min and Φ8 mm) [18]. The drill-exit surface is defined as the reference plane, and the drilling depth is defined as the distance between the chisel edge and the reference plane. Five representative positions have been analyzed in detail during the drilling process: Position One (P-I), when the drill chisel edge just reaches the reference plane; Position

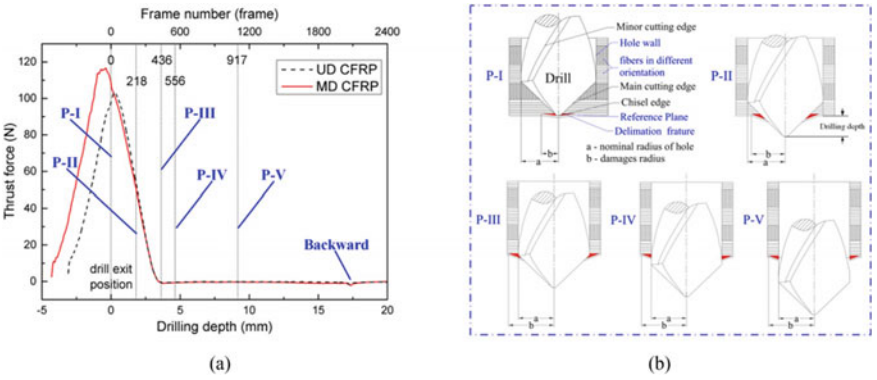

Fig. 12 Variation of thrust force curve with cutting depth **a** thrust force at different drilling depths, **b** schematic diagram of the corresponding drilling positions [18]

Two (P-II), when half of the main cutting edge passes the reference plane; Position Three (P-III), when the entire main cutting edge just passes the reference plane; Position Four (P-IV), when the minor cutting edge passes the reference plane by 1 mm; and Position Five (P-V), when the minor cutting edge passes 3 mm through the reference plane.

The drill-exit temperature peaked in the hole centre and gradually decreased outward, as shown in Table 1. The drill exit's temperature rise can be mainly attributed to the heat transferred from the drill and the machined materials. The peak temperature at P-I was about 58.2 °C for UD (unidirectional) CFRP and 54.3 °C for MD (multidirectional) CFRP. As drilling progressed, the temperatures kept increasing, peaked 105.4 °C in UD CFRP when the chisel edge was about 0.25 mm beyond the reference plane. For MD CFRP, a higher peak temperature (122.5 °C) took place at

Table 1 Gray and thermal images in different drilling depths [18]

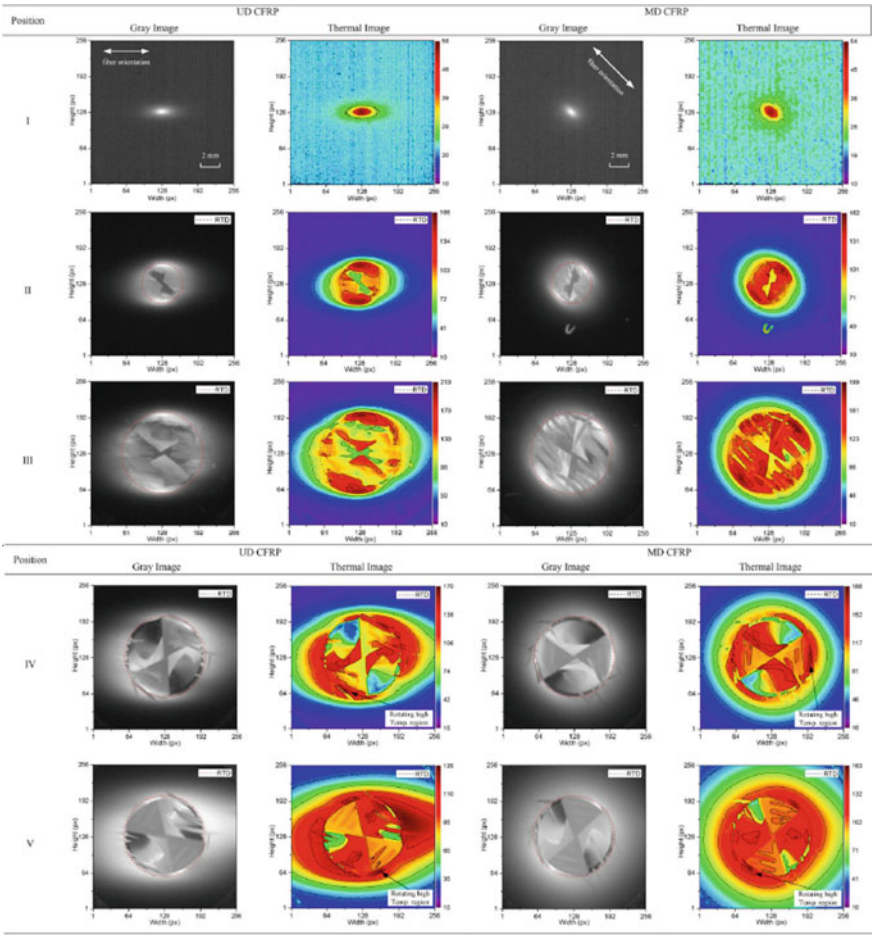

a similar location. The highest temperatures in the drilling of UD and MD CFRPs at P-II were above 160 °C. As the hole was being enlarged during drilling, the cutting velocity increased, leading to more cutting heat that further increased the cutting temperature (up to 210 °C from P-II to P-III).

4.2.3 Machining Quality of Drilling Surface

Typical damages caused by drilling are mainly fuzzing, tearing and delamination are shown in Fig. 13.

(1) Fuzzing. Fuzzing is generated by the failure of cutting of fibre. Due to the high strength of fibre, fuzzing is one of the common and most intuitive damages in the processing of FRPs.

(2) Tearing and delamination. Tearing is formed by a large-scaled separation between the part of materials on the surface and the bulk. Delamination refers to the degumming and separation of different layers caused by interlayer stress or manufacturing defect. Since tearing is the cracking between the surface material and the matrix materials, some scholars defined tearing as delamination damage. Size of the delamination (or tearing) is determined through surface observation [20].

(3) Mixed damages: Sometimes, a specific processing surface might have either the mixed defect of fuzzing, tearing and delamination, or internal micro-cracks or fibre pull-out. This is attributed to many reasons, such as different strengths of interlayer bonding agent, different performances of the fibre under different angles, as well as defects during material and component preparation, such as impurities, pores, etc.

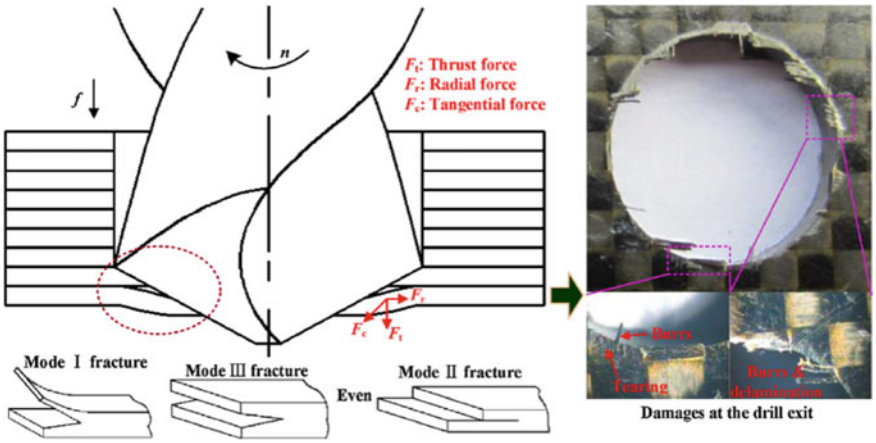

Fig. 13 Typical damages of CFPR caused by drilling [19]

Among typical machining damages of FRPs, delamination is the most critical damage and challenging failure mode during composite laminates drilling. Delamination production will decrease the fatigue life and load-carrying capacity of the composite component significantly [21]. During the drilling process, delamination is mainly produced at the entrance and exit of the hole. Severe delamination is often generated at the exit. At the exit of the hole, the remained material is easy to produce large deformations as a response to the thrust force. When the drill approaches the exit side of the hole, the uncut plies beneath the drill become more susceptive to deformation and in particular bending of this area due to the thickness's decrease. When the thrust force is higher than the material layers' interlaminate strength, the delamination is produced [22].

Hole wall quality is an essential factor that influences the utilization of materials. In particular, hole wall quality can influence the connection strength and fatigue life of composite structures. The machining quality of hole-surface depends on both cutting force and cutting temperature. Increasing temperature in the composite can change its properties, thus generating severe damage during the cutting process. Moreover, irreversible changes in composite performance occur quickly at temperatures that higher than glass transition temperature, which further decreases the usability of materials [23].

Fibre/matrix cracking, porosity formation and layer separation were shown on the hole surfaces, as shown in Fig. 14 [24]. Delamination and matrix loss/melt were observed from the early stages of drilling. The low thermal conductivity of composite materials induces that high temperature is easily generated during drilling, which is a contributory factor concerning resin melt. However, the damage is liable at lower temperature associated with the onset of plastic deformation.

Besides, small parallel grooves were generated under some conditions, as shown in Fig. 15. This may induce the interlaminar separation between fibre layers. Also, this may increase the surface roughness values associated with the holes.

Subsurface damage may be generated during machining; even good surface quality is obtained. Therefore, the subsurface is an essential factor during machining quality evaluation.

Fibre direction has a significant influence on the subsurface damage. Subsurface damage in fibre layer near the CFRP hole exit is shown in Fig. 16. When the cutting angle was fixed at 0°, there was transverse breakage on the subsurface CFRP hole wall. The strength of the matrix declined in response to the fibre layer's high cutting temperature at the outlet, thus causing the fibre to be crushed by the tool. At the cutting angle of 45°, there were regular breakage pits on the processed surface. The maximum depth of carbon fibre pitting was 24.8 μm. At the cutting angle of 90°, the subsurface of the hole walls developed two forms of damage: microcracks and debonding.

Furthermore, there was severe fibre bending behaviour near the hole walls. Microcracks are the consequence of the squeezing and bending fibres on the processed surface due to the vertical compressive stress. When the stress exceeds the carbon fibre's ultimate strength, the fibre-matrix interface on the processed surface may develop bending breakages, thus causing microcracks on the subsurface. At the

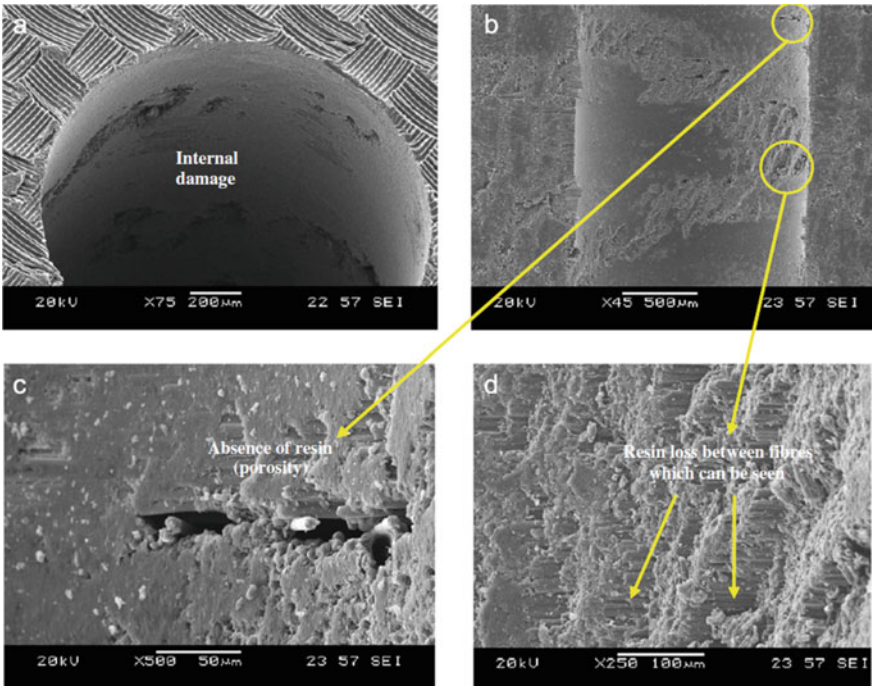

Fig. 14 Internal hole damage forms: **a** from hole exit, hole number 250 (speed: 3200 r/min, feed: 640 mm/min, drill: conventional); **b** test 3, sectioned hole, first hole (speed: 9600 r/min, feed: 960 mm/min, drill: conventional); **c** absence of resin between layers (porosity) and **d** resin loss [24]

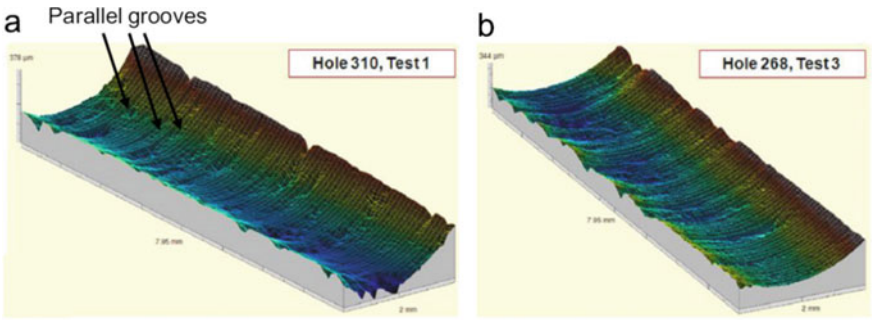

Fig. 15 3D topographic maps for the last hole drilled in CFRP [25]

cutting angle of 135°, there was severe subsurface damage. The maximum depth of subsurface damage was 45.2 µm. Subsurface damage was mainly manifested as bending breakage of fibres, causing cracks to diffuse toward the materials' internal structure. Since cutting temperatures close to the outlet were high, the matrix strength

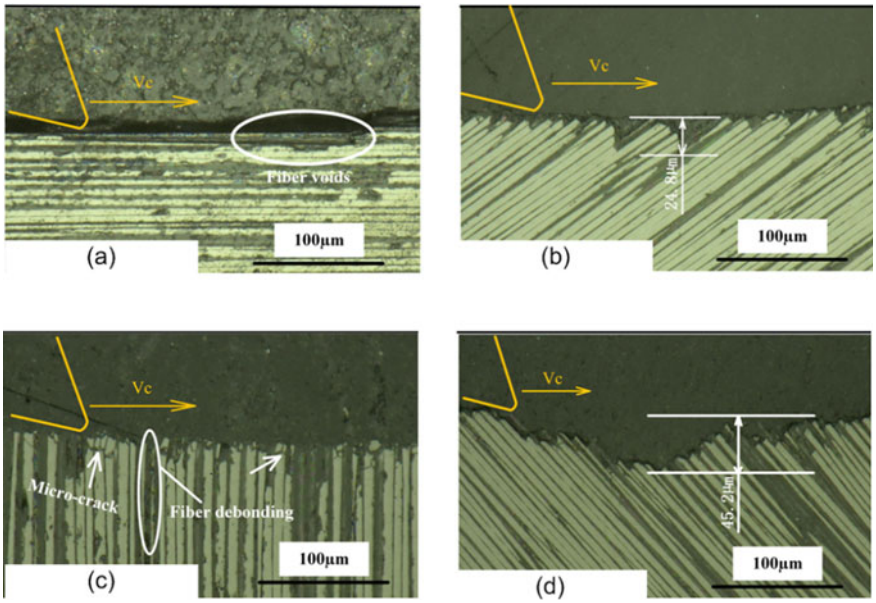

Fig. 16 Subsurface damage in fibre layer near the CFRP outlet (helical milling): **a** subsurface damage at 0° cutting angle; **b** subsurface damage at 45° cutting angle; **c** subsurface damage at 90° cutting angle; **d** subsurface damage at 135° cutting angle [26]

declined and decreased the bonding strength between fibre and matrix. This allows the fibre to bear a higher degree of bending deformation, which reduces chips' formation but favours crack initiation.

4.3 Milling Processes

A milling experimental study was carried out to study material removal in the milling process of FRPs and influencing factors of processing quality. A CFRP material was used in the experiment. The reinforced carbon fibre is T300, and the matrix material is AG-80 resin. A blind slot was milled by using a carbide milling cutter. The surface quality of the CFRP plate milled under different fibre directions is shown in Fig. 17 (feed per tooth, rotating speed, and milling depth are 0.01 mm/z, 4500 r/min and 0.9 mm, respectively).

Machining quality at two sides of the slot is smooth when $\theta = 0°$, without evident fuzzing. Since the compressive strength of carbon fibre is higher than the tensile strength of resin, resin develops interlayer separation when the squeezing reaches a certain extent. As the squeezing increases continuously, the separated carbon fibre breaks off when the bending stress reaches the ultimate bending strength of carbon

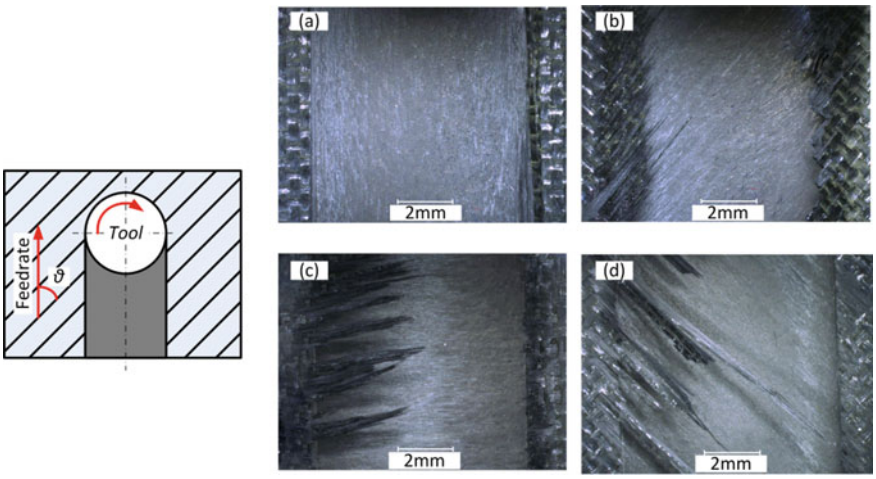

Fig. 17 Surface quality of CFRP milled under different fibre directions **a** 0°, **b** 45°, **c** 90°, **d** 135°

fibre, forming a cutting chip. Moreover, the rupture tends to extend toward the fibre direction. Hence, the milling quality at two sides of the blind slot is smooth.

A shear force perpendicular to the fibre direction is produced to respond to cutter's squeezing effect to the material when $\theta = 90°$. The carbon fibre is cut off when the shear stress exceeds the shearing strength of carbon fibre. Later, the carbon fibre is separated from matrix resin upon the squeezing effect of the cutter's rake face, which produces cutting chip.

When $\theta = 45°$, carbon fibre not only undertakes shear force perpendicular to the fibre direction but also bears tensile stress along the direction of carbon fibre. Hence, many un-cut carbon fibres are produced, which form fuzzing. The quantity of fuzzing when $\theta = 45°$ is significantly higher than that when $\theta = 90°$. The machining quality on the sidewall when $\theta = 90°$ is better than that when $\theta = 45°$.

Under $\theta = 135°$, the machining quality on the sidewall of the blind slot is inferior, manifested by long fuzzing and fibre tearing. Fuzzing is significantly longer than those during milling along with other directions.

During milling, along with different fibre directions, the machining quality on the right-side wall of the blind slot is higher than that on the left sidewall. When the milling tool cuts in the workpiece from the left side, the milling tool's rotating direction is opposite with the feeding direction of the workpiece. The thickness of the cutting layer increases gradually from zero to the peak, indicating that it belongs to the up milling. When the milling tool cuts out of the workpiece from the right side, the milling tool's rotating direction is the same as the feeding direction of the workpiece. The cutting layer thickness decreases gradually from the maximum to zero, indicating that the processing belongs to the climb milling. At the beginning of up milling, the cutting layer's thickness is zero, and it is smaller than the cutting edge radius. The cutter tooth squeezes and slides for a short distance on the machining

surface. The cutter produces strong friction on the workpiece surface, and it cannot produce cuttings effectively, which further influence the surface machining quality. The material can only be cut when the cutting layer's thickness is higher than the cutting edge radius. During climb milling, the cutter tooth will not produce squeezing and slippage phenomena when the thickness of the cutting layer decreases from the peak to zero, resulting in the good surface quality of workpieces.

To study the evolution of fibre cutting angle, typical surface morphologies during the orthogonal milling tests of UD-CFRP laminate are shown in Fig. 18 [27]. When the fibre cutting angle is 0°, a majority of the carbon fibres expose on the machined surface indicating the occurrence of fibre-matrix debonding. When the fibre cutting angle is 15°, fibre-matrix debonding is also observed, but the debonding length is smaller than that at the fibre cutting angle of 0°. Besides, the fibre fractures are parallel to the cutting velocity, and the fracture morphologies are rough due to the occurrence of the compression-induced fibre fractures. When the fibre cutting angle is 40°, the saw-tooth surface is generated, caused by the surface cavity defects. When the fibre cutting angle is 70°, bending induced fibre fractures were observed. When the fibre cutting angle is 120°, most of the fibre fractures are smooth, indicating the occurrence of the shear-induced fibre fractures. When the fibre cutting angle is 150°, the fibre fractures are perpendicular to the fibres' longitudinal direction, which can be attributed to the cutting edges' compression action.

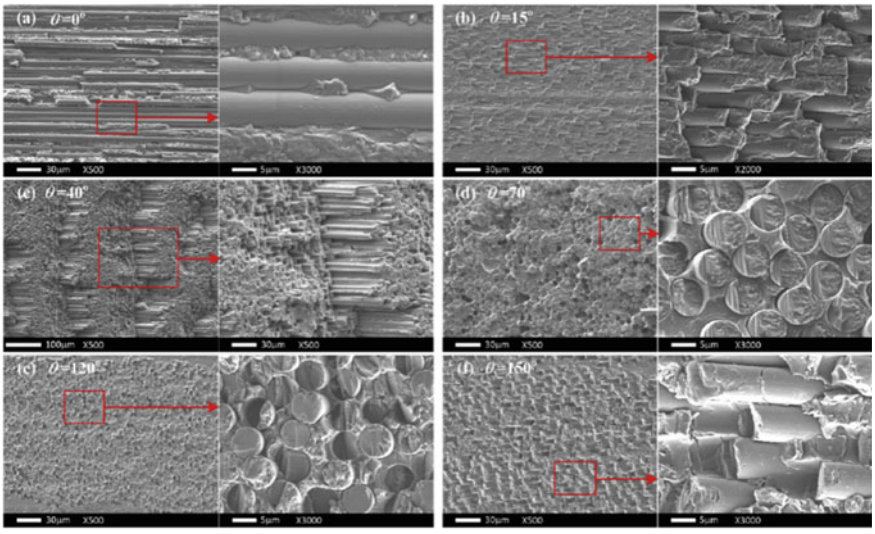

Fig. 18 Typical surface morphologies observed in the orthogonal milling of the UD-CFRP laminate disk [27]

5 Cutting Tools for Conventional Machining of FRPs

Selection of cutting tools mainly considers cutter materials and geometric parameters. Optimization of the cutter materials and geometric parameters mainly decreases cutting force and cutting temperature, aiming to assure the machining quality and machining efficiency. Currently, the demands for drilling are the largest in the processing of composite materials. Therefore, researches on cutting tool mainly concentrate on drilling cutter.

To improve the drilling quality of FRPs, many scholars proposed cutters with different geometric shapes, including tooth-shaped drill, candle-shaped drill, stepped drill and special-shaped drill [28]. Some drill bits with special drill geometries have been shown to produce lower delamination than conventional twist drills. Drill bit with special geometries is shown in Fig. 19.

The use of pilot hole strategies before finish sizing can considerably reduce thrust force due to the absence of contact between chisel edge and work material, thus further reducing delamination. The step drill bit with a suitable structure can avoid the initial damage exceeding the drill diameter effectively and have a good quality of the final hole. Furthermore, a one-shot drill bit is commonly applied for drilling CFRP parts to effectively reduce thrust force and improve drilled hole quality.

Although new drilling cutter can decrease machining damage, wearing the cutting tool, which is mainly produced of high-speed steel or carbide is still severe. Jain and Yang [31] proposed the cutting tool for core drilling to prolong the service life of the cutter and decrease thrust force produced by the chisel edge of the twist drill. The cutting edge of the core drill was fixed on the cutter body through super-hard abrasive particle sintering or electroplating, which assured the cutter's service life. Tsao and Hocheng [32] improved the core drill. Nevertheless, the core drill's hollow design makes the centre of the cutter easy to be blocked, which shortens the service life and processing efficiency of the cutter.

The electroplating diamond grinding-drilling combined cutter, formed by the organic combination of the traditional twist drill (or saw drill and candlestick drill) and diamond grinding, is a kind of composite cutter with promising prospects, as shown in Fig. 20. It has attracted great attention of production enterprises due to

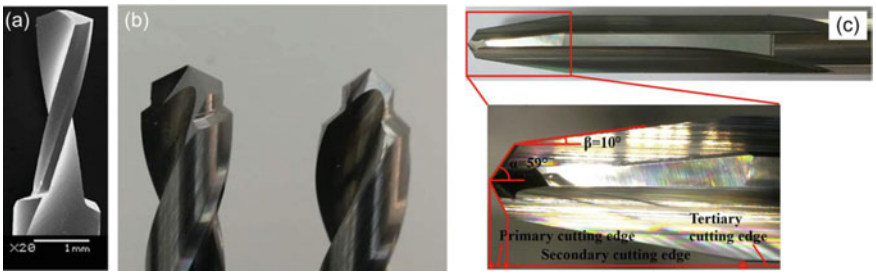

Fig. 19 Drill bit with special drill geometries **a** step drills A, **b** step drills B, **c** one-shot drill bit [24, 29, 30]

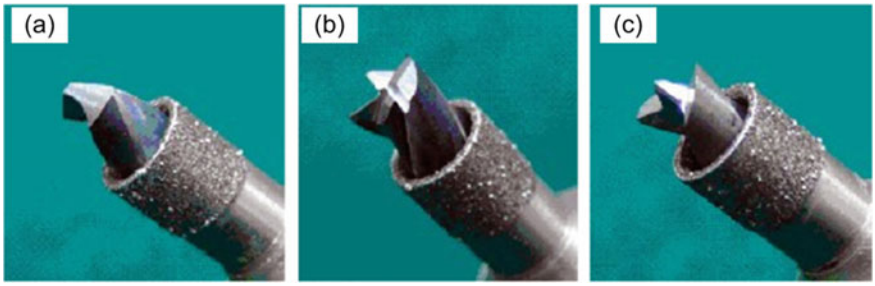

Fig. 20 Electroplated diamond drilling-grinding combined cutting tool **a** step-core-twist drill, **b** step-core-saw drill, **c** step-core-candlestick drill [33]

integrating processing procedures, and high machining quality. The front carbide drilling head (drilling the bottom hole) of the composite drilling cutter can gain a long service life through the secondary cutter sharpening. Hence, the cutter's service life is mainly determined by the service life of the electroplating diamond abrasive materials in the back end of the cutter (chambering and reaming).

6 Review Questions

(1) What are the main machining difficulties in traditional machining of different FRPs?
(2) Discuss the influence of cutting heat on cutting force and processing quality.
(3) Which are primary factors that influence the service life of cutter in machining of composite materials?
(4) How to design the cutter for different types of composite materials?
(5) What are the similarities and differences between grinding and drilling for composite materials?
(6) Discuss the influence of tool geometry on cutting force and cutting temperature.
(7) Discuss the influence of tool material on tool life and machining quality.
(8) Discuss the valuation of machining quality and how to monitor the machining quality during machining?
(9) Discuss the typical surface damage may be generated during turning.
(10) Discuss the subsurface damage may be generated during milling.
(11) Discuss the crack generation at different location of cutting edge during drilling using traditional twist drill.
(12) Discuss the role thermal conductivity of the cutting tool and workpiece in affecting tool life and machining quality.
(13) Discuss the role of fibre direction in determining the chip formation mechanism and the resulting surface topography in milling unidirectional composites.

(14) Discuss the effects of cutting speed and feed rate on cutting force in drilling FRPs.
(15) Discuss the difference of machining temperature during milling of CFRP and AFRP.
(16) Discuss the influence of plate thickness on the machining quality during drilling of CFRP.

Acknowledgements The editors would like to thank all the contributors (especially to Quan Wen from Northeastern University in China), who participated in scholarship and a desire to help in their busy schedules. This research is also supported by the National Natural Science Foundation of China (Grant No. 51875367).

References

1. Geng, D., Liu, Y., Shao, Z., Lu, Z., Cai, J., Li, X., Jiang, X., Zhang, D.: Delamination formation, evaluation and suppression during drilling of composite laminates: a review. Compos. Struct. **216**, 168–186 (2019)
2. Rawat, S., Attia, H.: Wear mechanisms and tool life management of WC-Co drills during dry high speed drilling of woven carbon fibre composites. Wear **267**(5–8), 1022–1030 (2009)
3. Freeman, W.-T., Kuebeler, G.-C.: Composite Materials: Testing and Design (Third Conference). ASTM International (1974)
4. Chatterjee, A.: Thermal degradation analysis of thermoset resins. J. Appl. Polym. Sci. **114**(3), 1417–1425 (2009)
5. Selzer, R., Friedrich, K.: Mechanical properties and failure behaviour of carbon fibre-reinforced polymer composites under the influence of moisture. Compos. Part A **28**(6), 595–604 (1997)
6. König, W., Graß, P.: Quality definition and assessment in drilling of fibre reinforced thermosets. CIRP Ann. Manuf. Technol. **38**(1), 119–124 (1989)
7. Xu, W., Zhang, L.: Tool wear and its effect on the surface integrity in the machining of fibre-reinforced polymer composites. Compos. Struct. **188**, 257–265 (2018)
8. Stone, R., Krishnamurthy, K.: A neural network thrust force controller to minimize delamination during drilling of graphite-epoxy laminates. Int. J. Mach. Tools Manuf. **36**(9), 985–1003 (1996)
9. Li, H., Qin, X., He, G., Price. M.-A., Jin, Y., Sun, D.: An energy based force prediction method for UD-CFRP orthogonal machining. Compos. Struct. **159**, 34–43 (2017)
10. An, Q., Cai, C., Cai, X., Chen, M.: Experimental investigation on the cutting mechanism and surface generation in orthogonal cutting of UD-CFRP laminates. Compos. Struct. **230**, 111441 (2019)
11. Liu, D., Tang, Y., Cong, W.-L.: A review of mechanical drilling for composite laminates. Compos. Struct. **94**(4), 1265–1279 (2012)
12. Vasudevan, H., Rajguru, R., Tank, K., Shetty, N.: Optimization of multi-performance characteristics in the turning of GFRP(E) composites using principle component analysis combined with grey relational analysis. Mater. Today Proc. **5**(2), 5955–5967 (2018)
13. Davim, J.-P., Mata, F.: A new machinability index in turning fiber reinforced plastics. J. Mater. Process. Technol. **170**(1–2), 436–440 (2005)
14. Henerichs, M., Voß, R., Kuster, F., Wegener, K.: Machining of carbon fiber reinforced plastics: influence of tool geometry and fiber orientation on the machining forces. CIRP J. Manuf. Sci. Technol. **9**, 136–145 (2015)

15. Rajasekaran, T., Palanikumar, K., Vinayagam, B.-K.: Application of fuzzy logic for modeling surface roughness in turning CFRP composites using CBN tool. Prod. Eng. **5**(2), 191–199 (2011)
16. Sivasankaran, S., Harisagar, P.-T., Saminathan, E., Siddharth, S., Sasikumar, P.: Effect of process parameters in surface roughness during turning of GFRP pipes using PCD insert tool. Procedia Eng. **97**, 64–71 (2014)
17. Hou, G., Zhang, K., Fan, X., Luo, B., Cheng, H., Yan, X., Li, Y.: Analysis of exit-ply temperature characteristics and their effects on occurrence of exit-ply damages during UD CFRP drilling. Compos. Struct. **231**, 111456 (2020)
18. Fu, R., Jia, Z., Wang, F., Jin, Y., Sun, D., Yang, L., Cheng, D.: Drill-exit temperature characteristics in drilling of UD and MD CFRP composites based on infrared thermography. Int. J. Mach. Tools Manuf. **135**, 24–37 (2018)
19. Su, F., Zheng, L., Sun, F., Wang, Z., Deng, Z., Qiu, X.: Novel drill bit based on the step-control scheme for reducing the CFRP delamination. J. Mater. Process. Technol. **262**, 157–167 (2018)
20. Hrechuk, A., Bushlya, V., Ståhl, J.-E.: Hole-quality evaluation in drilling fiber-reinforced composites. Compos. Struct. **204**, 378–387 (2018)
21. Persson, E., Eriksson, I., Zackrisson, L.: Effects of hole machining defects on strength and fatigue life of composite laminates. Compos. Part A Appl. Sci. Manuf. **28**(2), 141–151 (1997)
22. Ho-Cheng, H., Dharan, C.K.H.: Delamination during drilling in composite laminates. J. Eng. Ind. (Trans. ASME) **112**(3), 236–239 (1990)
23. Wang, B., Yang, B., Wang, M., Zheng, Y., Hong, X., Zhang, F.: Effect of cutting temperature on bending properties of carbon fibre reinforced plastics. Sci. Eng. Compos. Mater. **26**(1), 394–401 (2019)
24. Shyha, I.-S., Aspinwall, D.-K., Soo, S.-L., Bradley, S.: Drill geometry and operating effects when cutting small diameter holes in CFRP. Int. J. Mach. Tools Manuf. **49**(12–13), 1008–1014 (2009)
25. Shyha, I.-S., Soo, S.-L., Aspinwall, D.-K., Bradley, S., Perry, R., Harden, P., Dawson, S.: Hole quality assessment following drilling of metallic-composite stacks. Int. J. Mach. Tools Manuf. **51**(7–8), 569–578 (2011)
26. Wang, B., Wang, Y., Zhao, H., Sun, L., Wang, M., Kong, X.: Effect of a Ti alloy layer on CFRP hole quality during helical milling of CFRP/Ti laminate. Compos. Struct. **252**, 112670 (2020)
27. Wang, C., Liu, G., An, Q., Chen, M.: Occurrence and formation mechanism of surface cavity defects during orthogonal milling of CFRP laminates. Compos. Part B Eng. **109**, 10–22 (2017)
28. Hocheng, H., Tsao, C.-C.: Effects of special drill bits on drilling-induced delamination of composite materials. Int. J. Mach. Tools Manuf. **46**(12–13), 1403–1416 (2006)
29. Jia, Z., Zhang, C., Wang, F., Fu, R., Chen, C.: An investigation of the effects of step drill geometry on drilling induced delamination and burr of Ti/CFRP stacks. Compos. Struct. **235**, 111786 (2020)
30. Wang, F., Qian, B., Jia, Z., Fu, R., Cheng, D.: Secondary cutting edge wear of one-shot drill bit in drilling CFRP and its impact on hole quality. Compos. Struct. **178**, 341–352 (2017)
31. Jain, S., Yang, D.-C.-H.: Delamination-free drilling of composite laminates. J. Eng. Ind. **116**(4) (1994)
32. Tsao, C.-C., Hocheng, H.: Parametric study on thrust force of core drill. J. Mater. Process. Technol. **192–193**, 37–40 (2007)
33. Tsao, C.-C.: Investigation into the effects of drilling parameters on delamination by various step-core drills. J. Mater. Process. Technol. **206**(1–3), 405–411 (2008)

Nonconventional Machining Processes of Fibre Reinforced Polymer Composites

Ming Ming Wong Irina and Iskandar Bin Azmi Azwan

Abstract Driven by the need for lightweight and high-strength materials for parts and components in the aviation and automotive sectors, research activities aim to achieve these requirements exponentially. These research activities are not limited in material processing, testing and development, but also extended to the material's machinability. This chapter provides a comprehensive introduction which includes cutting mechanisms and critical process variables when machining fibre-reinforced polymer (FRP) composites using nonconventional machining processes, namely abrasive waterjet machining (AWJM), laser beam machining (LBM) and electrical discharge machining (EDM). Besides, the effects of machining process parameters on machinability outputs are also discussed.

Keywords Composite materials · Abrasive waterjet machining · Laser beam machining · Electrical discharge machining

1 Introduction

Fibre reinforced polymer (FRP) composites are frequently manufactured to near-net-shape, aiming to minimize the number of parts to assembly and reduce subsequent finishing processes. However, the inevitable presence of secondary machining processes, such as edge trimming and drilling in some cases, lead to choiceness quality and reliability of the composite part. Notably, these aspects are vital, especially for the aviation industry. Conventional machining may be challenging, which requires a sharp and hard-cutting tool to contact directly and mechanically shear the workpiece. In the conventional machining process, the high temperature would lead to the tool-chip interface, inaccurate composite dimensions, and decreasing tool

M. M. W. Irina (✉)
School of Engineering and Technology, University College of Technology Sarawak (UCTS), No. 1, Jalan Universiti, 96000 Sibu, Sarawak, Malaysia

I. B. A. Azwan
Faculty of Engineering Technology, Universiti Malaysia Perlis, Kampus UniCITI Alam Sungai Chuchuh, Aras 1, 02100 Padang Besar, Perlis, Malaysia

I. Shyha and D. Huo (eds.), *Advances in Machining of Composite Materials*, Engineering Materials, https://doi.org/10.1007/978-3-030-71438-3_4

life due to the possible thermal distortion. As a result of frequent tool changes, the manufacturing process requires more extended machining time, and hence nonconventional machining process can be the right candidate. Nonconventional machining processes refer to a group of processes, that apply various forms of energy to remove excess material without the cutting tool's absence. This chapter discusses different nonconventional machining processes used in FRPs industry, its feasibility, and influencing parameters for machining FRPs.

2 Overview of Nonconventional Machining Process for FRPs

The machining of composites material is different from machining metal. Specifically, it is challenging due to the heterogeneous and anisotropic nature of properties, low glass transition temperature, and high abrasion of fibre reinforcement [1]. Despite the significant effort made to minimize defects after the machining process, FRP composites remain susceptible to many failure modes due to the aforementioned unique properties. After the machining process, the common failure modes include fibre pull-out, fibre-matrix debonding, delamination, kerf angle, and low surface roughness. Defects in composite part led to redundant rework and scrap. Rework requires an additional inspection cost, yield losses, and loss of goodwill on the customer, resulting in wasting time and money for an organization. Research on various types of nonconventional machining processes of FRPs was highlighted among the research communities to surmount traditional processes' limitation to prevent these issues. Nonconventional machining processes refer to a group of processes that apply various energy sources, including the mechanical, thermal, electro-chemical energy, or combination of all energy types to form the workpiece's targeted final geometry. Comment types of nonconventional machining processes are presented in Fig. 1.

Three types of nonconventional machining processes are presented: mechanical, thermal electrical, and electrochemical machining. In the mechanical type, the erosion mechanism is implemented to remove the workpiece material using the high velocity of abrasive particles and hydraulic pressure as the media. Abrasive waterjet machining (AWJM) and ultrasonic machining (USM) are examples of mechanical machining. Furthermore, the thermal, electrical type employs highly amplified light or voltage to vaporize the unwanted workpiece material. Laser beam machining (LBM), electrical discharge machining (EDM), and wire electrical discharge machining (WEDM) are among the examples under this category. In an electrochemical machining (ECM) procedure, material removal occurs through ion displacement mechanism in an electrolyte solution under high electric current.

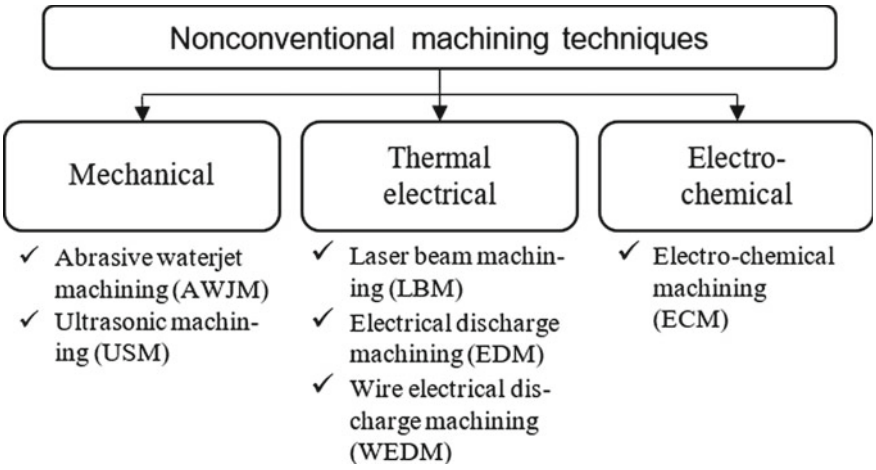

Fig. 1 Various types of conventional machining techniques for FRPs [2]

3 Classification of Nonconventional Machining Processes of FRPs

Among various nonconventional machining processes, AWJM, LBM and WEDM are the most favourable methods for the processing FRPs. Each method consists of specific benefits and drawbacks. This section provides an insight into the technology used in each process, it is cutting and damage mechanism for the machining of FRPs.

4 Abrasive Waterjet Machining (AWJM)

The AWJM procedure presents precise and "cold" cutting with a minimal thermal load. Presence of water in AWJM process has significantly minimized the effect of heat, allowing the composites to be cut without harming its intrinsic properties. A high-pressure water jet is combined with fine-grained garnet or aluminium oxide abrasive particles in an appropriate ratio, focusing on the specimen through a nozzle [3]. The material removal processes result from the erosion caused by the abrasive particles on the specimen surface.

The waterjet cutting is a nonconventional machining process that utilizes a highly pressurized water stream to cut through the material. The waterjet cutting system could be classified into two types, namely pure waterjet machining (WJM) and AWJM. Specifically, WJM employs high-pressure clean water to cut soft specimens, such as plastic, plywood, and rubber. In the case of the AWJM, the addition of abrasive mixes with waterjet in the mixing chamber enhances the machining process, which

allows the cutting of harder and brittle materials, such as building material, glass, and advanced composite material.

The AWJM process consists of three phases, as illustrated in Fig. 2. The high-pressure clean water enters the system through the orifice, which functions to convert the high-pressure water into a collimated jet and accelerate the pure waterjet for approximately three times as fast as the speed piston bullet [4]. Subsequently, the suction pressure generated by pure waterjet is sucked into the abrasive particles and air. Abrasive particles are only introduced into the mixing chamber after a specific time to prevent clogs in the mixing tube [5]. The abrasive particles, such as garnet and aluminium oxide, flow from the abrasive inlet and are integrated with high-velocity waterjet at the mixing chamber. Notably, these particles are frequently used to demonstrate the erosive effect of AWJM process. Lastly, the mixture of abrasive particles and waterjet accelerates and passes through the mixing tube with a typical dimension of 1 mm in internal diameter and 45 mm in length. The high-velocity exit jet stream passes through the jet nozzle to impinge on the workpiece.

The critical factor in producing a satisfactory quality product after machining by AWJM is selecting proper process parameters. As presented in Fig. 3, these process parameters are closely related to the process and could be broadly classified into the hydraulic, abrasive, workpiece, focusing tube, and cutting parameters. The output measures known as response parameters include the defect or geometrical damage of material after the AWJM process productivity and dimensional tolerance of FRPs.

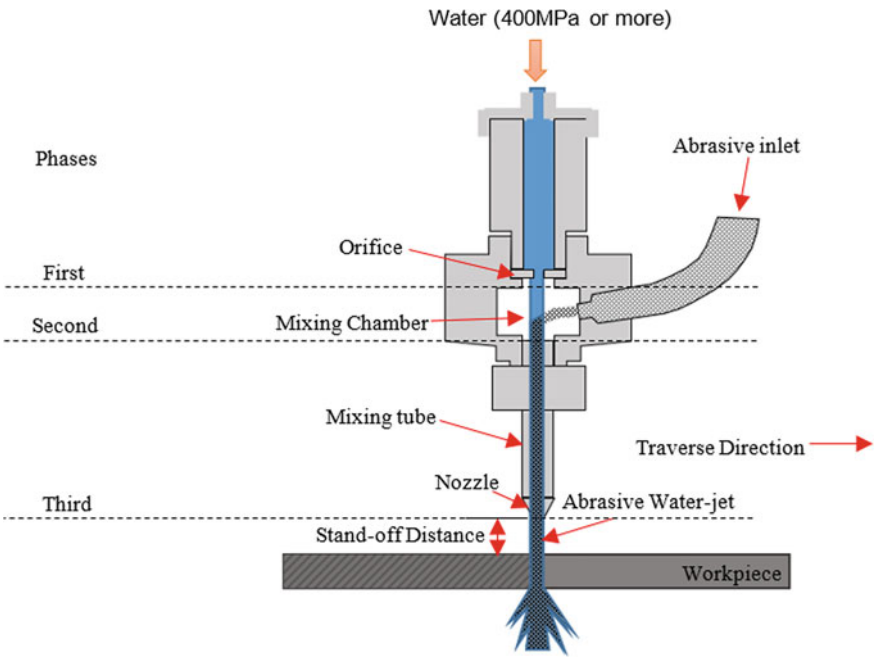

Fig. 2 The general structure of the cutting head system for AWJM

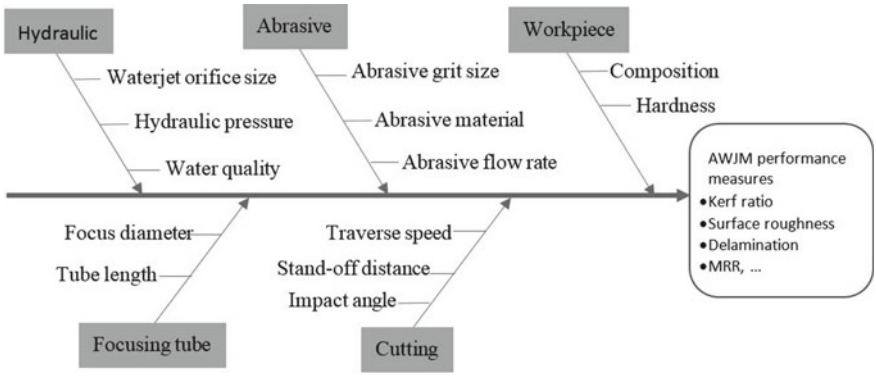

Fig. 3 Ishikawa cause and effect diagram or fishbone diagram for AWJM process [6, 7]

Several response parameters have been highlighted to achieve the desired output product quality, especially surface roughness, kerf ratio, and delamination. All these parameters impact the quality, efficiency, and economy of the overall process.

The AWJM process is considerably challenging in several process parameters, particularly the abrasive flow rate, standoff distance, hydraulic pressure, and traverse rate. Besides, FRP composites' brittle characteristics demonstrate the anisotropic and heterogeneous natures known as hard-to-machine material. Therefore, selecting the proper process parameter is essential to enhance the machinability for the FRP composite.

4.1 Material Removal Mechanisms of Abrasive Waterjet Machining

In abrasive waterjet machining, water is adopted as a medium to transfer the momentum of abrasive particles to the specimen. Initially, the high momentum abrasive particles possess more energy to cut the specimen on the top surface. However, the particles experience continuous loss of kinetic energy when the jet is propagated, leading to bent waterjet production. Furthermore, the low energy stream can only remove the matrix between the fibre and hence fibre/matrix delamination is apparently at the jet exit. The material removal process by AWJM could be classified into two types, namely micro-mechanism and macro-mechanism. Specifically, micro-mechanism of AWJM refers to the erosion of abrasive particles, which affect the machined specimen with high velocity. Meanwhile, macro-mechanism presents the kerf formation process. The cutting process takes place in a particular depth of penetration of abrasive waterjet and creating the cut's striated surface.

Micro-mechanism (or impact of the single solid particle) is the core material removal process of abrasive waterjet cutting with the high impact of solid abrasive

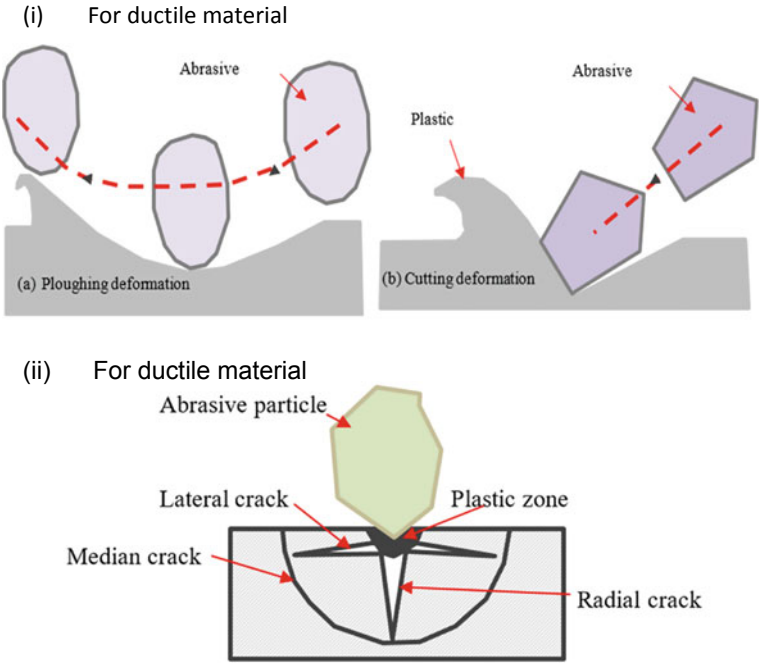

Fig. 4 Micro-mechanism of machining (**i**) ductile material and (**ii**) brittle material [9]

particle impingement. These mechanisms could be further separated based on the material's properties, which are brittle and ductile. When machining ductile materials, the removal process consists of two modes: ploughing and cutting deformation (see Fig. 4 (i)). In the case of the AWJM of brittle materials shown in Fig. 4(ii), the unwanted material would be machined due to crack initiation, propagation, and plastic deformation caused by the brittle failure of the material [8].

Macro-mechanism refers to the cutting process occurring at a particular penetration depth of the abrasive waterjet and striated cut surface development. Generally, the geometry of the generated cutting front ends at the striated or wave-cut surface. Notably, the machined surface has higher smoothness at the jet entrance (top), which eventually gains roughness towards the jet exit (bottom). The kerf wall roughness of FRP composite consists of three regions, including initial damage zone, smooth cutting zone, and rough cutting zone (refer to Fig. 5). These phenomena are attributed to the abrasive waterjet, which experiences a continuous loss of kinetic energy during the machining process. Figure 6 illustrates the kerf surface's deformation after machining by the sharp edge abrasive particles during AWJM.

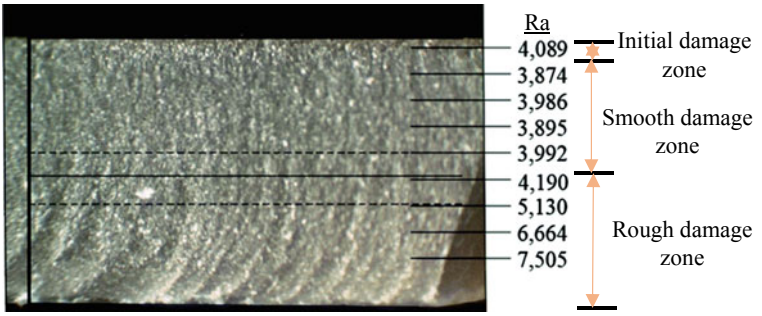

Fig. 5 Image of a micrograph of an AWJM glass FRP laminate [10]

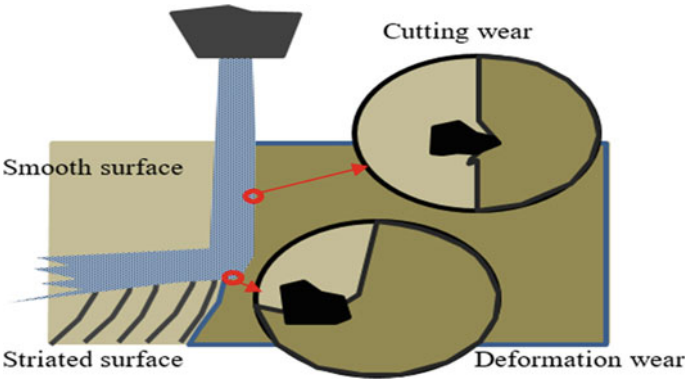

Fig. 6 Formation of distinct regions in AWJM

4.2 Abrasive Waterjet Machining Characteristics of FRPs

The AWJM process is a kind of nonconventional machining processes, which create no heat-affected zone and high machine versatility. Despite these advantages, challenges concerning the waterjet cutting of FRP composites are still present. Furthermore, the AWJM on FRP composites' layered nature still leads to defect, such as delamination, high surface roughness, and poor kerf geometry [11, 12]. As a result, low assembly tolerance and reduced structural integrity occur, resulting in in-service performance deterioration. Many studies recorded the machining features of FRPs using AWJM [13–15]. These research described the machining responses in terms of delamination damage, kerf taper, and FRP composites' surface roughness.

4.2.1 Delamination Damage

Delamination damage is a type of damage mechanism present in the machining of FRP composites. It is also a mode of cracks or interlaminar failure caused by adhesion loss between the two-layered fabric. Delamination has also been identified as one of the crucial modes, which reduce structural integrity and indirectly influence the long-term performance of FRPs. Delamination can be identified as the ratio of the maximum width of the delamination area (W_{max}) to the actual width of cut (W), which is as follows:

$$Delamination, F_d = \frac{W_{max}}{W} \tag{1}$$

The parametric study of delamination damage recorded that the abrasive flow rate, traverse rate, and hydraulic pressure significantly influenced delamination damage. A high number of abrasive particles strengthened the momentum of collision for the penetration to the workpiece area and worn away uncut fibre. Combining the higher hydraulic pressure with a lower travel speed could contribute to the abrasive particles' consistent kinetic energy. Meanwhile, the maintained kinetic energy of abrasive water streams could increase the overlap machining motion to cut through the composite laminate progressively while producing a clean kerf boarder. Accordingly, minimum delamination damage could be caused by incorporating high energy abrasive waterjet stream under low speed to cut the composite specimen.

It was recorded from the conventional process on the machining composite material that the delamination damage was more severe on the bottom side due to the thrust force. However, FRP composite material's delamination after AWJM was more critical on the upper ply than the laminate's bottom ply. This situation was caused by high-velocity abrasive particles that continuously impinge on the target FRP composite, which resulted in a substantial impact on the workpiece's surface. The strong exerted impact force over the inter-lamina adhesive force formed cracked tips on the lamina. The water flowing through the composite, a water wedge action, and the abrasive particles' embedment would be formed, which accelerated delamination [5].

Delamination increases with the increase in the traverse rate of the cutting nozzle. Higher nozzle travel speed that penetrating the workpieces leads to less abrasive particles overlapping the machining motion. The loss of kinetic energy from the abrasive waterjet leads to a challenge in obtaining a clean-cut surface. The high deflected waterjet stream and lack of cutting mechanisms in high-velocity abrasive waterjet generate bending fracture, which detaches the laminate plies at the fibre-matrix interface. This situation leads to visible delamination to the bottom plies of the laminate. In a study by Schwartzentruber et al. [16] on the modelling of delamination after the hole piercing of carbon FRP composite, it was found that increasing the hydraulic shock action formed large cracks in the bottom plies. This situation was due to the abrasive waterjet stream entering the final stages of piercing the laminate, which led to delamination damage, particularly on the bottom layer (refer to Fig. 7).

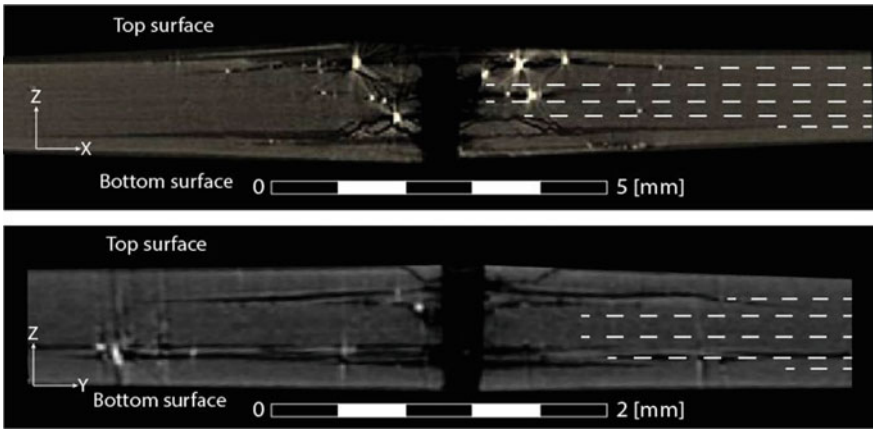

Fig. 7 X-ray scans along the centreline of the pierced holes of carbon FRP laminate after AWJM [16]

4.2.2 Kerf Taper

Kerf taper ratio is commonly identified through the kerf surface topography, such as roughness, waviness, and taper across the composite material thickness. It also represents one of the critical outcomes for the AWJM due to its impact on the process potential for fulfilling product requirements [17]. Generally, a tapered slot with a larger top kerf than the bottom kerf width will be opened by AWJM. The kerf ratio could be identified as the ratio of top kerf width (W_t) to the bottom kerf width (W_b), which is as follows:

$$Kerfration, T_R = \frac{W_t}{W_b} \tag{2}$$

It was recorded in the parametric research on the impact of kerf ration parameters that the standoff distance between the specimen and focusing nozzle was a critical factor of the kerf ratio. Doreswamy [18] experimentally demonstrated that the kerf width was reduced with the decreasing standoff distance and traverse rate. Furthermore, higher standoff distance allowed the expansion of waterjet with a lower density of abrasive particles on the diverging jet's outer circumference before the workpiece impinged. Based on the machined FRP composites' cross-sections from different standoff distance presented in Fig. 8, the significant variation between top and bottom kerf widths could be developed by increasing the standoff distance between the nozzle and workpiece.

It is noteworthy that the rise in the jet stream's divergence leads to a challenge in controlling the cutting width due to the loss of abrasive particles at the jet boundary [20]. This phenomenon leads to a considerable variation between the top and bottom kerf widths as the abrasive particle's kinetic energy continuously lost its ability to

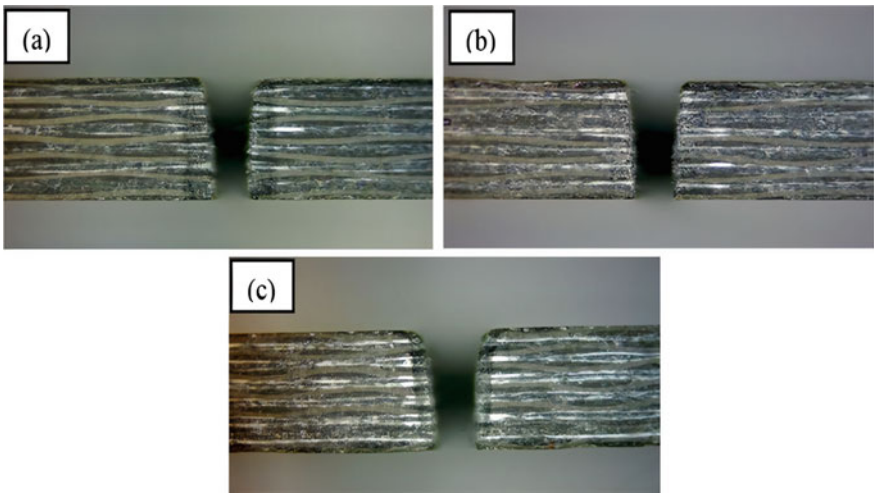

Fig. 8 Cross-section of FRP composite at different standoff distance cutting through AWJM. **a** 2 mm, **b** 5 mm, and **c** 8 mm [19]

penetrate the specimen. It was also found that the standoff distance ranging from 2 to 5 mm led to a notable influence on the response parameters, while the control over the kerf width was maintained.

The increase in traverse speed led to large kerf ratio. The abrasive water jet's rapid passing allowed low numbers of abrasive particles to penetrate the targeted area, which generated a narrower slot. Shanmugam et al. [5] manipulated the cutting angle ranging from 0° (normal cutting) to 5° to minimize or manage the kerf width damage. Subsequently, it was found that the cutting angle is one of the process parameters affecting the kerf width. It was also recorded that the compensated wall's kerf angle decreased with an increment on the other wall. Meanwhile, with the cutting angle of 4.5°, the kerf taper on the compensation wall was almost linear.

4.2.3 Surface Morphology

Surface roughness is an essential machined quality index, which is required for every machining product. The functional behaviour of a component is strongly impacted by the surface quality, especially the assembly parts. Three cutting regions are present in AWJM, namely initial damage zone, smooth cutting zone, and rough cutting zone (refer to Fig. 5). The surface finishes of FRP composite near the jet entrance comprise higher smoothness, directly progressing towards the jet exit.

The formation of the initial damage zone at the top of the workpiece is attributed to the penetration craters of a low-density abrasive particle of divergence waterjet at the periphery of the impact surface [21]. In general, standoff distance represents the most vital process parameter for the initial damage zone. The specimen exhibits smaller

initial damage zone under low standoff distance, while the zone width increases with high standoff distance. Moreover, a smooth cutting zone is a region with the highest surface quality as it does not receive the abrasive particle's impact. In contrast, the abrasive waterjet continues to provide adequate cutting capacity for machining the specimen.

A low surface finish could be developed while the traverse rate of AWJM is increased. Notably, the high traverse rate leads to a decreased exposure time of the abrasive waterjet stream to the targeted material. With the gradual loss of kinetic energy from the abrasive waterjet stream, jet deflection occurs, leading to the unwanted striate surface at the end of jet and severe surface roughness on the rough cutting zone. Figure 9 illustrates the AWJ machine hybrid carbon-glass FRP composite at the most and least attainable surface through different process parameters. The surface profiles demonstrate the transformation from the smooth cutting zone to the rough cutting zone.

In contrast, the composite surface's waviness appears at random due to different sets of the process parameter. High hydraulic pressure, low standoff distance, and slow traverse rate could produce an improved machined surface under high abrasive flow rate. Overall, the high kinetic energy abrasive particle results often increase the erosion rate under high pressure and enhance abrasive waterjet penetration to develop a smoother cutting surface.

Azmir et al. highlighted that FRP composites' machinability, namely GFRP [13] and AFRP [22] through AWJM process. Both of the composites produced higher-quality cut with a lower traverse rate. Meanwhile, a higher traverse speed often led to a lower amount of abrasive particle to impinge on the targeted material, which created a narrower cutting slot and rough surface finish. This situation might be attributed to shorter dwell time for the interaction between pressurized abrasive particles and workpiece when the jet travelled under high traverse speed [23].

Provided that surface waviness is generally a common defect in abrasive waterjet machined surface, a proper selection of process parameter is the key factor in producing sufficient surface quality of FRP composite for a successful application. Similar findings were developed on the unidirectional CRRP surfaces machined by AWJM using the Taguchi methodology [25]. The traverse rate and hydraulic pressure were recorded as the most vital influencing elements. Subsequently, high hydraulic pressure accelerated the momentum of abrasive particles and increased their ability for material removal.

5 Laser Beam Machining (LBM)

Among the various nonconventional machining processes, AWJM and LBM have received more attention among the researchers in composite manufacturing industries due to their superior capability of extensive operation on the layered nature of FRP composite. Despite being a cold and fast machining process, AWJM comprises several defects when machining on FRP composite. With the presence of water after

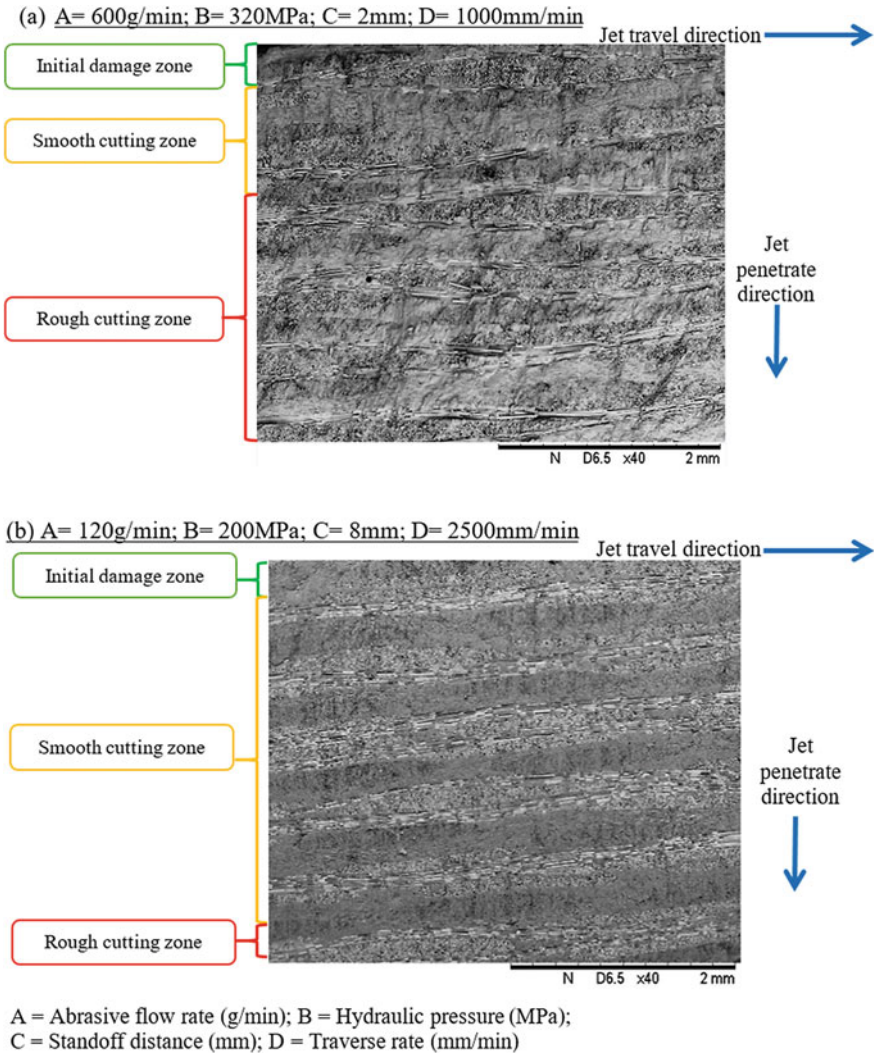

Fig. 9 Cross-section of hybrid carbon-glass FRP composite at different parameter setting through AWJM [24]

the AWJM process, the hygroscopic and layered nature of FRPs significantly reduces the mechanical strength of the composite. Therefore, the laser beam machining (LBM) has received considerable attention for machining FRP composites due to the dry mode machining without using a cutting tool. The highly concentrated monochromatic raw infrared beam is generally focused on a small spot with a diameter ranging from 0.1 to 1 mm [26].

LBM is a nonconventional machining process that uses the laser beam to produce heat for a thermal machining process. The letters in the word 'laser' originate from

"light amplification by stimulated emission of radiation". It utilizes light energy or laser to vaporize particles on the machined surface [27]. The LBM system consists of four main components: excitation source, laser discharge tube, laser delivery and focusing, and auxiliary devices, as shown in Fig. 10.

Besides, Fig. 11 below illustrates the principles of the laser beam. When electrons are exposed to an excitation source, the external energy will be absorbed. These electrons will move from the original energy level to a high energy level known as an excited state. However, provided that the high energy electrons are not stable under the excited state, the energy will be released in the form of photons and returned to the original energy level, which is identified as the transition state. In this state, the photons emitted in a spontaneous emission state would form incoherent light.

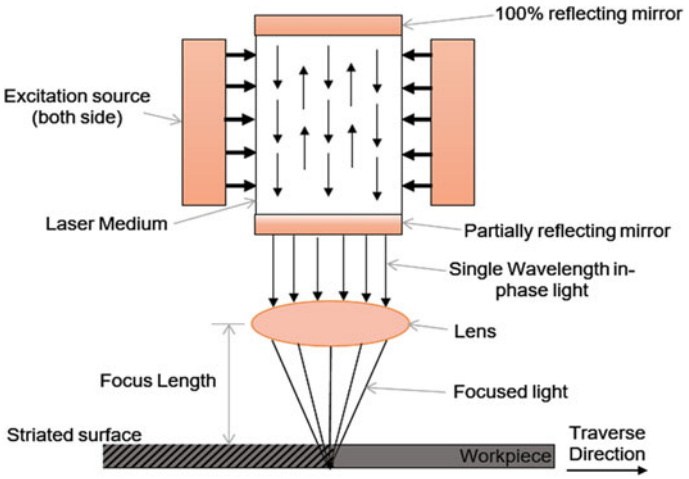

Fig. 10 Schematic of LBM [28]

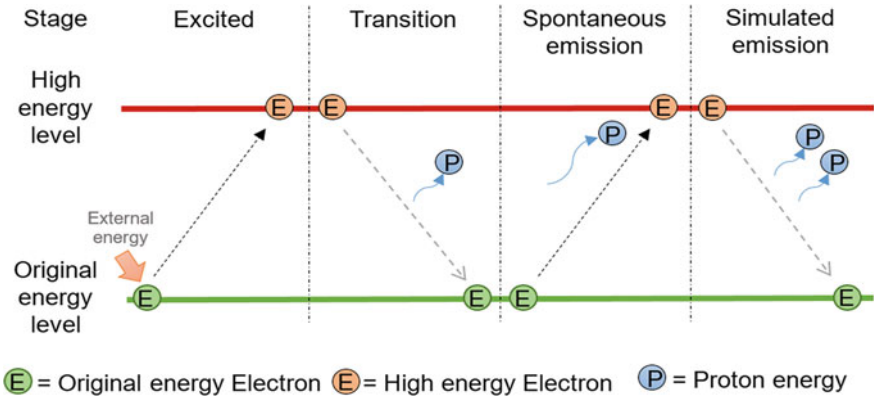

Fig. 11 Principle of the laser beam (adopted from [30])

In contrast, the stimulated emission involves the interaction between the emitted photons and other high energy electrons. This phenomenon induces the transition state in the same manner and leads to amplifying the emitted photons at high speed, which produces a coherent and focused beam known as the laser [29].

The excitation source provided sufficient energy to the laser medium by which the electrons are placed in their original energy state. The laser discharge tube function is filled with the laser medium to perform spontaneous and stimulated radiation emissions and create a coherent laser beam. The emitted laser beam characteristics are based on the laser medium, which may be in the solid, gaseous, or liquid laser form. The laser beam travels from the laser medium is then collected using the convex lens and directed for machining the FRPs to achieve complex sharp requirements for the board spectrum of application. Notably, auxiliary devices, such as the cooling system for the laser medium and auxiliary nozzle, are equally crucial for consistent productivity and quality of the machined material [31].

The laser cutting depends on the responses between the material workpiece and laser beam. High generated laser energy machining on FRPs has resulted in several defects, especially in terms of the heat-affected zone (HAZ), kerf width, and surface roughness. The process parameters, which could directly affect the process, are classified into the material parameter, laser system parameters, assist gas, focusing lens, and environment, as shown in Fig. 12.

In the process of LBM of FRPs, the laser source type was found to be the most significant factor due to its direct impact on the ability of the composite material to absorb the energy emitted by the laser beam. This phenomenon was also attributed to the energy absorption of a material based on the laser's wavelength. Notably, carbon dioxide (CO_2) and Nd: YAG laser cutting is the most common laser used to machining FRP materials in the industry [34]. Furthermore, the CO_2 laser is characterized as one of the gas lasers using carbon dioxide as the laser medium to produce high cutting efficiency and output power, while the solid-state of Nd: YAG laser can produce

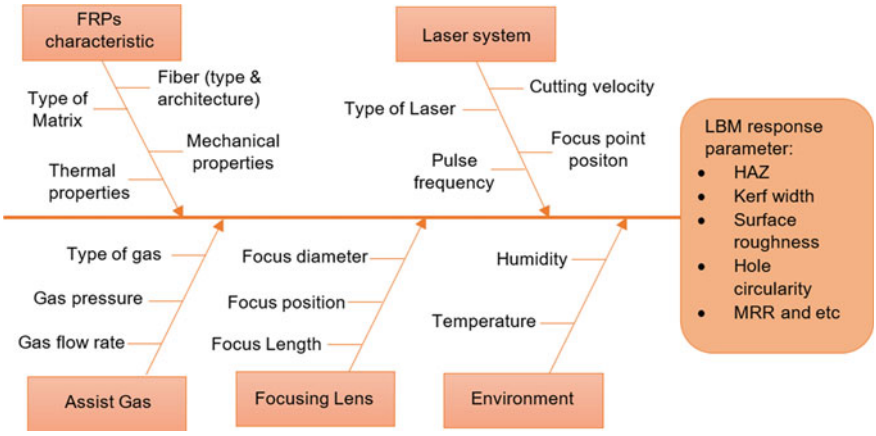

Fig. 12 Ishikawa cause and effect diagram for LBM process of FRPs [32, 33]

Table 1 Specification properties of CO_2 LASER and Nd:YAG laser [37]

Laser	CO_2	Nd:YAG
Type	Gas	Solid
Wavelength (μm)	9.4–10.6	1.06
Output power (kW)	Up to 20	Up to 16
Pump source	Electrical discharge	Flash lamp or laser diode
Mode of operation	CW or pulsed	CW or pulsed

improved focus and high beam intensity. The properties of CO_2 laser and Nd: YAG are illustrated in Table 1 below.

Herzog et al. [35] studied the influence of the CO_2, Nd: YAG, and disk (solid-state) laser source of LBM process on the machining quality of CFRPs. It was recorded from all the laser machined composites that HAZ took place through the specimens' cross-section after machining by a different laser source type (see Fig. 13). The Nd: YAG laser-produced smaller kerf width and HAZ in the machining of CFRPs, while a relatively severe HAZ could be observed on the CO_2 laser machined sample. This phenomenon could be attributed to the longer wavelength of CO_2 laser ($\lambda = 10.6$ μm), which produced high thermal conductivity with the presence of carbon fibre. Moreover, the CO_2 laser was competent in machining AFRP and GFRP due to fibre's low thermal conductivity [36]. Besides, the comparison between the kerf

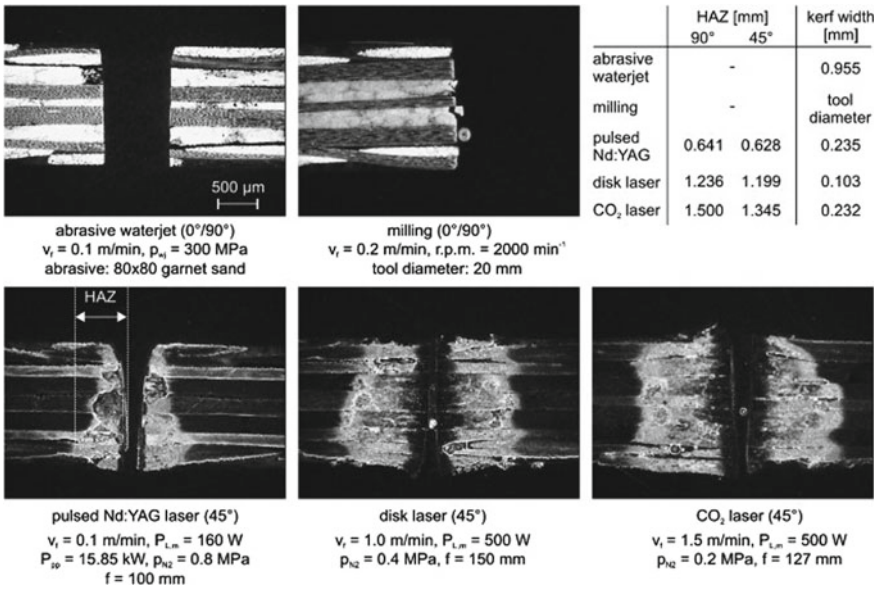

Fig. 13 Cross-section of CFRP samples processed using different cutting technologies [35]

width of CFRPs after machining showed that the kerf widths of laser machining were notably smaller than those of the AWJM and conventional milling process.

Pulse frequency and laser power are the process variables controlling the laser beam's thermal energy to the targeting material. Specifically, pulse frequency indicates the laser pulses striking the material in a short duration with several repetition rates. Furthermore, the laser beam acts in a similar way to a continuous wave at higher pulse frequency. Shyha et al. [38] studied the impact of laser power, gas pressure, cutting speed on CFRPs and GFRPs. It was reported that surface roughness increases in both materials with an increased laser power for a given cutting speed due to the less interaction time between the laser beam and workpiece at high cutting velocity.

Meanwhile, laser power refers to the laser beam's optical output power, which depends on the laser's operation mode. The high-power laser couple with high pulse frequency laser beam striking the material's surface would cause a significant amount of material to melt instantly, enhancing the HAZ and deteriorating the quality of cut [39]. Therefore, low laser power should be maintained when the pulse frequency is high to prevent the increase in HAZ width.

It is noteworthy that the high dependency of the process parameters of the actual laser sources on each other could be observed from the selectable level of one process parameter, which is based on the adopted level of the other parameters [40]. Therefore, a proper selection of process parameter range is essential to reduce the machining area's thermal damage and maintain optimum productivity.

5.1 Material Removal Mechanisms of Laser Beam Machining

In laser beam cutting, a small sport laser is used as the cutting tool to vaporize and shift the erosion to the machined workpiece, as illustrated in Fig. 14. With the release of the vapours, the molten material is moved by the high pressure assist gas, while the development of the kerf width leads to material removal. The LBM process mechanism for composite materials is complicated due to the anisotropic properties of FRPs, which consists of two different constituents of the material. At the same time, fibre reinforcement and matrix demonstrate substantially different thermal and physical properties.

When the spot laser strikes the specimen's surface during the LBM, the low thermal conductivity matrix material will be removed using the chemical degradation mechanism. When the high thermal laser beam melts or breaks the matrix's chemical bonds, decomposition of the matrix will occur. Notably, this material removal process is the most common in machining thermoset polymer, wood, and aramid composites, which have similar thermal properties with the polymer matrix. Furthermore, high conductivity of fibre (carbon or glass fibre) requires higher thermal energy and longer exposure time for rapid heating with the vaporization temperature.

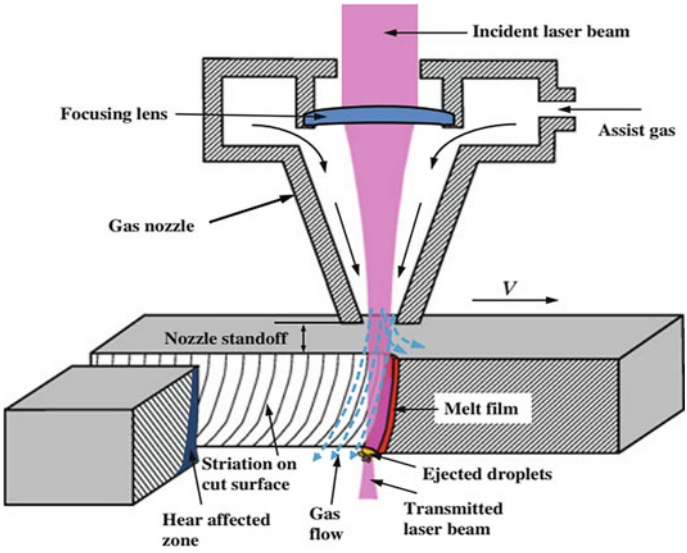

Fig. 14 Illustration of laser beam cutting process [41]

In the matrix's case, which melts when heated with the laser, the focused heat from a penetration cavity of the molten matrix will be removed by the shearing action of high-pressure assist gas. Striations appear on the cutting surface when the laser cutting process occurs to a certain depth of penetration. Notably, the frequency of striations depends on laser power and the cutting velocity of the laser nozzle. Subsequently, the machined surface gradually becomes rougher towards the laser beam exit due to the decrease in the laser nozzle's overlapping laser power and higher cutting velocity.

5.2 Features of Laser Beam Machining of FRPs

The laser machining of FRPs is a complex process due to its distinctive physical and thermal properties of two different constituent materials (fibre and matrix), demonstrating distinguished responses when exposed to the high thermal energy. The uneven material removal of fibre and matrix's relatively different vaporization properties leads to a severe form of HAZ, rougher surface finish with solidifying molten matrix at kerf exit known as dross. Many research works recorded the machining characteristics of FRPs using LBM, particularly CFRPs [33, 42] and GFRPs [34, 43].

5.2.1 Heat Affected Zone (HAZ)

The HAZ refers to substantial thermal energy conducted into the matrix at the adjacent area of machined surface, which results in surface region changes in the microscopic level, including laser power, cutting velocity and material thermal conductivity. Provided that heat conduction is the primary energy transfer process from the cutting zone to the vicinity surface. The width of HAZ is based on the process parameter, which would impede or promote heat conduction. Meanwhile, carbon fibre comprises the highest vaporization temperature and thermal diffusivity compared to glass fibre and aramid fibre.

Several challenges are present due to the notable difference between the thermal properties of the matrix constituent. Specifically, high thermal energy presents to vaporize the carbon fibre, more heat is conducted, and a severe HAZ is developed. Accordingly, an optimal set of laser power and cutting velocity is essential to reduce the machining process's interaction time due to broader HAZ generation before carbon fibre vaporization [40]. Figure 15 presents the micrographs recorded at the top and bottom machining hole surface of CFRP composites under different laser power and cutting velocity. It is also indicated that the wide HAZ was present in the unidirectional CFRPs along with the 0 ° fibre orientation, while a relatively low HAZ was present in 90° of fibre orientation.

The HAZ regularly follows the charred matrix residues and protruding fibres bound on the machined surface's kerf wall. An extension of the focused heat occurs into the specimen to a point where the temperature reaches the matrix's decomposition temperature. Meanwhile, high heat concentration could be generated by another set of process parameters, specifically the high pulse frequency with low

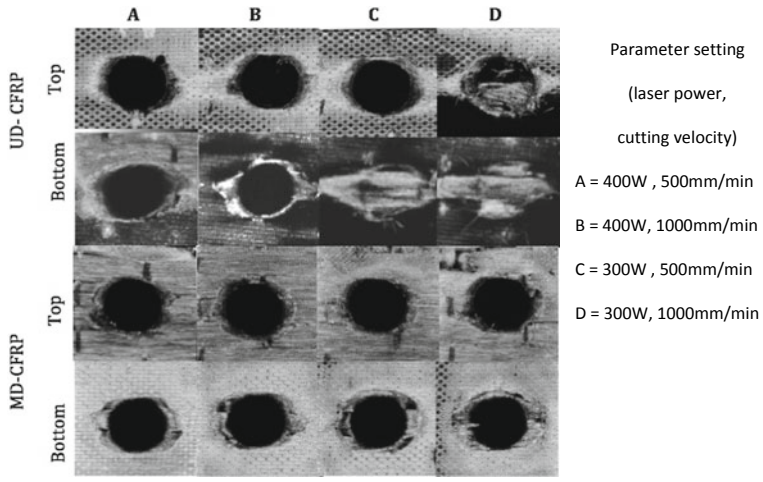

Fig. 15 C-scan images of unidirectional (UD-) and multidirectional (MD-) CFRP laminates cut by laser machining [31]

air pressure. The presence of high HAZ, heat, and resolidification of molten material leads to severe surface finish due to dross formation [44]. Therefore, lower HAZ could be achieved by proper optimization of selected process parameter range, which includes laser power, cutting velocity, pulse frequency, and air pressure to reduce the heat conduction of the machined surface.

5.2.2 Kerf Width

FRP composite is employed in high-end industries, especially the automotive and marine industries. Provided that luxury goods require high productivity and less tolerance, the LBM of FRPs has received substantial attention due to its high speed and precision machining, which could produce a cutting kerf of approximately 0.1 mm. However, the development of the kerf width is firmly based on the processing parameter.

In general, the machining of FRP composite through LBM would lead to a broader kerf width at the top than the bottom surface. This situation is due to the laser beam's first impinge on the machined surface, followed by the vaporization process through the workpiece. Notably, the cutting velocity is the most significant factor of the interaction duration between the laser beam and FRP materials. Lower cutting velocity increased the laser energy to vapour the fibre, resulting in a high amount of molten matrix on the cutting point and wider kerf, while poor HAZ is developed in the vicinity.

A study by Mishara et al. [45] on the kerf quality of hybrid carbon/basalt/Kevlar29 hybrid FRPs through LBM found that cutting speed is the most influential parameter for top and bottom kerf width compared to the laser power and assist gas pressure. Higher cutting velocity penetrating the machined surface led to less laser beam overlapping in the vaporization action, resulting in the narrow kerf.

Oh et al. [46] studied the cut quality of CFRP composite using fibre laser cutting. Figure 16 illustrates the kerf width obtained with different laser power and number of laser passes. The experimental results demonstrated that better kerf width and HAZ could be achieved under laser power of 1600 W, while sample specimen machining with laser power of 800 W showed higher performance in terms of surface finishing. It was also proven that higher laser light under high cutting speed would generate narrower kerf width and HAZ. The laser beam's high cutting speed reduced the overlapping laser beam on the composite and minimum heat conduction diffused to the vicinity to illustrate this finding.

5.2.3 Surface Morphology

Striations, matrix recessing, cavities, gross mark, and fibre pull-out are the general surface damages, which could be found at the cut surface of the workpiece after LBM. The development of striations at the inner kerf surface is caused by the cutting velocity or laser cutting mode. Relative high cutting velocity has significantly decreased the

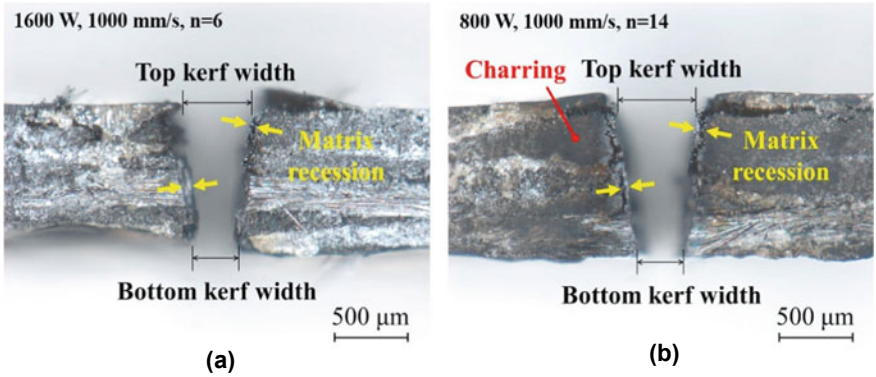

Fig. 16 Kerf formation under different laser power and number of passes [46]

laser beam's exposure time to vaporize the fibre, gradually losing its energy. Riveiro et al. [47] found that the in-pulse processing mode of machining pronounced striations on the inner kerf wall, as shown in Fig. 17. The pulse frequency is a significant control factor of striations. The slow pulse frequency would lead to rougher surface finish, and other defects, such as fibre-matrix debonding and fibre pull out.

The contrast between fibre and matrix constituents' thermal conductivity elevated the laser energy requirement to vaporize the fibre. Notably, this laser heat is stronger than the matrix's thermal conductivity, leading to a high molten matrix. Typically, the melting point of the epoxy-based matrix is in the range of 250–300 °C [38]. Although

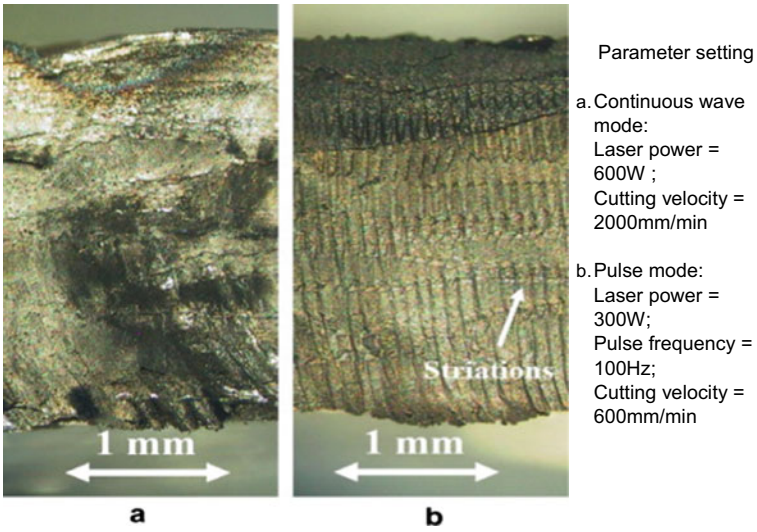

Fig. 17 Optical Image of the cut wall of sample processed **a** in continuous wave mode and **b** in pulsed mode [47]

high-pressure assist gas removes most of the molten matrix, several small solidified matrices remain on the kerf surface known as gross. A study by [31] recorded that severe matrix recession in the bare fibre due to the fibre removal by the thermal heat. The matrix was then evaporated near the inner kerf wall with the gas pressure [48].

6 Electrical Discharge Machining (EDM)

Electrical discharge machining (EDM) is also considered a potential alternative process to produce high dimensional accuracy and intricate shapes of FRPs. In contrast to AWJM and LBM, electrical discharge machining (EDM) consists of an electrode or wire as the tool to obtain material removal processes. However, the tool and the workpiece do not make actual physical contact allowing EDM to machine precision component for hard-to-machining and electrically conductive material easily [49]. The EDM could be classified into two types: die-sinking EDM (DS-EDM) and wire EDM (WEDM), as illustrated in Fig. 18. Both of these machining

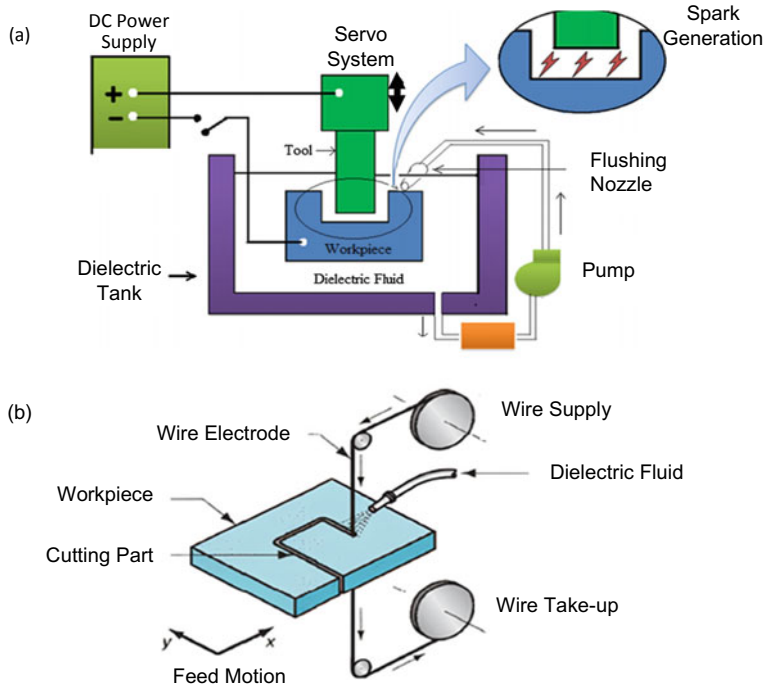

Fig. 18 Schematic of **a** DS-EDM [51] and **b** WEDM [52]

types use the same mechanism concept but the different shape of the electrode. DS-EDM machines are typically used for performing milling or through-hole drilling of CFRPs, whereas WEDM machines are used for cutting or trimming operation.

EDM is also known as "spark erosion" machining, is a thermal process that uses rapid recurring spark discharges to produce microscopically material removal between the tool and the workpiece in conjunction with the dielectric fluid. The dielectric fluid function controls the sparking-gap between tool and workpiece, acts as a coolant and removes the material waste from the sparking area. At the initial stage, no current flow in between the tool and workpiece due to the presence of dielectric fluid. As the on–off pulse from DC power supply is delivered to the tool and workpiece, the intense electrical field is generated to form a high-conductivity bridge across the gap [50]. The dielectric breaks down to form a transient spark discharges through the dielectric fluid; eventually, the high-temperature spark occurs to erode or melt the workpiece's surface.

Unlike aramid and glass fibre, carbon fibre is electrically conductive materials machined via EDM process. However, the semiconductive nature of CFRPs, which consists of distinct carbon fibre and polymer matrix properties, has increased the difficulty of being machined by EDM. The critical factor in producing a satisfactory quality product after machining by EDM is to select a proper set of the process parameter. Figure 19 depicted numerous processing parameters classified in terms of the workpiece, electrical, non-electrical and wire electrode parameters.

In the EDM process of CFRPs, the gap voltage, pulse on–off time, and tool material were the significant factors as these parameters control the power of discharge energy. Gap voltage refers to the width of the spark gap between the electrode and workpiece, whereas pulse on–off time refers to the frequency and duration of spark discharges on the machined surface. Lau et al. [54] carried out pioneering studies on the feasibility of using EDM to machining CFRPs. The experimental results showed that the copper

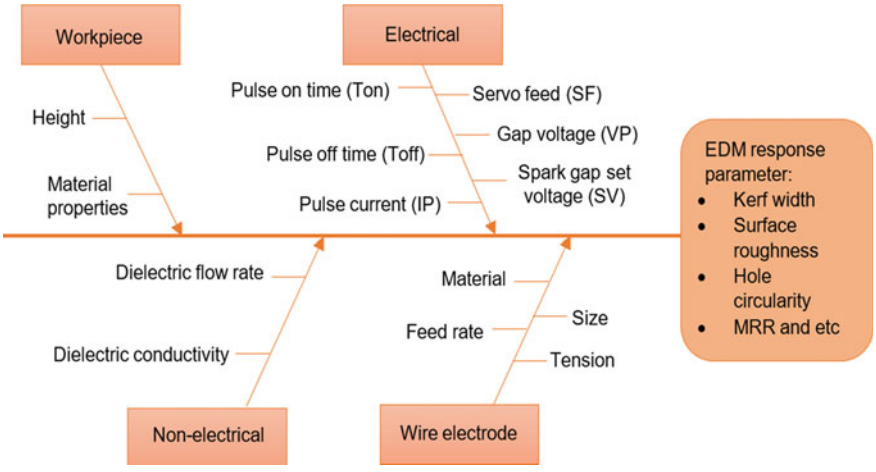

Fig. 19 Ishikawa cause and effect diagram for EDM process [53]

electrode produces better surface finish and tool wear than graphite electrodes. It was also reported that high current density would generate low material removal rate. Excessive thermal energy in the workpiece would lead to an excessive melted matrix that slows down the discharging process. A proper selection of process parameter range is essential to reduce the machining surface's thermal damage and maintain optimum productivity.

6.1 Material Removal Mechanisms of Electrical Discharge Machining

In EDM, material removal occurs through the thermal erosion after rapidly recurring spark discharges inducing between the electrode and the workpiece, as illustrated in Fig. 20. The intense electrical field is created between the gap as the pulse from DC is delivered to electrode and workpiece (pulse on time). The spark is generated due to the breakdown and deionization of a small portion of dielectric [50]. Generation of high-temperature spark discharge causes a small amount of material from the workpiece and electrode melts and vaporizes. As the pulse flow is momentarily stopped (pulse off time), the fresh dielectric fluid comes in position between the gap that removed the molten material and restored the insulating properties of the dielectric.

Besides, the EDM process mechanism for relatively low bulk electrical conductivity of CFRPs is currently not extensively investigated [55], due to the unique properties of CFRPs consisting of high conductive carbon fibres nonconductive matrix. Highly-localized concentration matrix has increased the rate of wire breakage failure during machine through conventional WEDM. Therefore, the recent research proposed and implemented a new WEDM-based machining process, namely preheating assisted WEDM (PAWEDM) process to make up a deficiency [56]. A sandwich assisting electrode method was applied prior WEDM process to improve

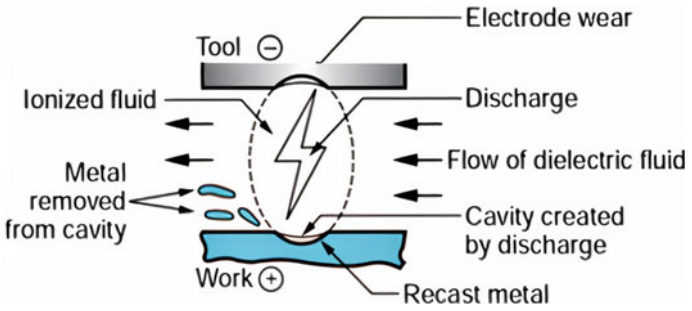

Fig. 20 Schematic of **a** basic EDM process and **b** close-up of the spark gap [52]

the mechanical performance of CFRPs. This process was adopted to spark erosion could be initiated effectivity despite the semiconductive nature of CFRP [57].

6.2 Features of Electrical Discharge Machining of FRPs

In addition to the LBM process, the EDM process represents another thermal machining method that utilizes the spark erosion for material removal. Machining through EDM process required a conductive material to conduct electricity through the sparking-gap. Thus, the EDM process is only applicable to CFRPs due to the presence of highly conductive carbon fibres. The low machining rate and frequent replacement of electrodes limit the use of EDM of CFRPs. The EDM on the layered nature of CFRPs also leads to defects, such as higher surface roughness and dimensional tolerance.

6.2.1 Material Removal Rate (MRR)

The MRR refers to the material removal per unit time, which directly relates to the process productivity. The MMR of CFRPS in EDM is much lower than those in AWJM and LBM due to the relatively low energy input and the material removal nature of the EDM process. The parametric study of MRR recorded that the gap voltage, pulse current and pulse on–off time, had a significant influence in MRR. Increase of gap voltage will significantly strengthen the discharge energy between the sparking gap and subsequently, high product temperature on the workpiece. After all, high pressure and temperature spark discharge lead to high material removal through the evaporation of fibre and melting of matrix [55]. Besides that, the higher pulse current eventually enhances the dissipation of heat energy between the electrode and workpiece.

Habib and Okada [58] studied the influence of EDM processes parameter of CFRP. Various cutting conditions such as open-circuit voltage, peak current, pulse on time and pulse off time was selected. The authors reported that MRR increases with a pulse on time and pulse off time. The electrode is subjected to move a significant number of positive charge when an increase of pulse on time. More heat will be generated in between the sparking gap, causing the increment of MRR. However, longer pulse off time also increases the melting rate of the matrix material. The molten matrix goes over the conductive carbon fibre surface and interrupts the discharging process, which results in a reduction of the MRR. A similar trend also indicated for pulse off time parameter. They increase the time interval results in an increment of breakdown voltage and discharge explosion, which generated a longer and deeper crater size. In addition to this, pulse off time more than 200 μs will decrease the MRR due to the fresh dielectric fluid moving into the gap, which stops the deposition process and commencing the cooling process and results in a lower spark efficiency [59, 60].

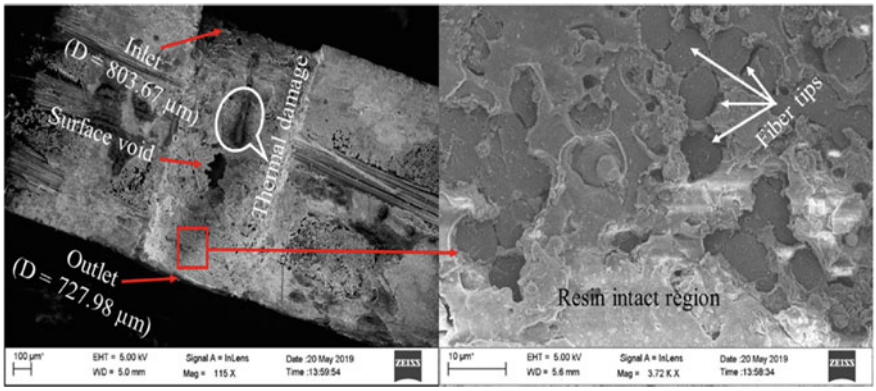

Fig. 21 FESEM image of the inner surface of the CFRP machined hole [61]

6.2.2 Surface Morphology

Lau et al. [54] reported that higher pulse current often led to rougher surface roughness. High pulse current increases the heat generated between the sparking gaps, causing the fibres' thermal expansion. Subsequently, it is debonding between the carbon fibre and matrix. Thus rougher surface finish appears. Besides that, Dutta et al. [61] studied the multi-objective optimization of hole dilation at inlet and outlet during machining of CFRP by µEDM using an assisting-electrode and rotating tool. Figure 21 illustrated the surface morphology of the machined hole's inner cylindrical surface at a voltage of 190 V, pulse duration of 20 µs and tool speed of 400 RPM.

The thermal damage and surface voids are visible in Fig. 21. This cavity occurred might be due to the evaporation and decomposition of the matrix in the resin-rich areas. Surface near to the outlet kerf width reveals the intact resin region. This is due to molten resin's presence under the sudden quenching by cold dielectric fluid that takes the shape of micro-spheres and finally settles on the bottom machined hole surface [61]. Besides, it can be observed that the size of the inlet kerf width is wider than the outlet kerf width, which creates a taper. This situation is associated with the sparking erosion process's exposure time on the electrode surface [62].

7 Summary

Among the nonconventional machining processes used to cut fibre reinforced polymer composites (FRPs), abrasive waterjet machining (AWJM), laser beam machining (LBM), and electrical discharge machining (EDM) have been the most notable approaches, which are currently adopted. However, each of the machining processes comprises limitation to machine FRPs. Specifically, AWJM as the cold machining process develops no heat-affected zone (HAZ) on the machined

composite. However, severe delamination within the lamina, especially on bottom kerf, has significantly reduced composite material's characteristic performance. Accordingly, LBM presents a possible alternative to machining composite and offers a high degree of flexibility and ability to cut difficult-to-machine materials under high cutting speed. Despite the dominance in terms of machinability output, the major drawbacks of LBM include the formation of HAZ and severe striations on the machined surface due to thermal cutting. The EDM process was implemented as an alternative process due to its precision and the capability to produce a burr-free machined surface with the absence of cutting force. Nevertheless, EDM is only practical for electrical conductivity material such as carbon fibre and provides relatively low MMR among the said machining processes. Notably, AWJM, LBM, and EDM processes can reduce machining damage through a careful selection of parameter setting. However, the multi-response optimization of these machining processes is another vital area that has received inadequate focus in past studies. Therefore, this area could be explored in future research.

8 Review Questions

(1) List the advantages and disadvantages of AWJM, LBM and EDM over the conventional process in the trimming of FRPs.
(2) Discuss the material removal mechanisms for the AWJM and LBM of FRPs.
(3) Discuss and explain the effect of hydraulic pressure, abrasive flow rate, traverse rate, and standoff distance on the delamination propagation damage in AWJM.
(4) Explain and compare the mechanisms of kerf formation between AWJM and LBM.
(5) In the case of LBM, the laser beam cannot produce a through the cutting of the machined material. What actions should be taken to produce a through cutting? What is the possible defect, which might appear in the machined material?
(6) In the case of LBM, the laser beam is required for the machining of unidirectional carbon FRPs. What actions should be taken to produce a clean through cutting?
(7) Discuss and explain the relationship between material properties and laser median of LBM.
(8) Discuss and explain the impact of laser power, cutting velocity, pulse frequency, and gas pressure in the laser machining of FRPs.
(9) What is the proposed action for reducing the delamination damage in AWJM and HAZ in LBM of FRPs?
(10) Compare the material removal mechanisms between LBM and EDM of FRPs.
(11) Discuss the role of dielectric fluid in EDM of CFRP.
(12) Explain why carbon FRPs are more amenable to EDM.
(13) Explain the strategies for increasing the conductivity of CFRPs in EDM.

(14) Discuss and explain the impact of pulse voltage, pulse current, electrode material and pulse on–off time in the EDM of CFRPs.
(15) What is the leading cause of kerf taper in AWJM, LBM and EDM?

Acknowledgements The author(s) would like to acknowledge that this chapter is a partially extended version of the paper entitled "Kerf taper and delamination damage minimization of FRP hybrid composites under abrasive waterjet machining" published at The International Journal of Advanced Manufacturing Technology, 2018.

References

1. Sedlacek, J., Slany, M.: Analysis of delamination in drilling of composite materials. Mod. Mach. Sci. J. **2**, 8–11 (2010)
2. Prasad, K., Chakraborty, S.: A decision guidance framework for nontraditional machining processes selection. Ain Shams Eng. J. **9**, 203–214 (2018)
3. Ibraheem, H.M.A.: Numerical optimization for cutting process in glass fibre reinforced plastic using conventional and nonconventional methods. Eastern Mediterranean University (2013)
4. Ramulu, M., Jenkins, M.G., Guo, Z.: Abrasive water jet machining mechanisms in continuous-fibre ceramic composites. J. Compos. Tech. Res. **23**(2), 82–91 (2001)
5. Shanmugam, D.K., Nguyen, T., Wang, J.: A study of delamination on graphite/epoxy composite in abrasive waterjet machining. Compos. Part A **39**, 923–929 (2008)
6. Gaidhani, Y.B.: Abrasive water jet review and parameter selection by AHP method. J. Mechan. Civil Eng. **8**(5), 1–6 (2013)
7. Kechagias, J., Petropoulos, G., Vaxevanidis, N.: Application of taguchi design for quality characterization of abrasive water jet machining of TRIP sheet steels. Int. J. Adv. Manuf. Technol. **62**, 5–8 (2012)
8. Jankovic, P., Igic, T., Nikodijevic, D.: Mosive water jet machining. Theoret. Appl. Mech. **40**(2), 277–291 (2013)
9. Momber, A.W., Kovacevic, R.: Material removal mechanism in abrasive waterjet machining. In: Principles of Abrasive Water Jet Machining. Springer, London (1998)
10. de e Lima C.E.A., Neis, P.D., Ferreira, N.F., Heck, D.J., Zibetti, T.F.: A new metric for assessing the surface roughness of agate plates cut by abrasive water jet. Int. J. Adv. Manuf. Technol. **106:**4903–4912 (2020)
11. Schwartzentruber, J., Papini, M., Spelt, J.K.: Characterizing and modelling delamination of carbon fibre epoxy laminates during abrasive waterjet cutting. Compos. Part A **112**, 299–314 (2018)
12. Selvam, R., Karunamoorthy, L., Arunkumar, N.: Investigation on performance of abrasive water jet in machining hybrid composites. Mater. Manuf. Process. **32**, 700–706 (2017)
13. Azmir, M.A., Ahsan, A.K.: A study of abrasive water jet machining process on glass/epoxy composite laminate. J. Mater. Process. Technol. **209**, 6168–6173 (2009)
14. Unde, P.D., Gayakwad, M.D., Patil, N.G., Pawade, R.S., Thakur, D.G., Brahmankar, P.K.: Experimental investigation into abrasive waterjet machining of carbon fibre reinforced plastic. J. Compos. **2015**, 1–9 (2015)
15. Dhanawade, A., Kumar, S.: Experimental study of delamination and kerf geometry of carbon epoxy composite machined by abrasive waterjet. J. Compos. Mater. **51**(24), 3373–3390 (2017)
16. Schwartzentruber, J., Spelt, J.K., Papini, M.: Modelling of delamination due to hydraulic shock when piercing anisotropic carbon-fibre laminates using an abrasive waterjet. Int. J. Mach. Tools Manuf. **132**, 81–95 (2018)

17. Xiao, S., Wang, P., Gao, H., Soulat, D.: A study of abrasive waterjet multi-pass cutting on kerf quality of carbon fibre-reinforced plastics. Int. J. Adv. Manuf. Technol. **105**, 4527–4537 (2019)
18. Doreswamy, D., Shivamurthy, B., Anjaiah, D., Sharma, N.Y.: An investigation of abrasive water jet machining on graphite/glass/epoxy composite. Int. J. Manuf. Eng. **2015**, 1–11 (2015)
19. Wong, M.M.I., Azmi, A., Lee, C., Mansor, A.: Kerf taper and delamination damage minimization of FRP hybrid composites under abrasive waterjet machining. Int. J. Adv. Manuf. Technol. **94**, 1727–1744 (2016)
20. Ramulu, M., Arola, D.: The influence of abrasive waterjet cutting conditions on the surface quality of graphite/epoxy laminates. Int. J. Mach. Tools Manuf. **34**, 294–313 (1994)
21. Natarajan, Y., Murugesan, P.K., Mohan, M., Ahmed, S.: Abrasive water jet machining process: a state of art of review. J. Manuf. Process. **49**, 271–322 (2020)
22. Azmir, M.A., Ahsan, A.K., Rahmah, A.: Effect of abrasive water jet machining parameters on aramid fibre reinforced plastics composite. Int. J. Mater. Form. **2**, 37–44 (2009)
23. Kong, M.C., Axinte, D., Voice, W.: Challenges on using waterjet machining of NiTi shape memory form alloys: an analysis of controlled-depth milling. J. Mater. Process. Technol. **211**(6), 959–971 (2011)
24. Wong, M.M.I., Azmi, A.I., Lee, C.C., Mansor, A.F.: Experimental study and empirical analyses of abrasive waterjet machining for hybrid carbon/glass fibre-reinforced composites for improved surface quality. Int. J. Adv. Manuf. Technol. **95**, 3809–3822 (2018)
25. Dhanawade, A., Kumar, S.: Multi Performance optimization of abrasive water jet machining of carbon epoxy composite material. Indian J. Eng. Mater. Sci. **25**, 406–416 (2018)
26. Abrate, S., Walton, D.: Machining of composite material. Part II: Nontraditional Methods, Compos. Manuf. **3**(2), 85–94 (1992)
27. Hocheng, H., Tsao, C.C.: The path towards delamination-free drilling of composite material. J. Mater. Process. Technol. **167**, 251–264 (2005)
28. Bakhtiyari, A.N., Wang, Z., Wang, L., Zheng, H.: A review on applications of artificial intelligence in modeling and optimization of laser beam machining. Opt. Laser Technol. **135**, 106721 (2021)
29. Parandoush, P., Hossain, A.: A review of modelling and simulation of laser beam machining. Int. J. Mach. Tools Manuf **85**, 135–145 (2014)
30. Keyence Corporation.: Laser Technical Guide: An Introduction (n.d.) https://www.academia.edu/35824583/LASER_TECHNICAL_GUIDE
31. Hejjaji, A., Singh, D., Kubher, S., Kalyanasundaram, D., Gururaja, S.: Machining damage in FRPs: laser versus conventional drilling. Compos. Part A **82**, 42–52 (2016)
32. Mathew, J., Goswami, G.L., Ramakrishnan, N., Naik, N.K.: Parametric studies on pulsed Nd:YAG laser cutting of carbon fibre reinforced plastic composites. J. Mater. Processing Technol. **89–90**, 198–203 (1999)
33. Goeke, A., Emmelmann, C.: Influence of laser cutting parameters on CFRP part quality. Phys. Procedia **5**, 253–258 (2010)
34. Choudhury, I.A., Chuan, P.C.: Experimental evaluation of laser cut quality of glass fibre reinforced plastic composite. Opt. Lasers Eng. **51**, 1125–1132 (2013)
35. Herzog, D., Jaeschke, P., Merier, O., Haferkamp, H.: Investigations on the thermal effect caused by laser cutting with respect to static strength of CFRP. Int. J. Mach. Tools Manuf. **48**, 1464–1473 (2008)
36. Lau, W.S., Lee, W.B., Pang, S.Q.: Pulsed Nd:YAG laser cutting of carbon fibre composite materials. CIRP Ann. **39**(1), 179–182 (1990)
37. Lee, H., Lim, C.H.J., Low, M.J., Tham, N., Murukeshan, V.M., Kim, Y.-J.: Lasers in additive manufacturing: a review. Int. J. Precision Eng. Manuf. Green Technol. **4**, 307–322 (2017)
38. Shyha, I.S., Kuo, C.L., Soo, S.L.: Workpiece surface integrity and productivity when cutting CFRP and GFRP composites using a CO_2 laser. Int. J. Mechatron. Manuf Syst **7**, 97–107 (2014)
39. Jain, A., Singh, B., Shriwastave, Y.: Reducing the heat-affected zone during the laser beam drilling of basalt-glass hybrid composite. Compos. Part B **176**, 107294 (2019)
40. Leone, C., Genna, S.: Heat affected zone extension in pulsed Nd: YAG laser cutting of CFRP. Compos. Part B **140**, 174–182 (2019)

41. Sun, S., Brandt, M.: Laser beam machining.In: Davim J.P. (Ed.), Nontraditional Machining Processes, pp. 35–96. London, Springer (2013)
42. Balakrishnan, V.S., Seidlitz, H., Yellur, M.R., Vogt, N.: A study on the influence of drilling and CO_2 laser cutting in carbon/epoxy laminates. J. Market. Res. **8**(1), 944–949 (2019)
43. Solati, A., Hamedi, M., Safarabadi, M.: Combined GA-ANN approach for prediction of HAZ and bearing strength in laser drilling of GFRP composite. Opt. Laser Technol. **113**, 104–115 (2019)
44. Jain, A., Singh, B., Shrivastava, Y.: Investigation of kerf deviations and process parameters during laser machining of basalt-glass hybrid composite. J. Laser Appl. **31**(3), 032017 (2019)
45. Mishara, D.R., Bajaj, A., Bisht, R.: Optimization of multiple kerf quality characteristics for cutting operation on carbon-basalt-Kevlar29 hybrid composite material using pulsed Nd: YAG laser using GRA. CIRP J Manuf Sci Technol Null (2019)
46. Oh, S., Lee, I., Park, Y.B., Ki, H.: Investigation of cut quality in fibre laser cutting of CFRP. Optics Laser Technol. **113:**129–140 (2019)
47. Riveiro, A., Quintero, F., Lusquiños, F., del Val, J., Comesaña, R., Boutinguiza, M., Pou, J.: Experimental study on the CO_2 laser cutting of carbon fibre reinforced plastic composite. Compos. Part A **43:**1400–1409 (2012)
48. Li, M., Li, S., Yang, X., Zhang, Y., Liang, Z.: Study on fibre laser machining quality of plain woven CFRP laminates. Appl. Phys. A **3**, 124–270 (2018)
49. Singh, M., Singh, S., Antil, P.: Secondary processing of reinforced polymer composites by conventional and nonconventional manufacturing processes. In: Bajpai P.K., Singh I. (eds.) Reinforced Polymer Composites, pp. 165–187. (2019)
50. Sheikh-Ahmad, J.Y.: Nontraditional Machining of FRPs, pp. 237–291. Springer, Machining of Polymer Composites New York (2009)
51. Mandaloi, G., Singh, S., Kumar, P., Pal, K.: Effect on crystalline structure of AISI M2 steel using tungsten-thorium electrode through MRR EWR, and surface finish. Measurement **90**, 74–84 (2016)
52. T. Saleh and R. Bahar, ELID griding and EDM for finish machining. In: Choudhury, I.A. (eds.) Comprehensive Material Finishing, pp. 364–407 (2016)
53. Choudhary, R., Singh, G.: Effects of process parameters on the performance of electrical discharge machining of AISI M42 high speed tool steel alloy. Materialstoday Proceedings **5**(2), 6313–6320 (2018)
54. Lau, W.S., Wang, M., Lee, W.B.: Electrical discharge machining of carbon fibre composite materials. Int. J. Mach. Tools Manuf **30**(2), 297–308 (1990)
55. Dutta, H., Debnath, K., Sarma, D.K.: A study of material removal and surface characteristics in mirco-electrical discharge machining of carbon fibre-reinforced plastics. Polym. Compos. **40**:4033–4041 (2019)
56. Wu, C., Cao, S., Zhao, Y.J., Qi, H., Liu, X., Guo, J., Li, H.N.: Preheating assisted wire EDM of semiconductive CFRPs: principle and anisotropy. J. Mater. Process. Technol. **288**, 116915 (2021)
57. Dutta, H., Debnath, K., Sarma, D.K.: A study of wire electrical discharge machining of carbon fibre reinforced plastic. In: Shunmugam M., Kanthababu M. (eds) Advances in unconventional machining and composites, pp. 451–460 Springer, Singapore, (2020)
58. Habib, S., Okada, A.: Influence of electrical discharge machining parameters on cutting parameters of carbon fibre-reinforced plastic. Mach. Sci. Technol. **20**(1), 99–114 (2016)
59. Abdallah, R., Soo, S.L., Hood, R.: A feasibility study on wire electrical discharge machining of carbon fibre reinforced plastic composites. Procedia CIRP **77**, 195–198 (2018)
60. Mazarbhuiya, R.M., Dutta, H., Debnath, K., Rahang, M.: Surface modification of CFRP composite using reverse-EDM method. Surf Interfaces **18**, 100457 (2020)
61. Dutta, H., Debnath, K., Sarma, D.K.: Multi-objective optimization of hole dilation at inlet and outlet during machining of CFRP by μEDM using assisting-electrode and rotating tool. Int J Adv Manuf Technol **110**, 2305–2322 (2020)
62. Sheikh-Ahmad, J.Y., Shinde, S.R.: Machinability of carbon/epoxy composites by electrical discharge machining. Int. J. Mach. Mach. Mater. **18**(1/2), 3–17 (2016)

Modelling Machining of FRP Composites

Alessandro Abena, Fadi Kahwash, and Khamis Essa

Abstract Machining of composite materials still represents a challenge in terms of controlling the process, especially to eliminate or minimise damage to the machined workpiece. Numerical models represent a powerful tool, usually used to investigate and optimize the process. For this reason, an overview of the state of the art of numerical techniques for simulating machining of composite materials at a macro-scale and micro-scale level is provided. Models based on the finite element method and mesh-free methods are discussed; advantages and drawbacks are highlighted. Finally, current models' ability to predict chip morphology, chip formation mechanisms, machining force and damages in the ma-chined workpiece is discussed.

1 Introduction

Machining composite materials still represents a challenge in controlling the process, especially eliminating or minimising damage to the machined workpiece. Numerical models represent a powerful tool, usually used to investigate and optimize the process. For this reason, an overview of the state of the art of numerical techniques for simulating machining of composite materials at both macro-scale and micro-scale level is provided. Models based on the finite element method and mesh-free methods are discussed, together with the advantages and drawbacks. Finally, current models' ability to predict chip morphology, chip formation mechanisms, machining force and damages in the machined workpiece is discussed.

The inhomogeneous and anisotropic nature of composite materials still represents a challenge in terms of machinability. Defects can arise during machining in each phase of the material. This involves the fibre, matrix, and fibre-matrix interface. The

A. Abena (✉) · K. Essa
Department of Mechanical Engineering, School of Engineering, University of Birmingham, Edgbaston, Birmingham B15 2TT, UK
e-mail: a.abena@bham.ac.uk

F. Kahwash
Faculty of Engineering and Environment, Northumbria University, Ellison Place, Newcastle upon Tyne NE1 8ST, UK

I. Shyha and D. Huo (eds.), *Advances in Machining of Composite Materials*, Engineering Materials, https://doi.org/10.1007/978-3-030-71438-3_5

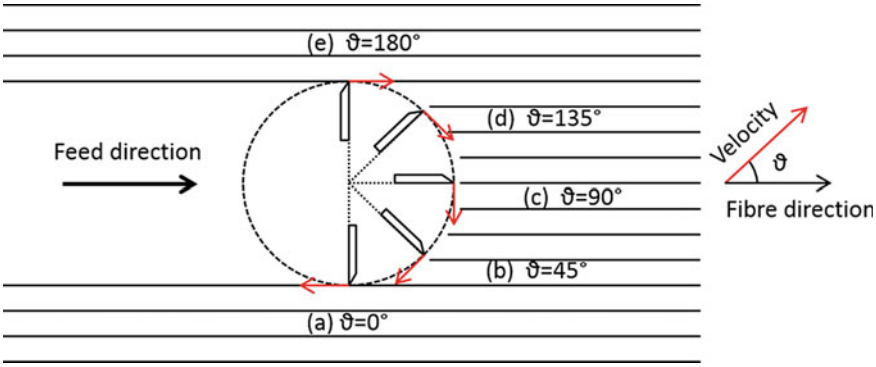

Fig. 1 Schematic of milling on FRP materials [1]

presence of such flaws can compromise surface integrity and lead to poor component in-service performance. The importance of minimizing or eliminating workpiece damage following machining has led industries and researchers to investigate these processes.

In the case of analysing conventional machining methods, processes such as drilling and milling represent complex operations. For instance, in the milling process, the local angle ϑ between the tool velocity vector and the fibre direction changes continuously during machining due to the tool revolution, as shown in Fig. 1, making the process challenging to investigate. Indeed, it has been observed that the chip formation mechanisms during machining of FRPs change depending on the fibre orientation, and so affecting the final quality of the component. In order to facilitate comprehension of events taking place during machining of FRPs and better understand the effect of fibre orientation, the following simplification is usually realised: a complex three-dimensional operation (e.g. milling) is downgraded to a multiple and simpler two-dimensional operation, which is represented by the study of the orthogonal cutting of FRPs for different fibre orientations [1].

Experimental studies on machining of FRPs represent a fundamental step to assess the tool-workpiece interaction and the material deformation and failure under specified machining conditions. However, the experimental approach can be expensive because of the cost of the material itself and the availability of expensive equipment to obtain and analyse the information about the process. In addition, the equipment available and the current technology also determine the level at which it is possible to analyse the process, often representing a limit in the ability to obtain the required and desired information, in particular at a micro-scale level. For these reasons, predictive models could help to overcome some of the limits, even if they still require the necessary experimental tests for validation purposes and assessing their degree of reliability. Different approaches, encompassing analytical, empirical and numerical methods, have been utilised to investigate composite materials machining [2].

Analytical approaches are usually based on strong assumptions, limiting their application [3–5]. Material removal complexity, due to different phases with which

different failure mechanisms are connected, and the fibre orientation's strong influence is difficult to capture using an analytical model. Many parameters involved and the complexity of their interaction make the development of an analytical model very challenging. The analytical approach has proven to be incapable of considering this complexity; thus, a few models have been developed, which were mainly only able to predict cutting force and thrust force.

Empirical approaches require experimental calibration [6–8]. This restricts the application to the range used for calibration. In addition, only the cutting force and thrust force can be obtained.

In contrast to previous approaches, numerical models represent a powerful tool, able to analyse the process at different levels of complexity. They seem to be the most flexible tool for studying CFRP machining and can provide detailed information at different spatial levels (from macro-scale to micro-scale) that could be difficult to obtain using different approaches (experimental, analytical and empirical). An example is a study of bouncing back, which represents the elastic recovery experienced by the workpiece after machining. It is well known for affecting the thrust force and the actual depth of cut, and since it takes place at the micro-scale level, it is difficult to investigate experimentally. Despite the advantages offered by numerical models, they still require validation by means of experiments and eventually, experimental tests, to obtain the specific material data (e.g. fibre, matrix and fibre-matrix interface properties). For the reasons mentioned above, numerical models' employment to investigate composite materials machining has become of fundamental importance.

The present chapter aims to provide an overview of the state of the art of numerical techniques for simulating machining of composite materials, and highlight advantages and drawbacks for each. Hence, this will provide a guideline for the model development, based on the information about the process of relevant interest to the user. A brief description of the chip formation mechanisms that occur when cutting FRPs is provided to facilitate the understanding of the simulation results.

2 Chip Formation Mechanisms of FRP Composites

The ability to interpret and understand results provided by numerical simulations and to improve current numerical models and techniques is strictly linked to the knowledge acquired about the process, derived from experiments. To this end, a brief description of the chip formation mechanisms when machining FRPs is provided in the present section.

Usually, orthogonal cutting is used to study the removal mechanisms when machining composite materials. Several chip formation mechanisms have been identified depending on fibre orientation (ϑ) and tool rake angle (α) [1, 9, 10], as shown in Fig. 2. For fibre orientation $\vartheta = 0°$ and a positive rake angle, the tool progression causes fibre-matrix interface damage with consequent fibre failure due to bending (Type I). For a negative rake angle, fibre failure due to buckling takes place (Type

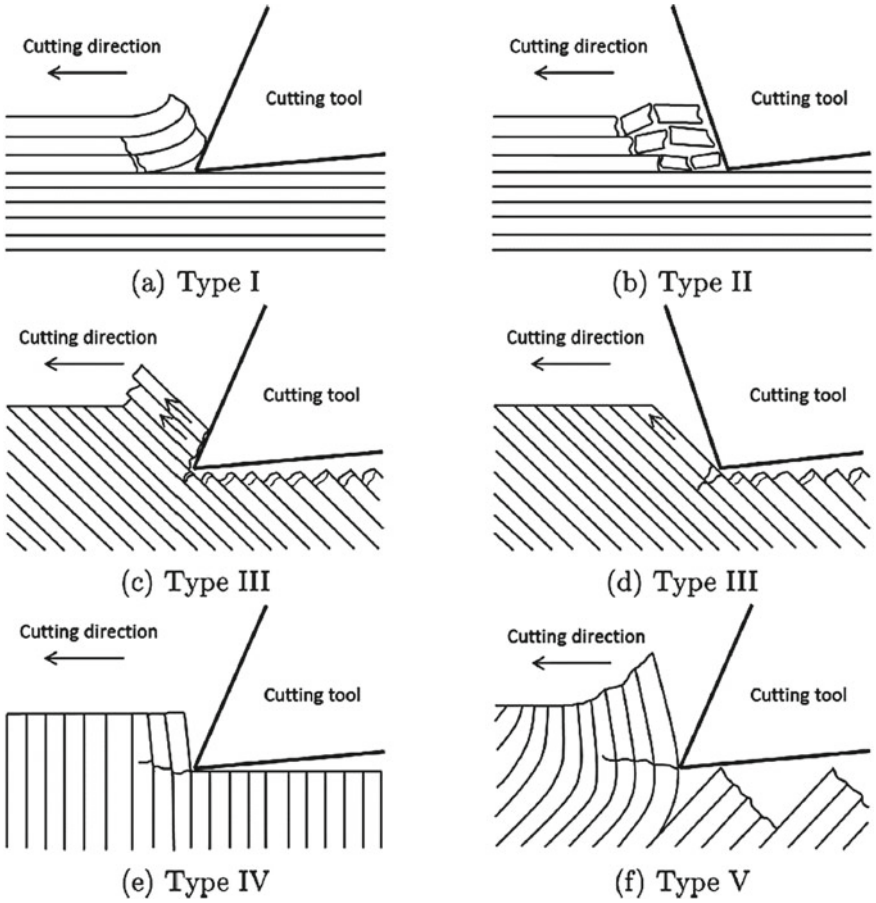

Fig. 2 Influence of fibre orientation and tool rake angle on the chip formation mechanisms [1]: **a** $\theta = 0° - \alpha > 0°$; **b** $\theta = 0° - \alpha < 0°$; **c** $\theta = 45° - \alpha > 0°$; **d** $\theta = 45° - \alpha < 0°$; **e** $\theta = 90° - \alpha > 0°$; **f** $\theta = 135° - \alpha > 0°$

II). For $0° < \vartheta < 75°$ and independently from the rake angle, the chip formation mechanism is caused by compression induced shear across the fibre axis, and shear fracture of the fibre-matrix interface along the fibre direction (Type III). The chip formation mechanism for $75° < \vartheta < 90°$ is characterized by compression induced fracture perpendicular to the fibre axis, and interface fracture due to shear along with the fibre-matrix interface (Type IV). For $\vartheta > 90°$ the chip formation mechanism involves considerable out-of-plane displacement; intra-laminar shear at the fibre-matrix interface; and bending deformations due to compression exerted by the tool, which leads to fibre and matrix failure usually below the cutting plane (Type V).

The chip formation mechanisms described are typical of machining carried out using a sharp cutting edge (nose radius of a few micrometres). When machining with a round cutting edge, a different chip formation mechanism has been observed

for $\vartheta = 90°$ [1, 11]; where the tool is not able to cut the fibre at the contact point, but it exerts compression loading on the sample causing fibre bending and failure below the cutting plane. When machining with a round cutting edge, it is possible to identify a part of the workpiece compressed under the tool. After the tool has passed, the material exhibits an elastic recovery. The amount of spring back the material undergoes is called bouncing back.

3 Classification of Numerical Modelling Techniques

Numerical modelling of a physical problem is composed of three main steps [12]: problem definition (idealisation and simplification of the problem); a mathematical model (definition of equations governing the problem); computer simulation (solving the mathematical model using numerical methods).

Different numerical methods have been implemented in simulations in order to predict tool-workpiece interaction, material deformation and failure, and machining force when machining FRPs. They can be mainly classified in the following categories:

- Finite element method (FEM)
- Mesh-free method (MM).

Mesh-free methods used so far in the literature for simulating machining of FRPs are smoothed particle hydrodynamics (SPH), the discrete element method (DEM) and the Galerkin method.

Independently on the numerical method chosen, it is possible to use three different approaches in order to model the composite material in a numerical analysis [2, 13]:

- Macro-mechanical approach
- Micro-mechanical approach
- Meso-scale approach.

The macro-mechanical approach involves representing the composite workpiece as an equivalent homogeneous material (EHM), whose properties can be derived using the rule of mixtures [14] from the knowledge of matrix and fibre material properties. The macro-mechanical approach can provide general information on the chip formation mechanisms, damage, and machining force prediction [15–18].

In contrast, the microscopic or micro-mechanical approach accounts for each material phase separately [19–21]; thus enabling more detailed simulation and analysis of material deformation and defect formation during machining. The micromechanical model represents a powerful approach to analysing processes at the microscopic level. However, it is still computationally prohibitive for simulating machining operations involving multiple materials, such as drilling, where the EHM approach has been widely used [22–24]. This led several researchers to develop a mesoscale formulation [25–27]. Here, the microscopic model is implemented in the vicinity of the tool, while the EHM approach is used for the rest of the model to provide

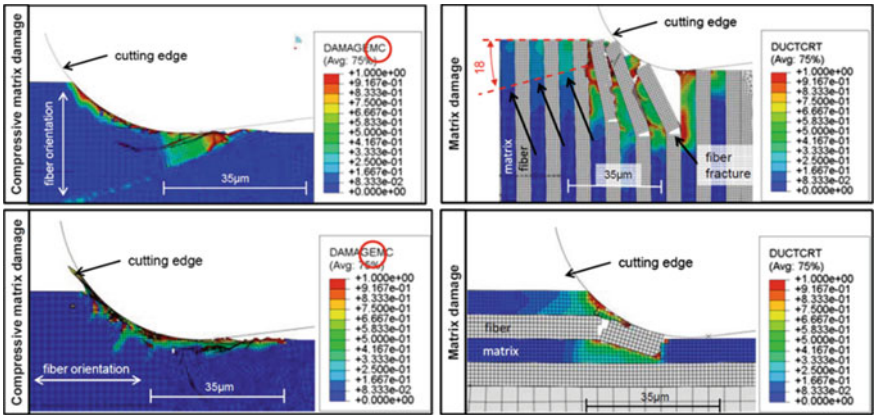

Fig. 3 Matrix damage distribution during orthogonal cutting of UD-CFRP for (left) the macroscopic approach; and (right) the mesoscale approach [28]. Reprint with kind permission from Elsevier—licence number 4587551218547

the necessary stiffness while minimising the computational cost. The advantage of using the mesoscale approach was highlighted in Rentsch et al.'s [28] work, where a comparison with the EHM approach was realized for the orthogonal cutting of UD-CFRP, as shown in Fig. 3. It was highlighted that the mesoscale approach provides further insight into the material removal mechanisms. It was used to investigate the matrix deformation and failure that plays a vital role in the material removal process.

Material models and failure criteria implemented in simulations depend on the approach chosen (macro-mechanical or micro-mechanical); in fact, they have to represent the material phase for which they are used.

Numerical simulations developed so far mainly try to replicate the experimentally observed chip formation mechanisms and predict machining force and damages or defects in the workpiece after machining. The chosen approach (macro-mechanical or micro-mechanical) affects the level at which it is possible to analyse the process and information provided in the output. When machining FRPs, defects can arise at the macro-scale and the micro-scale level; they involve matrix cracking, matrix burning, fibre fracture, fibre pullout, fibre-matrix debonding and delamination [10, 29]. In particular, matrix burning takes place when the temperature during machining exceeds the glass transition temperature of the matrix; debonding represents the detachment between the fibre and the matrix within a single-ply; delamination represents the detachment between two consecutive plies, and fibre pullout takes place when a fibre is removed from the matrix leaving a void. Therefore, defects such as debonding and fibre pullout can be predicted and studied only when a micro-mechanical approach is used. Instead, defects such as delamination are usually studied using a macro-mechanical approach due to the larger amount of material involved (two or more plies).

When developing a numerical model, geometrical assumptions also affect the researchers' ability to investigate the machining of FRPs. A two-dimensional model

allows a reduction of the computational cost of the analysis. However, it does not permit reproducing out-of-plane failure mechanisms and the simulation of quasi-isotropic laminates, which are commonly used for structural applications in the industry [17]. Such limits can be overcome using a three-dimensional model, which also allows simulating complex machining operations, such as drilling and milling.

4 Finite Element Modelling When Cutting FRP Composites

The finite element method has been the first and the most employed method for simulating composite materials machining. The degree of the complexity of models has increased over the years thanks to the growing computational power of computers; and to the improvement of the experimental equipment available to study the process, which has become able to provide more information, e.g. at the micro-scale level that can be used for the models' validation. An overview of models employing the finite element method is provided in the following.

4.1 Macro-Mechanical Approach

When the macro-mechanical approach is employed, an orthotropic homogeneous material with a pre-defined crack path allows several researchers to use the chip formation. Two fracture planes were considered by Arola et al. [30] as shown in Fig. 4, where the secondary shear plane was located ahead of the cutting tool at a distance equal to the mean primary fracture length.

Fracture planes were modelled with double nodes initially bonded together in pairs. Debonding occurred when the fracture criterion, reported in Eq. 1, was satisfied.

$$f = \sqrt{\left(\frac{\sigma_n^{'}}{\sigma^f}\right)^2 + \left(\frac{\tau_1}{\tau_1^f}\right)^2 + \left(\frac{\tau_2}{\tau_2^f}\right)^2}\,;\ \sigma_n^{'} = \max(\sigma_n, 0) \tag{1}$$

The symbols σ_n, τ_1 and τ_2 represent the in-plane normal and shear stress across the interface and the transverse shear stress, respectively. Instead, σ^f, τ_1^f and τ_2^f are the in-plane normal and shear strength and the transverse shear strength (out of plane) of the composite material. When the failure criterion ratio f reached the unit value, the overlapping nodes underwent debonding.

A similar approach was used by Bhatnagar et al. [31] and Nayak [32], who developed two-dimensional simulations of orthogonal cutting on GFRP for fibre angles $0° \leq \vartheta \leq 90°$, where duplicate nodes were positioned along the trim plane. Unlike Arola et al.'s [24] model, where a pre-defined secondary shear plane was located ahead of the cutting tool, a contour plot of the Tsai-Hill failure criterion was used to visualise

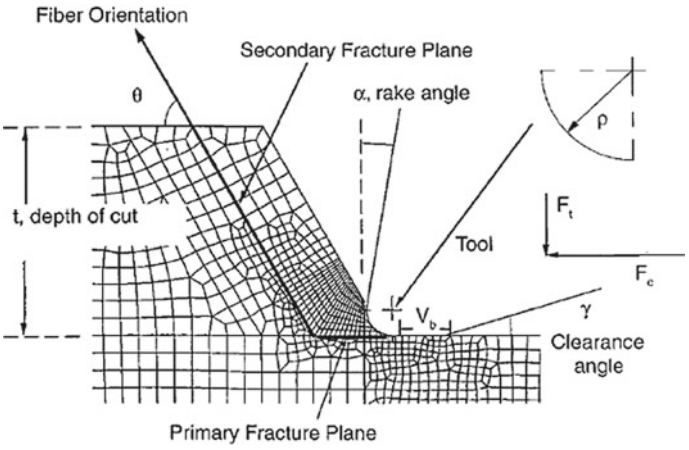

Fig. 4 Macro-mechanical finite element model implementing pre-defined fracture planes [30]. Reprint with kind permission from ASME

the crack propagation in the workpiece. Chip release took place where the Tsai-Hill contour met the sample's free edge when two consecutive nodes experienced debonding on the trim plane. A single fracture plane was also used by Arola and Ramulu [33], with secondary fracture promoting chip release identified employing Tsai-Hill and maximum stress criteria.

Venu Gopala Rao et al. [34] implemented a sacrificial layer, as well, with the node separation condition described similarly to that reported in Eq. (1). An estimation of chip release and damages in machined material was obtained using the Tsai-Wu failure criterion. In particular, the chip release occurred when the Tsai-Wu failure criterion was satisfied ahead of debonded nodes reaching the free edge of the sample.

Drawbacks of approaches based on a pre-defined sacrificial layer to simulate the chip formation include knowledge a priori of the chip formation mechanisms and the path followed by the crack during cutting. Such information is generally desired as output in a numerical model.

No pre-defined fracture plane was used by Lasri et al. [35]. The Hashin-Rotem's failure criterion [36] was implemented, and material stiffness properties' degradation was carried out according to the failure condition satisfied [35, 37]. Analysis' results show the damaged area and the failure mode responsible for it (Fig. 5). Since a user-defined subroutine was used to implement the material's constitutive model, user-defined field variables were used and linked with different failure mechanisms.

In particular, variables SDV2 and SDV3, reported in Fig. 5, were associated with fibre-matrix interface shear failure and fibre failure, respectively. The model is able to predict: the primary fracture plane formation, which propagates in a direction orthogonal to the fibre axis; and the secondary fracture plane, whose formation is due to the shear failure of the fibre-matrix interface.

In the models described above, tool advancement causes excessive deformation of elements and subsequent analysis interruption at some point of the machining.

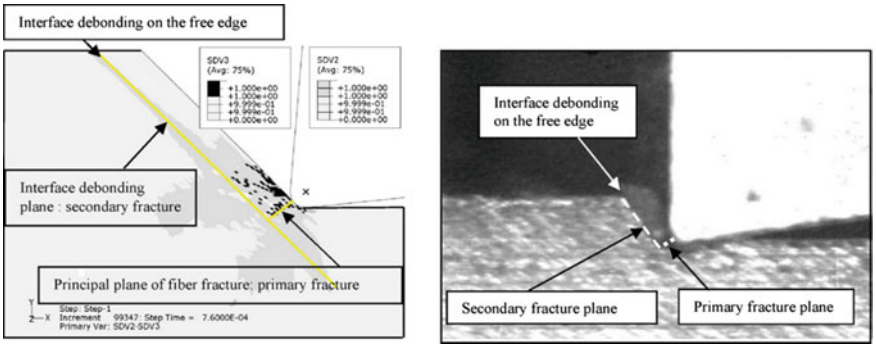

Fig. 5 Comparison of the damage when machining at $\vartheta = 45°$ between (left) numerical model implementing Hashin-Rotem's failure criterion; and (right) experimental image [37]. Reprint with kind permission from Elsevier—licence number 4587551053844

Two different techniques have been used to avoid analysis failure. An adaptive mesh technique was used by Mkaddem et al. [38]. It consists of repositioning the nodes in zones where elements reach a high level of distortion, and for this reason, it is generally computationally expensive. Differently, Soldani et al. [39] and Santiuste et al. [18] implemented properties' stiffness degradation once damage took place, with subsequent deletion of failed elements from the analysis. The latter technique makes it easier to visualise the path along which the cracks propagate. Nowadays, deletion of failed elements from the analysis is generally used.

Three-dimensional models have been developed by several researchers, simulating the composite as a homogeneous orthotropic material. The necessity of three-dimensional models was highlighted by Cantero et al. [16] when simulating cutting on quasi-isotropic laminates. Results showed significant out-of-plane stresses leading to delamination between different layers, representing a critical issue that can be adequately studied only by means of a 3D model. Damages in fibre, matrix and delamination during analysis are shown in Fig. 6.

A comparison between two-dimensional and three-dimensional models was carried out by Santiuste et al. [40]. It was found that the difference between 2

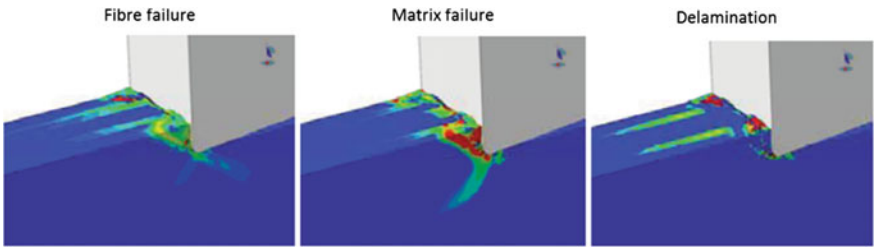

Fig. 6 Material damage during machining using a three-dimensional numerical model [16]. Reprint with kind permission from AIP Conference Proceedings—licence number 4587541138393

and 3D models' results reduces when decreasing the laminate thickness. The three-dimensional model predicts significant delamination, which is one of the most important causes for component rejection at the final stage of composite component manufacture.

A three-dimensional Tsai-Hill criterion, followed by material degradation until failure with element deletion from the analysis, was used by Venu Gopala Rao et al. [15]. Cutting force and thrust force obtained for fibre orientation $15° \leq \vartheta \leq 90°$ were compared with experimental results, showing good agreement for different depths of cut.

Santiuste et al. [17] implemented a three-dimensional model using Hou's theory, followed by material degradation until failure with element deletion from the analysis. Differently from the models previously mentioned, the delamination between plies was modelled by means of both Hou's criterion and cohesive elements for comparison purpose. A schematic of the model, boundary conditions applied, and cohesive elements' implementation is shown in Fig. 7.

Cohesive elements were positioned between consecutive plies; they were used to simulate the adhesion between them and consequently their eventual detachment during cutting, representing delamination damage. The results showed significant improvement in delamination damage prediction when using cohesive elements. In particular, it was highlighted how Hou's model underestimates the extension and amount of delamination damage. For this reason, the cohesive elements are usually used nowadays for simulating the interface between different plies. Santiuste et al.

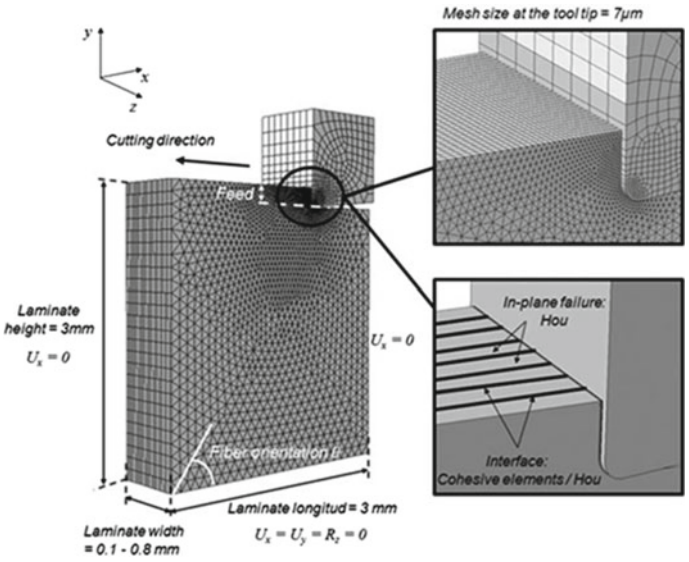

Fig. 7 Schematic of the model for orthogonal cutting of UD-CFRP material [17]. Reprint with kind permission from SAGE Publications—licence number 4587550660220

[17] also showed the three-dimensional model's capability to investigate the influence of the plies' staking sequence on the delamination damage.

4.2 Micro-Mechanical and Mesoscale Approaches

Unlike the macro-mechanical approach, the micro-mechanical and mesoscale approaches require the implementation of material models in terms of failure criteria and stiffness degradation for each phase of the composite material (fibre, matrix and fibre-matrix interface). Models developed up to date are generally two-dimensional [26–28, 41].

The composite materials implemented in numerical models mainly consist of glass or carbon fibres and an epoxy matrix. The epoxy matrix's mechanical properties are highly dependent on strain rate, temperature, and loading conditions [42–45]. This can usually be simplified and represented by a static stress–strain curve if the cutting speed is sufficiently low [26, 41]; which assures a low strain rate and low heat generation between tool and workpiece. In numerical models, the epoxy matrix is generally described as an elastoplastic curve to failure. The plastic region is defined employing Von Mises yield criterion and isotropic hardening [41, 46–48]. Material stiffness degradation can also be implemented until material failure takes place [25–27].

While glass fibres are isotropic and strain rate dependent [27], carbon fibres are orthotropic in nature and strain rate independent [29, 49, 50]. Over the past years, few experimental works have been carried out in order to assess fibre properties implemented in numerical analysis, causing a limitation in the employment of material models for their simulation. The Marigo model describes the brittle failure of carbon fibres by Dandekar and Shin [29];. In contrast, transversely isotropic and perfectly elastic behaviour, followed by maximum principal stress failure criterion was implemented by Abena et al. [41] and Venu Gopala Rao et al. [26]. Calzada et al. [25] imposed fibre failure occurring when stress along the fibre direction exceeds the fibre tensile strength for $\vartheta = 0°$ and $\vartheta = 135°$, or compressive strength for $\vartheta = 45°$ and $\vartheta = 90°$. A progressive damage model by Hashin was used for both the matrix and fibre by Rentsch et al. [28]; good results were found in terms of matrix/fibre failure mode, but the significant discrepancy between numerical and experimental cutting force and thrust force was attributed to the chosen material model.

The bond between fibre and matrix is usually realized by implementing a cohesive zone model. It was already utilised in a macro-mechanical approach by Santiuste et al. [17] to study the out-of-plane failure during orthogonal cutting of long fibre reinforced polymer (LFRP) composites. It was also implemented to simulate delamination for more complex machining operations, such as drilling [51, 52], and for impact problems on composites [53, 54].

In the micro-mechanical approach, modelling the matrix-fibre link is crucial for simulating the phases' debonding. It can be realized using cohesive elements [26, 27, 29, 41] or defining the cohesive property in the contact between the fibre and the

matrix [55]. A comprehensive and detailed study on the cohesive zone models was carried out by Abena et al. [56], where a qualitative and quantitative comparison was also realised.

Cohesive elements based on the traction–separation law are generally used to simulate very thin adhesive layers of bonded surfaces; implemented with a thickness value of zero [26, 27]. This approach's limitation has been highlighted by different works [25, 41, 56, 57] and resides in its inability to represent damage initiation and propagation to failure under compression; furthermore, the inability to produce any stress related to a membrane response [58]. In contrast, elements representing the surrounding phases (matrix and fibre) are able to fail under compression and membrane response and therefore, are deleted during the analysis. Hence, the cohesive elements could remain in the model even if their surrounding elements fail. When this happens, the cohesive elements lose their purpose, since they do not link the matrix and fibre anymore. They also usually experience excessive distortion since their nodes become free to move, as shown in Fig. 8.

Researchers have recently tried to overcome these drawbacks by extending the constitutive behaviour of the cohesive elements already implemented in the software [41]; or using traditional continuum elements for the interface [25, 57]. However, it is possible to assert that the previously described behaviour is common to all models reported in the literature in which interface elements are implemented and independently by their ability to experience compressive deformation and failure [25, 41, 57], whenever surrounding elements fail early. Besides, introducing a thickness in the interface elements to simulate the compressive behaviour does not correctly represent the real interface in a composite material. Generally, a composite material is realized via impregnating the fibre in the resin. Hence, the bond between the matrix and fibre is due purely to adhesion rather than a separate third phase having a finite thickness. For this reason, a cohesive model employing zero thickness cohesive elements based on the traction–separation law is a more appropriate solution.

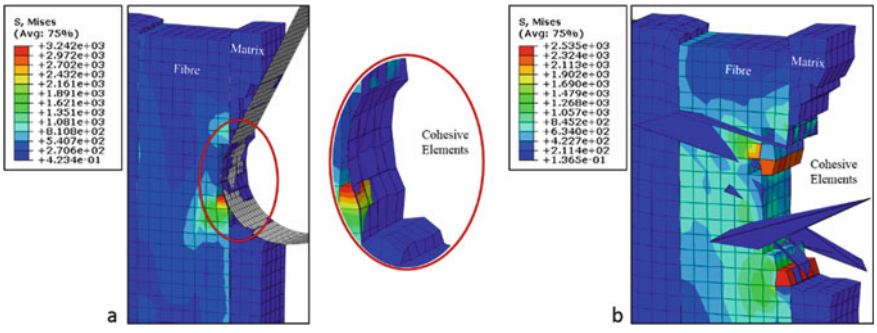

Fig. 8 Zero thickness cohesive elements: **a** matrix and fibre elements failure; and **b** excessive distortion experienced by cohesive elements with further advancement of the tool [56]. Reprint with kind permission from Elsevier—licence number 4599390029035

Drawbacks shown by interface elements can be overcome implementing "surface-based cohesive behaviour", where the cohesive behaviour is defined in terms of surface interaction property avoiding applying interface elements between the fibre and matrix phases. However, Abena et al. [56] highlighted that even if the absence of cohesive elements represents an advantage from a practical point of view, on the other hand, it makes it very difficult to recognise the interface failure, measure the debonding depth, and analyse the interface behaviour. In addition, this approach can be used only when a three-dimensional model is developed. It was also observed that debonding defect formation is almost absent or very low for all fibre orientations, making the matrix-fibre link stronger than cohesive elements based on the traction–separation law [56].

After studying and comparing existing cohesive zone models, Abena et al. [56] suggested a novel cohesive zone model in order to overcome limitations observed. The new approach employs zero thickness cohesive elements based on the traction–separation law, where cohesive elements failure is promoted by damage initiation and evolution due to tension and shear behaviour and surrounding element failure. The latter failure condition is called failure due to connectivity. Two connectivity matrices are obtained using a VUSDFLD subroutine, which stores the connection between cohesive elements and surrounding elements (matrix and fibre). During the analysis, the cohesive elements can deform elastically and experience damage evolution. In the meantime, the matrix and fibre deform under the loads applied during the machining and eventually fail. As one matrix/fibre element fails, a VUSDFLD subroutine searches in the connectivity matrices for the possible connected cohesive element, deleting it from the analysis. This criterion prevents the cohesive element from remaining in the model after the surrounding element fails, losing its purpose and potentially experiencing excessive deformation (Fig. 9).

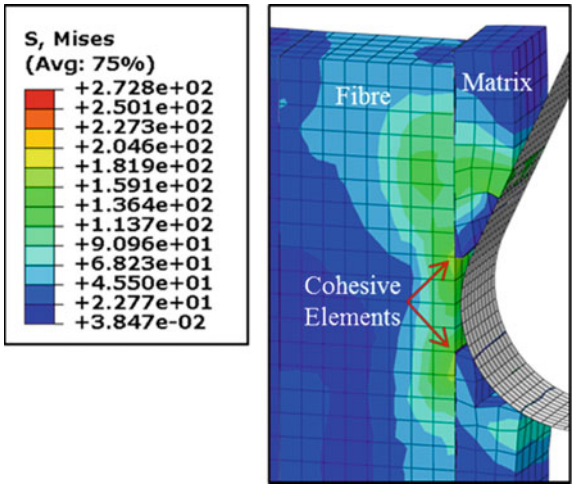

Fig. 9 Cohesive elements' deletion due to the surrounding element (matrix and fibre) failure [56]. Reprint with kind permission from Elsevier—licence number 4599390029035

Several studies have recently focused on developing more accurate and realistic cohesive models compared with the decohesion element with mixed mode capability proposed by Camanho and Davila [59]. For instance, dependence on strain rate has been introduced by May [60], and an elastoplastic phase in the constitutive law has been developed by Salih et al. [61]. Furthermore, new approaches for the interface simulation, such as the smoothed particle hydrodynamics (SPH) method [62], have been implemented. Such cohesive models could be applied to the simulation of machining of composite materials for predicting delamination or debonding.

Different studies have carried out comparable macro-mechanical and micro-mechanical approaches [28, 32, 34]; the advantages of the latter approach have been highlighted. Indeed, significant improvement in machining force prediction was observed by Venu Gopala Rao et al. [34]. In particular, a better agreement of the micro-mechanical model with the experimental results was detected in terms of thrust force prediction, highlighting the importance of considering each phase separately when modelling composite material. The macro-mechanical approach presented a maximum error on the thrust force prediction of ~11 N/mm at a fibre orientation of $\vartheta = 45°$; while the micro-mechanical approach differed only by ~2 N/mm. Finally, comparisons generally show the power of the micro-mechanical approach in analysing the chip formation mechanisms through single phases, providing detailed information on material deformation and failure mechanism during cutting, as shown in Fig. 9.

Three-dimensional models developed are quite limited in number. A three-dimensional model obtained extruding a two-dimensional model in a direction orthogonal to the cutting path (2D-extruded) was realized by Chennakesavelu [55] and Abena et al. [56]. A 2D-extruded model represents an intermediate step between two-dimensional models and the composite material's actual geometry, where cylindrical fibres are present. However, such an approach allows taking into account the three-dimensional effects using a simplified geometry.

Few three-dimensional models implementing cylindrical fibres have been developed [1, 57, 63]. A comparison between a 2D-extruded and a three-dimensional model was carried out by Abena [1] for different fibre orientations ($\vartheta = 0°, 45°, 90°, 135°$). A difference in terms of the material removal mechanism was found for $\vartheta = 0°$ and $\vartheta = 90°$.

For $\vartheta = 0°$, in a 2D-extruded model, cohesive elements separate the fibre from the matrix entirely. The tool tends to lift up the fibre and the matrix in contact with the rake face and push down the phases located below the cutting plane. The tool progression causes an increase in the fibre bending deformation and the propagation of cohesive failure (debonding) along the cutting direction. Fibre failure is due to bending, while in the cohesive elements, shear and tensile stresses contribute together to damage initiation and evolutions until failure. Differently, the three-dimensional model does not show debonding with consequent fibre bending until failure. The absence of debonding can be attributed to the change in the geometry, for the three-dimensional model, fibres are embedded in the matrix and surrounded by cohesive elements. Due to the different arrangement of cohesive elements, they absorb the loads' changes, affecting the chip formation mechanism. Hence, in a three-dimensional model, tool

advancement causes a failure of the fibre and matrix due to compression along the fibre axis.

For $\vartheta = 90°$, the three-dimensional model shows a cleaner cut with a crack propagating ahead of the tool orthogonally to the fibre axis; promoting a realistic chip formation mechanism. Differently from the 2D-extruded model, no multi-fracture was observed in the fibres. Cracks originated in the 2D-extruded model because of fibre bending, below the cutting plane, and the tool's compression at the contact point. Hence, damages in the fibre for the three-dimensional model were contained compared with the 2D-extruded model.

For $\vartheta = 45°$ and $\vartheta = 135°$, the chip formation mechanism was similar in both the 2D-extruded and three-dimensional models. However, the phases' different arrangement and geometry made the workpiece more compact for the latter, with less bending deformations shown for both orientations. Generally, the cohesive elements' failure and damaged areas were more extended in the 2D-extruded model than in the 3D model. The more compact behaviour during the cutting of the three-dimensional model caused a general increase in the cutting forces for all fibre angles, allowing a better prediction at $\vartheta = 0°$ and $\vartheta = 90°$ to be obtained. Instead, the thrust force is generally underestimated for both models.

A significant underestimation of thrust force has been observed and highlighted in several other works [25, 41, 57]. In particular, Calzada et al. [25] reported underestimating the thrust forces, which was one order of magnitude lower than the experimental values. This underestimation has been attributed to the failure and subsequent deletion of elements during the analysis along the cutting path; thereby causing relaxation in the force component due to the loss of contact between the tool and the workpiece [25, 41].

Quasi-static and explicit simulations have been carried out. A quasi-static simulation, involving the orthogonal cutting of UD-FRP at different fibre orientations and machining parameters, was developed by Venu Gopala Rao et al. [26, 34]. A tool displacement boundary condition was specified. The drawback of implementing a quasi-static analysis is that the model is limited to predicting failure only in the first fibre via an iterative approach. It is, therefore, unable to simulate chip formation progression. Unlike quasi-static analysis, dynamic simulations can predict the failure mechanism and illustrate material deformation during the chip formation process [25, 29, 41]. In such cases, a boundary condition based on tool velocity is typically implemented.

Independently on the approach chosen, macro-mechanical or micro-mechanical, the cutting tool is usually simulated as a rigid body [25–27, 41]; as its elastic modulus (e.g. Young's modulus for a tungsten carbide tool is in the range 500–700 GPa [64]) is much bigger than that of the fibres (e.g. Young's modulus along the fibre direction for carbon fibre is 230 GPa [10]) and the matrix (e.g. Young's modulus for an epoxy matrix is in the range 2.6–3.8 GPa [10]). An elastic material model was used by Ramesh et al. [65] in order to investigate the stress level in the tool during cutting. However, this model represents a simplistic approach; in fact, an appropriate elastoplastic material model should be associated with the tool to obtain

more reliable information on deformation and stress. Then deletion of failed elements could be added to simulate the tool wear during cutting.

5 Mesh-Free Modelling When Cutting FRP Composites

Models for simulating machining of composite materials usually employ the finite element method. The necessity of a mesh induces limitations in the capability of such a method to investigate the process. Firstly, the large deformation the material undergoes during cutting usually causes issues with a convergence of the solution. To avoid excessive deformation of the elements, when the failure condition is reached, the element is removed from the analysis. This causes a non-physical material loss, which is also usually followed by a loss of contact between the tool and the workpiece, affecting chip formation mechanisms, machining force and depth of cut. Deletion of elements due to failure allows the simulation of crack formation and growth in the workpiece, with element size affecting the minimum dimension of the crack that can be simulated. However, it is challenging to simulate cracks with arbitrary and complex paths, and also breakage of the material into a large number of fragments.

Mesh-free methods are usually employed in order to overcome the limitations related to the FE method. The workpiece is described as a cloud of particles, and it does not require any element connecting them. As for the FE method, mesh-free methods can implement macro-mechanical, micro-mechanical and mesoscale approaches. Mesh-free methods used for simulating machining of composite materials are mainly the following: smoothed particle hydrodynamics (SPH); the discrete element method (DEM) and the element-free Galerkin method (EFG).

5.1 Smoothed Particle Hydrodynamics

Being part of the mesh-free methods' family, the SPH method can handle large deformations and material opening due to tool action without element deletion. It has been successfully used for simulating orthogonal cutting in metals [66–70]. Particles used for representing the workpiece are linked through a specific constitutive behaviour assigned by the user. Material properties' degradation after the failure condition has been reached, allows particles to separate and therefore, the composite material to be cut.

A three-dimensional model for the orthogonal cutting of UD-CFRP implementing the SPH method was developed by Abena and Essa [63] using a mesoscale approach. Results were compared with those obtained employing a FE method and against experiments carried out by Calzada et al. [25]. The SPH method was more capable of simulating the chip formation mechanisms (Fig. 10). In general, the chip morphology predicted by the SPH method seemed to be more accurate when compared with high-speed camera images, being more prone to generate a continuous chip (Fig. 10). For

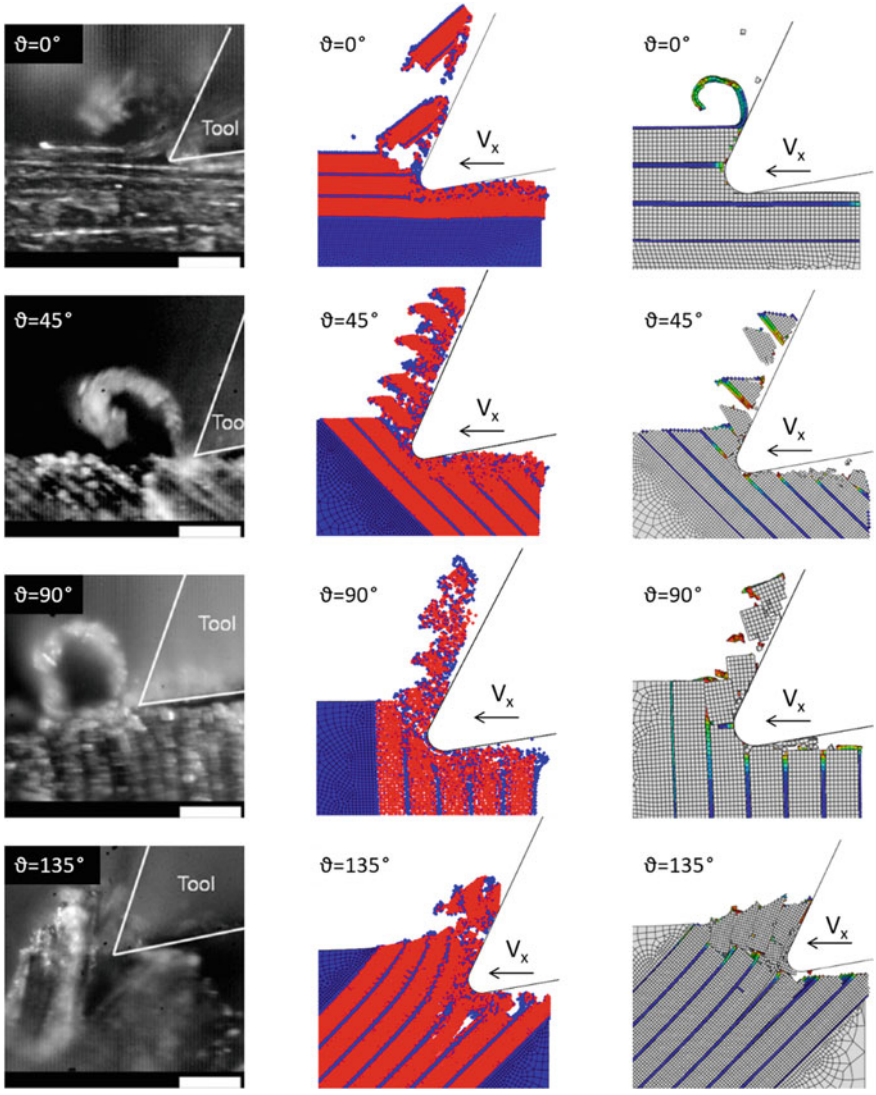

Fig. 10 Comparison of chip morphology and formation mechanisms for different fibre orientations considering: (left) experimental results [25]; (centre) SPH model [63]; and (right) FEM model [63]. Reprint with kind permission from Elsevier—licence number 4864431318474 and 4599390103074

all fibre orientations, damage extension was found larger when employing the SPH method due to the presence of damaged material around the tool, which causes an increase of material involved in the cutting.

When the SPH method was employed, the degradation of material properties after the failure condition was reached allowed particles to separate during cutting.

In this way, non-physical material loss observed in FE models was avoided, ensuring tool-workpiece contact during the whole cutting process, and improving the thrust force prediction. The thrust force is affected by bouncing back [10], representing the amount of elastic recovery the workpiece undergoes after the tool has passed.

The thrust force's contribution is due to the pressure the workpiece applies to the tool clearance face due to the elastic recovery after cutting. The bouncing back, i.e. the elastic recovery, also influences the depth of cut [10]. Differently from the FEM method where the element deletion usually leads to a gap between the tool clearance face and the machined surface, bouncing back and its effect on thrust force and the depth of cut can be simulated and studied when using the SPH method. The SPH model developed by Abena and Essa [63] predicted bouncing back equal to the cutting edge radius (~5 μm) when machining at fibre orientation $\theta = 0°$ (Fig. 11) and a depth of cut of 15 μm, in agreement with the literature. Therefore, the actual depth of cut was found to be of ~10 μm, instead of the set depth of cut of 15 μm.

The SPH method generally showed a better prediction in terms of cutting force than the FE method, with improvements reaching ~30% at $\theta = 0°$ [63]. Thrust force improved using the SPH method for all fibre orientations. In particular, the improvement was ~30% for $\theta = 90°$ and $\theta = 135°$, and ~26% for $\theta = 0°$ when compared to the FE method [63].

Finally, results obtained by Abena and Essa [63] showed that the SPH method could provide additional and vital information that it is not possible to obtain using the FE method, e.g. bouncing back; and it also allows achievement of a more accurate simulation of cutting of composite materials. However, differently from the FE method, the SPH method is not able to provide any information on the fibre-matrix interface, e.g. debonding damage, due to its inability to implement a cohesive model.

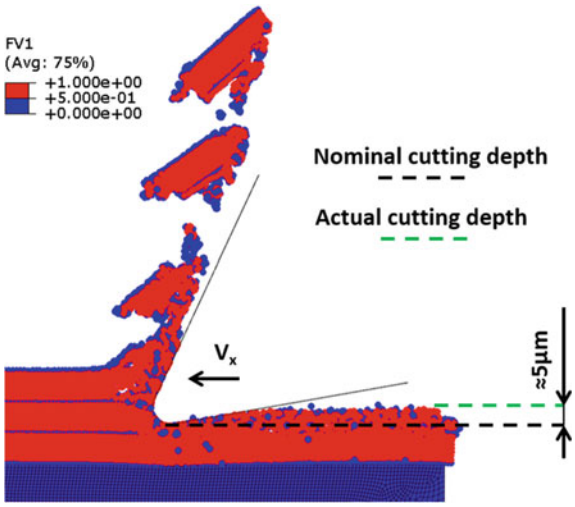

Fig. 11 Bouncing back amount calculated when employing the SPH method at fibre orientation $\theta = 0°$ [63]. Reprint with kind permission from Elsevier—licence number 4599390103074

5.2 Discrete Element Method

The discrete element method (DEM) is a numerical technique used to simulate the behaviour of assemblies of particles, first introduced by Cundall and Strack [71]. Particles can have different sizes and shapes and interact with each other through the contact implemented in the simulation. Contact properties (e.g. friction, damping, cohesion) affect the behaviour of the assembly of particles.

Iliesu et al. [21] employed the discrete element method to simulate the orthogonal cutting of UD-CFRP composites at the micro-scale level. To this end, they appropriately set the contact between particles in order to simulate fibre and matrix. The contact acted as a solid link between particles to simulate solid material. In particular, each fibre was simulated using two rows of particles across the diameter. Differently, no particles were used to model the matrix, which was simulated in terms of contact properties between adjacent particles of two consecutive fibres. For this reason, debonding between fibre and matrix could not be studied.

The model's behaviour during analysis is reported in Fig. 12. The developed model was able to capture the physical mechanism of chip formation. The cutting force and thrust force trends were found to be similar to the experimental results, even if underestimated or overestimated depending on the fibre orientation. It was highlighted that 80% of the computational time was spent searching for particles' contact and resulting forces, which was identified as a drawback of the DEM method.

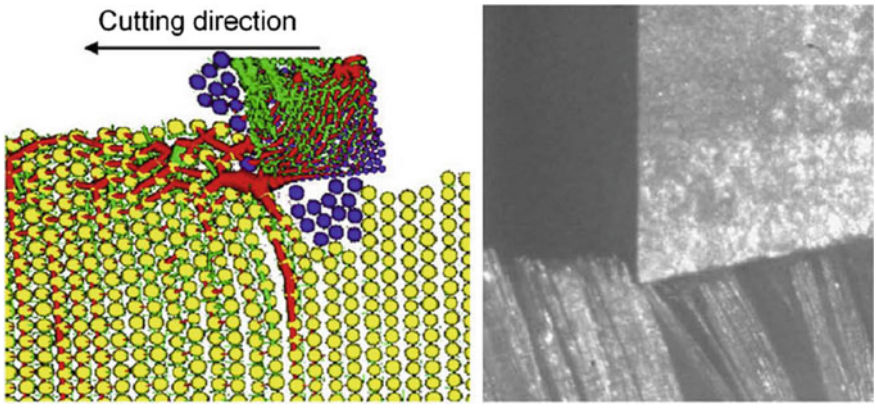

Fig. 12 Chip formation in orthogonal cutting of unidirectional composite at $\theta = 90°$: (left) DEM simulation; (right) high-speed video image [21]. Reprint with kind permission from Elsevier—licence number 4587550855774

5.3 *Element-Free Galerkin Method*

The Element-free Galerkin method (EFG) was conceived by Belytschko in 1994 [72]. The method was an improvement of the diffuse element method proposed by Nayroles et al. [73]. The EFG is based on a weak global form of the governing equations. It utilises Moving Least Squares (MLS) approximation in constructing the shape functions. No mesh is required to construct the discretised domain, only an adequately chosen weight function and nodal information. The EFG is well suited for fracture mechanics applications due to the lack of nodal connectivity and robustness with respect to the regularity of nodal distribution (ease of adaptive procedure). One drawback of the standard EFG was the difficulty in applying boundary conditions due to the lack of interpolating property of the MLS shape functions.

Kahwash et al. [74–76] proposed steady-state and dynamic models to simulate the orthogonal cutting of unidirectional composites based on the EFG method. The steady-state model is suitable for simulating cutting at low speed with an emphasis on cutting forces. Compared with experimental evidence and other simulations using FEM, a sample of the results is shown in Fig. 13. It can be seen that the trend of cutting forces is consistent between FEM and EFG. However, the force magnitude was generally under-predicted by the EFG. This was attributed mainly to the assumption of sharp tool nose in [74, 75] as opposed to 0.05 mm in the FEM study [35]. The effect of numerical parameters was studied and found that both the domain of influence size and weight function choice has a small effect on the results, indicating its robustness from a numerical point of view.

In Kahwash et al. [76], a dynamic model for orthogonal cutting was presented with several improvements over the steady-state model. The model is capable of modelling high-speed machining, including three failure criteria, non-linear constitutive model, and novel frictional contact force algorithm. The cutting forces were

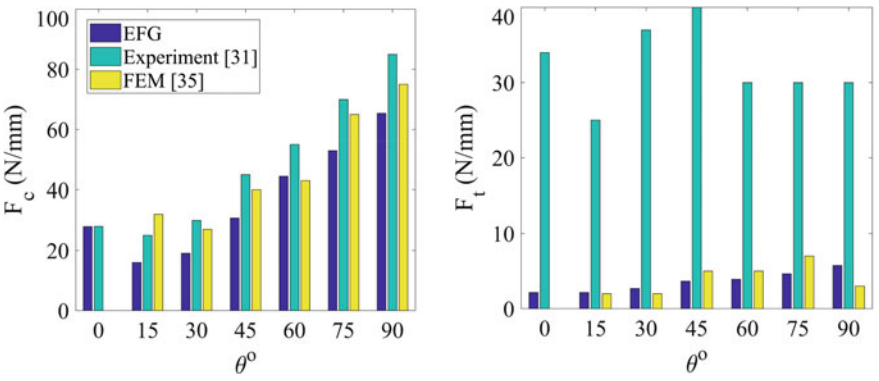

Fig. 13 Comparison of cutting force (left) and thrust force (right) between the EFG, FEM and experimental evidence cutting with 5° rake angle and 0.2 mm depth of cut, adapted from [75]. Reprint with kind permission from Elsevier—license number 4864730836751

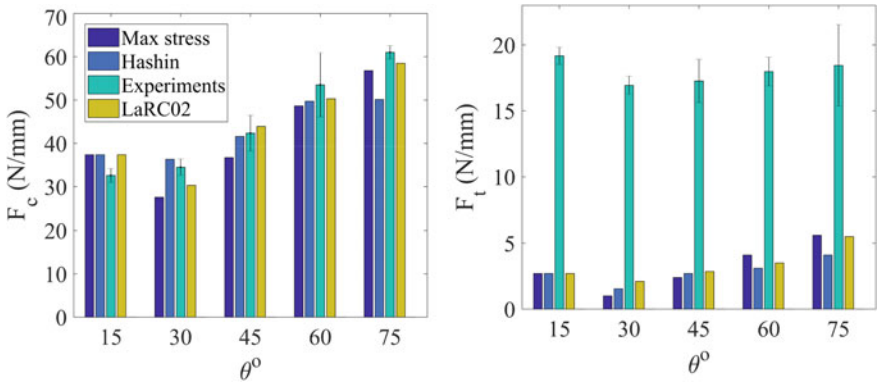

Fig. 14 Cutting force (left) and thrust force (right) utilising different failure criteria as compared to experiments, adapted from [76]. Reprint with kind permission from Elsevier—license number 4864731221487

compared against experimental evidence, as shown in Fig. 14. The main cutting force was predicted accurately, but the thrust force was under-predicted as is common in several studies of cutting forces. This could be attributed to the inability to capture the bouncing back effect.

Chip formation was also studied. The choice of failure criterion seems to play a more prominent role in predicting the onset and progression of chip formation than the prediction of cutting forces. Figure 15 shows fibre failure progression using Maximum stress, Hashin and LaRC02 failure criteria. It can be seen that fibre failure in compression, which is expected to be seen when cutting using a 0 rake angle is predicted by LaRC02 failure criteria and to a lesser extent by Hashin.

6 Summary

Machining of FRP composites still represents a challenge due to their inhomogeneous and anisotropic nature. Numerical methods are generally used to investigate the process at different scale levels and obtain predictions on variables of interest (e.g. type of damage, damage extension and machining force) when modifying the process' parameters (e.g. cutting speed, depth of cut and tool geometry).

Geometry assumptions (two-dimensional or three-dimensional model) and scale level of the simulation (macro-mechanical or micro-mechanical approach) affect the researchers' ability to investigate the process and the type of variables available in the output.

Different numerical methods have been used to simulate machining of FRP composites, each presenting advantages and drawbacks. The most used is the finite element method, which allows the implementation of cohesive zone models to simulate the bond between different plies and model the fibre-matrix interface. Therefore,

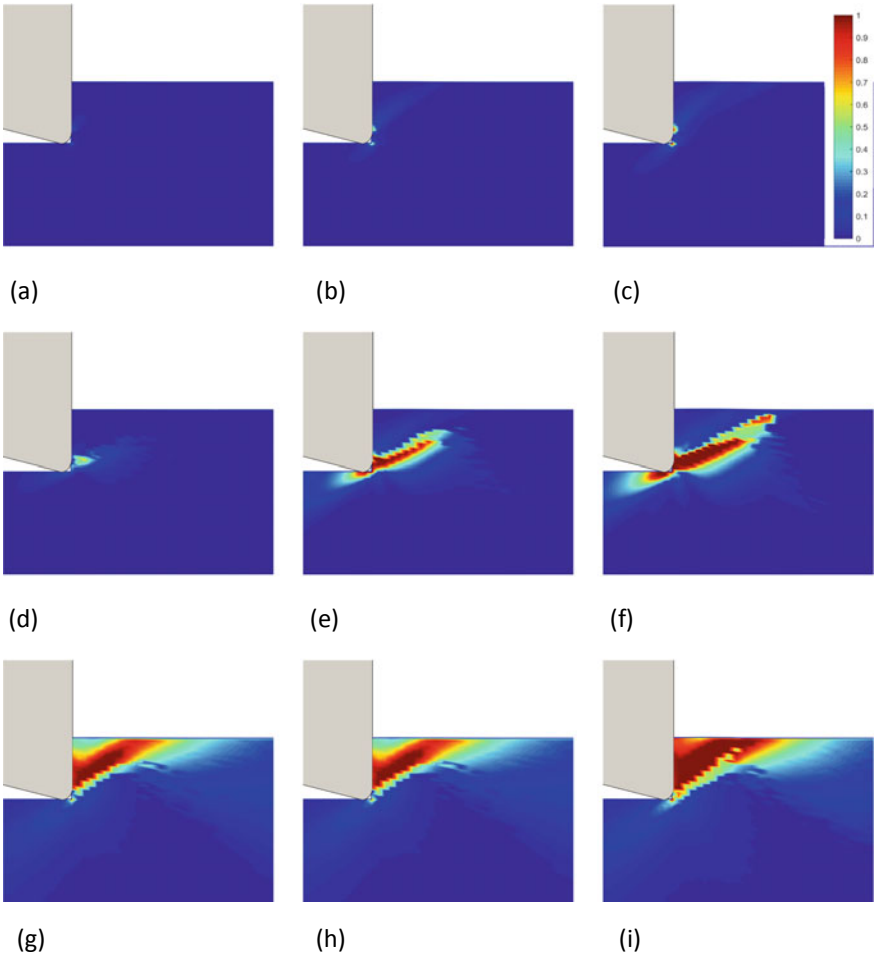

Fig. 15 Progressive fibre damage at $\theta = 30^o$ using maximum stress (**a**, **b**, **c**), Hashin (**d**, **e**, **f**) and LaRC02 (**g**, **h**, **i**) [76]. Reprint with kind permission from Elsevier—license number 4864731221487

the FE method enables the study of defect formation in terms of delamination and debonding. The main drawback of the FE method resides in the necessity of element deletion in order to simulate material opening and chip formation. This causes a non-physical material loss and a loss of contact between tool and workpiece. Hence, the FE method cannot simulate bouncing back and its effect on thrust force and depth of cut.

Mesh-free methods can overcome such limitations, being able to handle large deformations without element deletion. In particular, the SPH method has proved to be capable of predicting the bouncing back amount; therefore improving the prediction of thrust forces and providing a reliable measure of the actual depth of cut. Moreover, the prediction of chip type and chip formation mechanisms improved

when compared to the FE method. Other mesh-free methods have also been used for simulating the machining of FRP composites. The discrete element method has captured the physical mechanism of chip formation for different fibre orientations; however, it presents a high computational cost due to the search for the particles' contact and resulting forces. The Element-free Galerkin method was also applied to the machining of composites. The advantages of the method include accurate prediction of cutting force, ease of setting up the model and robustness concerning irregular nodal distribution.

Differently to models based on the FE method, mesh-free methods generally do not directly implement a cohesive zone model. For this reason, information on fibre-matrix interface behaviour is usually not available.

Finally, simulation of machining of FRP composites has improved over the past years. It will continue to do so by implementing other/novel available numerical methods, and the development of new material models for each phase of the material (e.g. fibre, matrix and fibre-matrix interface). The growing availability of material properties and in general of experimental data will also be fundamental to this journey.

7 Review Questions

(1) What is the process usually used to simplify the study of machining of FRP composites?
(2) What are the advantages of using numerical simulations to investigate FRP composites machining when compared with other available techniques?
(3) What is the effect of geometrical assumptions, two-dimensional or three-dimensional models, on the ability to investigate machining of FRP composites?
(4) What are the numerical methods usually used for simulating machining of FRP composites?
(5) What are the approaches that can be used for implementing composite materials in a numerical simulation?
(6) What are the advantages when using a macro-mechanical approach?
(7) What are the advantages when using a micro-mechanical approach?
(8) Why is a mesoscale approach usually used in the simulation of machining of FRP composites?
(9) What is the cohesive zone model used for in macro-scale and micro-scale approaches?
(10) What are the advantages and limitations of the usually used cohesive zone models, especially for simulation of debonding between fibre and matrix?
(11) What does "failure due to connectivity" mean for cohesive elements?
(12) What is the difference between quasi-static and explicit simulations in terms of results?
(13) Why are thrust forces generally underestimated when using the FE method?

(14) Which mesh-free methods are usually used for simulating machining of FRP composites?
(15) What are the advantages and limits of the SPH method when compared to the FE method?
(16) What does the bouncing back represent? How is the machining of FRP composites affected by bouncing back? How is it possible to simulate bouncing back?
(17) What is the discrete element method? How can the discrete element method be used for simulating machining of FRP composites? What is the main drawback when implementing the discrete element method?
(18) How can the tool be modelled when simulating machining of FRP composites?
(19) How are the shape functions constructed in the element-free Galerkin method? What is the information needed for constructing them?

References

1. Abena, A.: Advanced modelling for the orthogonal cutting of unidirectional carbon fibre reinforced plastic composites. Thesis (PhD) University of Birmingham (UK) (2017)
2. Che, D., Saxena, I., Han, P., Guo, P., Ehmann, K.F.: Machining of carbon fiber reinforced plastics/polymers: a literature review. J. Manuf. Sci. Eng. **136**, 1–5 (2014)
3. Zhang, L.C., Zhang, H.J., Wang, X.M.: A force prediction model for cutting unidirectional fibre-reinforced plastics. Mach. Sci. Technol. **5**, 293–305 (2006)
4. Jahromi, A.S., Bhar, B.: An analytical method for predicting cutting forces in orthogonal machining of unidirectional composites. Compos. Sci. Technol. **70**, 2290–2297 (2010)
5. Everstine, G.C., Rogers, T.G.: A theory of machining of fiber-reinforced materials. J. Compos. Mater. **5**, 94–106 (1971)
6. Langella, A., Nele, L., Maio, A.: A torque and thrust prediction model for drilling of composite materials. Compos. A Appl. Sci. Manuf. **36**, 83–93 (2005)
7. Kalla, D., Sheikh-Ahmad, J., Twomey, J.: Prediction of cutting forces in helical end milling fiber reinforced polymers. Int. J. Mach. Tools Manuf. **50**, 882–891 (2010)
8. Karpat, Y., Bahtiyar, O., Deger, B.: Mechanistic force modelling for milling of unidirectional carbon fiber reinforced polymer laminates. Int. J. Mach. Tools Manuf. **56**, 79–93 (2012)
9. Wang, D.H., Ramulu, M., Arola, D.: Orthogonal cutting mechanisms of graphite/epoxy composite Part I: unidirectional laminate. Int. J. Mach. Tools Manuf. **35**, 1623–1638 (1995)
10. Sheikh-Ahmad, J.Y.: Machining of polymer composites. Springer Science+Business Media (2009)
11. Pwu, H.Y., Hocheng, H.: Chip formation model of cutting fiber-reinforced plastics perpendicular to fiber axis. J. Manuf. Sci. Eng. **120**, 192–196 (1998)
12. Yip, S.: Handbook of materials modeling. Springer Science+Business Media (2007)
13. Dandekar, C.R., Shin, Y.C.: Modeling of machining of composite materials: a review. Int. J. Mach. Tools Manuf. **57**, 102–121 (2012)
14. Chawla, K.K.: Composite Material: Science and Engineering. Springer Science+Business Media (2012)
15. Venu Gopala Rao, G., Mahajan, P., Bhatnagar, N.: Three-dimensional macro-mechanical finite element model for machining of unidirectional-fiber reinforced polymer composites. Mater. Sci. Eng. A **498**:142–149 (2008)

16. Cantero, J.L., Santiuste, C., MarÍn, N., Soldani, X., Miguélez, H.: 2D and 3D approaches to simulation of metal and composite cutting. AIP Conf. Proc. **1431**, 651–659 (2012)
17. Santiuste, C., Olmedo, A., Soldani, X., Miguélez, H.: Delamination prediction in orthogonal machining of carbon long fiber-reinforced polymer composites. J. Reinf. Plast. Compos. **31**, 875–885 (2012)
18. Santiuste, C., Soldani, X., Miguélez, H.: Machining FEM model of long fiber composites for aeronautical components. Compos. Struct. **92**, 691–698 (2010)
19. Nayak, D., Singh, I., Bhatnagar, N., Mahajan, P.: An analysis of machining induced damage in FRP composites—a micromechanics finite element approach. AIP Conf. Proc. **712**, 327–331 (2004)
20. Dandekar, C.R., Shin, Y.C.: Multiphase finite element modelling of machining unidirectional composites: prediction of debonding and fiber damage. J. Manuf. Sci. Eng. **130**, 1–12 (2008)
21. Iliescu, D., Gehin, D., Iordanoff, I., Girot, F., Guetiérrez, M.E.: A discrete element method for the simulation of CFRP cutting. Compos. Sci. Technol. **70**, 73–80 (2010)
22. Palani, V.: Finite Element Simulation of 3D Drilling in Unidirectional CFRP Composite. Thesis (M.S.) Wichita State University (2006)
23. Isbilir, O., Ghassemieh, E.: Numerical investigation of the effects of drill geometry on drilling induced delamination of carbon fiber reinforced composites. Compos. Struct. **105**, 126–133 (2013)
24. Phadnis, V.A., Roy, A., Silberschmidt, V.V.: A finite element model of ultrasonically assisted drilling in carbon/epoxy composites. Procedia CIRP **8**, 141–146 (2013)
25. Calzada, K.A., Kapoor, S.G., De Vor, R.E., Samuel, J., Srivastava, A.K.: Modeling and interpretation of fiber orientation-based failure mechanisms in machining of carbon fiber-reinforced polymer composites. J. Manuf. Process. **14**, 141–149 (2012)
26. Venu Gopala Rao, G., Mahajan, P., Bhatnagar, N.: Micro-mechanical modelling of FRP composites—cutting force analysis. Compos. Sci. Technol. **67**:579–593 (2007)
27. Venu Gopala Rao, G., Mahajan, P., Bhatnagar, N.: Machining of UD-GFRP composites chip formation mechanism. Compos. Sci. Technol. **67**:2271–2281 (2007)
28. Rentsch, R., Pecat, O., Brinksmeier, E.: Macro and micro process modeling of the cutting of carbon fiber reinforced plastics using FEM. Procedia Eng. **10**, 1823–1828 (2011)
29. Dandekar, C.R., Shin, Y.C.: Multiphase finite element modeling of machining unidirectional composites: prediction of debonding and fiber damage. J. Manuf. Sci. Eng. **130**, 1–12 (2008)
30. Arola, D., Sultan, M.B., Ramulu, M.: Finite element modeling of edge trimming fiber reinforced plastics. J. Manuf. Sci. Eng. **124**, 32–40 (2002)
31. Bhatnagar, N., Nayak, D., Singh, I., Chouuhan, H., Mahajan, P.: Determination of machining-induced damage characteristic of fibre reinforced plastic composite laminates. Mater. Manuf. Process. **19**, 1009–1023 (2004)
32. Nayak, D., Bhatnagar, N., Mahajan, P.: Machining studies of UD-FRP composites part 2: finite element analysis. Mach. Sci. Technol. **9**, 503–528 (2005)
33. Arola, D., Ramulu, M.: Orthogonal cutting of fibre-reinforced composites: a finite element analysis. Int. J. Mech. Sci. **39**, 597–613 (1997)
34. Venu Gopala Rao, G., Mahajan, P., Bhatnagar, N.: Machining of UD-CFRP composites: experiment and finite element modelling
35. Lasri, L., Nouari, M., El Mansori, M.: Modelling of chip separation in machining unidirectional FRP composites by stiffness degradation concept. Compos. Sci. Technol. **69**, 684–692 (2009)
36. Hashin, Z., Rotem, A.: A fatigue failure criterion for fiber reinforced materials. J. Compos. Mater. **7**, 448–464 (1973)
37. Lasri, L., Nouari, M., El Mansori, M.: Wear resistance and induced cutting damage of aeronautical FRP components obtained by machining. Wear **271**, 2542–2548 (2011)
38. Mkaddem, A., El Mansori, M.: Finite element analysis when machining UGF-reinforced PMCs plates: chip formation, crack propagation and induced-damage. Mater. Des. **30**, 3295–3302 (2009)
39. Soldani, X., Santiuste, C., Muñoz-Sánchez, A., Miguélez, M.H.: Influence of tool geometry and numerical parameters when modelling orthogonal cutting of LFRP composites. Compos. Part A: Appl. Sci. Manuf. **42**, 1205–1216 (2011)

40. Santiuste, C., Miguélez, H., Soldani, X.: Out-of-plane failure mechanisms in LFRP composite cutting. Compos. Struct. **93**, 2706–2713 (2011)
41. Abena, A., Soo, S.L., Essa, K.: A finite element simulation for orthogonal cutting of UD-CFRP incorporating a novel fibre-matrix interface model. Procedia CIRP **31**, 539–544 (2015)
42. Hobbiebrunken, T., Fiedler, B., Hojo, M., Ochiai, S., Schulte, K.: Microscopic yielding of CF/epoxy composites and the effect on the formation of thermal residual stresses. Compos. Sci. Technol. **65**, 1626–1635 (2005)
43. Jordan, J.L., Foley, J.R., Siviour, C.R.: Mechanical properties of Epon 826/DEA epoxy. Mech. Time-Depend. Mater. **12**, 249–272 (2008)
44. Littell, J.D., Ruggeri, C.R., Goldberg, R.K., Roberts, G.D., Arnold, W.A., Binienda, W.K.: Measurement of epoxy resin tension, compression, shear stress-strain curves over a wide range of strain rate using small specimens. J. Aerosp. Eng. **21**, 162–173 (2008)
45. Chen, W., Zhou, B.: Constitutive behaviour of epoxy 828/T-403 at various strain rates. Mech. Time-Depend. Mater. **2**, 103–111 (1998)
46. Dunne, F., Petrinic, N.: Introduction to Computational Plasticity. Oxford University Press Inc (2005)
47. Rodney, H.: The Mathematical Theory of Plasticity. Oxford University Press (1998)
48. Hosford, W.F.: Fundamentals of Engineering Plasticity. Cambridge University Press (2013)
49. Zho, Y., Wang, Y., Xia, Y., Jeelani, S.: Tensile behaviour of carbon fiber bundles at different strain rates. Mater. Lett. **64**, 246–248 (2010)
50. Zho, Y., Wang, Y., Jeelani, S., Xia, Y.: Experimental study on tensile behaviour of carbon fiber and carbon fiber reinforced aluminium at different strain rate. Appl. Compos. Mater. **14**, 17–31 (2007)
51. Phadnis, V.A., Makhdum, F., Roy, A., Silberschmidt, V.V.: Drilling in carbon/epoxy composites: experimental investigations and finite element implementation. Compos. Part A: Appl. Sci. Manuf. **47**, 41–51 (2013)
52. Feito, N., López-Puente, J., Santiuste, C., Miguélez, M.H.: Numerical prediction of delamination in CFRP drilling. Compos. Struct. **108**, 677–683 (2014)
53. Zhang, J., Zhang, X.: Simulating low-velocity impact induced delamination in composites by a quasi-static load model with surface-based cohesive contact. Compos. Struct. **125**, 51–57 (2015)
54. Zhang, J., Zhang, X.: An efficient approach for predicting low-velocity impact force and damage in composite laminates. Compos. Struct. **130**, 85–94 (2015)
55. Chennakesavelu, G.: Orthogonal machining of uni-directional carbon fiber reinforced polymer composites. Thesis (B.Eng) Golden Valley Institute of Technology (2006)
56. Abena, A., Soo, S.L., Essa, K.: Modelling the orthogonal cutting of UD-CFRP composites: development of a novel cohesive zone model. Compos. Struct. **168**, 65–83 (2017)
57. Weixing, X., Zhang, L.C., Wu, Y.: Elliptic vibration-assisted cutting of fibre-reinforced polymer composites: understanding the material removal mechanisms. Compos. Sci. Technol. **92**, 103–111 (2014)
58. Abaqus Analysis User's Guide, chapter 32.5.1, (2013)
59. Camanho, P.P., Dávila, C.G.: Mixed-mode Decohesion Finite Elements for the Simulation of Delamination in Composite Materials. NASA/TM-2002-211737 (2002)
60. May, M.: Numerical evaluation of cohesive zone models for modeling impact induced delamination in composite materials. Compos. Struct. **133**, 16–21 (2015)
61. Salih, S., Davey, K., Zou, Z.: Rate-dependent elastic and elasto-plastic cohesive zone models for dynamic crack propagation. Int. J. Solids Struct. **90**, 95–115 (2016)
62. Mubashar, A., Ashcroft, I.A.: Comparison of cohesive zone elements and smoothed particle hydrodynamics for failure prediction of single lap adhesive joints. J. Adhes. **93**, 444–460 (2017)
63. Abena, A., Essa, K.: 3D micro-mechanical modelling of orthogonal cutting of UD-CFRP using smoothed particle hydrodynamics and finite element methods. Compos. Struct. **218**, 174–192 (2019)
64. https://en.wikipedia.org/wiki/Tungsten_carbide

65. Ramesh, M.V., Seetharamu, K.N., Ganesan, N., Sivakumar, M.S.: Analysis of FRP using FEM. Int. J. Mach. Tools Manuf. **38**, 1531–1549 (1998)
66. Zahedi, A., Li, S., Roy, A., Babitsky, V., Silberschmidt, V.: Application of smooth-particle hydrodynamics in metal machining. J. Phys: Conf. Ser. **382**, 1–5 (2012)
67. Spreng, F., Eberhard, P.: Machining process simulations with smoothed particle hydrodynamics. 15th CIRP Conference on Modelling of Machining Operations **31**:94–99 (2015)
68. Madaj, M., Píška, M.: On the SPH orthogonal cutting simulation of A2024-T351 alloy, 14th CIRP Conference on Modeling of Machining Operations **8:**152–157 (2013)
69. Zetterberg, M.: A critical overview of machining simulations in Abaqus. Thesis (M.S.) KTH Royal Institute of Technology (2014)
70. Limido, J., Espinosa, C., Salaün, M., Lacome, J.: SPH method applied to high speed cutting modelling. Int. J. Mech. Sci. **49**, 898–908 (2007)
71. Cundall, P.A., Strack, O.D.L.: A discrete numerical model for granular assemblies. Géotechnique **29**, 47–65 (1979)
72. Belytschko, T., Lu, Y.Y., Gu, L.: Element-free Galerkin methods. Int. J. Numer. Meth. Eng. **37**, 229–256 (1994)
73. Nayroles, B., Touzot, G., Villon, P.: Generalizing the finite element method: diffuse approximation and diffuse elements. Comput. Mech. **10**, 307–318 (1992)
74. Kahwash, F.: Element-free Galerkin modelling for cutting of fibre reinforced plastics. Thesis (PhD) Northumbria University (2017)
75. Kahwash, F., Shyha, I., Maheri, A.: Meshfree formulation for modelling of orthogonal cutting of composites. Compos. Struct. **166**, 193–201 (2017)
76. Kahwash, F., Shyha, I., Maheri, A.: Dynamic simulation of machining composites using the explicit element-free Galerkin method. Compos. Struct. **198**, 156–173 (2018)

Metal Matrix Composites

Wai Leong Eugene Wong and Sankaranarayanan Seetharaman

Abstract The chapter introduces the various types of matrix and reinforcements used in metal matrix composites (MMCs) and gives an overview of the types of MMCs, namely fibre reinforced MMCs; particle reinforced MMCs and multi-layer laminates. Standard manufacturing processes for MMCs include Solid-State Processing Methods such as powder metallurgy, mechanical alloying, diffusion bonding and deformation processing, Liquid Processing Methods such as stir casting, melt infiltration, squeeze casting and melt deposition are also presented in Sect. 3. In addition, in situ processes and additive manufacturing of MMCs are also introduced. In Sect. 4, equations are provided to allow the prediction of the properties of MMCs such as density, modulus and strength. Strengthening mechanisms for particle reinforced composites are briefly explained in Sect. 5. A review of various mechanical properties of MMCs produced by different manufacturing techniques is provided in Sect. 6. Lastly, the chapter provides the use of MMCs in various industries.

1 Introduction

This chapter provides an introduction to metal matrix composites. The common types of matrix and reinforcement materials and various manufacturing techniques such as traditional casting and powder metallurgy to modern additive manufacturing processes used in the fabrication of metal matrix composites are provided. Examples of the mechanical properties of MMCs with micron, nano-sized reinforcements are highlighted together with properties of MMCs produced by additive manufacturing techniques.

Materials have always been an essential part of the human civilisation and can be seen from the naming of the ages of civilisations: stone, bronze, iron and steel.

W. L. E. Wong (✉)
Mechanical Design and Manufacturing Engineering, Newcastle University in Singapore, Singapore, Singapore
e-mail: eugene.wong@newcastle.ac.uk

S. Seetharaman
Department of Mechanical Engineering, National University of Singapore, Singapore, Singapore

I. Shyha and D. Huo (eds.), *Advances in Machining of Composite Materials*, Engineering Materials, https://doi.org/10.1007/978-3-030-71438-3_6

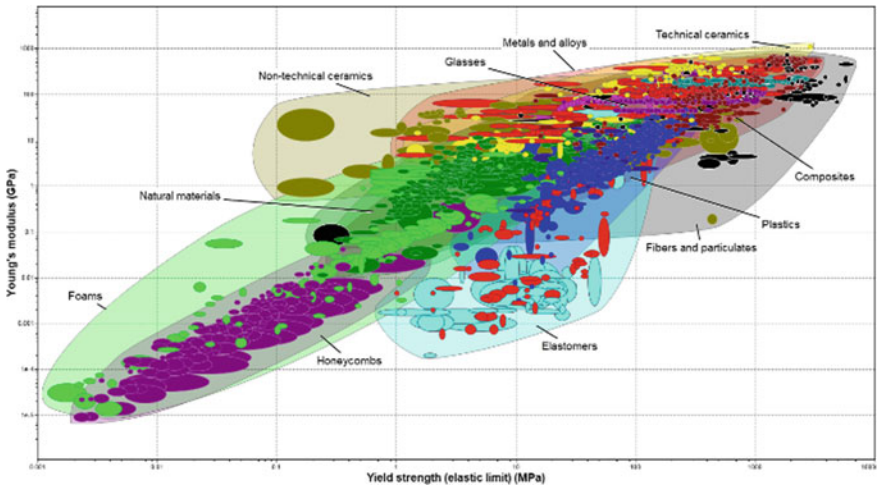

Fig. 1 Illustration of various classes of materials produced using CES Edupack software [3]

In the eighteenth and nineteenth century, iron and steel were used to make steam engines, railway and machines during the first and second industrial revolutions. In the twentieth century, polymers and silicon were ubiquitous in our daily lives. Many types of materials have been developed throughout the centuries from low stiffness and strength materials such as foams and honeycombs to high stiffness and strength materials such as metals and alloys, technical ceramics and composites as shown in Fig. 1.

Early civilisation used natural materials such as loam, mud, sand and straw to make composite bricks for buildings. Composite materials have found increasing applications in recent years. A composite material can be defined as combining two or more distinct materials to attain synergistic or superior properties over the individual constituents. In the aerospace industry, the latest aircrafts such as Airbus A350 and Boeing 787 Dreamliner uses at least 50% of carbon fibre composites in the structure [1]. Wind turbines also use glass-fibre reinforced composites in the turbine blades. However, polymeric composites suffer from low thermal resistance due to the polymer matrix's low melting temperature and low impact resistance with rapid deterioration in mechanical properties due to possible fibre cracking and delamination arising during service.

Metal matrix composites (MMCs) involve the combination of a continuous metallic matrix with reinforcements that typically comprise ceramic material or metallic material. The metallic matrix provides the potential for producing a composite with high mechanical and thermal properties compared to polymer matrix composites. Advantages of MMCs are summarized below [2].

- Higher stiffness and strength with the addition of reinforcements
- Higher service temperature for the metal matrix compared to the polymer matrix
- Higher toughness and ductility over ceramic matrix composites

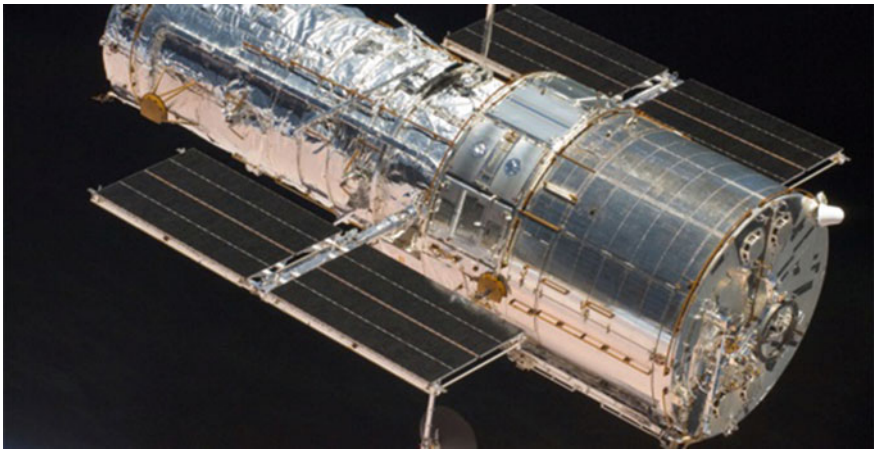

Fig. 2 Hubble space telescope utilises graphite-fibre/aluminium matrix composite for antenna booms. (Photo credit: DARPA)

- Good electrical and thermal conductivity compared to polymer and ceramic matrix
- Improved dimensional stability (e.g., lower thermal expansion with the addition of ceramic reinforcements of low coefficient of thermal expansion)
- Possible weight savings due to higher specific mechanical properties.

The ability to tailor the composites' properties using a combination of matrix and one or more reinforcements (metals or ceramics) makes it attractive for many applications. MMCs are used in various industries such as aerospace, automotive, defence, electronics and sports. For example, aluminium composite is used in the antenna booms for the NASA Hubble Space Telescope, as shown in Fig. 2.

Three entities can determine composite material characteristics: reinforcement, matrix, and interface explained in further details below.

1.1 Matrix

A variety of metals and their alloys are used as the matrix material for MMCs, and most of the research focused on lightweight metals such as aluminium, magnesium and titanium. Aluminium matrix composites are the most researched MMCs due to its low-cost relative to other light structural metals and can be found in aerospace and automotive industries. Magnesium matrix composites offer high specific stiffness and strength but are not widely used due to limited processing such as low extrusion rate and low corrosion resistance. Titanium matrix composites are used in jet engines and military jet landing gears. Other metals used as matrix include steel, copper, solder and nickel-based superalloys. Cobalt metal is also used as a matrix material for carbide reinforcements such as tungsten carbide to make hard metal cutting tools.

Table 1 Mechanical properties of common matrix materials [3]

Metal	Density (g/cm^3)	Modulus (GPa)	Yield strength (MPa)	Elongation (%)
Aluminium	2.67–2.73	69–72	28.5–31.5	37–43
Magnesium	1.73–1.75	44–45.5	65–100	12–20
Titanium	4.51–4.52	100–105	172–240	20–25
Copper	8.94–8.95	120–135	55–340	6–50
Cobalt	8.8–8.9	199–215	295–925	2–20
Iron	7.86–7.88	204–212	110–220	20–55
Nickel	8.85–8.95	190–220	80–795	2–60
Tungsten	19.3–19.4	340–350	1350–1680	10–25

Values of commercial purity metals obtained from CES EduPack software

The matrix's primary purpose is to bind the reinforcements and protect the reinforcements from mechanical and environmental damages. The matrix also allows the transfer of external forces to the reinforcement. Table 1 shows the properties of different metals used in MMCs.

1.2 Reinforcements

Reinforcements are added to improve the performance of the matrix material. The general characteristics of reinforcement are:

- Low density
- High Young's modulus
- High compression and tensile strength
- Good mechanical and chemical compatibility
- Good thermal stability.

The reinforcement can be classified as either continuous or discontinuous (short fibres, whiskers, micron and nano particulates).

Fibres are the most commonly used continuous reinforcement made of either carbon or ceramic. The ceramic types include alumina, silica, boron, alumina-silica, alumina-boria-silica, zirconia, magnesia, mullite, boron nitride, titanium diboride, silicon carbide, and boron carbide. For niche applications such as fighter jet engines, metallic wires made of tungsten are also used as continuous reinforcements for enhanced high-temperature creep resistance.

Fibre reinforced MMCs can provide high stiffness and strength along with the fibre orientation. The fibres are generally brittle and flaw sensitive. To avoid any unwanted reaction with the matrix and improve the bonding and wetting characteristics, the fibres are also often applied with protective coatings. As the fibres exhibit size effects,

Table 2 Types of reinforcements (Table adapted from [2])

Type	Aspect ratio	Diameter	Examples
Particle	1–4	1–25 μm	SiC, Al_2O_3, BN, B_4C, WC
Short fibres (whiskers)	10–1000	1–5 μm	C, SiC, Al_2O_3, Al_2O_3+SiO_2
Continuous fibres	>1000	3–150 μm	SiC, Al_2O_3, C, B, W, Nb-Ti
Nanoparticle	1–4	<100 nm	C, Al_2O_3, SiC
Nanotubes	>1000	<100 nm	C

i.e. the strength of these fibres decreases as the length increases, they can also be classified as either long fibres or short fibres.

As the metallic fibres usually fail due to the high density and the affinity for reaction with the matrix alloy, discontinuous reinforcement like short fibres or whiskers and ceramic particles are preferred for metal matrix composites. Whiskers are more costly than particles but offer higher strength due to their single-crystal structure.

For particle reinforcement, the type, size and distribution of the particles will affect the composite's performance. Classification of the types of reinforcements is shown in Table 2. While the size of particle reinforcement used in MMCs ranges from few nanometres to a few hundred micrometres, they are relatively cost-effective to produce in large quantities compared to continuous fibres. Existing production techniques such as casting or powder metallurgy followed by secondary shaping processing techniques including turning, milling, extrusion, forging and rolling can be applied for discontinuous reinforced MMCs. Also, the particle reinforced composites are known to display more isotropic properties.

Some of the most common particulate reinforcement types are alumina, boron carbide, silicon carbide, titanium carbide, and tungsten carbide. Similarly, whiskers made of silicon carbide, alumina and silicon nitride have also been used in MMCs. Silicon carbide is attractive due to its relatively high modulus, low density, and availability in many forms ranging from whiskers, powders and fibres. Alumina is attractive due to high chemical resistance and oxidation resistance. The properties of different reinforcement materials are shown in Table 3.

1.3 Interfaces

Interfaces refer to the bonding surface between the matrix and the reinforcement. Due to the small size of reinforcements, the bounding surface area occupied by the interface is very large and plays an essential role in determining the composites' final properties. Suitable interfaces free of voids and detrimental interfacial reaction products allow the effective transfer of mechanical forces from the matrix to the reinforcement without failure. Two types of bonding can exist at the MMC interface,

Table 3 Properties of common reinforcement materials [3]

Metal	Density (g/cm^3)	Melting point (°C)	Thermal expansion coefficient ($\mu m/°C$)	Modulus (GPa)	Yield strength (MPa)	Price (£/kg)
Al_2O_3	3.94–3.96	2050	7.7–8.5	450–460	1250–1340	25.2–31.5
AlN	3.27–3.33	2400–2510	4.6–4.8	323–348	218–242	78.7–126
B_4C	2.49–2.55	2400–2510	4.41–4.59	362–380	261–289	45.7–67.7
BN	2.2	2280–2380	2–6	48–50	27–30	26.8–39.4
SiC	3.15–3.2	2830–2840	3.9–4.3	450–480	2080–2500	23.6–39.4
Si_3N_4	3.15–3.21	2390–2500	3.23–3.37	288–302	240–270	26.8–40.9
TaC	1.34–1.39	3780–3880	6.6–7.4	360–375	194–250	50.4–75.6
TiB_2	4.45–4.54	2920–3050	6–8	410–430	339–374	14.–20.5
TiC	4.81–5.01	3160–3250	6.6–7.4	420–450	260–330	34.3–52
WC	1.53–1.59	2820–2920	4.5–7.1	600–670	373–530	14.2–22
ZrO_2	6.03–6.16	2550–2700	6–8.8	135–141	125–140	14.2–20.5
Be fibre	1.85–1.86	1280–1290	10.7	304–310	785–795	236–354
B fibre	2.46–2.57	2200	5.5–5.7	395–405	1750–2170	394–504
W fibre	19.4–19.6	3410	4.35–4.5	388–406	2250–2750	40.4–50.7
E glass	2.55–2.6	550–580[a]	4.9–5.1	72–85	1900–2050	1.24–2.48
C fibre (high strength)	1.8–1.84	3690–3830	−2–0.3	225–260	3750–4000	19.1–25.5

Properties are taken from CES EduPack and reflect bulk commercial purity material
[a]Glass transition temperature

namely, mechanical bonding and chemical bonding [2]. Mechanical bonding depends on the surface roughness while chemical bonding generally occurs at high temperature due to diffusion and chemical reaction between the matrix and reinforcement. Weak matrix-reinforcement bonding may lead to inferior mechanical properties of the composites and premature failure. An example of the interfaces between the magnesium matrix and carbon fibres is shown in Fig. 3.

Apart from cost, other limitations that prevent the widespread use of MMCs for engineering components lies in their tendency to fracture easily. The low ductility or brittleness is often caused by micro failure processes that invariably begin at the interfaces. Due to the thermal mismatch between the reinforcement and the matrix, high dislocation density will be generated at the interface. Hence the mechanical properties and overall performance of the MMCs are not limited by bulk properties but by interface properties and toughness. Detailed explanations of the importance of interfaces can be found in various references [1, 2, 4].

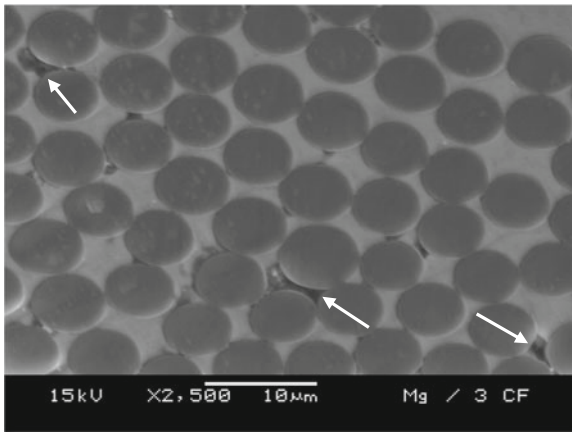

Fig. 3 Magnesium composite reinforced with carbon fibres with some voids marked by arrows

2 Classification of MMCs

Metal matrix composites can be classified in various ways. Depending on the matrix material, MMCs are classified into different categories like:

- Aluminium-based MMCs
- Magnesium-based composites
- Titanium-based composites
- Copper-based composites
- Super alloy-based composites.

Similarly, based on the reinforcement type, MMCs can be classified as fibre reinforced MMCs, particle reinforced MMCs and multi-layer laminates (see Fig. 4). The

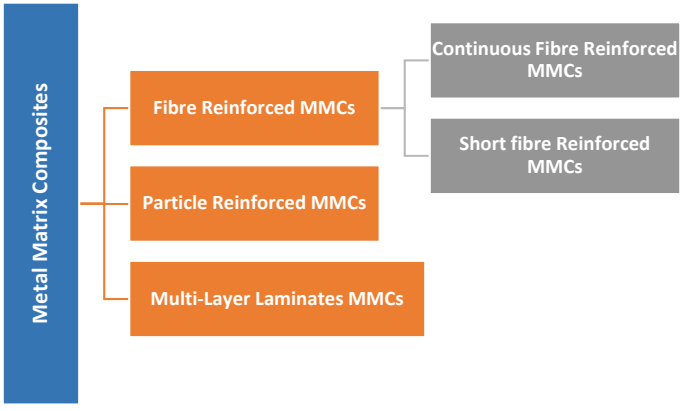

Fig. 4 Classification of metal matrix composites

fibre composites can be further classified as continuous and short (discontinuous) fibre reinforced composites.

2.1 Fibre Reinforced MMCs

The fibre reinforced MMCs can be broadly classified into (i) continuous fibre reinforced composites and (ii) short-fibre reinforced composites.

(i) Continuous fibre reinforced composites consist of a matrix reinforced by a dispersed phase in the form of continuous or long fibres.
(ii) Short-fibre reinforced composites consist of a matrix reinforced by a dispersed phase in the form of discontinuous fibres or whiskers (length < 100 * diameter).

2.2 Particle Reinforced Composites

Particle reinforced composites consist of a matrix reinforced by a dispersed phase in the form of particles. The particle dispersion within the matrix can be either random or with a specific orientation. Particle reinforced composites are relatively cheaper to manufacture due to the lower cost of the reinforcements and possess isotropic properties compared to fibre reinforced composites. An example of an aluminium composite reinforced with silicon carbide particles is shown in Fig. 5.

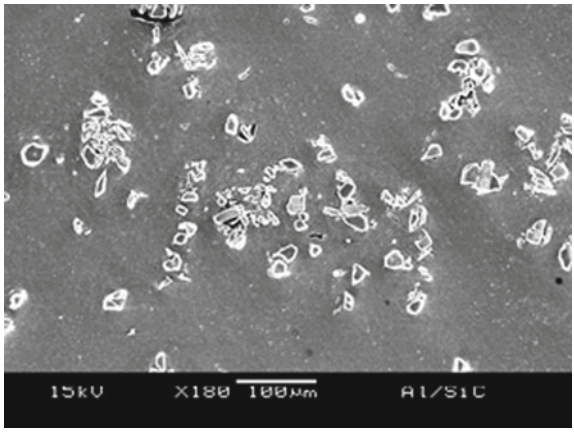

Fig. 5 Aluminium composite reinforced with silicon carbide particles

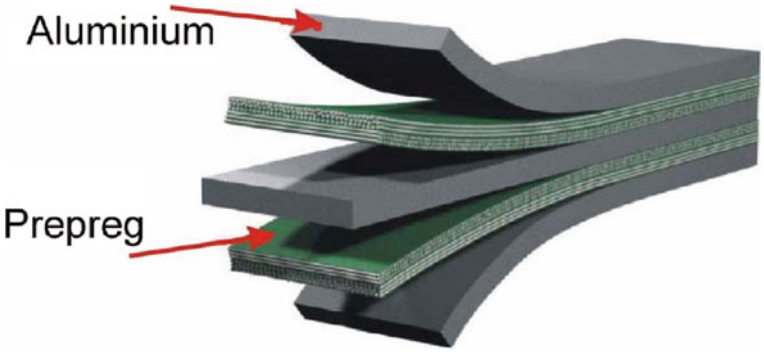

Fig. 6 An example of a cross-ply GLARE laminate, adopted from [6]

2.3 Multi-layer Laminate Composites

In laminated composites, layers of materials are stacked in a specific pattern to obtain a specific set of properties. One of the best known metal laminate composites is Glass laminate aluminium reinforced epoxy (GLARE) used in the aircraft such as Airbus A380 [5]. GLARE comprises alternating layers of thin aluminium sheets and glass fibre prepreg bonded together with epoxy, as shown in Fig. 6. The advantages of using GLARE include high specific strength and stiffness, excellent damage tolerance and impact properties.

3 Manufacturing Techniques of MMCs

Metal matrix composites can be produced using various methods that involve the processing of materials in either liquid, solid and vapour or gaseous state.

3.1 Solid-State Processing Methods

The advantages of using solid-state processing methods include reduced interfacial reactions between matrix and reinforcements due to lower processing temperature than liquid state processing and allowing for a higher volume fraction of reinforcements to be incorporated as the addition of reinforcements lead to an increase in viscosity of the liquid melt making it challenging to achieve a uniform distribution of reinforcement.

There are several solid-state processing techniques used to make particle or whisker reinforced MMCs, and the popular ones include (a) powder metallurgy, (b) mechanical alloying, (c) diffusion bonding, and (d) deformation processing.

a. **Powder metallurgy (PM)**

PM is an established method used for making particulate reinforced composites. In this method, a composite powder blend is prepared by mixing the metal alloy powder with the required amount of reinforcement whiskers or particulates [7]. After blending, the composite mixture is then compacted and sintered. Sintering is typically done in an inert nitrogen or argon atmosphere using electric or resistance heaters. A variant of the sintering is the use of hybrid microwave sintering to consolidate the green compact [8]. Hybrid microwave sintering allows for a significant reduction in sintering time and energy without compromising on the properties of the MMCs [9].

Further consolidation can take place via extrusion to obtain a near dense composite. The extrusion process can improve bonding between the reinforcement particle and matrix by fracturing the oxide film present on the surface of the metal particle. A schematic diagram of the PM process is shown in Fig. 7.

This method has been extensively used to fabricate aluminium and magnesium metal matrix composites with a reinforcement volume fraction of up to 30%. The particle size ratio between metal and reinforcement powders should be comparable to unity for uniform dispersion of reinforcement and avoid clustering [2, 4].

In the case of long continuous fibres, the fibre tows are first infiltrated by dry matrix powder, followed by hot isostatic pressing. However, cold-pressing and sintering are not preferred as the relatively high pressure necessary to achieve the required density can break the fibres. The sintering process can also degrade the fibre quality due to oxidation.

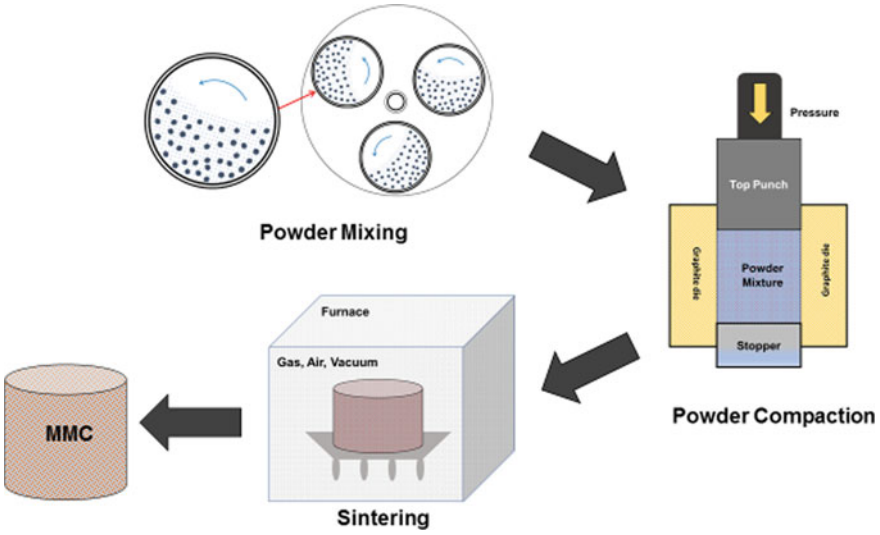

Fig. 7 A schematic showing the flow of powder mixing and consolidation

b. **Mechanical alloying**

Mechanical alloying involves repeated cold welding, fracturing, and re-welding of powder particles in a high energy ball mill. In this process, as shown in Fig. 8, the frictional heat developed at the particle interface results in local melting and consolidation of powder particles and the rapid heat extraction by the cooler particle interior causes rapid solidification. The composite powder mixture obtained is then cold compacted into a green billet that is then canned, degassed and hot-pressed at a temperature closer to the matrix alloy's solidus temperature. Using this method, various high strength equilibrium and non-equilibrium alloys and composites can be synthesised due to the high dislocation density and homogenous distribution of reinforcing constituents.

c. **Diffusion bonding**

Diffusion bonding is a solid-state joining technique used to process a wide variety of metal composites reinforced with continuous/discontinuous fibres. Strands or mats of fibres are sandwiched between metal foils and stacked in the desired order, as shown in Fig. 9. The laminate is then sealed in a can, heated and pressed to full density. Although there are many variants of the diffusion process, the basic principle involves interdiffusion of atoms and bonding between the mating contact surfaces under temperature and pressure. While the fibre orientation and volume fraction can be perfectly controlled, the processing time and cost are relatively high compared to other methods. Only objects of limited size and shape can be produced. Hot roll diffusion bonding is a variant of the diffusion bonding method used to produce sheet laminated metal matrix composites composed of different metals in the sheet

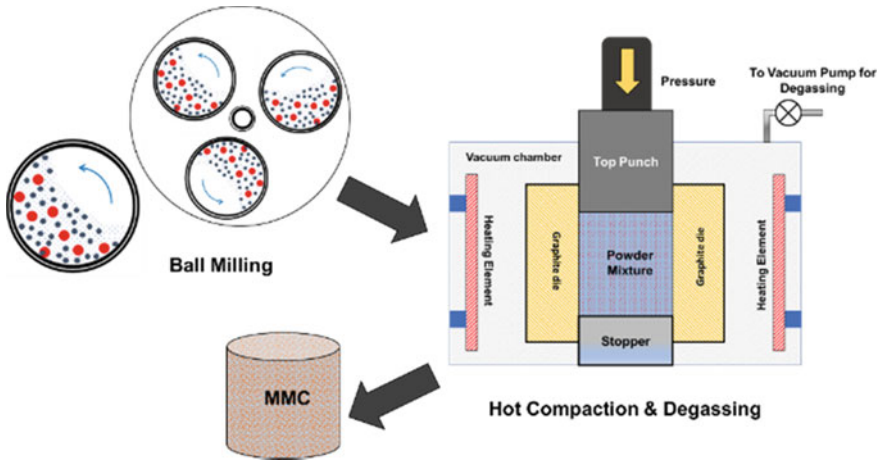

Fig. 8 Mechanical alloying technique

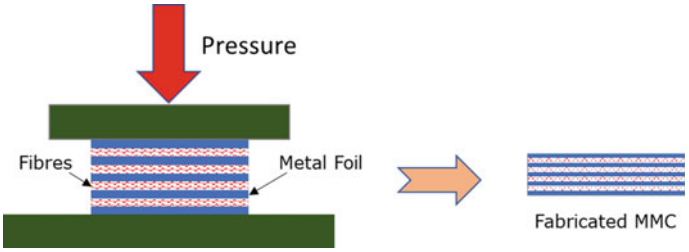

Fig. 9 Schematic of the diffusion bonding process

form. MMCs combinations of B/Al, Gr/Al, Gr/Mg and Gr/Cu have been manufactured using diffusion bonding into parts such as tubes, plates and panels for space applications [10].

d. **Deformation processing**

Mechanical processing methods such as swaging, extrusion, drawing or rolling can produce metallic composite made of a ductile two-phase metal. In this method, a two-phase alloy billet processed by casting or powder consolidation is subjected to mechanical deformation, causing the minor phase to elongate and become fibrous within the matrix. Hence, this method is limited to starting materials in which both phases are ductile and have similar flow stresses so that co-deformation occurs. Large total deformation strains may be employed. Heat treatments are often applied post deformation to promote required microstructural development. This technique is used to manufacture high-temperature superconductor wires comprising ceramic oxide superconductors and silver [1].

3.2 Liquid Processing Methods

Liquid processing methods for MMCs are commonly used due to the relatively lower cost for bulk materials than powder materials for solid-state processing and near net shape processing. In liquid processing methods, the reinforcement material is first dispersed into a molten matrix metal, and the composite slurry is then solidified into the required shape. The reinforcement can be dispersed into the molten matrix material in multiple ways:

- Stir casting—Direct mixing of reinforcement with the molten melt
- Melt infiltration—Infiltration of reinforcement preforms by molten metal
- Squeeze casting
- Melt deposition.

a. **Stir casting**

Stir casting is the most common and cost-effective method of producing composite materials. In this method, the reinforcement phase (short fibre or particles) is mixed with the molten matrix metal employing mechanical stirring or ultrasonic energy under an inert atmosphere. Conventional casting methods then cast the molten composite slurry. The properties of the MMCs produced using stir casting methods will depend on the processing parameters such as the temperature of the melt, stirring speed, stirring duration, and geometry of the stirrer, affecting the distribution of the reinforcements in the matrix. The dispersed phases are often coated with proper wetting agents to achieve better interfacial bonding with the matrix material and avoid any unwanted reaction and dissolution of reinforcement at high temperatures. In case of particulate reinforcement, careful attention must be paid to the particles' dispersion as they tend to form agglomerates for fine powder and segregation in the molten melt due to density difference between reinforcements and liquid melt. In general, the proper selection of processing parameters such as melt temperature, stirring speed, duration, and stirrer geometry, allows for the effective dispersion of particles (in size range 5–100 micrometre) up to 30% by volume. Superheating the molten melt by 50–100 °C is required for the higher volume fraction of particles due to an increase in the molten melt's viscosity. Figure 10 shows the schematic for stir casting where the reinforcement can be dispersed using a blade stirrer or ultrasonic energy.

b. **Melt infiltration**

In melt infiltration, a liquid metal alloy is infiltrated into the porous forms of fibres/whiskers reinforcements. The reinforcement volume can be between 10 and 70% depending upon the level of porosity of the preform.

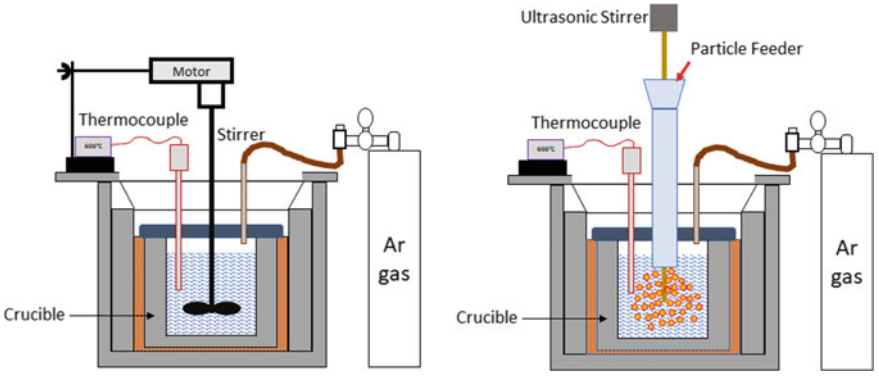

Fig. 10 Schematic diagram of stir casting (left) and application of ultrasonic for dispersion of reinforcements (right)

The infiltration of preforms can be conducted under atmospheric pressure in an inert atmosphere to minimise interfacial reactions between the matrix and reinforcements. However, the pressureless process involves long holding time at a high temperature of approximately 700–1000 °C for aluminium alloys for infiltration of the preform [2]. Infiltration of the preform can also be undertaken employing pressurized inert gas in which the gas pressure can be applied in two ways: (i) application of gas pressure to the melt surface after dipping the preform into the melt for infiltration, (ii) the applied gas first presses the molten metal and then infiltrates into the preform. Since the reaction time in both approaches is relatively short, reactive materials can be processed. However, comparing melt infiltration to squeeze casting, the processing times are relatively longer than in squeeze casting (Fig. 11).

c. **Squeeze casting**

In squeeze casting or pressure infiltration, the molten metal is forced into the preform, and pressure is applied until the solidification is complete. This method can be applied for both the fibres and particles reinforced composites. The prefabricated fibre (short Al_2O_3 fibre, carbon fibre) or particle preforms can be melt infiltrated and solidified under pressure. To avoid damage to the preforms, the melt is first pressed into the preform at low pressure, and then the pressure is increased for solidification. Since the melt solidifies under high pressure of 70–100 MPa, the squeeze cast composites are free from the common casting defects such as porosity and shrinkage cavities. As the infiltration duration is relatively short, the squeeze casting method can also be applied for reactive materials like magnesium and help to minimise interfacial reaction between the reinforcement materials and the matrix. The application of pressure during consolidation also provides the ability to fabricate parts with relatively complex geometry and allow composites with higher reinforcement volume fraction up to 55% to be obtained.

The squeeze casting can be classified into direct and indirect squeeze casting based on the mode of pressure application. In the direct squeeze casting method, the pressure for the infiltration of preforms is applied directly to the melt. However, in the

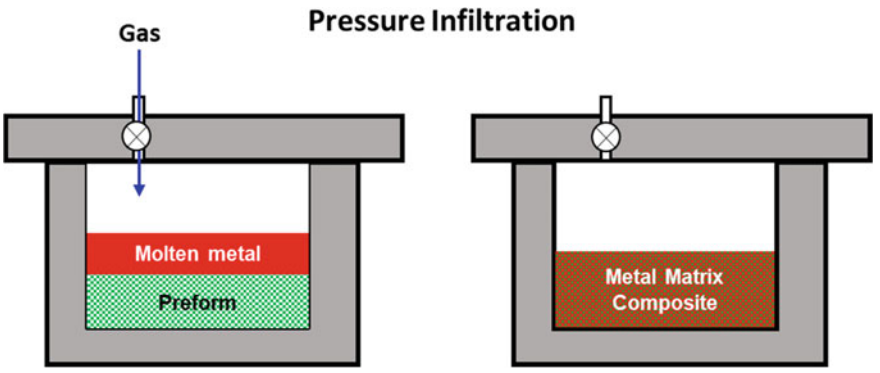

Fig. 11 Melt infiltration using pressurised inert gas

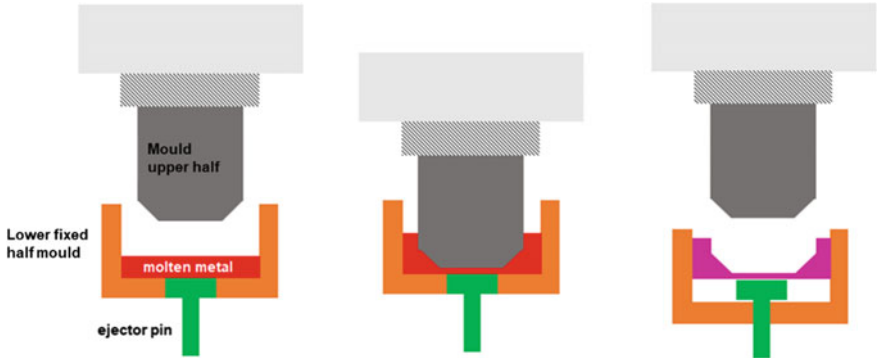

Fig. 12 Schematic diagram of the direct squeeze casting process

indirect squeeze casting, the melt is pressed into the preform through a gate system. Although the tooling is relatively simple for direct squeeze casting, the absence of a gate system necessitates the accurate determination of the melt volume. Another disadvantage is the presence of oxide residue in the composite, which is usually restricted by the indirect squeeze casting gate (Fig. 12).

d. **Melt deposition**

There are several deposition techniques available to produce metal matrix composites. While deposition methods like immersion plating, electroplating, chemical vapour deposition (CVD), physical vapour deposition (PVD) are only used for fibre reinforced MMCs, the spray deposition method can be used for both particle and fibre reinforced composites.

- ***Immersion plating***

This method is applicable for continuous fibre reinforcement which passes through baths of molten metal, slurry, sol, or organometallic precursors.

- ***Electroplating or electrodeposition***

In this method, the matrix metal coating is produced from a solution containing the ion of the desired material in the presence of an electric current. As this process is carried out at moderate temperatures, this method offers less/no damage to the reinforcing fibres. However, processing defects such as poor bonding and porosity are common for MMCs produced using this method. Also, only limited alloy matrices can be processed using this method.

- ***Chemical vapour deposition***

It involves chemical reaction or decomposition of a vaporized component on to the substrate to form a coating. Using this method, amorphous and crystalline (single

and polycrystals) coatings of oxide, carbide, nitride or pure metals can be made. When this method is used to deposit the matrix material on the reinforced preforms, it is called chemical vapour infiltration.

- ***Physical vapour deposition***

This method is highly suitable for producing fibre reinforced metal matrix composites in which the vapours of matrix metal were condensed to create coatings on the reinforcement fibres. The coated fibres are then consolidated by hot pressing or hot isostatic pressing. Based on the vapour generation techniques, the PVD processes can be classified into (i) evaporation based, (ii) sputtering and (iii) ion-plating. While the evaporation PVD methods include electron beam/arc evaporation, radiation heating, laser ablation and resistive heating, the sputtering techniques involve vaporization of the coating material from an ionized argon gas molecule via momentum transfer. Similarly, ion plating involves passing the vaporized component through an argon gas glow discharge around the substrate which ionizes and subsequently deposit the vapour onto the substrate. The primary advantage of PVD is the versatility in the coating's compositions and the superior bonding with the substrate. In addition, there are no chemical reaction by-products in these methods. However, PVD methods are relatively complicated and expensive.

- ***Spray deposition***

In spray deposition, reinforcements in the form of particles/whiskers are injected into the spray together with the atomized metal, creating a deposition layer on the substrate [4]. The depositions are then densified by suitable post-processing techniques. Similarly, for continuous fibre reinforcements, the molten matrix metal is sprayed onto the fibres with preferred orientation. In this method, fibre alignment can be easily controlled, and relatively faster solidification rates can be achieved.

- ***Spray-forming of Particle Reinforced MMCs***

It is a promising method for producing particle reinforced MMCs. It involves spray techniques which are used to develop monolithic alloys. Figure 13 shows an example of the spray forming process in which a spray gun is used to atomize the molten matrix metal into which the reinforcement particles are injected. The resulting metal matrix composite (about 97% dense) is then subjected to scalping, consolidation, and secondary finishing processes to produce wrought composites [1]. To facilitate the efficient transfer of particle reinforcement, optimum particle size and shape must be maintained.

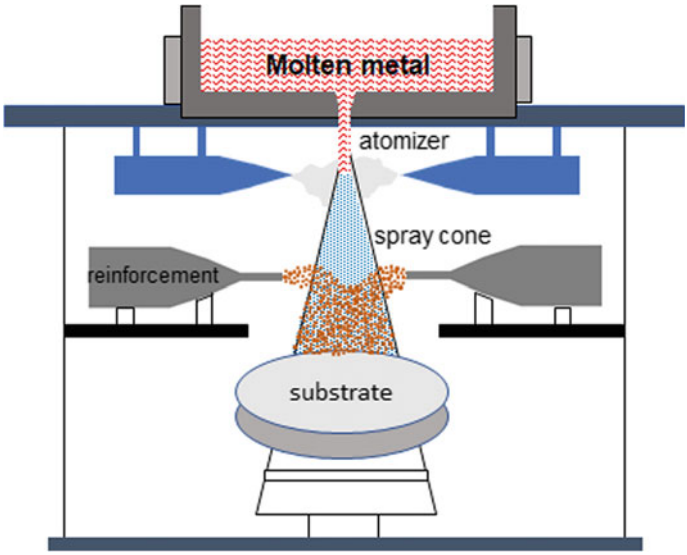

Fig. 13 Schematic diagram of the spray-forming process

3.3 In Situ Processes

In situ processing involves chemical reactions which results in the in situ formation of the reinforcing phase within a metal matrix. One of the classic examples of in situ processing is the controlled unidirectional solidification of a eutectic alloy, resulting in one phase being distributed in the form of fibres or ribbon in the other [2]. As the solidification rate controls the shape and distribution of the in situ reinforcement, better thermodynamic compatibility can be achieved at the matrix reinforcement interface, leaving the reinforcement surfaces free of contamination producing a stronger matrix-dispersion bond. However, in practice, the solidification rate is limited to a range of 1–5 cm/hour because of the need to maintain a stable growth front [2]. The patented XD process developed by Martin Marietta Corporation is an example of an in situ process where molten metal and compounds that will react exothermically come together to form ceramic reinforcement particles with sizes ranging from 0.2 to 10 μm [4]. The typical examples include aluminium MMCs reinforced with TiC and $TiB_{2,}$ which are formed according to the following reactions:

$$C + Ti + Al \rightarrow TiC + Al$$

$$2B + Ti + Al \rightarrow TiB_2 + Al$$

3.4 Additive Manufacturing

Additive manufacturing (AM) provides new opportunities for manufacturing MMCs with unique microstructure and properties and has been receiving increasing attention in recent years [11, 12]. Most of the research focus on the development of particle reinforced MMCs using AM processes. Both in situ and ex situ processes can manufacture MMCs with unique microstructure, design and mechanical properties. Figure 14 illustrates the AM processes that are employed for manufacturing MMCs. The processes include Powder Bed Fusion (PBF), Direct Energy Deposition (DED), Binder Jetting, Selective Laser Sintering (SLS), Selective Laser Melting (SLM) and Electron Beam Melting (EBM).

4 Predicting Properties of MMCs

Tailoring properties is one of the MMC applications' main advantages. The end properties of composite materials can be controlled by many variables, including reinforcement form, volume fraction, geometry, distribution, matrix/reinforcement interface, void content, and manufacturing process. The following sections will provide equations used in predicting the properties of metal matrix composites from the properties of the matrix and reinforcement.

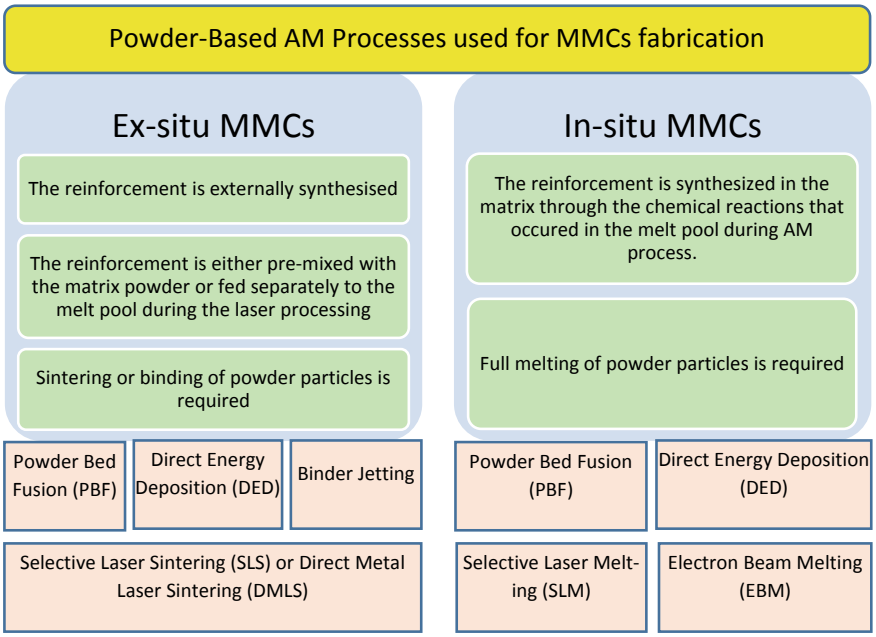

Fig. 14 Powder-based AM processes used for fabrication of MMCs (adapted from [12])

4.1 Volume and Weight Fractions

Based on mixtures' rule, composite materials' properties are the volume-weighted average of the phases (matrix and dispersed phase) properties. Hence, to estimate the mechanical properties of composite material, it is essential to know the relative proportions of matrix and reinforcement. The proportion can be expressed in terms of volume fraction of weight or mass fraction. Weight fractions are commonly used as it is easy to weigh the relative proportions of matrix and reinforcement using an analytical balance. The volume fraction is used in the computation of the properties of the composite. Therefore, knowing the conversion between weight and volume fraction is essential.

The weight fractions can be computed as follows:

$$W_M = \frac{w_M}{w_C} \tag{1}$$

$$W_R = \frac{w_R}{w_C} \tag{2}$$

$$W_M + W_R = 1 \tag{3}$$

where w_M, w_R and w_C are the respective weight of the matrix, reinforcement and composite material.

Similarly, the volume fractions can be computed as follows:

$$V_M = \frac{v_M}{v_C} \tag{4}$$

$$V_R = \frac{v_R}{v_C} \tag{5}$$

$$V_M + V_R = 1 \tag{6}$$

where v_M, v_R and v_C are the respective volumes of the matrix, reinforcement and composite material.

Making use of the relationship between weight, volume and density,

$$w_C = \rho_C v_C \quad w_M = \rho_M v_M \quad w_R = \rho_R v_R$$

where ρ_M, ρ_R, and ρ_C are the densities of the matrix, reinforcement and the composite material.

The relationships between the volume fractions and weight fractions can be expressed as follows:

$$W_M = \frac{w_M}{w_C} = \frac{\rho_M v_M}{\rho_C v_C} = \frac{\rho_M}{\rho_C} V_M$$

where the weight fraction of the matrix can be expressed as

$$W_M = \frac{\rho_M}{\rho_C} V_M \tag{7}$$

and the weight fraction of reinforcement is

$$W_R = \frac{\rho_R}{\rho_C} V_R \tag{8}$$

4.2 Density

The weight and volume fractions can be used to determine the density of the composite material. Using the total weight of the composite material,

$$w_C = w_M + w_R \tag{9}$$

$$\rho_C v_C = \rho_M v_M + \rho_R v_R \tag{10}$$

The density of the composite material can be determined by the volume fractions multiplied by the respective constituents' densities.

$$\rho_C = \rho_M V_M + \rho_R V_R \tag{11}$$

Using the total volume of the composite material, the composite's density can be computed based on the weight fractions divided by the densities of the respective constituents.

$$v_C = v_M + v_R \tag{12}$$

$$\frac{w_C}{\rho_C} = \frac{w_M}{\rho_M} + \frac{w_R}{\rho_R}$$

$$\frac{1}{\rho_C} = \frac{W_M}{\rho_M} + \frac{W_R}{\rho_R}$$

$$\rho_C = \frac{1}{\frac{W_M}{\rho_M} + \frac{W_R}{\rho_R}} \tag{13}$$

4.3 Coefficient of Thermal Expansion (CTE)

Based on the rule of mixtures, the thermal expansion coefficient of composite material can be computed as follows:

$$\boldsymbol{\alpha}_c = \boldsymbol{\alpha}_m V_m + \boldsymbol{\alpha}_r V_r \tag{14}$$

where $_c$, $_m$ and $_r$ refers to the thermal expansion coefficients of the composite, matrix and reinforcement materials.

For particle reinforced MMCs, the coefficient of thermal expansion can also be calculated based on the Turner model as below [1]:

$$\alpha_c = \frac{(\alpha_m V_m K_m + \alpha_r V_r K_r)}{(V_m K_m + V_r K_r)} \tag{15}$$

where K_m and K_r is the bulk modulus of matrix and reinforcement, respectively.

Similarly, for continuous fibre reinforced metal matrix composites, the thermal expansion coefficients along the longitudinal and transverse directions can be calculated as follows:

CTE in the longitudinal direction (along the fibres),

$$\alpha_{cl} = \frac{\alpha_m E_m V_m + \alpha_f E_r V_r}{E_m V_m + E_r V_r} \tag{16}$$

CTE in the transverse direction (perpendicular to the fibres),

$$\alpha_{ct} = (1 + \upsilon_m)\alpha_m V_m + \alpha_f V_r \tag{17}$$

where E_m, E_r are the elastic moduli of the matrix and the fibre reinforcement respectively, and $_m$ refers to the Poisson's ratio.

4.4 Modulus of Elasticity

The elastic behaviour of a composite depends on the type and volume fraction of the reinforcement, and it generally improves with the addition of the reinforcement, as shown below:

$$E_C = E_m V_m + E_r V_r \tag{18}$$

Along the transverse direction,

$$E_{ct} = \frac{1}{\left(\frac{V_m}{E_m} + \frac{V_r}{E_r}\right)} \tag{19}$$

For discontinuous fibres and particle reinforced composites, the elastic modulus can be calculated as follows:

$$E_c = \frac{E_m(1 + 2sqV_r)}{1 - qV_r} \tag{20}$$

where s is the particle aspect ratio and

$$q = \frac{\left(\frac{E_r}{E_m} - 1\right)}{\left(\frac{E_r}{E_m} + 2s\right)} \tag{21}$$

4.5 Tensile Strength

Addition of reinforcements to the matrix alloy generally enhances both yield and ultimate tensile strength. Based on the rule of mixtures, the tensile strength of the composites can be calculated as below:

$$\sigma_c = \sigma_m V_m + \sigma_r V_r \tag{22}$$

where σ_c, σ_m, σ_r refer to the tensile strength of the composite, matrix and the reinforcement, respectively.

However, for short-fibre reinforced composites, the tensile strength is calculated based on the fibre length. i.e. the length of fibre is critical in establishing the relationship.

$$\text{Case I:L} > \text{L}_\text{c};\ \sigma_c = \sigma_m V_m + \frac{L\tau_c V_r}{d}; \tag{23}$$

$$\text{Case II:L} < \text{Lc};\ \sigma_c = \sigma_m V_m + \sigma_r V_r\left(1 - \frac{L_c}{2L}\right) \tag{24}$$

where c is the shear strength of the bond between the matrix and the reinforcement fibre.

5 Strengthening Mechanisms

MMCs exhibit better strength than their unreinforced matrix metals as they can transfer much of the applied loads to the stronger reinforcement. Some of the common strengthening mechanisms applicable to particle reinforced metal matrix composites are discussed below.

5.1 Dislocation Strengthening

Generally, dislocation density in a composite matrix is higher than in unreinforced metal processed using similar methods. The increased dislocation density in the composites is due to the thermal stresses caused by CTE mismatch between matrix and reinforcement.

$$\Delta\sigma = 12\frac{\Delta\alpha\Delta T V_r}{bd} \tag{25}$$

where $\Delta\sigma$ is the increase in dislocation density, $\Delta\alpha$ is the CTE mismatch, ΔT is the temperature difference, b is Burgers vector, V_r is the reinforcement volume fraction, and d is reinforcement size. Hence, the dislocation density and the matrix strengthening increase with increasing reinforcement volume fraction and decreasing reinforcement size.

5.2 Grain Refinement Strengthening

The matrix grain size of metal matrix composites is usually smaller than that of the unreinforced counterparts. The smaller grain size implies greater grain boundary area and fewer dislocations in the pileups, thus resulting in larger stress requirements to cause yielding. The Hall-Petch equation can be used to explain the strengthening mechanism.

$$\sigma_{Hall-Petch} = \sigma_0 + \frac{k}{\sqrt{d}} \tag{26}$$

5.3 Orowan Strengthening

This strengthening mechanism is vital for dispersion strengthened materials in which the composite strength is improved by restricting the dislocation movement.

However, in other MMCs, the reinforcement particles are too large and too far apart to be considered a practical obstacle to the motion of dislocations. The Orowan-Ashby equation defines the Orowan stress as [13]:

$$\sigma_{Orowan} = \frac{0.13Gb}{\lambda} \ln \frac{d}{2b} \tag{27}$$

6 Review of Mechanical Properties of Developed MMCs

There are many various combinations of MMCs that have been developed by researchers and commercial companies. In recent years, there has been increasing research and development in using nano-size reinforcements. The advantages of using nano-size reinforcements include improvement in both strength and ductility and comparable or superior properties with small volume fraction compared to micron size reinforcement [7]. Examples of the mechanical properties of selected MMCs fabricated using different manufacturing techniques are shown in Table 4.

In addition to the use of nano reinforcements, various additive manufacturing techniques for the fabrication of metal matrix composites have increased exponentially in recent years. Examples of MMCs produced by AM techniques are shown in Table 5.

7 Application of MMCs

Metal matrix composites are used in a range of applications in the automobile, aerospace, power transmission, consumer electronics, and sports sectors. A summary of the various applications of MMCs is provided in Table 6.

The transportation sector has been one of the prime consumers of MMCs, and the applications in this field include drive shafts, pistons, engine and brake components. For example, Toyota introduced squeezed cast Al MMC piston reinforced with chopped fibre for a diesel engine in 1983 [44]. Al–Si matrix composite containing 12% Al_2O_3 and 9% carbon is used in the cylinder liner of Honda Prelude leading to a weight reduction of 20% in the aluminium engine block and improved wear resistance compared to cast iron [44]. Other popular automotive applications of MMC include connecting rod made of SiC-particle-reinforced aluminium–matrix composites to replace steel for lightweight. Duralcan supplied brake rotors of German high-speed train made of SiC particles reinforced AlSi7Mg composite with ~43% weight savings. Since the transportation sector is a high volume and high technology market, the manufacturing cost of MMCs should be as low as possible for their extended applications. Thus, reducing the manufacturing costs of MMC components will significantly aid in the replacement of conventional parts.

Table 4 Mechanical properties of MMCs

Composite	Technique	0.2%YS (MPa)	UTS (MPa)	Elongation (%)	Ref.
Al/13vol.%SiC	Stir casting + extrusion	88	215	9.5	[14]
Al/10wt%Si_3N_4	Stir casting	154	170	4	[15]
Al/5vol.%BN	PM + extrusion	258	377	–	[16]
Al/15vol.%Al_2O_3		260	425	–	
Cu/8wt%WC	Stir casting	–	237	~6	[17]
Al/4.8vol.%SiC	Disintegrated Melt Deposition (DMD) Technique	148	173	10	[18]
Mg/0.63vol.%Mo		123	198	9	[19]
Mg/30vol.%SiC	Stir casting	229	258	2	[20]
Mg/5vol.%Al_2O_3	PM with hybrid microwave sintering	159	214	3	[21]
Mg/10vol.%SiC		140	165	1.5	[22]
AZ91/15vol.%SiC	Stir casting	134	204	1.2	[23]
MMCs with nano reinforcements					
Al/1wt%SiC (as cast)	Stir casting and squeeze casting	203	323	5	[24]
Al4.5Mg/6wt%Al_2O_3	Stir casting	181	204	2	[25]
Al/1wt%CNT	Ultrasonic mixing and ball milling	190	290	5	[26]
Mg/1.3wt%CNT	Disintegrated Melt Deposition (DMD) Technique	140	210	13.5	[27]
Mg/0.97vol.%TiB2		110	173	16	[28]
Mg/0.6vol.%Cu	PM with hybrid microwave sintering	237	286	5.4	[29]
Mg/1.0vol.%SiC		157	203	7.6	[30]
Ti6Al4V + B_4C	Investment casting	954	1029	2.46	[31]
Ti6Al4V/5vol.% (TiB + TiC)	PM and spark plasma sintering	1267	1153	5.1	[32]
Commercially available MMCs					
AL2124/25vol.%SiC	PM using mechanical alloying	400	600	3–4	[33]
Al6061B/20vol.%SIC		410	490	7	
AA2009/25vol.%SiC	PM	448	593	3.4	[34]
AA6092/25vol.%SiC	PM	345	414	3	
AZ91/50%SiC	Squeeze casting	426	503	1.4	[35]
Ti/TiB	Wrought processing	650	810	7	

Table 5 Properties of MMCs fabricated by AM techniques

Composite	Observations	Ref.
AlSi10Mg/1wt%CNT	Fabricated using SLM Density >95%. Highest density 98.53% Hardness of 143.33 HV Tensile strength of 499 MPa and elongation of 7.6%	[36]
Al2024/3%TiB2	Fabricated using solid laser forming The average microhardness of composite is 108.5 HV compared to 75 HV for Al2024 alloy and 62 HV for cast Al2024 Composite achieved higher yield strength (163 MPa), tensile strength (284 MPa) and elongation (18%) compared to Al2024 alloy with 90 MPa yield strength, 202 MPa tensile strength and 7% elongation	[37]
Fe/25wt%WC	Fabricated using SLM Density achieved 98.5% with an average grain size of 0.82 to 1.24 μm Microhardness: 478.5–511.6HV	[38]
316L/3wt%V_8C_7	Fabricated using SLM Density achieved over 97% and the average grain size of ~.5 μm Highest UTS of >1400 MPa and elongation of 18% observed	[39]
Ti6AL4V/1.5%B_4C Ti6AL4V/3%B_4C	Fabricated using direct metal deposition (DMD) In situ formation of TiC and TiB Increased in hardness from 360 $HV_{0.5}$ to 455 $HV_{0.5}$ due to formation of 12vol.% TiB whiskers Improvement in elastic modulus from 115 GPa to 125 GPa For Ti6AL4V/1.5%B_4C composite, UTS is between 1000–1200 MPa in the longitudinal direction and 700 MPa in the transverse direction	[40]
Ti/5wt%B_4C Ti/5wt%BN Ti/2.5wt%B_4C + 2.5wt%BN	Fabricated using Laser engineered net shaping (LENS) Densities achieved range 96.1–97.4% Increase in compressive modulus to more than 152 GPa Highest compressive yield strength of 758 MPa observed in Ti/2.5 wt%B_4C + 2.5 wt%BN	[41]
Inconel 625/graphite Inconel 625/CNT	Fabricated using laser aided additive manufacturing (LAAM) Addition of graphite reinforcement improves yield strength (~688 MPa) and UTS (~970 MPa) but reduces ductility (~13%) compared to pure Inconel 625. Addition of CNT improves yield strength (695 MPa), UTS (~1006 MPa) and ductility (~21%)	[42]

(continued)

Table 5 (continued)

Composite	Observations	Ref.
CoCrFeMnNi HEA/4.8wt% TiN	Fabricated using SLM with remelting SLM built HEA/TiN: average UTS 1059 MPa and average elongation 15.3% Remelted SLM built HEA/TiN: average UTS > 1100 MPa and average elongation 18%	[43]

Table 6 Applications of MMCs

Industry	Applications	Desired properties
Aerospace	Support strut, landing gears, casing, fan and compressor blades, blade sleeve in helicopters	Low density, high strength, high stiffness, high fatigue strength, high fracture toughness
Automotive	Connecting rod, cylinder liner, brake disc, brake callipers, driveshaft, piston	Low density, high strength, high stiffness, high fatigue strength, good wear resistance, good thermal conductivity, good creep resistance
Military	Fins, missile body casings, armour, landing gears, nozzle actuator	Low density, high strength, high stiffness
Electronic	Heat sinks, casings, microprocessor and optoelectronic packaging	High thermal conductivity, low coefficient of thermal expansion
Sports	Bicycle frames, wheel rims, golf club heads, skis, tennis and badminton rackets	High stiffness, high strength, low density

The enhanced stiffness and strength of the MMCs make them highly suitable for military and commercial aircraft applications. For example, the aluminium access doors in the F-16 aircraft have been replaced with SiC particle reinforced MMCs for fatigue life improvement [2]. Similarly, the SiC mono fibre reinforced Ti-composites are used to replace the heavier IN718 and stainless-steel components of the F119 engine in the F-16. MMC has also replaced a CFRP fan-exit guide vane of a Pratt & Whitney engine on a Boeing 777 aircraft. The lower drag brace for the landing gear of F-16 is made of titanium reinforced with SiC fibres allowing a 40% weight reduction compared to the original part, which is made of high strength steel [45].

In the electronics industry, MMCs with controlled thermal expansion coefficients (by controlling the volume fraction of reinforcement and matrix) such as boron/graphite fibres or SiC particles reinforced aluminium composites are used in the new generation advanced integrated circuits to overcome the major concerns related to heat dissipation and thermal fatigue. Continuous Al_2O_3 fibre reinforced Al MMCs with adjustable CTE is also used as electrical conductors for power transmission applications.

The typical sporting applications of MMCs include fishing rods, bicycle frames, golf club heads, and tennis/squash rackets.

8 Review Questions

(1) What are the advantages and disadvantages of MMCs?
(2) Explain the function of the matrix and the reinforcement.
(3) Explain how the interface may affect the properties of MMCs.
(4) What can be done to prevent unwanted reactions between the fibres and the matrix?
(5) Describe the various types of reinforcement.
(6) Provide three examples of fibre reinforcement.
(7) Describe the process of powder metallurgy.
(8) Describe the differences between powder metallurgy and mechanical alloying.
(9) Describe the process of stir casting.
(10) What are the advantages and disadvantages of using squeeze casting over melt infiltration?
(11) How are reinforcements produced during in situ processing of MMCs?
(12) Describe the strengthening mechanisms for composites.
(13) How do the properties of AM manufactured MMCs compared to conventional MMCs produced by liquid or solid processing techniques?
(14) Provide examples of composites used in aerospace and the desired properties.
(15) Explain how it is possible to control the thermal expansion coefficient of MMCs?

References

1. Chawla, K.K.: Composite materials. Springer New York, New York, NY (2012). https://doi.org/10.1007/978-0-387-74365-3
2. Chawla, N., Chawla, K.K.: Metal matrix composites. Springer New York, New York, NY (2013). https://doi.org/10.1007/978-1-4614-9548-2
3. Granta Design Limited, CES Edupack, (2019)
4. Lloyd, D.J.: Particle reinforced aluminium and magnesium matrix composites. Int. Mater. Rev. **39**, 1–23 (1994)
5. Prasad, N.E., Wanhill, R.J.H.: Aerospace materials and material technologies. Springer Nature (2017)
6. Yang, J.-M., Hahn, T.H., Seo, H., Chang, P.-Y., Yeh, P.-C.: Damage tolerance and durability of fiber-metal laminates for aircraft structures (2010). http://www.tc.faa.gov/its/worldpac/techrpt/ar1018.pdf
7. Gupta, M., Wong, W.L.E.: Magnesium-based nanocomposites: lightweight materials of the future. Mater. Charact. **105** (2015). https://doi.org/10.1016/j.matchar.2015.04.015
8. Gupta, M., Wong, W.L.E.: Enhancing overall mechanical performance of metallic materials using two-directional microwave assisted rapid sintering. Scr. Mater. **52**, 479–483 (2005). https://doi.org/10.1016/j.scriptamat.2004.11.006
9. Gupta, M., Eugene, W.W.L.: Microwaves and metals (2011). https://doi.org/10.1002/9780470822746
10. Rawal, S.: Metal-matrix composites for space applications. JOM. 14–17 (2001)

11. Hu, Y., Cong, W.: A review on laser deposition-additive manufacturing of ceramics and ceramic reinforced metal matrix composites. Ceram. Int. **44**, 20599–20612 (2018). https://doi.org/10.1016/j.ceramint.2018.08.083
12. Almangour, B.: Additive manufacturing of emerging materials (2018). https://doi.org/10.1007/978-3-319-91713-9
13. Hull, D., Bacon, D.: Introduction to dislocations. Elsevier (2001). https://doi.org/10.1016/B978-0-7506-4681-9.X5000-7
14. Kazim, O.: Ductility and strength of extruded SiC p/aluminium-alloy composites mit Coen, Kazim nel* **62**, 275–282 (2002)
15. Raghavendra Rao, P.S., Mohan, C.B.: Study on mechanical performance of silicon nitride reinforced aluminium metal matrix composites. Mater. Today Proc. 2–6 (2020). https://doi.org/10.1016/j.matpr.2020.03.495
16. Dobrzański, L.A., Włodarczyk, A., Adamiak, M.: The structure and properties of PM composite materials based on EN AW-2124 aluminum alloy reinforced with the BN or Al2O3 ceramic particles. J. Mater. Process. Technol. **175**, 186–191 (2006). https://doi.org/10.1016/j.jmatprotec.2005.04.031
17. Girish, B.M., Basawaraj, B., Satish, B.M., Somashekar, D.R.: Electrical resistivity and mechanical properties of tungsten carbide reinforced copper alloy composites. Int. J. Compos. Mater. **2**, 37–43 (2012). https://doi.org/10.5923/j.cmaterials.20120203.04
18. Wong, W.L.E., Gupta, M., Lim, C.Y.H.: Enhancing the mechanical properties of pure aluminum using hybrid reinforcement methodology, Mater. Sci. Eng. A. **423** (2006). https://doi.org/10.1016/j.msea.2005.09.122
19. Eugene, W.W.L., Gupta, M.: Enhancing thermal stability, modulus and ductility of magnesium using molybdenum as reinforcement. Adv. Eng. Mater. **7** (2005). https://doi.org/10.1002/adem.200400137
20. Saravanan, R., Surappa, M.: Fabrication and characterisation of pure magnesium-30 vol.% SiCP particle composite. Mater. Sci. Eng. A. **276**, 108–116 (2000). https://doi.org/10.1016/s0921-5093(99)00498-0
21. Wong, W.L.E., Karthik, S., Gupta, M.: Development of high performance Mg–Al 2 O 3 composites containing Al 2 O 3 in submicron length scale using microwave assisted rapid sintering. Mater. Sci. Technol. **21**, 1063–1070 (2005). https://doi.org/10.1179/174328405X51758
22. Wong, W.L.E., Gupta, M.: Effect of hybrid length scales (Micro + nano) of SiC reinforcement on the properties of magnesium (2006). www.scientific.net/SSP.111.91
23. Poddar, P., Srivastava, V.C., De, P.K., Sahoo, K.L.: Processing and mechanical properties of SiC reinforced cast magnesium matrix composites by stir casting process. Mater. Sci. Eng. A **460–461**, 357–364 (2007). https://doi.org/10.1016/j.msea.2007.01.052
24. Zhu, J., Jiang, W., Li, G., Guan, F., Yu, Y., Fan, Z.: Microstructure and mechanical properties of SiCnp/Al6082 aluminum matrix composites prepared by squeeze casting combined with stir casting. J. Mater. Process. Technol. **283**, (2020). https://doi.org/10.1016/j.jmatprotec.2020.116699
25. Chandrashekar, A., Ajaykumar, B.S., Reddappa, H.N.: Mechanical, structural and corrosion behaviour of AlMg4.5/Nano Al2O3 metal matrix composites. Mater. Today Proc. **5**, 2811–2817 (2018). https://doi.org/10.1016/j.matpr.2018.01.069
26. Maqbool, A., Hussain, M.A., Khalid, F.A., Bakhsh, N., Hussain, A., Ho, M.: Mechanical characterization of copper coated carbon nanotubes reinforced aluminum matrix composites. Mater. Charact. **86**, 39–48 (2013). https://doi.org/10.1016/j.matchar.2013.09.006
27. Goh, C.S., Wei, J., Lee, L.C., Gupta, M.: Simultaneous enhancement in strength and ductility by reinforcing magnesium with carbon nanotubes. Mater. Sci. Eng. A **423**, 153–156 (2006). https://doi.org/10.1016/j.msea.2005.10.071
28. Meenashisundaram, G.K., Seetharaman, S., Gupta, M.: Enhancing overall tensile and compressive response of pure Mg using nano-TiB2 particulates. Mater. Charact. **94**, 178–188 (2014). https://doi.org/10.1016/j.matchar.2014.05.021
29. Wong, W.L.E., Gupta, M.: Development of Mg/Cu nanocomposites using microwave assisted rapid sintering. Compos. Sci. Technol. **67** (2007). https://doi.org/10.1016/j.compscitech.2006.07.015

30. Wong, W.L.E., Gupta, M.: Simultaneously improving strength and ductility of magnesium using nano-size SiC particulates and microwaves. Adv. Eng. Mater. **8**, 735–740 (2006). https://doi.org/10.1002/adem.200500209
31. Wang, J., Guo, X., Qin, J., Zhang, D., Lu, W.: Microstructure and mechanical properties of investment casted titanium matrix composites with B4C additions. Mater. Sci. Eng. A **628**, 366–373 (2015). https://doi.org/10.1016/j.msea.2015.01.067
32. Huang, L., Wang, L., Qian, M., Zou, J.: High tensile-strength and ductile titanium matrix composites strengthened by TiB nanowires. Scr. Mater. **141**, 133–137 (2017). https://doi.org/10.1016/j.scriptamat.2017.08.007
33. Materion Corporation (n.d.). https://materion.com/products/metal-matrix-composites/supremex/aluminum-silicon-carbide-composites
34. DWA Aluminum Composites USA (n.d.). https://www.dwa-usa.com/al-mmc-material-systems.html
35. Advanced Materials Technology (AMT) (n.d.). https://www.amt-advanced-materials-technology.com/materials/
36. Jiang, L.Y., Liu, T.T., Zhang, C.D., Zhang, K., Li, M.C., Ma, T., Liao, W.H.: Preparation and mechanical properties of CNTs-AlSi10Mg composite fabricated via selective laser melting. Mater. Sci. Eng. A **734**, 171–177 (2018). https://doi.org/10.1016/j.msea.2018.07.092
37. Wen, X., Wang, Q., Mu, Q., Kang, N., Sui, S., Yang, H., Lin, X., Huang, W.: Laser solid forming additive manufacturing TiB2 reinforced 2024Al composite: microstructure and mechanical properties. Mater. Sci. Eng. A **745**, 319–325 (2019). https://doi.org/10.1016/j.msea.2018.12.072
38. Gu, D., Ma, J., Chen, H., Lin, K., Xi, L.: Laser additive manufactured WC reinforced Fe-based composites with gradient reinforcement/matrix interface and enhanced performance. Compos. Struct. **192**, 387–396 (2018). https://doi.org/10.1016/j.compstruct.2018.03.008
39. Li, B., Qian, B., Xu, Y., Liu, Z., Zhang, J., Xuan, F.: Additive manufacturing of ultrafine-grained austenitic stainless steel matrix composite via vanadium carbide reinforcement addition and selective laser melting: Formation mechanism and strengthening effect. Mater. Sci. Eng. A **745**, 495–508 (2019). https://doi.org/10.1016/j.msea.2019.01.008
40. Pouzet, S., Peyre, P., Gorny, C., Castelnau, O., Baudin, T., Brisset, F., Colin, C., Gadaud, P.: Additive layer manufacturing of titanium matrix composites using the direct metal deposition laser process. Mater. Sci. Eng. A **677**, 171–181 (2016). https://doi.org/10.1016/j.msea.2016.09.002
41. Traxel, K.D., Bandyopadhyay, A.: Influence of in situ ceramic reinforcement towards tailoring titanium matrix composites using laser-based additive manufacturing. Addit. Manuf. **31**, (2020). https://doi.org/10.1016/j.addma.2019.101004
42. Zhang, B., Bi, G., Chew, Y., Wang, P., Ma, G., Liu, Y., Moon, S.K.: Comparison of carbon-based reinforcement on laser aided additive manufacturing Inconel 625 composites. Appl. Surf. Sci. **490**, 522–534 (2019). https://doi.org/10.1016/j.apsusc.2019.06.008
43. Li, B., Zhang, L., Yang, B.: Grain refinement and localized amorphization of additively manufactured high-entropy alloy matrix composites reinforced by nano ceramic particles via selective-laser-melting/remelting. Compos. Commun. **19**, 56–60 (2020). https://doi.org/10.1016/j.coco.2020.03.001
44. Hunt, W., Miracle, D.: ASM handbook vol. 21 composites. ASM International (2001). https://doi.org/10.31399/asm.hb.v21.9781627081955
45. Specialty Materials Incorporated (n.d.). http://specmaterials.com/f16landingbrace.htm

Conventional Machining of Metal Matrix Composites

Xiangyu Teng and Dehong Huo

Abstract This chapter provides an introduction to conventional machining of metal matrix composites (MMCs). The critical machining characteristics, namely chip formation mechanism, effects of cutting parameters, build-up edge, and tool wear with various types of cutting tool materials are discussed. In response to new developments on MMCs reinforced with nanoparticles, the state-of-the-art machining of both aluminium and magnetism-based nano-MMCs is presented, focusing on micro-machining as lots of products and applications using nano-MMCs are expected in microscale.

1 Introduction

The development of metal matrix composite (MMC) materials started in the early 1960s intending to satisfy the need for materials with superior mechanical properties and reduced weight [1]. In the early stages, MMC materials' major applications were employed in aerospace engineering such as aircraft structures, missiles, and space structures. However, new applications were subsequently found in various areas, including automotive, military, oil, and gas [2]. The form of reinforcement used can be classified as continuous fibre, discontinuous fibre (whiskers), particles, graphene, or nanotubes. As a cost-effective and isotropic composite material, the particulate reinforced MMCs have received close attention from both industries and academia due to their isotropic nature when compared to fibre reinforced alternatives [3]. Typically, metallic materials such as aluminium, magnesium, titanium alloys, and copper act as the matrix. Different metallic, intermetallic, ceramic, or organic compound materials, including Cu, Ti, SiC, Al_2O_3, ZrO_2, B_4N, and B_4C, act as reinforcement. Superior properties compared to the monolithic materials can be obtained, such as high strength to weight ratios, toughness, dimensional stability, fatigue endurance, and improved thermal and electrical conductivity [4].

X. Teng · D. Huo (✉)
Mechanical Engineering, School of Engineering, Newcastle University, Newcastle upon Tyne NE1 7RU, UK
e-mail: dehong.huo@newcastle.ac.uk

I. Shyha and D. Huo (eds.), *Advances in Machining of Composite Materials*, Engineering Materials, https://doi.org/10.1007/978-3-030-71438-3_7

The MMC components are usually fabricated in near-net-shapes; however, conventional machining, such as turning, milling, and drilling are necessary to achieve the desired accuracy and produce complex features [5, 6]. However, they bring significant challenges to the machining process due to the heterogeneous nature of MMCs and thus make them difficult-to-cut materials. The considerable tool wear and deteriorative machined surface finish can be introduced by abrasive particles with tool-like hardness. Therefore, broader applications have been restricted by the difficulties associated with the machining process.

Extensive research on the machining of particulate MMCs has been undertaken due to their unique isotropic nature, which exhibits a higher ductility compared to fibre-reinforced alternatives. Experimental and modelling work has been conducted to improve and quantify the machinability of MMCs in terms of optimizing machining parameters, selecting the reinforcement type, and the cutting tool materials and geometry.

The rest of the chapter introduces the chip formation mechanism, and discuss the critical machining characteristics, namely the effects of cutting parameters, built-up edge, and tool wear, which determine cost-effective machining of MMCs. Finally, the latest developments on micromachining of nano-MMCs are presented as many applications are anticipated in this field in the future.

2 Chip Formation Mechanism

Metal matrix composites contain the reinforced particulate and metallic matrix phase. The chip formation depends on the matrix, reinforcement, and interactions. The chip formation mechanism of MMCs is similar to that of monolithic metals but different in many aspects, in terms of cutting forces, chip morphology, machined surface characteristics. This section overviews the chip formation in machining particulate reinforced MMCs.

Figure 1 is a typical orthogonal cutting process of MMCs. It is assumed that the chip formation is due to shearing at the shear plane AB as shown in Fig. 1, because of the cutting tool edge radius, there will be a ploughing region BC around the cutting tool edge, where plastic deformation occurs with no chips formed. This is similar to the machining of monolithic metals. In machining of MMCs, in addition to ploughing, particle fracture and displacement also take place in this region, and the particle fracture and displacement occur mainly along the cutting line CD [7].

When the shear stress exceeds the maximum permissible value, the chip formation process would be initiated while the cutting tool penetrates the workpiece, causing it deforms elastically and plastically. The chip formation process can be affected by several factors in the machining process, such as cutting speed, material properties, microstructure, and the machine tool's dynamic features. The cutting parameters and volume fraction of reinforced particles are found to affect the chip formation significantly. The continuous chips are typically formed when the materials have sufficient deformability with uniform microstructure under a relatively high cutting

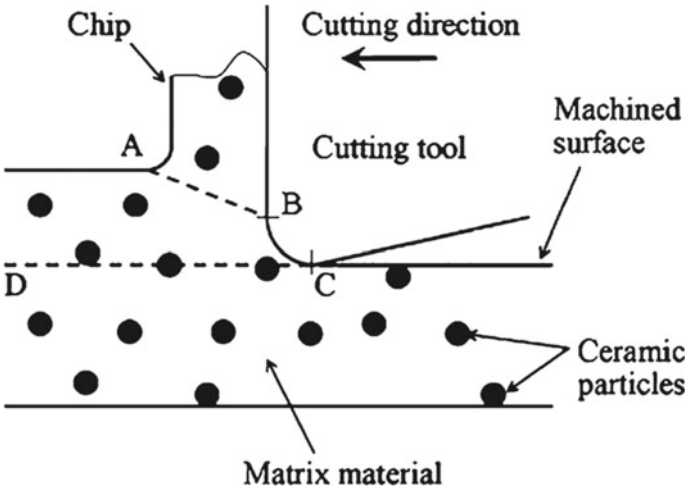

Fig. 1 Machining of particulate reinforced MMCs [7], with permission from Elsevier

speed. The addition of particles into monolithic materials leads to a sacrifice in their ductility. These characteristics lead to the fact that the continuous chips are less likely to be observed in the machining of particulate reinforced MMCs than the monolithic materials at the same cutting conditions.

Lin et al. [8] observed that the discontinuous chips are produced with SiC particles' addition when machining Al/SiC MMCs. This can be attributed to the addition of particles cause the fracture in the shear zone. During the machining process, the debonding and cracking of particles lead to the formation of a void at the shear zone. Finally, the fracture initiates with the propagation of the void. A similar chip formation mechanism was found by Karthikeyan et al. [9]. The Al/SiC MMCs with a low volume fraction would produce continuous chips. This could be verified by observing the chip root area with the absence of cracking root using the quick stop method. With increasing volume fraction, the chips tend to form discontinuously. In terms of the effect of cutting parameters on the chip formation, they also found that the continuous chips are observed at relatively high cutting speed, which is a general phenomenon observed by other researchers [10–12]. Small plastic deformation with periodic fracture was involved within the chip root region. Discontinuous chip with saw tooth appearance is generally produced at low cutting speed. This variation of chip formation can be attributed to the dramatically increased temperature associated with high cutting speed. One of the first equations of compression strength of MMCs (2024Al/SiC/vol.%20) regarding strain, strain rate, and the temperature is as follows [13].

$$\sigma = 815.64\dot{\varepsilon}^{0.1595}\ddot{\varepsilon}^{-0.0077} \text{ at } 150\,^{\circ}\text{C} \tag{1}$$

$$\sigma = 613.76\dot{\varepsilon}^{0.125}\ddot{\varepsilon}^{-0.0080} \text{ at } 250\,^{\circ}\text{C} \tag{2}$$

$$\sigma = 373.21\dot{\varepsilon}^{-0.00791}\left[\frac{t}{350}\right]^{-2.5} \text{ at } 350 - 450\,^{\circ}\text{C} \tag{3}$$

The thermal softening effect at high temperature dominates the strength of MMCs with little dependence on strain and strain rate. The deformation follows Eq. (3). The MMCs then present a decreased brittleness leading to an adiabatic shearing effect, and therefore the chips become more continuous with the elimination of the sawtooth profile. The deformation would follow the low temperature (1) at a low cutting speed which is a combination of ductile shearing and brittle fracture resulting in discontinuous chips with sawtooth appearance. A similar sawtooth pattern was found by Sahoo et al. [14] when machining 6061Al/SiC MMCs. They attributed the sawtooth-like pattern to be the high strain rate in the shear plane.

An improvement in the chip breakability due to the addition of particles was found by Paramrik et al. [15] when turning 6061 aluminium alloy reinforced with 20 vol.% SiC. Short chips were found at all cutting conditions. Figure 2 illustrates the effect of feed on chip formation. At feeds of 0.05 and 0.1 mm/rev, the chips are in the shape of a long spiral and straight chips. With increasing of feeds until 0.4 mm/rev, the chips become shorter of C shape. When comparing with non-reinforced alloy, the shape did not change with feeds. When machining MMCs, stress concentration with high strain and local deformations occurs due to particles' addition when increasing the feed, which can be attributed as the main reason leading the shorter chips with shape variation. At lower feed, the deformation is more homogeneous, which leads to longer chips.

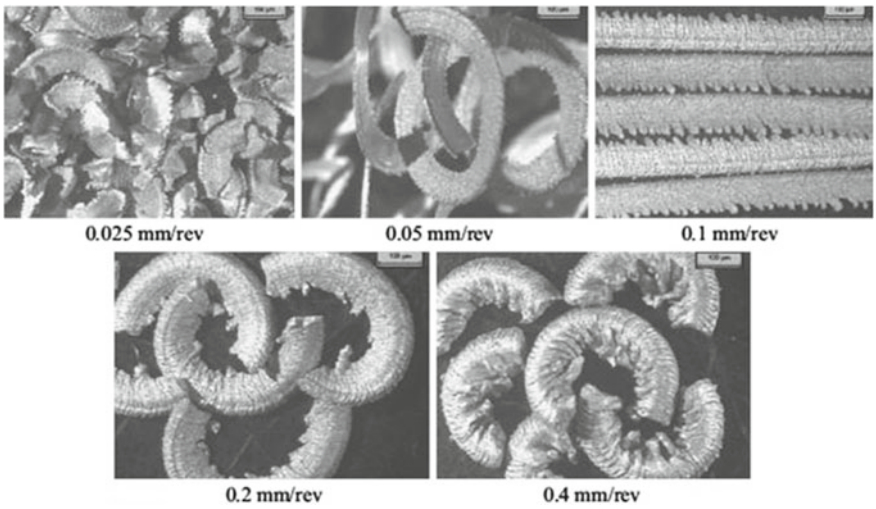

Fig. 2 Chip shapes of the MMC at different feeds (at speed 400 m/min and depth of cut 1 mm) (*Source* [15], with permission from Elsevier)

Dabade and Joshi [10] investigated the effect of size and volume fraction of particles on the chip formation mechanism by varying the cutting parameters (feeds, cutting speed) and tool geometry. Figure 3 demonstrates the variety of chips with cutting speeds, volume fraction, and particle size. When they increase the speed, the chips tend to become more continuous. This phenomenon can be explained by the soften effect due to increased temperature, resulting in a transition from brittle

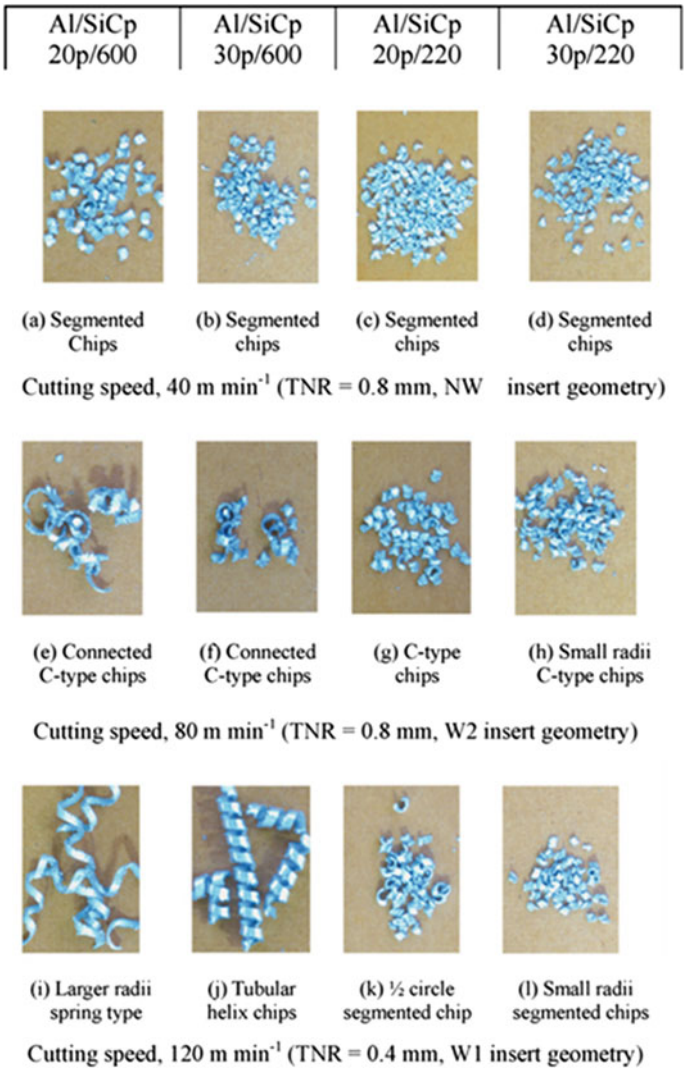

Fig. 3 Effect of cutting speed on chip form (feed = 0.2 mm/rev and depth of cut = 1 mm). (*Source* [10], with permission from Elsevier)

fracture regime to ductile regime. This trend is more evident in finer particles (see Fig. 3i–j) compared to that with coarser particles.

3 Effects of Cutting Parameters and Built-up Edge

3.1 Effects of Cutting Parameters

Cutting speed and feed rate were identified as significant contributors to surface quality, cutting force, and tool wear. The influence of various cutting parameters on cutting force and surface finish in turning Al/SiC MMCs was studied by Manna and Bhattacharayya [16, 17]. They found that surface roughness decreases when the cutting speed increases within a specific range. High cutting speed, low feed rate, and low depth of cut were suggested for achieving good surface quality.

El-Gallab and Sklad et al. [18] conducted a turning test on 20 vol.% Al/SiC to investigate the effect of cutting parameters on surface quality. The pull-out PCD grains caused by tool wear were thought to be another reason causing grooves on the machined surface. Moreover, voids and cracks were induced near the particles because of plastic deformation. The voids would join up when the feed rate increased, causing chip segmentation. High cutting speeds were also found to reduce surface roughness. The positive effect of increasing cutting speed on the surface finish has also been suggested in another research [19, 20]. The specific power consumption was identified as an indicator of machinability by Muthukrishnan et al. [21], and it was found to decrease with increasing cutting speed. Moreover, the better surface finish at high cutting speed was attributed to easier particle debonding.

Feed rate has been identified as the most significant factor influencing the cutting force and surface roughness [22–24]. Surface finish and integrity obtained in machining Al/SiC MMCs with different volume fractions (10 & 30 vol.%) were investigated by Dabade et al. [25]. Their statistical analysis indicated that the feed rate was the most significant factor affecting the cutting force for Al/30 vol.% SiC and Al/10 vol.% SiC. The MMCs with higher volume fraction exhibited higher cutting force. Additionally, by increasing the feed rate, the surface roughness increased, which is similar to the conclusion obtained by Kilickap et al. [26].

To reveal the mechanics and mechanism regarding the behaviour of MMCs during the cutting process, Kanna and Kishawy et al. [27] studied the deformation behaviour of the strain-hardened matrix materials and its relationship with cutting force during orthogonal machining. They stated that variation in average dislocation density could be characterized as one of the main factors that affect the cutting force. It was determined by variations in the size and volume fraction of reinforcement and cutting parameters such as feed rate and cutting speed.

3.2 Built-up Edge

Many researchers have conducted investigations of the formation mechanism of built-up edge (BUE) and its effect on the machinability of MMCs in terms of surface finish and tool wear. The benefit of BUE for the machining process is still a controversial topic [28]. The BUE is caused by the melt material that builds up at the tooltip, and therefore its formation is highly dependent on the temperature at the tool-materials interface [27]. The occurrence of BUE is found to depend on cutting speed firmly. Kumar et al. [12] investigated the BUE formation during the turning of Al/4.5% Vol Cu-based MMCs reinforced with TiC particles in dry conditions. They found an almost 50% decrease in the height of BUE when cutting speed increases from 40 m/min to 120 m/min. The BUE formation under the effect of cutting parameters was studied by Manna and Bhattacharayya [17]. They found no BUE is formed at high cutting speed (225 m/min) and low depth of cut and it increased as increasing the depth of cut. Similar observations were obtained from a study conducted by Sahin [29].

Muthukrishnan et al. [21] studied the BUE formation in machining Al/SiC MMCs using PCD cutting tools. The absence of BUE at high cutting speed can be attributed to the reduced adhesion characteristic due to the increased temperature. Moreover, extended tool life was obtained at a low cutting speed of 200 m/min. This can be attributed to the stable formation of BUE on the cutting edge, preventing it from undergoing abrasive wear. Acting as a sacrificial layer which is continuously replenished, the BUE protected the cutting edge from abrasive wear caused by the relative motion between the tool and abrasive particles [30, 31]. However, a detrimental effect of BUE on tool life was claimed by Kadirgama et al. [32]. They identified the built-up edge along with attrition/adhesion and oxidation as the primary wear mechanism. This is because, when the BUE falls off from the tooltip, a portion of the tool material would be removed, leading to adhesion wear. The BUE wear mechanism would become more significant when the cutting tool or coating has a high chemical affinity with workpiece materials.

In respect of surface finish, it was also concluded by Muthukrishnan et al. [21] that the formation of BUE causes the surface quality to deteriorate. This negative effect of BUE on the surface finish has been verified by other researchers [11, 33, 34]. The BUE would become unstable and fall off as the materials continuously build up. As a result, a portion of the broken BUE is smeared on the machined surface leading to low surface roughness.

4 Cutting Tools Wear for Machining of MMCs

The hard particles embedded in the matrix materials bring tremendous challenges in machining MMCs, leading to very short tool life. During the cutting process, hard particles separated from the substrate slide over the cutting edge during machining.

The direct contact between the cutting edge and particles that act as large numbers of small cutting edges leads to severe tool wear and reductions inaccuracy [35]. The tool wear mechanisms affecting the machining performance can be generally classified as abrasive wear, chipping on the cutting edge, fractures, and fatigue due to both thermal and mechanical load [35, 36]. Plenty of studies can be found regarding the tool wear modes and mechanism in the conventional machining process of MMCs.

Most researchers suggested that abrasive wear is the predominant wear mechanism in the machining of MMCs. For a given tool, matrix, and reinforcement materials, the tool wear mechanism will significantly depend on the cutting conditions and particle size and volume fraction. Ozben et al. [37] studied the effect of particle volume fraction and cutting speed on the tool wear in machining Al/SiC MMCs with different volume fractions. TiN-coated cemented carbide tools were used. It was reported that at a lower feed rate, tool wear rate would increase. This can be explained in terms of the increased contact length between the cutting tool and the abrasive particles at the lower feed rate. They also found that the lowest flank wear can be found at a low cutting speed of 50 m/min, and when cutting speed is increased to 150 m/min, flank wear increases. This can be attributed to the protective behaviours of the stable formation of BUE at low cutting speed. The importance of cutting speed is especially significant when machining MMCs with coarse particles. [38] Additionally, increased particle volume fraction from 5% to 15% resulted in increased tool wear. A similar observation was made by Sahin [29] where increasing either particle content or cutting speed leads to increased tool wear when machining Al alloy based MMCs reinforced with SiC particles. Mild abrasion and edge chipping were defined as the primary wear mechanisms. Li and Seah [39] also reported that the tool wear becomes severe when the particle volume fraction exceeds a threshold. An investigation of tool wear under the effect of reinforced particle size using coated and uncoated cemented was carried out by Ciftci [40]. Al/SiC MMCs with a constant volume fraction of 16% and various particle sizes of 30, 45, and 110 μm were used as specimens. Particle size was found to harm the tool. This observation was supported by Kannan [31].

Various cutting tool materials are employed in machining MMCs. Coated and uncoated cemented carbide, chemical vapour deposition (CVD), cubic boron nitride (CBN), and polycrystalline diamond (PCD) are the primary cutting tool materials used in the machinability studies of MMCs.

4.1 Uncoated Carbide Tools

Many studies have indicated that carbide tools generally exhibit rapid tool wear while machining MMCs, which means that carbide tool is not an ideal cutting tool for machining such materials [17, 37, 41, 42]. Carbide tools were found to be suitable in economic and short time run machining for roughing operation [43, 44]. Among these studies, carbide tools demonstrate a catastrophic failure when cutting speed exceeds 350 m/min, and thus the maximum cutting speed for such tools is limited

to 300 m/min. Boswell et al. [23] determined the optimum machining parameters in machining titanium based MMCs reinforced with 20 vol.% B4C using uncoated carbide tools. They concluded that the carbide tool is useful for producing the desired surface quality and its tool life is satisfactory. Hung et al. [44] suggested using the tungsten carbide tool in the roughing process and PCD tools in the finishing process. Kannan et al. [31] studied the progression of flank wear in machining Al6061 alloy based MMCs reinforced with SiC particles. It was concluded that low cutting speed and high feed rate could be used to maximize tool life. Ghani et al. [45] investigated the milling and turning process of AlSi/AlN MMCs using carbide cutting tools. Their results showed that uniform flank wear caused by abrasion was the dominant wear mechanism.

4.2 Coated Carbide Tools

To prolong the tool life, carbide tools with various ceramic coatings have been used to machining MMCs by many researchers. It was found by Sun et al. [46] that TiNAl- coated carbide tools demonstrate a satisfactory wear resistance with the cutting speeds from 10 to 40 m/min in the high-speed milling of Al/SiC MMCs with a volume fraction of 15%. Quigley et al. [47] studied the machinability of Al/SiC MMCs in terms of surface finish and tool wear using uncoated carbide tools and TiN-coated tools. The TiN-coated tools delivered improved wear resistance but worse surface finish when compared to uncoated carbide tools. Songmene and Balazinski [48] investigated TiCN-coated tools' performance in terms of flank wear and tool life in the machining Al-based MMCs reinforced with different types of particle materials. As the hardness of Al_2O_3 particles, at 2100–2300HV, is lower than that of TiCN coating (3000HV), the abrasive mechanism was not observed in the machining Al/Al2O3 MMCs leading to the most extended tool life and lowest flank wear rate. When machining the Al-based MMCs reinforced with SiC particles whose hardness is higher than TiCN coating, the cutting tool exhibited the shortest tool life and high flank wear rate. Overall, carbide tools with ceramic coating offer slight advantages in machining MMCs compared to uncoated tools. The wear resistance mainly depends on the reinforcement materials used.

The carbide cutting tools with a diamond coating made by chemical vapour deposition (CVD) have been identified as the most suitable cutting tools for machining MMCs. Compared with PCD, CVD diamond is harder, and it presents a lower friction coefficient, higher thermal conductivity, and better thermal stability. However, CVD cutting tools' main concern is considered the adherence between the coating and substrate carbide tool. Davim [49] compared the performance of CVD diamond coated and PCD tools in the machining of A356/SiC MMCs. The time taken for flank wear becoming visible in CVD tools was 10 times faster than that in PCD. The better performance of PCD in machining MMCs compared to CVD was also confirmed by Andrews et al. [50]. Kremer et al. [51] performed dry turning tests on Al/SiC MMCs using CVD diamond-coated tools. A range of relatively high cutting speed

of 400–900 m/min was used. The predominant wear mechanism was found to be coating failure caused by a process where the built-up edge welded onto the coating surface is regularly scratched away by hard SiC particles. Chou and Liu investigated coating failure [52]. They looked into the effect of cutting temperatures at the flank face of CVD cutting tools in the machining of Al/SiC MMCs. Greater interfacial stress was induced between the coating and substrate due to the different thermal expansion, contributing to the coating pull-out mechanism.

4.3 Cubic Boron Nitride Tools

Little research has been conducted on the tool wear of cubic boron nitride (CBN) when machining MMCs [26]. Ding et al. [53] studied the machinability of MMCs using various types of PCBN and PCD cutting tools in machining Al-based MMCs with SiC particles of 12.8 μm and 20% volume fraction. The built-up edge was significant with PCBN tools, which led to increased notch wear and deteriorated surface quality. PCBN tools exhibited a shorter tool life than PCD tools.

The performance of various cutting tools, including tungsten carbide, CBN, and PCD in machining Al/SiC, were tested by Hung et al. [54]. CBN and PCD tools fractured the SiC particles along their crystallographic planes, leading to minimum subsurface damage. The PCD tool lasted five times longer tool life than the CBN tool while machining at a cutting speed of 6 m/min, a feed rate of 0.07 mm/rev and a depth of cut of 5 mm.

Ciftci et al. [33] studied particle size's effect on cutting performance of CBN tools while turning Al/SiC. Tool fracture and abrasive and adhesion wear were identified as the primary wear mechanisms at particle sizes of 110 μm and 30 μm. It was concluded that the CBN tool is not suitable for cutting MMCs with the larger particles (110 μm).

4.4 Polycrystalline Diamond Tools

The earliest research on the machinability of aluminium alloy-based metal matrix composites reinforced with SiC particles (14 vol.%) was conducted by Tomac et al. [55]. They claimed that PCD tools could produce a very low cutting force as well as an excellent surface finish which is similar to that obtained from the grinding process.

Among those tools made from different materials, PCD cutting tools are the most preferred due to their acceptable life compared to others [8, 38, 56, 57]. This can be attributed to the low friction coefficient of PCD and its low chemical affinity with workpiece materials as well as the fact that the hardness of PCD tools is higher than most commonly used particle materials such as SiC and Al2O3 [49, 58]. These unique features make it an ideal tool material for the machining of MMCs.

Muguthu et al. [59] found that PCD tools exhibited lower power consumption and higher wear resistance than polycrystalline cubic boron nitride (PCBN) in the turning of Al_2O_3/SiCp MMCs. While the PCD tools provided admirable performance in machining MMCs, the machining cost is also significantly higher due to manufacturing costs, consequently restricting their use [8, 53, 56].

Huang et al. [60] conducted a drilling experiment on Al/SiCp with a high volume fraction (56%). The average particle size is 60 μm. Extremely rapid flank wear was found on PCD drills, and it was concluded that the primary mechanisms include abrasive and adhesive wear. The results indicated that the PCD tool is suitable for machining Al/SiCp MMCs with high volume fractions and large particle size.

An abrasive wear mechanism was identified in earlier work conducted by Tomac and Tonnessen [55]. The results obtained from their research showed that the PCD tool exhibits over 30 times longer tool life than the carbide tool with the same cutting parameters. El-Gallab and Sklad [56] machined Al/SiC MMCs using PCD tools and found abrasion to be the primary wear mechanism, which was verified by the flank face with grooves parallel to the chip flow direction. They attributed the formation of grooves to the following three reasons: (1) Aluminium seizure and the pull-out process of PCD grains, (2) formation of Al_2O_3 on the cutting edge, (3) SiC abrasive particles.

5 Micromachining of MMCs

As a relatively new technique developed in the past two decades, non-lithography based micro manufacturing including micro EDM, laser beam machining, micromechanical cutting, etc. is capable of manufacturing with a broader range of workpiece materials and producing components with complex 3D shapes. Micro cutting involves a mechanical material removal process used to machine highly accurate 3D components with a dimension or feature size ranging from several microns to hundreds of microns on various engineering materials including metals, polymers, glasses, ceramics, and composites. The processes can be categorized as micro turning, micro-milling, micro-drilling, and micro-grinding. Micro milling is recognized to be one of the most flexible and versatile micro mechanical cutting processes with high accuracy. Thus it has received considerable attention in the last decade [61]. This section focuses on the state-of-the-art in micromachining of MMCs, focusing on micro-milling drawn on authors' work on this topic.

To produce micro features, micro endmills ranging from 50–1000 μm are typically used. Although micro-milling is kinematically similar to its conventional counterpart, several issues including size effect and minimum chip thickness arise from the fact that uncut chip thickness is comparable to the cutting edge radius in micro-milling [61]. The attainable accuracy, as well as the surface quality and the integrity of products, can be influenced by numerous factors such as cutting edge geometry, material microstructure, and strengthening mechanisms. These issues mean that the

material removal mechanism in micro-milling is different from that in conventional milling. These problems encountered with micro-milling also limit its industrial applications.

5.1 Size Effect in Micromachining

In the conventional macro milling process, the cutting edge can be assumed to be ideally sharp as the cutting edge radius is much smaller than the uncut chip thickness. In this case, the effect of cutting edge radius can be neglected, and the shearing mechanism dominants the material removal process. In the micro-milling process, with the decreasing of uncut chip thickness dimensionally close to the same magnitude as the cutting edge radius, the effective rake angle becomes highly negative, which changes the material removal mechanism from shearing to ploughing [62]. In this case, the materials being ploughed off mainly undergo an elastic deformation which in turn produces a large frictional force between the cutting tool and the workpiece. As a result, the specific cutting energy (energy consumed in removing a unit volume of material) would suffer a nonlinear increase when the uncut chip thickness decreases below a specific value. This usually significantly affects aspects of the cutting process, such as surface finish, surface integrity, and tool wear. Therefore, the size effect caused by the decreasing ratio of uncut chip thickness to cutting edge radius is considered as one of the main factors affecting the cutting mechanism in the micro-milling process.

5.2 State-of-the-Art of Micromachining of Metal-Based Nanocomposites

Typically, the improvement of ultimate tensile and yield strengths of the matrix can be achieved by adding the micro-sized particles. However, some restrictions of conventional micro-MMCs in specified applications are discovered due to the sacrifice in ductility caused by the large volume fraction of particles when compared to their matrix material [63, 64]. In recent years, MMCs reinforced with nanoparticles (nano-MMCs) as promising materials are receiving increasing attention in both academia and industries. It is noticed that the MMCs with a small volume fraction of nanoparticles are found to exhibit even better mechanical properties, and the temperature creeps resistance than those reinforced with the larger volume fraction of micro-sized particles without compromising in ductility [65]. Unlike the most commonly used particle size ranging from 50 to 500 μm in conventional micro-MMCs, the size of particles reinforced within nano-MMCs is usually less than 100 nm.

Although plenty of studies have investigated the machinability of MMCs with micro-sized particles, fewer publications can be found on the machining of MMCs

reinforced with nano-reinforcement. Latest developments on machining of both aluminium and magnesium-based nano-MMCs are reviewed in this section.

5.2.1 Aluminium Based Nano-MMCs

El-Kady et al. [66] conducted a turning experiment on Al-based nano-MMCs with nano SiC particles. They found that, by increasing the content of SiC particles from 1 to 5 wt%, surface finish improvement occurs, and the cutting force increases due to the increase in hardness. Moreover, the surface roughness decreased with increasing cutting speed. This phenomenon is similar to that observed in the machining micro-sized particle reinforced MMCs.

The machining characteristics of the Al and Al–Si alloys (LM6 and LM25) and Al/Al–Si-based nano-MMCs reinforced with carbon nanotube were investigated by Gangadharan et al. [67] using recurrence plots (RP) and recurrence quantification analysis (RQA) technique. Results indicated that the machinability in terms of vibration damping ability and stability of LM6 could be future improved by adding 0.5 wt% CNT. The improved machinability of CNT reinforced nano-MMCs was also observed by Sasimurugan and Palanikumar [68]. They found that compared to the ordinary hybrid Al/SiC-Al_2O_3 MMCs, the negative effect of increasing feed rate on the surface finish is reduced to a large extent in machining Al/CNT-Al_2O_3 nano-MMCs.

The effect of the addition of graphite reinforcement on machining MMCs have been studied by various researchers. The negative effect of adding graphite reinforcement in Al/SiC MMCs on machined surface roughness was found by Basavarajappa et al. [69]. This surface degradation was attributed to the voids generated on the surface caused by the smearing and removal of graphite particles.

The optimization of cutting parameters in the turning of hybrid Al-based nano-MMCs reinforced with nano SiC particle and graphite was performed by Priyadarshi and Sharma [70] using a response surface methodology. A positive effect of cutting speed on the surface finish was also observed. Higher surface roughness could be induced at a higher feed rate due to the increased heat generation. Moreover, the cutting force was significantly influenced by the feed rate and depth of cut.

5.2.2 Aluminium Based Nano-MMCs

Recently, magnesium receives increasing attention from the biomedical area due to its biocompatibility, biodegradability, and similar mechanical properties to human cortical bone [71, 72]. Therefore, magnesium-based nanocomposites show great potential in use for implant materials, micro clips, and suture wire [73] due to their improved corrosion resistance.

The demand for miniaturized components with complex features and admirable mechanical properties in microscale has rapidly increased in many applications such as bioengineering, aerospace, medical, and electronics in the last decade. Figure 4 indicates some specific micro-scale applications which demand the miniature size

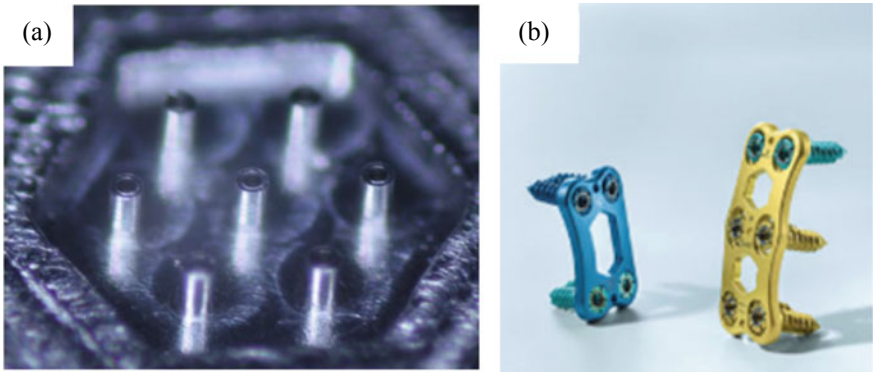

Fig. 4 Micro-scale applications of MMCs: **a** micromachined electrospray atomizers (hole inner diameter 50 μm fabricated in RISE lab); **b** bio-implant: bone plates

and high dimensional accuracy made by MMCs [74]. To satisfy such increasing demands, mechanical micromachining is recognized as one of the most versatile micro-manufacturing processes. With the decreasing ratio of either the uncut chip thickness or microstructure of workpiece material to the cutting edge radius, the grain size and material microstructure become the predominant factors which raise the issues such as size effect and minimum chip thickness effect during the material removal process.

Therefore, it is believed that those obstacles mentioned above in conventional machining of MMCs will become significant in the micromachining process. Besides, from the strengthening mechanism point of view, Orowan strengthening effect plays a vital role in strengthening nano-MMCs, which is different from that for micro-MMCs due to the reduced particle size and volume fraction. Therefore, it is believed to make the material removal mechanism significantly different from their micro-sized counterparts. The development of the conventional machining method has attracted researchers on various micro-MMCs materials for approximately two decades, and a large number of experiments and modelling related studies have been done. However, a gap exists in the development of micromachining on the magnesium-based MMCs reinforced with the nanoparticles.

Liu [75] conducted a micro-milling experiment on Mg-based nano-MMCs with a relatively high content of SiC particles (5, 10, and 15 vol.%), and it was found that increasing SiC nano-reinforcements volume fraction improves the yield and fracture strength of MMCs and consequently resulted in an increased cutting force. Moreover, the cutting force profiles were not as smooth as those of pure Mg as a result of nanoparticles, which influences the chip formation of Mg MMCs.

Teng et al. [76] conducted the micro machinability investigation on the two types of Mg-based MMCs reinforced with Ti and TiB2 nanoparticles, respectively considering the size effect. The effect of cutting parameters on the surface morphology and cutting force was studied. As illustrated in Fig. 5, severe top burrs on the slot edge and worse surface finish with a large crack area were observed at a small feed per

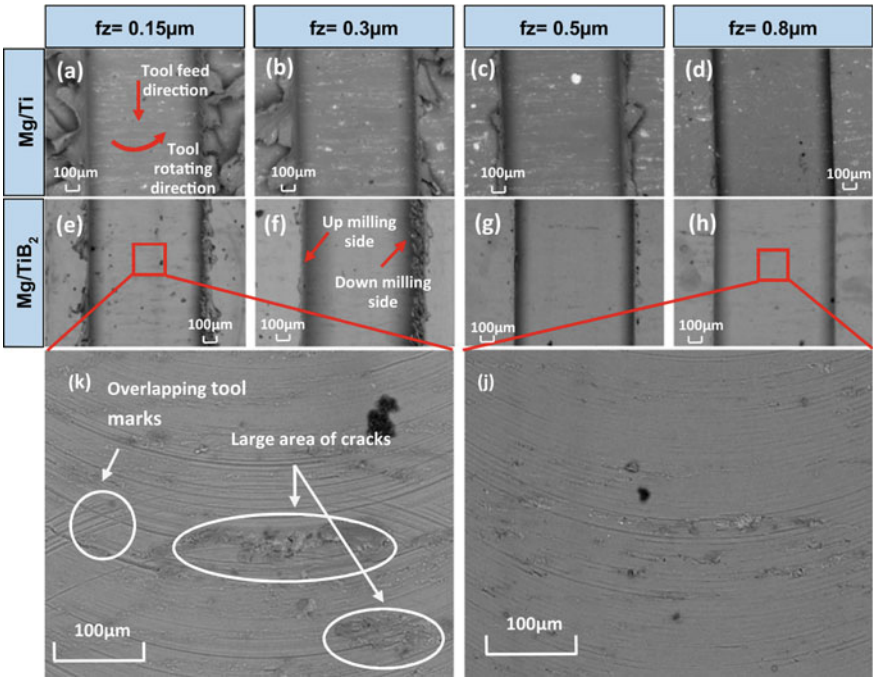

Fig. 5 SEM micrographs of micromachined slots for Mg/TiB2 MMCs and Mg/ Ti MMCs at spindle speed: 40,000 rpm depth of cut: 200 µm **a** and **e** feed per tooth: 0.15 µm/tooth; **b** and **f** feed per tooth: 0.3 µm/tooth; **c** and **g** feed per tooth: 0.5 µm/tooth; **d** and **h** feed per tooth: 0.8 µm/tooth; **k** Magnified image of **e**; **j** magnified image of **h** (*Source* [77], Creative Commons CC BY license)

tooth (0.15 and 0.3 µm) for both MMCs due to the size effect. When increasing the feed per tooth, the size of burrs was found to be decreased, and the surface finish is improved. Mg/TiB2 exhibited an improved machined surface quality at all cutting conditions. The cutting force of Mg/Ti MMCs was found to be two times larger than that of Mg/TiB2 MMCs at various feeds and the same cutting speed and depth of cut, which can be considered as the main reason leading to a worse surface finish for Mg/Ti MMCs. Moreover, the minimum chip thickness was determined to be 0.8 µm, namely 53% of the cutting edge radius based on analyzing the relationship between specific cutting energy and various feed per tooth.

5.3 Tool Wear Mechanism in Micromachining of MMCs

The size effect caused by scaling effects in micro-milling plays an essential role in the material removal mechanism and the underlying mechanics during the machining process. The ploughing region's size where material elastically deforms and recovers to its original position after the tool passes cannot be neglected in micro-milling.

Consequently, high friction and stress are induced between the cutting tool and the materials, making the cutting edge the most loaded portion of micro endmills [78]. Therefore, unpredictable tool life and the premature failure of micro endmills have been recognized as the main micro-milling barriers [79]. The flank wear is considered as the main wear criterion in the conventional milling process, but it becomes less significant in the micro-milling process. The wear mechanisms and failure types in micro-milling are diverse and complex.

Additionally, the tool wear measurement is challenging due to the miniaturized size of endmills in micro-milling. A literature survey shows that the current state-of-the-art lacks generic tool wear criteria and assessment methods in micro-milling. Some attempts in investigating tool wear mechanisms in the micro-milling of engineering materials are summarised below.

Ucun et al. [80] compared endmills' performance with different coatings (AlTiN, TiAl&AlCrN, AlCrN, TiAl&WC/C, and diamond-like carbon) during the micro-milling of Inconel 718 superalloy. Effective tool diameter and cutting edge corner were measured to quantitatively define tool wear condition (Fig. 6). Flank wear due to abrasion and chipping was reported as the dominant wear modes. Local fractures resulting from fatigue and burr formation were observed due to the excessive friction on a part where smeared by workpiece material, and the size effect dominated this at small uncut chip thickness. Diamond-like carbon and TiAlN&WC/C coatings exhibited better wear resistance compared to others.

Overall, diverse wear mechanisms have been reported in the machining of different engineering materials. However, only a few publications have investigated wear mechanisms during the machining of MMCs reinforced with nanoparticles. It is believed that the enhanced mechanical properties of MMCs would make the machining process more challenging than that in the conventional machining process. Therefore, it is crucial to comprehensively understand the material removal mechanism in the micromachining of nano MMCs. Teng et al. [81] investigated the tool wear mechanism in micromachining of Mg-based MMCs reinforced with vol.% 1.92

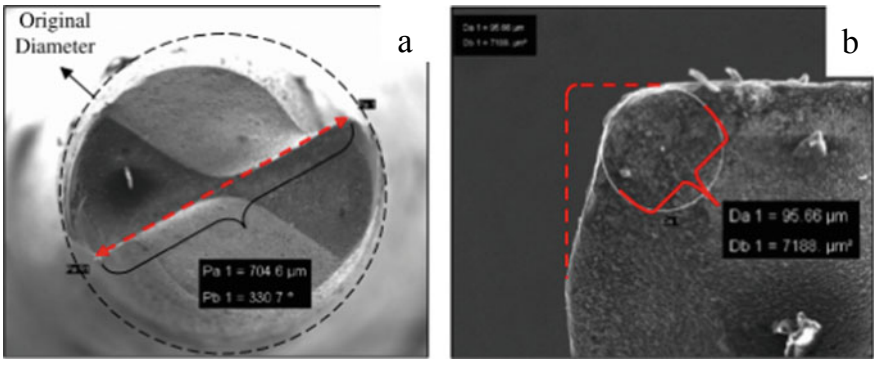

Fig. 6 Tool wear criteria: **a** effective tool diameter; **b** cutting edge radius. (*Source* [80], with permission from Elsevier)

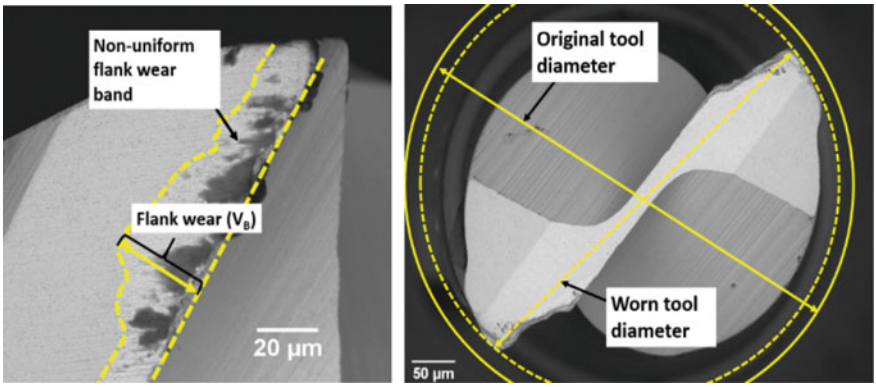

Fig. 7 Measurement of **a** flank wear, VB and **b** effective tool diameter (DE). (*Source* [82], with permission from Springer)

nano-sized titanium particles by studying the effect of various cutting parameters on the tool wear progression. As shown in Fig. 7, the effective tool diameter DE and average flank wear VBA were selected as the tool wear criteria. A finite element model was established to explain the matrix deformation and abrasive wear mechanism caused by an interaction between tool-particle. Abrasive wear and chip adhesion were defined as the primary tool wear mechanism. Figure 8 demonstrates the tool wear conditions under a constant depth of cut of 100 µm and various cutting speeds and feed per tooth. The smallest wear was observed at the highest cutting speed of 125.6 µm/min, which is opposite to that in the machining of MMCs reinforced with micro-sized particles where tool wear would accelerate at relatively high cutting speed. The BUE observed at the cutting edge can be attributed to being the main reason protecting the tool from abrasive wear. Whereas the highest cutting speed also produced a relatively deteriorative surface due to the existence of BUE. The partial BUE detached from the cutting edge was squeezed by the cutting edge and adhered on the machined surface leading to a deteriorative surface. Moreover, due to the elastically dominated cutting mechanism caused by the size effect, the largest tool wear was observed at the lowest feed per tooth of 0.75 µm/tooth.

6 Summary

This chapter provided a comprehensive review of the state-of-the-art machining of metal matrix composites, with both macro and micromachining processes discussed. Although tool wear remains the main issue in cost-effective machining of MMCs due to the reinforcements' abrasive nature, conventional machining is still the major secondary manufacturing process to fabricate components made of MMCs. The

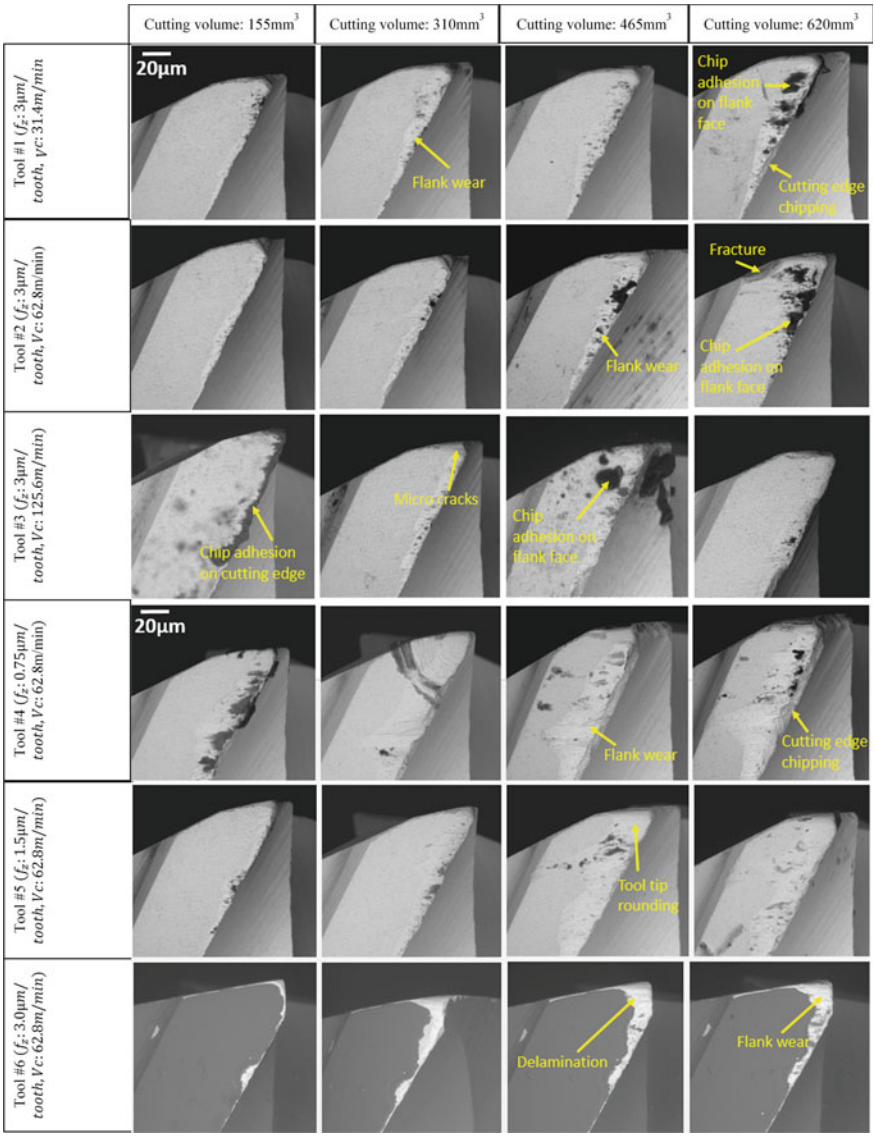

Fig. 8 Micrographs of tool wear progression at a constant depth of cut of 100 μm and various cutting speeds and feed per tooth. (*Source* [82], with permission from Springer)

machinability of commonly used Al/SiC MMCs has been thoroughly investigated, and optimal machining parameters and tooling are readily available in the literature. However, machining other types of MMCs such as magnesium-based MMCs and nano-MMCs are still under-researched, attracting increasing attention from the machining research community.

7 Review Questions

(1) Explain why machining is necessary for the fabrication of MMCs products.
(2) What are the main challenges in conventional machining of MMCs?
(3) State briefly the chip formation mechanism difference between machining of MMCs and monolithic materials.
(4) How do the cutting parameters affect the machinability when machining particulate metal matrix composites?
(5) Discuss the reasons causing the different chip morphology/shapes.
(6) Discuss how built-up edge affect the machinability of MMCs in terms of tool life.
(7) What is the dominant difference between the conventional and micromachining of metal matrix composites in terms of machinability?
(8) What are the main tool wear modes in the machining of MMCs?
(9) Please specify the tool wear characteristics exhibited by each type of cutting tool (uncoated carbide, coated carbide, CBN, and PCD) when machining MMCs and how it varies with various cutting parameters and reinforcement materials?
(10) What does 'size effect' in micromachining refer to?

References

1. Teti, R.: Machining of Composite Materials. CIRP Ann. Manuf. Technol. **51**, 611–634 (2002). https://doi.org/10.1016/S0007-8506(07)61703-X
2. Satyanarayana, K.G.: Handbook of ceramics and composites. Marcel Dekker, INC, New York, USA (1989)
3. Chawla, B.N., Shen, Y.: Mechanical behavior of particle reinforced metal matrix composites. Adv. Eng. Mater. **3**, 357–370 (2001). https://doi.org/10.1002/1527-2648(200106)3:6%3c357:AID-ADEM357%3e3.3.CO;2-9
4. Shukla, M., Dhakad, S.K., Agarwal, P., Pradhan, M.K.: Characteristic behaviour of aluminium metal matrix composites: a review. Mater. Today Proc. **5**, 5830–5836 (2018). https://doi.org/10.1016/j.matpr.2017.12.180
5. Sekhar, R., Singh, T.P.: Mechanisms in turning of metal matrix composites: a review. J. Mater. Res. Technol. **4**, 197–207 (2015). https://doi.org/10.1016/j.jmrt.2014.10.013
6. Hung, N.P., Loh, N.L., Xu, Z.M.: Materials technology cumulative tool wear in machining metal matrix composites part II: machinability (1996)
7. Zhang, L.C.: Cutting composites: a discussion on mechanics modelling. J. Mater. Process. Tech. **209**(9), 4548–4552 (2009)
8. Lin, J.T., Bhattacharyya, D., Lane, C.: Machinability of a silicon carbide reinforced matrix composite aluminium metal. Matrix **183**, 883–888 (1995)
9. Karthikeyan, R., Ganesan, G., Nagarazan, R.S., Pai, B.C.: A critical study on machining of Al/SiC composites. Mater. Manuf. Process. **16**, 47–60 (2001). https://doi.org/10.1081/AMP-100103696
10. Dabade, U.A., Joshi, S.S.: Analysis of chip formation mechanism in machining of Al/SiCp metal matrix composites. J. Mater. Process. Technol. **209**, 4704–4710 (2009). https://doi.org/10.1016/j.jmatprotec.2008.10.057

11. El-Gallab, M., Sklad, M.: Machining of Al/SiC particulate metal matrix composites Part II: Workpiece surface integrity. J. Mater. Process. Technol. **83**, 277–285 (1998). https://doi.org/10.1016/S0924-0136(98)00072-7
12. Kumar, A., Mahapatra, M.M., Jha, P.K.: Effect of machining parameters on cutting force and surface roughness of in situ Al-4.5%Cu/TiC metal matrix composites. Meas. J. Int. Meas. Confed. **48**, 325–332 (2014). https://doi.org/10.1016/j.measurement.2013.11.026
13. Gururaja, S., Ramulu, M., Pedersen, W.: Machining of MMCs: a review. Mach. Sci. Technol. Int. J. **17**(1), 41–47 (2013)
14. Sahoo, A.K., Pradhan, S., Rout, A.K.: Development and machinability assessment in turning Al/SiCp-metal matrix composite with multilayer coated carbide insert using Taguchi and statistical techniques. Arch. Civ. Mech. Eng. **13**, 27–35 (2013). https://doi.org/10.1016/j.acme.2012.11.005
15. Pramanik, A., Zhang, L.C., Arsecularatne, J.A.: Machining of metal matrix composites: effect of ceramic particles on residual stress, surface roughness and chip formation. Int. J. Mach. Tools Manuf **48**, 1613–1625 (2008). https://doi.org/10.1016/j.ijmachtools.2008.07.008
16. Manna, A., Bhattacharayya, B.: Influence of machining parameters on the machinability of particulate reinforced Al/SiC-MMC. Int. J. Adv. Manuf. Technol. **25**, 850–856 (2005). https://doi.org/10.1007/s00170-003-1917-2
17. Manna, A., Bhattacharayya, B.: A study on machinability of Al/SiC-MMC. J. Mater. Process. Technol. **140**, 711–716 (2003). https://doi.org/10.1016/S0924-0136(03)00905-1
18. El-Gallab, M.S., Sklad, M.P.: Machining of aluminum/silicon carbide particulate metal matrix composites: part IV. Residual stresses in the machined workpiece. J. Mater. Process. Technol. **152**, 23–34 (2004). https://doi.org/10.1016/j.jmatprotec.2004.01.061
19. Ozcatalbas, Y.: Investigation of the machinability behavior of Al4C3 reinforced Al- based composite produced by mechanical alloying technique. Compos. Sci. Technol. **63**, 53–61 (2003)
20. Palanikumar, K., Muthukrishnan, N., Hariprasad, K.S.: Surface roughness parameters optimization in machining A356/SiC/20p metal matrix composites by PCD tool using response surface methodology and desirability function. Mach. Sci. Technol. **12**, 529–545 (2008). https://doi.org/10.1080/10910340802518850
21. Muthukrishnan, N., Murugan, M., Prahlada Rao, K.: Machinability issues in turning of Al-SiC (10p) metal matrix composites. Int. J. Adv. Manuf. Technol. **39**, 211–218 (2008). https://doi.org/10.1007/s00170-007-1220-8
22. Basavarajappa, S., Chandramohan, G., Davim, J.P.: Some studies on drilling of hybrid metal matrix composites based on Taguchi techniques. J. Mater. Process. Technol. **196**, 332–338 (2008). https://doi.org/10.1016/j.jmatprotec.2007.05.043
23. Boswell, B., Islam, M.N., Davies, I.J., Pramanik, A.: Effect of machining parameters on the surface finish of a metal matrix composite under dry cutting conditions. Proc. Inst. Mech. Eng. Part B J. Eng. Manuf. **231**, 913–923 (2017). https://doi.org/10.1177/0954405415583776
24. Muthukrishnan, N., Davim, J.P.: Optimization of machining parameters of Al/SiC-MMC with ANOVA and ANN analysis. J. Mater. Process. Technol. **209**, 225–232 (2009). https://doi.org/10.1016/j.jmatprotec.2008.01.041
25. Dabade, U.A., Joshi, S.S., Balasubramaniam, R., Bhanuprasad, V.V.: Surface finish and integrity of machined surfaces on Al/SiCp composites. J. Mater. Process. Technol. **192–193**, 166–174 (2007). https://doi.org/10.1016/j.jmatprotec.2007.04.044
26. Kiliçkap, E., Çakir, O., Aksoy, M., Inan, A.: Study of tool wear and surface roughness in machining of homogenised SiC-p reinforced aluminium metal matrix composite. J. Mater. Process. Technol. **164–165**, 862–867 (2005). https://doi.org/10.1016/j.jmatprotec.2005.02.109
27. Kannan, S., Kishawy, H.A., Deiab, I.: Cutting forces and TEM analysis of the generated surface during machining metal matrix composites. J. Mater. Process. Technol. **209**, 2260–2269 (2009). https://doi.org/10.1016/j.jmatprotec.2008.05.025
28. Nicholls, C.J., Boswell, B., Davies, I.J., Islam, M.N.: Review of machining metal matrix composites. Int. J. Adv. Manuf. Technol. **90**, 2429–2441 (2017). https://doi.org/10.1007/s00170-016-9558-4

29. Sahin, Y.: The effects of various multilayer ceramic coatings on the wear of carbide cutting tools when machining metal matrix composites. Surf. Coatings Technol. **199**, 112–117 (2005). https://doi.org/10.1016/j.surfcoat.2005.01.048
30. Pedersen, W., Ramulu, M.: Facing SiCp/Mg metal matrix composites with carbide tools. J. Mater. Process. Technol. **172**, 417–423 (2006). https://doi.org/10.1016/j.jmatprotec.2005.07.016
31. Kannan, S., Kishawy, H.A., Balazinski, M.: Flank wear progression during machining metal matrix composites. J. Manuf. Sci. Eng. **128**, 787 (2006). https://doi.org/10.1115/1.2164508
32. Kadirgama, K., Abou-El-Hossein, K.A., Noor, M.M., et al.: Tool life and wear mechanism when machining Hastelloy C-22HS. Wear **270**, 258–268 (2011). https://doi.org/10.1016/j.wear.2010.10.067
33. Ciftci, I., Turker, M., Seker, U.: CBN cutting tool wear during machining of particulate reinforced MMCs. Wear **257**, 1041–1046 (2004). https://doi.org/10.1016/j.wear.2004.07.005
34. Hung, N.P., Yeo, H., Oon, B.E.: Effect of cutting fluid on the machinability of metal matri × composites. J. Mater. Process. Technol. **67**, 151–161 (1997)
35. Weinert, K., Lange, M.: Machining of magnesium matrix composites. Adv. Eng. Mater. **3**, 975–979 (2001). https://doi.org/10.1002/1527-2648(200112)3:12%3c975:AID-ADEM975%3e3.0.CO;2-L
36. Takács, M., Verö, B., Mészáros, I.: Micromilling of metallic materials. J. Mater. Process. Technol. **138**, 152–155 (2003)
37. Ozben, T., Kilickap, E., Çakir, O.: Investigation of mechanical and machinability properties of SiC particle reinforced Al-MMC. J. Mater. Process. Technol. **198**, 220–225 (2008). https://doi.org/10.1016/j.jmatprotec.2007.06.082
38. Yanming, Q., Zehua, Z.: Tool wear and its mechanism for cutting SiC particle-reinforced aluminium matrix composites. J. Mater. Process. Technol. **100**, 194–199 (2000)
39. Li, X., Seah, W.K.H.: Tool wear acceleration in relation to workpiece reinforcement percentage in cutting of metal matrix composites. Wear **247**, 161–171 (2001). https://doi.org/10.1016/S0043-1648(00)00524-X
40. Ciftci, I., Turker, M., Seker, U.: Evaluation of tool wear when machining SiCp-reinforced Al-2014 alloy matrix composites. Mater. Des. **25**, 251–255 (2004). https://doi.org/10.1016/j.matdes.2003.09.019
41. Heath, P.J.: Developments in applications of PCD tooling. J. Mater. Process. Technol. **116**, 31–38 (2001). https://doi.org/10.1016/S0924-0136(01)00837-8
42. Aramcharoen Mativenga PT, Yang S, A., Mativenga, P.T., Yang, S., et al.: Evaluation and selection of hard coatings for micro milling of hardened tool steel. Int. J. Mach. Tools Manuf **48**, 1578–1584 (2008). https://doi.org/10.1016/j.ijmachtools.2008.05.011
43. Narahari, P., Pai, B.C., Pillai, R.M.: Some aspects of machining cast Al-SiCp composites with conventional high speed steel and tungsten carbide tools. J. Mater. Eng. Perform. **8**, 538–542 (1999). https://doi.org/10.1007/s11665-999-0006-6
44. Hung, N.P., Boey, F.Y.C., Khor, K.A., et al.: Machinability of cast and powder-formed aluminum alloys reinforced with SiC particles. J. Mater. Process. Tech. **48**, 291–297 (1995). https://doi.org/10.1016/0924-0136(94)01661-J
45. Ghani, J., Haron, C., Kasim, M.: Wear mechanism of coated and uncoated carbide cutting tool in machining process. J. Mater. 1–7 (2015). https://doi.org/10.1557/jmr.2015.382
46. Sun, F., Wu, Z., Zhong, J., Chen, M.: High speed milling of SiC particle reinforced aluminum-based MMC with coated carbide inserts. Key Eng. Mater. **274–276**, 457–462 (2004). https://doi.org/10.4028/www.scientific.net/KEM.274-276.457
47. Quigley, O., Monaghan, J., O'Reilly, P.: Factors affecting the machinability of an A1/SiC metal-matrix composite. J. Mater. Process. Technol. **43**, 21–36 (1994)
48. Songmene, V., Balazinski, M.: Machinability of graphitic metal matrix composites as a function of reinforcing particles. CIRP Ann. Manuf. Technol. **48**, 77–80 (1999). https://doi.org/10.1016/S0007-8506(07)63135-7
49. Davim, J.P.: Diamond tool performance in machining metal-matrix composites. J. Mater. Process. Technol. **128**, 100–105 (2002). https://doi.org/10.1016/S0924-0136(02)00431-4

50. Andrewes, C.J.E., Feng, H., Lau, W.M.: Machining of an aluminum/SiC composite using diamond inserts. J. Mater. Process. Technol. **102**, 25–29 (2000)
51. Kremer, A., Devillez, A., Dominiak, S., et al.: Machinability of Al/SiC particulate metal-matrix composites under dry conditions with CVD diamond-coated carbide tools. Mach. Sci. Technol. **12**, 214–233 (2008). https://doi.org/10.1080/10910340802067494
52. Chou, Y.K., Liu, J.: CVD diamond tool performance in metal matrix composite machining. Surf. Coatings Technol. **200**, 1872–1878 (2005). https://doi.org/10.1016/j.surfcoat.2005.08.094
53. Ding, X., Liew, W.Y.H., Liu, X.D.: Evaluation of machining performance of MMC with PCBN and PCD tools. Wear **259**, 1225–1234 (2005). https://doi.org/10.1016/j.wear.2005.02.094
54. Hung, N.P., Boey, F.Y.C., Khor, K.A., et al.: Machinability of aluminum alloys reinforced with silicon carbide particulates. J. Mater. Process. Technol. **56**, 966–977 (1996). https://doi.org/10.1016/0924-0136(95)01908-1
55. Tomac, N., Tannessen, K., Rasch, F.O.: Machinability of particulate aluminium matrix composites. CIRP Ann. Manuf. Technol. **41**, 55–58 (1992). https://doi.org/10.1016/S0007-8506(07)61151-2
56. El-Gallab, M., Sklad, M.: Machining of Al/SiC particulate metal-matrix composites part I: tool performance. J. Mater. Process. Technol. **83**, 151–158 (1998). https://doi.org/10.1016/S0924-0136(98)00054-5
57. El-Gallab, M., Sklad, M.: Machining of Al/SiC particulate metal matrix composites. Part III: comprehensive tool wear models. J. Mater. Process. Technol. **101**, 10–20 (2000). https://doi.org/10.1016/S0924-0136(99)00351-9
58. Paulo Davim, J., Monteiro Baptista, A.: Relationship between cutting force and PCD cutting tool wear in machining silicon carbide reinforced aluminum. J. Mater. Process. Technol. **103**, 417–423 (2000). https://doi.org/10.1016/S0924-0136(00)00495-7
59. Muguthu, J.N., Dong, G., Ikua, B.: Optimization of machining parameters influencing machinability of Al2124SiCp (45%wt) metal matrix composite. J. Compos. Mater. **49**, 217–229 (2013). https://doi.org/10.1177/0021998313516141
60. Huang, S.T., Zhou, L., Chen, J., Xu, L.F.: Drilling of SiCp/Al metal matrix composites with polycrystalline diamond (PCD) tools. Mater. Manuf. Process. **27**, 1090–1094 (2012). https://doi.org/10.1080/10426914.2011.654152
61. Cheng, K., Huo, D.: Micro cutting: fundamentals and applications. John Wiley & Sons Ltd, Chichester, UK (2013)
62. Liu, X., DeVor, R.E., Kapoor, S.G., Ehmann, K.F.: The mechanics of machining at the microscale: assessment of the current state of the science. J. Manuf. Sci. Eng. **126**, 666 (2004). https://doi.org/10.1115/1.1813469
63. Ye, H.Z., Liu, X.Y.: Review of recent studies in magnesium matrix composites. J. Mater. Sci. **9**, 6153–6171 (2004). https://doi.org/10.1023/B:JMSC.0000043583.47148.31
64. Mazahery, A., Abdizadeh, H., Baharvandi, H.R.: Development of high-performance A356/nano-Al2O3 composites. Mater. Sci. Eng. A **518**, 61–64 (2009). https://doi.org/10.1016/j.msea.2009.04.014
65. Gupta, M., Wong, W.L.E.: An insight into processing and characteristics of magnesium based composites. In: Alderman, M., Manuel, M.V., Hort, N., Neelameggham, N.R. (eds.) Magnesium technology 2014, pp. 423–428. Springer International Publishing, Cham (2016)
66. El-Kady, E.Y.: The effect of machining parameters on the cutting forces, tool wear, and machined surface roughness of metal matrix nano composite material. Adv. Mater. **4**, 43 (2015). https://doi.org/10.11648/j.am.20150403.11
67. Gangadharan, K.V., Umashankar, K.S., Desai, V.: Machining characteristics of multiwall-CNT reinforced Al/Al-Si composites using recurrence quantification analysis. Jordan J. Mech. Ind. Eng. **5**, 345–351 (2011)
68. Sasimurugan, T., Palanikumar, K.: Experimental studies on machining characteristics of hybrid aluminium metal matrix composite and carbon nano tubes added hybrid aluminium metal matrix composite. Int. Conf. Nanosci. Eng. Technol. ICONSET **2011**, 159–162 (2011). https://doi.org/10.1109/ICONSET.2011.6167944

69. Basavarajappa, S., Davim, J.P.: Influence of graphite particles on surface roughness and chip formation studies in turning metal matrix composites. Mater. Res. **16**, 990–996 (2013). https://doi.org/10.1590/S1516-14392013005000098
70. Priyadarshi, D., Sharma, R.K.: Optimization for turning of Al-6061-SiC-Gr hybrid nanocomposites using response surface methodologies. Mater. Manuf. Process. **31**, 1342–1350 (2016). https://doi.org/10.1080/10426914.2015.1070427
71. Li, N., Zheng, Y.: Novel magnesium alloys developed for biomedical application: a review. J. Mater. Sci. Technol. **29**, 489–502 (2013). https://doi.org/10.1016/j.jmst.2013.02.005
72. Staiger, M.P., Pietak, A.M., Huadmai, J., Dias, G.: Magnesium and its alloys as orthopedic biomaterials: a review. Biomaterials **27**, 1728–1734 (2006). https://doi.org/10.1016/j.biomaterials.2005.10.003
73. Gupta, M., Wong, W.L.E.: Magnesium-based nanocomposites: lightweight materials of the future. Mater. Charact. **105**, 30–46 (2015). https://doi.org/10.1016/j.matchar.2015.04.015
74. Liu, J., China, B.S.: Experimental study and modeling of mechanical micro-machining of particle reinforced heterogeneous materials. PhD thesis, University of Central Florida (2011)
75. Liu, J., Li, J., Xu, C.: Cutting force prediction on micromilling magnesium metal matrix composites with nanoreinforcements. J. Micro. Nano-Manuf. **1**, (2013). https://doi.org/10.1115/1.4023286
76. Teng, X., Huo, D., Wong, E., et al.: Micro-machinability of nanoparticle-reinforced Mg-based MMCs: an experimental investigation. Int. J. Adv. Manuf. Technol. **87** (2016). https://doi.org/10.1007/s00170-016-8611-7
77. Teng, X., Huo, D., Wong, E., et al.: Micro-machinability of nanoparticle-reinforced Mg-based MMCs: an experimental investigation. Int. J. Adv. Manuf. Technol. 1–14 (2016). https://doi.org/10.1007/s00170-016-8611-7
78. Li, P., Oosterling, J.A.J., Hoogstrate, A.M., et al.: Design of micro square endmills for hard milling applications. Int. J. Adv. Manuf. Technol. **57**, 859–870 (2011). https://doi.org/10.1007/s00170-011-3330-6
79. Tansel, I., Rodriguez, O., Trujillo, M., et al.: Micro-end-milling—I. Wear and breakage. Int. J. Mach. Tools Manuf **38**, 1419–1436 (1998). https://doi.org/10.1016/S0890-6955(98)00015-7
80. Ucun, I., Aslantas, K., Bedir, F.: An experimental investigation of the effect of coating material on tool wear in micro milling of Inconel 718 super alloy. Wear **300**, 8–19 (2013). https://doi.org/10.1016/j.wear.2013.01.103
81. Teng, X., Huo, D., Shyha, I., et al.: An experimental study on tool wear behaviour in micro milling of nano Mg/Ti metal matrix composites. Int. J. Adv. Manuf. Technol. (2018). https://doi.org/10.1007/s00170-018-1672-z
82. Teng, X., Huo, D., Shyha, I., et al.: An experimental study on tool wear behaviour in micro milling of nano Mg/Ti metal matrix composites (2018). https://doi.org/10.1007/s00170-018-1672-z
83. Manna, A., Bhattacharyya, B.: Investigation for optimal parametric combination for achieving better surface finish during turning of Al/SiC-MMC. Int. J. Adv. Manuf. Technol. **23**, 658–665 (2004). https://doi.org/10.1007/s00170-003-1624-z
84. Ramaswami, R.: The effect of the built-up-edge(BUE) on the wear of cutting tools. Wear **18**, 1–10 (1971). https://doi.org/10.1016/0043-1648(71)90059-7

Non-conventional Machining of Metal Matrix Composites

Justin Dunleavey, Sundar Marimuthu, and Mohammad Antar

Abstract The machining of monolithic materials such as metals and alloys is a well-established process and is used extensively in a wide range of applications in many sectors of the aerospace, medical and automotive industries. However, metal matrix composites (MMCs) are particularly challenging due to the differences in the chemical and physical properties of the hard reinforcement and the metal matrix. Non-conventional machining (NCM) is an excellent tool for the processing of advanced materials such as metal matrix composites. This chapter provides an overview on the machining of metal matrix composites using a range of non-traditional manufacturing techniques including laser processing, electrical discharge machining, waterjet machining and selected others. Productivity and surface integrity aspects such as roughness and delamination are reviewed and discussed. The advantages and disadvantages against conventional methods are also discussed in detail.

1 Introduction

The machining of monolithic materials such as metals and alloys is a well-established process and is used extensively in a wide range of applications in many sectors of the aerospace, medical and automotive industries. However, metal matrix composites (MMCs) are particularly challenging due to the differences in the chemical and physical properties of the hard reinforcement and the metal matrix. Non-conventional machining (NCM) is an excellent tool for the processing of advanced materials such as metal matrix composites. This chapter provides an overview of the machining of metal matrix composites using a range of non-traditional manufacturing techniques including laser processing, electrical discharge machining, waterjet machining and selected others. Productivity and surface integrity aspects such as roughness and delamination are reviewed and discussed. The advantages and disadvantages of conventional methods are also discussed in detail.

J. Dunleavey (✉) · S. Marimuthu · M. Antar
The Manufacturing Technology Centre, Coventry CV7 9JU, UK
e-mail: Justin.Dunleavey@the-mtc.org

I. Shyha and D. Huo (eds.), *Advances in Machining of Composite Materials*,
Engineering Materials, https://doi.org/10.1007/978-3-030-71438-3_8

From a machining perspective, the key consideration in processing metal matrix composites is the distinct and discrete characteristics of the reinforcement within the effective primary material. While the most commonly encountered matrices such as aluminium, titanium, magnesium, cobalt and nickel are well understood in materials processing, the presence of reinforcement presents further challenges to non-conventional methods. In comparison to mechanical and physical attributes that dominate the tool-based processing of MMCs, management of the differences in electrical and thermal properties of the metallic matrices and the typically ceramic reinforcements are the main factors for non-conventional approaches.

1.1 MMC Material and Machining Characteristics

The Chapter "Nonconventional Machining Processes of Fibre Reinforced Polymer Composites" reviewed non-conventional machining of fibre reinforced polymers (FRPs). In comparison to FRPs and other plastic matrix composites (PMCs), general differences in the material characteristics of MMCs include:

- Increased ductility.
- Increased thermal and electrical conductivity.
- Increased range of operational temperatures (dependant on the alloy used).

These characteristics result in different machining considerations between PMCs and MMCs. The ability to handle increased thermal and electrical loads open up a range of opportunities for NCM processes that are limited in the processing of carbon fibre reinforced polymer (CFRP) and similar materials. While the heat from a laser is often sufficient to critically damage a plastic matrix through localized, asymmetrical and excessive burning, a metallic matrix can generally facilitate ample distribution of the thermal loading with its increased conductivity, specific heat and higher melting and boiling points.

The key challenges in relation to the traditional processing of metal matrix composites are similar to those encountered with reinforced plastics. These are listed below:

- Layer delamination
- Fibre pull-out/particle displacement
- Uncut fibres or unremoved particles
- Layer breakout
- Matrix damage (thermal damage or fracture)
- Reinforcement fracture
- Voids resulting from the unwanted removal of reinforcement.

Underlying the challenges of processing MMCs by either conventional means or otherwise is a generally low amount of research. According to an examination of available literature, fewer than 10 studies per year were conducted until 1993, with

20–40 publications each year between 1993 and 2006. Only in the period after 2006 has consistently high levels of research been conducted [1].

Progress has been further inhibited by a developing understanding of the fundamental behaviour of composite materials under the relevant machining conditions. The single shear plane cutting models that form the basis of the understanding of the monolithic material process are unsuitable for use with MMCs [2]. Few predictive models of MMCs processing exist, which can further limit the understanding and knowledge required for high quality and predictable machining [3].

Researching, understanding and optimization of the processing of MMCs by conventional or non-conventional means are expected to accelerate in line with the industrial uptake of these advanced materials. While there are currently some specialist applications, barriers to full exploitation exist in the form of high cost, immature supply chains, established alternatives and competition from PMCs.

In terms of the existing solutions in conventional machining methods, many of these have additional considerations based on ancillary processes and longevity—for example, high rates of tool wear, expensive tool materials and lubricant requirement. Among the advantages of non-conventional machining methods is a decreased need for consumables, which often include expensive and specialist tools with carbide tips, TiN coated HSS, cubic boron nitrate tools and PCD coatings, the effectiveness of which are still limited to short run production due to wear [4].

1.2 Non-conventional Machining of Composites

Non-conventional machining processes in the context of this chapter refers to methods in which a process that is primarily non-mechanical in terms of interaction energy used for material removal. This is in contrast to the shearing action that is present in most of the tool or other contact-based systems such as milling, turning or grinding. The alternatives to traditional tool-based methods include the application of thermal or electrical energy. Despite the highly kinetic and impact-based nature of processes such as waterjet machining, these are also considered non-conventional due to the use of a non-solid medium to deliver the necessary mechanical forces. In some instances, mechanical energy is applied—albeit with some assistance that is considered non-standard. An example of such assistance is ultrasonic vibration.

As mentioned above, a key factor for the use of a non-conventional process is the reduced influence of the characteristics of the reinforcement materials. With MMCs, these are generally a hard and brittle ceramic material which is taxing of machining tools in terms of wear. As will be discussed in further detail, NCM processes are based on the removal of the matrix with secondary expulsion of the reinforcement, or purely non-contact means that machine both constituent materials. In these circumstances, the challenges presented by the hardness of the reinforcements are reduced.

For example, the laser and electrical discharge machining processes represent thermal processing, while the chemical and electrochemical methods rely on the elemental breakdown of the workpiece. Neither relies on mechanical shearing energy

for the machining operations, and this represents a major alternative to tool-based operations. Thermal damage is less of a concern as the metallic matrices are conductive and allow generated heat to dissipate much better than plastic matrices. In most cases, the thermal or chemical breakdown of the matrix will occur more readily than the breakdown of the reinforcement.

The following non-conventional machining technologies are examined in this chapter:

- Laser drilling
- Waterjet guided laser drilling
- Electrical discharge machining
- Abrasive waterjet machining
- Chemical and electrochemical machining
- Ultrasonic and vibration-assisted machining.

2 Laser Processing

Multiple industries, including the aerospace and automotive sectors, are seeking novel lightweight materials and their fabrication technologies to reduce structural weight without compromising strength. At the same time, environment protection measures and the need for energy efficiency in transport methods are gaining increased attention. Particle reinforced aluminium metal matrix composites have huge potential in the automotive industry due to their lightweight and strength properties. This section discusses the laser drilling of silicon carbide (SiC) particle reinforced aluminium by pulsed laser and waterjet guided laser means. Experimental work, unless otherwise referenced, has been conducted by the authors.

2.1 Laser Drilling of Aluminium Metal Matrix Composites

For experiments in laser drilling of MMCs, a cast aluminium (Al) silicon carbide (SiC) metal matrix composite (Al MMC) of 2 mm thickness was used as the base material. The volume fraction of SiC was ~40%. Figure 1 shows the microstructure of the Al MMC discussed in this section.

As discussed by Marimuthu [5], of all the non-conventional machining processes, laser machining is considered to be the preferred technique for hole drilling due to its high productivity and its unique ability to drill holes in components at steep angles. Laser drilling in traditional materials, including metals and alloys, is extensively used in manufacturing industries to create holes of various sizes (0.25–1 mm) and shapes.

Depending on the hole size, shape and quality requirements, four types of laser drilling processes are widely used in industries. These include helical drilling, trepanning, single-pulse drilling and percussion drilling. Laser processing of composite materials is inherently challenging due to the immense difference in the thermal

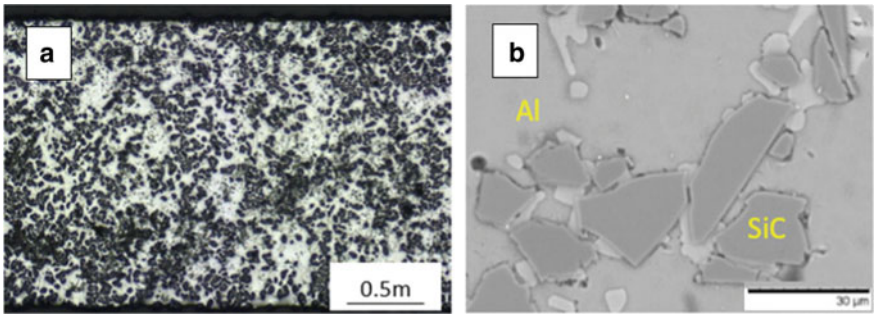

Fig. 1 Image showing the microstructure of the SiC reinforced Al MMC

properties of the matrix and the reinforcement [6]. To achieve better drilling quality for composites such as MMCs, it is vital to control the heat input and heat distribution [7] within and around the laser interaction zone.

Most of the laser drilling currently carried out in industries, either using percussion or trepan techniques, is performed using millisecond (ms) pulsed lasers that have a peak power density between $1e^6$ and $1e^9$ W/cm^2. As a thermal process, the millisecond laser drilling mechanism is based on heating, melting, vaporization and melt ejection. The percussion drilling technique is used for applications that require a large number of holes at high speed. However, it is associated with a number of adverse effects including irregular hole shapes, higher recast layer, higher dross at the exit and spatter over the top surface. Trepanning drilling is the most widely used drilling technique and is used for high-value components where the quality requirements are stringent; however, its material removal rate is slower than percussion drilling technique by a factor of five to ten.

The laser trepanning drilling discussed in this section was carried out using an IPG millisecond pulsed fibre laser. The fibre laser can operate at pulse durations ranging from 0.2 to 10 ms, with a maximum average power of 2 kW and a maximum peak power of 20 kW. The optical arrangement consists of a 120 mm collimator and a 150 mm focusing lens, which images the end-of-fibre beam to the workpiece surface.

Key requirements of the laser drilling process include minimal thermal damage (i.e. recast layer or heat-affected zone (HAZ)), minimum dross at the hole exit, minimum spatter over the hole entrance, high hole circularity, consistent hole profile and high drilling speed. Figure 2 shows the influence of speed on hole quality for constant frequency and energy. As can be seen from this image, low speed produces much better drilling performance in terms of recast layer thickness, hole circularity, and hole profile. This is attributed to the fact that specific energy increases with reduced scanning speed. The specific energy for the speed of 250 mm/min and 750 mm/min was 480 J/mm and 160 J/mm, respectively. Higher specific energy,

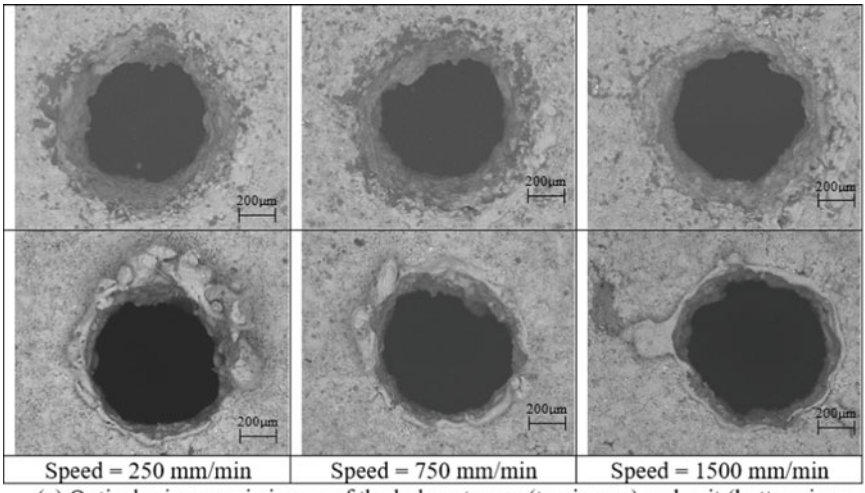

(a) Optical microscopic image of the hole entrance (top image) and exit (bottom image)

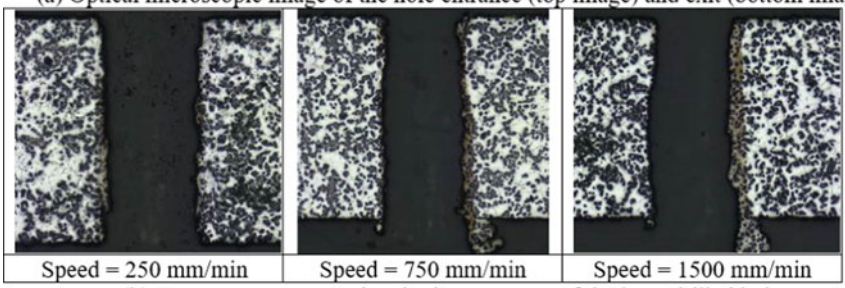

(b) Transverse cross-sectional microstructure of the laser drilled holes

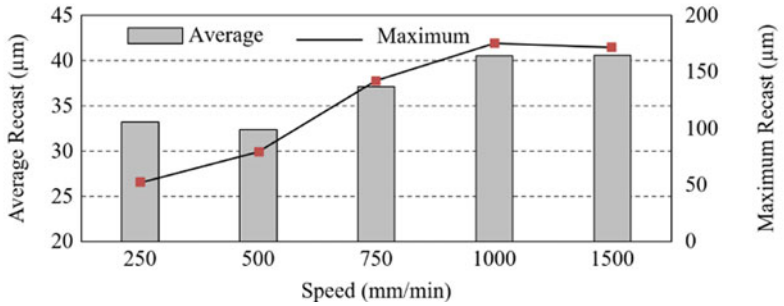

Fig. 2 Effect of trepanning speed on laser drilling hole quality (Energy = 20 J, No. of orbit = 1, pulse duration = 1 ms, Frequency = 100 Hz)

along with high pressure assist gas jet, helps to efficiently remove the recast layer and the dross at the hole exit.

Assist gas composition has a significant effect on laser drilling characteristics, and it also represents a significant proportion of the laser drilling cost. As noticed from Fig. 3, the holes drilled with argon assist gas demonstrated the lowest recast layer thickness, followed by nitrogen assist gas. Both oxygen and compressed air resulted in excessive recast layer and irregular hole profile, possibly due to the reactive nature of these gases with aluminium at high temperature.

Figure 4 shows microstructural images of the laser trepanned drilled Al MMC sample. The figure shows the influence of ms laser drilling on SiC particles and the melt ejection characteristics. The SiC particles within the recast layer (Fig. 4a, b: material that was melted but not removed), spatter (Fig. 4c), and dross (Fig. 4f: material that was melted and ejected from the hole) are very similar to the SiC in the base material (Fig. 4d). No melting or degradation of SiC particles was observed in Fig. 4, which suggests that the SiC particles do not absorb the laser beam and are removed along with the molten aluminium by melt ejection. This is a unique

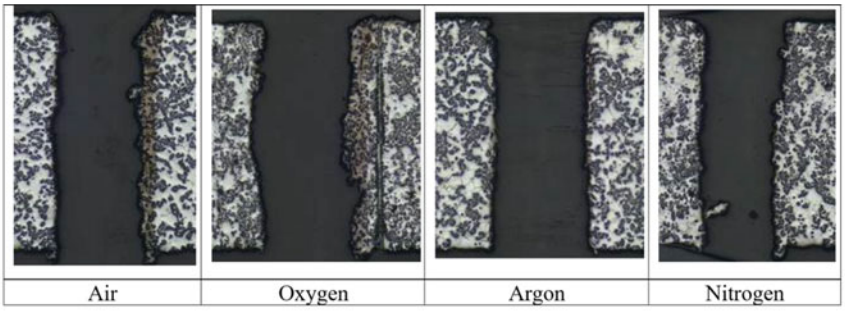

(a) Transverse cross-sectional microstructure of the laser drilled holes

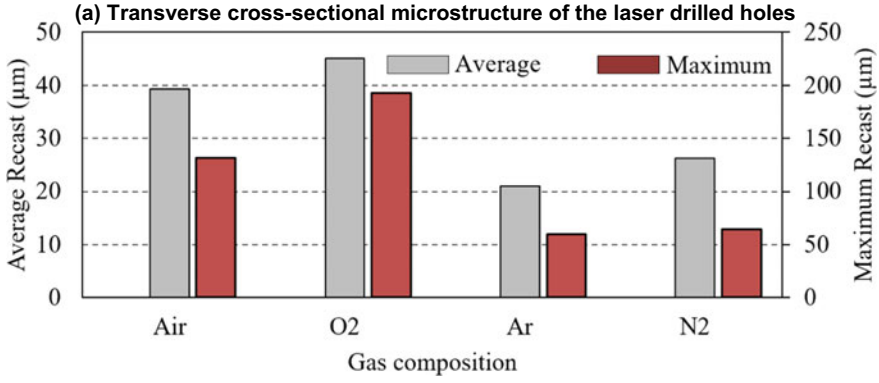

(b) Thickness of average and maximum recast layer

Fig. 3 Effect of assist gas composition on laser drilling hole quality (Energy = 20 J, Speed = 750 mm/min, pulse duration = 1 ms, Frequency = 100 Hz, No. of orbit = 1)

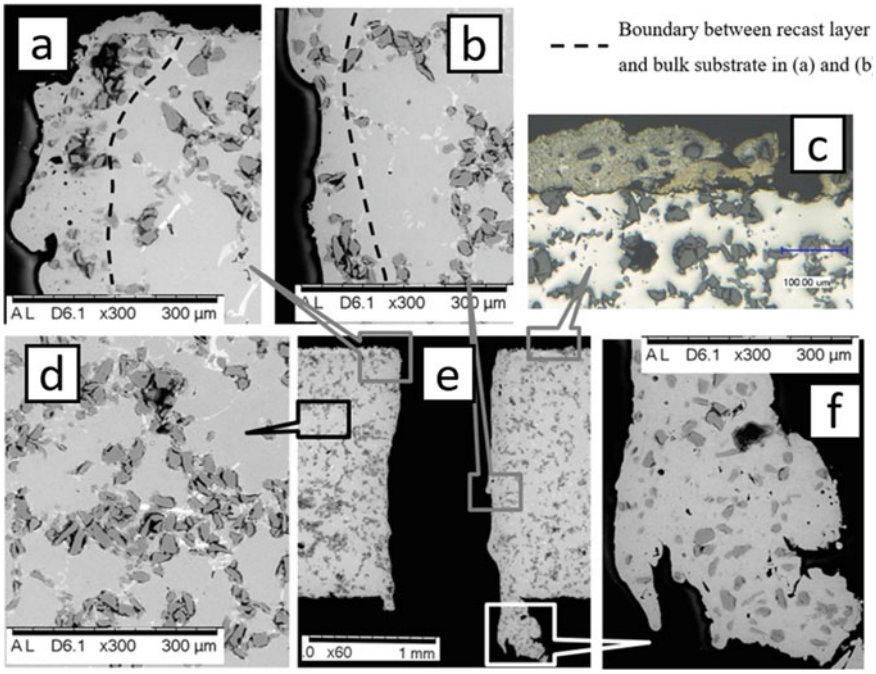

Fig. 4 Image showing the microstructure of the laser drilled hole at various region (**a**: Recast layer; **b**: Recast layer; **c**: Spatter; **d**: Unaffected parent material; **e**: A full cross-sectional view of the laser drilled hole; **f**: Dross) (Energy = 20 J, Speed = 750 mm/min, pulse duration = 1 ms, Frequency = 100 Hz, No of orbit = 1)

observation that demonstrates the advantage of millisecond laser drilling of MMCs, which is not observed in applications in laser material processing of carbon fibre composites [8].

From Fig. 5, the initial laser interaction with the Al MMC resulted in a bright plasma plume, which corresponds to the vaporization of the top melt layer (at 109 μs) followed by the melt-ejection. Melt-ejection from the hole entrance (Fig. 5) is driven mostly by vapour pressure that is being generated due to the vaporization of aluminium metal. As seen in this image, during the melt ejection process, the material first moves outwards and then upwards before being ejected out of the laser irradiation zone. The depth of the hole increases as the material (both molten aluminium and SiC particles) continues to be removed from the hole. The laser drilled hole quality is directly related to the melt ejection process. Inefficient melt ejection can result in excessive heat affected zones and recast layer, which was not the case with ms laser drilling of Al MMC.

Both the initial vaporization and the melt ejection process were more violent in Al MMC laser drilling when the process was repeated on the monolithic equivalent material. This could be attributed to the fact that the Al MMC behaves like a porous medium as SiC is transparent to the 1070 nm fibre laser beam. The increase in melt

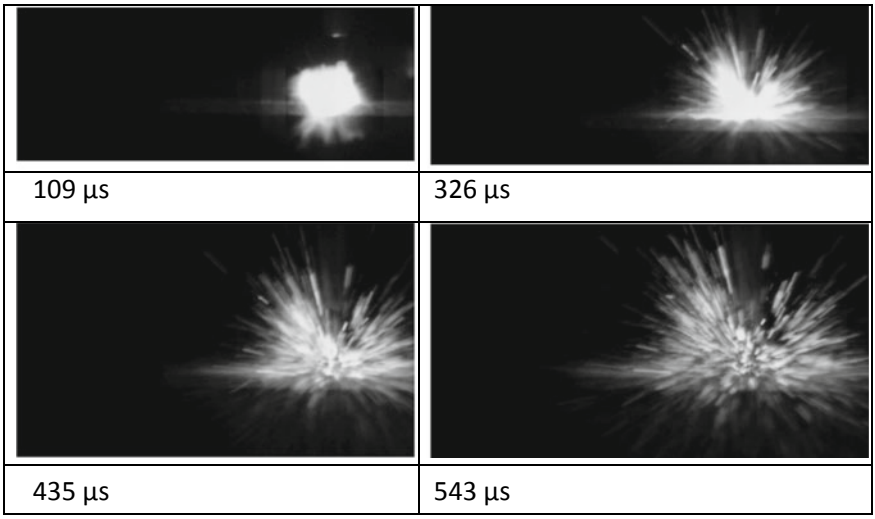

Fig. 5 High-speed photographic images of the millisecond pulse laser drilling of 2 mm thick Al MMC and 2 mm thick isotropic Al alloy

ejection is attributed to the ~40% volume fraction of SiC, which does not absorb the laser beam but is ejected as solid particles with the molten aluminium. This is one of the main reasons for increased efficiency in laser drilling of Al MMC compared to the non-reinforced alloy. The peak power of 2.5 kW, which produced better drilling performance, is much lower in comparison to the optimal range of parameters reported in previous investigations for drilling non-reinforced alloys [5].

Good internal surface finish is associated with positive effects in the overall performance of laser drilled components. Figure 6 shows the effect of laser input parameters on hole surface roughness. Laser parameters have a significant effect on hole surface finish, and this effect seems to be more significant in the drilling of composites like MMC than in laser drilling of metals or alloys, as observed by Marimuthu et al. [9]. As noticed from Fig. 6, the roughness of the hole increases as average laser power increases. The hole surface seems to have a metallic finish at low average power (500 W) and an abrasive like surface condition at higher average power (1000 W). The abrasive like structure at high power is attributed to the increase in the concentration of SiC particles along the surface of the laser drilled hole. At high average power, more material (Al) is melted, and due to the melt pool convection, the SiC particles migrate to the outer edge of the hole (close to the mushy zone of the melt), increasing the surface roughness of the drilled hole.

Figure 7 shows the resulting microstructure from the ms laser interaction with the Al MMC for one to three laser pulses, with a pulse energy of 20 J, pulse duration of 1 ms and frequency of 100 Hz. This figure shows the evolution of the hole and the melt ejection from the hole. As noticed in Fig. 7a, material removal is not linear in

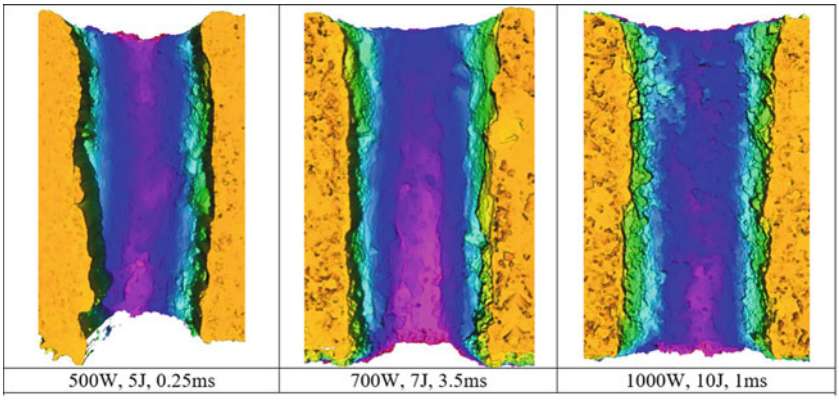

Fig. 6 Effect of laser parameters on hole surface finish (Speed = 750 mm/min, Frequency = 100 Hz, No of orbit = 1)

relation to the number of pulses. The melt is removed during the first two pulses by vaporization induced melt ejection, but the vaporization based melt ejection was not sufficient to remove all of the molten material. Often the role of melt pool motion is overlooked in laser based material removal processes like laser drilling or cutting. This is true for laser drilling of metals and alloys; however, it seems that melt pool motion has a significant influence on the laser drilling of MMCs. From Fig. 7a, after two pulses a slightly higher concentration of SiC particles was observed in the recast material, which indicates the significance of melt pool motion during the laser drilling of the material.

It seems there was some movement of molten material from the laser interaction zone other than that of the melt ejection process. The melt ejection process, as shown in Fig. 5 (images from high speed camera), is responsible for most of the material removal through the hole entrance and exit. However, as seen in Fig. 7b, there was some steady-state movement of melt from the laser-material interaction zone to the hole periphery (top surface), which was deposited around the top edge of the hole in addition to the melt spatter. Another noticeable inference from Fig. 7b is that the SiC particles were ejected without melting or decomposition.

2.2 Water-Jet Guided Laser Drilling of Aluminium Metal Matrix Composites

Water-jet guided (WJG) laser machining was first demonstrated by Richerzhagen in 1994 [10] and has securely established itself in various industrial applications, especially for the machining of advanced materials. The waterjet guided laser process is

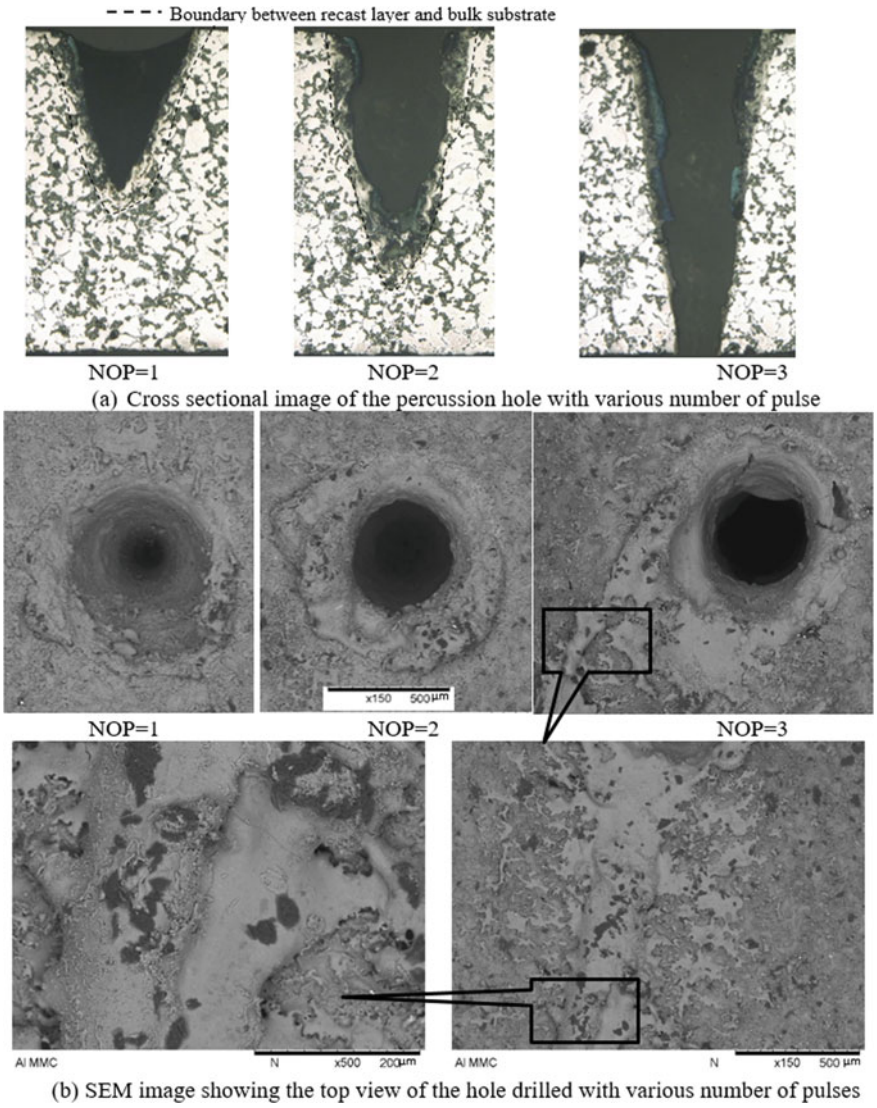

Fig. 7 Image showing the hole formation characterizes during millisecond pulse laser drilling of Al MMC (Energy = 20 J; pulse duration = 1 ms, Frequency = 100 Hz)

based on the concept of using a pressurized micro waterjet as a laser beam guide., The laser beam is guided through the pressurized waterjet by means of total internal reflection (at the air/water interface). This is similar to a laser beam travelling through multimode glass fibre. A Q-switch diode pumped solid-state laser operating at nanosecond pulse durations, and a wavelength of 532 nm is commonly used as the laser source

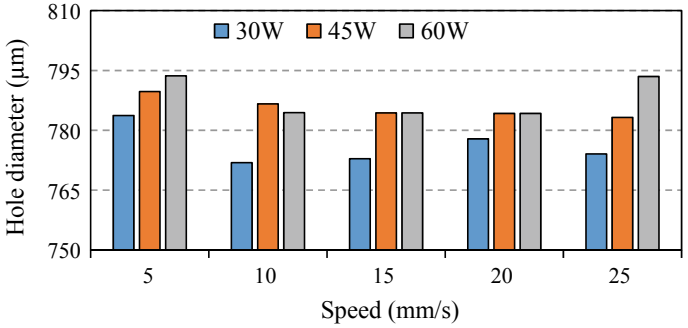

Fig. 8 Effect of trepanning speed and average laser power on hole diameter during WJG laser drilling (pulse duration = 200 ns, waterjet pressure = 300 bar and frequency = 800 Hz)

for WJG laser process. The waterjet also offers additional benefits including efficient removal of melted material and reduced thermal impact.

The cast aluminium (Al) silicon carbide (SiC) metal matrix composite (Al MMC) to be discussed in this section is same as one explained in Sect. 2.1, Fig. 1. Figure 8 shows the influence of laser average power and trepanning speed on the average hole diameter. As seen from the graph, the increase in laser power results in increased hole diameter. Here, the heat generation at the laser-material interaction zone increases, which ultimately increases the hole diameter. Though small, a reverse effect was noticed with the increase in speed, i.e. the increase in speed slightly decreases the hole diameter. With the increase in scanning speed, the number of pulses per position (or pulse offset) reduces, which reduces the total heat load to the material (Figs. 9 and 10).

Figure 9 shows the optical microscopic image of the hole entrance and exit for drilling at various speeds and laser powers. Irrespective of laser power and speed, WJG laser drilling produced holes of excellent circularity. In general, no spatter nor dross nor hole erosion was observed at the hole entrance and exit. Figure 10 shows the hole taper for drilling at various laser speeds and powers. As expected, both speed and power influence the hole taper. There is a slight increase in hole taper with the increase in speed and laser power. However, the values of the hole taper were extremely low compared to conventional laser drilling, in which a hole taper of 1.5–3° is reported for fibre laser drilling of Al MMC [11]. The extremely low taper observed with WJG laser drilling is attributed to the fact that the beam propagates within the waterjet.

Figure 11 shows cross-sectional images of the WJG laser drilled holes for various laser powers. Irrespective of laser drilling parameters, no thermal damage such as recast layer, oxide layer, heat affect zone or bell mouth were observed during the WJG laser drilling process. The nanosecond laser pulse width combined with the waterjet aided in avoiding the thermal defects, which are commonly observed in the conventional laser drilling processes. The only noticeable defect from the WJG laser drilling process is the hole taper. Hole taper was observed either at high scanning

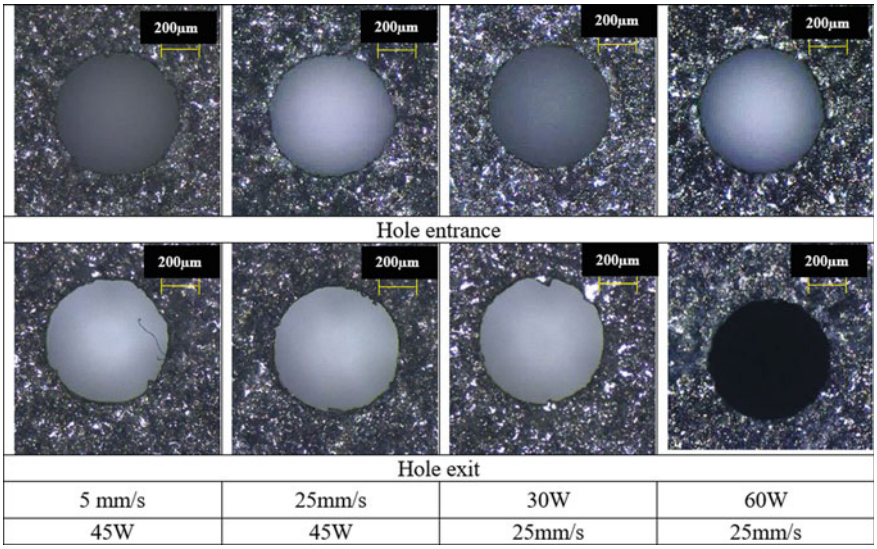

Fig. 9 Optical microscopic image showing the hole entrance and exit for various trepanning speeds and power during WJG laser drilling (pulse duration = 200 ns, waterjet pressure = 300 bar and frequency = 800 Hz)

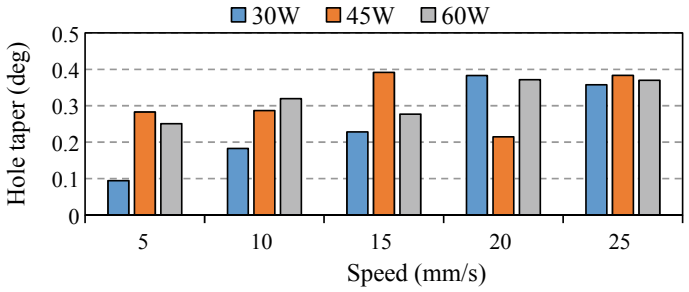

Fig. 10 Effect of trepanning speed and average laser power on hole taper during WJG laser drilling (pulse duration = 200 ns, waterjet pressure = 300 bar and frequency = 800 Hz)

speed or at low laser power, both of which are attributed to the insufficient energy during the drilling process. As noticed from the figure, the microstructure of the WJG laser drilled hole surface is similar to the base material with no noticeable heat affected zone, recast layer or oxide layer.

Figure 12 shows the influence of laser average power and trepanning speed on the surface roughness of the internal hole profile. The top image shows the isometric colour map of the internal hole surface obtained using an Alicona infinite focus measurement system. From the graph, the scanning speed of 5 mm/min shows relatively higher roughness compared to other scanning speeds. This should be due to

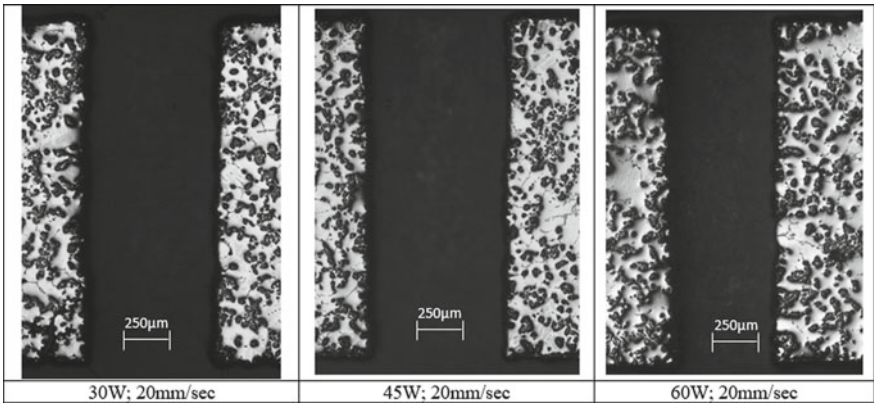

Fig. 11 Microscopic image showing the hole cross-sections for various laser powers during WJG laser drilling (pulse duration = 200 ns, waterjet pressure = 300 bar and frequency = 800 Hz)

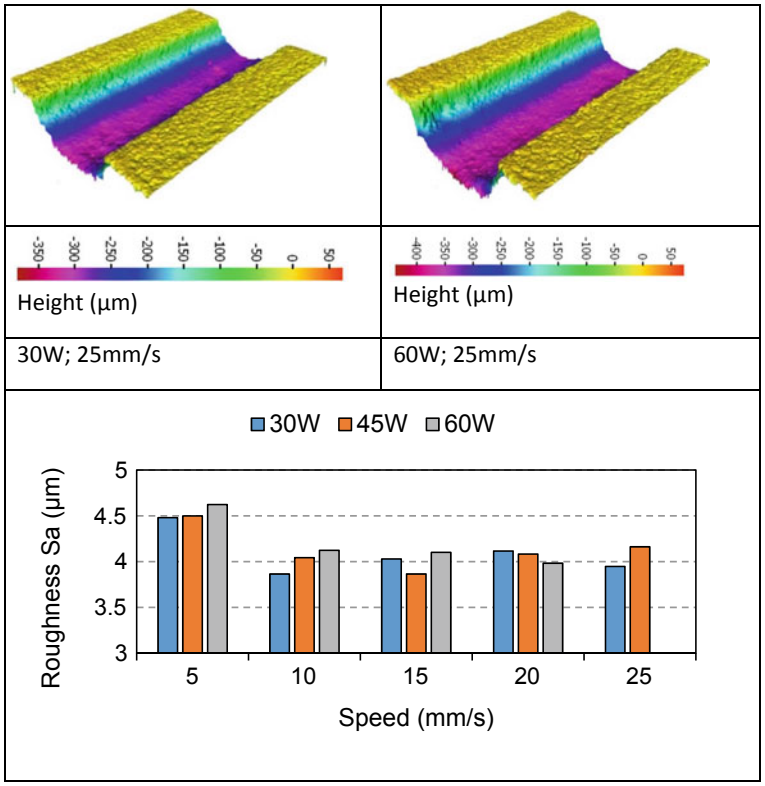

Fig. 12 Effect of trepanning speed and average laser power on hole roughness during WJG laser drilling (pulse duration = 200 ns, waterjet pressure = 300 bar and frequency = 800 Hz)

the high heat input at reduced speed, which leads to coarse ablation of the material and slightly higher surface roughness. Overall, laser power has minimal impact on the hole surface roughness.

When comparing the millisecond pulsed and waterjet guided laser drilling systems, Fig. 13 shows images of the Al MMC holes obtained in these processes. From Fig. 13, the material removal characteristic of millisecond laser drilling seems to be melting, followed by melt ejection. Also, due to melt pool convection, no evidence of SiC particles was observed at the hole surface. It seems due to the melt pool convection [12], the SiC particles have migrated to the subsurface of the melt pool. On the contrary, the surface condition of WJG laser-drilled Al MMC seems to be like a cold-machined [13] surface condition, i.e., there is no visible evidence of Al melting or SiC redistribution.

In summary, millisecond/continuous wave laser processing of Al MMC is readily capable of rapidly drilling particulate MMCs but tends to result in significant thermal damage. During the laser drilling of Al MMC, the SiC particles are ejected un-melted along with the molten aluminium, which makes the drilling process more efficient

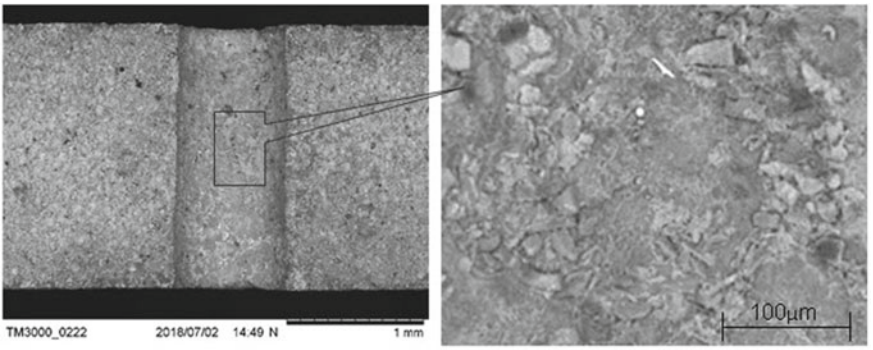

Fig. 13 Scanning electron microscope (SEM) image showing the hole surface characteristic of WJG laser drilling process (20 mm/s; 45 W)

compared to laser drilling of isotropic materials. Thus, less energy and lower peak power are required. In addition, trepanning speeds of up to 1000 mm/min can be achieved without compromising the drilling quality, which represents a significant increase in speed in comparison to the drilling of monolithic metals and alloys. Waterjet guided laser drilling appears to be an appropriate choice for advanced materials like Al MMCs. During the WJG laser drilling/cutting of Al MMC, the material is removed by cold ablation, without leaving any residual melt layer within the bulk material. Both matrix and reinforcement particles are removed by the same process, similar to that of cold ablation. However, the process is slow in comparison to the millisecond/continuous wave laser processing.

3 Electrical Discharge Machining

The material removal mechanism of electrical discharge machining (EDM) depends on the conductivity of the metal matrix and tool electrode, and the opposing electrical polarity of these two elements. Separation of the tool electrode and workpiece by a non-conducting medium is also vital. These factors facilitate the flow of electrons into the non-conducting medium, which results in the formation of the spark that is the primary source of the machining energy. This section describes the EDM of particle and fibre reinforced MMCs. Experimental work on SiC particle reinforced aluminium and alumina fibre reinforced aluminium, unless otherwise referenced, has been conducted by the authors.

EDM is an established technology for the machining of several common MMC matrix materials. While traditionally reserved for hard, brittle, or otherwise difficult-to-machine components, it is also well equipped for aluminium—the most common matrix material in MMCs. Occasionally EDM would be used on monolithic aluminium alloys if intricate features or deep, narrow holes were required. EDM is commonly used on materials such as titanium alloys, nickel superalloys and refractory metals.

While the matrix materials are readily conductive, the most common reinforcement elements encountered in metal matric composites have an electrical conductivity that is prohibitive to the EDM process. These values may exceed the limit of EDM capability. One exception is the electric resistivity of reasonably conductive carbon fibres—these fibres are the basis of the spark formation in carbon fibre reinforced polymer processing by EDM. However, carbon fibre reinforcements are not commonly encountered in traditional metal matrix composites—sandwich structures of CFRP and aluminium layers are common.

Generally, EDM can be successfully applied to single-phase ceramics, cermets, and ceramic/matrix composites, as far as they exhibit an electrical resistivity lower than 100–300 Ω cm [14]. Additionally, the hardness of the reinforcement material is near irrelevant—matrix conduciveness and the relative amount of it are the main considerations.

While the EDM process and parameters for monolithic metal materials are well understood and have been refined to provide the capability of producing accurate machining actions with high surface integrity, the volume of research for MMCs is lower.

3.1 EDM of Particulate Reinforced Metals

Existing research indicates that the EDM processing of PMMCs is moderately uninhibited by the reinforcement materials, as long as the percentage of reinforcement is sufficiently low. In a comparative examination between unreinforced Al356 aluminium alloy and a SiC particle reinforced Al356 alloy (40% vol) a two-step process using industrially available parameters for aluminium was performed in order to gauge the effects of the reinforcement on a WEDM machining process. The two-step process involved an initial cut followed by additional passes for the improvement of surface finish.

In terms of speed, the initial cutting cycle was quicker in the MMC, taking only 59% of the time taken to cut the unreinforced alloy. The finishing passes, however, were some seven times longer in duration, giving a complete process for the MMC that was ~2.5 longer. The increase in speed in the initial cutting is likely due to the forceful expulsion of particles when using the more aggressive parameters. As the melting point of the reinforcement is significantly higher than that of the matrix, they were likely expulsed whole along with the molten aluminium, resulting in a more efficient removal process. While the EDM plasma region temperature is estimated at 8,000–12,000 °C (sufficiently high for melting/vaporization of SiC, the reinforcement) the much lower temperature of aluminium alloys suggests that the rate of machining and melt depth will be much higher in this phase of the material. This theory of the melting of the matrix and dislodgement of the particles from the interface by dielectric flushing is also raised by Vishwakarma [15] in the EDM machining of Al–5% SiC–5% B4C and Al–5% SiC–5% glass prepared by stir casting.

Conversely, the extension of the finishing phases is likely due to surface level or near-surface level SiC particles. As these are less conductive than aluminium, the interface to be machined becomes less conductive as there is less material that will readily spark under the finishing parameter conditions. Ramulu also outlines the idea of surface-level particles shielding the matrix for reduced material removal rate (MRR) in a review of EDM processing of SiC reinforced alloys [16].

No significant difference in resultant surface roughness was observed between the aluminium alloy and MMC. However, the recast layer was higher in the MMC. Other authors have commented on the low influence of SiC particulate reinforcement in surface roughness—however, this was not as widely observed when working with alumina reinforcements [17].

Workpieces may be prone to irregularities directly related to particulate reinforcement, but the observances of these were rare. One example is the excessive loss of material, which is believed to be due to particle clusters near the surface (Fig. 14).

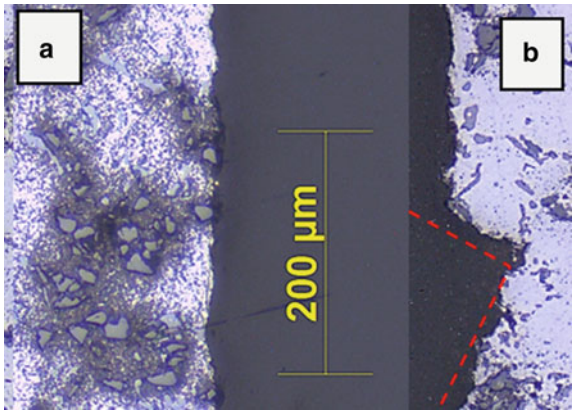

Fig. 14 Kerf detail of WEDM cut SiC reinforced Al356 alloy. Shown are a cluster of particles near surface level (**a**) and a section of cut material in which a larger mass of material has been removed (**b**)

The machining energy is believed to have been sufficient to remove the cluster, taking with it the surrounding matrix.

Examining surface morphology, the wire EDM cut aluminium alloys demonstrated large, smooth craters, even during the coarse machining parameter sets. The appearance of the MMC was similar for the roughing parameters used. With finishing parameters, SiC particles are visible on the workpiece surface and have disrupted the formation of regular craters (Fig. 15).

Other works have examined the effect of wire material in the cutting of MMCs. Patil [18] examined the use of plain brass and brass coated copper wires in cutting an A359/SiCp composite. The study reports a 58% improvement in process speed with the use of the coated wire. This could be attributed to the higher electrical conductivity of the diffusion annealed wire due to its copper core, combined with the low vapour point temperature zinc on the wire surface. The electrical conductivity of the wire electrode is an important factor in the WEDM process, affecting electrical discharge current peak value, the time required to reach the peak current, and consequently the machining characteristics such as material removal rate (cutting rate), surface finish and kerf width.

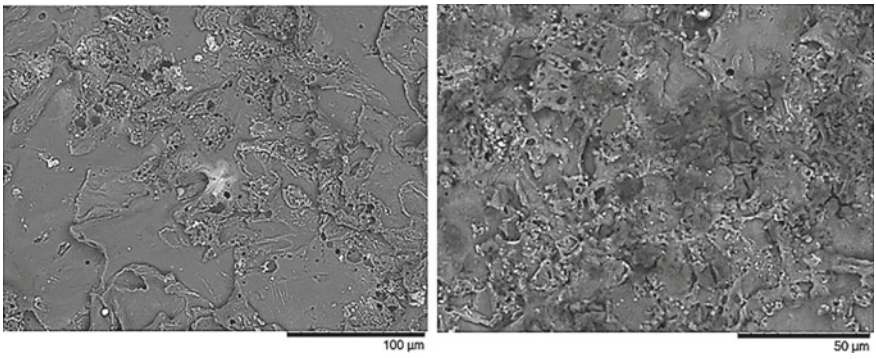

Fig. 15 SEM images of WEDM cut AL356 (L) and 40% volume SiC reinforced Al 356 (R)

3.2 Die-Sink EDM of Particle Reinforced Metals

Most of the existing research in EDM processing of MMCs is based on the die-sink method. Even when fibre reinforced composites are considered, the die-sink method is preferred due to the propensity of wire breakages resulting from the continuous ceramic fibres.

In a comparative study on SiC particle reinforced Al356 alloy (40% vol) and its unreinforced equivalent using industrially available parameters for aluminium, the presence of reinforcement extended the machining process duration by 60% and 32% with the use of graphite and copper electrodes respectively. In these instances, a 3.2 μm Ra surface finish target was applied. With a 0.8 μm Ra target the process duration for the MMCs was extended by 20% with graphite electrodes. In contrast, with copper electrodes, the duration for machining the monolithic alloy and MMC were roughly equivalent. Surface roughness was approximately 0.3 μm higher in the MMCs throughout. Recast layer thicknesses in the MMCs, and monolithic alloys were similar when machined with graphite, whereas recast was roughly doubled in the MMC with the use of copper tools.

The presence of the ceramic particles prohibited the formation of regular EDM craters, leaving irregular surfaces. Lower target surface roughness resulted in increased amounts of surface-level reinforcement particles as gentler parameters were applied. In Fig. 16, the AlSiC material shows an irregular surface in comparison to the regular craters seen in the Al356 material. Emerging SiC particles are highlighted in broken lines.

Recast was observed to be porous when in proximity to the SiC particles. The presumption is that the molten material that would under normal circumstance be recast is not able to form as readily on the ceramic particles, or that the emerging low conductivity SiC particles hinder the regular spark formation at surface level (Figs. 17 and 18).

Nanimina [16] investigated the die-sink EDM of a 30 vol% alumina particle reinforced aluminium composite, examining responses to parameters changes in the MMC and monolithic equivalent. It was reported that increases in peak current resulted in a greater material removal rate in both materials, but that the MRR for the standard alloy increased more rapidly. Low current (<10 amps) resulted in a similar MRR between both materials.

A similar trend was noted for pulse on time, however, the MRR was consistently higher for the monolithic material in the ranges tested, with the greatest difference in MRR seen at approximately 100 μs. The effects of increases to pulse off time resulted in MRR decreases. In both cases the MRR for the standard alloy was routinely higher, but both observed a similar trend of a rapid decrease as the off time increased to 50 μm, with a reduced effect observed with further off time increases.

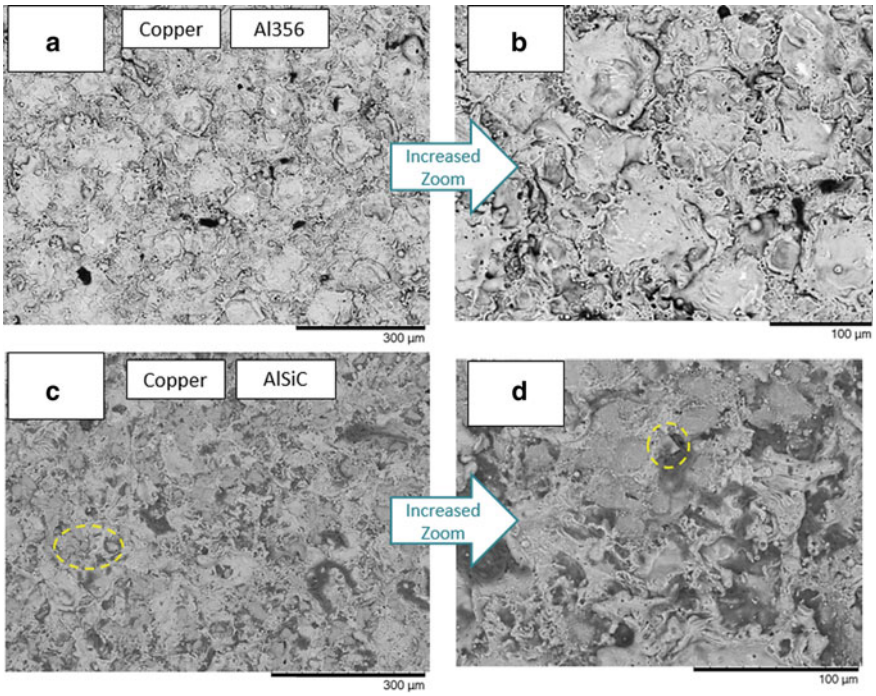

Fig. 16 SEM images of Al356 (**a**, **b**) and AlSiC MMC (**c**, **d**) die-sink EDM machined using copper electrodes

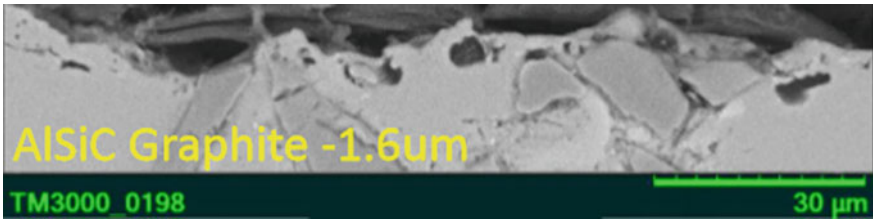

Fig. 17 Recast layer in a cross section image of AlSiC MMC machined with a graphite electrode

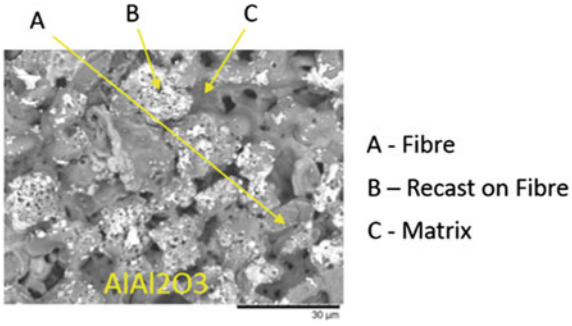

Fig. 18 WEDM cut Al-Al_2O_3 showing fibre, matrix and recast layer

Tooling wear rate (TWR) was also examined under the conditions outlined above. Wear rate was lower for the MMC at lower peak currents but normalised across both at higher currents. Tool wear observed when machining the MMC was more responsive in relation to changes in pulse duration, whereas wear seen when working the monolithic Al6061 was more stable, with the exception of operating at pulse off times lower than 10 μs.

3.3 EDM of Fibre Reinforced Metals

EDM processing of fibre reinforced metals is challenging due to the more consolidated and continuous nature of the reinforcement. In a comparative study between an alumina fibre reinforced aluminium and its monolithic equivalent, the use of established industrial parameters for WEDM was trialled on the MMC and monolithic equivalent. The process involved one set of initial cuts (roughing) and further finishing cuts to improve surface finish (finishing).

Process speed for the initial cut was much lower in the WEDM cutting of the MMC. Speeds of 5.17 mm/min were recorded when cutting the monolithic alloy, reducing to 0.16 mm/min when cutting in the cross fibre direction of the MMC. Both samples were 4 mm thick. Roughness values were similar with roughing parameter sets at 3 μm Ra, but in finishing the values obtained for the MMC were much higher—5.6 μm versus 3 μm.

The increase in surface roughness is likely due to the material removal mechanism. The electrical discharges are reliant on the aluminium matrix. While the fibres may be vaporized or melted, the surfaces observed in the cross section imply that there is also a degree of brittle fracture. The pressure from the vaporization of the dielectric and matrix and collapse of the plasma channels is the likely cause. Fractured sections of the fibre can be seen embedded in the rough cut surface (Fig. 19, shown in broken lines).

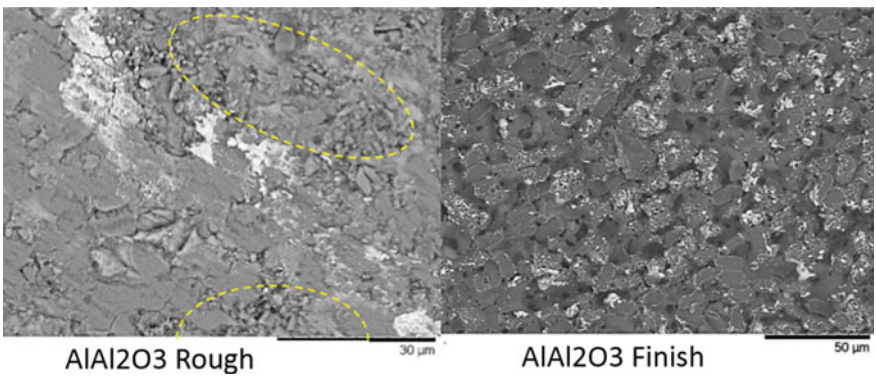

Fig. 19 Aluminium reinforced with an aluminium fibre cut by WEDM using roughing parameters (L) and finishing parameters (R)

The rough cuts are likely to have deposited a high level of recast, coating the fibres and leaving a reasonably smooth surface. The finish cut would then erode the recast deposited on the fibres while preserving the fibres themselves. Nearby aluminium, with its lower melting point, would be removed, leaving the fibres exposed and increasing the roughness.

Ramulu and Taya [16] investigated the machinability of whisker reinforced aluminium MMCs. Aluminium matrix composites with 15 and 25 vol% SiC whisker/2124 were die-sink EDM processed using copper and brass tools. It was found that the material removal rate increases at higher current, but that material removal rate was negatively affected by increased whisker content. Additionally, micro-hardness tests on SiCw/Al composite have revealed that the machining causes surface softening at slower cutting speed. It was also found that higher cutting speed results in micro-damage in the surface and sub-surface area. Material removal rate obtained by using a copper electrode was 5–10% less than that of obtained when using the brass electrode.

Although reliant on the metallic matrix, the EDM process is readily capable of cutting particulate MMCs. When targeting lower surface roughness, the machining duration is increased, especially at high reinforcement concentrations. Parameters for monolithic alloys tend to provide satisfactory results, although parameter optimizations have been performed on aluminium MMCs. Generally, die-sink EDM is preferred for fibre MMCs due to wire breakages and slow machining with WEDM. With both methods, when smooth surfaces finishes are desired there tends to be surface-level reinforcement as low energy sparks strip away the matrix material. Most of the published work is on SiC reinforced metal matrix composites. Not as much work is reported on Al_2O_3 reinforced MMCs.

4 Abrasive Waterjet Machining

Waterjet machining uses a high-pressure, high-velocity stream of water that cuts through workpiece material. High pressure pumps and specialist nozzles allow the stream to gain sufficient kinetic energy to remove material from surfaces it impacts. Abrasive waterjet machining (AWJM) or abrasive jet machining (AJM) incorporates an abrasive into the stream which increases its kinetic and erosive potential. Abrasive waterjet can be used to cut almost all metallic or ceramic engineering materials. The cutting of MMC is well established and common, especially in thicker material sections that would present issues to other cutting technologies such as laser or mechanical cutting.

4.1 Material Removal Mechanism

The material removal mechanism of AWJM is complex and composed of multiple modes. Initially, as the jet strikes, there is material removal by compressive failure. At the impact point, the fluid pressure exceeds the local compressive strength leading to localized failure and material removal [17]. As the jet spreads and flows outward after impact, erosive shearing takes place. After this initial action, as the kerf is established, the kerf walls are exposed to more erosive shearing, leading to gradual deformation wear of the kerf walls [19].

There are some other differences when the material characteristics of the workpiece are considered. For particularly ductile materials, material removal is characterized by more plastic deformation. With more brittle materials, fracturing becomes the common mechanism. Taken independently, the metallic matrix material in MMCs are more prone to the erosive shearing, while the ceramic reinforcements are largely machined by progressive crack propagation and spontaneous fracturing [20].

AWJM is an established technology for the cutting of many common MMC matrix materials, including aluminium and titanium. Process variables include abrasive particle size, particle material and particle flow rate, jet pressure, jet diameter, transverse speed and stand-off distance between nozzle and workpiece. Cutting of common reinforcement materials such as alumina and SiC is also well established.

4.2 Particle Reinforced Metal Matrix Composites

In the abrasive waterjet-based processing of MMCs, the presence of reinforcements affects the basis of the material removal process but does not present any major barriers to successful machining. For example, with particle reinforced metals, the particles that emerge at the surface level, as the kerf progresses, are largely dislodged, rather than machined—fundamentally different to the brittle based material removal methods seen in monolithic ceramic materials. As with WEDM, the inclusion of particles in the material does not offer any major obstacle to AWJ cutting.

Materials such as reinforced aluminium are readily machinable. A study conducted on 30% volume SiC particulate/6061-T6 aluminium [21] established that the material is comfortably processed by AWJM. The surface finish varied dependant on the cutting depth and relation to the jet direction, but the maximum Ra surface roughness values were generally below 3 μm. However, some damage was observed at the cut entrance due to the cutting erosion and dislodgement of surface-level particles. Additionally, burrs were observed at the cut exit, implying that the plastic deformation based shearing expected of an aluminium matrix has not been affected by the presence of the reinforcing particles. It could be assumed that a hybrid material removal mechanism is taking place, with a combination of the shearing of the matrix and sporadic dislodgment of the particles.

Feed rates for aluminium based PMMCs tend to appear longer than those recorded for unreinforced aluminium, although few direct comparisons exist. Compared to other MMCs technologies, AWJ is among the fastest in terms of transverse speed. One study on monolithic aluminium recorded speeds of up to 4 mm/s in processing a 60 mm thick example [22], in contrast to the 2.5 mm/s for 50.8 mm thick AMMC or 4 mm/s for processing Al/Al_2O_3 [23].

The concentration of reinforcing particles has a significant effect on the effectiveness of AWJ machining in delivering a high quality surface. Generally, the higher the concentration of the particulate reinforcement, the higher the degree of taper and surface waviness will be [24]. This indicated a greater resistance to the propagation of the jet, which is due to the decreased ratio of relatively soft, ductile metal to hard ceramic reinforcement that will deflect and absorb oncoming kinetic impact.

The effect of the concentration of particle reinforcement in aluminium MMCs appears predictable, in terms of qualitative assessment. Surface roughness will generally rise with increases in the percentage content of reinforcement. Figure 20 shows results gathered for surface roughness measurements in a comparative study between monolithic Al6061 and Al6061 with SiC reinforcement of 5, 10 and 15% [25].

From these graphs, it appears that a lower jet pressure and lower abrasive feed rate resulted in lower or equal overall roughness for the MMC, with a decreased influence of the reinforcement at depths below 18 mm. In contrast, high pressure and high abrasive rates gave more consistent results at low depths, including better surface roughness in these areas.

In addition to the concentration of particular reinforcement, the relationship between the reinforcement size and the size of the abrasive particle included in the AWJ stream appears to be of critical importance. If the reinforcing particles are significantly larger and of similar strength, mass deflection of the waterjet delivered abrasive into the kerf sidewall may result in kerf enlargement and increased surface roughness through pitting or embedment [26]. Also, proposed in this study is a gradual blunting of the abrasive particles by the SiC particles as an explanation for higher roughness.

Stand-off distance also appears closely related to the kerf taper, with a nearly linear relationship in the AJW machining of AlSiC reported by [21]. Here, increased stand-off distance resulted in a predictable increase in kerf taper. This is common in most AWJ cutting reports due to decreased kinetic energy and is exaggerated by higher transverse speeds. Hole piercing is feasible in the particle reinforced examples; however, the damage was present and appeared to be random. Standoff distance is a key factor in maintaining reasonable hole quality with AWJ piercing of MMCs [21].

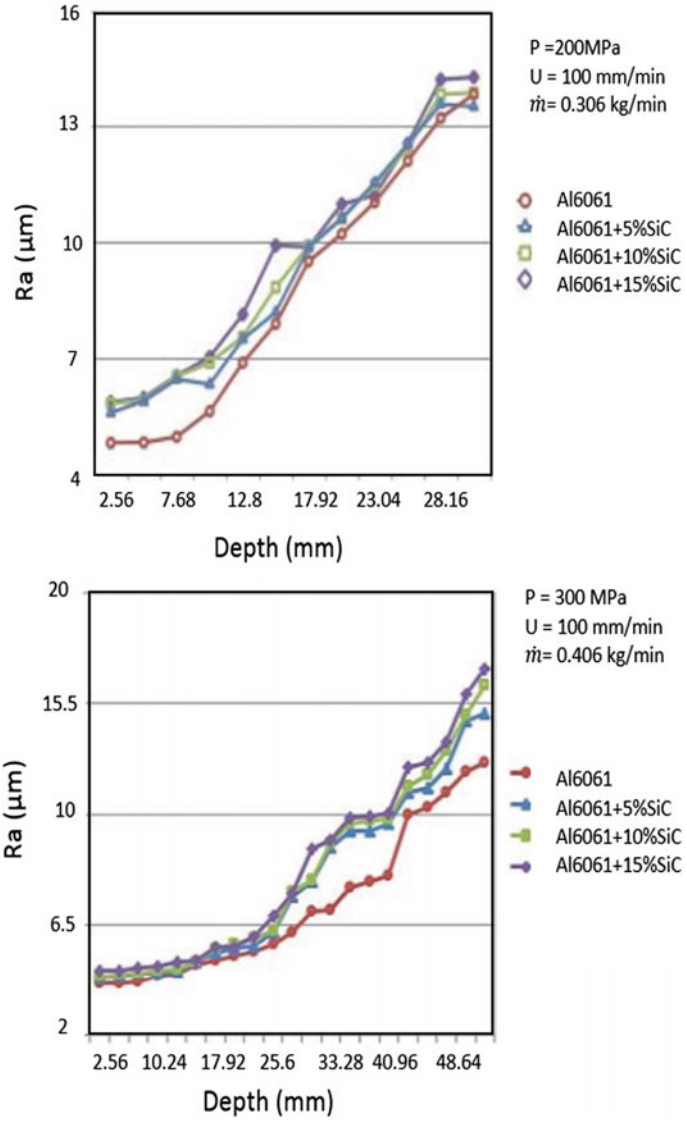

Fig. 20 Effect of SiC particle concentration on resultant surface roughness in AWJ machining of aluminium-SiCp composites using high and low pressure and abrasive flow rate [25]

4.3 Fibre Reinforced Metal Matrix Composites

AWJ machining of fibre reinforced metals is less developed, with the challenges believed to reflect those encountered in CFRP processing by AWJ means—delamination being the prevalent concern. However, metal matrices are less susceptible to the brittle fracture failure mode, which would cause exit delamination.

A study on Titanium/Graphite (Ti/Gr) metal composite laminates revealed distinct machining zones that varied with depth. Rounded edges at the entrance kerf were followed by smooth and rough regions of machining. The titanium contingent was machined by ductile deformation, while the fibres were removed by microchipping, brittle fracture, and bending failure. Kerf taper was positive in the range of 0.065–0.115 mm/mm, and there was a general absence of delamination [27]. Similar to the water-wedging phenomenon seen in AWJ cutting of CFRPs, with advanced FRP-Metal stacks AWJ cutting sometimes leads to non-uniform geometries or holes and kerfs with a high degree of taper.

AWJM appears to be a promising technology for the processing of PMMCs in terms of capability and speed. Particle size and density affect the output quality, with increases in size and density leading to larger kerfs and higher roughness through deflection of the abrasive particles to the kerf wall. Processing of FMMCs is less common, but successful trials have been conducted on titanium-graphite laminates with successful cutting and low taper.

5 Electrochemical Machining

Electrochemical machining uses electrical energy to generate the chemical breakdown of a workpiece. The method draws comparison to EDM. Similar to EDM, there is a reliance on the workpiece being electrically conductive. However, there are key differences in the material removal mechanism (spark based versus dissolution) and the role of the fluid (electrical insulation versus electrical conduction). ECM is a comparably rapid process with little tool wear, so it is used for high-output precision machining actions such as those required for aero-engine components. As the majority of the reinforcements in metal matrix composites are much less electrically conductive than the metallic matrices, the material removal mechanism is reliant on the tool-matrix interactions.

5.1 Material Removal Mechanism

The key process parameters associated with ECM are the applied voltage-current characteristics, electrolytic concentration, electrolyte flow rate and pulse-on time,

pulse-off time and feed rate of the tool. A study by Kumar [28] outlines this observation in the ECM of aluminium reinforced with 5, 10 and 15% SiC particles by volume, noting that silicon carbide is inactive in the chemical reaction that dissolves the matrix.

Parameter studies on the electrolyte, feed rate and voltage settings show that increases to these input values increase the MRR in aluminium PMMCs with 10% SiC. However, aside from the voltage augmentation, these increases come at the expense of surface quality [26]. Electrolytic concentration will influence the ionization of the workpiece material, which gives way to the surface dissolution. With increases in the electrolytic concentration, the more rapid dissolving of the surface is efficient in evacuating the reinforcing elements. The localized effect of the particles is decreased due to the higher concentration of ions, but this gives way to less accurate machining and a higher overcut. The electrolyte type also plays a major role; for example, NaCl gives better surface finish when compared with $NaNO_3$ [29]. Further research infers that lower current density leads to dragging of aluminium particles from the matrix [30]. This is generally not uniform and causes poor surface finish.

The majority of the issues encountered in ECM of PMMCs are due to the interaction of the reinforcing particles with the reactions occurring between the conductive machining elements and the electrolytic fluid. With ECM, there is a definite positive relationship between the relative content of ceramic reinforcement and the process duration. Increases in the concentration of reinforcing particles used decreases the overall conductivity of the workpiece. Thus, MRR is lower than with monolithic equivalents.

With tube and cylindrical tool shapes, work based on Al/5% B4Cp revealed through statistical modelling that voltage, feed rate and electrolyte concentration affect the radial overcut dimension by 65.44%, 30.22% and 4.31% respectively in electrochemical drilling of small diameter holes. Radial overcut is defined as the difference between the radii of the machined hole and ECM tool used to create it [31].

5.2 Hybridization

A recurring issue in the ECM of particle reinforced composites is the trade-off between machining speed and surface quality, with parameter alterations that are beneficial to MRR often being detrimental to resultant surface roughness. The irregular removal of particles with certain parameter combinations can also be challenging to control.

For these reasons, several attempts at process improvement through hybridization have been made. Examples include abrasive assisted ECM, ECM-EDM hybridization and ECM assisted grinding. Methods of including abrasive matter in the electrolyte flow have also been trialled to increase MRR and improve surface roughness (abrasive assisted ECM processing).

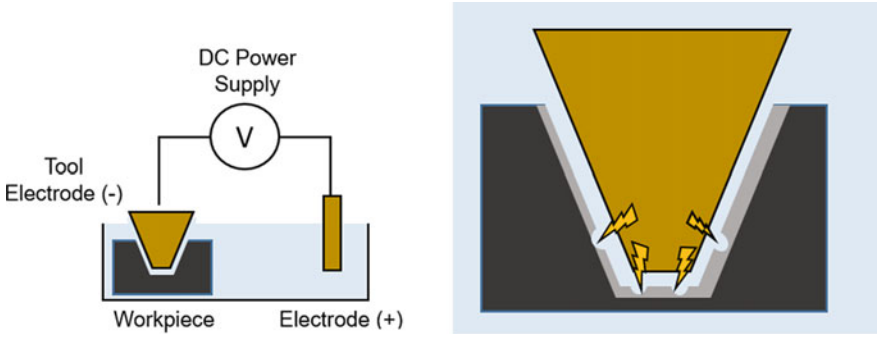

Fig. 21 Electrochemical discharge machining, (L) general process and (R) machining interface. (Image adapted from [32])

Sankar [30] reported that the inclusion of 50 μm diameter SiC particles in the electrolytic fluid had resolved the issue of decreased MRR that is caused by the non-conductive reinforcing particles in the workpiece material. The additional abrasive both removes additional workpiece material and smooths the machined surface. These trials were carried out on aluminium reinforced with boron carbide and graphite particles, machined with cylindrical ECM tools.

Electrochemical discharge machining (ECDM) uses both the material removal mechanisms of ECM and EDM. The hybrid process attempts to utilise the positive aspect of each method while addressing ECM's low efficiency and surface quality limitations, and EDM's low MRR and tool wear issues (Fig. 21).

With ECDM the metal removal is the combined effect of erosion and electrochemical machining. The combined effect of the two modes of material removal can readily remove the ceramic phases of the MMC, as the dissolution of the metallic phase accelerates the EDM process. This results in higher MRR and greater potential to form a defect-free surface. The electrolytic fluid, as well as the ECM dissolution, improves the EDM process. The conductive fluid permits a wider machining gap which is used to maintain distance and quality during the material removal [32].

Under certain conditions, reasonably high surface qualities can be achieved. Examinations have investigated the specifics of machining of composites with ECDM, in which it was found that a very high current density exists between the matrix and particle interfaces. It was found that this high current density can improve surface finish by up to 40% [32].

Unlike in unassisted ECM, it appears that there may be an ideal range for operating voltage. It appeared previously that increases in voltage within a sensible range would lead to a greater MRR. In a study by Vani [33], it is seen that operations at 100 V are distinctly less efficient than those taking place at 60 V. The reason for the decrease in MRR is higher voltages leading to excessive removal of the bulk material with little opportunity for the particles trapped in the spark gap to be removed by the electrolyte flow.

Further to this, it was shown that reinforcing particles have the effect of controlling the heat from propagating into the bulk material during EDM alone, which results in a lower molten pool volume than would be seen in a monolithic equivalent. This leads to a reduction in the MRR. The use of ECM for dissolving the metallic material can reduce the consequences of a smaller melt pool. In ECDM, the pulse duration is another critical consideration that is seen to have a suitable range. Outside of this range, there are adverse effects which lead to higher surface roughness. At low pulse duration, only ECM activity was observed, negating the advantages of the hybrid process. Conversely, at appropriate pulse duration, both EDM and ECM activities are present that easily removes the machining debris and produces better surface finish [32]. Excessively high pulse duration may lead to larger discharge craters which result in higher surface roughness.

Hydrogen formation is a by-product in the ECDM process. Hydrogen gas is liberated in the form of bubbles at the cathode due to electrochemical reaction. The bubbles gradually grow in size, and after attaining a critical size, they detach from the electrode surface. The hydrogen bubbles affect the circuit voltage and may lead to electrochemical arc machining, which is several times more efficient in MRR than EDM or ECM alone [34].

In summary, due to the differences in electrical conductivity in MMC materials, the reinforcement tends to be inactive in the reaction brought about by ECM. High concentrations of reinforcement in particle MMCs has been seen to increase the overall process duration by decreasing the MRR. A machining interface of decreased overall conductivity and hindered propagation of the generated heat appear to be the main externalities of the reinforcement.

Altering parameters, such as increasing electrolytic concentration and current, can increase the processing speed, but this tends to be at the expense of surface quality. Attempts at process hybridization have been made, most with EDM due to the thermo-electrical basis of the material removal mechanism. This has been shown to increase the material removal rate while maintaining reasonable surface quality.

6 Ultrasonic and Vibration Assisted Machining

Ultrasonic machining (USM) is a method that uses gradual erosion by abrasive particles as a means of machining the workpiece. A vibrating tool (or sonotrode) aggravates abrasive particles through high frequency, low amplitude vibration at the tool-workpiece interface.

While USM can provide ~1 μm Ra surface finishes in MMCs [35], the material removal rate has been reported as low—some 10′s of mg/min. This makes it less competitive than other methods. Regarding the material removal mechanism, the same study reported cleavage fracture and brittle fracture in SiC particles and ductile failure when Al_2O_3 was used as the abrasive type. Ultrasonic machining tends not to be preferred as the process is slow, and the ductility of the matrix does not necessitate such a gentle machining method.

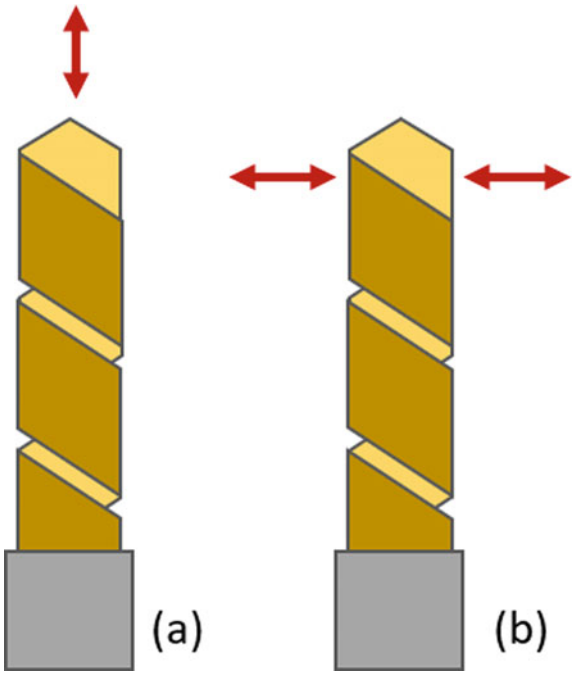

Fig. 22 Simplified axial (**a**) and transverse (**b**) modes of vibration

Ultrasonically assisted (UA) machining differs in that a standard tool can be used for machining, and the process is not entirely reliant on the vibration for the machining process. Instead, the vibrations reduce the axial force and torque that is required [36]. This section focuses on UA machining due to the higher concentration of research in this field.

6.1 Ultrasonically Assisted Machining of MMCs

Common issues with the conventional milling or turning of MMCs are centred on tool wear and surface quality. The abrasive nature of the reinforcement has a major effect on the rate of tool wear. At the same time, phenomena such as displaced surface level particles can lead to voids—this affects surface roughness verification and surface integrity.

The motivation for introducing ultrasonic assistance (UA) is to reduce the force required for machining. The axial force and torque are generally decreased as the tool is vibrated [36]. The material removal mechanism differs significantly from standard drilling, milling or turning as the torque and force are reset through vibration. The reduction in force is believed to reduce tool wear. Some verification of this exists for monolithic materials and CFRP, but there are few definitive studies in relation to the processing of MMCs.

Work conducted on the ultrasonically assisted turning of an A359/SiC/20p (20 vol% SiC) material [37] yielded good results with regards to the machined surface. The roughness of the MMC surface turned with vibrations was better than that turned without vibrations. In comparison with an unassisted equivalent and with all other parameters remaining constant, ultrasonic vibration with an amplitude of 3.7 μm resulted in a ~20% reduction in Ra. Values for surface roughness were 0.071 μm and 0.090 μm for ultrasonically assisted and standard turning, respectively. With ultrasonic assistance, the surface height overall range (Rt) was seen at 0.56 μm, compared to the value of 0.86 μm seen in the standard operation.

With the use of vibration, other factors such as cutting speed, depth of cut and feed rate still have a significant effect on the output roughness. When the speed or feed values were increased to a higher setting, the Rt value was effectively tripled.

In addition, the ultrasonic assistance effectively normalized the surface appearance. A regular pattern was established by the oscillations of the vibrating tool. This is in contrast to the irregular surfaces seen in standard machining, where particle influence can lead to peaks, troughs and striations. This experiment did, however, rely on sophisticated diamond cutting tools.

Ultrasonically assisted drilling (UAD) is another UA application. The mechanism and application differ from UA turning, although similar benefits are reported—reduced force, superior surface finishing and greater machinability. With regards to composites, most of the work has focused on particle reinforced aluminium alloys.

As with turning, the key factors in UAD are the vibration characteristics such as amplitude and frequency, but also the general relative motion resulting from the vibration. Axial and transverse vibration, for example, will have differing general effects on the produced workpiece.

Swarf formation and the material removal mechanism are directly altered by the ultrasonic vibration. The axial oscillation adds to the cutting edge movement towards the feeding direction, resulting in a reduced machining force and the formation of smaller chips. In addition, with increasing amplitude, the axial oscillation of the tool amplifies, and better surface roughness is obtained. This low force and high amplitude motion smooth the surface at regular intervals. Most cases reported that some of these particles remain on the finished surface, others are pulled out, while some of the SiC particles fracture under the pressure of the cutting tool [38].

Research on ultrasonically assisted drilling of SiC particle reinforced aluminium has examined the performance differences between standard drilling and UAD in terms of drilling force, surface roughness and burr height for variable SiC particle concentrations. In almost all instances of drilling with a TiN coated 5 mm HSS drill, preferable output was generated with the use of ultrasonic assistance. A study by Kadivar [38] examined values for the average axial force encountered in drilling the various aluminium-SiC particle composite configurations. Across the various SiC content values (5%, 15%, 20%), UA appears to have at least halved the required axial force. In addition, the UA process appears less susceptible to the effects of increased SiC content—the values recorded for all percentages of SiC inclusions fell within a ~80 N range, even at higher vibration amplitudes. In contrast, standard

operations demonstrated a ~200 N increase in mean drilling force when moving from a SiC concentration of 5 to 20% concentration.

The same study reports that surface roughness values and burr height were also improved by the ultrasonic assistance. While the force reduction was near uniform in its effectiveness at various vibration amplitudes, amplitude variation has opposing effects on surface roughness and burr height. Lower amplitude frequencies were effective in minimizing burr height, while high amplitude delivered lower surface roughness. Two different vibration systems were trilled in these experiments—one which resulted in primarily axial movement, and one which resulted in primarily lateral movement. The axial movement was seen as preferable in the tests. Higher surface roughness was observed with higher lateral vibration, which created a greater contact area between the tool and the hole walls, leading to extra surface damage and inferior surface finish.

Burrs are undesirable side effects encountered in machining actions in which additional material is built up around the machined edge. High drilling forces can push bulk material to the hole edge area in drilling. Deburring operations are often time consuming and expensive, accounting for up to 30% of the total cost of some high precision parts [39]. Kadivar [40] specifically examined ultrasonic assistance in the reduction of burr formation in drilling AlSiC composite material using TiN coated HSS drills. It was reported that UAD can be used to reduce burr height by approximately 80%, even at higher feed rates and spindle speeds. Increases in spindle speed did increase burr height in both standard and UA drilling. However, the burr height response to increases in feed rate was low. UAD resulted in some reduction in burr width. The use of UAD resulted in lower values but was susceptible to changes in feed rate and spindle speed in the same manner as standard drilling.

In summary, ultrasonic machining is capable of machining MMCs to a high surface finish, reporting various reinforcement fracture modes depending on the material composition. However, USM alone is uncommon due to the long durations and ductility of the matrix. Applying ultrasonic vibration assistance to other methods is better documented in exiting literature. Ultrasonically assisted drilling and turning bring some improvement to surface roughness and standardization of the surface profile, and there are few drawbacks aside from the specialist transducers and higher energy consumption in applications such as turning. While reasonable characterization and demonstration of the beneficial elements have been completed, there is still limited development of the specific understanding of the specific tool-reinforcement interactions.

7 Summary

The conventional tool-based machining of advanced materials such as MMCs is challenging due to the abrasive nature of the reinforcement. Over the last few decades, non-conventional machining processes have been making a significant impact in modern manufacturing, especially for machining of advanced materials like MMCs.

Despite the widely recognized merits of these methods in the manufacturing industries in general, there are some negative aspects, including high capital cost, low productivity and lack of robust in-process monitoring systems. The recent developments in non-conventional machining, including next-generation ultrasonic-assisted machine tools and high-power ultrafast lasers, are expected to significantly improve the machining quality and process lead-time in composite processing.

8 Review Questions

(1) Why may the laser drilling of a particle reinforced aluminium be more efficient, and require a lower peak power, than the drilling of a standard aluminium alloy?
(2) In laser drilling of aluminium PMMCs, few ceramic particles are seen on the hole wall—why is this, and how does this redistribution of particles take place?
(3) Limited machining of SiC particles takes place in millisecond drilling of Aluminium-SiC MMCs as they are ejected in the melt. This is not the case in waterjet guided laser drilling. What factors and differences between the two laser-based processes lead to changes in the SiC removal mechanism?
(4) The cutting action of Wire EDM is at times quicker in particle reinforced MMCs than in the unreinforced equivalent. Describe how the influence of the particles affect the material removal process and how this may positively affect the material removal rate in rough machining.
(5) EDM surfaces are characterized by round, overlapping craters. Why does the presence of ceramic particles disrupt the crater formation process?
(6) EDM is a well-understood machining technology with well-developed parameters for engineering materials. Why do parameters that result in low surface roughness in monolithic materials sometimes increase surface roughness in particle and fibre reinforced MMCs?
(7) Explain how the size and hardness of reinforcing particles in PMMCs relative to the size and hardness of the abrasive materials in an abrasive waterjet stream affect the roughness and morphology of the side walls in AWJ cutting.
(8) How do the material failure modes of the metal matrix and ceramic fibres differ in terms of AWJ machining?
(9) Metal composite laminates such as Ti/Graphite fibre cut by AWJM can exhibit non-uniform kerf width that varies with machining depth—how do the laminate properties affect this?
(10) How does higher reinforcement concentrations decrease the machining speed of MMCs when using ECM?
(11) Why is it difficult to control the surface finish in the ECM of PMMCs when using low electrical current?
(12) In hybrid EDM-ECM, how does the surface dissolving effect of the ECM process increase the machining efficiency of the electrical discharges?

(13) Explain how applying ultrasonic vibration to the tool in the turning of PMMCs results in a normalized surface, as opposed to surface that may have exposed particles or voids?
(14) Why is axial vibration preferred over lateral vibration in the ultrasonically assisted drilling of MMCs?

References

1. Nicholls, C.J., Boswell, B., Davies, I., Islam, M.N.: Review of Machining Metal Matrix Composites. Department of Mechanical Engineering, Curtin University, Perth (2014)
2. Quan, Y.M., Zhou, Z.H., Ye, B.Y.: Cutting process and chip appearance of aluminum matrix composites reinforced by SiC particle. J. Mater. Process. Technol. **99**(1–3), 231–235 (1999)
3. Dabade, U.A., Dapkekar, D., Joshi, S.S.: Modeling of chip–tool interface friction to predict cutting forces in machining of Al/SiCp composites. Int. J. Mach. Tools Manuf **49**(9), 690–700 (2009)
4. Durante, S., Rutelli, G.: Aluminum-based MMC machining with diamond-coated cutting tool. Surf. Coat. Technol. **94–95**(1), 632–640 (1997)
5. Marimuthu, S., Antar, M., Dunleavey, J., Hayward, P.: Millisecond fibre laser trepanning drilling of angular holes. Int. J. Adv. Manufac. Technol. 1–11 (2019)
6. Diaz, O., Luna, G., Liao, Z., Axinte, D.: The new challenges of machining Ceramic Matrix Composites (CMCs): review of surface integrity. Int. J. Mach. Tools Manuf **139**, 24–36 (2019)
7. Negarestani, R., Sundar, M., Sheikh, M.A., Mativenga, P., Li, L., Li, Z.L., Chu, P.L., Khin, C.C., Zheng, H.Y., Lim, G.C.: Numerical simulation of laser machining of carbon-fibre-reinforced composites. J. Eng. Manufac. **224**(7), 1017–1027 (2010)
8. Li, Z., Chu, P., Zheng, H., Lim, G., Li, L., Marimuthu, S., Negarestani, R., Sheikh, M., Mativenga, P.: Laser machining of carbon fibre-reinforced plastic composites. In: Advances in Laser Materials Processing, pp. 136–177. Woodhead Publishing (2010)
9. Marimuthu, S., Antar, M., Dunleavey, J., Chantzis, D., Darlington, W., Hayward, P.: An experimental study on quasi-CW fibre laser drilling of nickel superalloy. Opt. Laser Technol. **94**, 119–127 (2017)
10. Richerzhagen, B.: Development of a System for Transmission of Laser Energy, Doctoral dissertation, Ph.D. Thesis work, EPFL, Switzerland, (1994)
11. Arindam, G., Manna, A.: Response surface method based optimization of ytterbium fiber laser parameter during machining of Al/Al2O3-MMC. Opt. Laser Technol. **46**, 67–76 (2013)
12. Sharma, S., Mandal, V., Ramakrishna, S., Ramkumar, J.: Numerical simulation of melt hydrodynamics induced hole blockage in Quasi-CW fiber laser micro-drilling of TiAl6V4. J. Mater. Process. Technol. **31**(262), 131–148 (2018)
13. Phillips, K., Gandhi, H., Mazur, E., Sundaram, S.: Ultrafast laser processing of materials: a review. Adv. Opt. Photonics, **31** 7(4), 684–712 (2015)
14. Lopez-Esteban, S., Gutierrez-Gonzalez, Mata-Osoro, G., Pecharroman, C., Diaz, L.A., Torrecillas, R., Moya, J.S.: Electrical Discharge Machining of Ceramic/Semiconductor/Metal nanocomposites. CINN, Llanera
15. Vishwakarma, M., Parashar, V., Khare, V.K.: Advancement in electric discharge machining on metal matrix composite materials in recent: a review. Int. J. Sci. Res. Publ. **2**(3), (2012)
16. Ramulu, M., Taya, M.: EDM machinability of SiCw/Al composites. J. Mater. Sci. **24**, 1103–1108 (1989)
17. Lavoi, F.J.: Abrasive Jet Machining. In: Machine Design, pp. 135–139 (1973)
18. Patil, N.G., Brahmankar, P.K., Thakur, D.G.: On the effects of wire electrode and ceramic volume fraction in wire electrical discharge machining of ceramic particulate reinforced aluminium matrix composites. Procedia CIRP **42**, 286–291 (2016)

19. Bhattacharyya, B., Doloi, B.: Mechanisms of material removal. In: Modern Machining Technology: Advanced, p. 107. Micro Machining and Super Finishing Technology, Hybrid (2019)
20. El-Domiaty, A.A., Abdel-Rahman, A.A.: Fracture mechanics-based model of abrasive waterjet cutting for brittle materials. Int J Adv Manuf Technol **13**, 172–181 (1997)
21. Ramulu, M., Hamatani, G.: Machinability of high temperature composites by abrasive waterjet. J. Eng. Mater. Technol. (1990)
22. Chithirai Pon Selvan, M., Mohanasundararaju, N., Sachidananda, H.: Effects of process parameters on surface roughness in abrasive waterjet cutting of aluminium. Frontiers Mech. Eng. **7**(4), (2012)
23. Abrate, S., Walton, D.: Machining of composite materials. Part II: Non-traditional methods. Compos. Manufac. **3**(2), 85–94 (1992)
24. Hashish, M.: Machining of advanced composites with abrasive-waterjet. Manufac. Rev. **2**, 142–150 (1989)
25. Prabhu Swamy, N.R.: An investigation on surface roughness of aluminium metal matrix. In: IOP Conference Series: Materials Science and Engineering (2018)
26. Davim, J.P.: Modern Manufacturing Engineering. Springer, Berlin (2015)
27. Ramulu, M., Pahuja, P., Hashish, M., Isvilonanda, V.: Abrasive waterjet machining effects on kerf quality in thin fiber metal laminate. In: 2015 WJTA-IMCA Conference and Expo. New Orleans (2015)
28. Senthil Kumar, K.L., Sivasubramanian, R., Kalaiselvan, K.: Selection of optimum parameters in non conventional. Portugaliae Electrochim Acta **27**(4), 477–486 (2009)
29. Goswami, R.N., Mitra, S., Sarkar, S.: Experimental investigation on electrochemical grinding (ECG) of alumina-aluminum interpenetrating phase composite. Int. J. Adv. Manufac. Technol. **40**(7–8), 729–741 (2009)
30. Sankar, M.V., Gnanavelbabu, A., Kumar, R.: Effect of reinforcement particles on the abrasive assisted electrochemical machining of Aluminium-Boron carbide-Graphit composite. Procedia Eng. **97**, 381–389 (2014)
31. Rama, R.S., Padmanabhan, G., Naidu, K.M., Reddy, R.A.: Multi-response optimization of electrochemical machining of Al-Si/B4 composites using RSM. Int. J. Manufac. Mater. Mech. Eng. **3**(3), 42–46 (2013)
32. Vijaya Vani, V., Kumer Chak, S.: A review on electro chemical discharge machining (ECDM) of al-based metal matrix composites (MMC). Int. J. Mech. Prod. Eng. **4**(8), (2016)
33. Liu, J.W., Guo, Z.N.: Wire electrochemical discharge machining of Al_2O_3 particle reinforced aluminium alloy 6061. Mater. Manufac. Process **24**, 446–453 (2009)
34. Nandi, D., Baran Puri, A., Basak, I.: Behaviour of bubbles generated in electro-chemical discharge machining. Int. J. Eng. Sci. Technol. (2011)
35. Singh, G., Kumar, D., Sharma, N., Kumar, B.: Investigation Into machining characteristics of trialumane zirconium particle reinforcement in metal matrix composite using ultrasonic machining process. Intern. J. Res. Eng. Technol. 2321–7308 (2014)
36. Roy, A., Silberschmidt, V.V.: Ultrasonically assisted machining of Titanium alloy. In: Machining of Titanium Alloy, pp. 131–147. Springer, Heidelberg (2014)
37. Zhong, Z.W., Lin, G.: Diamond turning of a metal matrix composite with ultrasonic vibrations. Mater. Manuf. Process. **20**(4), 727–735 (2005)
38. Kadivar, M.A., Akbari, J., Yousefi, R., Rahi, A., Ghahramani Nick, M.: Investigating the effects of vibration method on ultrasonic-assisted drilling of Al/SiCp metal matrix composite. Robot. Comput.-Integr. Manufac. **30**(3), 344–350 (2014)
39. Silva Costa, E., Bacci da Silva, M., Rocha Machado, A.: Burr produced on the drilling process as a function of tool wear and lubricant-coolant conditions. J. Braz. Soc. Mech. Sci. Eng. **31(**1), (2009)
40. Kadivar, M.A., Yousefi, R., Akbari, J., Rahi, A., Nikouei, S.M.: Burr size reduction in drilling of Al/SiC metal matrix composite by ultrasonic assistance. Adv. Mater. Res. **410**, 279–282 (2012)

Finite Element Modelling of Machining of Metal Matrix Composites

Xiangyu Teng, Dehong Huo, and Islam Shyha

Abstract The fundamental material removal mechanism is central to understanding the machining process of metal matrix composites and improving such materials' machinability. Numerical models have been used extensively in the investigation of the machining process. It offers many advantages over experimental methods, particularly for examining the micro-scale phenomena that are hard to observe through experiments. This chapter will focus on the most widely used modelling method—finite element (FE) modelling. It starts from an overview of FE modelling on machining of MMCs. Then the general finite element model formulation is introduced. Finally, a case study using FE modelling on the cutting mechanism of Mg-MMCs reinforced with micro-sized and nano-sized particles.

1 Introduction

As one of the most common numerical simulation methods, the finite element (FE) modelling technique has been widely employed in the machining process studies to understand the material removal mechanism better. FE modelling can predict the cutting force, stress, strain, and temperature and chip formation during the cutting process. When compared to experimental research and other modelling techniques such as analytical modelling and molecular dynamics simulations, finite element method presents a better capability in predicting the behaviours of the material which is closer to reality: (1) tool-particles interaction, (2) particle fracture, (3) the merging of voids caused by debonding of particles, (4) surface generation during machining process [1]. As one of the most commonly used modelling methods, finite element modelling has gained increasing attention on studying the machining mechanism

X. Teng · D. Huo (✉)
Mechanical Engineering, School of Engineering, Newcastle University, Newcastle upon Tyne NE1 7RU, UK
e-mail: dehong.huo@newcastle.ac.uk

I. Shyha
School of Engineering and the Built Environment, Edinburgh Napier University, Edinburgh EH10 5DT, UK

I. Shyha and D. Huo (eds.), *Advances in Machining of Composite Materials*, Engineering Materials, https://doi.org/10.1007/978-3-030-71438-3_9

of MMCs in the past two decades. This chapter reviews the state-of-the-art in FE modelling of machining of MMCs, with emphasis on nano-MMCs. An overview of materials constitutive models, fracture criteria, and friction models is also presented. A case study on modelling of Mg-MMCs with SiC nanoparticles is given along with its micro-sized counterpart.

2 Review of FE Modelling on Machining of MMCs

Various numerical techniques have been used to model the machining process of MMCs in the past two decades. The modelling process can be achieved at two levels, namely in macro-mechanical and micro-mechanical models. Within macro-mechanical models, MMCs are treated as macroscopically anisotropic materials without considering fundamental characteristics such as particle size, interfaces between particles and matrix, and the fracture properties of particles. On the other hand, micro-mechanical models focus on the materials' local behaviour during the machining process. Thus they can predict the behaviour of particles such as debonding and fracturing during tool-particles interaction. Therefore it produces more visible details about the materials removal mechanism when compared to experimental approaches.

Different materials removal mechanism can be found in the machining of MMCs, which can be classified as follows: (1) the nucleation of voids due to debonding at the interface between particles and matrix, (2) particles failure. (3) growth and merging of voids in the matrix [1]. Those unique failure mechanisms in machining MMCs mean that their behaviour is different from that of homogeneous materials. According to numerous studies of finite element modelling on MMCs, it has been proven that various phenomena can be successfully simulated during the cutting process including particle failure, the flow of the particles in the tool-workpiece contact zone, debonding of the reinforcement in the secondary and primary deformation zones, and tool-workpiece interaction which leads to severe and premature tool wear.

The earliest attempt was conducted by establishing numerical investigation of the micromechanics involved during the machining of A356 aluminium alloy with 35% volume fraction of SiC particulate-based MMC using FORGE2 code [2, 3]. The whole simulation process was split into two stages. A homogeneous material was modelled to obtain the hydrostatic pressure in the first stage. The resultant loading output was applied in the second stage, accomplished using ANSYS, an elastoplastic FEA code. Using pressure data from aluminium alloy simulations, the particle–matrix interface failure, sub-surface damage, tool wear and residual stress were studied. Later, instead of simulating the two phases separately, a transient dynamics FE model was established to investigate the diamond turning process of Al6061/SiCp MMCs [4]. The normal and shear stresses field was studied in four different cases, namely tool facing/ploughing of aluminium matrix/SiC element respectively, and found that the relative position of the SiC element and cutting tool motion produced different

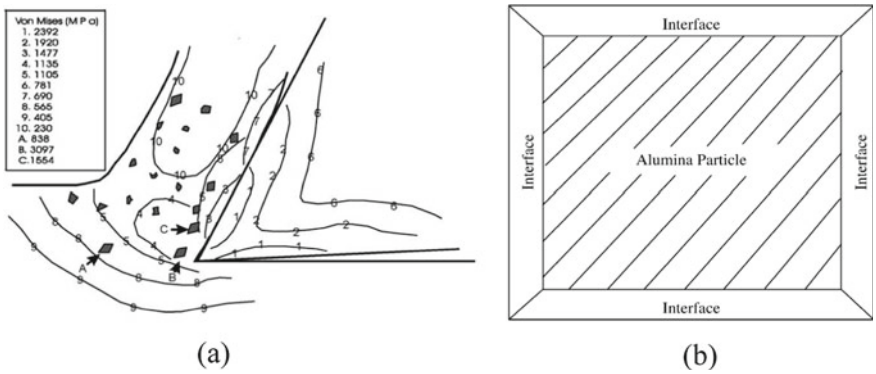

Fig. 1 **a** Von Mises stress distribution within matrix material; **b** modelling of particle interface. *Source* [5], with permission from Elsevier

magnitudes and patterns of stress. However, to better understand the material removal mechanism during machining, studying the interaction between the two phases is essential. Therefore, Zhu and Kishawy presented a plane-strain thermo-elastoplastic finite element model of orthogonal machining of Al6061/Al_2O_3 MMCs (Fig. 1) [5]. Temperature-dependent material properties were incorporated into this simulation. The effective and shear stresses on reinforcements and different machining deformation zones were investigated. The interface failure model between the matrix material and particles (e.g. particle debonding) was used to explain tool wear development. Although reinforcement was considered in this model, detailed cutting behaviours such as tool-particles interaction and particles' effect on the chip formation process were not simulated.

As the cutting tools pass through different phases of materials in the machining process, namely, soft matrix phase and hard. The abrasive nature of the reinforcement would cause the severe tool wear. This abrasive mechanism is hard to capture in machining experiment. Therefore, the interaction between particles and the cutting tool was studied through three scenarios with particles either above, along with or below the cutting path (Fig. 2) [4]. The variations in tensile and compressive stresses at the particles and the surrounding matrix as the tool advanced was investigated in these three scenarios and were used to explain the occurrence of particles fracture and to debond from the matrix. Additionally, the machined surface was considered hardened due to particles' indentation in the machined surface caused by interaction with the cutting tool. Apart from the excessive tool wear caused by machining MMCs, severer sub-surface damage compared with other machinable alloy is another challenge.

A multi-step 3D finite element model of sub-surface damage after the machining of MMCs was provided [6] (Fig. 3). The cutting data obtained from the initial step using an equivalent homogenous material (EHM) model was applied to a local multi-phase model. This multi-step method provided an accurate prediction of particle

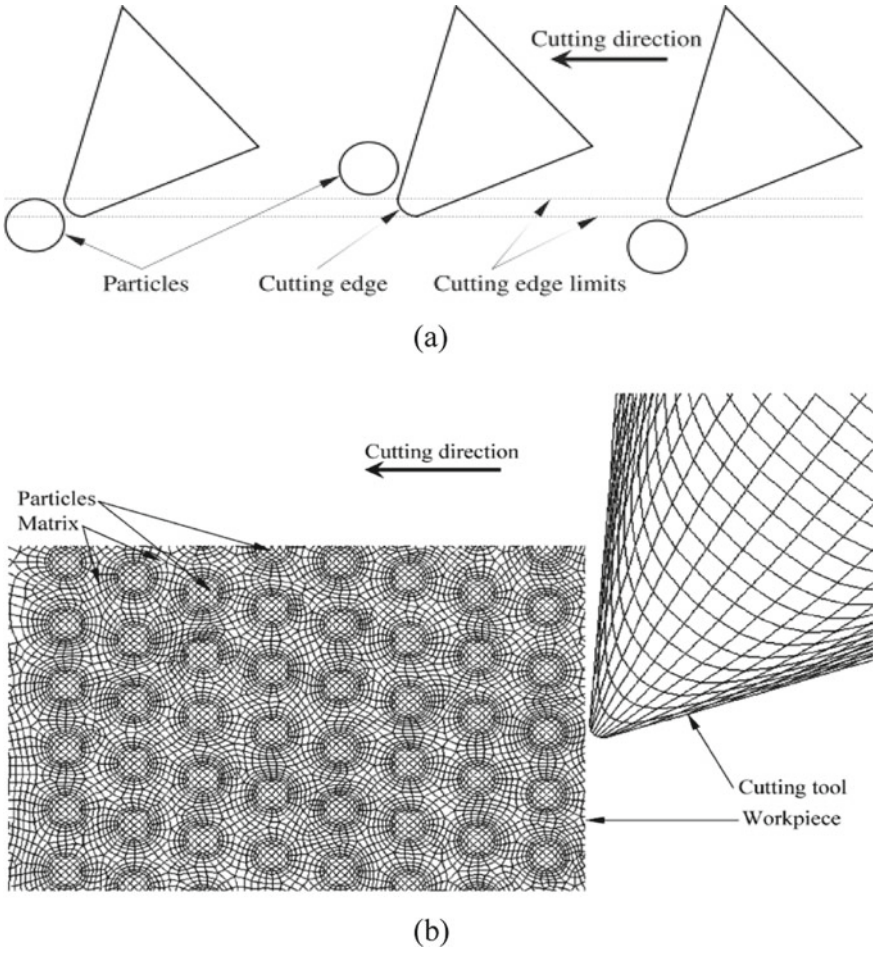

Fig. 2 **a** Three scenarios of tool-particles interaction; **b** Schematic representation for MMCs machining simulation. *Source* [4], with permission from Elsevier

fracture behaviour and the relationship between cutting force and depth of sub-surface damage.

Zhou et al. studied the removal mechanism by looking into the von Mises equivalent stress distributed locally within matrix and particle phases [7]. However, this simulation model exhibited an inability to globally simulate the chip formation process and stress/strain distribution under the particles' effect. To overcome this problem, the edge defects near the exit of orthogonal cutting by creating a FE model with randomly distributed particles was studied in later work [8]. The brittle fracture of particles and plastic flow of the matrix was found in the simulation process resulting in fragmented chips. The machined surface defects are also contributed

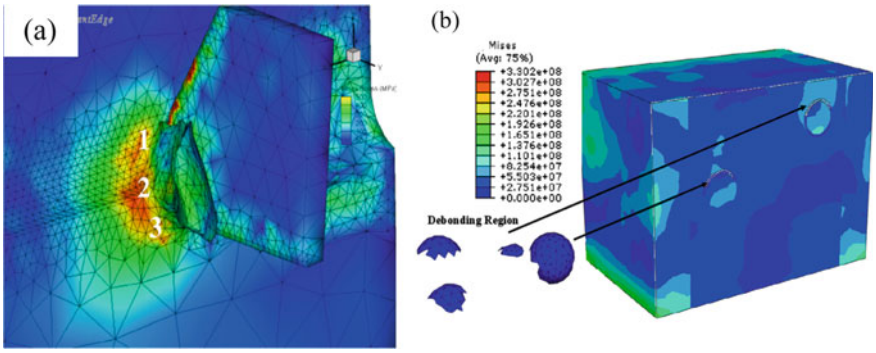

Fig. 3 **a** Stress distribution obtained from the machining EHM model; **b** sub-surface damage at a depth of 40.7 μm. *Source* [6], with permission from Elsevier

by particles failure behaviours such as debonding, microfracture, big cleavage, and cutting through particles [9].

Different model setting-up methods were attempted. A cohesive zone with predefined elastic modulus was added between the reinforcement and matrix phases [10]. The model with a cohesive zone element was more accurately predicted by cutting forces and chip morphology than the model without a cohesive zone. By introducing the cohesive zone, more local behaviours such as tool-particles interaction considering the effect of cutting speed by incorporating all phases of MMCs, including the matrix, particles and the interface between matrix and particles [11, 12]. Moreover, plastic deformation in the machining of Al6061/Al_2O_3 MMCs was analysed using the adaptive meshing technique to avoid mesh quality deterioration.

So far, most of the finite element modelling investigations have focused on machining MMCs with micro-sized particles. Only a few attempts have been made on machining of nano-MMCs. Teng et al. established a two-dimensional micromechanical finite element model to simulate the micro orthogonal machining of Mg-based MMCs reinforced with nanoparticles [13]. Unlike the fragmented chips obtained in machining MMCs with micro-sized particles, they found that continuously formed chips with a saw-tooth appearance were predominant. The reduction in particle size could induce significant changes in the material removal mechanism.

3 Overview of Finite Element Model Formulation

Several input factors for FEM such as the assignment of workpiece material properties (material constitutive model), criteria of chip separation (fracture criteria), friction within tool-chip interface, and mesh generation strategies are essential to provide a realistic model. The selection of appropriate factors critically affects the quality of output during the simulation. Among these factors, materials constitutive models, fracture criteria and friction models have been recognised as the three most important factors.

3.1 Materials Constitutive Model Formulation

An accurate material constitutive model is one of the most critical aspects to describe the behaviour of material deformation during the machining process. In reality, the workpiece material undergoes extreme conditions such as high strain, strain rate, and temperature increase. A high level of plasticity was observed in the primary and secondary shear zones. Meanwhile, a work hardening effect triggered by the fast strain rate of workpiece plays a vital role in determining its instantaneous mechanical properties, whilst the material properties measured in quasi-static conditions no longer govern the plastic behaviour. The material constitutive models used to describe stress and strain response and its dependence on strain and strain rate hardening and temperature softening effect have been proposed by researchers.

Among these material constitutive models, Johnson–Cook equation [14] has been widely used in FEM with adiabatic transient dynamic simulations. The factors affecting the workpiece's flow stress were classified into three terms: the elastic–plastic term representing the strain hardening. This viscosity presents increased flow stress with high strain rate and the temperature softening effect (Eq. 1).

$$\overline{\sigma} = \left[A + B\left(\overline{\varepsilon}^{pl}\right)^{n}\right]\left[1 + C\ln\left(\frac{\dot{\overline{\varepsilon}}^{pl}}{\dot{\varepsilon}_0}\right)\right]\left[1 - \left(\frac{T - T_{room}}{T_{melt} - T_{room}}\right)^{m}\right] \tag{1}$$

where $\overline{\sigma}$ is the flow stress, $\overline{\varepsilon}^{pl}$ is the plastic strain, $\dot{\overline{\varepsilon}}^{pl}$ is the plastic strain rate, $\dot{\varepsilon}_0$ is the reference strain rate, T is the workpiece temperature, T_{melt} and T_{room} are the material melting and ambient temperature. Coefficient A is the yield strength, B is the hardening modulus, C is strain rate sensitivity coefficient, n is the hardening coefficient, m is the thermal softening coefficient and these material coefficients are determined by experiments.

By considering the crystalline structure of a material, Zerilli and Armstrong [15] proposed a material constitutive model (Eqs. 2 and 3) based on the theory of dislocation mechanics. Two models based on the workpiece's lattice structure, including the body centre cubic (BCC) and face centre cubic (FCC), were established, as described respectively.

$$\overline{\sigma} = C_0 + C_1\exp\left[-C_3T + C_4T\ln\left(\dot{\overline{\varepsilon}}^{pl}\right)\right] + C_5\overline{\varepsilon}^{pl} \tag{2}$$

$$\overline{\sigma} = C_0 + C_2\overline{\varepsilon}^{pl}\exp\left[-C_3T + C_4T\ln\left(\dot{\overline{\varepsilon}}^{pl}\right)\right] \tag{3}$$

where $C_0 - C_5$ are materials constants determined through experiments. T is the absolute temperature.

The selection of material constants in constitutive models can critically affect outcomes such as stress and strain distribution, cutting force, temperature field, and chip morphology. Acquisition of these constants experimentally is a relatively

complex process since the experimental data is necessary to be acquired under the deformation conditions that cover an extensive range of strains, strain rate and temperature. Several constitutive models are also available to model the workpiece such as Mecking-Kocks [16] model with 23 material constants and a physical-based model with more necessary constants from 8 to 12 presented by Nemat-Nasser [17]. As J–C model and Z-A model require fewer constants than the two models mentioned earlier, they are widely used in material modelling studies.

3.2 Fracture Criterion

Materials separation is a complex process, including many physical mechanisms occurring at the micromechanical level [1]. Stress and strain were recognised as two main tensors that cause the initiation and evolution of materials fracture. In commercial FE software, the fracture mechanism can be classified into the ductile fracture and shear fracture. In ductile fracture, the voids would undergo the nucleation, growth and coalescence and eventually fracture. The mechanism in the shear fracture is mainly based on the shear band localisation. Recently, several fracture criteria for the ductile metal have been proposed and are widely used in various areas such as impact, fatigue analysis and metal forming process, which are (1) constant strain criterion and maximum shear stress criterion, (2) Johnson–Cook fracture criterion and (3) Cockcroft-Latham fracture criterion. Some of them are either built-in commercially available software or implanted through the user-defined subroutine.

3.2.1 Constant Strain Criterion

Constant strain criterion (Eq. 4) has been employed in many pieces of research regarding metal cutting and forming [5, 18, 19]. This criterion is assumed to be satisfied when the equivalent plastic strain reaches a critical value (equivalent strain at the onset of fracture). The workpiece's nodal point in front of the tooltip will be separated, resulting in the chips' separation. The disadvantage of this fracture criterion requires a high computational cost.

$$\omega_D = \int \frac{d\overline{\varepsilon^{pl}}}{\overline{\varepsilon_f^{pl}}} = 1 \tag{4}$$

where ω_D is a state variable.

The equivalent plastic strain at the onset of fracture is assumed to be a function of stress triviality and strain rate [20]:

$$\overline{\varepsilon}_f^{pl}\left(\eta, \dot{\overline{\varepsilon}}^{pl}\right) \tag{5}$$

where $\eta = -\mathrm{p/q}$ is the stress triaxiality, p is the pressure stress, q is the von Mises equivalent stress, $\dot{\overline{\varepsilon}}^{pl}$ is the equivalent strain rate.

3.2.2 Johnson–Cook Fracture Criterion

Johnson–Cook fracture criterion (Eq. 6) is a function of strain and strain rate hardening effect and temperature softening. It has been widely used to define the fracture criterion in metal machining. The equivalent plastic strain at the onset of fracture, $\overline{\varepsilon}_f^{pl}$, is defined as

$$\overline{\varepsilon}_f^{pl} = \left(d_1 + d_2 e^{d_3 \eta}\right)\left[1 + d_4 \ln\left(\frac{\dot{\overline{\varepsilon}}^{pl}}{\dot{\varepsilon}_0}\right)\right]\left[1 + d_5\left(\frac{T - T_{room}}{T_{melt} - T_{room}}\right)\right] \tag{6}$$

where $\mathrm{d_1} - \mathrm{d_5}$ are fracture parameter obtained from experiments, $\eta =$ is the stress triaxiality and $\dot{\varepsilon}_0$ is reference strain rate.

A damage parameter D is defined in each analysis increment, and the element would be deleted once damage parameter D reaches the unit value.

$$D = \sum \frac{\Delta \overline{\varepsilon^{pl}}}{\overline{\varepsilon_f^{pl}}} \tag{7}$$

Johnson–Cook simi-empirical fracture criterion and the constants can be determined through the tensile test, shear test or Hopkinson bar torsion with extensive strain rate and temperature [1].

3.2.3 Cockcroft-Latham Fracture Criterion

The Cockcroft-Latham fracture criterion was initially proposed for bulk forming operations (Eq. 8). However, a modified criterion was applied in machining simulation by numerous researchers [21–23]. The main disadvantage of this criterion is that it can be only used in small and negative triaxiality [1]. Same as other criteria as mentioned earlier, the onset of fracture initiates when the critical damage value, C, obtained through integration of the normalised maximum principal stress reaches the predefined value determined from the tensile test.

$$C = \int_0^{\varepsilon_f} \sigma^* d\overline{\varepsilon} \tag{8}$$

where $\sigma^* = \frac{\langle \sigma_1 \rangle}{\overline{\sigma}}$, the value of σ_1 is defined to be unity within this function if $\sigma_1 > 0$, and zero if $\sigma_1 < 0$, $\overline{\sigma}$ is equivalent stress.

3.2.4 Fracture Criterion Coupled with Damage Evolution Step

Generally, damage evolution step which is based on the accumulation of stress and strain can be used in combination with the fracture criteria aforementioned to model the progressive damage and failure of workpiece material. The materials failure process was divided into two steps, and the first step introduces the damage imitation while the second introduces the damage evolution. Two approaches can be employed to define the evolution process, including dissipated energy and effective plastic displacement.

Figure 4 presents the stress–strain response during the damage process. From point A to B, the material undergoes plastic strain with the hardening effect. Damage initiation is not satisfied at point B until the damage parameter D reaches unity, and σ_{y0} and $\overline{\varepsilon}_0^{pl}$ are the yield stress and equivalent plastic strain. After point B, the material undergoes the damage evolution process whilst the load-carrying capability is reduced until it reaches the failure state [20].

During the damage evolution process, the strain–stress response cannot illustrate the damage behaviour since it can cause a strong mesh-dependency based on strain localisation. Therefore, a fracture energy-based approach (Eq. 9) was proposed by Hillergorg [24]. The energy, G_f, was defined as a material parameter required to open a unit area of the crack. By utilising this approach, the mesh dependency is reduced, and the damage behaviour after the onset of fracture is decreased through a stress-displacement response.

$$G_f = \int_{\overline{\varepsilon}_0^{pl}}^{\overline{\varepsilon}_f^{pl}} L\sigma_y d\overline{\varepsilon}^{pl} = \int_0^{\overline{\mu}_f^{pl}} \sigma_y d\overline{\mu}^{pl} \tag{9}$$

where L is the characteristic length, $\overline{\mu}^{pl}$ is the equivalent plastic displacement.

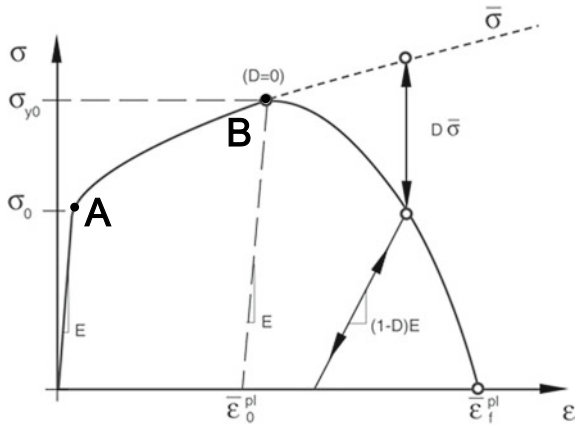

Fig. 4 Stress–strain curve of the damage evolution process

This approach introduces the equivalent plastic displacement, $\overline{\mu}^{pl}$ as the fracture work conjugate of the yield stress after the damage initiation point. The value of $\overline{\mu}^{pl}$ is defined as zero before the damage initiation and $\overline{\mu}^{pl} = L\overline{\varepsilon}^{pl}$ once the damage initiation criterion is satisfied.

For the damage evolution defined in terms of equivalent plastic displacement, a damage variable d (d = 0 at damage initiation point) was determined.

$$\mathrm{d} = \frac{L\overline{\varepsilon}^{pl}}{\overline{\mu}_f^{pl}} = \frac{\overline{\mu}^{pl}}{\overline{\mu}_f^{pl}} \tag{10}$$

Once damage variable d reaches unity, it can be thought that the load-carrying capability of a material is fully degraded, namely the failure of workpiece would occur. With the damage evolution defined in terms of energy, the equivalent plastic strain at failure can be expressed as:

$$\overline{\mu}_f^{pl} = \frac{2G_f}{\sigma_{y0}} \tag{11}$$

3.3 Friction Between Tool-Chip Interface

The friction characteristic at the tool-chip interface is one of the factors that significantly affect the simulated results. There are two shear zones taking place at the cutting tool's vicinity; primary shear zone due to the large strain and strain rate, secondary shear zone due to the friction at the tool-chip interface. The friction characteristic is very complicated. A large amount of heat can be generated due to friction at the tool-chip interface with high cutting speed leading to a high temperature field, which eventually facilitates the process of excessive tool wear. The simplest way is to experimentally acquire a constant coefficient of friction and apply it along with the tool-chip interface.

In most studies, Coulomb friction law combining with the sticking-sliding theory is applied to simulate friction stress. Two regions, including sticking and sliding, are established along with the tool-chip interface. A sticking region forms at the cutting tool's vicinity and the friction shear stress (Eq. 12) is equal to the average shear flow stress in the chips, k_{chip} [25]. Once the shear stress at interface reaches a critical value (limiting shear stress), sliding regime (Eq. 13) govern the friction process. Sliding region forms along the remainder region along with the interface and the friction shear stress can be determined using a coefficient of friction, μ.

$$\tau_{sticking} = k_{chip} \text{ when } \mu\sigma_n < \tau_{lim} \tag{12}$$

$$\tau_{sliding} = \mu\sigma_n \text{ when } \mu\sigma_n \geq \tau_{lim} \tag{13}$$

where τ_{lim} is the limiting shear stress, σ_n is normal stress distribution along the rake face, $\tau_{sticking}$ is friction shear stress along the sticking region, $\tau_{sliding}$ is friction shear stress along the sliding region, μ is the friction coefficient.

4 FE Modelling on the Cutting Mechanism of Nano-Particles MMCs

In this section, a comprehensive introduction on the study of finite element modelling of MMCs reinforced with nanoparticles conducted by Teng et al. [13] will be presented.

4.1 Modelling Procedures

The model is based on the micro-milling of Mg-MMCs reinforced with SiC nanoparticles. An assumption [26] has been made for simplifying 2D micro-milling process to orthogonal machining process. In micro milling experiment conducted within this study, the maximum uncut chip thickness t (less than 2 μm) is much smaller than the diameter of micro endmill (500 μm) as shown in Fig. 5a. It results in a relatively small variation of uncut chip thickness (2 μm) when compared with the travel distance of cutting edge in 180° of tool rotation (~392.5 μm), it can be thought that the variation of uncut chip thickness will not make a significant influence on results (e.g. cutting force and chip morphology). Therefore, the uncut chip thickness in the micro-milling process can be considered equivalent to that in the orthogonal machining process, as shown in Fig. 5b.

A two-dimensional micro-mechanical finite element model is established to simulate the micro-orthogonal machining process of nano Mg/SiC MMCs using commercially available software ABAQUS/Explicit v6.14–4. Since the nonlinearity, immense strain and strain rate are involved in the machining process, arbitrary Lagrangian–Eulerian (ALE) formulation is selected to avoid severe distortion of elements. The schematic representation of the established model is shown in Fig. 5. The cutting tool which moved horizontally into the workpiece with a predefined speed. To better understand the machining process details, two phases materials, including matrix and particles, are assigned individually in this model. The particle diameter is defined as 100 nm, with a volume fraction of 1.5%. The machining parameters are listed in Table 1.

A particles distribution strategy that makes the particles distributed at different relative locations of cutting path is used in this model, as shown in Fig. 6a. Within this strategy, the distance between each particle in X and Y direction is the same. In contrast, the distance between the uppermost particles and top surface of the workpiece is 50 nm larger in Y direction than the last column from right to the left

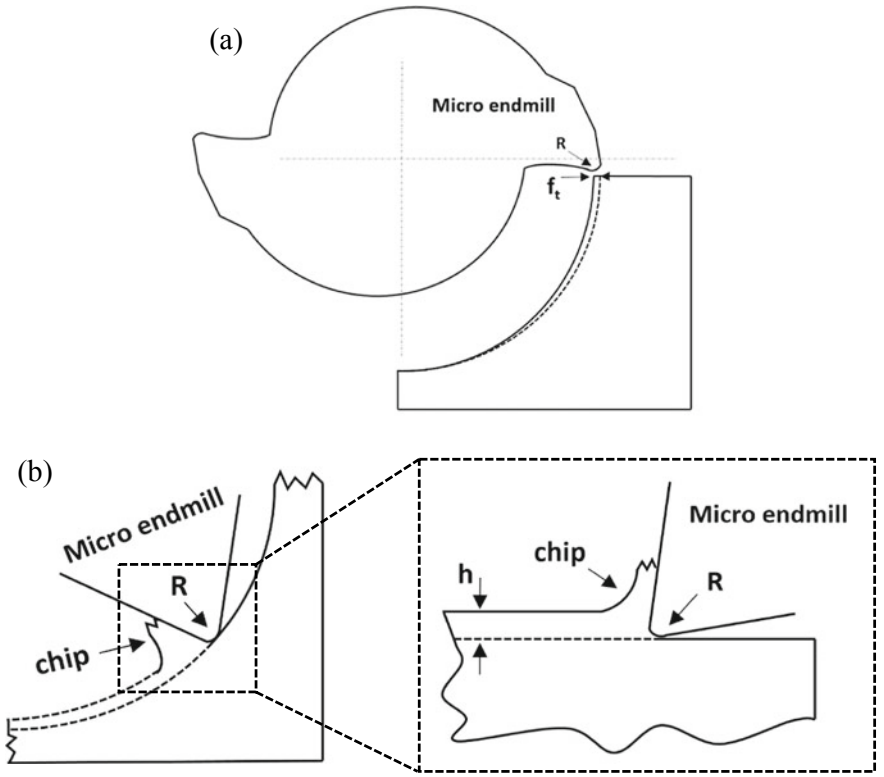

Fig. 5 **a** Schematic diagram of the 2D milling process in 180° of tool rotation; **b** Relationship between 2D milling process to the orthogonal machining process. *Source* [13], with permission from Elsevier

Table 1 Machining parameters in the FE model

Cutting speed, V_c (m/min)	125.64
Uncut chip thickness, t (μm)	0.1, 0.2, 0.5, 1, 2
Tool rake angle, α (Degree)	10
Tool clearance angle, β (degree)	6
Cutting edge radius, (μm)	1

side. For example, particles along line A distribute further away from bottom cutting edge limits, representing the diversity of particles locations relative to the cutting path in reality.

Magnesium matrix is treated as a deformable thermo-elastic–plastic material with quadrilateral continuum element and fracture criteria. Johnson–Cook constitutive model is used to describe the plasticity behaviour of magnesium matrix during the machining process. Johnson–Cook fracture equation is used to define the materials failure criterion for magnesium matrix. SiC particles were assumed to be a brittle

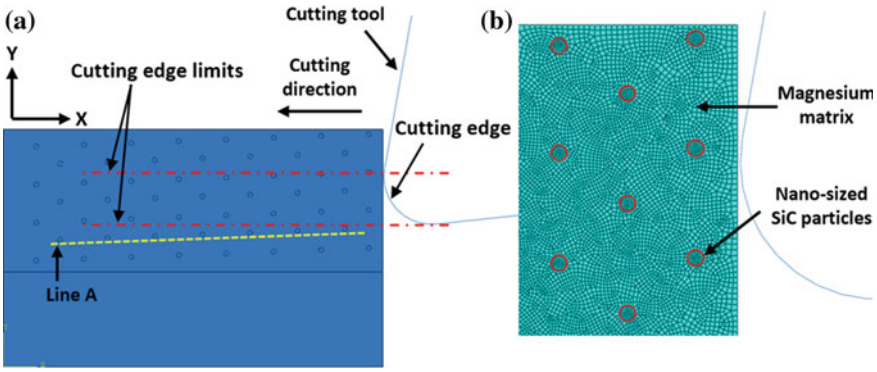

Fig. 6 **a** Schematic representation of the established models for micro orthogonal machining of Mg/SiC MMCs; **b** Local zooming of mesh element. *Source* [13], with permission from Elsevier

cracking body with brittle failure definition to investigate its behaviour during the cutting process. Free thermal-displacement quad-dominated meshing technique is used to advance the front algorithm for both matrix and particles. Mesh size of particles and matrix surrounding particles is defined to be 25 and 40 nm. The bottom surface of the models was fixed in all directions. The surface-to-surface contact model is applied between the external surface of the tool and node points of the machining area.

4.2 Chip Formation Process Analysis

Figure 7 illustrates the simulated chip formation process under the uncut chip thickness of 1 μm. As shown in Fig. 7a, when the tool firstly engages with the workpiece, highly concentrated stress is induced leading to an irregular shear zone closely formed in front of the cutting edge, which is different from that in macro machining of MMCs where an apparent primary shear zone can be formed at the initial cutting stage.

As the tool advances, the primary shear zone can be observed in Fig. 7b. Additionally, the particles take more stress than matrix material, especially those particles located near the primary shear zone. This is attributed to the high elasticity of SiC particles. The maximum von Mises stress is found at the particles located under cutting edge, 3109 MPa. This is different from machining monolithic materials where the maximum stress occurs in the primary shear zone.

Moreover, another difference can be obtained by observing the von Mises stress distribution pattern in Fig. 8. The addition of nanoparticles significantly alters the pattern of stress field within the matrix. A distorted stress contour can be found at the vicinity of each particle. This observation can be explained by particles' existence in the matrix, restricting the progression of plastic stress flow within the matrix during the machining process. The stress is accumulated and results in a high plastic strain

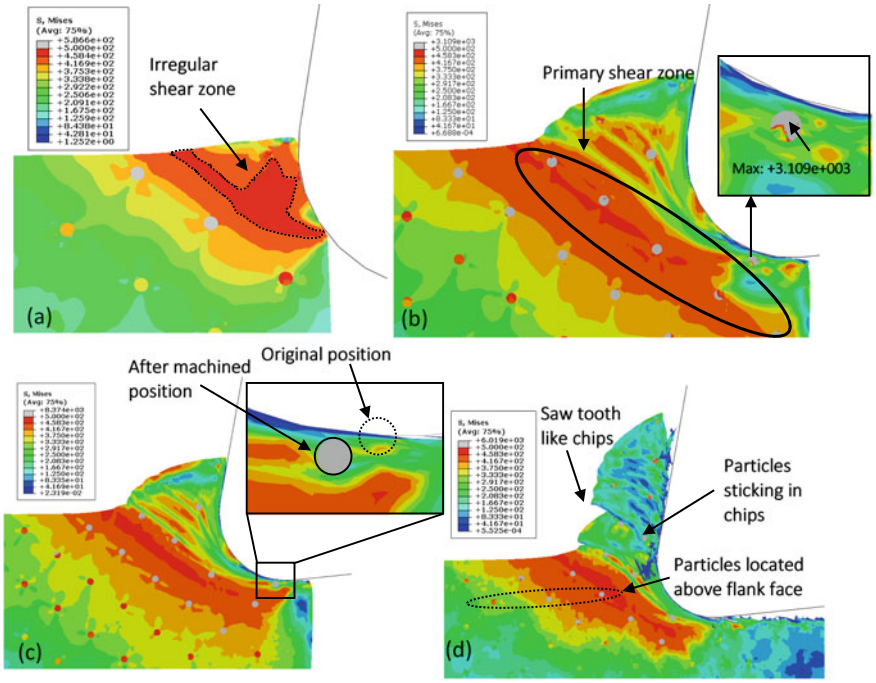

Fig. 7 Chip formation process during the micro-machining of nano Mg/SiC MMCs. *Source* [13], with permission from Elsevier

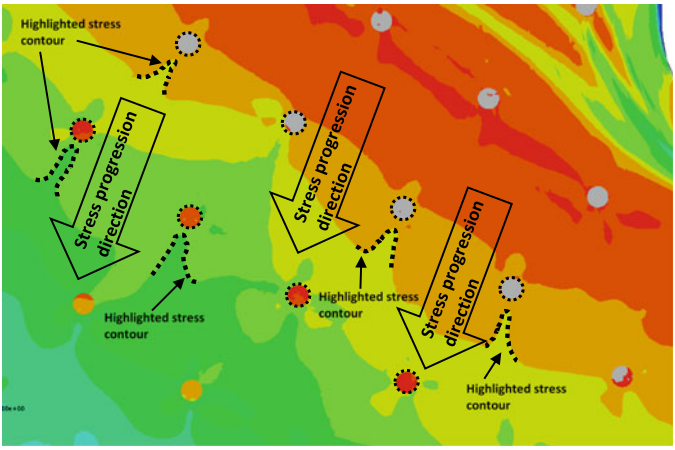

Fig. 8 Effect of addition of nanoparticles on the distribution pattern of von Mises stress contour. *Source* [13], with permission from Elsevier

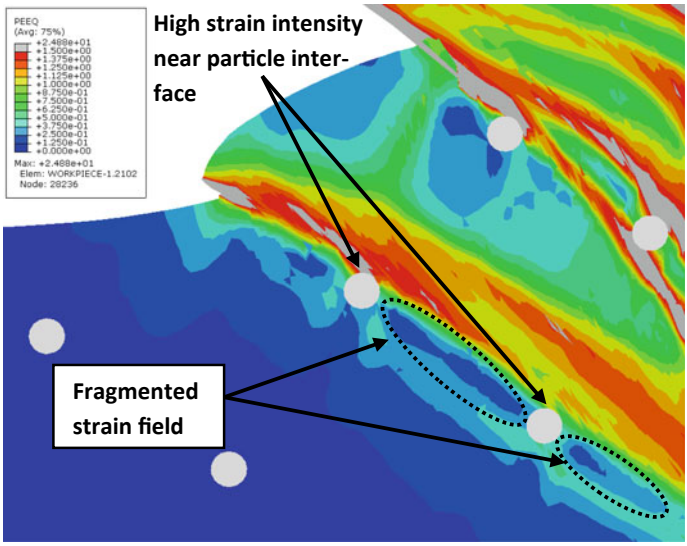

Fig. 9 Distribution of equivalent plastic strain within nano Mg/SiC MMCs. *Source* [13], with permission from Elsevier

field at particle interface, as shown in Fig. 9. The existence of nanoparticles also fragments strain field. Similar phenomena were reported by Pramanik et al. [5] in the machining of micro-sized Al/SiC MMCs.

As the tool continuously moves, Fig. 7c shows the behaviour of a particle located immediately under the flank face of the cutting tool when the tool is approaching it. Comparing with the original position of this particle moves horizontally with the highly deformed matrix in cutting direction without any direct contact with the cutting edge. Evolution of von Mises stress on the matrix element surrounding the particle with the cutting edge approach is studied in Fig. 10 in details. Initially, von Misses stress is found to increase to a maximum value of 454 MPa (C) with the tool's advancement. At this stage, the particle is found at primary shear zone. As mentioned earlier, this particle acting as a barrier restricts plastic stress progression within the matrix, which results in high compressive stress acting on the matrix close to the particle interface. This is different from the macro machining process. The maximum stress usually happens at the matrix between cutting edge and particles due to the indention caused by the cutting edge [4].

Consequently, this results in concentrated stress ranging from 540 to 650 MPa acting at particles. A sudden drop in von Mises stress is followed from C to E as the primary shear zone moves horizontally passing through this particle. At this period, the restricting behaviour on plastic stress flow of particle becomes less dominant as particles move with the surrounding matrix with further advancement of the tool. It is believed that the matrix element experiences a highly plastic deformation within this stress drop process (C to E). Finally, von Mises stress releases and decreases to

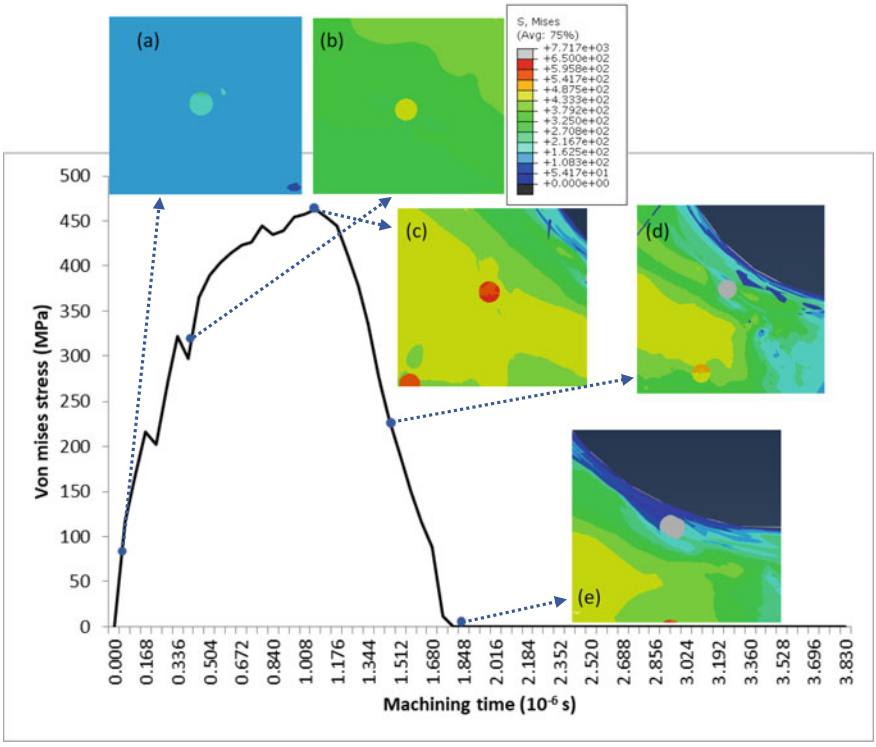

Fig. 10 Evolution of von Misses stress distribution on the matrix element close to the interface of particle. *Source* [13], with permission from Elsevier

0 MPa when the cutting edge passes through it, failing the matrix surrounding this particle. As a result, this particle is subjected to debonding from the matrix.

The premature tool wear caused by the high contact stress between the cutting tool and hard particles has been recognised as one of the crucial factors affecting the machinability of MMCs. The interaction process between the cutting tool and particles should be better analysed to predict the tool wear. Figure 11a–d illustrates the stress distribution on the particles located immediately below the cutting edge with the tool's advancement. Based on the observation of Fig. 11a and b, the increase in von Mises stress can be observed on the particle due to the compressing of the surrounded matrix with tool approaching the particle. The direct contact between tool and particles can be found in Fig. 11c. Highly concentrated stress on the particle's upper part is generated due to the ploughing between particle and flank face. This particle is then debonded and slide over the flank face (Fig. 11d). During the sliding process, particle acting as a sharp cutting edge scratches the flank face leading to abrasive wear. Smoother wear at the flank face is expected due to the nanoparticles. Additionally, it is evident from this figure that the particle is still intact, which is

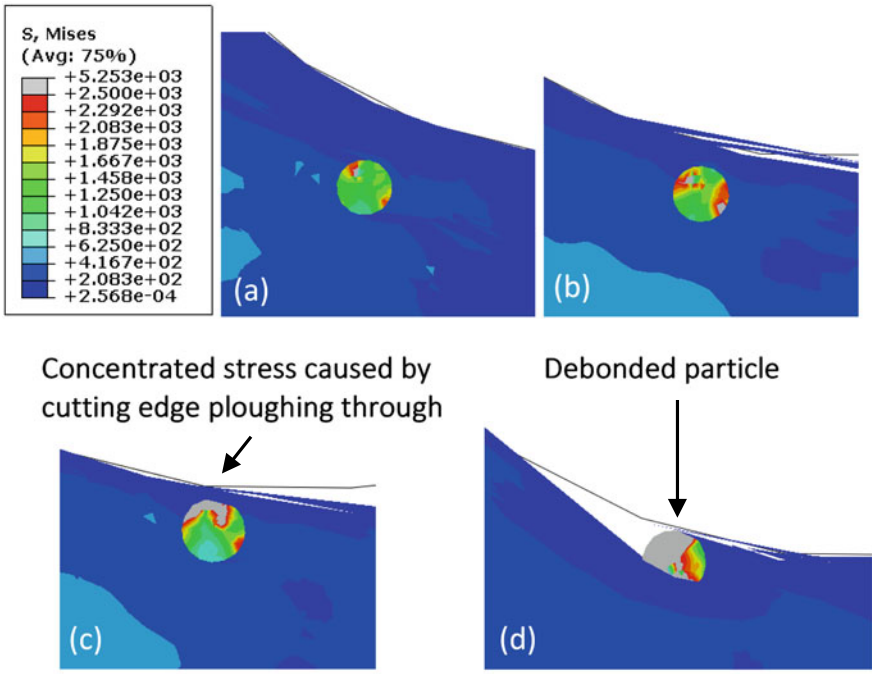

Fig. 11 Evolution of von Misses distribution on the particle located immediately below cutting edge with the cutting tool's advancement. *Source* [13], with permission from Elsevier

different from that in the machining of micro-sized MMCs where particle fracture is observed.

Upon the advancement of the cutting tool, the chip is completely formed (Fig. 7d). A complete chip-tool contact area is achieved with chip flow happening along the rake face. In this stage, the particles located above the cutting tool's flank face initially move with the surrounding matrix and enter into the formed chips as the cutting edge approaches. Figure 7d also illustrates a continuous chip with saw tooth appearance. This phenomenon can be explained by studying the equivalent plastic strain distributed in the chip. As shown in Fig. 12, a large deformation is observed at the chip and cutting tool interface.

Moreover, it can be seen that several highly strained bands are distributed across the chips at the vicinity of particles, which can be considered as the main reason contributing to the lamellate structure of chips. Those highly strained bands are mainly caused by localised high plastic von Mises stress bands (Fig. 13). Figure 13 illustrates the formation of high-stress bands within chip with the advancement of the cutting tool. At the initial stage, the primary shear zone is observed in Fig. 13a. As the tool further moves, the transition stage is achieved (Fig. 13b). The concentrated stress field is observed at the particles' interface as the primary shear zone passing

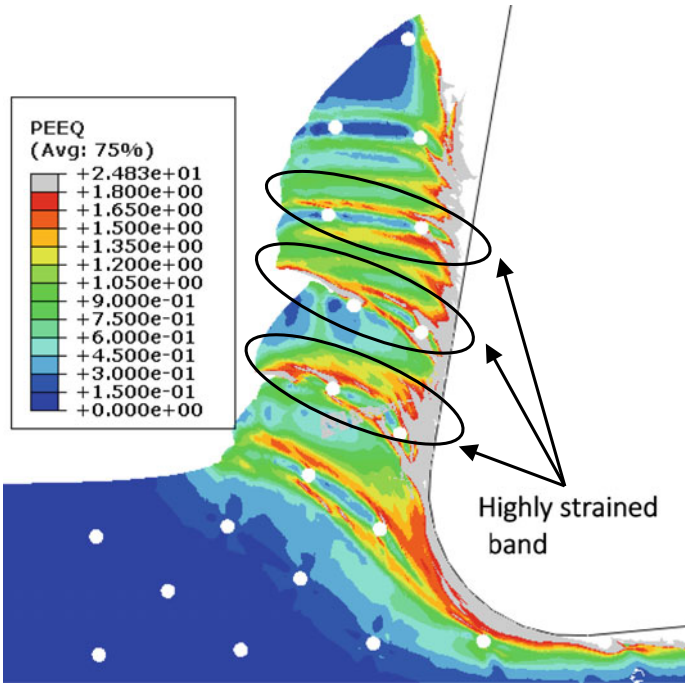

Fig. 12 Distribution of equivalent plastic strain within formed chips. *Source* [13], with permission from Elsevier

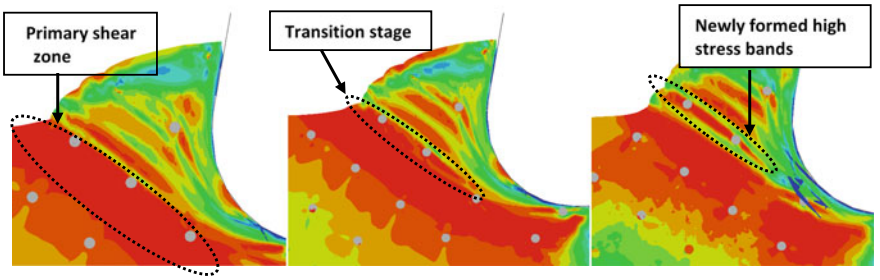

Fig. 13 Formation of high-stress bands within chips with the advancement of the cutting tool. *Source* [13], with permission from Elsevier

through due to particles' restricting behaviour to plastic stress flow, as mentioned earlier. Figure 13c shows that eventually, the high-stress bands is formed within chips.

4.3 *Effect of Uncut Chip Thickness*

Specific cutting force can be calculated by dividing the resultant cutting force by the section area of the cutting area. Figure 14 shows the specific cutting force at different uncut chip thickness obtained from the machining experiment and simulation model. A sudden decrease can be observed when the uncut chip thickness is less than 0.5 μm. Then the specific cutting force decreases mildly with the increase of uncut chip thickness.

Several differences will appear when the machining features decrease from macro to micro-scale. One of the significant concerns is the size effect leading a transitional regime associated with intermittent shearing and ploughing in the material removal process [27]. In this section, the chip morphology of micromachining on nano Mg/SiC MMCs under various uncut chip thickness is investigated through FE models (Fig. 15). Minimum chip thickness is determined based on the studying of chip morphology. The uncut chip thickness is selected to be 0.1, 0.2, 0.5, 1 and 2 μm. As shown in Fig. 15, the highly concentrated stress region can be considered the primary shear zone observed within workpiece materials with different locations underneath the cutting edge at all uncut chip thickness.

At uncut chip thickness of 0.1 μm, it can be found from Fig. 16 that there is no continuous chip formed in the cutting process. The small amount of material is initially elastically 'pushed' and accumulated in front of cutting edge (Fig. 16a). With the tool continuously moving, the equivalent strain at the chip root increases, resulting in plastic deformation. Figure 16c illustrates the continuous cutting stage. The maximum equivalent plastic strain is distributed at the accumulated material, which finally leads to a complete failure and stress within workpiece is released. The fragmented chip is therefore formed by this discontinuous removal mechanisms. The chip formation process at an uncut chip thickness of 0.2 μm exhibits a similar behaviour like that of an uncut chip thickness of 0.1 μm. When the uncut chip

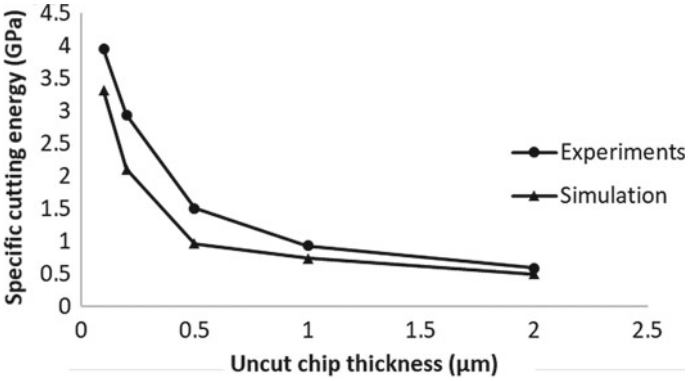

Fig. 14 Specific cutting force at different uncut chip thickness. *Source* [13], with permission from Elsevier

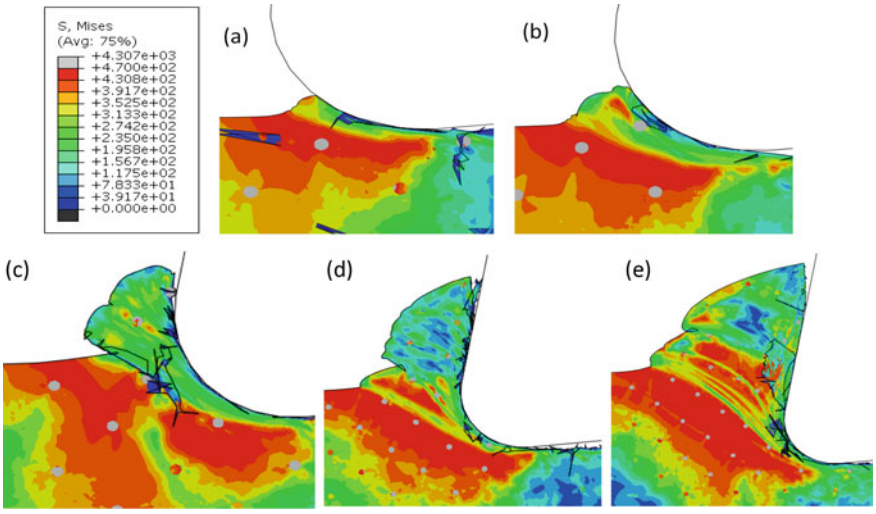

Fig. 15 Chip morphology at uncut chip thickness of **a** 0.1 μm; **b** 0.2 μm; **c** 0.5 μm; **d** 1 μm; and **e** 2 μm. *Source* [13], with permission from Elsevier

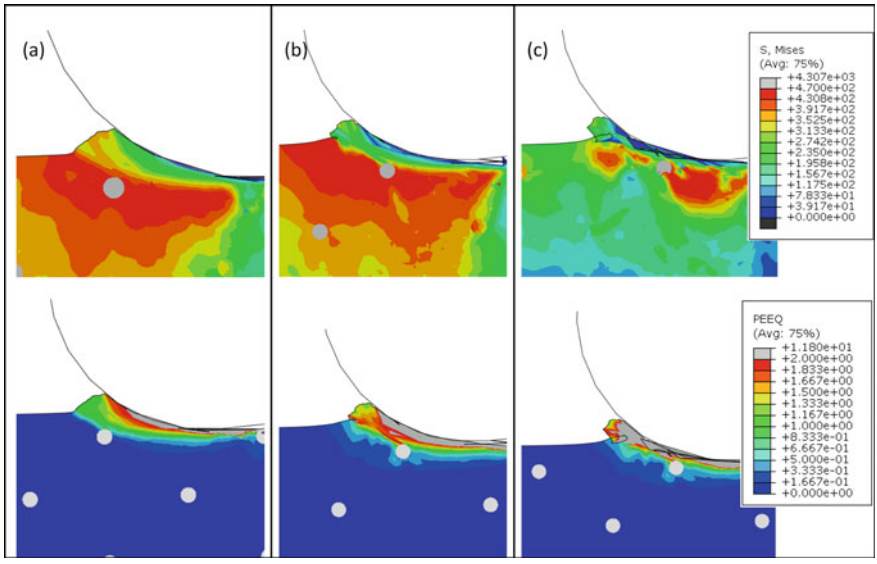

Fig. 16 Stress and strain distribution within workpiece at material removal process under the uncut chip thickness of 0.1 μm. *Source* [13], with permission from Elsevier

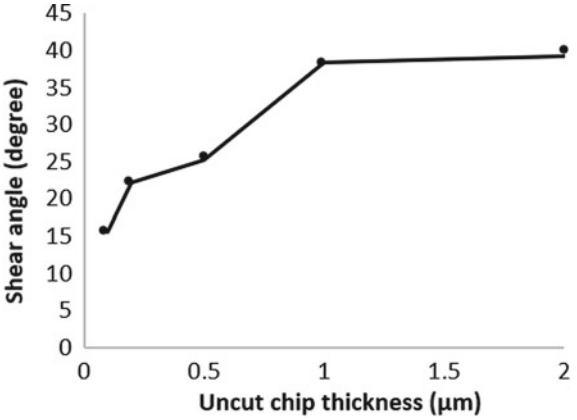

Fig. 17 The variation of shear angle with uncut chip thickness in the FE model. *Source* [13], with permission from Elsevier

thickness increase to 0.5 to 2 µm, an irregular segmented chip is formed. Based on these results, the minimum chip thickness can be proposed to be 0.5 µm (0.5R) under the input parameters utilised in this FE model. This result is consistent with that obtained from research carried by Teng et al. [28], which is 0.53R in micromachining of Mg/Ti with a volume fraction of 1.98%. Moreover, an increase in the shear angle can be found with the uncut chip thickness (Fig. 17).

5 Comparison Between Micro-Sized and Nano-Sized Particles Reinforced MMCs

In this section, simulation models machining of two types of MMCs reinforced with micro-sized particles and nanoparticles were developed respectively. This section presents a comparison between machining of micro and nano-MMCs in terms of chip formation, stress/strain distribution, tool-particles interaction and machined surface morphology. Finally, validation of FE models is conducted by investigating tool wear, chip morphology and machined surface morphology obtained from micro-milling experiments.

5.1 Von-Mises Stress Distribution in the Cutting Area

Chip formation process accompanying with the stress distribution when micromachining of Al/SiC MMCs reinforced with nano-sized and micro-sized particles were illustrated in Figs. 18 and 19, respectively. Figures 18a and 19a show the initial contact stage between the deformed workpiece and cutting tool before chip formation. Particles distributing at the matrix experiencing with highly concentrated stress

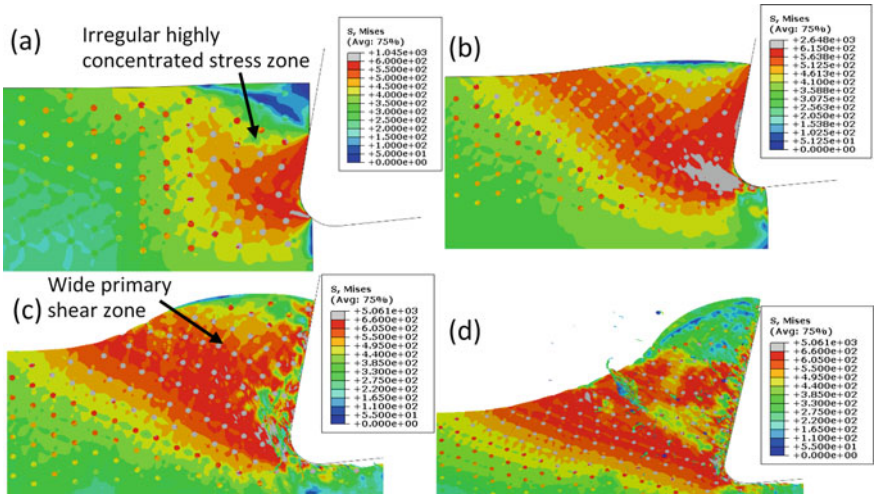

Fig. 18 Chip formation when micromachining of Al/SiC MMCs reinforced with nano-sized particles (0.2 μm diameter). *Source* [29], with permission from Elsevier

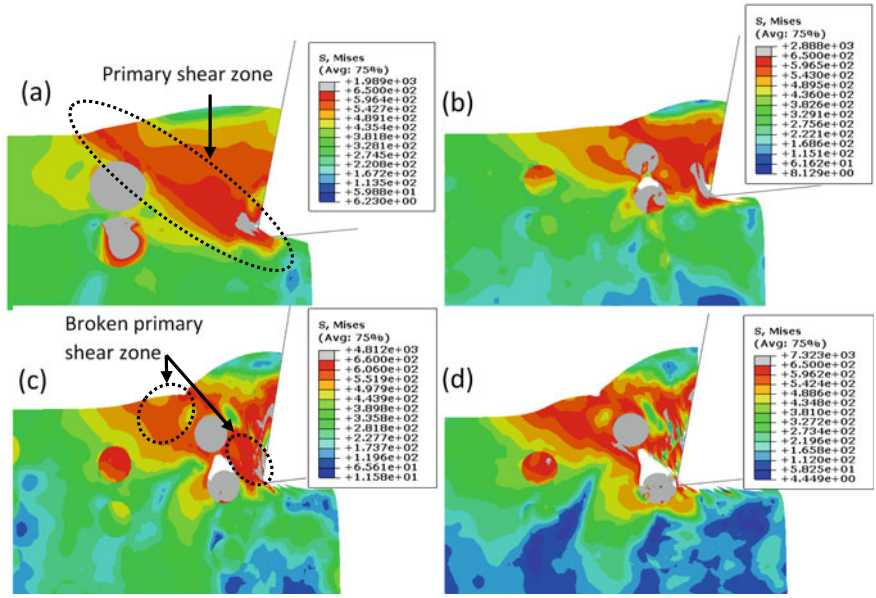

Fig. 19 Chip formation when micromachining of Al/SiC MMCs reinforced with micro-sized particles (10 μm diameter). *Source* [29], with permission from Elsevier

zone bear the greatest stress at both models. It proves the fact that hard SiC particles carry most of the load transferred from matrix materials. This can be attributed to the high elasticity of SiC particles. A different phenomenon in terms of von Mises stress distribution pattern within the matrix can be found between these two models when machining nano-MMCs (Fig. 18a), a narrow straight primary shear zone can be commonly found in machining homogeneous materials is not apparent. Instead, an irregular, highly concentrated stress zone was observed in the tool-workpiece interface, and the stress from the tooltip progresses to the upper surface with decreasing magnitude. With the cutting tool advances (Fig. 18b and c), a larger primary shear zone, when compared to that in machining homogeneous matrix materials (Fig. 20), becomes evident. In contrast, the primary shear zone can be observed when the cutting tool firstly engages with the workpiece and lasts during chip formation process in the model of machining micro-MMCs (Fig. 19a). The difference in the von Mises stress distribution between the two models implies that particles' location and size play a significant role in determining the stress propagation mechanism with the cutting tool's advancement.

In the model of machining nano-MMCs, a significant reduction in particle size tends to increase the number of particles involved in the machining area (uncut chip thickness) when compared to that in the machining of micro-MMCs. Unlike the highly concentrated stress region confined to the narrow primary shear zone in machining homogeneous materials (Fig. 20), these particles acting as barriers restrict

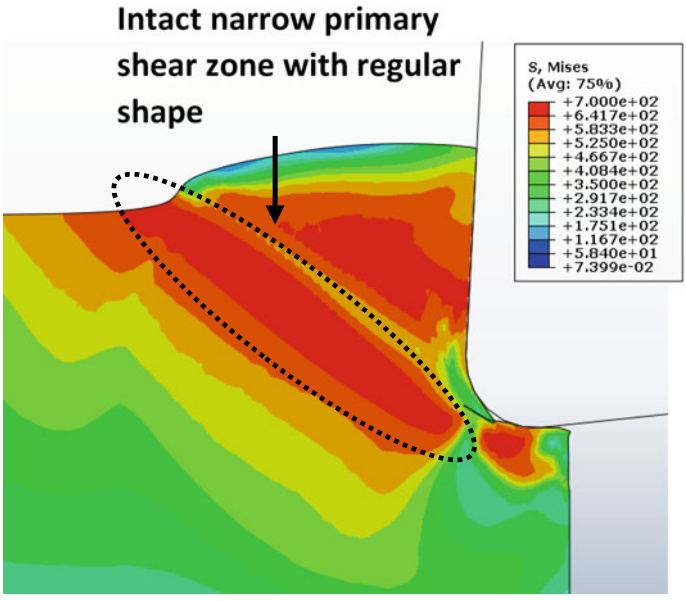

Fig. 20 Von Mises stress contour in machining pure Aluminium using the same cutting parameters of nano Al/SiC MMCs machining. *Source* [29], with permission from Elsevier

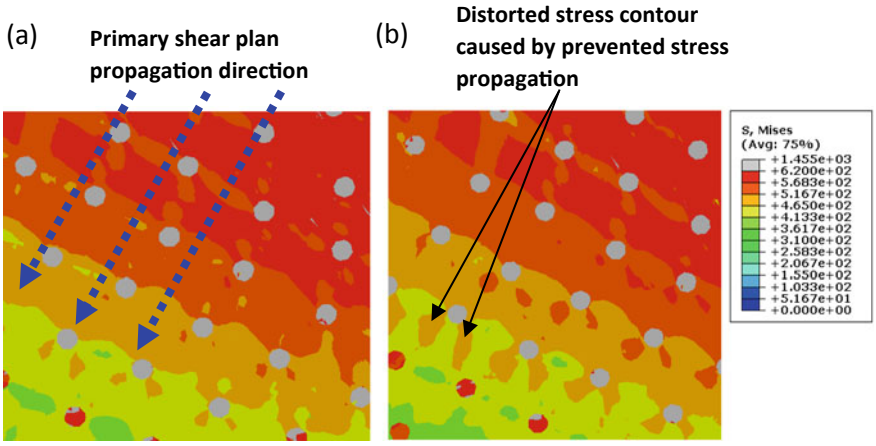

Fig. 21 Effect of nanoparticles on primary shear zone propagation **a** primary shear zone propagation direction; **b** distorted stress contour caused by prevented stress propagation. *Source* [29], with permission from Elsevier

the propagation of stress and force the highly concentrated stress to propagate to the surrounding area. This is believed to be the main reason leading to an irregular stress zone at the tool-workpiece interface at the initial cutting stage and larger shear zone with the cutting tool's advancement. A detailed study on restricting nanoparticles' behaviour is conducted by observing the primary shear zone propagation, as shown in Fig. 21. With the propagation of the primary shear plane, higher magnitude stress attempts to bypass the nanoparticle, which causes the irregular stress contour at the interface of each particle. As a result, a fragmented plastic strain field within matrix materials is formed due to the matrix's ability to deform plastically and particles' inability, see Fig. 22. The stress is therefore accumulated near the interface of particles and causes the highly concentrated plastic strain filed.

When the ratio between the particle diameter to uncut chip thickness increases, the particle's effect on stress distribution would be more dominant than that in nano-MMCs. By observing the von Mises stress pattern in the model of machining micro-MMCs, a significant difference when compared to that in machining nano-MMCs is that the particle size becomes comparable with the width of the primary shear zone (Fig. 19b–d). Similarly, micro-sized particles act as a barrier restricting the propagation of the primary shear zone. However, the primary shear zone is broken into two regions with a similar particle area and thus spread to surrounding when it is bypassing the micro-sized particle. Thus, greater compressive stress is generated on the particles under the squeezing action of cutting tool and matrix, resulting in a concentrated stress zone and maximum plastic strain on the tool-particle interface as shown in Fig. 23.

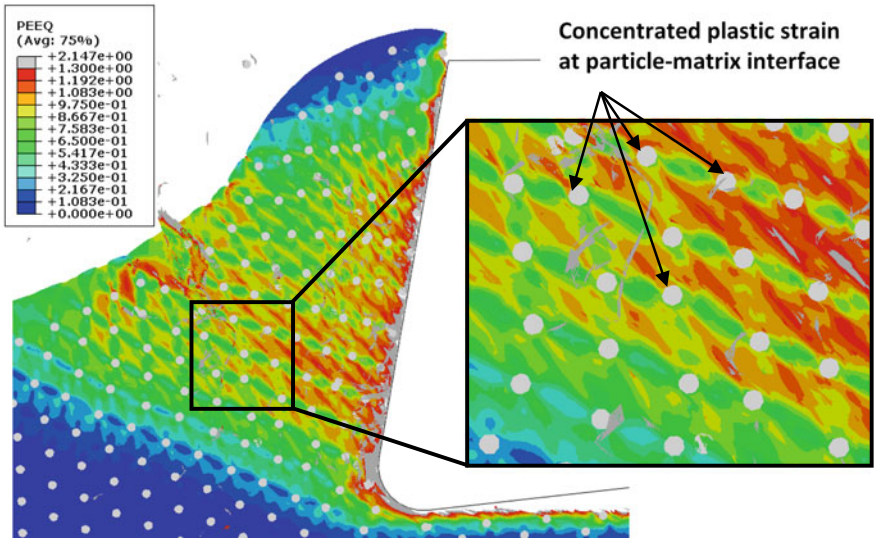

Fig. 22 Distorted plastic strain field in machining nano Al/SiC MMCs. *Source* [29], with permission from Elsevier

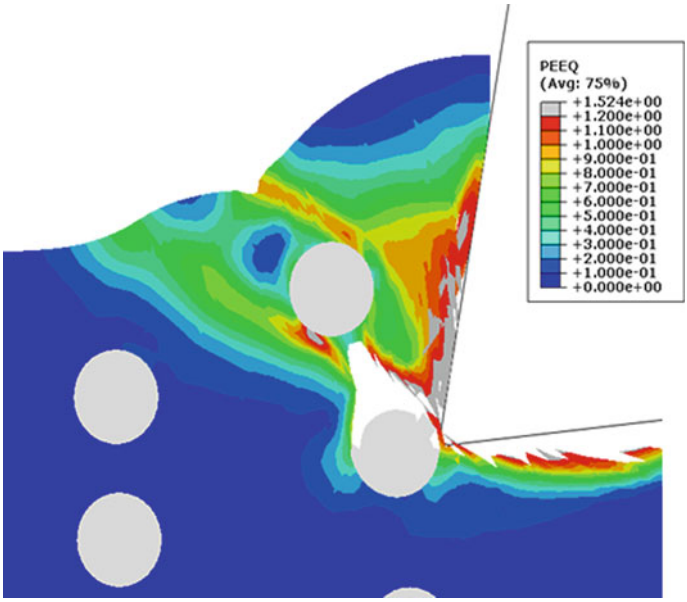

Fig. 23 Distribution of plastic strain filed in the machining of micro Al/SiC MMCs. *Source* [29], with permission from Elsevier

5.2 Tool-Particles Interaction

It is believed that the significant reduction in particle diameter from micro to nanoscale influence not only the stress distribution but also the tool-particle interaction. Figures 24 and 25 illustrate the tool-particle interaction in machining nano-MMCs and micro-MMCs, respectively. It can be observed from Fig. 24 that with the formation of a continuous chip, the particle embedded within formed chips slides over the rake face generating high localised stress at the tool-particle contact zone, which is similar as that for micro-MMCs. However, the nanoparticles are more likely to be squeezed by cutting edge due to their significantly large size difference, which leads to a relatively even distribution within particles. Also, the nanoparticles exhibit good mobility within the matrix, as mentioned earlier. As a result, nanoparticles keep intact without cleavage and fracture. In contrast, the micro-sized particles are observed to experience fracture.

Different behaviours of a particle interacting with the cutting tool in micro-MMCs machining process are shown in Fig. 25. It can be seen that the partially debonded particle is embedded within fragmented chips and slide along the cutting tool, resulting in the particle sliding behaviour on the tool rake face and a high localised contact region (Fig. 25a), which in turn would contribute to the tool wear. The particle located in the cutting path suffers a fracture. It was partially imbedded within the newly formed machined surface, which might be considered one of the main factors contributing to surface deterioration (Fig. 25b). Some particles located along or below the cutting path are pressed into the matrix (Fig. 19c). These particles acting as sharp cutting edge lead to the increased residual stress or severe plastic deformation on the machined surface. The particle detachment from the machined surface leading to the cavity can be observed from Fig. 25d. This phenomenon is

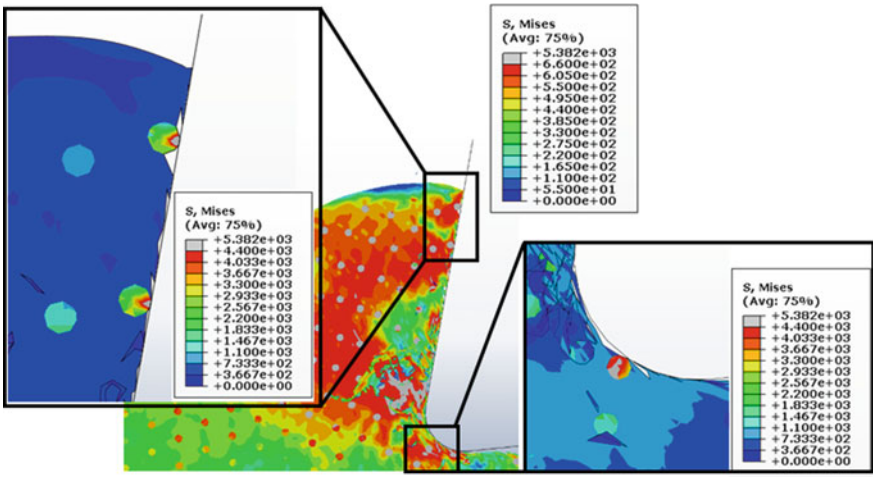

Fig. 24 Nanoparticles interacting with the cutting tool. *Source* [29], with permission from Elsevier

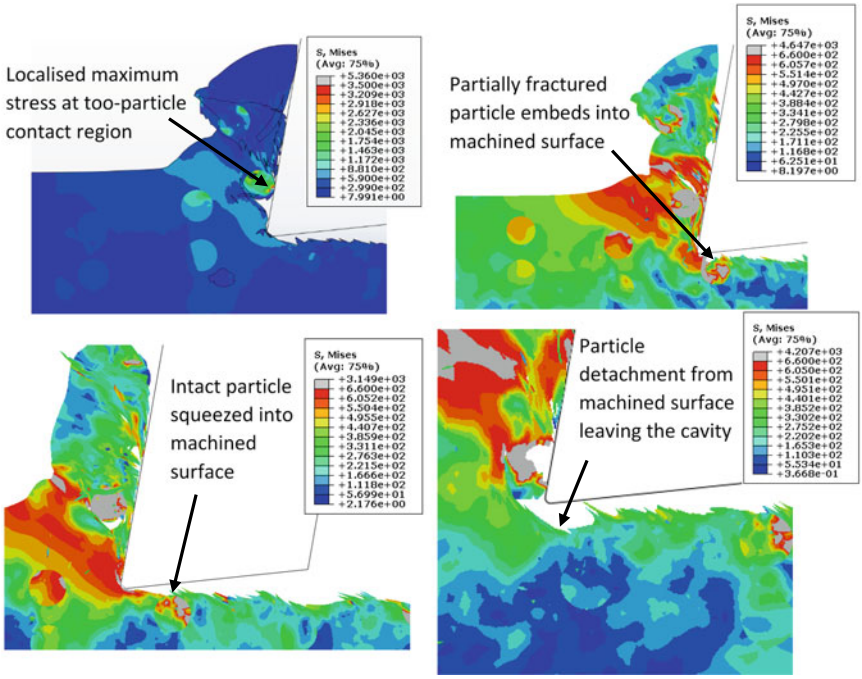

Fig. 25 Different tool-particle interaction behaviours in machining micro Al/SiC MMCs. *Source* [29], with permission from Elsevier

widely acknowledged by previous researchers in both experimental and simulation works.

The tool particle interaction can be visualised by analysing characteristics of the cutting force profile obtained from these two models (Fig. 26). Cutting forces from machining the homogeneous matrix material under the same cutting parameters are also plotted in Fig. 26. A larger cutting force fluctuation caused by the tool-particle interaction and fragmented chip formation is observed in the micro-MMCs machining process compared to homogeneous matrix materials. By comparison, apparent instability in cutting force obtained from machining nano-MMCs cannot be observed compared to that in machining homogeneous matrix. The larger cutting force fluctuation in machining micro-MMCs can be explained as results of various tool-particle interaction behaviours and the large particles' increased kinetic energy.

Generally, the tool-particle interface's high contact stress has been recognised as the main reason causing the tool wear. Various tool wear patterns can be obtained from machining nano and micro-MMCs, as shown in Fig. 27. Tooltip rounding and relatively smooth abrasive wear can be observed on the micro endmill's flank face in machining nano-MMCs (Fig. 27b). This can be attributed to the relatively small size of nanoparticles resulting in small kinematic energy compared to micro-sized particles during tool-particle interaction. Besides, good mobility of nanoparticles

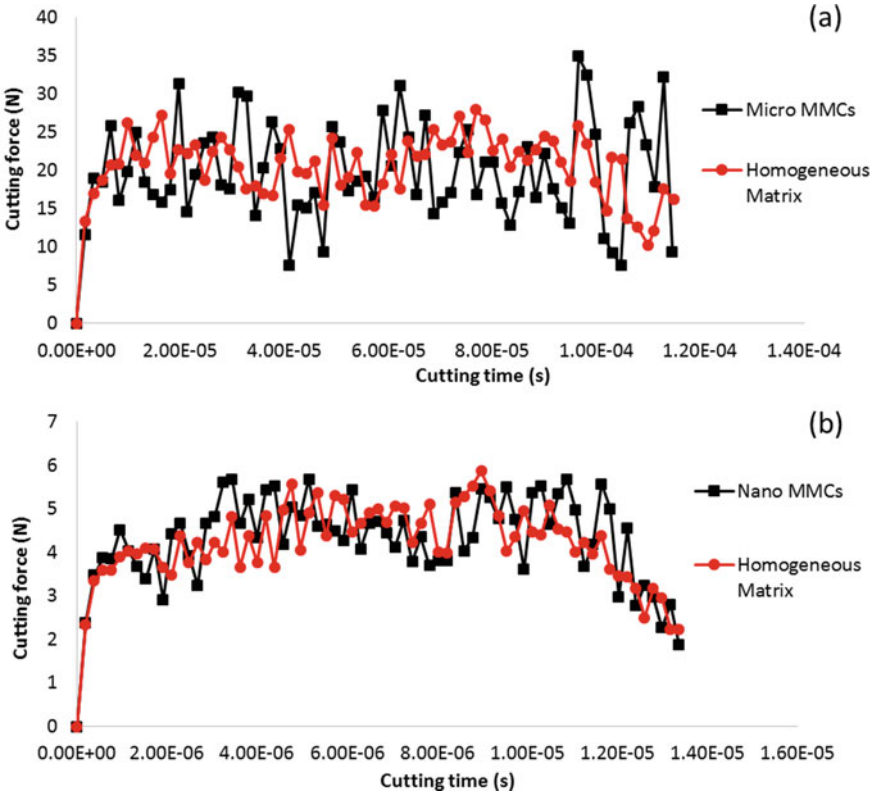

Fig. 26 Simulated cutting forces of micromachining Al/SiC MMCs reinforced with **a** micro-sized particles; **b** Nanoparticles. *Source* [29], with permission from Elsevier

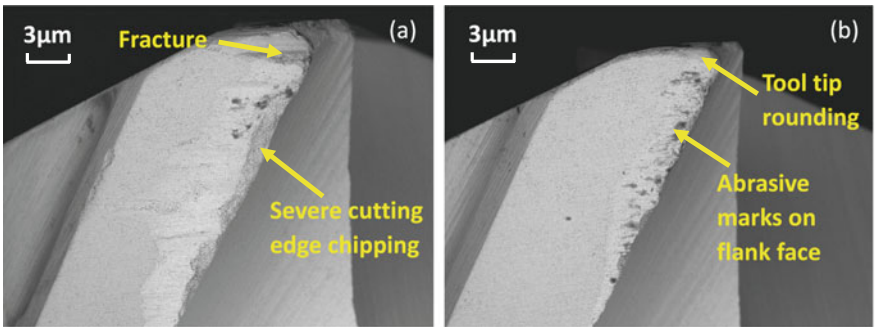

Fig. 27 SEM micrographs of main cutting edge wear of micro endmill obtained from machining Al/SiC MMCs reinforced with Vol. 10% **a** micro-sized particles (Φ:10 µm); **b** Nano-sized particles (Φ:0.2 µm) under feed per tooth of 4 µm/tooth, cutting speed of 125.64 m/min and depth of cut of 30 µm. *Source* [29], with permission from Elsevier

with matrix deformation is another crucial factor contributing to the smooth abrasive wear pattern. However, the low mobility of micro-sized particles within matrix materials and increased kinetic energy of micro-sized particles are believed to be the main reason that leads to a more severe edge chipping and fracture of tooltip on the endmill used in machining micro-sized MMCs, see Fig. 27a. Moreover, the unstable and fluctuating nature of the machining process caused by different tool-particles interaction behaviours accelerates the wear process.

5.3 Chip Formation Process

To analyse the chip morphology characteristics in machining the two MMC materials, it is necessary to understand the matrix's stress distribution. The size and location of particles play a significant role in the stress distribution pattern in the machining process. Figure 28 demonstrates the fragmented chips formation with stress distribution immediately after the chip formation shown in Fig. 19. Initially, the particles along the cutting path partially deboned without any direct contact with a tooltip, see Fig. 19b. With the tool advances, bypassing the primary shear plane occurred due to restricting the particle initiation behaviour. A highly concentrated stress zone is formed between the particle interface and upper surface of the workpiece in the shear plane and leads to crack initiation in the matrix, as shown in Fig. 28a. This crack initiation can be further proved by observing the high plastic strain field near this particle in Fig. 24. The plastic deformation mainly governs the MMCs workpiece behaviour in machining. As the tool advances, the matrix crack propagates towards the upper workpiece surface, as shown in Fig. 28b. Figure 28c shows the fragmented chips form.

Chips were collected from micro and nano-MMCs machining experiments to validate the chip formation models. The increased discontinuity can be observed at the sawtooth structure of the chips obtained from the machining of micro-MMCs (Fig. 29a). In contrast, continuous chips with saw tooth structure were found in machining nano-MMCs, as shown in Fig. 29b. The same observation was obtained from the experimental work conducted by Teng et al. [13]. It should be noted that although fragmented chips are formed in 2D FE simulation because the axial depth

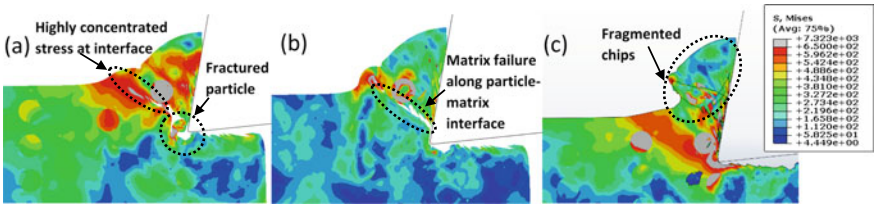

Fig. 28 Fragmented chips formation when micromachining of micro Al/SiC MMCs. *Source* [29], with permission from Elsevier

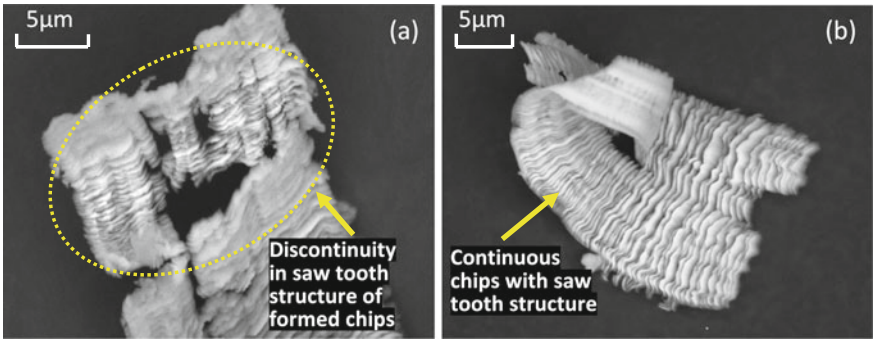

Fig. 29 SEM images of chips obtained from machining Al/SiC MMCs reinforced with Vol. 10% **a** micro-sized particles (Φ:10 μm); **b** Nano-sized particles (Φ:0.2 μm) under feed per tooth of 4 μm/tooth, cutting speed of 125.64 m/min and depth of cut of 30 μm. *Source* [29], with permission from Elsevier

of cut in the milling experiment is much greater than the micro-sized particle and also the micro-sized particles are randomly distributed in the matrix, the actual chips may not break along the width of the chip. Therefore, when observing a crossed section of the actual chips, the simulated chips morphology of micro and nano-MMCs shows high consistency with experimental results.

The highly concentrated stress zone can also be found at the particle–matrix interface in both models, as mentioned earlier. Therefore, it might not be the main reason for fragmented chips in the micro-MMCs machining process. The chip formation mechanism in machining micro-MMCs is depended on the size and location of particles which is the main factor determining the way of stress propagation. By comparing the width of the primary shear zone with particle size in these two models, it can be found that the shear zone is keeping intact during chip formation process in nano-MMCs rather than being fragmented in micro-MMCs. The existence of nanoparticle only affect the stress distribution pattern, and it does not significantly affect the overall integrity of the primary shear zone during its propagation. In other words, the restricting behaviour of micro-sized particles is more dominant than that in nanoparticles, which results in low mobility of particles within matrix deformation. This might be due to the sizeable uncut chip thickness to particle diameter in machining nano-MMCs. It can be thought that the location of nanoparticles has little effect on the chip formation mechanism in the nano-MMCs machining process. Therefore, the ratio of uncut chip thickness to particle size might be considered the fundamental reason was determining the chip formation mechanism. Finally, the intact primary shear zone means that the material removal is achieved by shear sliding in the nano-MMCs machining process. For micro-MMCs, as the result of strong restricting behaviour of micro-sized particles, the particle detachment from matrix caused by highly concentrated stress at its interface can be recognised as one factor promoting the formation of fragmented chips.

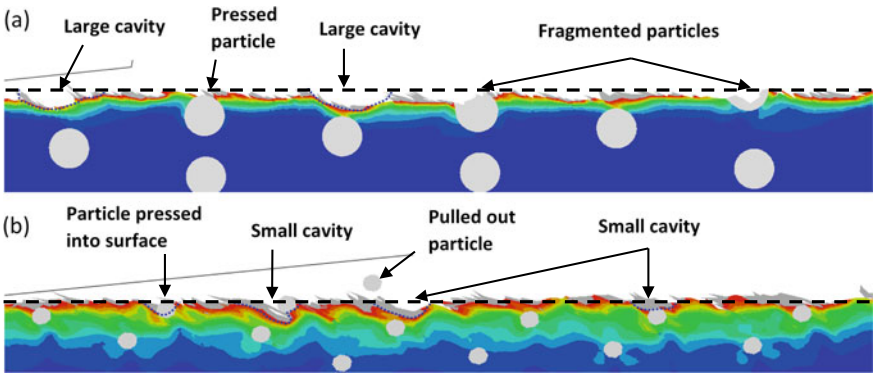

Fig. 30 Simulated surface morphology from machining **a** micro-MMCs; **b** Nano-MMCs. *Source* [29], with permission from Elsevier

5.4 Machined Surface Morphology

Different tool-particles interaction behaviours can be found in machining nano and micro-MMCs, leading to different machined surface morphology. Figure 30 shows the simulated surface morphology in machining micro and nano-MMCs. The surface deterioration in machining micro-MMCs can be attributed to the surface defects such as cavities, scratch marks, fragmented particles embedded within matrix and particles pressed into matrix causing excessive strain, which leads to a matrix failure (Fig. 30a). The abovementioned phenomenon obtained from simulation model can be easily observed from experimental results. It can be observed from Fig. 31a and b that the large cavity is formed when the majority of particles located in the cutting path are pulled away from the matrix during tool-particle interaction. Also, the fragmented particle embedded within the matrix is observed in Fig. 31a, consistent with simulated results. Excessive compressive stress would be caused by the particles pressed into the machined surface leading to the matrix failure or irreversible plastic deformation.

Moreover, during the cutting process, scratch marks on the machined surface will be formed when the fragmented particles act as sharp cutting edge being ploughed through between the flank face of the cutting tool and matrix. The magnified images of scratch marks marked in region i and ii can be found in Fig. 31b. Similar surface morphology can be observed in the simulation model of machining nano-MMCs (Fig. 30b). However, they are not observed in machined surface obtained from experimental works. Distinct milling tool path can be observed on the machined surface (Fig. 31c). Micro defects can be found at the tool path which broke its continuity. This might be caused by the scratching of residual chips containing nanoparticles at the tool-matrix interface during high-speed machining. It can be said that the significant reduction in particles size is beneficial for improving the machined surface quality.

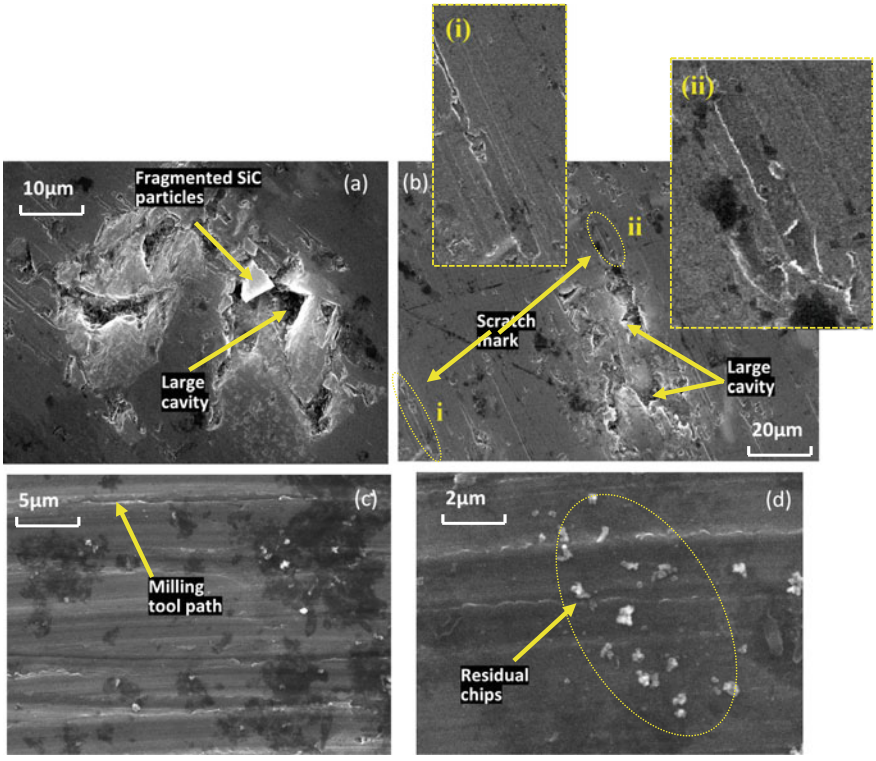

Fig. 31 SEM micrographs of the machined surface from experimental works **a** and **b** micro-MMCs; **c** and **d** nano-MMCs under the feed per tooth of 4 μm/tooth, cutting speed of 125.64 m/min and depth of cut of 30 μm. *Source* [29], with permission from Elsevier

6 Review Questions

(1) Please state the differences between macro-mechanical and micro-mechanical models.
(2) What are the primary materials removal mechanism revealed by the finite element modelling method when machining particulate MMCs?
(3) According to the simulation results, how do the reduced particles from micro-sized to nano-sized affect machinability? How do these relate to the results obtained from machining experiments?
(4) Please state the chip formation process of nano MMCs.
(5) Why do the particles near the primary shear zone take more stress than matrix materials?
(6) Please explain what can cause the distorted stress contour located at the vicinity of nanoparticles in FE analysis.
(7) Why would the addition of particle accelerate the progression of tool wear?
(8) What causes the lamellate structure of chips?

(9) How does the ratio of particle to uncut chip thickness affect the stress distribution during machining process?
(10) Please give the different behaviours of particles interacting with cutting tool in the machining process of micro MMCs.
(11) Please give the main types of surface defects in machining micro and nano MMCs and explain the reasons.
(12) How does the size effect affect the specific cutting energy?
(13) What causes different tool wear patterns when machining micro and nano MMCs?

References

1. Dandekar, C.R., Shin, Y.C.: Modeling of machining of composite materials: A review. Int. J. Mach. Tools Manuf. **57**, 102–121 (2012)
2. Monaghan, J., Brazil, D.: Modeling the sub-surface damage associated with the machining of a particle reinforced MMC. Comput. Mater. Sci. **9**(1–2), 99–107 (1997)
3. Monaghan, J., Brazil, D.: Modelling the flow processes of a particle reinforced metal matrix composite during machining. Compos. Part a Appl. Sci. Manuf. **29**(1–2), 87–99 (1998)
4. Pramanik, A., Zhang, L.C., Arsecularatne, J.A.: An FEM investigation into the behavior of metal matrix composites: Tool-particle interaction during orthogonal cutting. Int. J. Mach. Tools Manuf. 47(10), 1497–1506 (2007)
5. Zhu, Y., Kishawy, H.A.: Influence of alumina particles on the mechanics of machining metal matrix composites (tie constrains). Int. J. Mach. Tools Manuf. **45**(4–5), 389–398 (2005)
6. Dandekar, C.R., Shin, Y.C.: Multi-step 3-D finite element modeling of subsurface damage in machining particulate reinforced metal matrix composites. Compos. Part Appl. Sci. Manuf. **40**(8), 1231–1239 (2009)
7. Zhou, L., Huang, S.T., Wang, D., Yu, X.L.: Finite element and experimental studies of the cutting process of SiCp/Al composites with PCD tools. Int. J. Adv. Manuf. Technol. **52**(5–8), 619–626 (2011)
8. Zhou, L., Wang, Y., Ma, Z.Y., Yu, X.L.: Finite element and experimental studies of the formation mechanism of edge defects during machining of SiCp/Al composites. Int. J. Mach. Tools Manuf. **84**, 9–16 (2014)
9. Wang, B., Xie, L., Chen, X., Wang, X.: The milling simulation and experimental research on high volume fraction of SiCp/Al. Int. J. Adv. Manuf. Technol. **82**(5–8), 809–816 (2016)
10. Umer, U., Ashfaq, M., Qudeiri, J.A., Hussein, H.M.A., Danish, S.N., Al-Ahmari, A.R.: Modeling machining of particle-reinforced aluminum-based metal matrix composites using cohesive zone elements. Int. J. Adv. Manuf. Technol. **78**(5–8), 1171–1179 (2015)
11. Ghandehariun, A., Kishawy, H.A., Umer, U., Hussein, H.M.: Analysis of tool-particle interactions during cutting process of metal matrix composites. Int. J. Adv. Manuf. Technol. **82**(1–4), 143–152 (2016)
12. Ghandehariun, A., Kishawy, H.A., Umer, U., Hussein, H.M.: On tool-workpiece interactions during machining metal matrix composites: investigation of the effect of cutting speed. Int. J. Adv. Manuf. Technol. **84**(9–12), 2423–2435 (2016)
13. Teng, X., Huo, D., Chen, W., Wong, E., Zheng, L., Shyha, I.: Finite element modelling on cutting mechanism of nano Mg/SiC metal matrix composites considering cutting edge radius. J. Manuf. Process. 32 (2018)
14. Johnson, G., Cook, W.: A constitutive model and data for metals subjected to large strains, high strain rates and high temperatures. In: Proceedings of the 7th International Symposium on Ballistic, pp. 541–547 (1983)

15. Zerilli, F.J., Armstrong, R.W.: Dislocation-mechanics-based constitutive relations for material dynamics calculations. J. Appl. Phys. **61**(5), 1816 (1987)
16. Follansbee, P.S., Gray, G.T.: An analysis of the low temperature, low and high strain-rate deformation of Ti−6Al−4V. Metall. Trans. A **20**(5), 863–874 (1989)
17. Nemat-Nasser, S., Guo, W.-G., Nesterenko, V.F., Indrakanti, S.S., Gu, Y.-B.: Dynamic response of conventional and hot isostatically pressed Ti–6Al–4V alloys: experiments and modeling. Mech. Mater. **33**(8), 425–439 (2001)
18. Shi, J., Liu, C.R.: On predicting chip morphology and phase transformation in hard machining. Int. J. Adv. Manuf. Technol. **27**(7–8), 645–654 (2006)
19. Simoneau, A., Ng, E., Elbestawi, M.A.: Chip formation during microscale cutting of a medium carbon steel. Int. J. Mach. Tools Manuf. **46**(5), 467–481 (2006)
20. Abaqus/Explicit V6.14 User manual (2016)
21. Aurich, J.C., Bil, H.: 3D Finite Element Modelling of Segmented Chip Formation. CIRP Ann. Manuf. Technol. **55**(1), 47–50 (2006)
22. Ceretti, E., Lucchi, M., Altan, T.: FEM simulation of orthogonal cutting: serrated chip formation. J. Mater. Process. Technol. **95**(1), 17–26 (1999)
23. Hua, J., Shivpuri, R.: Influence of crack mechanics on the chip segmentation in the machining of Ti-6Al-4. In: Proceedings of the 9th ISPE International Conference on Concurrent Engineering, pp. 357–365 (2002)
24. Hillerborg, A., Modéer, M., Petersson, P.-E.: Analysis of crack formation and crack growth in concrete by means of fracture mechanics and finite elements. Cem. Concr. Res. **6**(6), 773–781 (1976)
25. Maekawa, K., Obikawa, T., Yamane, Y., Childs, T.H.C.: Metal Machining: Theory and Applications. Wiley, New York (2000)
26. Lai, X., Li, H., Li, C., Lin, Z., Ni, J.: Modelling and analysis of micro scale milling considering size effect, micro cutter edge radius and minimum chip thickness. Int. J. Mach. Tools Manuf. **48**(1), 1–14 (2008)
27. Liu, X., Devor, R.E., Kapoor, S.G., Ehmann, K.F.: The mechanics of machining at the microscale: assessment of the current state of the science. J. Manuf. Sci. Eng. **126**(4), 666–678 (2004)
28. Teng, X., Huo, D., Wong, E., Meenashisundaram, G., Gupta, M.: Micro-machinability of nanoparticle-reinforced Mg-based MMCs: an experimental investigation. Int. J. Adv. Manuf. Technol. 1–14 (2016)
29. Teng, X., Chen, W., Huo, D., Shyha, I., Lin, C.: Comparison of cutting mechanism when machining micro and nanoparticles reinforced SiC/Al metal matrix composites. Compos. Struct. **203**(July), 636–647 (2018)

Drilling of Fibre Reinforced Polymers and Hybrid Stacked Materials

Ahmed Sadek, Zhongde Shi, Mouhab Meshreki, Ireene Sultana, and Helmi Attia

Abstract Hole making represents the majority of the machining operations of composites and hybrid stacked aerospace-structures. Conventional drilling induced part defects, such as delamination of layers and thermal damage of the matrix, are of major economic and safety concerns for aerospace manufacturers. This chapter discusses selected emerging non-conventional processes for drilling of composites and hybrid stacks, which could effectively prevent the sources of drilling induced damage without compromising the process productivity. The discussion in this chapter has focused on process optimization based on understanding the mechanics of the process. Additionally, a new online cyber-physical adaptive control (CPAC) capability is presented, which demonstrates the maximization of tool life and process productivity while preserving the part quality based on integrated advanced process modeling and smart real-time tool wear detection.

1 Introduction

In recent years, composites have gained enormous acceptance as a key material in the manufacturing of aircraft. Holes in composites are commonly made for structure joining, avionics and weight reduction. In addition, it is common to drill through hybrid composite metallic structures (stacks) due to the co-existence of different materials in the aero-structure.

Tremendous research efforts have been exerted towards improving the conventional drilling processes' performance and introducing new nonconventional drilling processes to provide root solutions to the drilling induced material damage. The research carried out on conventional drilling of fibre reinforced polymers FRPs [1,

A. Sadek (✉) · Z. Shi · M. Meshreki · H. Attia
Aerospace Manufacturing Technologies Center, National Research Council of Canada, Montreal, Canada
e-mail: Ahmad.sadek@nrc-cnrc.gc.ca

M. Meshreki · I. Sultana · H. Attia
Department of Mechanical Engineering, University of McGill, Montreal, Canada

I. Shyha and D. Huo (eds.), *Advances in Machining of Composite Materials*, Engineering Materials, https://doi.org/10.1007/978-3-030-71438-3_10

2] indicated that the conventional drilling of FRPs and hybrid stacks in dry conditions tends to require low feeds combined with high rotational speeds for most of the cases in order to reduce mechanical damage. Operating at low feeds compromises the processes productivity and increases the tool-workpiece contact time. This promotes tool wear and thermal damage of the FRP material, mostly when drilling is performed at the high range of the so far investigated rotational speeds. Therefore, a motivation to modify the conventional drilling process in order to untie this conflict was created. Intermittent or interrupted cutting processes were introduced for drilling of FRPs and stacks to eliminate continuous engagement of one or more cutting edges of the tool with the workpiece [3], leading to force and temperature reduction [4]. The reduction of cutting forces can be attributed to less contact time and length between the chip and the tool's rake face, which reduces the frictional force component [5]. These features reduce or eliminate the drilling-induced damage when drilling FRPs and hybrid FRP/metal stacked materials, such as entry and exit delamination, thermal damage (matrix burnout), fibre pull-out, and interlaminar delamination. The deflection of the CFRP layer under the drilling tool's axial forces' action is one of the leading causes of the machining induced interlaminar delamination, which is the most widely experienced serious FRP type of damage that undermines the material mechanical properties.

In orbital drilling (OD), the cutting tool rotates about its axis and simultaneously about the desired cylindrical hole axis at an eccentric distance. It is fed along with the hole depth following a helical path. This process has demonstrated its potential in avoiding the types mentioned above of damage [6], due to the axial force reduction and the elimination of the axial dwell of the stationary drilling tool centre over the uncut material thickness [7]. Although this process produces delamination-free holes with allowable geometric accuracy, it reduces productivity due to the helical path that the tool has to follow compared to the linear axial feed in conventional drilling. This is compounded by the limitations on the maximum speed and acceleration that the machine can achieve to deliver the helical tool motion when OD is performed on a CNC machining centre. Super-abrasive orbital drilling (SAOD) using diamond tools is a new promising process for drilling FRP parts and hybrid stacks. It has shown to significantly extend the tool life while preventing drilling-induced damage [8]. Its limitation in producing low surface finish is addressed in this chapter.

The vibration-assisted drilling (VAD) process is another example of an intermittent cutting process that can provide practical solutions to overcome the challenges of drilling FRP and hybrid stacked materials. In the VAD process, a harmonic motion is superimposed over the conventional feed motion in the axial direction [9]. This type of mixed motion is believed to combine the mechanical and thermal benefits of the intermittent cutting state, and at the same time preserve the process productivity by maintaining the conventional axial feed motion [10]. Such unique capabilities have placed VAD as a powerful candidate to be implemented in most of the aerospace manufacturing facilities.

For further process development and optimisation of intermittent drilling processes, it is imperative to reach a deeper understanding of the physics and

phenomena associated with such processes. Following a summary of the characteristics of the conventional drilling process of hybrid stacks, the subsequent sections of this chapter will provide insight into the fundamental mechanics and research advances of the orbital and vibration-assisted drilling processes of FRP composites and hybrid FRP/metal stacks.

2 Conventional Drilling of Hybrid Stacks

Extensive research work has been on-going to better understand the process and overcome the challenges of drilling through two or three different materials, each with its different thermal and mechanical properties. The most common type of stacks is made of Titanium (Ti) and/or Aluminium (Al) with Carbon Fibre Reinforced Polymer (CFRP). Several factors affect the process, namely, the stack materials, the sequence and thickness of the materials, the tool geometry, tool wear, the chip evacuation, as well as the type of lubricant and coolant, if any.

The complexity of the process is also dependent on the overall thickness of such stacks, which can range from thin (~5 mm) to deep (~80 mm) thicknesses for aerostructures applications. The stack sequence refers to the order in which the layers of the stacks are assembled. Each sequence comes with its special challenges. For example, Ti-CFRP stacks, where titanium is drilled first, the thermal damage at the Ti-CFRP interface is commonly encountered. Due to Titanium's low thermal conductivity and heat capacity, the material experiences a substantial temperature rise. Simultaneously, given that the CFRP constrains the Ti layer, this temperature rise is associated with damage on the composite's surface.

On the other hand, negligible thermal damage is experienced in the reversed sequence, whereby the CFRP is at the entry, and the Ti is at the exit. In this case, another challenge arises, mainly due to the titanium chip evacuation, which damages the surface of the CFRP hole and causes flute clogging. In the drilling of Al/CFRP/Ti, the titanium chips' transport causes erosion and delamination of the CFRP layers. The depth of the erosion can reach up to 300 μm [11].

The FRP- metal drilling sequence may prevent the exit delamination as the metallic layer has a backing effect at the FRP exit plan. Despite such a favourable effect, the reverse sequence of metal-FRP is still widely used to avoid the erosion and delamination of the FRP layer resulting from the transport of the metallic chips.

With such configurations, the drilling forces need to remain below a specific critical limit for each layer of the stack to avoid inducing damage. Figure 1a and b shows an example of the axial force and torque (moment) in conventional drilling of Ti-CFRP stacks [12]. The forces and torques in the Ti component are almost three-fold higher than in the CFRP layer, as has been confirmed in most of the research work regardless of the tool geometry, coating, lubrication or stack sequence [13]. In order to capture the effect of the cutting feed and speed on the force, analysis of variance ANOVA has frequently been performed [14]. In general, it was found that the feed has a dominant effect on the forces and torque. For example, in [15],

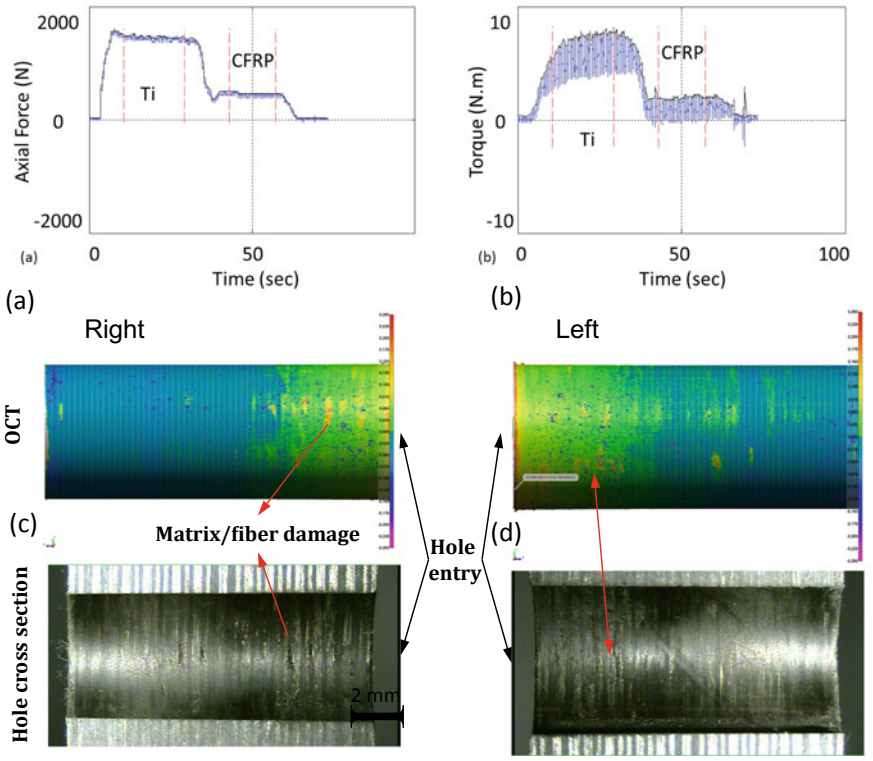

Fig. 1 **a** Thrust force and **b** moment in drilling Ti-CFRP stacks. **c** right and **d** left cross-section of CFRP after drilling Ti-CFRP [12]

it was found that feed and the drill's tool diameter have a higher effect in CFRP-Al stack drilling compared to the speed. It was also found that their effect was higher in aluminium than in CFRP.

The cutting temperature is one of the crucial parameters in stack drilling. It affects the tool performance and life, and the hole quality in terms of thermal damage and dimensional errors. Several approaches have been undertaken to control the temperature including flood cooling, minimum quantity lubrication or air cooling.

In the CFRP-Al drilling, the temperature was found to be proportional to the speed [16]. When drilling the CFRP, the temperature rises rapidly (up to 230 °C), whereas when drilling the Al layer, the temperature drops quickly from the peak value to 115 °C. The higher temperature in CFRP as compared to the aluminium is attributed to the abrasive nature of the carbon fibres and the low thermal conductivity of CFRP, as compared to the high conductivity of Al. It was also shown that it is not likely for the heat generated during aluminium drilling to affect the CFRP due to its high thermal diffusivity [17].

As indicated earlier, titanium's low thermal conductivity and heat capacity result in higher cutting temperature, affecting the tool wear. In the drilling of CFRP-Ti, it

was shown that the thermomechanical damage of the CFRP is caused by insufficient extraction of metallic Ti-chips which are reaming at the newly generated bore surface [18]. In case of Ti-CFRP, the high temperature of titanium causes (1) thermal damage on the entry surface of CFRP, and (2) adherence of chips on the tool surface, causing damage to the internal surface of the CFRP hole [12]. Figure 1c and d shows the cross-section of a CFRP hole and the corresponding optical computed tomography (OCT) scan, following the drilling of a Ti layer [12]. As can be seen, internal delamination and surface damage caused by the tool wear. In some cases, it was noticed that the drilling temperature was not affected by speed for the CFRP [19].

3 Vibration-Assisted Drilling of FRPs and Hybrid Stacks

The vibration-assisted drilling (VAD) is based on superimposing an axial vibratory motion on the primary conventional axial feed to produce a cyclic separation between the tool and the workpiece [3]. Figure 2a shows the mean conventional path of the cutting edges in the cylindrical hole [20]. Figure 2b shows the combined conventional and vibratory motion of the tool edges in an opened hole presentation. The figure

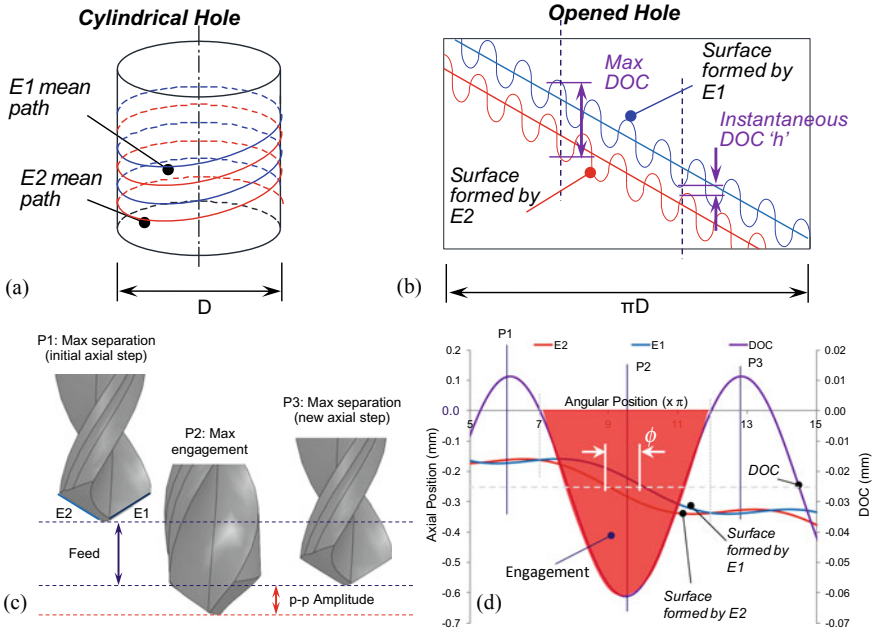

Fig. 2 **a** Mean paths of the tool cutting edges in the cylindrical hole, **b** the vibratory path of the tool cutting edges represented in the opened hole. **c** Positions of the tool edge through the VAD engagement and the separation cycles **d** Axial and angular positions of the machined surfaces formed by the cutting edges during VAD, and the resultant DOC [20]

shows that at a specific angular position, the depth of cut (DOC) is determined by the vertical difference between a point on the previously formed surface and a point on the surface about to be formed at the same angular position. The chip thickness varies according to the phase difference between the variations on the two surfaces, controlled by the process parameters feed rate 'f_r', rotational tool frequency 'ω_T', axial modulation frequency 'ω_m', and axial modulation amplitude 'A_m'. Based on the frequency range of study, VAD is classified as low-frequency (LF-VAD), where the modulation frequency is $\leq$1000 Hz, and high frequency (HF-VAD), where the modulation frequency is >1000 Hz. The associated maximum modulation amplitudes (peak-to-peak) with LF-VAD and HF-VAD are 600 μm and 20 μm, respectively.

Figure 2d shows a plot of the axial and angular positions of the points on the machined surfaces formed by the cutting edges $E1$ and $E2$ according to the combined conventional and vibratory motion of the tool. The tool positions P1, P2, and P3 described in Fig. 2c are marked on the plot in Fig. 2d, showing the maximum disengagement and engagement positions. The figure shows that the sinusoidal forms of the two surfaces formed by $E1$ and $E2$ are not in phase, which results in a dynamic DOC during VAD. The phase difference between the two surfaces controls the instantaneous DOC value. Therefore, the rotational speed and the modulation frequency possess a non-monotonic effect on the maximum DOC when the tool is at the maximum engagement position and on the maximum axial force accordingly. For constant f_r and A_m, the increase in the phase difference 'ϕ_n', for $\phi_n \leq \pi$, increases the maximum DOC, which is defined by the maximum distance between the peaks of both surfaces as shown in Fig. 2b. This is followed by a decrease in the maximum DOC for $\pi < \phi_n \leq 2\pi$. At the position of full separation, the DOC drops to a value of zero. The effect of different combinations of the VAD parameters on the maximum DOC and axial force will be discussed in the following sections.

The chip's width is also determined by the duration of the engagement cycle controlled by the modulation frequency and the rotational speed. Such factors have a direct impact on cutting energy, which is translated into drilling forces and temperatures. Experimental results showed the capability of VAD to reduce the drilling forces compared to conventional drilling of FRPs [21]. The beneficial effect of low frequency-high amplitude (LFHA) VAD includes the increase in tool life by nearly twofold before reaching the critical thrust force, cutting power or tool wear [21]. Significant temperature reduction in LFHA-VAD of metallic materials was reported in [22]. Further understanding of the VAD parameters' effect on the drilling forces and the temperature was provided in [20] through a systematic experimental analysis. The VAD parameters were controlled independently.

3.1 Drilling Forces in Vibration-Assisted Drilling (VAD)

The research work presented in [23] examined the effect of the low-frequency LFHA-VAD conditions, shown in Table 1, on the drilling forces and torques in hybrid CFRP/Al stacks. Analysis of the results presented in Fig. 3 showed the dominant

Table 1 VAD of CFRP/test conditions of VAD of CFRP/Al stacks [23]

Test No	Cutting speed (m/min)		f_r (mm/rev)	ω_m (Hz)	A_m (mm)
	CFRP	AL			
1	130	200	0.04	45	0.005
2	130	200	0.06	50	0.02
3	130	200	0.08	55	0.05
4	150	200	0.04	45	0.005
5	150	200	0.06	50	0.02
6	150	200	0.08	55	0.05
7	170	200	0.04	45	0.005
8	170	200	0.06	50	0.05
9	170	200	0.08	55	0.02

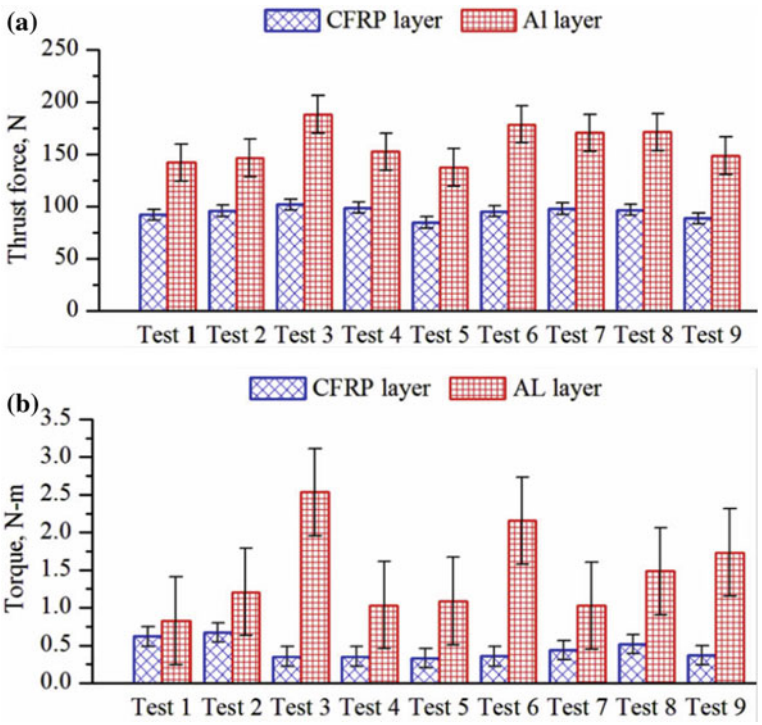

Fig. 3 Measurements of **a** thrust force and **b** torque in the CFRP and Al layers [23]

effect of the modulation amplitude 'A_m', followed by the feed 'f_r' on the measured forces in the CFRP and Al layers.

The independent VAD parameters investigated in [20] were found to have non-monotonic effects on the drilling forces. This is due to the competing effects of cutting force reduction and increase via progressive material removal and localised increased DOC, respectively. This investigation showed a consistent direct relationship of the maximum axial force with the modulation amplitude and the feed. This is due to the increase in a maximum depth of cut with increasing the feed or the amplitude, which requires higher energy to remove a larger chip volume. The higher frequency $\omega_m = 60$ Hz increased the axial force concerning the lower frequency $\omega_m = 30$ Hz. Such an increase is due to the increase in the phase difference 'ϕ_n', which increased the maximum DOC for $\phi_n \leq \pi$. On the other hand, the maximum axial force was shown to have an inverse relationship with the rotational speed 'n' for the same frequency. Increasing the rotational speed means increasing the number of rotational cycles of the cutting edges for the same number of vibration cycles, which reduces the maximum chip thicknesses.

In the HF-VAD regime, Fig. 4 shows the effect of the modulation amplitude and frequency on the measured axial force in the CFRP and Ti-6Al-4 V layers at a rotational speed n = 2000 rpm. For the investigated drilling feeds, the HF-VAD showed a 20–30% reduction in the thrust force in the CFRP and Ti6Al4V layers,

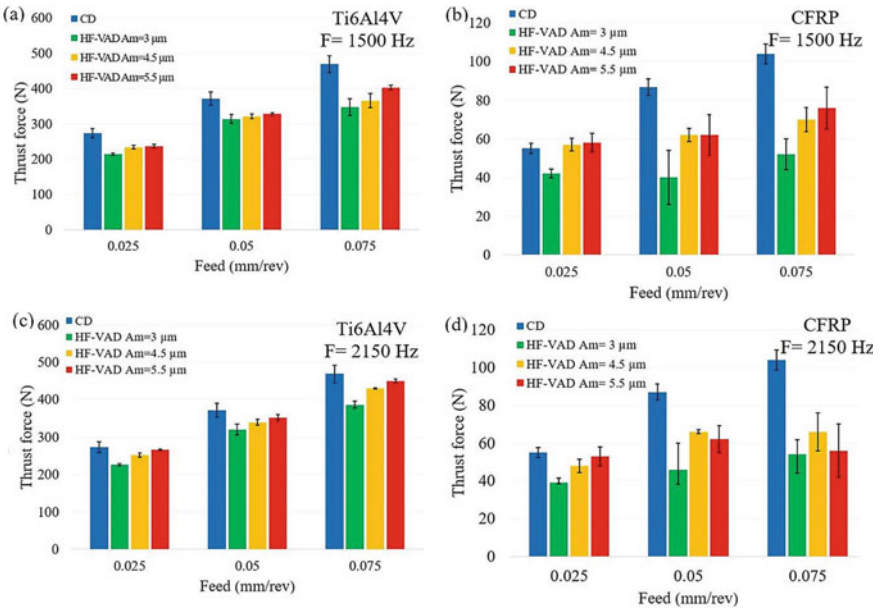

Fig. 4 Effect of feed and HF-VAD modulation frequency and amplitude and n = 2000 rpm on the thrust (axial) force in the Ti6Al4v layer at **a** $\omega_m = 1500$ Hz and **c** $\omega_m = 2150$ Hz and CFRP layer at **b** $\omega_m = 1500$ Hz and **d** $\omega_m = 2150$ Hz [24]

compared to conventional drilling. The following are the main factors that contributed to the force reduction in LF-VAD and HF-VAD:

- The progressive removal of smaller volumes of chip consumes less energy during the duty cycles.
- The broken metallic chips facilitate chip evacuation and reduce the frictional forces on the rake face.
- The elimination of the extrusion/pressing effect under the chisel edge, allowing more tangential cutting by the primary cutting edges.
- Some theories related the force reduction in the HF-VAD to the so-called knifing effect, which resemblances the high stress state formed while cutting with serrated edges.

3.2 *The Thermal Aspect of Vibration-Assisted Drilling (VAD)*

The thermal aspect of VAD is critical, especially in the drilling of CFRP/Ti stacks due to the low thermal diffusivity of the Titanium layer during the transient stage of drilling through the CFRP/Ti interface. This results in heat flow towards the CFRP layer, which burns out the matrix and damages the FRP layer. The VAD has exhibited up to 43% temperature reduction than conventional drilling of CFRP/Ti stacks, as reported in [25]. It was also shown that the vibration amplitude should reach a certain threshold level to have such a favourable effect. This is clearly shown in Fig. 5a where the temperature was found to significantly drop at amplitudes greater than or equal to Am = 0.07 mm. The explanation of the cooling effect in VAD is based on the size of the air gap formed during the separation cycle as well as the flow of the air inside such a gap. As shown in the analysis reported in [26], the confined air gap between the tool and the machined surface resembles a closed enclosure in a rotor–stator system. The airflow regime in the gap depends on the rotational speed 'n' and the gap width 'g' between the tool (rotor) and the workpiece (stator). Low rotational speeds produce a three-dimensional laminar airflow in the gap, driven by

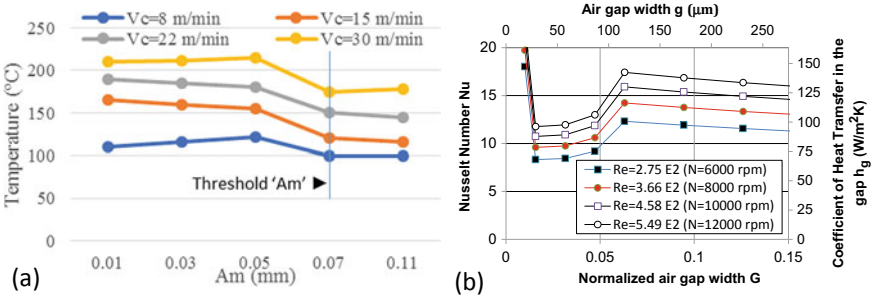

Fig. 5 **a** Effect of independent VAD parameters on temperature in the Ti-6Al-4 V layer f = 0.1 mm/rev [25]. **b** Effect of rotational speed and air gap on the coefficient of heat transfer 'h_g' [26]

the imbalance of centrifugal forces in the annulus. For higher rotational speeds and gap width, Reynolds number 'Re' reaches a critical value 'Re_{cr}' and toroidal Taylor vortices are formed. The coefficient of heat transfer CHT across the air gap 'h_g' can be expressed in terms of the dimensionless parameters: Nusselt Number 'Nu', Reynolds Number 'Re', and the normalised gap width 'G = g/R', where 'R' is the rotating tool radius. The plot in Fig. 5b shows the Nu correlations [26, 27].

Figure 5b shows that at G = 0.01, h_g is much higher than that of the free rotor in open space. At intermediate gap widths $0.02 \leq G \leq 0.06$, the CHT 'h_g' drops to a minimum level at $G \approx 0.02$ and then increases to a maximum level at G ~0.063. For larger gap widths, G >0.06, the increase in the air gap leads to a decoupling effect between the tool and workpiece surfaces, which reduces h_g. A significant enhancement in the CHT can be achieved when low frequency vibration (40–120 Hz) is imposed on the rotating body. This correlation explains the sudden temperature reduction behaviour at the threshold amplitude (Am = 0.07 mm) shown in Fig. 5a.

Figure 6 shows the effect of the modulation amplitude and frequency on the drilling tool tip maximum temperature at the hole exit plane. The figure shows a general trend of temperature reduction of around 35% for the tested HF-VAD conditions compared to conventional drilling [24] due to the lower cutting energy and the improved chip evacuation efficiency unlike the broad range of modulation amplitude and air gap in LF-VAD, the limited range of Am variation that could be provided by the piezoelectric HF-VAD actuator used in [24] resulted in marginal variations in temperature reduction.

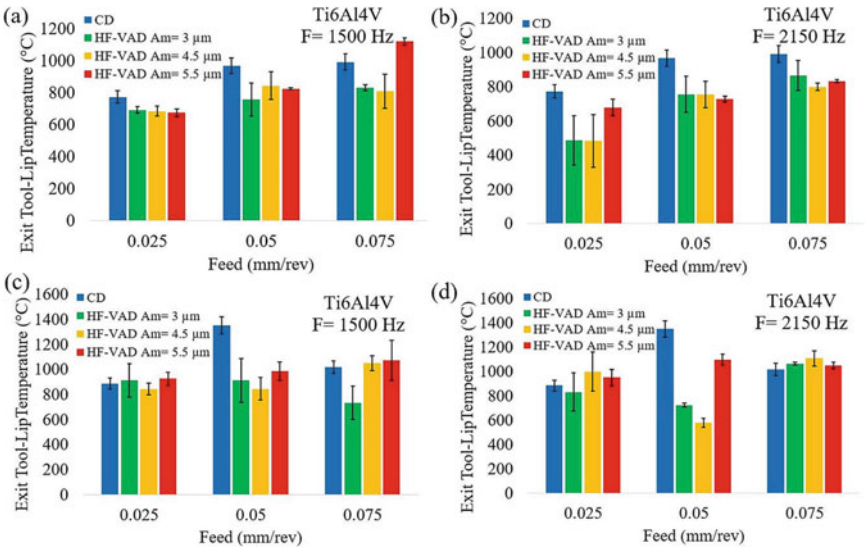

Fig. 6 Effect of modulation amplitude and frequency **a**, **c** 1500 Hz and **b**, **d** 2150 Hz on the exit tool-lip temperature for different feeds at **a**, **b** n = 2000 rpm and **c**, **d** n = 3000 rpm [24]

3.3 Hole Quality and Surface Integrity in VAD

The reduced axial forces in VAD has reduced the burr height measured at the exit plane of the Ti-6Al-4 V layer from 1.5 mm to 0.1 mm, respectively [18]. In CFRP, Fig. 7a shows the effect of "ω_m" and "A_m" on the exit delamination factor ($\varphi_d = (D_m - D_h)/D_h$), *where "$D_m$" is the maximum diameter of the circle encompassing the observed delamination, and "D_h" is the nominal hole diameter at the hole exit plane*). At low feed, delamination free holes could be produced. The exit delamination factor did not follow a clear trend with respect to the modulation frequency and amplitude. The feed has exhibited the most dominant effect, where the delamination factor increased from acceptable ($\varphi_d < 0.5$) at the low feed to unacceptable levels ($\varphi_d > 0.5$) at higher feeds. Although the highest exit delamination factor took place at the low rotational speed, the entire range of high rotational speed combined with high feed rates resulted in delamination factors beyond the acceptable limit ($\varphi_d < 0.5$) due to the high axial feed that increases the chances of push-out delamination.

Compared to conventional drilling, while the mean surface roughness "R_a" of the hole walls drilled in Ti6Al4V by VAD was improved by 50% [18], a slight reduction in Ra was observed for the CFRP. Figure 7b shows that Ra's dependence on the modulation frequency and amplitude did not follow a clear trend. The figure also shows that the surface roughness was controlled mainly by the rotational speed and feed interactions. The maximum surface roughness (>3.0 μm) was associated with the 9000 rpm and 12,000 rpm rotational speeds at the low feed. This could be attributed to tool dynamics at high speeds and low damping at low feeds.

The hole size error percentage is evaluated as $HD_e = (D_A - D_h)/D_h \times 100$, where "$D_A$" is the actual hole diameter, and *"D_h"* is the nominal hole diameter. A negative error indicates that the produced hole size is smaller than the nominal size. Based on the specification adopted by leading aerospace manufacturers, the allowable tolerance limits of the hole size errors for low load carrying holes are − 0.7 to 0.4%. In conventional drilling, oversized CFRP holes are produced due to the reaming effect of the long Ti6Al4V chips transmitted upwards to the CFRP layer during drilling.

This effect is eliminated in the VAD process through the breakage of Ti6Al4V chips, allowing their easy evacuation through the tool flutes. As a result, the hole size error in the CFRP and Ti6Al4V stacked layers can be reduced to the acceptable hole size tolerance range, as shown in Fig. 7c. Holes produced at high speed combined with low and high feeds were over the upper tolerance limit. This could be due to the effect of tool dynamics at high speeds combined with low damping at low feed and excessive tool deflection in the case of high feed.

The elimination of the exit delamination, shown in Fig. 8a, is attributed to the reduced HF-VAD axial forces. Figure 8b compares the Ti-6Al-4Vexit burr height obtained by HF-VAD and the reference conventional drilling process. For the investigated HF-VAD conditions, lower burr height was obtained [24]. The reduced HF-VAD exit temperature has prevented burr formation due to material softening, contributing to up to 85% burr reduction.

(a)

Feed (mm/rev)		0.05		0.10		0.15	
rpm	Amp. (mm)	Frequency (Hz)					
		30	60	30	60	30	60
6000	0.04			0.5-1.5		>1.5	
	0.10	0.0 – 0.50					
	0.20	0.5 – 1.5					
	0.40						
9000	0.04						
	0.10	0.0 – 0.5		0.5 – 1.5			
	0.20						
	0.40						
12000	0.04						
	0.10	0.5 – 1.5					
	0.20	0.0-0.5		0.0-0.5			
	0.40						

(b)

Feed (mm/rev)		0.05		0.10		0.15	
rpm	Amp. (mm)	Frequency (Hz)					
		30	60	30	60	30	60
6000	0.04	1.5 µm – 3.0 µm					
	0.10						
	0.20	1.5 – 3.0					
	0.40						
9000	0.04				<1.5 µm		
	0.10	<1.5 µm					
	0.20	1.5 µm – 3.0 µm					
	0.40						
12000	0.04	> 3.0 µm		1.5 µm – 3.0 µm			
	0.10						
	0.20	<1.5 µm					
	0.40						

(c)

Feed (mm/rev)		0.05		0.10		0.15	
rpm	Amp. (mm)	Frequency (Hz)					
		30	60	30	60	30	60
6000	0.04						
	0.10						
	0.20						
	0.40	<-0.7%		<-0.7%			
9000	0.04						
	0.10	-0.7% to 0.4%					
	0.20						
	0.40	<-0.7%					
12000	0.04	>0.4%				>0.4%	
	0.10						
	0.20						
	0.40						

Fig. 7 **a** Effect of the LF-VAD parameters on the (**a**) exit delamination factor, **b** surface roughness (Ra) and **c** hole size error % [28]

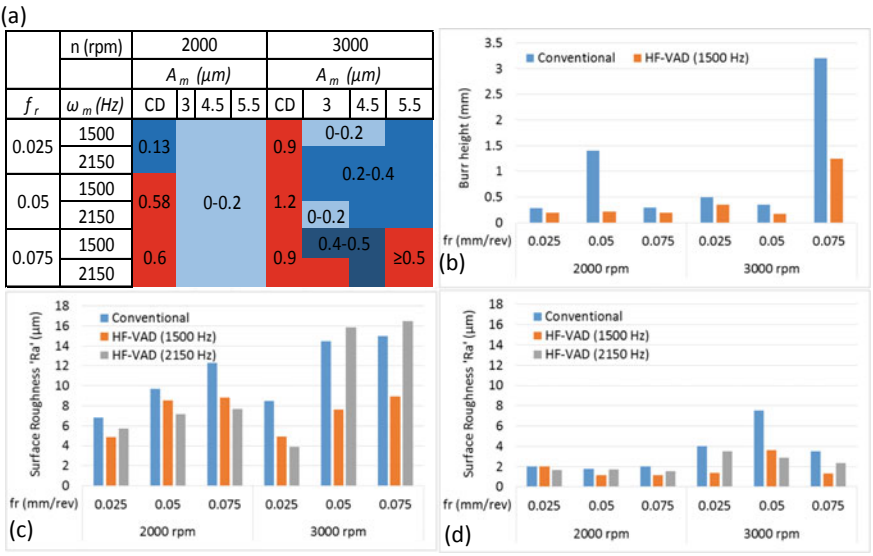

Fig. 8 Effect of the HF-VAD parameters on the **a** exit delamination factor (CFRP), **b** burr height (Ti-6Al-4 V, **c** Surface roughness (CFRP) and **d** surface roughness (Ti-6Al-4 V) [24]

Figure 8c compares the effect of modulation frequency on the measured surface roughness (Ra) for CFRP at the modulation amplitude Am = 3 μm. The percentage of changes in Ra are relative to the reference case of conventional drilling. The surface roughness generally increased with the feed rate and cutting speed. The investigated HF-VAD conditions exhibited up to 55% reduction in the Ra value, which could be attributed to the improved Ti chip evacuation. The Ra values for the Ti stack layer were in the same range of improvement, as shown in Fig. 8d.

4 Orbital Drilling (OD) of FRPs and Hybrid Stacks

The orbital drilling (OD) process is characterised by cyclic engagement and disengagement between the tool and the work-piece [29, 30]. Linear elastic fracture mechanics (LEFM) modelling for delamination in conventional drilling of FRP laminates showed that exit delamination occurs when a specific critical limit of axial force is exceeded [31]. The research work carried out in [6] extended the LEFM model to investigate the unique characteristics of the orbital drilling (OD) process from a new energy perspective. The primary feed component in the OD tool motion is along the tangential direction, not the axial direction, as in conventional drilling. This directs a major component of the total work done by the tool in the tangential direction while the axial force component is significantly reduced. The redistribution of the cutting

energy eliminates a considerable source of delamination in OD because FRP laminates are more susceptible to delamination damage under the action of axial forces rather than tangential forces.

4.1 Cutting Forces in Orbital Drilling (OD)

The study conducted in [32] on orbital drilling of AlCuMg2/CFRP/Ti-6Al-4 V hybrid stacks demonstrated the significant reduction in axial forces and temperatures in all layers, in Ti due to the redirection of the major work components to the tangential cutting direction. Figure 9a shows the reduction in axial forces and a corresponding increase in the tangential OD forces. The distributed loading of the axial force on the remaining FRP layers, shown in Fig. 9b, was proven to result in less deflection and delamination than the concentrated loading mode in conventional drilling, see Fig. 9c.

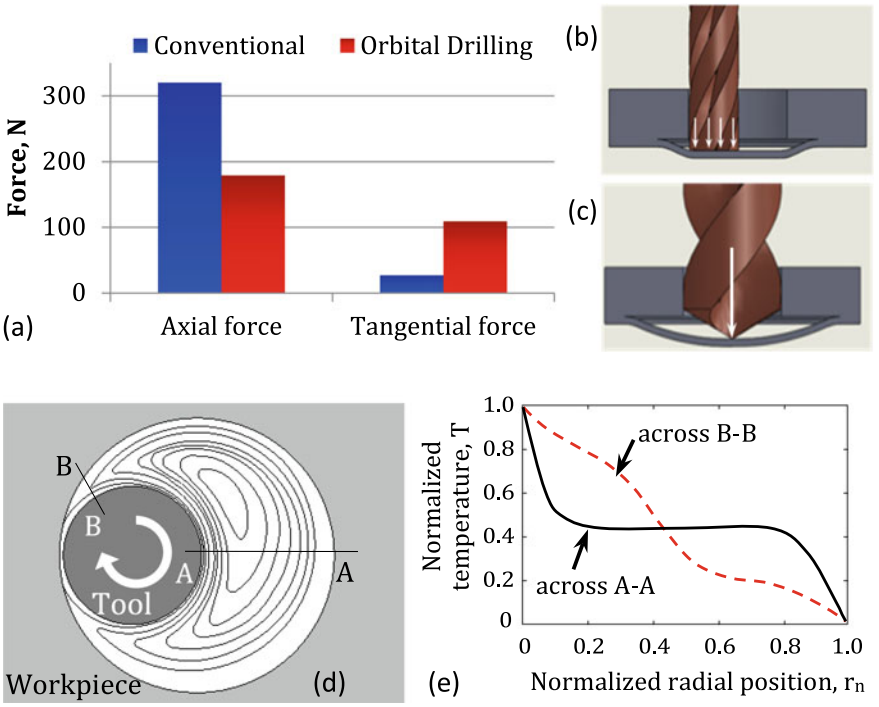

Fig. 9 **a** redistribution of the axial into tangential OD force components and loading modes of the **b** OD and **c** Conventional drilling on the remaining FRP layers at the exit. **d** Orbital drilling eccentric tool-workpiece configuration and **e** dimensionless radial temperature distribution narrow and wide gaps [6, 33]

4.2 The Thermal Aspect of Orbital Drilling (OD)

OD's intermittent cutting nature reduces the heat input to the tool and workpiece compared to conventional drilling. This is because the instantaneous tool-workpiece engagement in OD is limited to a single cutting edge intermittently, as opposed to conventional drilling where the cutting edges of a point drill remain in continuous contact with the workpiece thought out the drilling process. The air gap between the tool and the hole walls in OD enables the formation of flow vortices and the combined convection and radiation mode of heat transfer. Such phenomenon represents an additional unique feature that contributes to enhancing the cooling of the tool in OD. The analysis in [6] has shown that the low rotational speeds 'n' and small air gap width 'b' between the tool and the hole surface results in a steady airflow and minimal convective heat transfer. At increased tool rotational speed ($n \geq 3500$ rpm) and/or the annulus width, the airflow in the annulus forms was found to form flow vortices that can result in effective cooling of the tool and workpiece via convective heat transfer. A schematic presentation of such vortices' typical flow streamlines in an eccentric annulus [34] is shown in Fig. 9d For an adiabatic airflow in a concentric annulus, the overall convective coefficient of heat transfer 'hc' between the tool and the hole walls yields the relationship with Taylor Number Ta, and the rotational speed 'n' [35]. The distribution of the air temperature 't' in the gap is shown in Fig. 9e [33], where the dimensionless temperature $T = (t - t_c)/(t_h - t_c)$ is normalised with respect to the local surface temperatures of the rotating hot cylinder and the cold stationary hole, t_h and t_c, respectively. The radial position 'r_n' in the gap, measured from the tool surface, is normalised concerning the local gap width 'b'. The central region of large gaps in Fig. 9e is nearly flat because of the Taylor vortices, which act as effective mixing agent. Therefore, the resulting temperature gradient at the tool and hole surfaces are considerably steeper than those for laminar flow, yielding a sharp increase in 'hc' [6]. This analysis explains the up to 60% rake face temperature reduction in OD compared to conventional drilling in the Al, CFRP and Ti layers.

4.3 Hole Quality and Surface Finish in OD

The accuracy of hole size in OD is mainly affected by the tool deflection, the precision of the helical path generated by the machine tool controller, and the tool dynamics (whirling). The hole size error is defined as the ratio of the difference between the actual hole diameter "D_a", and the nominal hole diameter "D_n" to the nominal hole diameter (Hole Size Error (%) $= (D_a - D_n)/D_n) \times 100$. Figure 10a shows the hole size errors map for holes produced using OD in CFRP [36]. The produced size of each hole resulted from the two competing effects of tool dynamics and tool deflection. The general observation in [36] was that OD produced higher hole size errors than the conventional drilling, due to the smaller size of the tool and the higher tangential forces. Drilling at high axial feed (180–360 mm/min) and low

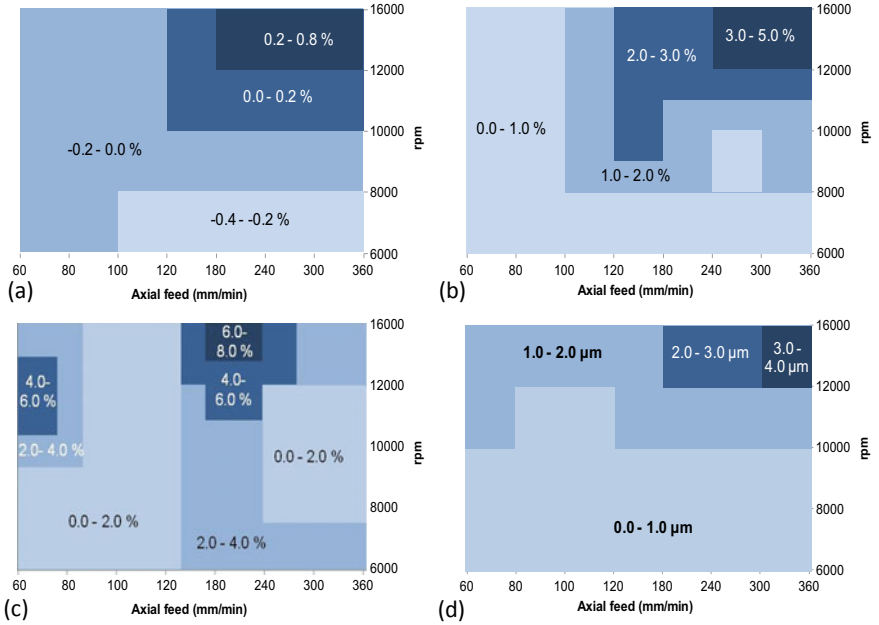

Fig. 10 Effect of OD axial feed and rotational speed on **a** hole size errors, **b** circularity, **c** concentricity and **d** surface roughness in CFRP [36]

rotational speeds (6000–8000 rpm) produced undersized holes outside the acceptable tolerance limit. This is attributed to the tool deflection towards the hole centre under the action of higher feed forces. For the same range of high axial feeds, the hole size error approaches zero at the rotational speed of 10,000 rpm due to the reduced tool deflection under lower feed forces. Positive hole size error starts to develop with higher rotational speeds (12,000–16,000 rpm), possibly due to the effect of tool whirling.

For higher feeds and rotational speeds, the hole circularity errors are shown in Fig. 10b are three times higher than those obtained at lower feeds, due to the increased in-plane forces. The effect of speed is more pronounced for the higher pitch where the circularity increased with increased speed. In general, the concentricity errors, shown in Fig. 10c, are below the standard industrial requirements of 25 µm. No definite trend is seen for all the conditions. It can be noticed that at low orbital feed, the concentricity tends to increase with speed, but at the highest speed of 16,000 rpm, there is a considerable reduction in error.

In the surface roughness map shown in Fig. 10d [36], the mean surface roughness 'Ra' was measured along with the hole depth in CFRP. For rotational speeds 'n' in the range of 6000–10,000 rpm, Ra was found to be less sensitive to the effect of axial feed. It remained below a value of 1 µm, compared to 1.83 µm obtained in conventional drilling. However, at higher rotational speeds in the range of 12,000–

16,000 rpm, Ra increased significantly primarily with higher axial feeds, due to the fibre pull-out and the growing effect of tool dynamics that resulted in poor fibre cutting.

5 Orbital Drilling of CFRPs with Super Abrasive Tools

Super abrasive materials refer to diamond and cubic boron nitride (CBN), which are the hardest material known so far, respectively. As with conventional abrasive wheels, super abrasive wheels are also made in various sizes, shapes, and bonds. However, they can be made with a single layer of abrasives by electroplating or brazing abrasive grains on precisely machined wheel cores. Such wheels are not periodically trued or dressed and are more suitable for profile grinding and possess unique advantages for running at a high peripheral velocity over conventional wheels. In addition, single layer super abrasive wheels can be made with the geometry of milling cutters or drills.

Fundamental understanding of the material removal mechanisms of carbon/epoxy machined by a single diamond grain was carried out by Thomson et al. [37]. The FE and experimental investigation showed that the primary material removal mechanism when the fibre's relative orientation to the direction of cutting motion is 0°, and 90° is longitudinal compressive or shear damage, followed by fibre bending failure. For 45° relative orientation, it is the transverse tensile failure that dominates at the beginning of machining. As the grain advances, deboned fibres undergo bending and eventually fail. Using Hashin's damage criteria [38], a generalised model was developed to predict damage evolution and predict cutting forces in orbital drilling, resulting from the ploughing, friction, and chip formation processes. For 95% confidence interval, the force prediction errors were found to be $<\pm 5\%$ [39]. This development allowed the design and optimisation of the drilling process and the cutting tool, as presented in the coming sub-sections.

5.1 Tool Performance and Hole Surface Quality

The performance of single-layer diamond tools and the hole surface quality for orbital drilling were experimentally evaluated in terms of forces, temperatures, surface roughness, delamination, surface burning, hole geometric accuracies, and tool geometries [40]. The test materials were 6.35 mm thick carbon/epoxy plates having a $[0/\pm 45/90]_{24\,s}$ stacking sequence. Ball-end and flat-end diamond tools were used. The diameters of the tool and hole were 9.525 and 12.180 mm, respectively. The spindle speed n_s, orbital feed rate v_w, and axial feed rate v_a for a pitch $p =$ 0.5 mm were 40,000 rpm, 1500 mm/min, and 97 mm/min.

The variations of forces, temperatures, hole surface roughness, circularity, and diametrical accuracies versus the accumulative number of holes for the 60-grit ball-end tool are given in Fig. 11. During the first hole, the forces obtained are the initial forces to drill a hole at the test condition using a new tool. With continued drilling, both peripheral and thrust forces increased by approximately 90% and 93%, respectively from the 1st to the 220th hole. The forces increased quickly up to the 45th hole, followed by a reduction in the rate of force increase. Peripheral force increased by about 1% per hole up to the 45th hole, which reduced to a 0.18% increment per hole after that.

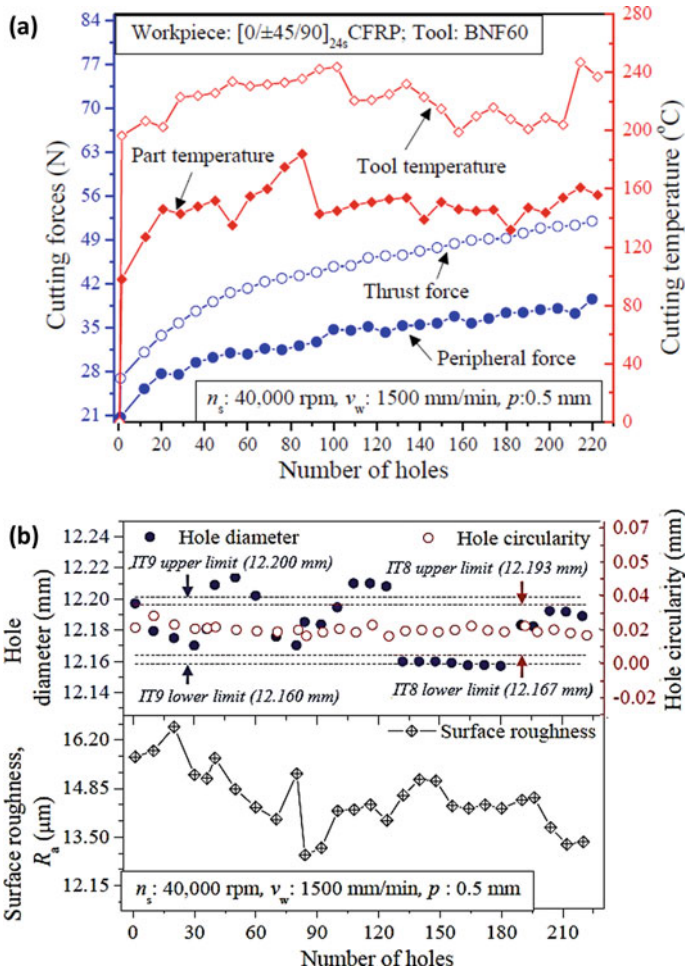

Fig. 11 Results for OD with a 60-grit single-layer ball-end diamond tool: **a** Forces and temperatures versus the number of holes, and **b** Geometric accuracies and surface roughness [40]

Similarly, the thrust force increased by 1 and 0.18% per hole from hole 1 to hole 45 and hole 46 to hole 220, respectively. This observation can be explained by two factors. One is the tool clogging, in which crushed polymers and fractured fibres occupy inter-grain pockets. Therefore, with the continuation of hole drilling, contact pressure increases at the tool-workpiece interface. The fresh chips generated during drilling try to flow through these pockets; thus, squeezing the clogged debris. Clogged debris can be partially cleaned by applying high air pressure onto the tool surface. Due to the higher adhesion of carbon particles to elastomers, as compared to diamonds, rubber strips/adhesives were found to be effective to some extent to pull out carbon particles from inter-grain pockets. The other factor is the tool wear. The new cutting edges of the grains are usually sharp, which rapidly become blunt during machining within a short time. Beyond this stage, grain wear is slower. Hence, typical wear versus time relationship closely resembles the trends of the time variation of forces.

Similar reasons can explain the variations of cutting temperatures measured at the holes' exit plane with an IR camera. It can be seen in Fig. 11a that the part temperature increased from about 98–184 °C for the first 84 holes. It then dropped to 143 °C during drilling hole 90 and maintained a steady state with a slight inclination of 12 °C. No burn marks on the hole surfaces were observed. This is also expected because the resin's glass transition temperature (toughened epoxy) is around 200 °C [41]. In orbital drilling, the tool continuously rotates along its orbital path; therefore, the point of heat generation at the tool workpiece interface continuously moves. This prevented heat accumulation in a single location on the workpiece surface and eventual thermal damage. High speed rotation of the tool also facilitated heat convection.

It can be seen from the top plots of Fig. 11b that about 50% and 80% of the hole diameters are within IT8 (27 μm) and IT9 tolerance (43 μm), respectively as compared with 19% in IT8 with conventional drilling using a carbide tool. The average hole diameter was 12.180 mm, with 18.4 μm standard deviation. Hole circularity was well within IT8. Surface roughness *R*a shown in the bottom plot of Fig. 11b varied between 13.0 and 16.6 μm, increasing the number of holes. The *R*a values gradually decreased during the drilling of the first 80 holes. At the beginning of drilling, fresh grains usually tended to cut surfaces while generating sharp grooved profiles on the hole surface. As drilling continued, the grain tips quickly flattened to reach a steady state with slightly reduced protrusion heights as compared to the initial heights. This, in turn, generated truncated, grooved profiles on the hole surface with a lower peak to valley distances, which eventually lowered the *R*a values.

A picture is given in Fig. 12a showing a hole boundary, highlighted damage zones and types of damage. A damage ring concentric to the hole centre was utilised for quantifying the fuzzing defect. The ratio of the diameters corresponding to the damage ring and hole was defined as the damage factor. The minimum damage factor of 1 was obtained during drilling of the first 27 holes, which increased to about 1.06 at the end of drilling 220 holes. With ball-end tools, the diamond grains at the ball end of the tool removed materials both axially and radially. The tool exerted both axial and radial forces to the workpiece. The radial force can trigger resin damage

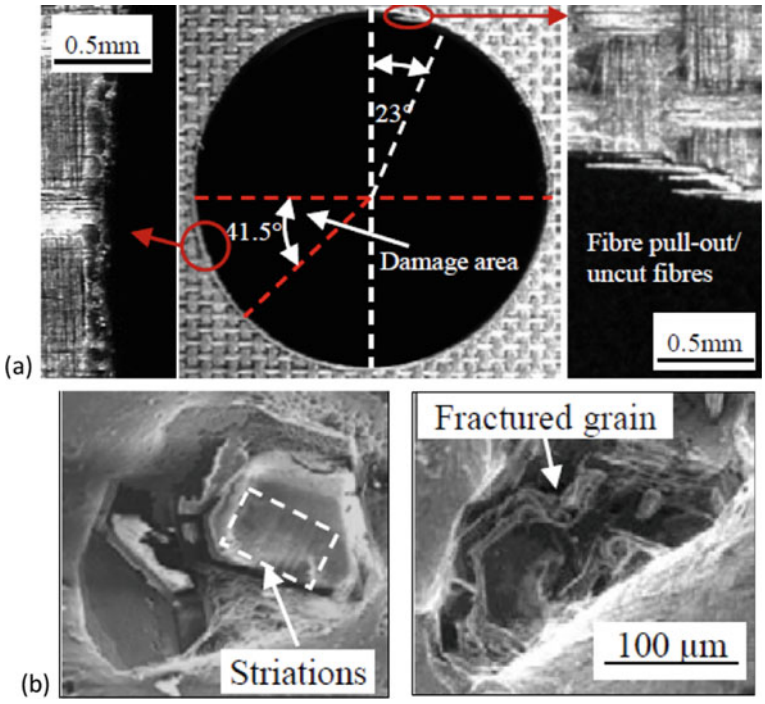

Fig. 12 Results for OD with a 60-grit single-layer ball-end diamond tool: **a** Fibre pull-out/uncut fibres, and fuzzing, and **b** grain attrition wear and fracture [40]

between inter-plies resulting in slight separation of the top ply from adjacent ply and eventual fuzzing of the hole edge. Delamination was observed at the entrance side for 2.3% of the drilled holes. A delamination factor was calculated following the same method as that used to obtain the damage factor. The minimum and maximum delamination factors were observed for hole 28 and hole 92 with factors of 1.04 to 1.40, respectively. Almost 99% of the drilled holes had no exit delamination.

The variations of the tool performance and the machined hole qualities were attributed to the tool wear with continued drilling. SEM observations revealed the presences of both attrition wear and grain fractures, as shown in Fig. 12b. Grain fractures and attrition wear accounted for up to 33 and 0.08% of the projected tool surface area, respectively. Therefore, the contribution of attrition wear in increasing forces is negligible compared to that of the clogging. No grain dislodgement was observed although fine abrasion lines were formed on the bond surface.

The effects of tool geometry on tool performance and machined hole qualities were also investigated with 60-grit diamond flat-end tools (F60) and ball-end tools (B60). The forces are compared in Fig. 13 under the same cutting condition. It can be seen in Fig. 13a that the tool B60 generated approximately twice the tangential force of the tool F60. This is because the ball-end tool started cutting with very low cutting speed due to the small radii near the lowest point of the ball-end. For F60, the

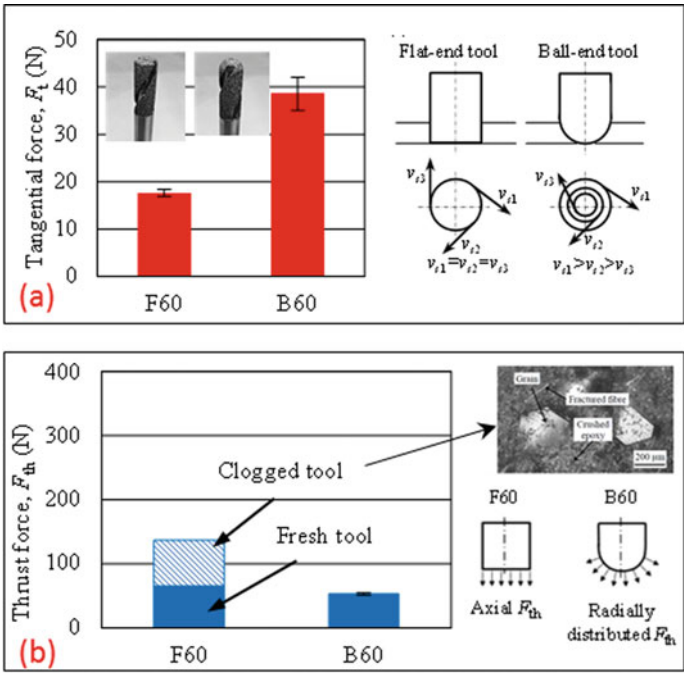

Fig. 13 Effect of tool geometry on **a** tangential forces, and **b** thrust forces

cutting speed was constant along the tool axis. Low speed caused an increase in the chip thickness, which, in turn, increased cutting forces. The thrust force generated by a fresh flat-end tool, as shown in Fig. 13b was slightly higher than that of a ball-end tool. However, a flat-end tool was more prone to clogging. Once clogged, the flat-end tool generated almost twice thrust force as compared to a new tool. For the tool F60, the forces normal to the tool face acted along the tool axis and contributed 100% to the thrust force. However, for the tool B60, only the force component along the tool axis contributed to the thrust force. Such components decreased with increasing inclination of the force to the tool axis.

Like forces, the tool temperature at the centre of the tool bottom surface, part temperature along the periphery of the hole, and hole surface roughness are also affected by the tool geometry. The tool and part temperatures were about 210 and 160 °C with the F60 tool, respectively. However, the temperatures with the B60 tool were lower, reaching 150 °C for the tool and 92 °C for the part. For both tools, the tool temperatures were significantly higher than the corresponding part temperatures. The large difference between the tool and part temperatures was due to the air gap between the tool and the hole surfaces in orbital drilling, which allowed the creation of vortices in this gap. This, in turn, enhances the cooling process. The tool and part contact area with the B60 tool was bigger than that with the F60 tool, which reduced the heat intensity or heat flux with the B60 tool and lower temperatures. No

signs of thermal burn were found on the hole surfaces. This was expected since the part temperatures with both tools were lower than the critical burning temperature of about 280 °C [42]. The tool temperatures were slightly higher than the polymer's glass transition temperature with the F60 tool, implying clogging and adherence of the polymer material to the tool surface was present. R_a values obtained were about 9 μm with the F60 tool, and 12 μm with the B60 tool. The R_a values were higher than generally required for hole surfaces, necessitating taking measures to lower surface roughness.

5.2 *Overcoming the Hole Surface Roughness Challenge*

It is evident from the test results that orbital drilling using diamond tools generated less cutting forces and holes without delamination or fibre pull-out. However, the surface roughness was much higher than what was obtained in orbital drilling with end mills. To overcome this limitation of the tools, two approaches were investigated and proved to be very effective. One approach utilised the concept of the hybrid tool by combining a diamond tool and an end mill. The other approach utilised a hybrid process. Conventional orbital drilling was carried out using a single diamond tool to generate holes followed by an oscillatory finishing operation to achieve the final required surface roughness and hole dimensions.

The concept of the hybrid tool shown in Fig. 14 contained sections of both abrasive grains for rough cut and conventional milling cutting edges for finish cut [43]. The former section was indicated as section 'A' in the figure and comprised of coarse grains (40–60 grit diamond) brazed or electroplated on the tool core. From the tool geometry aspect, ball-end tool is preferable because of its ability to transfer thrust forces radially. The latter section was indicated as section 'B' where four slots were provided in the tool body to accommodate cutting inserts. Depending on the process requirements, a different number of slots can be integrated into this section. Each

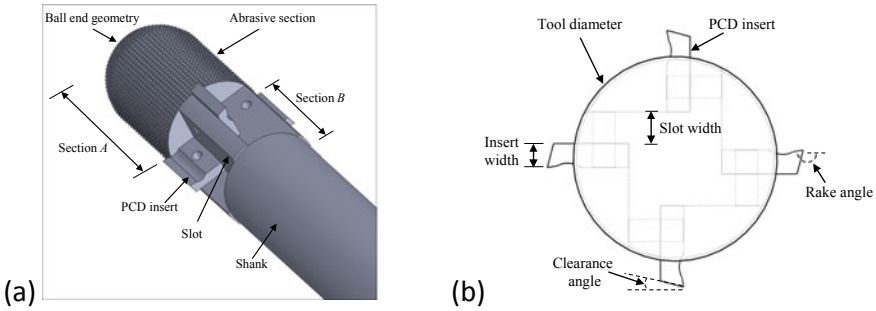

Fig. 14 **a** 3D model of hybrid tool **b** tool cross-section [43]

insert was provided with a rake angle of 7–10° and a clearance angle of 10–15°. The values of these angles were based on commercially available end mills.

To test the concept of the hybrid tools, orbital drilling with a four fluted tungsten carbide (WC) end mill on pre-drilled holes of 12 mm was carried out. The tool had a diameter of 9.525 mm. The workpiece material was CFRP of $[(0/\pm 45/90)_6]_S$ stacking sequence. The holes were pre-drilled with a 60-grit diamond tool. In the finishing step with the end mill, the spindle speed, orbital feed rate, and axial pitch were 40,000 rpm, 1500 mm/min, and 0.5 mm, respectively. The final hole nominal diameters were 12.25 mm.

The surface roughness *R*a of the pre-drilled holes was in the range of 7.5–10 μm. After the orbital finishing with the end mill, the roughness was reduced to 0.5–4 μm. The big variation of Ra was due to the wear of the end mill. The reason that an end mill reduced surface roughness over a diamond tool during orbital drilling was due to having continuity along a cutting edge, unlike diamond tools in which there was a space between consecutive abrasive grains leading to discontinuity.

Delamination and thermal burn were not seen during this step of finishing the pre-drilled holes. However, fibre pull-out was detected in some sections of a hole. This can be explained by the fact that tungsten carbide end mills were used for drilling carbon/epoxy composites. Because of the abrasive nature of carbon fibres, the cutting edges were abraded and broken off. Therefore, the tool could not remove and cut the fibres entirely resulting in the fibre pull-outs. The phenomenon became aggravated after completing 2–3 holes using one end mill. It is worth mentioning that carbide cutting edges were not suggested due to excessive edge wear with them. Based on the preliminary investigations, using single layer diamond grains for the rough cut and incorporating PCD cutting edges in the same tool for the finish cut is expected to increase cutting tool life significantly than any other commercially available tools without increasing cost. In case of smaller tool diameter, clamping PCD inserts to the slots is difficult. In this case, the tool core can be machined to provide the geometry of a PCD insert. Then, the cutting edges can be coated with PCD.

In the hybrid process approach shown in Fig. 15a, the drilling was done in two steps, where conventional orbital drilling (COD) is carried out to generate holes, then followed by an oscillatory finishing operation (OFO) using the same diamond tool [8]. A small amount of additional material or radial allowance is then removed in the OFO step at the same spindle speed, but a relatively higher axial feed rate and lower orbital feed rate. In the OFO step, the rotating tool oscillates at a frequency f and amplitude l along its axis while following an orbital path. Unlike the COD operation, the tool is continuously in contact with the whole thickness of the drilled hole all the time during OFO. The axial oscillation of the tool is repeated until the full hole circumference is machined.

The key to the success for OFO to improve the surface roughness is to use a lower orbital feed rate and a higher axial feed rate or an axial oscillating frequency. This combination leads to the formation of an angle between the resultant tool feed direction and the direction of tool surface speed. It was analysed and experimentally validated that forming an angle between the feed and tool surface speed directions increases the equivalent grain packing density per unit grinding width, leading to the

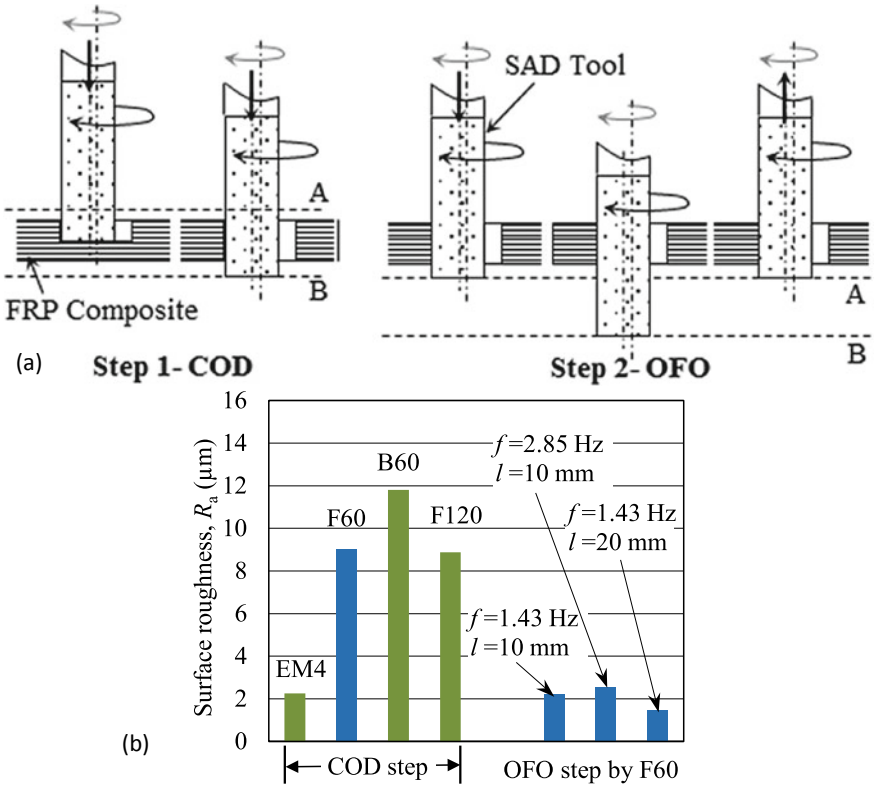

Fig. 15 **a** Process schematic, and **b** Ra for different tools produced by tool F60 [8]

smoothing effect to ground surfaces [44]. A higher ratio of axial feed rate to orbital feed rate will lead to a larger speed angle and smoother ground surfaces. However, a higher ratio will compromise productivity.

The process was experimentally validated. Surface roughness R_a values for the holes produced by fresh flat-end 60-grit diamond tool (F60), flat-end 120-grit tool (F120), ball end 60-grit tool, and an end mill (EM4) in the COD operation, and by the F60 tool in the OFO operation are compared in Fig. 15b.

It can be seen that the F60 and F120 tools produced practically the same R_a in the COD step. On average, EM4 generated approximately 75% lower R_a compared to the super abrasive diamond (SAD) tools. The OFO process produced, on average, approximately 80% lower R_a as compared to those in the COD process.

In summary, it has been demonstrated that the application of SAD tools in orbital drilling effectively produces delamination free IT8-IT9 holes in CFRP materials. Also, with proper selection of cutting conditions and tool geometry, orbital drilling using SAD tools can significantly reduce cutting forces and improve tool life compared to carbide tools. High surface roughness generated by SAD tools can be

eliminated by adopting oscillatory orbital drilling or implementing the concept of hybrid tools. Thus, compared to PCD tools, SAD tools offer comparable outcomes at a lower cost.

6 Predictive Model-Based Adaptive Drilling of Composite/Metal Stacks

Unlike the case of chip formation by plastic deformation during machining of ductile metals, the chip is formed by a series of consecutive fractures of matrix and fibres during the machining of FRPs [28]. Moreover, the mechanical properties are theoretically homogenous and isotropic for metals, while they are known to be dependent on the fibre orientation for FRP laminates. These two significant differences in the principles of machining of metals versus FRPs justify the importance of introducing a new model that gives an in-depth understanding of the mechanics of the drilling process of FRP laminates. The model needs to consider the tool geometry and fibres directionality as the main load carrying component of the composite material, which merely control the FRP machinability due to the fibre significantly higher strength compared to the matrix [45].

The anisotropy of the FRP laminates is the leading cause for the dynamically changing drilling forces with the drilling tool's rotation. Such behaviour adds to the model's complexity, which aims to capture the force fluctuation and maximum force due to the material anisotropy.

The considerable research on empirical force modelling showed good predictions of the average force values within the limited range of the drilling parameters used for model calibration. Therefore, this approach does not meet the industrial need of a generalised predictive modelling capability.

The models presented in [46, 47] adopted the shear plane concept reported in [48] for modelling the drilling forces of multidirectional FRPs, ignoring the fundamental differences between metal and FRP cutting, outlined above. This explains the inability of these model to predict the principal features of the force signal.

Finite element modelling of drilling of FRPs [49] has encountered the challenge of enormous computational cost, especially for modelling a highly complex process. This stems from the need to employ very fine mesh and adaptive meshing of the tool and the workpiece over small time steps to capture the dynamically changing directional properties of the material on the fibre scale. Other sources of error included defining the material properties used to predict chip formation by the fracture on the fibre scale. The nonlinearity of the contact problem with the machined FRP surface, as well as identifying the coefficient of friction between the tool and the workpiece adds to the complexity of the problem.

To overcome the limitations of the approaches mentioned above, mechanistic modelling emerges as a viable solution. It can represent the effect of different machining phenomena encountered while drilling of FRPs, in the form of cutting

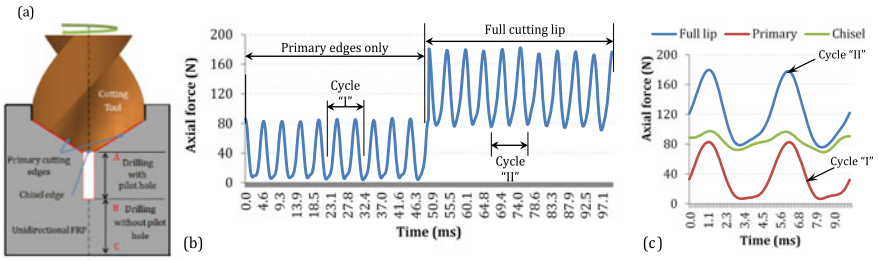

Fig. 16 **a** Hole preparation for the calibration experiment to split the behaviour of the primary and chisel cutting edges during drilling of FRP **b** The measured force signal showing the effect of the engagement of the chisel edge after drilling through the air gap of the pilot hole. **c** Separated axial force behaviours of the full cutting lip, the primary cutting edges and the chisel edge during the defined cycles of tool rotation (n = 6000 rpm, and fr = 0.15 mm/rev)

coefficients. Limited calibration tests are required to account for the directional material property with respect to the fibre orientations. In this approach, the different behaviours of the cutting tool's primary and chisel edges are recognised, and the cutting pressures of each of these cutting edges are separately identified, using a special preparation of the hole being drilled for the calibration tests [28]. This is shown in Fig. 16a, where a blind pilot has drilled ahead of the chisel edge till the middle of the hole depth. Drilling through the blind pilot hole is represented by the first portion of the force signal shown in Fig. 16b, where the measured axial force was lower compared to the second half of the drilling pass where the full cutting lip is engaged. The force and torque fluctuations due to the variation of the fibre orientations as the tool rotates can be seen. A full cycle of the tool in each of the signal sections can be identified, where "cycle I" is for the primary edges, and "cycle II" is for the full cutting lip. Each of these cycles gives information on the force's value at every fibre orientation that the cutting edges have engaged with during cutting. The isolated effect of each section of the cutting tip can be obtained, as shown in Fig. 16c. The relationship of the calibrated cutting pressures and θ_e is identified through the obtained variation of the axial force with θ_e and the area of the uncut chip on the primary and chisel cutting edges. The same sequence can be applied to identify the effect of θ_e on other force components and at different levels of cutting conditions and flank tool wear (VB) to calibrate the full database of cutting pressures.

Equations 1–3 show the model formulation, in a functional form, for predicting the drilling force components $F_{zp,L}$ *and* $F_{zc,L}$ at the primary and chisel edges, respectively, in each of the stack material layers *L*. The calibrated cutting pressures $K_{F,p}$ and $K_{F,c}$ for the primary and chisel tool edges, respectively, are identified as functions of the process variables: tool wear '*VB*' in hybrid metals and FRPs stacks, cutting velocity *v*, chip thickness *d*, normal rake angle of the cutting edge α and the effective material property or fibre orientation angle θ_e. The total axial force $F_z(t)$, at an instant of time *t,* for drilling the stack layers is computed from the integration of the elemental forces $F_{zp,L}$ of the *primary cutting edges Np and* $F_{zc,L}$ of the chisel edge. Knowing $F_z(t)$, one can predict if mechanical and thermal damages took place [50].

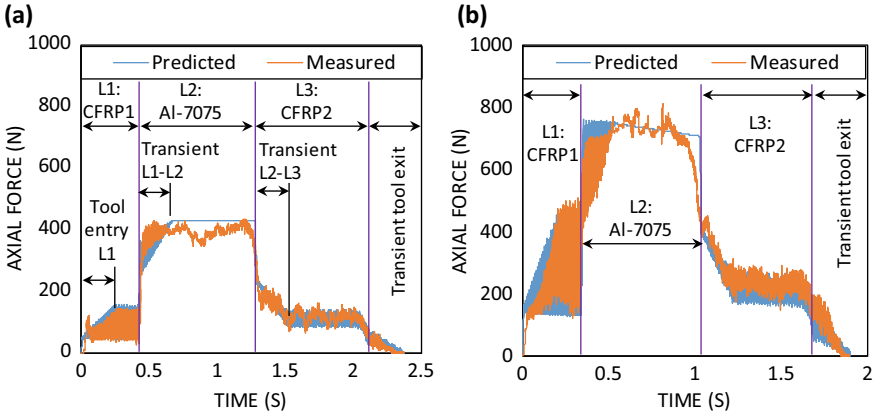

Fig. 17 Predicted versus measured axial drilling forces in CFRP-1/Al-7075/CFRP-2 at n = 6000 rpm, f = 0.075 mm/rev, **a** VB = 0 μm and **b** VB = 135 μm [50]

$$F_{\boldsymbol{Z,p,L}}(t) = Np.\boldsymbol{K}_{\boldsymbol{F,p,L,i}}(VB_L, v_i, d_{p,L,i}, \theta_{e,L,i}, \alpha_{L,i,t}, t).d_{p,L,i}(t).\boldsymbol{l}_{\boldsymbol{p,L,i}}(t) \quad (1)$$

$$F_{\boldsymbol{Z,c,L}}(t) = \boldsymbol{K}_{\boldsymbol{F,c,L,j}}(VB_L, v, d_{c,L,j}, \theta_{e,L,j}, t).\boldsymbol{d}_{\boldsymbol{c,L,j}}(t).l_c \quad (2)$$

$$F_Z(t) = \sum F_{zp,L}(t) + \sum F_{zc,L}(t) \quad (3)$$

where i and j are the indices of the elements engaged with the primary and chisel edges, respectively.

Figure 17 shows the accurate force model predictions compared to the measured axial force signal for CFRP1/Al7075/CFRP2 stack drilling, including the transient and steady-state features, for a new tool and a worn tool ($VB = 135$ um).

Effective adaptive control system for drilling of stacks requires synchronising real-time feedback from the actual drilling process, with the cyber computational space, where two interactive models are involved: (a) Machine learning tool wear prediction and (b) cutting force prediction to optimise and continuously control the tool feed rate to maintain the drilling axial force F_z below a critical level F_{cr}.

To maximise productivity, *offline* feed rate model-based optimisation maximises feed rate f within the safe limit. For the case tested in [50], $f = 0.147$ mm/rev at $n = 7500$ rpm and $VB = 0$ mm for the initial hole through the CFRP stack layers. The initial feed rate $f = 0.075$ mm/rev was maintained for layer L2 (AL-7075). The force model showed that at the exit plane of CFRP layer L1, the effective force $F_{eff} < F_{cr}$, due to the support from the underneath undrilled stack layers. The predicted F_{eff} at the exit plane of the last unsupported CFRP layer L3 increased with the VB growth. Therefore, the AC system reduced the actual feed f obtained from the CNC controller in steps of 15% each time the model predicted that F_{cr} was approached. This ensured drilling the following set of holes using an updated safe value of f.

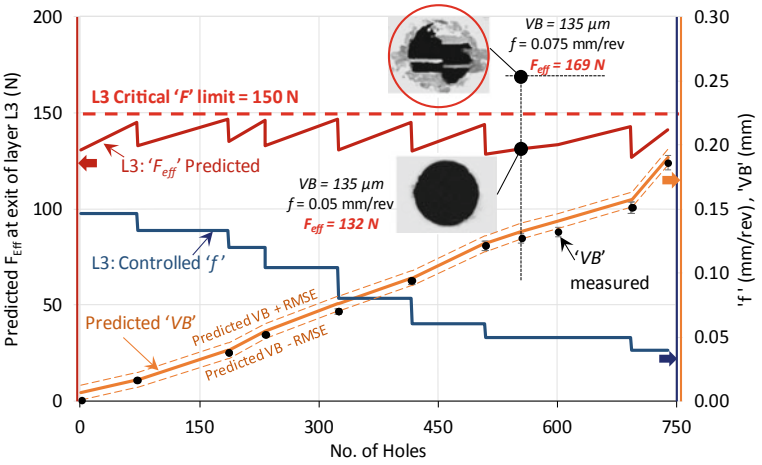

Fig. 18 Model-based adaptive control system performance curve with experimental validation of *VB* and delamination predictions at the exit plane of L3-CFRP [50]

Figure 18 demonstrates an example for controlling the feed rate in the third layer L3 of the CFRP1-Al7075-CFRP2 stack to maximise the life of one drilling tool to a maximum VB = 200 um, without exceeding the critical force limit F_{cr}. The demonstrated model-based adaptive control system enabled drilling a total of 740 holes with acceptable hole quality using a single tool and operating at a near optimum feed rate to maximise productivity and prevent part damage. The figure depicts the validated case of acceptable hole quality ($\varphi_d < 0.05$) when $VB = 135$ µm and feed rate was reduced by the AC to 0.05 mm/rev. In the absence of the AC system, considerable delamination of $\varphi_d = 0.53$ was observed at this wear level ($VB = VB = 135$ µm) and the pre-set feed rate $f = 0.075$ mm/rev. The predicted tool wear from the spindle power signals was in good agreement with the measured tool wear validated after each feed reduction. Drilling the same total number of acceptable quality holes, at the initially optimised conditions without engaging adaptive control would have required seven tool changes that correspond to the incidents where the force has exceeded the critical limit for the VB level. This translates to more than a *four-fold* increase in cost while achieving a marginal productivity gain of 5%. Using the force and wear prediction models, the CPAC system performance was compared to 3 drilling strategies to produce the same number of holes: (1) Eliminating tool change, by keeping the feed rate at a constant low-level $f = 0.042$ mm/rev for all stack layers to keep the tool wear $<VB_{max}$, (2) Allowing a single tool change, by maintaining the initial feed rate (before off-line optimisation) $f = 0.075$ mm/rev, for all stack layers, and (3) Following strategy-2, but allowing two premature tool changes, to simulate the commonly followed practice to avoid part damage. Compared to strategies 1–3, the activation of the CPAC system reduced the total cycle time (drilling and tool change) by 50%, 10% and 13%, respectively. The corresponding reduction in the process cost

is estimated to be 34%, 35% and 50%, respectively. This analysis demonstrates the significant saving in cost reduction and productivity improvement when the proposed CPAC system is implemented.

7 Review Questions

(1) What are the main factors that control the quality of the hole in the drilling of hybrid metal/FRP stacks?
(2) How is the axial drilling force affected by the non-monotonic behaviour of the vibration assisted drilling (VAD) parameters?
(3) What is the principal mechanism of tool cooling in low frequency high amplitude VAD? What impact do the rotational speed and modulation amplitude have on such a mechanism?
(4) How does the feed rate in the drilling of FRPs impact the hole quality in terms of exit delamination?
(5) What is the principal mechanism of axial force reduction in orbital drilling (OD)? How can this impact the hole exit delamination in FRPs?
(6) In OD of FRP holes, how significant are the effects of axial feed and rotational speed on the hole surface roughness? What is the primary type of defect that results in a high surface roughness?
(7) What differentiates super abrasive tools as compared to conventional abrasive tools?
(8) Explain the evolution of the hole surface roughness obtained by super abrasive OD with the number of drilled holes. What are the proposed process modifications that can improve the hole surface quality in super abrasive OD?
(9) What are the main limitations of adopting classical numerical and empirical methods in modelling machining of FRPs?
(10) What are the main parameters that need to be considered for accurate force prediction in machining hybrid stacks? What can be an effective means of calibrating such parameters?
(11) Model-based cyber-physical adaptive control (CPAC) has demonstrated direct gains in extended tool life and process productivity. What are other anticipated industrial economic and environmental gains associated with the implementation of such technology?
(12) The demonstrated CPAC system integrates 2 major modules: predictive force modelling and online tool wear monitoring. What other modules can be developed and integrated within the system to improve the process cost effectiveness further?

References

1. Hocheng, H., Puw, H.Y.: On drilling charachteristics of fiber-reinforced thermoset and thermoplastics. Int. J. Mach. Tools Manuf **32**(4), 592–601 (1991)
2. Rawat, S., Attia, H.: Characterization of the dry high speed drilling process of woven composites using machinability maps approach. CIRP Ann. Manuf. Technol. **58**(1), 105–108 (2009)
3. Brehl, D.E., Dow, T.A.: Review of vibration-assisted machining. Precis. Eng. **32**(3), 153–172 (2008)
4. Ezugwu, E.O., Okeke, C.I.: Tool life and wear mechanisms of tin coated tools in an intermittent cutting operation. J. Mater. Process. Technol. **116**(1), 10–15 (2001)
5. Itoigawa, F., Takeuchi, D., Nakamura, T., Childs, T.H.C.: Experimental study on lubrication mechanism in mql intermittent cutting process. Mach. Sci. Technol. **11**(3), 355–365 (2007)
6. Sadek, A., Meshreki, M., Attia, M.H.: Characterization and optimization of orbital drilling of woven carbon fiber reinforced epoxy laminates. CIRP Ann. Manuf. Technol. **61**(1), 4 (2012)
7. Brinksmeier, E., Fangmann, S., Meyer, I.: Orbital drilling kinematics. Prod. Eng. Res. Devel. **2**(3), 277–283 (2008)
8. Sultana, I., Shi, Z., Attia, H., Thomson, V.: A new hybrid oscillatory orbital process for drilling of composites using superabrasive diamond tools. CIRP Ann. **65**(1), 141–144 (2016)
9. Arul, S., Vijayaraghavan, L., Malhotra, S.K., Krishnamurthy, R.: Influence of tool material on dynamics of drilling of GFRP composites. Int. J. Adv. Manuf. Technol. **29**(7–8), 655–662 (2006)
10. Astashev, V.K., Babitsky, V.I.: Ultrasonic processes and machines. In: Babitsky, V.I., Wittenburg, J. (ed.). Springer, Berlin (2007)
11. Brinksmeier, E., Janssen, R.: Drilling of multi-layer composite materials consisting of carbon fiber reinforced plastics (CFRP), titanium and aluminum alloys. CIRP Ann. Manuf. Technol. **51**(1), 87–90 (2002)
12. Meshreki, M., Damir, A., Attia, M.H.: Drilling of composites and stacked material: process optimization and evaluation of the effects of drilling-induced defects on structural integrity. National Research Council Canada, NRC-Internal report (2013)
13. Shyha, I., Soo, S.L., Aspinwall, D.K., Bradley, S., Dawson, S., Pretorius, C.J.: Drilling of titanium/CFRP/aluminium stacks c3—key engineering materials. In: ICoPE2010 and 13th ICPE International Conference on Precision Engineering, pp. 624–633 (2010)
14. Zitoune, R., Krishnaraj, V., Collombet, F., Le Roux, S.: Experimental and numerical analysis on drilling of carbon fibre reinforced plastic and aluminium stacks. Compos. Struct. **146**, 148–158 (2016)
15. Krishnaraj, V., Zitoune, R., Collombet, F., and Davim, J.P.: Challenges in drilling of multi-materials. In: Materials Science Forum, pp. 145–168. Trans Tech Publications Ltd. (2013)
16. Wang, C.Y., Chen, Y.H., An, Q.L., Cai, X.J., Ming, W.W., Chen, M.: Drilling temperature and hole quality in drilling of CFRP/aluminum stacks using diamond coated drill. Int. J. Precis. Eng. Manuf. **16**(8), 1689–1697 (2015)
17. Montoya, M., Calamaz, M., Gehin, D., Girot, F.: Numerical simulation of workpiece thermal field in drilling CFRP/aluminum alloy c3—key engineering materials. In: 17th Conference of the European Scientific Association on Material Forming, ESAFORM 2014, pp. 1226–1235. Trans Tech Publications Ltd., Espoo (2014)
18. Pecat, O., Brinksmeier, E.: Low damage drilling of CFRP/titanium compound materials for fastening c3—procedia cirp. In: 2nd CIRP Conference on Surface Integrity, CSI 2014. Elsevier B.V., Nottingham (2014)
19. Wei, Y., An, Q., Ming, W., Chen, M.: Effect of drilling parameters and tool geometry on drilling performance in drilling carbon fiber-reinforced plastic/titanium alloy stacks. Adv. Mech. Eng. **8**(9), 1–16 (2016)
20. Sadek, A., Meshreki, M., and Attia, M.H.: Effect of tool kinematics on the drilling forces and temperature in low frequency high amplitude vibration assisted drilling (46438): p. V02AT02A035 (2014)

21. Arul, S., Vijayaraghavan, L., Malhotra, S.K., Krishnamurthy, R.: The effect of vibratory drilling on hole quality in polymeric composites. Int. J. Mach. Tools Manuf. **46**(3–4), 252–259 (2006)
22. Okamura, K., Sasahara, H., Segawa, T., Tsutsumi, M.: Low-frequency vibration drilling of titanium alloy. JSME Int. J. Ser. C **49**(1), 76–82 (2006)
23. Kuo, C., Li, Z., Wang, C.: Multi-objective optimisation in vibration-assisted drilling of CFRP/al stacks. Compos. Struct. **173**, 196–209 (2017)
24. Hussein, R., Sadek, A., Elbestawi, M.A., Attia, M.H.: Elimination of delamination and burr formation using high-frequency vibration-assisted drilling of hybrid CFRP/ti6al4v stacked material. Int. J. Adv. Manuf. Technol. **105**(1), 859–873 (2019)
25. Pecat, O., Brinksmeier, E.: Tool wear analyses in low frequency vibration assisted drilling of CFRP/ti6al4v stack material. In: Procedia CIRP. Elsevier (2014)
26. Sadek, A., Attia, M.H., Meshreki, M., Shi, B.: Characterization and optimization of vibration-assisted drilling of fibre reinforced epoxy laminates. CIRP Ann. **62**(1), 91–94 (2013)
27. Boutarfa, R., Harmand, S.: Local convective heat transfer for laminar and turbulent flow in a rotor-stator system. Exp. Fluids **38**(2), 209–221 (2004)
28. Sadek, A.: Vibration assisted drilling of multidirectional fiber reinforced polymer laminates. In: Mechanical Engineering Dept. University of Mcgill (2014)
29. Sadek, A., Meshreki, M., Zhongde, S., Attia, H.: A comparative study on conventional and orbital drilling of woven carbon fiber reinforced epoxy laminates. In: 2nd International Conference, Process Machine Interactions. Vancouver (2010)
30. Sadek, A., Meshreki, M., Attia, M.H.: Characterization and optimization of orbital drilling of woven carbon fiber reinforced epoxy laminates. CIRP Ann. Manuf. Technol. **61**(1), 123–126 (2012)
31. Tsao, C.C.: Experimental study of drilling composite materials with step-core drill. J. Mater. Des. **29**, 1740–1744 (2008)
32. Brinksmeier, E., Fangmann, S., Rentsch, R.: Drilling of composites and resulting surface integrity. CIRP Ann. Manuf. Technol. **60**(1), 57–60 (2011)
33. Mota, J.P.B., Rodrigo, A.J.S., Saatdjian, E.: Optimization of heat-transfer rate into time-periodic two-dimensional stokes flows. Int. J. Numer. Meth. Fluids **53**(6), 915–931 (2007)
34. Shu, C., Wang, L., Chew, Y.T., Zhao, N.: Numerical study of eccentric couette? Taylor flows and effect of eccentricity on flow patterns. Theoret. Comput. Fluid Dyn. **18**(1), 43–59 (2004)
35. Becker, K.M., Kaye, J.: Measurements of diabatic flow in an annulus with an inner rotating cylinder. J. Heat Transfer **84**(2), 97 (1962)
36. Sadek, A., Meshreki, M., Attia, H.: Experimental optimization of orbital drilling of woven carbon fiber reinforced epoxy laminates. In: The 19th International Conference on Composite Materials. Montreal, Quebec, Canada (2013)
37. Thomson, V., Sultana, I., Shi, Z., Attia, H.: Material removal mechanism of carbon/epoxy composites in single diamond grain machining (2013)
38. Hashin, Z., Rotem, A.: A fatigue failure criterion for fiber reinforced materials. J. Compos. Mater. **7**(4), 448–464 (1973)
39. Thomson, V., Sultana, I., Shi, Z.: An analytical model to predict cutting force during machining of composites by superabrasive tools (2014)
40. Sultana, I., Shi, Z., Attia, M.H., Thomson, V.: Surface integrity of holes machined by orbital drilling of composites with single layer diamond tools. Procedia CIRP **45**, 23–26 (2016)
41. Cytec Engineered Materils, Technical Data Sheet, CYCOM® 977-2 Epoxy resin system, AECM-00007 Rev-01, March 2012
42. Lee, L.-H.: Mechanisms of thermal degradation of phenolic condensation polymers. II. Thermal stability and degradation schemes of epoxy resins. J. Polym. Sci. Part A: Gen. Pap. 3(3), 859–882 (1965)
43. Sultana, I., Shi, Z., Attia, H., Thomson, V.: High speed orbital drilling of composites and a proposed new tool design. In: Canadian International Conference on Composites. Edmonton, Alberta, Canada (2015)
44. Shi, Z., Meshreki, M., Lamarre, J.-M., Attia, H., Aghasibeig, M.: An experimental study for lowering surface roughness in grinding with electroplated superabrasive wheels. In: 21st International Symposium on Advances in Abrasive Technology-Toronto (2018)

45. Sheikh-Ahmad, J.Y.: Mechanics of chip formation. In: Machining of Polymer Composites. New York, Springer (2009)
46. Guo, D.-M., Wen, Q., Gao, H., Bao, Y.-J.: Prediction of the cutting forces generated in the drilling of carbon-fibre-reinforced plastic composites using a twist drill. J. Eng. Manuf. 226 (2011)
47. Elhachimi, M., Torbaty, S., Joyot, P.: Mechanical modelling of high speed drilling. 2: predicted and experimental results. Int. J. Mach. Tools Manuf. **39**(4), 569–581 (1999)
48. Zhang, L.C., Zhang, H.J., Wang, X.M.: A force prediction model for cutting unidirectional fibre-reinforced plastics. Mach. Sci. Technol. **5**(3), 12 (2001)
49. Singh, I., Bhatnagar, N., Viswanath, P.: Drilling of uni-directional glass fiber reinforced plastics: experimental and finite element study. Mater. Des. **29**(2), 546–553 (2008)
50. Sadek, A., Hassan, M., Attia, M.H.: A new cyber-physical adaptive control system for drilling of hybrid stacks. CIRP Ann. **69**(1), 105–108 (2020)

Ceramic Matrix Composites (CMCs)

Jibran Khaliq

Abstract Ceramic matrix composites (CMCs) are a class of composite materials in which filler are incorporated within a ceramic matrix. As a result of filler addition to ceramic matrix, specific properties can be altered. There are various ways to manufacture ceramics and CMCs, mainly depending upon the filler material and the final application. One such property is a reduction in crack propagation. Although their constituents are brittle, CMCs have found their applications in the vast majority of the area, including space, refractories, energy storage, and automotive. This chapter considers classification and manufacturing CMCs. This chapter summarises state of the art for CMCs and their manufacturing techniques and lays the foundation for their micromachining.

1 Introduction

Traditional Structural materials which possess higher temperature resistance are becoming popular for use in the extreme environmental conditions. One group of materials that has been explored is ceramics such as Silicon Carbide (SiC) [1] Boron Carbide (b_4C) [2], Cubic Boron Nitride (c-BN) [3] which can perform efficiently at temperatures above 1500 °C. Out of all the excellent properties, ceramic materials tend to have intrinsic brittleness and failure to absorb energy before failing. To overcome these drawbacks, significant progress has been reported in the last two decades. The most important development appeared to overcome these drawbacks is in the form of composites, i.e. the combination of multiple constituent phases with suitable microstructures to improve specific structural or functional properties.

Ceramic Matrix Composites (CMCs) are those classes of materials which contain ceramic as a matrix (or binding agent) together with fillers such as particles [4], fibres (short or long) and nano-materials [5]. Ceramics matrix composites have filler ranging from ceramics to polymers [6] and various shapes and sizes. These

J. Khaliq (✉)
Department of Mechanical and Construction Engineering, Faculty of Engineering and Environment, Northumbria University, Newcastle upon Tyne N1 8ST, UK
e-mail: jibran.khaliq@northumbria.ac.uk

I. Shyha and D. Huo (eds.), *Advances in Machining of Composite Materials*, Engineering Materials, https://doi.org/10.1007/978-3-030-71438-3_11

fillers also improve the ceramic matrices' inherent catastrophic failure ability due to different strengthening mechanisms being active under service conditions. Few of these strengthening mechanisms are filler pullout, crack propagation and deflection. Various fillers behave differently in a ceramic matrix due to their shape and size, resulting in different strengthening mechanisms. CMCs offer superior strength to weight ratios than polymer or metal matrix composites due to these strengthening mechanics. CMCs are 33% lighter than the nickel based superalloys, which dramatically reduce the cost and increase performance [7]. On top of superior strength to weight ratio, their operating temperatures are also nearly 400 °C higher than nickel-based superalloys [8]. Due to their higher service temperatures and lower thermal conductivities, the engines continuously run at higher temperatures, increasing fuel economy and efficiency, resulting in fewer pollutants. According to Markets and Markets, the CMCs are projected to grow at CAGR of 9.65% to a total value of $7.51B by 2026.

Similarly, CMCs in industrial power turbines could reduce emissions and the cost of electricity. Owing to their higher operating temperatures and better mechanical properties than other materials, CMCs find their applications in extreme and demanding environments such as aerospace, furnace parts and turbine blades.

2 Classification of Ceramic Matrix Composites

Generally, ceramics-based composites are classified according to the physical shape of the filler material, however in this chapter; the composites are classified according to the nature of the filler materials such as micro filler or nano-filler as depicted in the schematic Fig. 1.

2.1 Micro Composites

Generally, ceramics-based composites are classified according to the filler material's physical shape; however, in this chapter; the composites are classified according to the nature of the filler materials such as micro fillers nano filler as depicted in the schematic Fig. 2.

2.2 Nanocomposites

Those composites in which the fillers have one of the so-called nano range (<100 nm) are called nanocomposites. The examples of such fillers are Carbon Nanotubes (CNTs) [9], Graphene [10] and other carbonaceous [11] and non-carbonaceous nanoparticles. Nanofillers are defect-free as they contain close to 'perfect' crystal

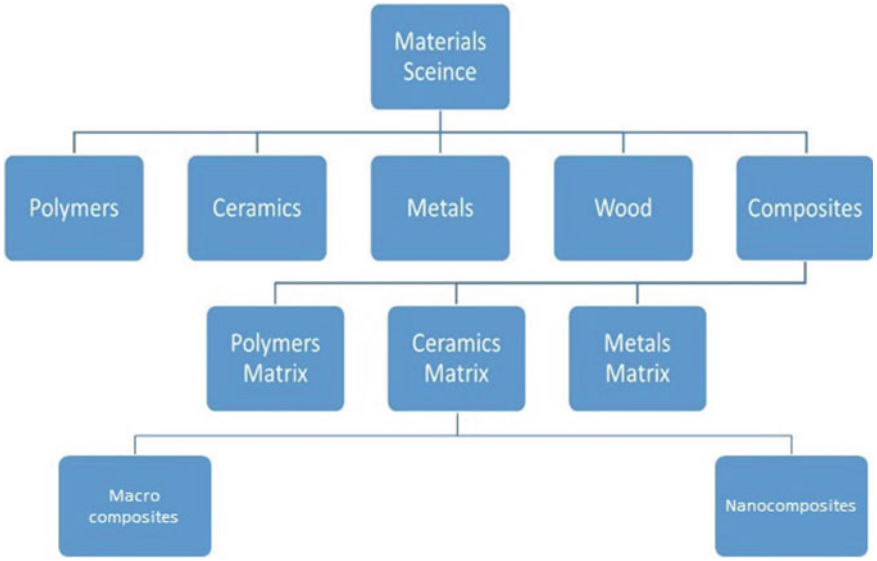

Fig. 1 Classification of different engineering materials

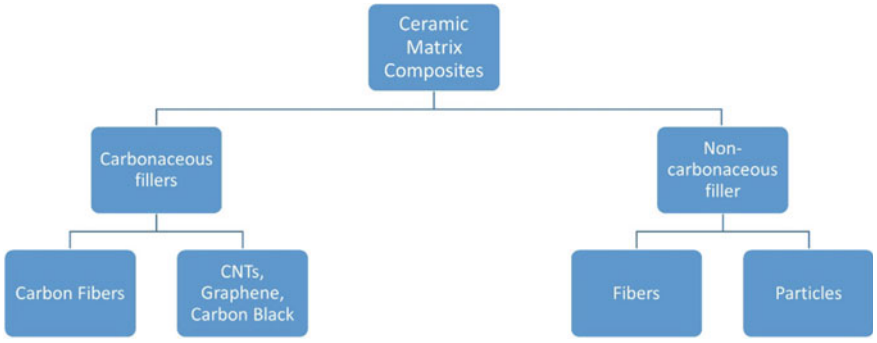

Fig. 2 Classification of different ceramic composite materials

structure. The lower volume of nanofillers additions (5–10%) demonstrates the same level of improvement in properties as achieved by adding 15–40% of micro fillers hence reducing the weight which is a crucial factor in the aerospace industry [12]. Incorporating nanofiller especially CNTs into ceramics, is not straightforward as it comes with a common challenge of CNT dispersion inside a matrix. CNTs tend to agglomerate when dispersed inside a matrix due to van de Waal forces and their low compatible interaction with a matrix [13]. Moreover, the fabrication of ceramics and ceramics-based materials predominantly requires high temperatures for sintering, which deteriorate/oxidize CNTs and other carbonaceous nanofillers [14]. As a result,

instead of improving the desired properties, the resultant ceramic possesses higher porosity than anticipated after densification.

3 Properties of Ceramic Matrix Micro Composites

Ceramics, in general, possess high fracture toughness and resistance to crack deformation. During a loading cycle, ceramics generally crack through crack propagation when the load is higher than their fracture toughness values. These fracture toughness values can be increased by adding fillers such as fibres, rapheme sheets, other ceramic fillers etc. the embedded fillers in CMCs bridge the crack and hence stop the propagation of crack [5]. This mechanism helps to avoid a brittle fracture and material move towards a ductile fracture. Ductile fractures are more advantageous compared to brittle fractures as they give a sign of warning before failure. The ductile fracture can only be observed when there is a weak bond between the fibre and the matrix for the bridging to occur. A strong matrix-filler bond will result in a brittle failure as it will not provide time to create a so-called bridge between filler and matrix. In some case, the fibres are arranged in a 2-dimensional manner, and the resulting material behaves as an anisotropic material. Due to this anisotropy, the cracks are not bridged, the way they should be which results in.

Single Edged Notch Bend tests were generally carried out to measure crack resistance which uses a single notch as a starting crack [15]. Due to the cracks' complex nature, the measured data is normalized to generate the stress intensity factor. This requires identical geometry for comparing different samples.

3.1 Mechanical Properties

Monolithic ceramics follow the linear stress–strain curve as they do not tend to have bridging as observed in CMCs. CMCs, on the other hand, show nonlinear stress–strain curves. This non-linearity portrays as the material is deforming plastically; this phenomenon is called quasi-plastic. This phenomenon is caused by micro cracks due to the bridging effect as the load increases. The Elastic modulus of the fibres used in CMCs is generally lower than that of the matrix or (monolithic ceramics); hence, the stress–strain slope decreases gradually with increasing load [16].

Carbon fibres are commonly used as reinforcing agents in different polymer and ceramic matrices to improve mechanical properties at a low cost. Carbon fibre performs better in polymer matrices compared to ceramic matrices due to the difference in processing conditions. During ceramic processing, the matrix is exposed to high temperatures and pressure, which can induce corrosion, oxidation, and mechanical failure of the fibre. The fibres are coated with a protective coating using chemical

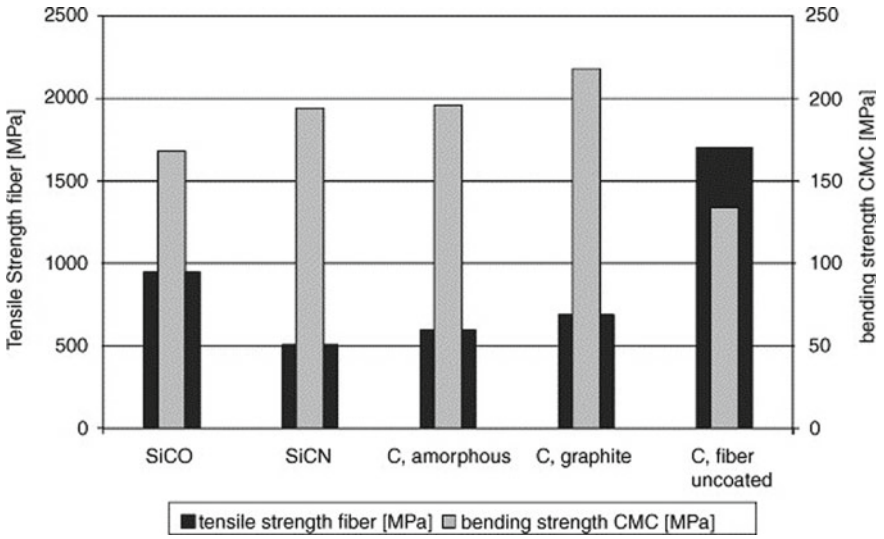

Fig. 3 A comparison of bending and tensile strength of reinforced fibres [17]

vapour deposition (CVD) to overcome these challenges. CVD is a relatively expensive coating technique with low deposition rates. Due to this reason, CVD is only used to coat fibres which are to be used in aerospace applications.

Fibre-matric adhesion is another property in CMCs that can be improved using a protective coating on fibres typically in the range of 100–500 nm. An inexpensive technique called continuous liquid phase coating (CLPC) is used to coat fibres at a large scale. In CLPC, commercial fibres are thermally downsized under nitrogen environment followed by a continuous coating of a polymeric precursor solution. The polymeric coating is then dried, cured and calcined in an inert environment in order to achieve homogenous and dense coating on each fibre. Figure 3 compares the bending and tensile strength of fibres reinforced with various materials [17].

3.2 Electrical Properties

Thermal and electrical properties of CMCs depend upon multiple factors such as matrix, porosity, filler type/ratio and heat treatment. Ceramics and CMCs are excellent electrical insulators due to the covalent bonding making up the crystal structure. These CMCs and ceramics can be made electrically conductive by adding conducting fillers such as carbon/metallic particles [18] or changing their electronic configuration [19]. The electronic configuration, more commonly called stoichiometry, can be disturbed using doping or using heat treatment to reduce conditions. $SrTiO_3$ or similar perovskites have been researched to enhance electrical conductivity using reduction heat treatment or doping such as La [20]. The electrical conductivity of

materials depends upon the electron mean free path, which is the minimum distance an electron travels before being hindered. In CMCs, the phonons mean free path can be reduced using fillers, reducing electrical conductivity. On the other hand, the addition of conductive filler can enhance the electrical conductivity by replacing 'insulating' matrix with a conducting part which will suppress the decreased phonon mean free path [21].

3.3 Thermal Properties

Ceramics possess an inherent ability to have low thermal conductivities than materials such as metals due to lack of ionic and metallic bonding. Thermal conductivity of a material depends upon similar factors as mentioned for electrical conductivity. Aluminium nitride (AlN) is one of the ceramics having high thermal conductivity (140–180 W/mK) [22] and a low coefficient of thermal expansion. However, this value can vary significantly depending upon processing conditions, starting material, porosity and if any sintering additives are added. Sintering dense AlN for efficient heat transfer is challenging due to its low diffusive nature; hence a very high processing temperature of over 1900 °C in a reducing atmosphere is applied [23]. Addition of sintering aids to manufacture CMCs has proved to be an effective strategy. CeO_2 [24], Y_2O_3 [25], CaO [26] and $CaZrO_3$ [27] have been added by researchers to improve densification and hence thermal conductivity.

Another useful material with high thermal conductivity is Si_3N_4 with values in the range of 70–180 W/m K. Typical sintering temperature for these ceramics is above 1500 °C; however, special attention needs to be paid to Si vacancies as they negatively affect thermal conductivity values [28]. In ordered to achieve the best possible values researchers have used, raw materials with low oxygen contents, non-oxide additives and texturing to utilize anisotropy in the material.

3.4 Corrosion Resistance

Ceramics are known for their excellent corrosion resistance and are utilized in various applications such as aerospace, turbines, and heat exchange tubes. Metals and polymers tend to oxidize at higher temperatures and prone to chemical attacks. Due to strong covalent bonding in ceramics and CMCs, they choose materials to be used in extreme conditions. CMCs are often used as protective coatings to prevent the damage of the base material. One of the design solutions for protective coating is to have multilayer coating. There is often a bond layer, active layer and outer layer with outer layer behaving as an oxygen/erosion-resistant layer [29]. In SiC/c composites, the bond layer is made upon SiC with the outer layer comprising either SiC [30] or Si_3N_4 [31]. The functional layer (central layer) is composed of mixtures from Si-B-C system. The three layers together can also prove to be self-healing.

4 Properties of Ceramics Matrix Nanocomposites

One of the significant purposes of making composites is to enhance the properties such as structural or functional. Addition of a small amount of fillers can dramatically improve the properties. For example, the addition of small amounts of carbonaceous filler to a ceramic matrix (an electrical insulator) can make it an excellent electrical conductor. A so-called percolation threshold of 0.64 has been reported, which is low compared to other micron-sized filler materials. This low value has been attributed to the large aspect ratio of nano-fillers [32].

Similarly, ceramics' thermal conductivity with strong covalent bonds is caused mainly by the lattice vibration of phonons [33]. Addition of fillers can disrupt the lattice vibrations and reduce the phonon mean free path, resulting in a reduced thermal conductivity value since nano-fillers are either 1 or 2 dimensional. The typical processing method for nano-filer based ceramic composites is the use of high pressure and high temperature. Generally, hot pressing or spark plasma sintering is used to manufacture ceramic nanocomposites. Although the ceramics with carbonaceous fillers can be manufactured using these methods, they come with an associated directionality in the properties which impart anisotropy within the material [34]. During pressing, the fillers tend to align themselves in the direction perpendicular to the applied pressure/load, as shown in the image Fig. 4.

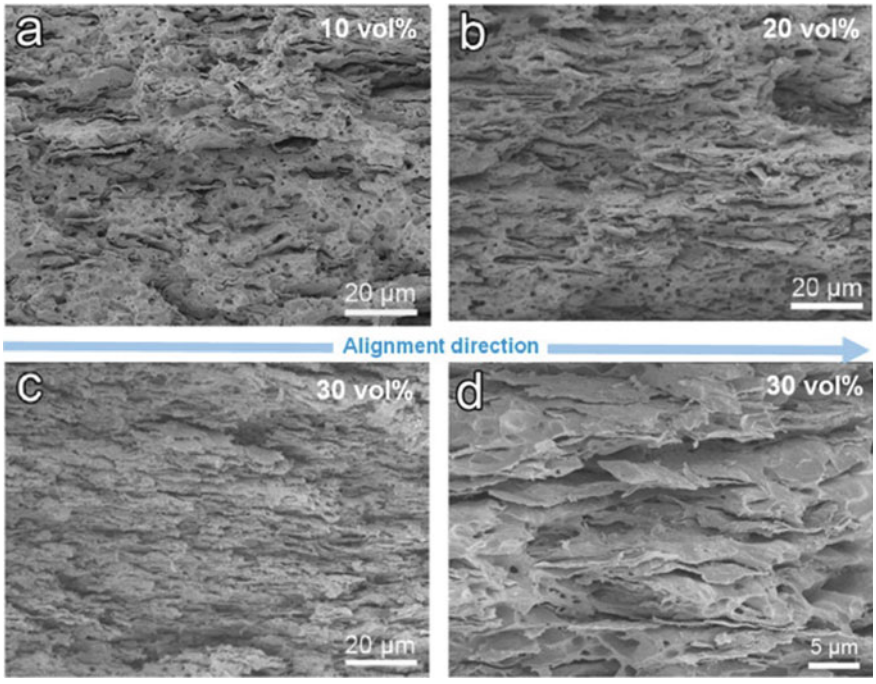

Fig. 4 SEM image of fractured graphene copper nanocomposite [34]

Table 1 Mechanical properties of CMC Nanocomposite

Material	Hardness (GPa)	Fracture toughness (MPa $m^{1/2}$)	Flexural strength (MPa)	Young's modulus (GPa)
Si_3N_4/GNP 1.5 vol% [35]	–	6.6 (235%)	–	–
Si_3N_4/RGO 4.3 vol% [36]	15.9 (−22%)	10.4 (135%)	1040 (10%)	264 (−19%)
Si_3N_4/MGN 1 wt% [37]	16.3 (0.6%)	8.5 (35%)	–	–
Si_3N_4/GPL 1 wt% [38]	13.9 (−4%)	8.7 (15%)	892 (20%)	–
Si_3N_4/FLG 3 wt% [39]	14.3 (−5%)	3.6 (−10%)	900 (−13%)	245 (−6.5%)
Al_2O_3/GPL 0.22 wt% [40]	17.66 (−2%)	4.49 (27.2%)	523 (30.8%)	–
Al_2O_3/RGO 2 vol% [41]	21.17 (7%)	10.5 (150%)	380 (8%)	–
SiC/RGO 5 vol% [42]	–	8.3 (162%)	600 (60%)	–
SiC/GNP 4 vol% [43]	25.6 (2%)	6.6 (34%)	–	424.3 (23%)

Some mechanical and physical properties (such as elastic modules) of CMC can potentially be predicted using the rule of a mixture. Rule of mixture is a mathematical expression that expects particular property of a composite in terms of the constituent ratios and is given below.

$$\rho = V_f \rho_f + V_m \rho_m$$
$$E = V_f E_f + V_m E_m$$

Some of the properties of ceramic composites are given below in the Table 1.

5 Manufacturing of Ceramics Matrix Composites (CMCs)

Ceramic matrix composites (CMCs) offer a unique combination of favourable properties required to substitute traditional materials. For instance, they provide the low density and thermal stability, high operating temperature (to name a few) for structural applications where long-term exposure to extreme environmental condition is inevitable. There are various manufacturing techniques available to manufacture CMCs. Mechanical, functional and thermal properties of CMCs depend upon the

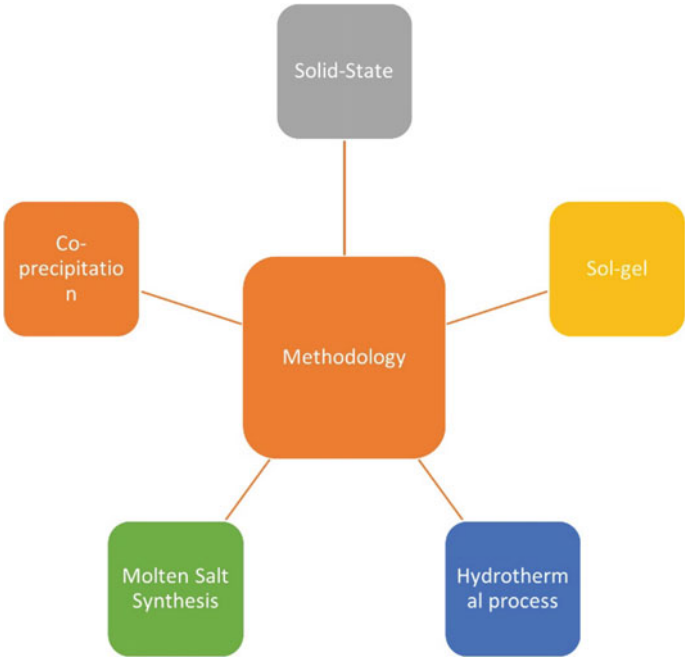

Fig. 5 Different synthesis techniques for ceramics powder

manufacturing technique used. Since ceramics require high pressure and high temperature processing to form the composites' final shape, carbonaceous materials make the processing difficult as they tend to oxidize at ceramics' sintering temperatures.

The first step in manufacturing the composites is the manufacturing (synthesis) of the matrix (and/or filler) powders which can then be consolidated into monolithic ceramics. The following Fig. 5 outlines the few commonly used techniques for ceramic powder synthesis.

5.1 Manufacturing of CMC Micro Composites (Powder Synthesis Methods)

5.1.1 Solid-State Reaction

One of the oldest yet most used ceramic powder fabrication techniques is the solid-state reaction (SSR). In this techniques, the reactant powders are initially weighed according to their stoichiometric ratios, mixed using a ball mill and calcined at high temperatures (the temperature depends upon the nature of the reaction and can be above 1000 °C) [44]. Different calcination temperatures have been investigated in solid-state reactions and an essential factor in controlling the particle size and

the crystal morphology [45]. Higher temperatures tend to increase the particle size, which will have a larger grain once the powder is sintered. This is relevant to the reduced surface energy mechanism occurring at elevated temperatures, leading to grain boundary enlargement and particle size growth [46]. The images shown in the Fig. 6 illustrate micrographs of rectangular-shape like zinc niobium oxide calcined at different temperatures which results in varying particle sizes [47].

Besides the undesired elevated temperatures required to synthesize ceramics, single-phase ceramic synthesis can be challenging [48]. There can be multiple reasons to prevent a pure phase formation such as the thermodynamics favouring a different

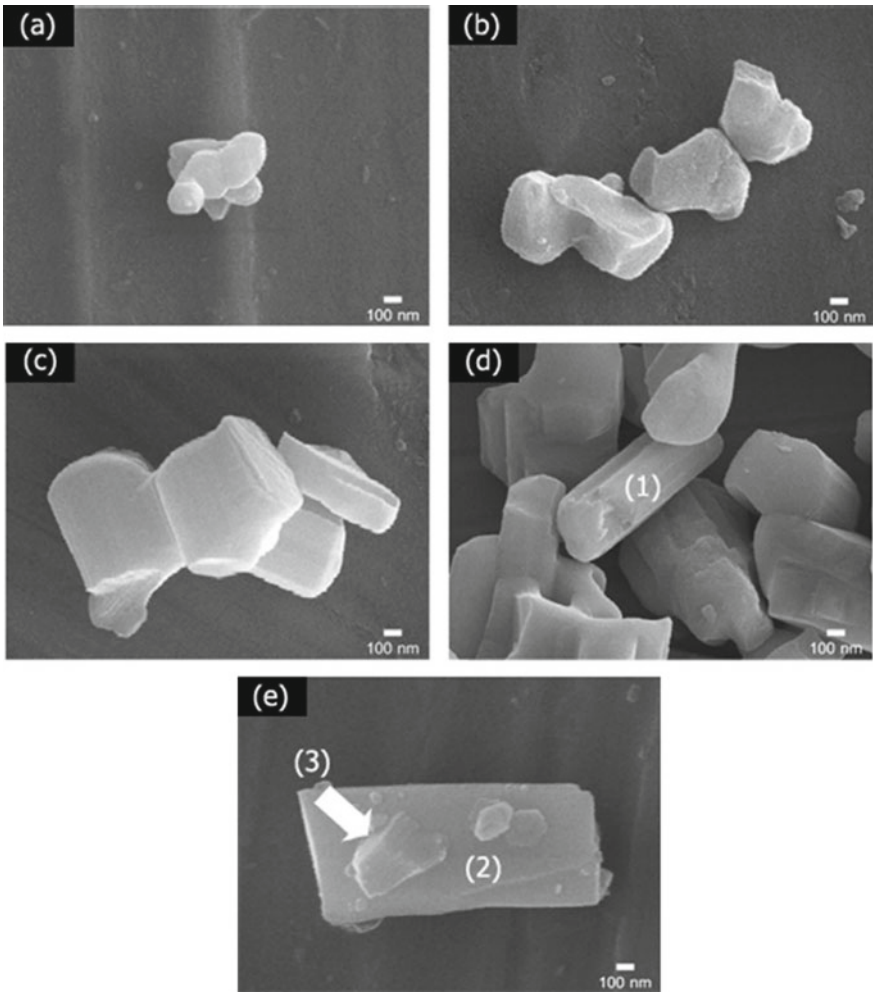

Fig. 6 SEM images of $Zn_2Nb_{34}O_{87}$ calcined at **a** 900 °C **b** 1000 °C **c** 1100 °C **d** 1200 °C and **e** 1300 °C at a heat rate of 5 °C/min [47]

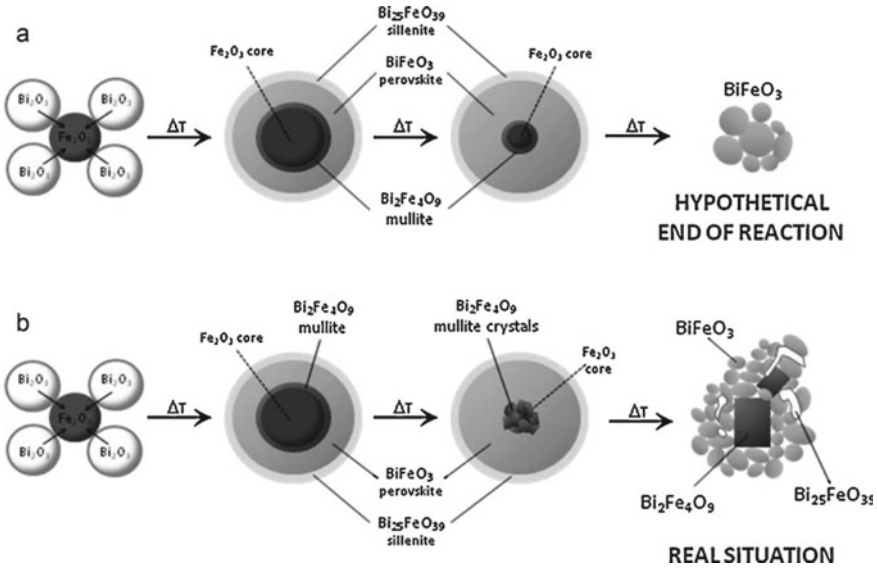

Fig. 7 A schematic of the solid-state synthesis if $BiFeO_3$ **a** Hypothetical end of the reaction **b** Real situation [49]

phase than desired, availability of impurities. For instance, in $BiFeO_3$ systems [49], upon mixing stoichiometric ratios of BiO and Fe_2O_3, the diffusion of the Bi-ions in Fe_2O_3 will form undesirable compounds (sillenite and mullite), as shown in the Fig. 7 initially. Upon further increasing the temperature, diffusion of Bi ions increased, and the undesired compounds completely decomposed until eventually a perovskite phase of $BiFeO_3$ is formed.

Hydrothermal Synthesis Method

Hydrothermal synthesis technique uses aqueous solutions, acids and bases, to crystallized single-crystal ceramic at elevated pressure and relatively low temperature compared to synthesis temperature in the solid-state procedure (temperature usually between 80 and 240) [50]. A Teflon lined steel pressure vessel called an autoclave is used to carry out the synthesis reaction at various temperatures. Since the reaction is carried out in a closed system, and the contents can later be recycled, this technique is considered 'environmentally friendly' [51, 52]. The relatively low reaction temperature required in the hydrothermal process is deemed to be advantageous as it is energy efficient. The reaction can be carried out in a conventional oven or an oven equipped with microwave radiation. Figure 8 displays a process chart for the steps involved in the hydrothermal and the microwave-assisted hydrothermal process. Hydrothermal synthesis offers other advantages: lower reaction times (compared to conventional solid-state process), uniform particles size and lower related cost [52].

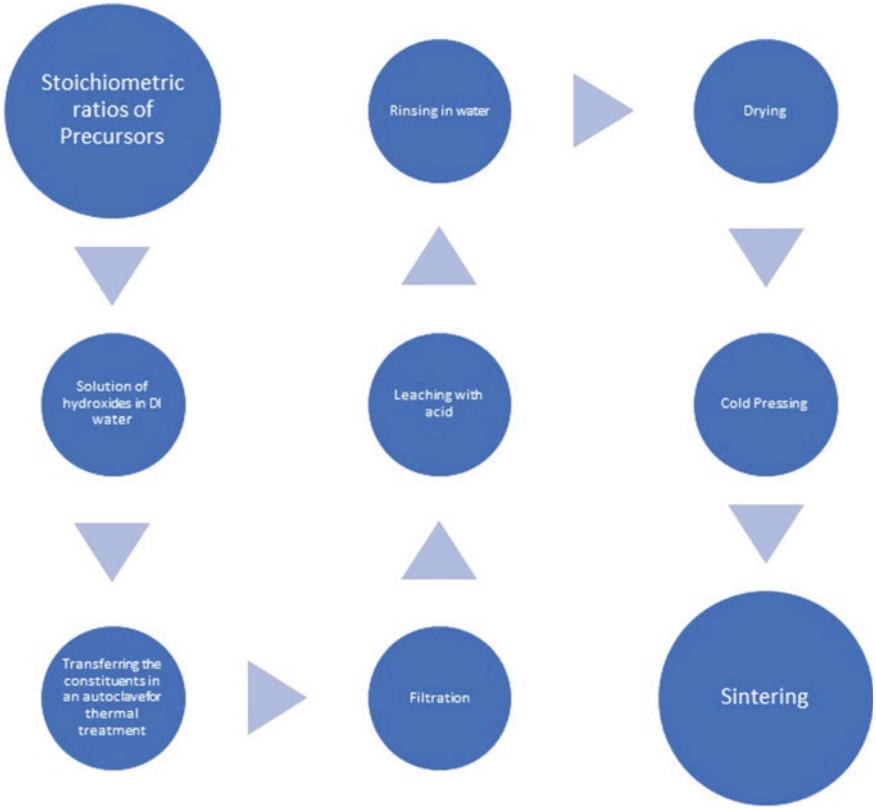

Fig. 8 Flux diagram of the hydrothermal synthesis and the microwave-assisted hydrothermal process adapted from [52]

Molten Salt Synthesis

Molten salt synthesis (MSS) is a technique where salt (or a mixture of salts) is used as a solvent in a molten state, to nucleate the particles during the reaction. It enables accelerated reaction times compared to the solid-state reaction technique, due to the small diffusion distances in the melt-solid and higher oxides mobility in the melt [53]. Higher quantities of salt are typically added to the reactants and heated above the salt's melting temperature. The flowchart shown in the figure gives an overview of the steps related to the molten salt synthesis technique and the controlling factors affecting the final particle characteristics at each step. In this technique, the reactants such as oxides and the salt are mixed in an alumina crucible and heated to a high temperature in a furnace (the typical synthesis temperature is close to 1100 °C). The heating temperature and reaction duration depend upon the powder characteristics, thermodynamics, and salt used. The resulting product mass will be afterwards washed with deionized water, to remove the salt (thus water-soluble salts are used in molten salt synthesis). Sometimes, repeated washing is recommended as the salt may require

a longer time to dissolve according to salt's solubility. To desorb ions efficiently, the application of hot water is recommended.

The particle's shape and morphology in the molten salt synthesis technique are usually associated with two main reaction mechanisms: dissolution–precipitation and template-growth, depending on the reactants' relative dissolution rates in the molten salt. They take place during the reaction stage [54].

Co-precipitation Method

In contrast to the various synthetic techniques mentioned above, the co-precipitation synthesis method aims to produce a final multicomponent ceramics to form intermediate precipitates that are usually hydrous oxides oxalates [77, 78]. The steps involved in the co-precipitation process are illustrated in Figure. In this method, the final product's structure and the resulting microstructure of the particles depend upon various factors such as secondary processing exhibited such as Ostwald ripening/centrifugation, stirring rate and the pH of the solution.

The stages carried out in the co-precipitation synthesis method are very similar to those in the solid-state synthesis technique; however, the calcination temperature required in co-precipitation is much lower together with its simplicity and quick processing. The following figure demonstrates the reaction process to synthesize $BaTiO_3$ powder using co-precipitation technique [55] (Fig. 9).

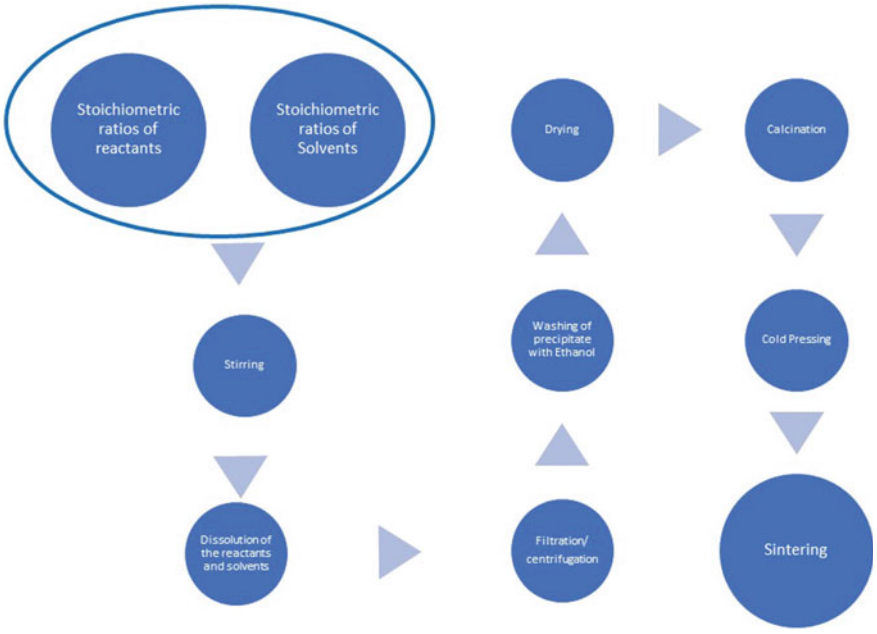

Fig. 9 Flowchart displaying $BaTiO_3$ powder synthesis using co-precipitation method adapted from [55]

Sol–Gel Method

Sol–gel is a chemical procedure in which a colloidal solution called a "sol" is formed, gradually transforming and creating a gel-like biphasic system. This biphasic system contains both a solid and a liquid whose morphologies can vary from individual particles to a continuous network which is generally polymeric [56]. Sometimes, the colloidal solution has a low volume fraction of particles, and a large amount of liquid needs to be extracted for the gel formation to occur. Removal of liquid can be accomplished in two ways, either letting the particles sediment down or then pouring off the liquid or using centrifugation. Centrifugation is quicker and saves time in phase separation. After the liquid is removed, the residue is dried, followed by densification. Distribution of the gel's porosity determines the solvent removal rate, which ultimately determines the final microstructure of component.

5.2 Manufacturing of CMC Nanocomposites

CMCs with carbonaceous fillers such as CNTs, Graphene or carbon fibres require special processing techniques due to relatively higher sintering temperature for ceramics. One of the methods to make ceramic-CNT composite is in-situ growth of ceramics on CNTs [57], jet-milling with diamond nozzle [58], high-pressure [59]. Wet mixing [60] is another technique through which ceramic nanocomposites can be manufactured. This process can create homogenous dispersion of CNTs initially; however, they tend to re-agglomerate after the solvent is removed. CNTs tend to re-agglomerate even if they are functionalized, which decreases colloidal stability. This issue can be resolved using metal catalyst-chemical vapour deposition (CVD) [61] however; it generates other negative features such as a porous interface, or CNT/interface heterogeneous structure. These processing techniques, although they are frequently used but are not suitable for high loading of CNTs. Acid-treated CNTs are mixed individually in water with Al_2O_3 nanoparticles, and the process is assisted by electrostatic forces [62]. The re-agglomeration of CNTs after solution removal and further drying steps were eliminated due to the arrest of CNTs in ceramic nanoparticles which subsequently created a homogenous distribution of CNTs. Another advantage of this processing technique was the use of high loadings of CNTs which was not feasible in other processing techniques due to their agglomeration. Similar results of CNT dispersion, post-sintering integrity and interface interaction were demonstrated by employing spark plasma sintering (SPS) technique [14, 63]. Fully dense monolithic composites [64] or functionally gradient nanocomposites [65] have also been reported. These fabrication techniques have demonstrated their effects on composites, electrical, mechanical, thermal, and other properties nanocomposites.

Graphene exhibits similar enhancement in electrical, thermo-mechanical properties compared to CNTs since both are allotropes of carbon. Therefore, due to their similar reinforcement nature in ceramic matrices, it is feasible to apply the same

processing methods to graphene nanocomposites used with CMCs with CNTs as fillers [66]. The main difference between graphene and CNT structures is the aspect ratio. Due to higher aspect ratios of CNTs, they tend to agglomerate more while graphene use can get rid of this issue, improving distribution and leading to homogeneous properties. Another distinct advantage of using graphene is getting rid of functionalization step as CNTs require them to detangle. Two common methods to disperse graphene in the ceramic matrix include powder and colloidal processing [67, 68]. The basic principle for both techniques is similar as they are using shear force such as ball milling and ultra-sonication to incorporate graphene into a ceramic matrix. In powder processing, graphene is first mixed with a solvent such as alcohol using an ultra-sonication tip. This way graphene is dispersed homogeneously in the solvent, and ceramic powder is subsequently added in the same solution through ball milling. In colloidal mixing, a prior mixture of ceramic-graphene is prepared in the form of colloidal suspensions using slow magnetic stirring and/or ultra-sonication. However, in colloidal processing, surface modification of both matrix and filler such as functionalization [69] or surfactant [35] is usually required, which is an added step compared to powder processing. Besides the above processing techniques, sol–gel processing has also generated a homogenous distribution of graphene in a ceramic matrix with assisted precursors [70, 71].

When methods mentioned earlier are not suitable for graphene-ceramic nanocomposite, polymer derived ceramics (PDC) is another option to manufacture graphene-ceramic nanocomposites [72]. This technique's general principle is to create a liquid preceramic-polymer mixed with graphene [73]. This manufacturing process has demonstrated high thermal, mechanical properties and chemical durability compared to other manufacturing techniques. Another added advantage of this technique is that it can accommodate higher filler loading of graphene.

In terms of characterisation of different properties, graphene reinforced ceramic matrix nanocomposites are subjected to fracture toughness, flexural and hardness and tensile test. Using graphene has remarkably improved the ceramic matrices' physical, electrical, and mechanical properties. Colloidal and molecular mixing have proved to be better processing techniques to enhance graphene-ceramic nanocomposites properties than powder processing due to the reasons mentioned above [74].

CMCs Containing Textiles

Fibres are commonly used as reinforcing agents in the polymer matrices to enhance mechanical properties of the polymers. Textiles made of fibres have gained popularity as they tend to achieve isotropic properties compared to the unidirectional fibres [75]. The manufacturing processes for polymer-based composites are well understood and have taken inspiration to be applied in the fabrication of CMCs. In one of the techniques, fabrics are first dipped in the ceramic matrix slurry followed by draping [76]. A roller or scraper is used to press different green composite layers, followed by firing at high temperature. This method is used where the components' lower mechanical strength is required as the volume fraction of fibres is on the lower side in this technique.

In the second method, fibre fabrics dipped in matrix slurry are stacked up in layers and put into a press mould. The mould is compacted using high pressure which can be changed depending upon the final thickness needed, and the parts are dried at relatively low temperatures in an oven. After pressing, the part is dried in a drying oven under moderate temperatures. The parts can also be dried while pressing using a hot press which eliminates the drying step. This method produces composites with a high-volume fraction of filler and has better mechanical strength than the first method.

The methods described above are mostly used for small items, and with increasing demand for composites, automated and reproducible processes are required. Pre-peg fabrication is one way to speed up the manufacturing process and reproduce the products with the same quality level. The pre-pegs are produced with defined material quantity such as mass and volume of ceramic and organic binder and can be kept in storage for several weeks.

Sintering

Sintering is a process in which ceramic or metallic powders are compacted and formed into a solid shape. In sintering diffusion of atoms occurs across the particles in which small particles are "eaten up" by larger particles to form large grains. As a result of this process, the individual particles of powder stick to forming a dense, compact shape. Sintering can take place at a higher temperature generally lower than the melting point of the ceramic matrix. In some instances, some of the constituents can also melt and its termed as liquid phase sintering. Ceramics such a B_4C, SiC, W_4C, SiN require incredibly high temperature and sintering is the preferred method to consolidate the particles [77]. Sintering of ceramics can be accomplished through various techniques such as Conventional Sintering [78], Spark Plasma Sintering (SPS) [44] and Microwave Sintering [79]. Conventional sintering is a process in which powder is compacted through the application of pressure which is also a vital part of sintering. However, pressing can take place either before or after the application of high temperature. Conventional sintering in which the process in which pressure is applied during sintering has been subdivided into two sections below.

Hot Pressing (HP)

HP is a consolidation process of powders (ceramics or metals). The powder's porosity is reduced by simultaneous heat and pressure, which in turn increases the density. This increment in density and porosity reduction will eventually improve the mechanical, electrical, and physical properties of ceramics and ceramics-based composites. In hot pressing, the powders are filled in a reshaped die and compressed along the vertical direction to compact the powder alongside increasing the temperature. In other hot-pressing method called Hot Isostatic Pressing, the powder-filled die is subjected to a high temperature in a high-pressure vessel and an inert gas applying pressure. Most used gases are inert such as Argon as they do not react with the reactants. To apply the pressure, the vessel is heated to a high temperature. The gas is pumped through an external source.

Metallic powders can also be compacted using hot isostatic pressing. In this method typically the pressure and inert gas exert in the range of 50–300 MPa [80] while the sintering temperature depends upon the individual materials and can be as high as 2400 °C for B_4C [81] based CMCs or as low as 500 °C for aluminium based metallic powders [82]. During hot isostatic pressing, the densification of the CMCs is achieved through a combination of enhanced diffusion, plastic deformation, and grain growth due to increased temperature and pressure.

Spark Plasma Sintering

Spark Plasma Sintering (SPS) is one of the processing routes to sinter variety of ceramics and metallic powder, monolithic, functionally gradient or composites. SPS's main advantage over the conventional sintering technique is that it takes only a few minutes to achieve the required sintering temperature and completes the sintering process in far less time than traditional sintering. Conventional sintering typically takes hours to complete, however using SPS. The same sintering process can be accomplished within minutes (this depends upon the type of ceramics used as carbides and nitrides may take an hour or so to sinter). This quick processing is made possible in SPS due to high heating rates (nearly 400 °C/min) achieved in the SPS. In conventional sintering, a heating rate of 5–10 °C/min is typically used to achieve a temperature of 1200 °C, and it usually requires 2–4 h. In SPS, however, this temperature can be reached in 3 min, making the process much quicker. As high pressure is simultaneously applied together with the temperature, it leads to higher densification of the powder at a relatively lower sintering temperature (on average, 200–300 °C lower than conventional sintering) [83].

On top of that, due to the sample being heated internally compared to the external heating that occurs in conventional sintering processes, the powder achieves better densification. It reaches a theoretical density value of closer to 100%. As the sintering time is too short in SPS, grain growth/coarsening does not occur. It is exceptionally beneficial to sinter nanosized particles into nanocomposites without defect structures compared to conventional sintering. These nanocomposites exhibit excellent mechanical properties such as high strength, hardness, toughness etc. In conventional sintering, a green compact usually needs to be prepared using a die and a cold press before sintering in a furnace. In SPS, the powders to be sintered are directly put into the suitable graphite dies with matching punches which will act as pressure applicators during SPS processing as shown in the Fig. 10.

The entire graphite die assembly is then put inside the SPS chamber followed by a closing chamber using the controller buttons. The control unit is programmed according to the requirements, and the sintering process is carried out. Controlling the sintering atmosphere is more convenient in SPS than conventional furnaces, and the powders can be sintered under vacuum or inert environments. Nearly all types of materials can be sintered using SPS, and due to the high heating rate, unwanted reactions can be eliminated paving the way for desired compositions.

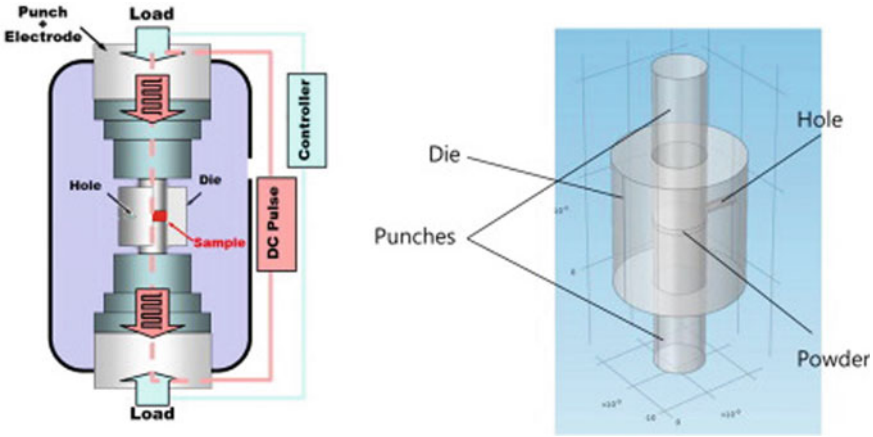

Fig. 10 A schematic of spark plasma sintering furnace [84]

Microwave Sintering

Microwaves are a form of electromagnetic waves in which the frequency range lies from 300 MHz to 300 GHz. In microwave heating, the material absorbs the electromagnetic microwaves and transforms it into heat. This heating is different from the conventional heating as in traditional heating; the heat is transferred through conduction or convection. There is a temperature gradient in conventional heating due to the surface of the material being heated firs compared to the core. On the contrary, in microwave heating, the core of the material heated first due to the heat being generated within the material. This kind of heating can be advantageous to the ceramic processing, and hence microwave sintering is used to manufacture ceramics and CMCs. Following are the few advantages of using microwave sintering over the conventional sintering: high heating rates, low processing times, decreased sintering temperatures; enhanced density due to improved diffusion hence enhanced mechanical, electrical and thermal properties. However, despite these apparent advantages due to the nature of the processing parameters required during ceramics' sintering, they can make microwave sintering process a challenging one. These requirements can be, for example, high temperatures and high or uniform heating rates. The fundamental differentiating element between microwave and conventional sintering lies in the heating mechanism of the ceramic. The microwave sintering is potentially an economic sintering process that possesses short processing time and expected to overcome the conventional sintering process's deficiencies. There has been an apparent interest in microwave sintering to manufacture ceramics and ceramic-based composites for these reasons. Microwave sintering has been picked up worldwide as a novel strategy for sintering an assortment of powders because it offers numerous benefits, as mentioned earlier.

6 Machining of CMCs

The conventional method to machine fibre reinforced CMCs uses diamond coated tools such as saws, wheels, drill bits and cutting tools [85]. The tools are used to cut out different shapes and patterns CMCs or to create threads. CMCs can also be machined using high alloy steel or diamond cutters for complex shapes. This is a faster method than diamond-based grinding techniques; however, it produces comparatively rougher surfaces. On the other hand, laser machining provides high precision and can be used for various items. The alternative to laser cutting is waterjet cutting which uses an abrasive medium and water to cut the CMCs. Chapter "Machining of Ceramic Matrix Composites" presents more details on machining of CMCs.

7 Application of CMCs

As mentioned earlier, ceramics are inherently brittle and prone to failure under sudden load. The introduction of CMC has solved the major challenges of conventional structural ceramics. Their most common uses are under extreme environments where resistance to high temperature or corrosion is desired. Following are a few examples where CMCs are traditionally used.

7.1 Space Application

During exit and re-entry to earth's atmosphere, the space vehicle is exposed to high temperature in the range of 1500 °C. Traditional ceramics can easily handle such high temperature; however, they cannot handle the thermal shock that comes with high temperature exposure. CMCs can overcome thermal shock with added advantages of higher strength to weight ratios and reusability. At such temperatures, CMCs with oxide fibres are not possible due to increased creep values. On the other hand, silicon carbide fibres are not strong enough due to re-crystallization above 1250 °C [86]. Carbon fibres in a silicon carbide matrix (C/SiC) are used in development programs for these applications.

7.2 Brake Disk

Currently, carbon-based composites are used in the automotive sector for racing cars and aeroplane brakes. Under normal conditions, the car brakes experience temperatures as high as 500 °C. At these temperatures, Carbon-based composites can degrade or lose their performance. SiC-based composite with carbon addition as a filler is

paving its way to the automotive sector and currently operating for luxury cars. CMCs based brake disc offers an excellent lifetime, typically in the range of 300,000 km as they tend to wear at a very low rate. On top of that, CMCs offer corrosion and humidity resistance, which prolong these brake discs' life span.

7.3 Bearings

A plain bearing is the simplest form of bearings without any rolling elements. As they are used in pumps to push liquids, excellent corrosion resistance against all kinds of media and low wear rate and low friction levels are generally required. Under continuous load, the CMC based bearing has a low risk of failure. In larger pumps, the risk of failure increases due to the changing requirements as they pump several thousand cubic meters of liquid over various heights.

7.4 Manufacturing

Aluminium Nitride and Silicon Nitride ceramic composites are being developed to be used in the tool's coating. These tools can perform dry, wet, turning and milling without any enhanced degradation of the tool. Similarly, the ceramics composites in the form of nano-coatings are used in the automotive sector to manufacture different parts and applications in fuel cells, filters and units that can convert energy. Moreover, lightweight bodies, with improved strength to weight ratios compared to conventional ceramic/metallic parts, are also being produced and used in the automotive sector.

7.5 Magnetic Application

Composites in which magnetic fillers are dispersed inside either nonmagnetic or magnetic matrices have found their applications in quite a few sectors such as recording, Refrigeration and magnetoresistance. Composite magnets have both matrix and filler as magnetic materials are practically useful due to their high residual magnetism and high BH values where B is magnetic flux density and H is the magnetic field strength, compared to conventional magnets. There are two types of magnetic materials, and they are termed as Soft and Hard Magnets. Soft magnets are magnets that are easy to magnetize and demagnetize while hard magnets are difficult to magnetize. Composites had $Nd_2Fe_{14}B$ as hard magnetic matrix and $Sm_2Fe_{17}N_3$ as a soft magnetic filler offer enhanced magnetic properties [87]. In another study, composites having nano FePt and Fe_3O_4 particles were fabricated using self-assembly to obtain $FePt/Fe_3Pt$. In this composite, FePt acted as a hard magnet while and Fe_3Pt was a

soft magnet. An optimum set of properties can be achieved by adjusting the building blocks' particle size and ratios [88].

8 Review Questions

(1) What is the fundamental processing difference between ceramics and metals?
(2) What are the main differences between structural CMCs and functional CMCs?
(3) Explain the difference between Ceramic based nanocomposites and Micro-composites.
(4) How can you control the electrical and thermal conductivities of ceramic-based composites?
(5) What is the difference between hydrothermal synthesis and conventional powder synthesis?
(6) How can you make sure that your synthesised ceramic powders are composed of one or multiple phases?
(7) How ceramics and ceramic-based composites can be incorporated into fabrics.
(8) Explain the primary fracture mechanism in monoliths ceramics.
(9) How a crack propagates in ceramic-based micro composites compared to a ceramic-based nanocomposite.
(10) What are the challenges in manufacturing carbon fibre reinforced composites compared to nanocomposites?
(11) What are the challenges in grinding monolithic ceramics and CMCs?

References

1. Ghasali, E., et al.: Preparation of silicon carbide/carbon fiber composites through high-temperature spark plasma sintering. J. Asian Ceram. Soc. **5**(4), 472–478 (2017)
2. Shirvanimoghaddam, K., et al.: Boron carbide reinforced aluminium matrix composite: physical, mechanical characterization and mathematical modelling. Mater. Sci. Eng., A **658**, 135–149 (2016)
3. Zhang, J., Tu, R., Goto, T.: 23—Cubic boron nitride-containing ceramic matrix composites for cutting tools. In: Low, I.M. (ed.) Advances in Ceramic Matrix Composites, pp. 570–586. Woodhead Publishing (2014)
4. Nuruzzaman, D.M., Kamaruzaman, F.F.B.: Processing and mechanical properties of aluminium-silicon carbide metal matrix composites. IOP Conf. Ser. Mater. Sci. Eng. **114**, 012123 (2016)
5. Porwal, H., et al.: Graphene reinforced alumina nano-composites. Carbon **64**, 359–369 (2013)
6. Khaliq, J., et al.: Effect of the piezoelectric ceramic filler dielectric constant on the piezoelectric properties of PZT-epoxy composites. Ceram. Int. **43**(2), 2774–2779 (2017)
7. Li, L.: Modeling cyclic fatigue hysteresis loops of 2D woven ceramic matrix composites at elevated temperatures in steam. Materials **9**(6) (2016)

8. Zhang, K., et al.: Joining of Cf/SiC ceramic matrix composites: a review. Adv. Mater. Sci. Eng. **2018**, 15 (2018)
9. Curtin, W.A., Sheldon, B.W.: CNT-reinforced ceramics and metals. Mater. Today **7**(11), 44–49 (2004)
10. Miranzo, P., Belmonte, M., Osendi, M.I.: From bulk to cellular structures: a review on ceramic/graphene filler composites. J. Eur. Ceram. Soc. **37**(12), 3649–3672 (2017)
11. Al Sheheri, S.Z., et al.: The preparation of carbon nanofillers and their role on the performance of variable polymer nanocomposites. Des. Monomers Polym. **22**(1), 8–53 (2019)
12. Rathod, V.T., Kumar, J.S., Jain, A.: Polymer and ceramic nanocomposites for aerospace applications. Appl. Nanosci. **7**(8), 519–548 (2017)
13. Chu, B.T.T., et al.: Fabrication of carbon-nanotube-reinforced glass–ceramic nanocomposites by ultrasonic in situ sol–gel processing. J. Mater. Chem. **18**(44), 5344–5349 (2008)
14. Inam, F., et al.: Electrically conductive alumina–carbon nanocomposites prepared by spark plasma sintering. J. Eur. Ceram. Soc. **30**(2), 153–157 (2010)
15. Dassios, K.G., Matikas, T.E.: Damage assessment in a SiC-fiber reinforced ceramic matrix composite. J. Eng. **2013**, 6 (2013)
16. Mechanical properties of ceramic matrix composites exposed to rig tests. In: 28th International Conference on Advanced Ceramics and Composites B: Ceramic Engineering and Science Proceedings, pp. 153–159
17. Gadow, R., Kern, F., Ulutas, H.: Mechanical properties of ceramic matrix composites with siloxane matrix and liquid phase coated carbon fiber reinforcement. J. Eur. Ceram. Soc. **25**(2), 221–225 (2005)
18. van de Goor, G., Sägesser, P., Berroth, K.: Electrically conductive ceramic composites. Solid State Ionics **101–103**, 1163–1170 (1997)
19. Khaliq, J., et al.: Utilizing the phonon glass electron crystal concept to improve the thermoelectric properties of combined Yb-stuffed and Te-substituted $CoSb_3$. Scripta Mater (0)
20. Sparks, T.D., Fuierer, P.A., Clarke, D.R.: Anisotropic thermal diffusivity and conductivity of La-doped strontium niobate $Sr_2Nb_2O_7$. J. Am. Ceram. Soc. **93**(4), 1136–1141 (2010)
21. Galusek, D., Galusková, D.: Alumina matrix composites with non-oxide nanoparticle addition and enhanced functionalities. Nanomaterials **5**(1), 115–143 (2015)
22. Wozniak, M., et al.: Thermal conductivity of highly loaded aluminium nitride–poly(propylene glycol) dispersions. Int. J. Heat Mass Transf. **65**, 592–598 (2013)
23. Streicher, E., et al.: Densification and thermal conductivity of low-sintering-temperature AlN materials. J. Eur. Ceram. Soc. **6**(1), 23–29 (1990)
24. Choi, H.-S., et al.: Structural, thermal and mechanical properties of aluminum nitride ceramics with CeO_2 as a sintering aid. Ceram. Int. **42**(10), 11519–11524 (2016)
25. Fabrichnaya, O., et al.: Liquid phase formation in the system Al_2O_3–Y_2O_3–AlN: Part II. Thermodynamic assessment. J. Eur. Ceram. Soc. **33**(13), 2457–2463 (2013)
26. Molisani, A.L., Goldenstein, H., Yoshimura, H.N.: The role of CaO additive on sintering of aluminum nitride ceramics. Ceram. Int. **43**(18), 16972–16979 (2017)
27. Lee, H.M., Kim, D.K.: High-strength AlN ceramics by low-temperature sintering with $CaZrO_3$–Y_2O_3 co-additives. J. Eur. Ceram. Soc. **34**(15), 3627–3633 (2014)
28. Yonezawa, T., et al.: Pressureless sintering of silicon-nitride composites. Compos. Sci. Technol. **51**(2), 265–269 (1994)
29. Cheng, L., et al.: Corrosion of a 3D-C/SiC composite in salt vapor environments. Carbon **40**(6), 877–882 (2002)
30. Niu, M., et al.: SiC/(SiC + glass)/glass coating for carbon-bonded carbon fibre composites. RSC Adv. **6**(66), 61228–61234 (2016)
31. Herrmann, M.: Corrosion of silicon nitride materials in aqueous solutions. J. Am. Ceram. Soc. **96**(10), 3009–3022 (2013)
32. Ahmad, K., Pan, W., Shi, S.-L.: Electrical conductivity and dielectric properties of multiwalled carbon nanotube and alumina composites. Appl. Phys. Lett. **89**(13), 133122 (2006)

33. Ishikawa, T., et al.: A tough, thermally conductive silicon carbide composite with high strength up to 1600 °C in air. Science **282**(5392), 1295 (1998)
34. Chu, K., et al.: Thermal properties of graphene/metal composites with aligned graphene. Mater. Des. **140**, 85–94 (2018)
35. Walker, L.S., et al.: Toughening in graphene ceramic composites. ACS Nano **5**(4), 3182–3190 (2011)
36. Ramirez, C., et al.: Extraordinary toughening enhancement and flexural strength in Si_3N_4 composites using graphene sheets. J. Eur. Ceram. Soc. **34**(2), 161–169 (2014)
37. Kvetková, L., et al.: Influence of processing on fracture toughness of Si_3N_4 + graphene platelet composites. J. Eur. Ceram. Soc. **33**(12), 2299–2304 (2013)
38. Zhang, Y., et al.: Effect of graphene orientation on microstructure and mechanical properties of silicon nitride ceramics. Process Appl Ceram **12**(1), 27–35 (2018)
39. Tapasztó, O., et al.: Dispersion patterns of graphene and carbon nanotubes in ceramic matrix composites. Chem. Phys. Lett. **511**(4–6), 340–343 (2011)
40. Liu, J., Yan, H., Jiang, K.: Mechanical properties of graphene platelet-reinforced alumina ceramic composites. Ceram. Int. **39**(6), 6215–6221 (2013)
41. Lee, B., et al.: Simultaneous strengthening and toughening of reduced graphene oxide/alumina composites fabricated by molecular-level mixing process. Carbon **78**, 212–219 (2014)
42. Belmonte, M., et al.: Toughened and strengthened silicon carbide ceramics by adding graphene-based fillers. Scripta Mater. **113**, 127–130 (2016)
43. Pereira dos Santos Tonello, K., et al.: Fabrication and characterization of laminated SiC composites reinforced with graphene nanoplatelets. Mater. Sci. Eng. A **659**, 158–164 (2016)
44. Khaliq, J., et al.: Reduced thermal conductivity by nanoscale intergrowths in perovskite like layered structure $La_2Ti_2O_7$. J. Appl. Phys. **117**(7), 075101 (2015)
45. Guo, X., et al.: Effect of calcining temperature on particle size of hydroxyapatite synthesized by solid-state reaction at room temperature. Adv. Powder Technol. **24**(6), 1034–1038 (2013)
46. James, N.K., et al.: High piezoelectric voltage coefficient in structured lead-free (K, Na, Li)NbO_3 particulate—epoxy composites. J. Am. Ceram. Soc. **99**(12), 3957–3963 (2016)
47. Amonpattaratkit, P., Ananta, S.: Effects of calcination temperature on phase formation and particle size of $Zn_2Nb_{34}O_{87}$ powder synthesized by solid-state reaction. Mater. Chem. Phys. **139**(2), 478–482 (2013)
48. Khaliq, J., et al.: Utilizing the phonon glass electron crystal concept to improve the thermoelectric properties of combined Yb-stuffed and Te-substituted $CoSb_3$. Scripta Mater. **72–73**, 63–66 (2014)
49. Bernardo, M.S., et al.: Reaction pathways in the solid state synthesis of multiferroic $BiFeO_3$. J. Eur. Ceram. Soc. **31**(16), 3047–3053 (2011)
50. Suchanek, W.L., Lencka, M.M., Riman, R.E.: Chapter 18—hydrothermal synthesis of ceramic materials. In: Palmer, D.A., Fernández-Prini, R., Harvey, A.H. (eds.) Aqueous systems at elevated temperatures and pressures, pp. 717–744. Academic Press, London (2004)
51. Zhou, Y., et al.: Hydrothermal synthesis and piezoelectric property of Ta-doping $K_{0.5}Na_{0.5}NbO_3$ lead-free piezoelectric ceramic. Ceram. Int. **35**(8), 3253–3258 (2009)
52. Villafuerte-Castrejón, E.M., et al.: Towards lead-free piezoceramics: facing a synthesis challenge. Materials **9**(1) (2016)
53. Cai, Z., et al.: Molten salt synthesis of lead lanthanum zirconate titanate ceramic powders. J. Alloy. Compd. **454**(1), 466–470 (2008)
54. Cai, Z., et al.: Large-scale synthesis of $Pb_{1-x}La_xTiO_3$ ceramic powders by molten salt method. J. Alloy. Compd. **420**(1), 273–277 (2006)
55. Adelina, I., Sophie, G.-F., Bernard, D.: BaTiO3 thick films obtained by tape casting from powders prepared by the oxalate route. Process. Appl. Ceram. **3**(1–2), 65–71 (2009)
56. Afrin, R., et al.: Synthesis of multiwalled carbon nanotube-based infrared radiation detector. Sens. Actuators, A **187**, 73–78 (2012)
57. Mazumder, S., et al.: Carbon nanotubes-porous ceramic composite by in situ CCVD growth of CNTs. Mater. Chem. Phys. **171**, 247–251 (2016)

58. Llorente, A., et al.: Jet milling as an alternative processing technique for preparing polysulfone hard nanocomposites. Adv. Mater. Sci. Eng. **2019**, 8 (2019)
59. Roy, S., et al.: Magnetic properties of glass-metal nanocomposites prepared by the sol-gel route and hot pressing. J. Appl. Phys. **74**(7), 4746–4749 (1993)
60. Palmero, P.: Structural ceramic nanocomposites: a review of properties and powders' synthesis methods. Nanomaterials **5**(2), 656–696 (2015)
61. Rodiles, X., et al.: Carbon nanotube synthesis and spinning as macroscopic fibers assisted by the ceramic reactor tube. Sci. Rep. **9**(1), 9239 (2019)
62. Kim, E.-H., Jung, Y.-G., Paik, U.: Microstructure and mechanical properties of Al_2O_3 composites with surface-treated carbon nanotubes (CNTs): dispersibility of modified carbon nanotubes (CNTs) on Al_2O_3 matrix. J. Nanosci. Nanotechnol. **12**(2), 1332–1336 (2012)
63. Sikder, P., et al.: Improved densification and mechanical properties of spark plasma sintered carbon nanotube reinforced alumina ceramics. Mater. Chem. Phys. **170**, 99–107 (2016)
64. Han, X.-X., et al.: Microstructure, sintering behavior and mechanical properties of SiC/$MoSi_2$ composites by spark plasma sintering. Trans. Nonferrous Metals Soc. China **28**(5), 957–965 (2018)
65. Tan, X., et al.: Functionally graded nano hardmetal materials made by spark plasma sintering technology. J. Metastable Nanocrystalline Mater. **23**, 179–182 (2005)
66. Kinloch, I.A., et al.: Composites with carbon nanotubes and graphene: an outlook. Science **362**(6414), 547 (2018)
67. Sun, J., Gao, L., Li, W.: Colloidal processing of carbon nanotube/alumina composites. Chem. Mater. **14**(12), 5169–5172 (2002)
68. Gallardo-López, Á., et al.: Spark plasma sintered zirconia ceramic composites with graphene-based nanostructures. Ceramics **1**(1), 153–164 (2018)
69. Wang, K., et al.: Preparation of graphene nanosheet/alumina composites by spark plasma sintering. Mater. Res. Bull. **46**(2), 315–318 (2011)
70. Hintze, C., et al.: Facile sol–gel synthesis of reduced graphene oxide/silica nanocomposites. J. Eur. Ceram. Soc. **36**(12), 2923–2930 (2016)
71. Giampiccolo, A., et al.: Sol gel graphene/TiO_2 nanoparticles for the photocatalytic-assisted sensing and abatement of NO_2. Appl. Catal. B **243**, 183–194 (2019)
72. Román-Manso, B., et al.: Polymer-derived ceramic/graphene oxide architected composite with high electrical conductivity and enhanced thermal resistance. J. Eur. Ceram. Soc. **38**(5), 2265–2271 (2018)
73. Ji, F., et al.: Electrochemical performance of graphene nanosheets and ceramic composites as anodes for lithium batteries. J. Mater. Chem. **19**(47), 9063–9067 (2009)
74. Porwal, H., et al.: Toughened and machinable glass matrix composites reinforced with graphene and graphene-oxide nano platelets. Sci. Technol. Adv. Mater. **14**(5), 055007 (2013)
75. Selzer, R., Friedrich, K.: Mechanical properties and failure behaviour of carbon fibre-reinforced polymer composites under the influence of moisture. Compos. A Appl. Sci. Manuf. **28**(6), 595–604 (1997)
76. Mouchon, E., Colomban, P.: Oxide ceramic matrix/oxide fibre woven fabric composites exhibiting dissipative fracture behaviour. Composites **26**(3), 175–182 (1995)
77. Sadighzadeh, A., et al.: Study of sintering temperature on the structure of silicon carbide membrane. J. Theor. Appl. Phys. **8**(4), 169–173 (2014)
78. Yin, C., et al., NaCa4V5O17: A low-firing microwave dielectric ceramic with low permittivity and chemical compatibility with silver for LTCC applications. J. Eur. Ceram. Soc. (2019)
79. Oghbaei, M., Mirzaee, O.: Microwave versus conventional sintering: a review of fundamentals, advantages and applications. J. Alloy. Compd. **494**(1), 175–189 (2010)
80. Ohtaka, O., et al.: High-pressure and high-temperature generation using diamond/SiC composite anvils prepared with hot isostatic pressing. High Pressure Research **25**(1), 11–15 (2005)
81. She, J., Guo, J., Jiang, D.: Hot isostatic pressing of α-silicon carbide ceramics. Ceram. Int. **19**(5), 347–351 (1993)

82. Zulfia, A., et al.: Effect of hot isostatic pressing on cast A357 aluminium alloy with and without SiC particle reinforcement. J. Mater. Sci. **34**(17), 4305–4310 (1999)
83. Grasso, S., et al.: Low-temperature spark plasma sintering of pure nano WC powder. J. Am. Ceram. Soc. **96**(6), 1702–1705 (2013)
84. Byon, C., et al.: Numerical study of a SiC mould subjected to a spark plasma sintering process. Scripta Mater. **96**, 49–52 (2015)
85. Gavalda Diaz, O., et al.: The new challenges of machining Ceramic Matrix Composites (CMCs): review of surface integrity. Int. J. Mach. Tools Manuf **139**, 24–36 (2019)
86. Després, J.-F., Monthioux, M.: Mechanical properties of C/SiC composites as explained from their interfacial features. J. Eur. Ceram. Soc. **15**(3), 209–224 (1995)
87. O'Donnell, K., Kuhrt, C., Coey, J.M.D.: Influence of nitrogen content on coercivity in remanence-enhanced mechanically alloyed Sm-Fe-N. J. Appl. Phys. **76**(10), 7068–7070 (1994)
88. Akbari, H., Zeynali, H., Bakhshayeshi, A.: Interparticle interactions of FePt core and Fe_3O_4 shell in FePt/Fe_3O_4 magnetic nanoparticles. Phys. Lett. A **380**(7), 927–936 (2016)

Machining of Ceramic Matrix Composites

Jinguang Du, Haizhen Zhang, Yongmiao Geng, Wuyi Ming, Wenbin He, Jun Ma, Yang Cao, Xiaoke Li, and Kun Liu

Abstract Carbon fibre-reinforced ceramic matrix composites have many excellent physical and mechanical properties, such as high specific strength, hardness, and fracture toughness compared to their matrix, and they also possess good performance in wear, heat and ablation resistance and dimensional stability. They are an ideal choice for thermal protection and high-temperature structural materials. However, their characteristics of high hardness and abrasive nature make these materials difficult to machine, which limits their large-scale industrial application. This chapter reviews research on the machining of carbon fibre-reinforced ceramic matrix composites, including conventional and unconventional machining processes. The problems arising with various machining methods and possible solutions are discussed.

1 Introduction

A ceramic matrix composite is a kind of material composed of ceramic matrix and various fibres. Because the fibres can prevent the growth of cracks, fibre-reinforced ceramic matrix composites with excellent toughness can be obtained. Carbon fibre is currently widely used in ceramic matrix composites as the reinforcement phase, while some also use silicon carbide. Carbon fibres have attractive properties such as low density, high tensile modulus and strength, low thermal expansion coefficients and high thermal conductivity [1, 2], and are often compounded with a matrix such as resin, metal or ceramic to form a structural composite. Currently, fibre-reinforced composites are widely applied in many fields.

Carbon fibre-reinforced ceramic matrix composites (CFRCs) and carbon fibre-reinforced polymer matrix composites (CFRPs) have attracted close research attention [3, 4]. CFRCs have many excellent propertiesm including low weight, chemical stability, corrosion, wear and fatigue resistance as well as high strength, and can

J. Du · H. Zhang · Y. Geng · W. Ming · W. He · J. Ma (✉) · Y. Cao · X. Li · K. Liu
Henan Provincial Key Laboratory of Intelligent Manufacturing of Mechanical Equipment, Zhengzhou University of Light Industry, No. 5 Dongfeng Road, Zhengzhou, China
e-mail: majun@zzuli.edu.cn

I. Shyha and D. Huo (eds.), *Advances in Machining of Composite Materials*, Engineering Materials, https://doi.org/10.1007/978-3-030-71438-3_12

be applied widely in aerospace [5], energy, advanced structural, brake system [6], sporting goods, and defence applications [7, 8].

Although CFRCs are usually manufactured in near-net shapes, the composite component is generally subjected to secondary machining after manufacture in order to achieve the required and designed dimensional tolerance, shape and positional accuracy [9]. Secondary machining is mainly used to finish the surface shaping, trimming and drilling the structural parts by conventional or unconventional machining. The machining mechanism for CFRCs is more complicated than that of traditional metals and their alloys [10, 11] due to the complicated internal relationship between carbon fibre and the reinforcing phase as well as the non-homogeneous and anisotropic properties of these composites.

At present, many of the material fabrication methods for carbon fibre composites have been thoroughly researched and tested, but secondary machining requires further study. The machinability and surface integrity of CFRCs can directly affect their performance, which is one of the most critical issues in their manufacture and use. When machining these composites, tool wear is severe, residual stress is generated, and the carbon fibres may be pulled out causing delamination. This limits their wider application. Recently, achievements have been made in understanding defect formation and microscopic material removal mechanisms, and in evaluating and characterizing surface quality during the machining of these composites. However, further study on precision and efficient machining technologies for these composites is imperative.

The machining of CFRCs can be classified as conventional or unconventional. At present, traditional machining methods such as milling, grinding, and drilling have become means to study the cutting mechanism and reduce defect generation while machining composites. Unconventional methods mainly refer to laser-beam machining and water-jet cutting, which help overcome the disadvantages of conventional machining. Meanwhile emerging hybrid methods like ultrasonic vibration- and laser-assisted machining are also regarded as unconventional machining.

Therefore, this chapter reviews the current status of conventional and unconventional machining methods for ceramic matrix composites such as C/SiC and SiC/SiC composites and discusses the material removal mechanisms before summarizing the problems with various machining methods.

2 Conventional and Unconventional Machining of Ceramic Matrix Composites

2.1 Conventional Machining

Conventional machining methods (turning, milling, grinding and drilling) occupy an important position in the machinery industry, since most precision parts need secondary processing. Compared to traditional metal materials, ceramic matrix

composites are usually anisotropic and possess higher strength and hardness and wear resistance. Using conventional methods in machining these composites, the mechanism of traditional machining and surface formation progress can be quite different from those for plain metal materials. Therefore many scholars have studied the conventional machining processes and machining mechanisms of these composite materials, and their most significant findings are summarised in this section.

2.1.1 Milling

The outstanding physical and mechanical properties of carbon fibre-reinforced composites lead to increasing demand for aerospace structural parts with thin-wall geometrical characteristics such as deep cavities and narrow grooves. Milling is a standard method used in machining these structural parts. For ceramic matrix composites that have a certain level of brittleness, however, few published reports cover milling. Some studies have considered the milling of CFRCs using cemented carbide and super—hard diamond tools. For example, PCD tools in general exhibit better cutting performance than tungsten carbide with the same machining conditions, whilst a K10 cemented carbide end mill was found to be unsuitable due to severe wear [12].

By observing surface/subsurface damage in milling experiments with C/SiC composites using PCD tools, surface formation mechanism has the manifestation modes of laminated fracture, and the pull-out and fracture of the carbon fibre bundle. Higher cutting speed and a small axial depth of cut can reduce cutting force, eventually improving surface quality [13]. Varying the feed rate of 20 mm/min to 320 mm/min had little effect on edge breakage and burr generation when milling C/SiC composites, and the desired machining results were obtained, and a smaller depth of cut caused only a few edge breakages and burrs on the machined surface [14]. Fibre orientation had a notable effect on surface quality, and fibre orientations at angles of 0° and 135° exhibited the best and worst surface quality respectively [14].

In practice, one can also optimize the machining process by considering multiple factors. For example, a profile of the CNC milling process for carbon fibre-reinforced ceramic composite has been completed using many technological trials [15]. After tool selection, cutting depth calculation, and tool path design, and taking into consideration compactness and the processing rigidity of C/SiC composites, better machining accuracy, surface quality and higher machining efficiency can be obtained by selecting an appropriate cutting speed or higher feed rate.

2.1.2 Grinding

Grinding is often considered to be a finishing method which also has advantages in the machining of hard and brittle material. Grinding plays an crucial role in the

machining of precision parts. In the grinding of CFRCs, grinding force, fibre removal mode, and surface quality have been the main focus of researchers.

The use of single-particle diamond tools and finite element modelling via ABAQUS have become an effective means to study the material removal mechanism. A single particle diamond model was established using ABAQUS for the grinding of C/SiC composite which can be simulated with different grinding parameters [16]. The results showed that grinding forces were small, surface quality improved, and the scale of surface cracking decreased with an increased rate of rotation of the grinding wheel. The finite element simulation of single-diamond abrasive grinding provided an effective method and a good theoretical basis for an understanding of the grinding mechanism of ceramic matrix composite [16]. In Li's study, to fully elucidate the material removal mechanisms in the grinding of unidirectional C/SiC composites, a single-abrasive scratch tool was used to carry out experiments in two cutting directions, as shown in Fig. 1 [17]. With the same cutting depth, it was found that the tangential force is larger than the normal force, which is similar to the results of work by Du et al. [18], and the grinding forces in both longitudinal and transverse cutting directions display being different [17]. Brittle fracturing plays a vital role in the material removal mode when scratching C/SiC composites. Ding et al. pointed out that the grinding force of C/SiC composite was small, at 35–76% of the cutting force of SiC under the same grinding parameters [19].

The machining process has also been analysed using the empirical formula for grinding force. Given the complexity of the grinding process and the diversity of composite structures, it is more difficult to establish a mathematical model for grinding force than for milling. Based on the removal mechanism mainly involving brittle fracture, theoretical expressions of grinding force for the surface friction layer of 2D C/SiC composite have been proposed when grinding these composites using a resin-bond diamond wheel as follows [20]:

$$F_t \propto K a_p^{0.75} v_s^{-0.5} v_w^{0.5} \tag{1}$$

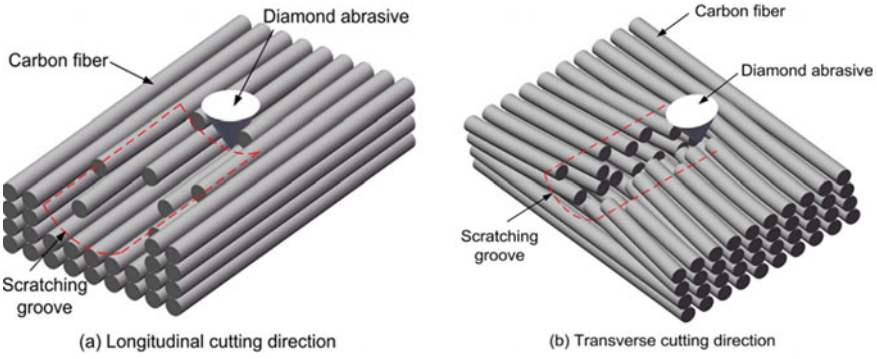

Fig. 1 Two typical cutting directions [17] (Reprinted with permission from Elsevier: licence number 17)

$$F_n \propto K' a_p^{0.75} v_s^{-0.5} v_w^{0.5} \tag{2}$$

where F_t and F_n are tangential and normal grinding forces respectively, K and K' are scale factors, a_p is grinding depth, v_s is wheel speed, and v_w is workpiece speed.

From the above theoretical expressions of grinding force, it is determined that the biggest influence on grinding force is grinding depth, while grinding wheel and workpiece speeds had roughly the same effect [26]. Further modelling work is needed to account for the effect of fibre orientation and fibre removal modes.

Most research on the grinding of C/SiC composites focuses on the machining and material removal mechanisms. The orientation of the carbon fibres affects the removal process and surface formation, the details of which have been verified experimentally. The removal of C/SiC composite material is related to its microstructure, the grinding parameters and fibre orientation, and many studies suggest that brittle removal is the primary mode.

Research into the formation mechanism of the surface morphology of C/SiC composite with the two-dimensional orthogonal woven structure subjected to grinding using a resin-bonded diamond wheel shows that the grinding parameters significantly influence surface roughness [21], which increases with feed rate and depth of cut but is reduced with faster wheel speed [21], as with common metal materials. Due to the nature of the braided structure, the primary formation mechanism of the ground surface of C/SiC composites involves the layered brittle fracture of the carbon fibre. The fracture of fibres in bundles oriented at 0° was more severe than for those at 90°. Moreover, in analysing the grinding of C/SiC composite in three directions, Zhang et al. [22] employed the relevant basic grinding theory and concluded that fibre orientation and the grinding parameters affected the grinding force and had a significant effect on the surface topography. In addition, the anisotropy of the C/SiC composite was the main reason for the changes in grinding force and surface topography in the three specific directions [22].

Du et al. investigated the influence of fibre orientation and grinding parameters on cutting force and surface quality in the machining of 2D C/SiC composite using an electroplated diamond wheel, and they obtained some different findings [18]. Furthermore, carbon fibre removal was analysed in depth taking into consideration the relationship between machining direction and fibre orientation. Figure 2 [18] shows the modes of fibre removal in machining this composite. Some fibres were cut off from the entire fibre or were pulled out and broken to form the machined surface. Feed rate may have some influence on the fracture of the fibre. At high feed rates, there is little time to remove the fibre, resulting in the phenomenon of extrusion fracture [18]. When grinding C/SiC composites with different weave structures, the grinding parameters in the machining process vary slightly.

The ground surface quality of C/SiC composites with different grinding parameters was studied by Ding et al. [19]. Both the carbon fibres and SiC matrix were removed in the manner of brittle fracture. Fibre removal involved laminar fracture and fibres being pulled out, which is not sync with the removal of SiC matrix. As a result, the machined surface roughness of C/SiC composite was higher than that

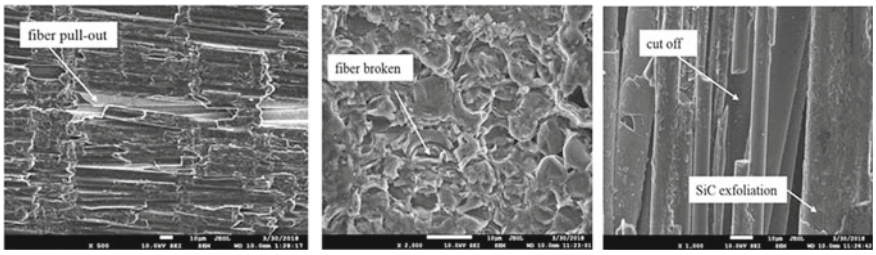

Fig. 2 Primary surface defects when grinding C/SiC composites [18] (Reprinted with permission from Elsevier: licence number 18)

of SiC with the same grinding parameters [19]. Based on the orthogonal grinding of C/SiC composite, the effects of grinding parameters on inner-cone surface roughness have also been analysed, and the main factor influencing the surface quality of the internal vertebral body during grinding was the operating table speed, followed by workpiece speed, unit feed, and grinding wheel speed [23]. It is therefore proposed that the optimization of grinding parameters can improve the vertical working table speed.

Besides, the grinding parameters also have influence on the grinding chips for grinding of C/SiC composite. As shown in previous research [24], the removal form of grinding chips affects the formation of surface defects. When machining this composite, the SiC matrix is mainly removed by forming debris. On the other hand, the removal of carbon fibre generates two kinds of CF fragments and debris, and the characteristics of chips and material removal correlate with aspects of the grinding mechanism. When the bending stress inside the carbon fibre is greater than its ultimate strength, it will peel off and break [24]. Deboned cracks and grooves and fibre pull-out can be observed when the diamond grit acts on the fibres in both orientations. Overall, it was concluded that brittle fracture plays a central role in the progress of material removal during the grinding of this composite.

The effects of fibre orientation and grinding depth on the surface integrity and grinding force of unidirectional C_f/SiC was investigated in Qu et al.'s study [25]. Three reference planes based on the positional relationship between the grinding wheel and carbon fibres were defined. In each reference plane, different fibre deflections were used to evaluate the characteristics of the grinding process. The trends of surface quality and grinding force showed a certain regularity, and the primary forms of damage were matrix cracks, fibre wear, fracture, and pull-out, and interfacial debonding [25].

Research into the grinding of ceramic matrix composite also investigates machinability using new cutting tools. One study employing WA and s of the machining of C/C–SiC composite [12] found that the machining performance of a porous vitrified bonded diamond wheel was better than that of a WA wheel. Elsewhere, a new design of a segmented wheel was developed for grinding ceramic matrix composites [26], and correlation analysis showed that it could reduce grinding forces, wheel wear and increase material removal rate (MRR). The proposed wheel has relatively little static

cutting edges, contributing to fewer momentary engagements of the cutting edges and lower rubbing and ploughing power. Meanwhile, the conventional grinding (CG) of surfaces is generally better than intermittent grinding (IG) with the T-Tool wheel [26]. A genetic algorithm (GA) can be used to optimize the grinding process with multiple objectives, and relevant studies indicate that grinding parameters such as depth of cut, table feed, and the size and density of grit could be varied to obtain higher values of MRR, better surface finish and less surface and subsurface damage [27].

At present, the industry is changing traditional manufacturing models and promoting green technology. Different types of lubrication have a significant influence on the grinding of ceramic matrix composites, and greener cooling systems will play an increasingly important role in machining. The minimum quantity lubrication (MQL) method offers significant advantages, where compressed gas (such as air, nitrogen or carbon dioxide) is mixed with a minimal amount of lubricating oil and vaporised to form a oil mist consisting of micron-level droplets, which is sprayed into the cutting area through a nozzle at high speed. The grinding of C_f/SiC ceramic matrix composite using MQL can achieve better surface quality and comparatively small grinding forces, as shown in Fig. 3, as well as reducing air pollution [28]. The nozzle direction, air pressure, oil flow rate and nozzle distance in MQL all influence the machining process. The effects of spray area, air pressure, oil flow rate and nozzle distance on the surface roughness and cutting forces in grinding of unidirectional C_f /SiC composite have been investigated using single factor experimentation to obtain a suitable combination of MQL parameters [28]. To gain higher surface quality and lower cutting force in the grinding of unidirectional carbon fibre reinforced ceramic matrix composites, a method of carbon nanofluid minimum quantity lubrication has been proposed [29] which further improves the surface quality and reduces cutting force.

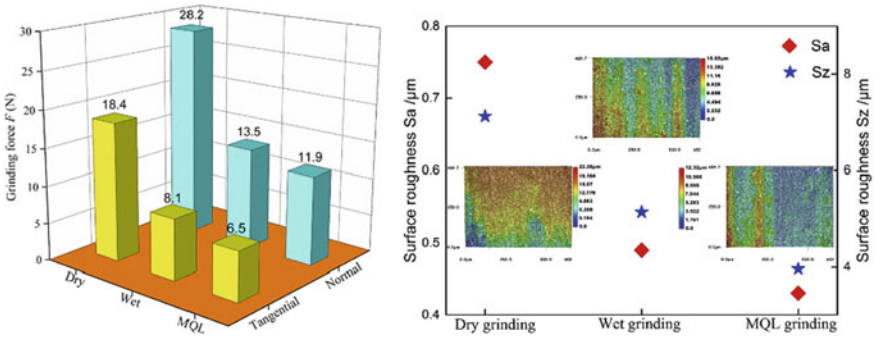

a) Grinding force b) Surface roughness

Fig. 3 Effect of lubrication conditions on the grinding of C_f/SiC composites [28] (Reprinted with permission from Elsevier: licence number 28)

The effect of grit geometry and fibre orientation on the material removal mechanism in the machining of silicon carbide fibre-reinforced silicon carbide matrix composite (SiC/SiC CMC) using abrasive grains with different sizes and arrangements has been analysed using scratch tests [30]. The shape of the abrasive grit was found to have a greater effect on cutting force than fibre orientation. Smaller square grit caused less resistance to penetration, allowing effective engagement with the workpiece in matrix-rich areas. However more lateral damage to transverse fibres was produced [30]. Gong et al. [31] compared the different machining properties of SiC and C/SiC composites in experiments with a diamond grinding wheel and found that the grinding forces with SiC were greater than for the C/SiC composites used. The material removal process of SiC and C/SiC composites took different forms, but involved the same removal mode of brittle fracture.

2.1.3 Drilling

Drilling is a method of machining holes using drills or reamer tools. Many scholars have conducted theoretical and empirical research into the effects of drilling force ad torque and the quality of drilled holes in machining carbon fibre-reinforced composites. Experimental studies have most often employed carbide, coated and uncoated, and PCD drills and cutters.

In one study, three different diameter carbide cutters were used to investigate the effects of spindle speed, feed rate, feed amount and drill diameter on axial force [32], which was found to decrease with spindle speed. Meanwhile, the ratio of cutting speed to feed rate increased with drill diameter and feed rate. The drilling of small holes with a diameter of 3 mm in carbon fibre-reinforced resin matrix composites using carbide twist drill was reported by Wen et al. [33]. When the number of holes drilled increased, their quality deteriorated, and tool wear was severe. Errors in drilled hole diameter error increased as spindle speed increased and decreased as feed rate increased.

Different type of cutting tools show various wear properties when drilling composite materials. PCD cutting tools are suitable for drilling holes with higher quality. PCD and diamond-coated cutters have been considered foe the drilling of CFRCs [34], and it was found that the quality of the hole made by PCD cutters was better than that of diamond coating cutters.

Hole exit quality and machined surface integrity are important indices in evaluating the quality of drilling for 2D C_f/SiC composites. Feed rate and cutting speed influence the brittle fracture modes of carbon fibres, which include micro brittle fracture inside the carbon fibre as well as macro brittle fracture. Due to the micro-brittle fracturing of fibres, the drilled surface remains relatively flat when drilling 2D C_f/SiC composites using PCD tools [35]. In analysing the influence of tool angle on the drilling machinability of 2D C_f/SiC composites, Zou et al. [36] determined the effect of the clearance and point angles of PCD drill tools on thrust force, drilling torque, hole surface quality, and the material removal mechanism. Their findings showed that a larger point angle of the cutting tool, in this case 150°, can help gain

better surface quality of the machined hole and hole exits, but that changing the clearance angle had a relatively small effect on machined surface roughness. Also, the main material removal mechanisms in the drilling of 2D C_f/SiC composites were fibre fracture, matrix removal, and fibre-matrix debonding [36]. To understand how the drilling process influences the micro-structure of SiC/SiC ceramic matrix composites, Diaz et al. [37] conducted experiments using a diamond-coated twist cutting tool. The results showed that the brittle fracture of fibres is dominant, and the primary plastic mechanism for the SiC matrix region and debonding mechanism was due to SiC particles being pulled out [37].

Some specially designed electroplated diamonds have been proposed for the drilling of this composite to improve the quality of drilled holes and overcome the shortcomings of other cutting tools. Zhang [38] adopted brazed diamond bit and electroplated diamond bit drills with C/C–SiC composites and conduced a correlation analysis to determine the influence of drilled material and machining parameters on drilling force. The brazed diamond bit was found to be superior to the electroplated bit when machining C/C–SiC composite, and the feed rate significantly affected drilling force. The main defects oin holes included delamination, tearing, and edge collapse, and the quality of the hole entrance was better than the exit [38]. Xing et al. studied the effects of machining parameters on axial force, machined quality and tool wear in drilling unidirectional C/C–SiC using brazed diamond drills as shown in Fig. 4 [39], and the delamination of the hole entrance, drilled hole quality were strongly influenced by drilling direction and fibre orientation. A graphite plate was used to improve hole exit quality, and can prevent the workpiece from bending as shown in Fig. 5 and the experimental results demonstrate reduced damage to the hole exit.

The above conventional machining methods of carbon fibre-reinforced ceramic matrix composites have the advantages of simple operation and low investment in equipment. However, in traditional machining methods, cemented carbide tool wear is relatively severe, resulting in frequent changes of cutting tools, low machining efficiency, and higher machining costs. Although the wear of PCD tools is lower, and the machined quality better, the cost of the cutting tools is also high. Furthermore, conventional machining methods are not wholly suitable for the processing requirements of complex structural parts. To reduce the defects caused by traditional

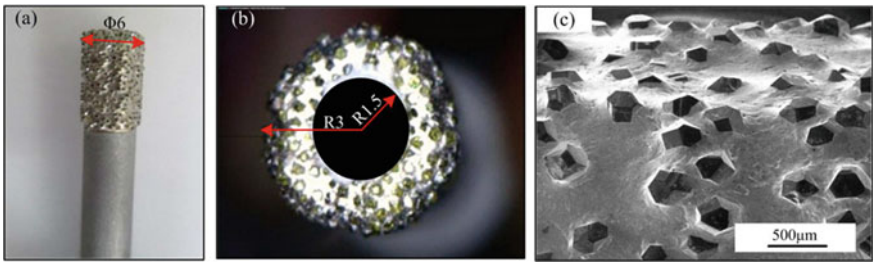

Fig. 4 Brazed diamond drills [39] (Reprinted with permission from Elsevier: licence number 39) (**a**) and (**b**) optical topography of brazed diamond tools, (**c**) SEM topography of diamond grains

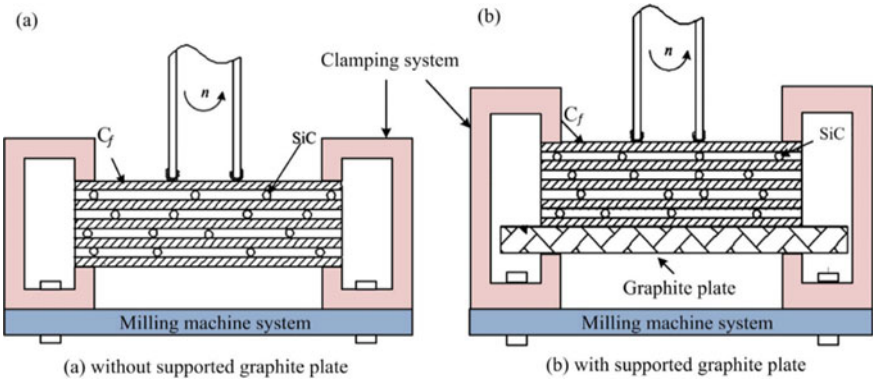

Fig. 5 Schematic diagram of drilling with and without supported graphite plate [39] (Reprinted with permission from Elsevier: licence number 39)

machining, new tools and optimized machining parameters continue to be explored by scholars.

2.2 Unconventional Machining

With the development of new machining technology, unconventional machining is gradually being applied to the machining of carbon fibre-reinforced ceramic matrix composites. Various such machining methods have been developed to improve surface quality, reduce machining defects and tool wear. Unconventional machining technology is generally a form of phase transformation that removes the material at high temperature, high pressure, or high-frequency vibration using special equipment. The machining mechanisms are different from those in conventional shear removal. Current research on unconventional machining methods for carbon fibre-reinforced ceramic matrix composites mainly focuses on high-pressure water jet, laser beam and/or laser-assisted machining, as well as ultrasonic-assisted and electric discharge machining (EDM).

2.2.1 High-Pressure Water Jet Machining

The high-pressure water jet machining methodis the cold machining method, which has no heat-affected zone and low machining force. Moreover, the structure of the cut material does not change, and almost no stress and strain are produced [40]. Hashish [41] proved the feasibility of the abrasive water-jet turning of hard-brittle carbon, metal and ceramic materials inby experiments to have high efficiency and complete surface. Subsequent reports show that this method can be used to cut carbon fibre-reinforced ceramic/polymers matrix composites [42]. The machining

principle of abrasive water jet was expounded by Liu et al. [43], who concluded that the surface quality and size control of three-dimensional parts in the abrasive water jet machining of holes and shafts needed to be further improved. These studies demonstrate the feasibility of water jet machining of fibre-reinforced composites, but there exists delamination on the machined surface.

The cutting mechanism of the abrasive water-jet cutting of carbon fibre composite mainly realtes to the impact of abrasive grit on the composite surface at high speed to generate cracks. Then, the high water pressure promotes crack propagation and ultimately material removal [44]. In a study by Xue et al. [45], an ultra-high-pressure water machining centre was designed, and the water machining head was connected to the vertical shaft end of a five-axis linkage machine tool. This was deemed suitable for the machining of large-scale curved carbon fibre-reinforced composite such as that used in aeroplane wings.

Water-jet cutting technology is relatively mature, but the theory and processes involved in abrasive water-jet machining for milling, turning, and drilling require further research. Another aspect to focus on is the precise control of machining dimensions and surface roughness by choosing appropriate parameters. The optimisation of combinations of machining parameters, quantitative control of machining dimension, and improvement of surface quality will have has far-reaching significance for the application of water jet processing.

2.2.2 Laser-Beam and Laser-Assisted Machining

Laser-beam machining uses light to achieve a laser beam with high energy density after focusing through a lens, in a process governed by the photothermal effect. Its high energy produces high temperatures up to tens of thousands of degrees Celsius locally on the workpiece surface to melt or vaporise the material [46]. Laser-beam machining requires no cutting tools and involves fast machining speeds and low levels of deformation in the machining of various materials. surface Meanwhile, laser-assisted machining mainly provides heat for other machining methods such as milling and drilling. The laser-beam machining of carbon fibre composite can avoid the problem of tool wear, but also brings new challenges due to the anisotropy of these composites such as in the formation of heat-affected zones after laser cutting, fibre pull-out, delamination and fibre end swelling [47].

For laser beam machining/laser-assisted machining of carbon fibre composite, a suitable selection of laser and machining parameters plays a crucial role in machined quality and the material removal mechanism. Relevant material removal mechanisms include pyrolysis, photochemical action and mechanical ablation. Peng et al. [48] investigated the effect of laser parameters of intensity, frequency and duty cycle on ablation heat during the cutting of C/SiC composites. It was found inappropriate to simply use ablation heat to characterize the ablation resistance of high-temperature-resistant materials, since the ablation heat obtained using different parameters varied widely [48].

Additionally, the effects of different machining parameters such as scanning speed, filling pitch and laser power on the morphology of machined C/SiC composites using 800 nm femtosecond (fs) lasers were determined by Zhai et al. [49]. The micro-grooves machined by a high energy density fs laser were of relatively high quality. Theoretical analysis and simulation were also used to analyse the laser-beam machining process. Zhang et al. reported the effect of machining parameters on the laser-beam machining of the same composites [50]. They found that smaller spiral width and spacing helped to improve the machined quality of the holes. The effects of energy density, feed rate, machining mode (single loop scanning and spiral scanning) on the machining properties of C/SiC composites with picosecond laser have been investigated by Liu et al. [51, 52]. Energy density and feed rate had a substantial effect on the quality of machined micropores. It was shown that the selection of laser-beam machining parameters greatly influences the machining process and quality. The optimisation of these parameters yielded relatively good results in terms of the width and depth of the slits.

It is challenging to avoid problems associated with heat-affected zones in laser-beam machining [53]. However, the situation can be improved with a reasonable selection of machining parameters to improve machined quality. Femtosecond laser beam machining can enable 'cold' ablation, avoid heat-affected zones and greatly improve machined quality. However, the structure of femtosecond laser machine tools is complex, and they are expensive, and exhibit unstable performance, making it difficult to achieve broad industrial application.

Scholars have researched other ceramic matrix composites such as SiC/SiC composites. Different parameters of machining modes and laser power influence the process of pico-second laser machining of SiC/SiC composites. Li et al. [54] found that different results in terms of machined surface morphology and structure can be gained with the machining modes of single ring and helical line scanning. Increased laser power can lead to a linear increase in the width of grooves, but their depth reached a maximum and then remained constant. When drilling SiC/SiC composites using a pico-second laser, energy density and feeding speed significantly affect the quality of micro-holes and, at the laser entry side, energy density has little effect on their roundness while these parameters substantially influenced the quality of micro-holes at the laser exit side [55]. The femtosecond laser can be also used to machine silicon carbide ceramic matrix composites.

According to Zhai et al. [56], the use of high-frequency femtosecond laser for the machining of SiC/SiC prompted an oxidation phenomenon occurring on the machined surface. As laser power, repetition frequency and scanning times increased, more obvious oxidation could be observed, while higher scanning velocity resulted in less oxidation. Machining parameters such as spot overlap and helical line overlap ratios, laser processing power and processing steps all had significant effects on the surface morphology and geometry of micro-holes in the femtosecond laser drilling of SiC/SiC composites [57].

From the above discussion, the water-jet cutting of carbon fibre composite material mainly causes delamination defects, whereas the laser-assisted/laser-beam machining of C/SiC composites gebnerates heat-affected zones, delamination, and

end expansion. To compensate for the shortcomings of individual processing methods, combinations of methods have also been applied. Combining water-jet machining with laser cutting is a relatively new concept. The water jet has the function of cooling and scouring, so that water-jet-assisted laser cutting can reduce the size of heat-affected zones and improve machined morphology, which makes it superior to conventional laser-beam machining.

2.2.3 Ultrasonic Vibration-Assisted Machining and Rotary Ultrasonic Machining

Ultrasonic assisted machining involves the application of high frequency and a small amplitude to the machine tool spindle or workpiece during conventional machining. The material is removed by hammering, grinding, polishing and scratching, which can reduce cutting force, inhibit the occurrence of damage and improve the machined quality [58, 59].

Studies show that ultrasonic vibration-assisted machining has obvious advantages compared to the conventional milling, drilling and grinding of carbon-fibre composite. Some studies conclude that ultrasonic torsional vibration milling can significantly reduce cutting force, chipping and burr formation [60, 61]. A cutting force prediction model was developed which first considered the dynamics of machining, and the relevant parameters and variables associated with the rotary ultrasonic side-milling (RUM) of C/SiC composite [62]. It was found that simulation results using model differed from measured values in most cases by less than 10%, so that machining efficiency and quality could be improved. Liu et al. [63] conducted an experimental study of tool wear when using a diamond-coated cutter in the ultrasonic vibration-assisted milling of C/SiC composites, and showed that abrasive wear and the peeling of coating were the main wear mechanism and form respectively. Tool wear in the ultrasonic-vibration milling of C/SiC composites is clearly less severe than that in traditional milling, and can improve the machined surface quality of 2D C_f/SiC composites [64].

In addition to ultrasonic vibration-assisted milling, ultrasonic vibration-assisted grinding is also employed in the machining of this composite and exhibits higher machining efficiency and lower surface damage than conventional grinding. The use of an electroplated diamond tool for machining C/SiC composite under the action of ultrasonic torsional vibration can reduce surface roughness. Liu et al. [65] reported the effect of machining parameters on cutting force in the cases of the conventional and ultrasonic-vibration grinding of C/SiC composites using electroplated diamond grinding wheels. Compared with traditional machining, the cutting force can be reduced by more than 50% under the same conditions. Ding et al. [66] used ultrasonic-assisted grinding (UAG) and conventional machining (CG) in machining C/SiC composites. Surface roughness with UAG was significantly reduced, the grinding force was reduced by up to 45% and, after comparisons of surface topography, grinding force, force ratio and unconventional grinding energy, it was found that the grinding energy could be reduced by 18–39%. Azarhoushang

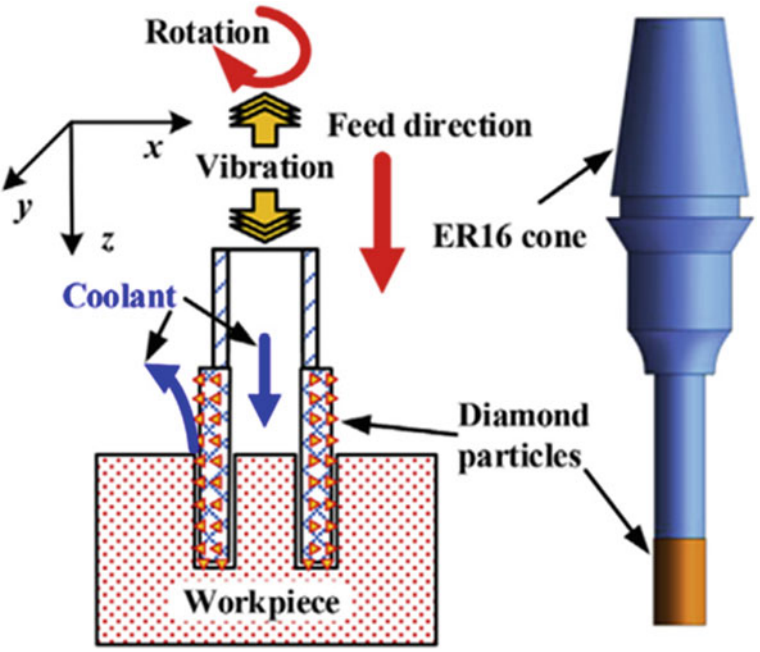

Fig. 6 Schematic diagram of RUM [71] (Reprinted with permission from Elsevier: licence number 71)

et al. developed a specially designed block ultrasonic sonotrode exhibiting multiple resonant frequency behaviour [67]. Changes in grinding force and surface roughness according to machining parameters and workpiece material were reported, and a large reduction in grinding force and surface roughness could be achieved [67], wheel wear characteristics were also analysed.

Rotary ultrasonic machining (RUM), as shown in Fig. 6 [71], and ultrasonic-assisted drilling can improve the quality of the drilled hole to a certain extent. Ultrasonic-assisted drilling can reduce defects such as micro-cracks, fibre pull-out, delamination and burring compared to conventional drilling. Comparative studies of the rotary ultrasonic machining and ultrasonic-assisted drilling of carbon fibre composites [68–72] demonstrate the effects of ultrasound and machining parameters and fibre orientation on drilling force and surface morphology and quality.

Hocheng et al. reported the effects of various process parameters on material removal rates (MRR), edge quality, hole clearance, and tool wear [68], showing that the ultrasonic-assisted drilling of C/SiC composites can improve machinability and reduce costs compared with other feasible machining processes. In the RUM of C/SiC composites, a generally positive correlation can be found between the extent of tearing defects and thrust force [69]. Hole defects can be evaluated indirectly according to trends in the changes of thrust force. RUM can reduce hole exit defects compared with conventional grinding, and thus has potential value in improving

machined quality. Variations in cutting force at the entrance hole reflect the influence of penetration depth and, compared with the conventional grinding this composite, cutting force can be substantially reduced using RUM [70]. Cutting force also has an important effect on hole exit quality. The understanding that the machined quality of holes can be improved by controlling cutting force is a major advance, and fibre cutting direction relative to fibre orientation also has a large influence on surface morphology both in conventional machining and the RUM of C/SiC composites [71].

Combined with conventional rotary ultrasonic drilling (Con-RUD) with only one-dimensional longitudinal ultrasonic vibration, a rotary ultrasonic drilling (RUD) method with longitudinal and torsional coupled (LTC) vibration has been developed for the machining of C/SiC laminates [72]. The LTC-RUD tool's longitudinal and torsional coupling (LTC) vibrations allowed the diamond abrasive to vibrate in a 2D trajectory in the cutting plane. Using the LTC-RUD can reduce cutting forces by more than 50% compared to Con-RUD in the machining of C/SiC composites, dramatically improving machining efficiency and reducing the occurrence of delamination. For existing Con-RUDs, the LTC-RUD can be retrofitted with simple modifications without replacing the ultrasonic machine to significantly improve machining performance.

The mathematical modelling of the cutting mechanism in the ultrasonic-assisted drilling of ceramic matrix composite is a very useful tool which can provide a theoretical basis for parameter optimization and the physical simulation of the machining process for deformation prediction and control. A mathematical axial drilling force and torque model for rotary ultrasonic drilling (RUD) of C/SiC composites has been proposed [73] based on indentation fracture theory to understand the material removal mechanism, and experimental results showed that this model is feasible.

The ultrasonic vibration-assisted machining and RUM of ceramic matrix composites has some advantages in reduce cutting force and improving machined surface quality. Rotary ultrasonic machining can reduce the machining defects at the drilled hole entrance and exit, and is a method with considerable development potential and prospects for application.

2.2.4 Electrical Discharge Machining

Electrical discharge machining is a method of removing workpiece material by electrolytic erosion using a pulse discharge between tool and workpiece electrodes in a specific medium. It produces instantaneous high temperature which causes metal to be melted locally, vaporised and etched away. Because fibre-reinforced composites contain ceramic matrix or plastic, they exhibit poor electrical conductivity. The rate of material removal using EDM is very low, and few studies have investigated the EDM of these composites.

Wei et al. [74] reported on the machining mechanism of fibre-reinforced ceramic composites by EDM and proposed methods to improve the material removal rate (MRR) and surface integrity. The removal mechanism involves the cracking of the

ceramic matrix by thermal shock, and the fibre is removed by brittle fracture [74]. It is been observed that in the EDM of carbon fibre-reinforced carbon composites, lower pulse energy can obtain a better machined effect, and the best parameters to improve the MRR was described by Guu et al. [75].

W. B. He et al. found that the carbon fibre orientation relative to machining direction and machining parameters in the WEDM of 2D C/SiC composite all influence the machining mechanism and resulting quality [76]. Using different machining directions relative to carbon-fibre orientation had a significant effect on surface quality. The transverse and longitudinal fracture of carbon fibres and micro cracks are the most important form of material removal, and pits and recast layers occur on the machined surface. Interfacial debonding between carbon fibres and the SiC matrix was also observed.

In order to study the effect of thermal stress on material removal in the discharge process during the EDM of ceramic matrix composite, a thermal–electric–mechanical coupling simulation model was developed, as shown in Fig. 7 [77]. Based on the

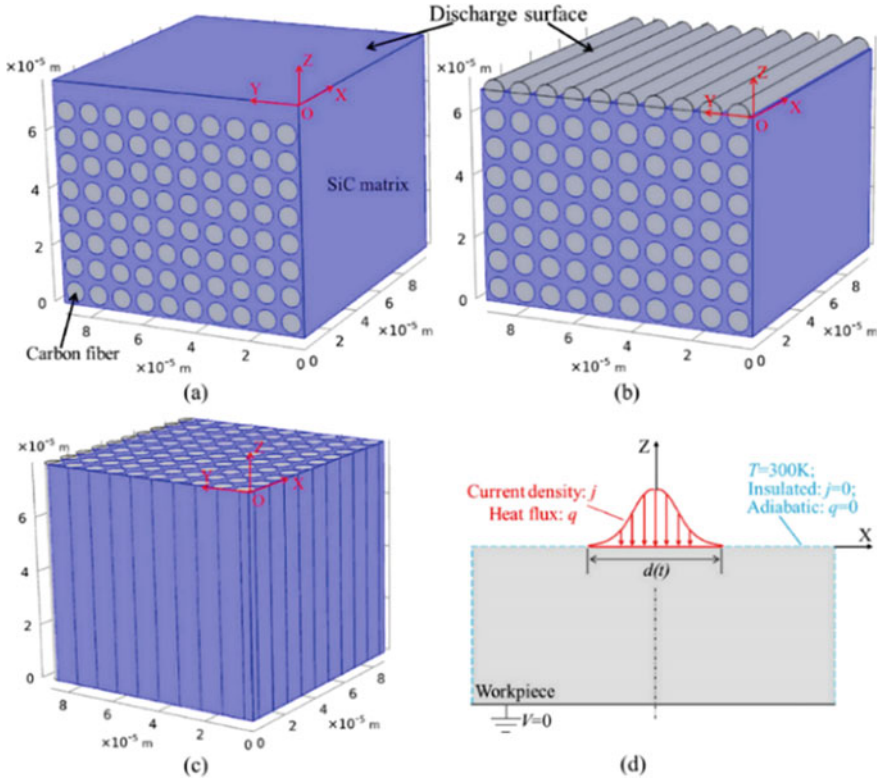

Fig. 7 Schematic of the 1/4 simulation model: **a** discharge on the SiC coating; **b** discharge on the parallel surface; **c** discharge on the vertical surface; **d** boundary conditions exerted in the simulation model [77] (Reprinted with permission from Elsevier: licence number 77)

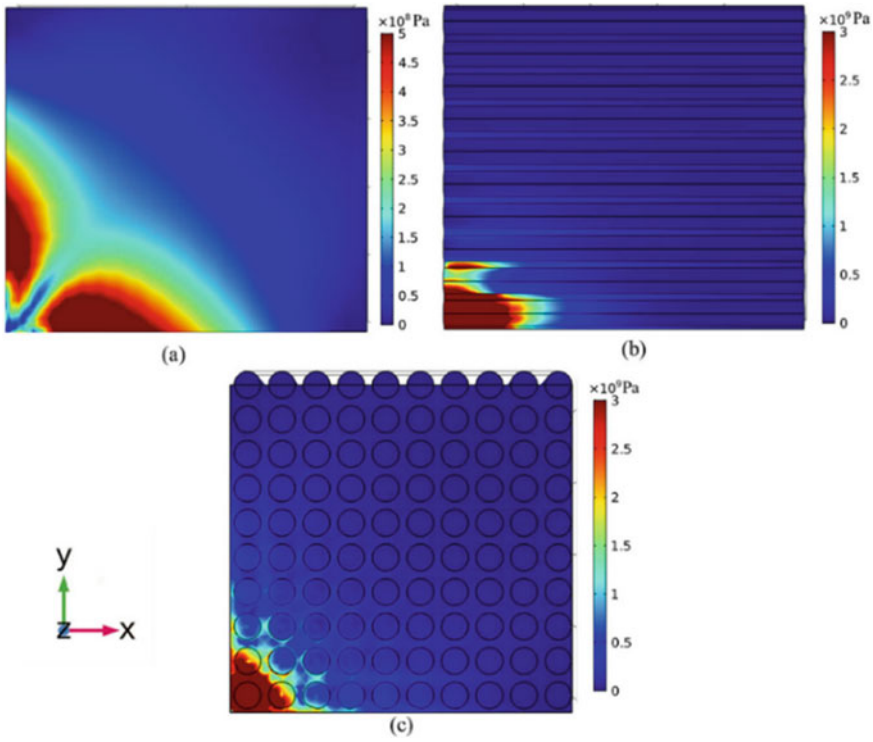

Fig. 8 Stress distribution of the 1/4 model at t = 5 μs: discharges on the **a** SiC coating; **b** parallel surface; **c** vertical surface [77] (Reprinted with permission from Elsevier: licence number 77)

1/4 simulation model, the stress distribution after 5 μs with discharges at different workpiece positions are shown in Fig. 8 [77]. It can be seen that the high thermal stress on the SiC coating on the parallel and vertical discharge surfaces of the C_f/SiC composite were all far higher than the corresponding tensile strengths of the SiC coating, carbon fibre, and SiC matrix [77]. At present, the EDM of C_f/SiC composites is not suitable for large-scale industrial application due to relatively low machining efficiency and machined surface quality.

In addition, there are also reports of the effect of EDM machining parameters with other ceramic composites such as ZrB_2–SiC and TiN/Si_3N_4 composites [78, 79]. Guo et al. [78] selected material removal rate, side gap, and surface roughness as indicators in analysing the influence of the polarity of the electrode, peak current, pulse-on time and pulse-off time in the EDM of ZrB_2–SiC. It was found that polarity also affects surface morphology. Larger molten drops occurred on the machined surface where the workpiece was attached to the anode, while a polygonal material layer and cylindrical flat areas were observed on the machined surface at the site of attachment to the cathode [79].

From the above reports on the machining of carbon fibre-reinforced ceramic matrix composites, unconventional machining technology shows excellent machining performance compared with conventional machining. Non-contact machining realised using special equipment produces high temperature and pressure and the high-frequency vibration phase removal of material. Moreover, the contact stress is small, damage to the material can be minimized, and common defects such as chipping, burrs, cracking, and fibre pull-out are effectively reduced. The surface quality is obviously improved and these methods thus have great potential for development.

3 Discussion

Up to now, many scholars have conducted many studies of the machining of carbon fibre-reinforced ceramic matrix composites using both conventional and unconventional methods. There are still various problems that need to be solved, which are briefly described here.

(1) Comparisons of the systems used for the cutting of carbon fibre-reinforced composites with different carbon fibre content and structures require further attention. At present, research into the cutting mechanisms used for composites with different carbon fibre content is relatively scarce. Such analyses of the machinability of composites could facilitate the design and improvement of material preparation and provide additional information concerning the optimisation of fabrication procedures so as to improve production efficiency.
(2) The establishment of a database for tool optimisation is an important aim. More research can be carried out into the selection of tool geometry and material capable of producing the same or better surface quality of machined carbon fibre-reinforced composites with different carbon fibre types and weaving methods. In the process of machining these composites, studies of the relationships between various machining parameters and the machine tool system can be conducted in order to obtain higher machined quality and machining efficiency.
(3) Reliable theoretical models are needed to further develop techniques for the evaluation of surface quality of composites. Patterns of defects such as delamination, layered brittle fracture, crack, and fibre pull-out during machining are completely different from those occurring in the machining of metallic composite materials. Indicators such as surface roughness are often used to evaluate surface quality after machining, but these measures may not fully reflect surface quality. Therefore, it is necessary to establish and improve surface quality evaluation systems and methods for these composites.

4 Conclusions

(1) Conventional machining methods have the advantages of simple operation, mature technology, and less investment in equipment, but tool wear is severe especially when using carbide tools where the hard point of cutting rubs directly against the cutting edge of the tool. The shearing of the matrix, fracture of fibres, friction between the cutting edge and the chips produced and the machined surface are accompanied by the generation of heat. Cutting heat is concentrated near to the tool's cutting edge, resulting in the ablation of the surface of the tool, reducing its cutting performance. PCD and CBN cutters have excellent properties which are suitable for machining ceramic matrix composites.

(2) Conventional machining produces many types of defects in carbon fibre-reinforced composites, such as tearing and burrs. These composites have low interlayer bonding strength. The cutting force exceeds the strength of the bonding between layers in the direction of vertical fibre lay-up during processing, cause defects associated with delamination. When drilling these composites, the outermost material deforms and retreats owing to the action of axial force, causing delamination, tearing and bulging defects. The carbon fibres are pulled out of the matrix and form burrs without being sheared. The fracture of carbon fibres is the main removal mode.

(3) Unconventional machining methods can to some extent reduce defects such as machining damage, delamination, cracks, and fibre pull-out. A combination of water-jet machining and laser-beam machining can significantly reduce the heat-affected zone due to the scouring and cooling of the water jet, and the machined surface morphology is improved, which is more advantageous than conventional laser-beam machining in some respects. Ultrasound-assisted machining and rotary ultrasonic machining are relatively mature techniques for the machining of carbon fibre-reinforced ceramic matrix composites, and can not only reduce cutting forces and machining defects such as chipping, burrs, cracks, and fibre pull-out, but also may improve machining efficiency and surface quality. Such approaches have greater application potential for the machining of these composites than traditional machining methods.

5 Review Questions

(1) Describe the differences between FRP, CFRC and CFRP.

(2) Why are ceramic matrix composites difficult-to-machine materials and what aspects of the difficulty in machining them mainly reflect?

(3) Why are there so few reports on the turning of fibre-reinforced ceramic matrix composites, such as C/SiC and SiC/SiC composites and CFRC?

(4) What is the difference between the machining of fibre-reinforced ceramic matrix composites, and that of traditional metal materials in terms of the material removal and surface formation mechanism?

(5) What are the main aspects of the influence of fibre orientation on cutting force and surface quality in the conventional machining process used for fibre-reinforced ceramic matrix composites and CFRP?
(6) What is the difference between ultrasonic machining and ultrasonic-assisted machining?
(7) Why can ultrasonic machining milling, grinding and drilling reduce cutting force and improve surface machining quality compared with the corresponding conventional machining methods?
(8) What kind of damage appears in the machining of fibre-reinforced ceramic matrix composites using an abrasive water jet?
(9) What are the advantages of the use of lasers in the machining of ceramic matrix composites?
(10) In the use of EDM, how do the electrical machining parameters and the polarity of the workpiece affect the machining process of fibre-reinforced ceramic matrix composites?
(11) What are the limiting factors for the EDM and WEDM of processing fibre-reinforced ceramic matrix composites?
(12) What other unconventional machining methods can be applied to the machining of ceramic matrix composites?

Acknowledgements The author(s) would like to thank the National Natural Science Foundation of China [grant number 51505434]; the Young Talents Lifting Project of Henan Province in 2019 [sequence number 34]; the Natural Science Foundation of Henan Province, China [grant numbers 182300410170 and 182300410215]; and the Program for Innovative Research Team in Science and Technology at the University of Henan Province [grant number 18IRTSTHN015].

References

1. Krenkel, W.: Carbon fibre reinforced silicon carbide composites (C/SiC, C/C–SiC). In: Bansal, N.P. (ed.) Handbook of Ceramic Composites, pp. 117–148. Springer, Boston (2005)
2. Chung, D.D.L.: Carbon fibers, nanofibers, and nanotubes. In: Chung, D.D.L. (ed.) Carbon Composites: Composites with Carbon Fibers, Nanofibers and Nanotubes, pp. 1–87. Elsevier, Cambridge (2017)
3. Chung, D.D.L.: Ceramic-matrix composites. In: Chung, D.D.L. (ed.) Carbon Composites: Composites with Carbon Fibers, Nanofibers and Nanotubes, pp. 467–531. Elsevier, Cambridge (2017)
4. Che, D.M., Saxena, I., Han, P.D., Guo, P., Ehmann, K.F.: Machining of carbon fiber reinforced plastics/polymers: a literature review. J. Manuf. Sci. Eng.-Trans. ASME **136**(3) (2014)
5. Padture, N.P.: Advanced structural ceramics in aerospace propulsion. Nat. Mater. **15**(8), 804–809 (2016)
6. Fan, S.W., Zhang, L.T., Cheng, L.F., Tian, G.L., Yang, S.J.: Effect of braking pressure and braking speed on the tribological properties of C/SiC aircraft brake materials. Compos. Sci. Technol **70**(6), 959–965 (2010)
7. Schmidt, S., Beyer, S., Knabe, H., Immich, H., Meistring, R., Gessler, A.: Advanced ceramic matrix composite materials for current and future propulsion technology applications. Acta Astronaut **55**(3), 409–420 (2004)

8. Ahmad, J.Y.S.: Machining of Polymer Composites. Springer, Boston (2009)
9. Wang, D.H., Ramulu, M., Arola, D.: Orthogonal cutting mechanisms of graphite/epoxy composite. Part I: unidirectional laminate. Int. J. Mach. Tools Manuf. **35**(12) 1623–1638 (1995)
10. König, W., Wulf, Ch., Graß, P., Willerscheid, H.: Machining of fibre reinforced plastics. CIRP Ann-Manuf. Technol. **34**(2), 537–548 (1985)
11. Komanduri, R.: Machining of fiber-reinforced composites. Mach. Sci. Technol **1**(1), 113–152 (1997)
12. Tashiro, T., Fujiwara, J., Takenaka, Y.: Grinding of C/C–SiC composite in dry method, pp. 351–352. Springer, London (2007)
13. He, T., Fu, Y.C., Su, H.H., Ding, K.: Study on surface integrity in milling of C/SiC composite. J. Nanjing Univ. Aeronaut. Astronaut. **46**(5), 701–706 (2014)
14. Be, M.Z.: Experimental research on drilling and milling of C/SiC composites. Dalian University of Technology, Dalian (2013)
15. Zhou, D.H., Fan, H.X., Wang, Z.L.: NC machining technology of C/SiC fiber reinforced ceramic material profile. Aerosp. Manuf. Technol. (5), 14–17 (2012)
16. Li, J.D., Ren, C.Z., Lv, Z., Zhang, L.F.: Finite element simulation of single diamond abrasive surface grinding C/SiC. J. Mater. Sci. Eng. **32**(5), 686–715 (2014)
17. Li, Y.C., Ge, X., Wang, H., Hu, Y.B., Ning, F.D., Cong, W.L., Ren, C.Z.: Study of material removal mechanisms in grinding of C/SiC composites via single-abrasive scratch tests. Ceram. Int **45**(4), 4729–4738 (2019)
18. Du, J.G., Ming, W.Y., Ma, J., He, W.B., Cao, Y., Li, X.K., Liu, K.: New observations of the fiber orientations effect on machinability in grinding of C/SiC ceramic matrix composite. Ceram. Int **44**(12), 13916–13928 (2018)
19. Ding, K., Fu, Y.C., Su, H.H., Gong, X.B.: Effect of C/SiC composites material structure on grinding forces and machined surface quality. China Mech. Eng. **24**(14), 1886–1890 (2013)
20. Liu, J., Li, H.B., Zhang, X.Y., Hong, Z.L., He, Z.B., Zhang, Y.: Investigation of grinding characteristics and removal mechanisms of 2D-C/SiC in high speed deep grinding. Acta Materiae Compositae Sinica **29**(4), 113–118 (2012)
21. Liu, Q., Huang, G.Q., Xu, X.P.: Surface forming mechanism of grinding 2D-C/SiC Composites. J. Fuzhou Univ. (Nat. Sci Ed.) **46**(2), 228–233 (2018)
22. Zhang, L.F., Ren, C.Z., Ji, C.H., Wang, Z.Q., Chen, G.: Effect of fiber orientations on surface grinding process of unidirectional C/SiC composites. Appl. Surf. Sci **366**, 424–431 (2016)
23. Chi, X., Wu, F., Suo, X.H.: Research of grinding parameters about C–SiC ceramic matrix composite. Aviat. Precis. Manuf. Technol. (1), 41–43 (2012)
24. Liu, Q., Huang, G.Q., Xu, X.P., Fang, C.F., Cui, C.C.: A study on the surface grinding of 2D C/SiC composites. Int. J. Adv. Manuf. Technol. **93**(1), 1–9 (2017)
25. Qu, S.S., Gong, Y.D., Yang, Y.Y., Wen, X.L., Yin, G.Q.: Grinding characteristics and removal mechanisms of unidirectional carbon fibre reinforced silicon carbide ceramic matrix composites. Ceram. Int. (2018)
26. Tawakoli, T., Azarhoushang, B.: Intermittent grinding of ceramic matrix composites (CMCs) utilizing a developed segmented wheel. Int. J. Mach. Tools Manuf. **51**(2), 112–119 (2011)
27. Agarwal, S.: Optimizing machining parameters to combine high productivity with high surface integrity in grinding silicon carbide ceramics. Ceram. Int. **42**(5), 6244–6262 (2016)
28. Qu, S., Gong, Y.D., Yang, Y.Y., Sun, Y., Wen, X.L., Qi, Y.: Investigating minimum quantity lubrication in unidirectional Cf/SiC composite grinding. Ceram. Int. **46**(3), 3582–3591 (2020)
29. Qu, S.S., Gong, Y.D., Yang, Y.Y., Wang, W.W., Liang, C.Y., Han, B.: An investigation of carbon nanofluid minimum quantity lubrication for grinding unidirectional carbon fibre-reinforced ceramic matrix composites. J. Clean. Prod. **249**, 119353 (2020)
30. Luna, G.G., Axinte, D., Novovic, D.: Influence of grit geometry and fibre orientation on the abrasive material removal mechanisms of SiC/SiC ceramic matrix composites (CMCs). Int. J. Mach. Tools Manuf. **157**, 103580 (2020)
31. Gong, Y.D., Qu, S.S., Yang, Y.Y., Liang, C.Y., Li, P.F., She, Y.B.: Some observations in grinding SiC and silicon carbide ceramic matrix composite material. Int. J. Adv. Manuf. Technol. **103**, 3175–3186 (2019)

32. Zhang, H.J., Fan, Y., Chen, W.Y., Chen, D.C.: Investigation of cutting force for high speed drilling carbon fiber composite. Aeronaut. Manuf. Technol. (12), 76–79 (2006)
33. Wen, Q., Zhao, Y., Gong, Y.D.: Experimental study on small hole machining of carbon fiber reinforced composites. Mach. Des. Manuf. (1), 86–89 (2018)
34. Tong, M.L.: Research on Finite Element Analysis and Experiment of Drilling of Carbon Fiber Reinforced Polymer Composites. Harbin University of Science and Technology, Harbin (2014)
35. Chen, J., An Q.L., Ming, W.W., Chen, M.: Hole exit quality and machined surface integrity of 2D Cf/SiC composites drilled by PCD tools. J. Eur. Ceram. Soc. **39**(14), 4000–4010 (2019)
36. Zou, F., Chen, J., An, Q.L., Cai, X.J., Chen, M.: Influences of clearance angle and point angle on drilling performance of 2D Cf/SiC composites using polycrystalline diamond tools. Ceram. Int. **46**(4), 4371–4380 (2020)
37. Diaz, O.G., Axinte, D.A., Butler-Smith, P., Novovic, D.: On understanding the microstructure of SiC/SiC ceramic matrix composites (CMCs) after a material removal process. Mater. Sci. Eng., A **743**, 1–11 (2019)
38. Zhang, G.D.: Experimental study on drilling C/C–SiC composites. Shandong University, Jinan (2015)
39. Xing, Y.Q., Deng, J.X., Zhang, G.D., Wu, Z., Wu, F.F.: Assessment in drilling of C/C–SiC composites using brazed diamond drills. J. Manuf. Process. **26**, 31–43 (2017)
40. Hashish, M.: A modeling study of metal cutting with abrasive waterjets. J. Eng. Mater. Technol. **106**(1), 88 (1984)
41. Hashish, M.: Turning with abrasive-waterjets—a first investigation. J. Eng. Ind. **109**(4), 2496–2503 (1987)
42. Liu, Z.W.: Study on removal mechanisms of hard-brittle materials and pre-mixed micro abrasive water jet polishing technology. Shandong University, Jinan (2011)
43. Liu, Q., Meng, F.Z., Tian, X.L., Tang, X.J.: Research progress of machining ceramics by abrasive water jet. Tool Eng. **52**(4), 3–6 (2018)
44. Wang, W.: Study on the experiment of carbon fiber composite materials with high-pressure awj cutting. Harbin University of Science and Technology, Harbin (2015)
45. Xue, S.X., Meng, J.K., Ren, Q.L., Han, C.H., Chen, Z.W., Li, Y.F.: Research on working condition and cutting mechanism of water cutting equipment for large scale curved composite component. Fluid Mach. **44**(12), 25–28 (2016)
46. Wang, R.G., Pan, W., Jiang, M.N., Chen, J., Luo, Y.M., Sun, R.F.: Development in machinable ceramics and machining technology of engineering ceramics. Bull. Chin. Ceram. Soc. **20**(3), 27–35 (2001)
47. Negarestani, R., Li, L., Sezer, H.K., Whitehead, D., Methven, J.: Nano-second pulsed DPSS Nd:YAG laser cutting of CFRP composites with mixed reactive and inert gases. Int. J. Adv. Manuf. Technol. **49**(5–8), 553–566 (2010)
48. Peng, G.L., Zhang, X.H., Wang, Y.H., Yan, H., Gao, Y.J., Zheng, Y.L.: Effect of laser parameters on C/SiC composites material ablation heat. Chin. J. Lasers **40**(11), 132–136 (2013)
49. Zhai, Z.Y., Wang, W.J., Zhao, J., Mei, X.S., Wang, K.D., Wang, F.C., Yang, H.Z.: Influence of surface morphology on processing of C/SiC composites via femtosecond laser. Compos. Pt. A-Appl. Sci. Manuf. **102**, 117–125 (2017)
50. Zhang, R.H., Li, W.N., Liu, Y.S., Wang, C.H., Wang, J., Yang, X.J., Cheng, L.F.: Machining parameter optimization of C/SiC composites using high power picosecond laser. Appl. Surf. Sci. **330**, 321–331 (2015)
51. Liu, Y.S., Wang, C.H., Li, W.N., Zhang, L.T., Yang, X.J., Cheng, G.H., Zhang, Q.: Effect of energy density and feeding speed on micro-hole drilling in C/SiC composites by picosecond laser. J. Mater. Process. Technol. **214**(12), 3131–3140 (2014)
52. Liu, Y.S., Wang, C.H., Li, W.N., Yang, X.J., Zhang, Q., Cheng, L.F., Zhang, L.T.: Effect of energy density on the machining character of C/SiC composites by picosecond laser. Appl. Phys. A-Mater. Sci. Process. **116**(3), 1221–1228 (2014)
53. Riveiro, A., Quintero, F., Lusquinos, F., del Val, J., Comesana, R., Boutinguiza, M., Pou, J.: Experimental study on the CO_2 laser cutting of carbon fiber reinforced plastic composite. Compos. Pt. A-Appl. Sci. Manuf. **43**(8), 1400–1409 (2012)

54. Li, W.N., Zhang, R.H., Liu, Y.S., Wang, C.H., Wang, J., Yang, X.J., Cheng, L.F.: Effect of different parameters on machining of SiC/SiC composites via pico-second laser. Appl. Surf. Sci. **364**, 378–387 (2016)
55. Liu, Y.S., Wang, J., Li, W.N., Wang, C.H., Zhang, Q., Yang, S.J., Cheng, L.F.: Effect of energy density and feeding speed on micro-holes drilling in SiC/SiC composites by picosecond laser. Int. J. Adv. Manuf. Technol. **84**, 1917–1925 (2016)
56. Zhai, Z.Y., Wei, C., Zhang, Y.C., Cui, Y.H., Zeng, Q.R.: Investigations on the oxidation phenomenon of SiC/SiC fabricated by high repetition frequency femtosecond laser. Appl. Surf. Sci. **502**, 144131 (2020)
57. Liu, Y.S., Zhang, R.H., Li, W.N., Yang, X.J., Cheng, L.F., Zhang, L.T.: Effect of machining parameter on femtosecond laser drilling processing on SiC/SiC composites. Int. J. Adv. Manuf. Technol. **96**, 1795–1811 (2018)
58. Yuan, S.M., Song, H., Lu, Y.L.: Research for cutting force and torque in rotary ultrasonic drilling of carbon fiber reinforced polymers. Aeronaut. Manuf. Technol. **535**(16), 96–102 (2017)
59. Ding, K., Su, H.H., Fu, Y.C., Cui, F.F., Li, Q.L., Lei, W.N.: Ultrasonic assisted machining of ceramic matrix composites. Aeronaut. Manuf. Technol. **510**(15), 42–49 (2016)
60. Wang, M.H., Jiang, Q.J., Wang, B., Xu, Y.X.: Mechanism of reduction of damage during ultrasonic torsional vibration milling of C/SiC composites. Mod. Manuf. Eng. (3), 103–109 (2016)
61. Wang, M.H., Jiang, Q.J., Liu, D.X., Xu, Y.X.: Study on surface roughness by ultrasonic torsional vibration milling C/SiC composites. Mod. Mach. Tool Autom. Manuf. Tech. (6), 12–16 (2015)
62. Yuan, S.M., Fan, H.T., Amin, M., Zhang, C., Guo, M.: A cutting force prediction dynamic model for side milling of ceramic matrix composites C/SiC based on rotary ultrasonic machining. Int. J. Adv. Manuf. Technol. **86**(1–4), 37–48 (2016)
63. Liu, Y., Liu, Z.B., Wang, X.B., Huang, T.: Experimental study on tool wear in ultrasonic vibration–assisted milling of C/SiC composites. Int. J. Adv. Manuf. Technol. **107**, 425–436 (2020)
64. Chen, J., Ming, W.W., An, Q.L., Chen, M.: Mechanism and feasibility of ultrasonic-assisted milling to improve the machined surface quality of 2D Cf/SiC composites. Ceram. Int. **46**(10), 15122–15136 (2020)
65. Liu, Y., Zhen, J.Z., Chen, A.D., Sun, S.L.: Study of single processing parameter of cutting force of C/SiC composites by ultrasonic vibration method. Mach. Build. Autom. (6), 35–37 (2017)
66. Ding, K., Fu, Y.C., Su, H.H., He, T., Yu, X.Z., Ding, G.Z.: Experimental study on ultrasonic assisted grinding of C/SiC composites. Key Eng. Mater. **620**, 128–133 (2014)
67. Azarhoushang, B., Tawakoli, T.: Development of a novel ultrasonic unit for grinding of ceramic matrix composites. Int. J. Adv. Manuf. Technol. **57**(9–12), 945–955 (2011)
68. Hocheng, H., Tai, N.H., Liu, C.S.: Assessment of ultrasonic drilling of C/SiC composite material. Compos. Pt. A-Appl. Sci. Manuf. **31**(2), 133–142 (2000)
69. Feng, P.F., Wang, J.J., Zhang, J.F., Zheng, J.Z.: Drilling induced tearing defects in rotary ultrasonic machining of C/SiC composites. Ceram. Int **43**(1), 791–799 (2017)
70. Wang, J.J., Feng, P.F., Zhang, J.F., Guo, P.: Experimental study on vibration stability in rotary ultrasonic machining of ceramic matrix composites: cutting force variation at hole entrance. Ceram. Int. **44**(12), 14386–14392 (2018)
71. Wang, J.J., Zhang, J.F., Feng, P.F.: Effects of tool vibration on fiber fracture in rotary ultrasonic machining of C/SiC ceramic matrix composites. Compos. Pt. B-Eng. **129**, 233–242 (2017)
72. Wang, J.J., Feng, P.F., Zhang, J.F., Guo, P.: Reducing cutting force in rotary ultrasonic drilling of ceramic matrix composites with longitudinal-torsional coupled vibration. Manuf. Lett. **18**, 1–5 (2018)
73. Islam, S., Yuan, S.M., Li, Z.: Mathematical modeling and experimental studies on axial drilling load for rotary ultrasonic drilling of C/SiC composites. Int. J. Adv. Manuf. Technol.s **107**, 1309–1326 (2020)
74. Wei, C.J., Liu, J., Xu, Z.H., Xu, Q.Q.: EDM of ceramic matrix composite with fiber reinforcement. Electromach. Mould (1), 25–29 (2015)

75. Guu, Y.H., Hocheng, H., Tai, N.H., Liu, S.Y.: Effect of electrical discharge machining on the characteristics of carbon fiber reinforced carbon composites. J. Mater. Sci. **36**(8), 2037–2043 (2001)
76. He, W.B., He, S.T., Du, J.G.: Fiber orientations effect on process performance for wire cut electrical discharge machining (WEDM) of 2D C/SiC composite. Int. J. Adv. Manuf. Technol. **102**(1), 507–518 (2019)
77. Yue, X.M., Li, Q., Yang, X.D.: Influence of thermal stress on material removal of Cf_SiC composite in EDM. Ceram. Int. **46**(6), 7998–8009 (2020)
78. Guo, Y.F., Feng, Y.R., Wang, L., Kelie, D., Ma, C.J., Lin, T.: Experimental investigation of EDM parameters for ZrB_2-SiC ceramics machining. Procedia CIRP **68**, 46–51 (2018)
79. Selvarajan, L., Rajavel, R., Prakash, B., Mohan, D.G., Gopi, S.: Investigation on spark electrical discharge machining of Si3N4 based advanced conductive ceramic composites. Mater. Today Proc. **27**(3), 2174–2178 (2020)

Nano-structured Polymer-Based Composites

Abhishek Gaikwad, Kishore Debnath, and Manoj Kumar Gupta

Abstract Nano-structured polymer-based composites have gained much importance in recent years due to their improved and excellent properties compared to their bulk-sized equivalents. In nanostructured polymer composites, nano-sized particles are added to the matrix material as nanoparticles have a too high surface to volume ratio, resulting in improved composites' overall properties. In this chapter, various nano-structured polymer-based composites are discussed based on their suitable applications. The properties of nano-structured polymer-based composites such as thermal, mechanical, flame retardancy, electrical and optical properties, barrier properties, anticorrosive properties, and adsorption behaviour and factors affecting the properties are discussed. This chapter also presents the different manufacturing techniques of nano-structured polymer-based composites.

1 Introduction

Since ancient times advancement in material science is the root cause of technological development. The term nanocomposite is used in the early 1980s. These materials possess excellent mechanical, physical, biological, electrical, and chemical properties which make them superior to conventional materials. High surface area to mass ratio, large surface area, and high aspect ratio are some other attractive characteristics of nanomaterialz [1]. The ratio of surface to volume increases with decreasing particle size, significantly affecting the material's properties.

A. Gaikwad
Mechanical Engineering Department, Sam Higginbottom University of Agriculture, Technology and Sciences, Prayagraj, India

K. Debnath (✉)
Mechanical Engineering Department, National Institute of Technology Meghalaya, Shillong, India

M. K. Gupta
Mechanical Engineering Department, Motilal Nehru National Institute of Technology Allahabad, Prayagraj, India

I. Shyha and D. Huo (eds.), *Advances in Machining of Composite Materials*, Engineering Materials, https://doi.org/10.1007/978-3-030-71438-3_13

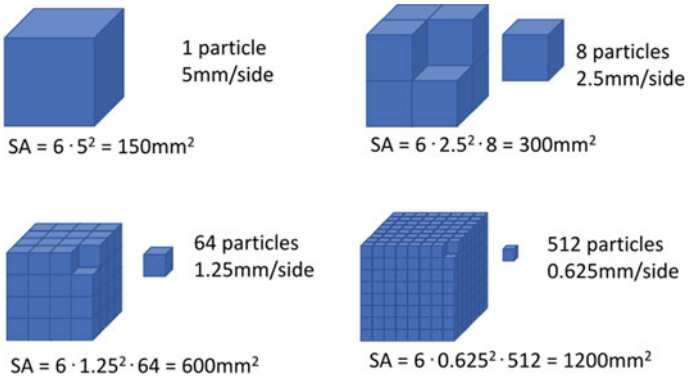

Fig. 1 Relationship between particle size and surface area [3]

The influence of the surface area had been demonstrated in the form of a particle [2]. The breaking of large particles into smaller particles results in an increased surface area. The rate of the reaction also increases as more surface area is available for the reaction. As shown in Fig. 1, the particle has an edge length of 5 mm. Therefore, the total surface area of the particle is 150 mm^2. Reducing the particle's edge length to 2.5, 1.25, and 0.625 mm, the total surface area becomes 300, 600, and 1200 mm^2.

When the composites' components have at least one dimension in the nanometre scale, they are termed nanocomposites. Most commonly it is the reinforcement phase which includes nano clay, nanotubes, or nanoparticles [4]. Nanostructured polymer composites can be obtained by using an appropriate polymer matrix and incorporating nanomaterials into it [5]. Few examples of nano-sized objects are DNA molecules having a diameter of 25 nm and proteins having a typical length of 10 nm.

Out of various nanocomposites, polymer nanocomposites are considered as a leading area of current research and advancement. It exhibits many beneficial properties (a) dimensional variability, (b) film-forming ability, and (c) activated functionalities [6]. Polymer nanocomposites have shown remarkable progress in electronics and communications, energy and data storage, aerospace, biomedical, agricultural sectors, food and water purification, environmental, sporting materials, automobiles, and packaging and defence applications [7]. The properties of polymers can be modulated precisely through the incorporation of nanofillers. Products made of nanocomposite in electronic and medical components, storage devices, stain-free fabrics, and nano paints are already commercialised. Nanocomposites are termed as 'materials of the future' as it has overcome present constraints of micro composites and monolithic.

Nanocomposites are used the first time in the early 1990s by Toyota Central R&D Laboratory to fabricate the car's belt cover using nylon-montmorillonite (MMT) clay nanocomposites [8, 9]. Nanoparticles, carbon nanotubes (CNTs), carbon nanofillers, graphene, nanocellulose, nanowires, nano-silica, and nano clay are extensively used engineered nanomaterials in medical, industrial, and consumer products. These are all tested for their reinforcing ability and showed tremendous improvement in the properties of nanocomposites [10–12]. Improved mechanical properties, high thermal

stability, and lower gas permeability are the few characteristics of polymer-matrix nanocomposites [13]. The market of polymer nanocomposites is anticipated to reach above USD 5100 million by 2020 [14].

2 Classification of Nanocomposites

Nanocomposites are categorized based on the type of materials (i.e., reinforcing and matrix material) employed for fabrication, as shown in Fig. 2 [15]. The different types of nanocomposites are (a) polymer-matrix nanocomposites, (b) ceramic-matrix nanocomposites, and (c) metal-matrix nanocomposites.

Both academicians and industrialists carry out extensive research activities in the field of polymer nanocomposites due to their outstanding properties such as (a) high modulus and stiffness, (b) high toughness, and (c) high strength with the incorporation of nano additives. Wear resistance, flame retardancy, barrier resistance, electrical, optical, and magnetic properties are also found excellent for polymer nanocomposites [16]. The properties of polymer nanocomposites are far better than conventional micro composites and metals. Thus, in this chapter, the discussion is focussed on nanocomposites that consist of the polymer as matrix material.

2.1 Polymer-Matrix Nanocomposites

In this type of nanocomposites, the polymer is used as matrix material, and different nano additives (nanomaterials) are used as reinforcements. The nanomaterials can be classified based on the number of dimensions in the nano range (=100 nm) where 1 nm

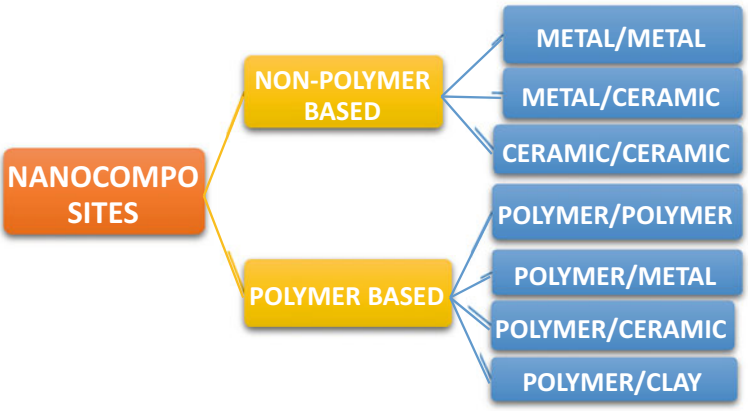

Fig. 2 Classification of nanocomposites [17]

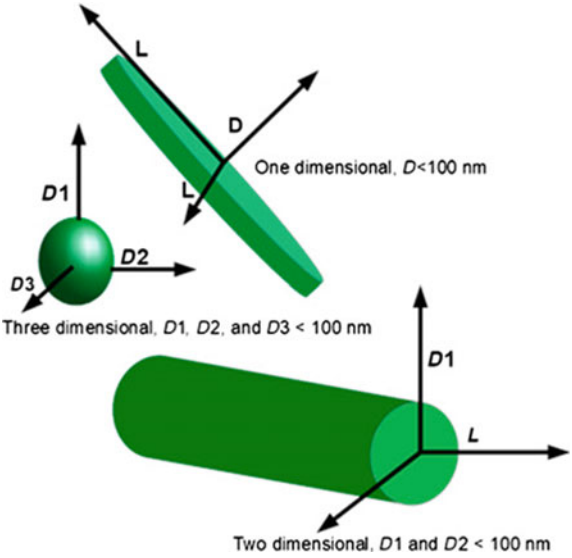

Fig. 3 Classifications of nanofillers [20]

$= 10^{-9}$ m [18]. The nanofillers' applications in polymer composite are differentiated based on their dimensions, as shown in Fig. 3 [19].

2.1.1 One-Dimensional (1D) Nanomaterials

Nanofiller with at least one of its dimensions <100 nm is considered one-dimensional (1D). It is in the form of a sheet. It has various applications in microelectronics, biosensors, sensors, biomedical, and coatings. It possesses extraordinary electrical, magnetic, and optic properties—examples: nano clay, nanoplatelets, nanosheets, and montmorillonite (MMT) clay.

a. **Polymer–clay nanocomposites**

C.A. Bower in 1949 first mentioned polymer–clay nanocomposites during conducting DNA engross from the montmorillonite clay [21]. The advancements in polymer–clay nanocomposites result in their usage in numerous applications. Polymer–clay nanocomposites are termed as multiphase systems. It consists of a contentious phase of polymer and dispersed phase of silicate (filler) with at least one dimension in the nanometre scale—the chemical bonding between filler and polymer results in the composites' superior properties. To achieve high strength, smectite clay (saponite, montmorillonite, and hectorite) are used as filler materials out of which the most common is montmorillonite (MMT) [22]. When dimensions of the filler are in nanoscale, their properties also change significantly [23]. Tests are conducted on various nanofillers like graphene, CNTs, nano-silica, and nanocellulose to find their strengthening ability (reinforcing). Currently, clays are the most demanded layered silicates used for the fabrication of polymer nanocomposites.

b. **Structures of polymer–clay nanocomposites**

The polymer–clay nanocomposite properties' improvement depends on the extent of the clay particles' dispersion in the polymer matrix. The dispersion of clay nanoparticles in polymer mainly depends on two parameters. These are:

1. Physical and chemical compatibility between polymer and clay nanoparticles, and
2. The method used for the production of polymer–clay nanocomposite.

The microstructure of polymer–clay nanocomposites is dependent on the interphase bonding between polymer and clay nanoparticles. The possible types are described below, and the same is presented in Fig. 4 [24].

1. **Phase-separated structure**: This structure is produced when the interface bonding between polymer and clay nanoparticles is very delicate. It is difficult to obtain the polymer intercalation in the clay layers during mixing between the organic polymer and inorganic clay (unmodified clay). As a result, clay is scattered as lump or particles stacked in aggregation with the polymer. The structure of composites is achieved because of phase separation. The properties

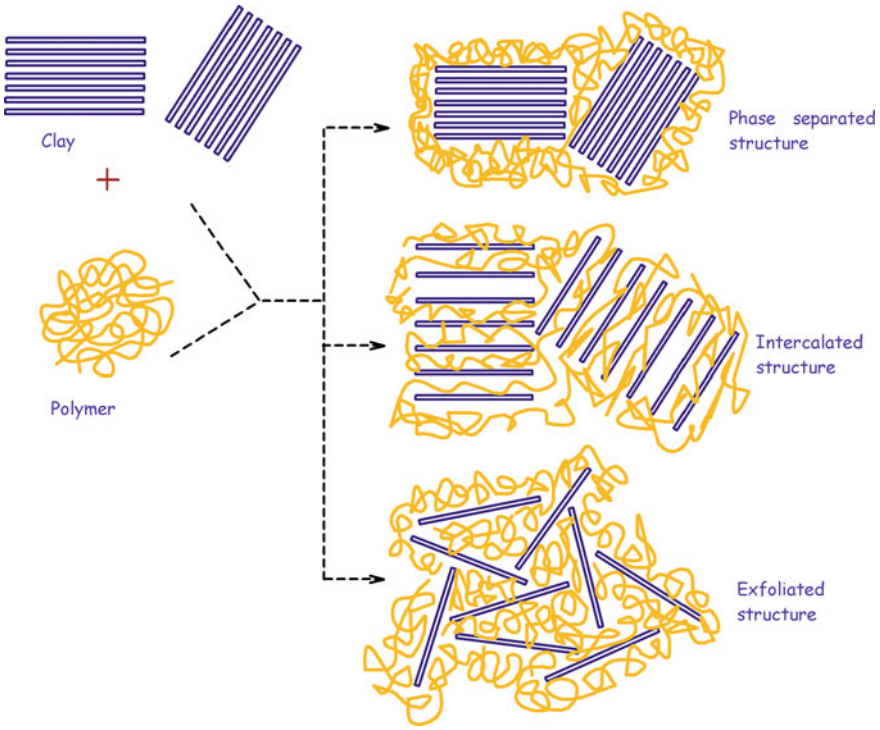

Fig. 4 Structures of polymer–clay nanocomposites [24]

of phase-separated composites are similar to conventional micro composites. Hence, it is anticipated that polymer–clay nanocomposites of such category show a downturn in their properties [25].

2. **Intercalated structure**: When the polymer–clay nanocomposite polymer chains are intercalated to a limited extent between the clay layers, it produces intercalated structure. The distance between the interlayer and clay layers increases due to the polymer intercalation, and it is termed as intercalated polymer–clay nanocomposites.
3. **Exfoliated structure**: The delaminated or exfoliated structure is obtained when individual clay layers randomly separated as sheets are dispersed in the continuous polymer at a suitable gap that relies on the clay charge. If the interlayer spacing increases more than 8–10 nm due to polymer chains, the structure obtained is considered as exfoliated structure. Improvement in the mechanical, barrier and thermal properties of the resultant nanocomposites depend on the uniform dispersion of exfoliated clay in the polymer. It is challenging to achieve complete exfoliation. In exfoliated nanocomposites, better dispersion of individual clay layers can result in lower clay content and higher aspect ratio. Large surface interaction between polymer and clay id the main reason behind the most notable advancement in polymer properties [26].

2.1.2 Two-Dimensional (2D) Nanomaterials

In 2D nanomaterials at least two dimensions of nanofillers should be <100 nm. Filaments, fibres, or tubes are generally used as 2D nanomaterials. In energy, sensors, catalysis, electronics, and optoelectronics, 2D nanofillers are extensively used. Examples: CNTs, nanofibers, nanowires, nanorods, whiskers, and 2D graphene [27].

a. **Polymer-carbon nanotube (CNT) composites**

In 1985, buckminsterfullerene (C_{60}) which is the latest form of carbon, was discovered [28]. CNTs comprising long and thin cylinders of carbon were first discovered in 1991 by employing an arc-discharge method [29]. CNTs differ from other carbon materials like fullerene, diamond, and graphite. It has carbon with an aspect ratio of >1000 [30]. CNTs are divided into two types based on the fabrication process [31]. The essential properties of different CNTs are shown in Table 1.

Table 1 Physical properties of different CNTs [32]

Properties	SWCNTs	MWCNTs
Density (gcm^{-3})	0.8	1.8
Electrical conductivity (S/cm)	10^2–10^6	10^3–10^5
Thermal conductivity (W/mK)	6000	2000
Thermal stability in the air (°C)	>600	>600

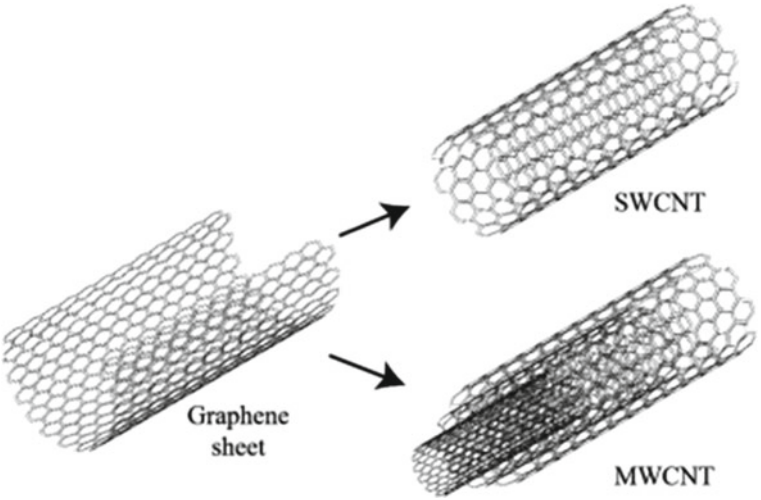

Fig. 5 Schematic presentation of SWCNT and MWCNT produced from graphene sheets [33]

- Single-walled CNTs: SWCNTs comprise a graphene layer rolled into a seamless (smooth and continuous) cylinder (Fig. 5). The diameter of an SWCNT is approximately 0.5–5 nm [34].
- Multi-walled CNTs (MWCNTs): MWCNTs are a special form of fullerene comprising two or more than two concentric cylindrical graphene sheets (Fig. 5) separated by Van der Wall forces. Inner and outer diameter reported for an MWCNT is 1.5–15 nm and 2.5–50 nm. The most usual interlayer distance is in the range of 0.32–0.35 nm and can vary slightly due to defects and other several factors [35, 36].

  It is made up of large macromolecules having a unique shape, size, and exceptional mechanical properties. Nanotubes are differentiated based on their diameter, length, chirality, or twist. By employing different processing techniques, CNTs can be fabricated into various aspect ratios, and their lengths can also be varied. Superb mechanical properties, lightweight characteristics, and high specific surface area of CNTs have attracted researchers to use them as reinforcements in polymer composite [37–40]. Its diameter is <100 nm and can be thinner than 5 nm. CNTs are used for several purposes such as (a) fabrication of energy and hydrogen storage systems, (b) manufacturing of automotive and aerospace components, (c) creation of nano filters and sensors, (d) identification of cancer cell and tissue engineering, (e) drug and gene delivery, (f) production of electronics devices and microchip, artificial implants, hard and flexible materials, and (g) solution of environmental problems [41]. The global CNTs market is forecasted to reach USD 6.8 billion by 2023 from USD 1.6 billion, the market valuation in 2016 [42].

An investigation is performed to determine the effect of CNT pre-localisation on the properties of ultra-high-molecular-weight polyethene (UHMWPE) nanocomposites [43]. It is concluded that a high concentration of CNT results in enhanced strain-hardening and yield stress of CNT-UHMWPE nanocomposites. Another study showed that the mechanical properties like tensile strength and impact toughness of graphene-polyvinyl chloride (PVC) composites could be improved remarkably by steady dispersions at very low loading graphene (i.e., 0.3 wt%) [44]. A study was conducted on multi-layered graphene-reinforced polymer composites to analyse the nano-indentation properties through molecular dynamics (MD) simulation. The results revealed that the indentation resistance is considerably using single and multi-layered graphene sheets [45]. Arash et al. [46] employed the MD simulation method to record the nanocomposites' total potential energy for calculating CNT-polymer nanocomposites' properties. The results showed that Young's modulus of (polymethyl methacrylate) (PMMA) strengthened by infinite long CNTs is remarkably increased compared with pure PMMA. The mechanical properties of grapheme-polymer composites are evaluated by applying MD simulation [47]. The results showed that shear modulus, hardness, and Young's modulus increased approximately 27.6, 35, and 150% by reinforcing graphene nanosheets into the polymer.

b. **Structure of carbon nanotubes (CNTs)**

The electronic configuration of carbon atom is $1s^2\ 2s^2\ 2p^2$ which shows that in 1 s orbit it has 2 strong bound electrons. In 2 s and 2p orbitals, 4 relatively weak bound electrons are called valence electrons. Carbon atom enters different hybridization stages like sp, sp^2, and sp^3 in different materials due to a slight difference in energy between 2 s and 2p levels. The hybridization flexibility allows the atomic orbitals to organize themselves in the structures of various dimensions such as nanoparticles (3D), CNTs (2D), and nano clays (1D) [48, 49].

Defects such as pentagons and heptagons sometimes formed on the external layer to form curved and spiral-type nanotubes. The longest grown CNTs currently are above 0.5 m [50] and cycloparaphenylene is considered the shortest CNT [51]. The thinnest CNT with a diameter of 0.3 nm is armchair CNTs [52]. CNTs are observed to hold the maximum density of 1.6 gcm^{-3} (generally, 1–1.4 gcm^{-3}) [53]. MWCNT's tensile strength is 63 GPa (9,100,000 psi) [37], for stainless steel it is 0.38–1.55 GPa. Pressure up to the level of 25 GPa can easily withstand by standard SWCNTs without permanent deformation. The geometry and most of the properties of CNTs depend on the diameter and chiral angle (θ), also known as helicity [54]. There are three conditions to differentiate SWCNT based on the chiral index. According to the conditions given below, SWCNT is also named armchair, zigzag (achiral nanotubes), and chiral (Fig. 6).

1. If chiral indices are equal (i.e., $n = m$), then the chiral angle is 30°.
2. If anyone of the chiral index is 0, i.e., (n, 0) or (0, m), then the chiral angle is 0°.
3. In the last case, $n \neq m$, if the chiral angle is $0° < \theta < 30°$ [55].

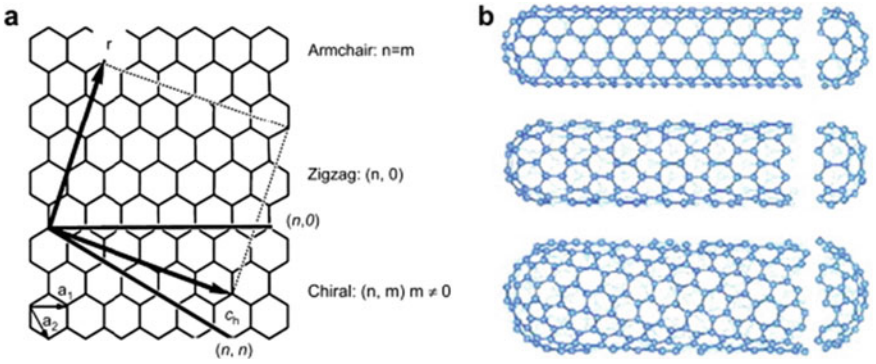

Fig. 6 **a** Representations of rolling of a graphene sheet and **b** different types of CNTs [48]

2.1.3 3D Nanomaterials

In 3D nanomaterials, all three dimensions are in nano range and mostly in cubical and spherical shapes. It is also referred to as iso-dimensional nanoparticles or zero-dimensional nanoparticles. To fabricate nanocomposites, it is essential to find the inherent properties of 3D nanofillers. Applications in which 3D nanomaterials are applied when combined with suitable matrix (polymer) are coatings, filtration, and biomedicine. Examples: nanoparticles (nanocellulose), nanogranules, and nanocrystals.

a. **Polymer-nanocellulose composites**

Nanocellulose can be explained as particles with diameters below micrometre (0.1 μm or 100 nm). In other words, nanocellulose is considered as particles whose size defines its optical, electrical, or magnetic properties [56]. Nanocellulose is extracted from a plant cell wall which is known as a natural nanomaterial. Nanocellulose has some striking features such as (a) high strength, (b) high surface area, and (c) excellent stiffness. Cellulose fibre combined with hydroxyl groups and strong hydrogen bonding networks renders into outstanding mechanical and physical properties [57]. Nanocellulose, which is a natural fibre, can be extracted from cellulose. Nanocellulose fibre gained special attention due to its size as its diameter is less than 100 nm and length is several micrometres. Nanocellulose holds outstanding strength property, low density (around 1.6 gcm^{-3}), and is considered as biodegradable nanofiber. It has high stiffness (220 GPa) which is better than the Kevlar fibre. It also has a high tensile strength (10 GPa) which is better than cast iron and strength to weight ratio is about eight times higher than stainless steel. Nanocellulose can be functionalized into various surface properties as it is transparent and consists of a reactive surface of hydroxyl groups [58].

b. **Structure of polymer-nanocellulose composites**

Cellulose is an extensive, renewed, natural organic polymer. The primary origin of cellulose is cotton that contains 95% pure cellulose. The primary material properties can enhance by accurate dispersion of cellulose in nanocomposites [59]. Cellulose nanocrystals or nanowhiskers are extracted from cellulose fibres through acid hydrolysis. Nanocellulose can be divided into two types:

i. nanostructured materials (cellulose microfibrils and cellulose microcrystals), and
ii. nanofibers (cellulose nanocrystals, cellulose nanofibrils, and bacterial cellulose) [60, 61].

Several nanocellulose forms can be produced using different methods from various cellulosic sources, as shown in Fig. 7 [62]. Characteristics like morphology, size, etc. of nanocellulose depend on the (a) isolation and processing conditions, (b) cellulose origin, and (c) possible pre-treatment or post-treatment. Nanocomposites fabricated using nanocellulose comprises of exceptional properties like (a) lightweight, (b) high mechanical strength, (c) transparent, and (d) high thermal properties [63].

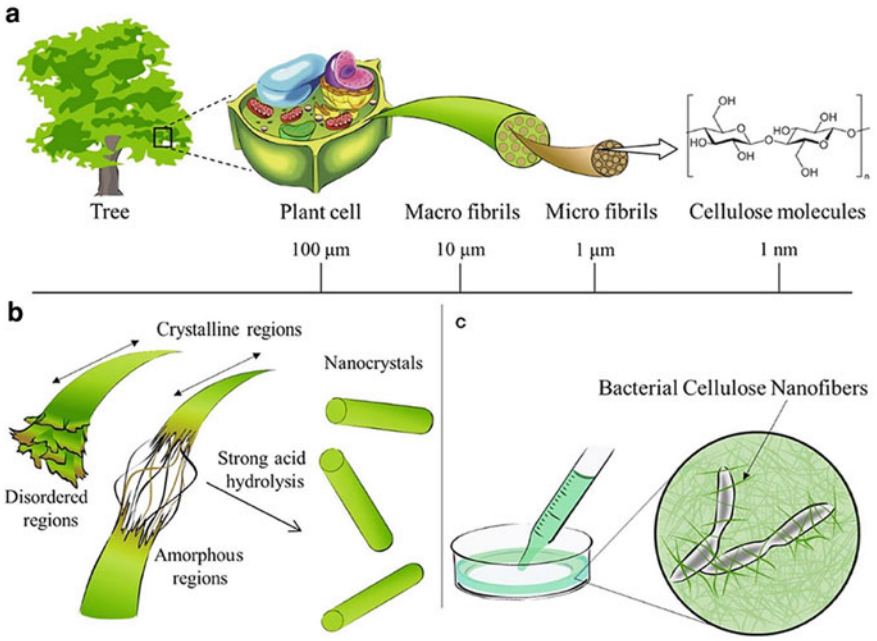

Fig. 7 **a** Extraction of cellulose from trees, **b** reaction between cellulose and strong acid to obtain nanocellulose, and **c** representation of bio nanocellulose cultured from cellulose-synthesizing bacteria [64]

3 Properties of Composites Reinforced with Nanofillers

Nanofillers are incorporated in a matrix (polymers) to improve the structured nanocomposites' characteristics for suitable applications. Nanofillers also hindered the drawbacks of polymers used for the manufacturing of nanocomposites. The improvement in the property is challenging as it may affect the other characteristics. The study revealed that the polymer's nature and properties, fabrication conditions, and methodology affect the final characteristics of nanocomposites [65]. The different properties of polymer nanocomposites are discussed in the following sections.

3.1 Mechanical Properties

Nanofillers as reinforcing agent play a significant role in improving the mechanical properties of polymer nanocomposites [66]. While reinforcing soft matrix with rigid nanofiller, the considerable amount of applied load is borne by nanofillers subject to adequate interactions between filler and matrix [67, 68]. Increased value of modulus can be attained by increasing the ratio of filler in the nanocomposites. Nanocomposites possess better mechanical properties than the neat polymer. CNTs demonstrated exceptional mechanical properties with Young's modulus of 1.2 TPa and tensile strength of 50–200 GPa. CNTs are considered as the most suitable candidate as reinforcement because of their superior properties including (a) low density, (b) high surface area, and (c) high aspect ratio [32]. A study showed an increase in clay content results in higher storage modulus of polyvinylidene fluoride/clay nanocomposites at 100–150 °C [69]. Research conducted on nylon-6-clay nanocomposites showed significant improvement in the properties as its modulus doubled and strength increased by 50% at clay loading of 4.2 wt.% [70, 71].

3.2 Thermal Properties

Many researchers reported that polymer structured nanocomposites have superior thermal stability than pure polymers due to nanofillers' incorporation into the polymer matrices [72, 73]. Polystyrene-clay nanocomposites have higher degradation temperature, i.e., around 30–40 °C in comparison to pure polystyrene under nitrogen and air heating degradation conditions [74]. Outstanding thermal conductivity of CNTs attracted many researchers to fabricate nanocomposites with improved thermal conductivity by reinforcing CNTs into various polymer matrices [75, 76]. Thermal conductivity in the case of CNTs-polymer nanocomposites relies on several factors (a) CNTs content, (b) aspect ratio, (c) dispersion, (d) CNT-polymer interfacial interactions, and (e) existence of metal impurities. According to the report,

thermal conductivity at room temperature increases by 300% and magnetic alignment increases by approximately 10% with a SWCNTs loading of 3 wt.% in epoxy [77]. Similarly, in an infiltration method, the thermal conductivity is increased to 220% by combining epoxy and SWCNTs (2.3 wt.% l) [78]. CNTs can improve the thermal stability of the polymer due to its better heat dissipation characteristic. The thermal property of nylon-6-clay thermoplastic nanocomposites is enhanced with an increase in the heat distortion temperature (HDT) by 80 °C when compared one-on-one with pristine polymer [70–74].

3.3 Flame Retardancy

Polymers are extensively used in domestic applications, and thus, their flammability needs to be reduced. Presently common chemical additives are used as flame retardants to reduce the ignition and control burning. Conventionally, phosphorous and several halogen-based compounds are used as a flame retardant without affecting the other properties and quality of polymer [79, 80]. Polymer nanocomposite is investigated for high-temperature applications using epoxy, nylon-11, etc. Nano clay plays a significant role in decreasing the flammability as flammability is considered an important aspect for many applications [81]. Nanocomposites produced from the nylon, polystyrene, epoxy, or vinyl ester possess low flammability compared with pure polymer.

3.4 Electrical and Optical Properties

Many research groups study the influence of adding nanotubes in polymers to improve electrical properties. In some studies, nanotubes are employed to improve relatively low-cost polymers' conductivity as an alternative to presently used filler like carbon black. Other studies investigated the incorporation of nanotubes in conducting polyaniline polymer. However, further work needs to be performed, aiming specific applications such as photovoltaic devices or supercapacitors. In many cases, improvement in mechanical properties is an additional advantage of the incorporation of nanotubes.

3.5 Barrier Properties

The addition of clays in polymer improves the barrier properties of the polymer as clay sheets are impermeable. Barrier properties are enhanced due to the maze or tortuous path that slowdown the gas molecule diffusion through polymer [82, 83]. The degree of advancement in barrier properties directly relies on the degree of tortuosity

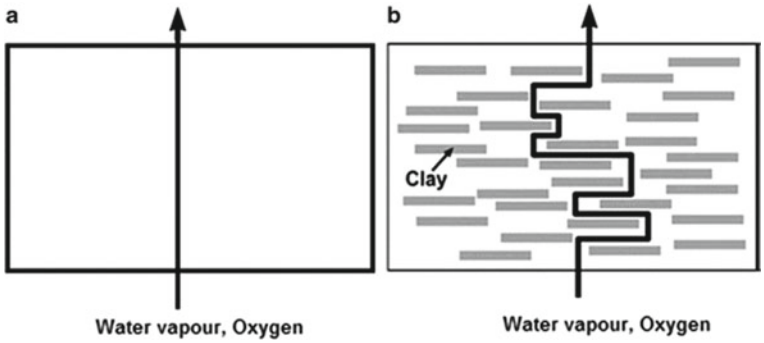

Fig. 8 Illustration of the tortuous pathway [86, 87]

produced by clay layers in the diffusion way of molecules through polymer film. The ratio of actual distance covered by diffusive molecule to the shortest distance to diffuse is a tortuous factor. It is mostly influenced by the aspect ratio of clay dispersed in the matrix. Barrier properties in the polymer can be further improved by increasing exfoliation or dispersion and the clay sheet's lateral length. Many researchers have reported that barrier properties are against diffusion of gases and vapours in polymer–clay nanocomposites [84, 85]. Figure 8 shows the tortuous path formed in polymer film due to the incorporation of exfoliated clay nanoplatelets.

a. Pathway taken by migrating gas molecules is perpendicular to the film orientation when average diffusion occurs.
b. Diffusing molecules must navigate impenetrable particles or platelets and through interfacial zones with distinct permeability features than those of virgin polymer. The mean gas diffusion length increased due to the tortuous pathway.

3.6 Anticorrosive Properties

Anticorrosiveness of the polymer can be improved by incorporating platelet fillers like layered silicate as it increases the length of the diffusion pathways. Clay reduces the permeability of polymer coating films by increasing the diffusion pathways shown in Fig. 8. The structured polymer nanocomposites of different polymers such as polystyrene, polyimide, polyaniline, and epoxy with unmodified and organically modified clays are investigated as anticorrosive coatings on metals [88].

3.7 Adsorption Behaviour

Incorporation of nanoparticles in polymer matrix turns polymer nanocomposites into highly tuneable adsorptive material. The adsorptive behaviour of nanocomposites

can be utilized for many applications such as (a) water purification, (b) fuel cell technology, (c) drug delivery, and (d) chemical sensor. Toxic materials like metal ions, dyes, and microorganisms from water or wastewater can be removed using polymer nanocomposites due to their adsorptive behaviour.

Apart from the properties discussed above, polymer structured nanocomposites possess few more properties. The properties of nanocomposites depend not only on the properties of individual components but also on the structured polymer nanocomposites' properties. These are (a) process used to fabricate nanocomposite, (b) types of filler material, (c) orientations of filler material, (d) degree of combining two phases, (e) interfacial adhesion, (f) volume fraction, (g) nature of the interphase, (h) shape and size of nanofiller materials, and (i) system morphology [89].

Nanomaterials play a critical role in enhancing nanocomposites' properties by dispersing and distributing nanofillers in the matrix. Sometimes, if it is not appropriately dispersed, agglomeration of particles takes place, and thus, nanocomposites' characteristics deteriorate, affecting the nanocomposite's performance improvement. Figure 9 shows different types of distribution and dispersion of nanoparticles in the matrix.

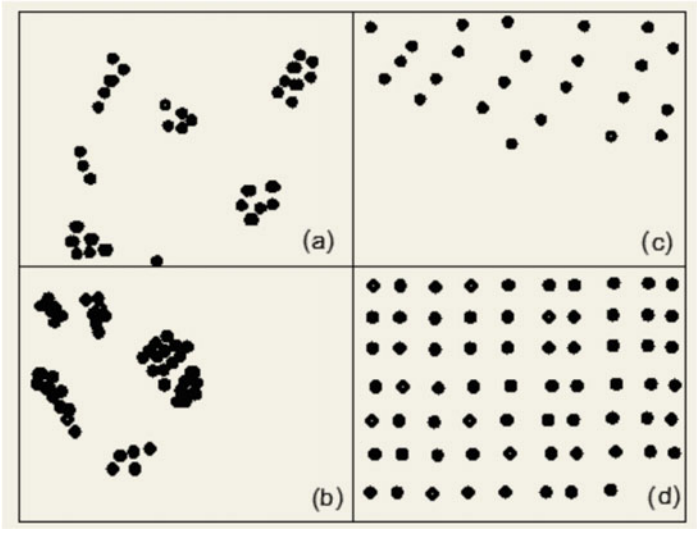

Fig. 9 Representations of distribution and dispersion of nanoparticles in matrix **a** good distribution but low dispersion, **b** poor distribution and poor dispersion, **c** poor distribution but good dispersion, and **d** good distribution and good dispersion [90]

4 Manufacturing Techniques of Nano-Composites

Manufacturing of polymer nanocomposites can be done either by mechanical or chemical processes. The difficulties associated with polymer nanocomposite manufacturing are uniform and homogeneous dispersion of nanoparticles in the polymer. Intricate polymerization reactions, chemical reactions, and surface modification of filler are approaches to solve this problem [91]. The processes used for the manufacturing of nanocomposites depend on the matrix material types, i.e., organic or inorganic [92]. The different methods involved in the fabrication of polymer nanocomposites are:

1. In-situ polymerization
2. Intercalation method.
    a. Chemical technique
    b. Mechanical technique.
3. Sol–gel method (other emerging synthesis methods)
4. Direct mixing of nanofillers and polymer [93].
    a. Melt compounding/blending
    b. Solvent method.
5. Latex technology
6. Ex-situ Synthesis
7. Other methods.

1. **In-situ polymerization**: It is considered the first evolved method moderately used to dispersion nanoparticles in the monomer. The process is schematically shown in Fig. 10. It is an efficient method that improves the compatibility between the nanofillers and polymer [94]. In this technique, the formation of the polymer occurs between the intercalated sheets [95]. This technique provides

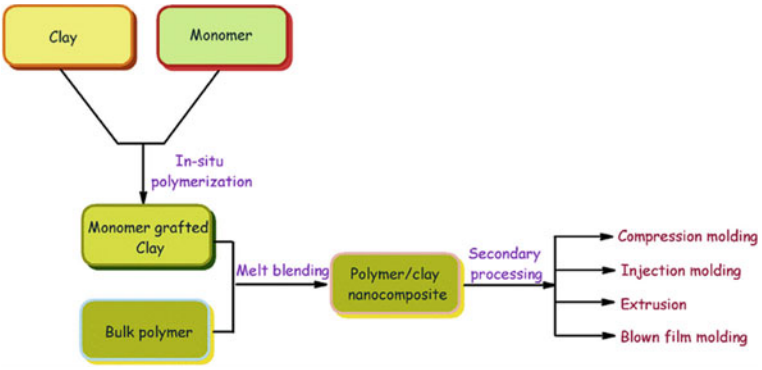

Fig. 10 Schematic representations of the stages of the in-situ polymerization method [16–24]

uniform dispersion of nanoparticles in the matrix. Swelling of nanoparticles takes place in monomer solution when low-molecular-weight monomer solution is discharged between nano clay layers [96]. Monomers are polymerized after mixing with nanoparticles through addition or condensation reactions with the help of an initiator and/or the catalyst at an elevated temperature either in presence or absence of solvent. The benefit of using this method is the formation of covalent bonding between polymer and functionalized CNTs, resulting in improved composites' properties. The reports showed the application of in-situ polymerization method for manufacturing of epoxy-based nanocomposites [97–99]. High-temperature synthesis causes decomposition of polymer, and slow rate of reaction is the disadvantage of the process [100].

2. **Intercalation method**: In this method, the nanoplatelets type of nanomaterials disperses into the polymer. Properties like flammability, shrinkage, and stiffness improved due to the addition of clays (nanomaterial) into the polymer. Swollen of clay takes place in solvent and intercalation of polymer chains occurs between the layers. Precipitation or vaporization method is used to obtain intercalated nanocomposite by removing the solvent [101]. Two different techniques can be used to disperse nanoplatelets homogeneously [102].

    a. ***Chemical technique***: It uses the in-situ polymerization method in which polymerization reaction occurs after the dispersion of nanoparticles in the monomer. In this method, nanocomposites are produced through chemical reactions in a liquid environment. It holds an additional polymerization process after nanoplatelets are distributed into the polymer. Nanoplatelets are swollen in the monomer solution, and the emergence of the polymer takes place between the intercalated sheets due to polymerization method. It results either in compact nanocomposite material or nanocomposite particles [103, 104].
    b. ***Mechanical technique***: It involves polymer and nanoplatelets direct intercalation using solution mixing. Co-solvent is used to dissolve polymer and solvent to swollen up the nanoplatelet sheets. Mixing of these two solutions allows the polymers chain to intercalate into the nanoplatelets layers and displace the solvent [16].

3. **Sol–gel method**: It is also termed as template synthesis [105]. The bottom-up approach is employed in the sol–gel method, and its principle is different from the preceding methods. The dispersion of solid nanoparticle in monomer solution results in a colloidal suspension of solid nanoparticles termed sol. In the gel, 3D interconnecting network formed between phases by polymerization reactions followed by hydrolysis procedure. In this method, the polymer is considered a nucleating agent assisting in developing layered crystals. As it grows, the polymer is oozed between layers and nanocomposite is formed [96]. Various other methods are applied for preparing polymer nanocomposites includes electrospinning, self-assembly, and phase separation. The method used

to manufacture nanofibers with the help of electrostatic force is known as electrospinning. The nanofibers in the range of 40–200 nm in diameter are manufactured using this unique synthetic method [106, 107]. Producing nanofibers with the electrospinning help is based on the polymer's viscoelastic behaviour and the electrostatic forces [108, 109]. Electrospun nanofibers possess special properties such as (a) cost-effectiveness, (b) permeability, (c) superior directional strength, (d) low basis weight, (e) high porosity, (f) flexibility, (g) layer thinness, and (h) high surface area per unit mass [110]. The molecule-mediated technique used for fabricating several nanocomposite films with desirable thicknesses is self-assembly [111]. Nanoparticles are connected by weak van der Waals hydrogen bond and electric/magnetic dipole interactions, rather than strong chemical bonds [112]. Production of nanofibrous matrices from polymer solutions requires thermally induced gelation, solvent exchange, and freeze-drying called phase separation [113].

4. **Direct mixing of nanofillers and polymer**: In nanocomposite fabrication, direct mixing of nanofillers and polymer transpire as a top-down approach. It is based on the breaking of cluster nanofillers during mixing. This method is most suitable for fabricating polymer nanocomposites as it necessitates two common ways of blending the polymer and nanofillers.

   a. ***Melt compounding/blending***: In this method, polymer and nanofillers combine in the absence of solvents above the polymer's glass transition temperature. In melt compounding/blending shear stress or hydrodynamic force instigate viscous drag to melt polymer and breakdown the aggregates of nanofiller using shear stress, which boosts homogeneous and uniform distribution of nanofiller in the polymer (Fig. 11).
   b. ***Solvent method***: In the solvent method, nanoparticles are distributed in solution employing solvent and polymer is dissolved in co-solvent (Fig. 12). Solvent evaporation or solvent coagulation is used to retrieve resulting nanocomposites from solvent methods. The shear stresses induced in the polymer during the solvent method are lower than melt compounding. The sonication method is employed to pre-disperse nanofillers in the solvent

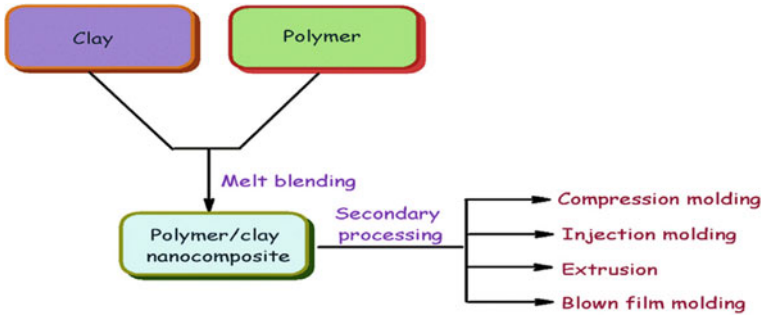

Fig. 11 Schematic of the steps involved in melt-blending [16–24]

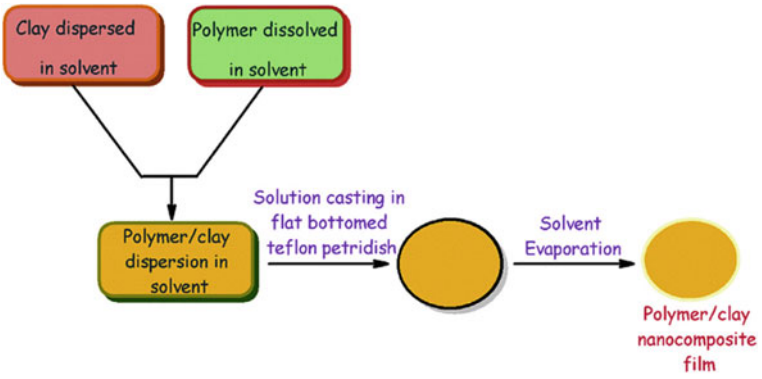

Fig. 12 Schematic representations of stages involved in solution-blending [16–24]

and breakdown aggregates of nanofiller. This method is also known as solution mixing.

5. **Latex technology**: It is a new technique to incorporate CNTs into polymer [114, 115]. In this method, distinct polymer particle colloidal dispersion occurs in an aqueous medium. It is used in polymers produced by emulsion polymerization or brought into the emulsion to disperse CNTs. It is an easy process as it comprises two simple aqueous components, flexible, reproducible, dependable, and permits integration of individual CNTs into a highly viscous polymer matrix. The procedure is safe, environmentally friendly, and economical as water is used as a solvent for CNT dispersion.
6. **Ex-situ synthesis**: It is also termed a blending or direct compounding technique in which nanofillers are synthesized by the external synthesis process and then added or combined to a monomer or resin. This is also used to fabricate polymer nanocomposites when mass production is desired. The process is economical and has operational convenience. At first, nanofillers and polymer are individually produced and compounded by solution melt blending, emulsion, or mechanical forces [116, 117]. The nanoparticles show a significant tendency to form large clusters during blending.
7. **Other methods**: To obtain nanocomposites with high CNT content, the latest processes developed are (a) pulverization, (b) spinning of coagulant, (c) layer-by-layer deposition, and (d) densification. Table 2 provides a summary of the technique, benefits, and CNTs used in these methods. It should be noted that many researchers have conducted tests to devise the latest processing methods that can develop nanocomposites with unique structure and properties for specific applications.

Table 2 New techniques for manufacturing of CNT-polymer nanocomposites

No	CNT	Fabrication technique	Benefits	Method
1	As received CNTs	Polymer and CNTs are mixed and pulverized by pan mill or twin-screw	Possible grafting of polymers on CNTs, easy scale-up, and solventless process	Pulverization [118, 119]
2	Pre-distribution of CNTs using surfactant solution	Coagulation of CNT into mesh by wet spinning into polymer solution and transforming the mesh into the solid fibre by slow draw procedure	Used to fabricate CNT-polymer fibre	The spinning of coagulant [120]
3	Pre-distribution of CNTs in solvent	Dipping of a solid substrate of CNTs into polymer solutions by the following curing	Structural flaw arises from the phase segregation of polymer	Layer by layer deposition [121]
4	As grown CNTs forest	CNT forest is produced and shifted to a pool of uncured epoxy. The matrix is infused into CNT forest and then cured	CNT vol.% can be controlled by varying the densification of CNT forest and aligning CNTs in nanocomposites	Densification [122]

If the polymer nanocomposites are prepared by using any one of the above techniques then they have to go for final processing by employing conventional manufacturing methods like (a) injection moulding, (b) calendaring, (c) casting, (d) compression moulding, (e) blow moulding, (f) rotational moulding, (g) extrusion moulding, and (h) thermoforming.

5 Applications of Nanocomposites

With nanotechnology, polymer nanocomposites came into limelight as it possesses many advanced features and improved properties. Nanomaterials have extensive applications in various sectors, as discussed below [123, 124]:

1. **Aerospace:** The primary concerns for the aerospace structure are weight, strength and stiffness, performance, thermal stability, retardancy, and durability [125]. Nanocomposites have exceptional structural properties, including favourable coefficient of thermal expansion. These properties are critical in aerospace research focusing on telescopes and antennas [126].
   Weight reduction: Reduced vehicle weight can increase payload capacity and reduce fuel consumption and emissions. In aircraft and spacecraft industries, the current trend is to maximize the use of lightweight composites. Boeing 787

is made up of a large volume of composites (50%) in comparison to Boeing 777 in which only 7% is used. A nano porous polymers density is 1/5th of a fully dense polymer, i.e., 0.2 g cm^{-3}. Enhancement in mechanical properties like strengthening nanopore walls is achieved by adding nanofillers (CNTs, nano clay, and graphene). Composite weight can be reduced by using CNT fibres that possess higher tensile properties [127].

Strength and stiffness: Organic polymer-nanocomposites possess remarkably higher modulus and strength. The fracture toughness of composites is increased from 3.4 to 4.2 MPa/m^2, i.e., 24% with the incorporation of 10 vol% MWCNT in alumina composites [128]. The addition of 1% nanotubes increases the elastic stiffness of CNT-polystyrene composites by 36–42% and tensile strength by 25% [129].

Thermal stability and fire retardancy: It is considered an essential property to meet market-driven performance and cost requirements. It plays a vital role in many applications, such as aircraft, military applications, and many sensing systems. Experimental results showed enhancement in the flame retardant, thermal, and mechanical properties of the polymer nanocomposite and confirmed their use in aerospace applications [130, 131].

2. **Automobile:** Polymer–clay nanocomposites are first used to fabricate car parts as they possess high stiffness and thermal stability. The first industry used nanocomposites in the automobile was General Motors. The use of nanocomposites resulted in the reduction of component weight by approximately 1 kg [132]. Toyota Central R&D Laboratory performs extensive research in 1986 to determine the properties of nylon-6-clay nanocomposites used as timing belt covers in automobile [133, 134]. In recent times, nanocomposites are the most commonly used material for manufacturing of car parts like side moulding, doors, seatbacks, console, cargo bed bridge, panels, trim, handles, rear view mirror, components of the gas tank, engine cover, bumper, etc. as it produces stiffer, lighter, less brittle at cold temperature, and more scratch-resistant parts. The weight of any part fabricated using 5 wt% clay can be reduced by 25% compared to glass fibre reinforced nylon. The addition of nano clays also results in increased thermal distortion temperature from 65–152 °C. In the late 1990s, CNTs were found in most automobiles' fuel system where they are typically blended with nylon to prevent static charge build-up. The whole automotive world is currently using polymer nano clay-composites as a potential substitute because of low emission, low cost, and high performance. The use of nanomaterials in automobile tires is one of its earliest applications. Future applications of nanocomposites to the automotive industry include (a) sensors and switches, (b) fuel cells, (c) batteries, (d) hydrogen storage, (e) fire-retardant interiors, (f) LED lighting, and (g) miniaturized systems based on NEMS.
3. **Nanostructured membranes:** Membranes possesses internal nanostructures that are termed as nanostructured membranes [135]. In recent years, the advancement of nanostructured membranes in the different field covers:

Nanostructured membranes for reverse osmosis: CNTs and graphene oxide are considered the most favourable nanomaterials for reverse osmosis application. These materials can be synthesized to have non-tortuous pores in a few nanometres to transport water molecules in the desalination process [136–139].
Nanostructured membranes for ultrafiltration: Ultrafiltration is basically for water treatment based on the membrane separation process. The phase inversion method is used to fabricate ultrafiltration membranes whose pores are generally in the nanoscale range (1–100 nm) [140].
Nanostructured membranes for gas separations: Nanomaterials like silica (SiO_2) and CNTs are incorporated into the polymer to prepare nanostructured membranes for gas separation. The selection of nanomaterial and polymer is the subject of extensive research [141–146]. Silica can improve the thermal and mechanical stabilities as well as gas separation property of membranes. CNTs have excellent mechanical and thermal stabilities and potentiality to minimize the compaction effect in high-pressure gas separation. The improvement is attributed to the ability of MWNTs to improve the mechanical strength and anti-compaction property of the mixed matrix membranes.

4. **Water treatment processes**: In water treatment, nanostructured polymer composites are employed in diverse roles and capacities (like catalyst, adsorbents, and membrane filters) and as monitoring purposes and detecting microbial agents. Nanomaterials and polymers used in composites play a crucial role in determining its utilization for the treatment process. Methods of preparation and synthesis polymer nanocomposites also influence the performance of the application for water treatment [147].
Polymer nanocomposites as photocatalysts: Application of polymer nanocomposites as catalysts during wastewater treatment has received enormous attention among researchers. Polymer nanocomposites have great potential as catalysts due to the unique characteristics such as superior influence on the rate of chemical reactions, specific surface area, and inherent electronic properties. Studies revealed that polymer nanocomposites could function as photocatalysts in chemical reactions when light is absorbed, bringing excitation in higher energy levels [145]. The suitability of polymer nanocomposites as efficient photocatalysts for water treatment purposes is based on the quality of nanocomposites used and their ability to irradiate light source [146].
Polymer nanocomposites as adsorbents: The most straightforward and efficient procedure of separating water and contaminants is adsorption [148, 149]. When substances like liquid, solid, or chemical species gather and transform into a solid surface is termed as adsorption [150]. When transferring the adsorbate molecule from solution to the available binding sites on the adsorbent, the procedure is considered adsorption. According to various reports, numerous sorbents used to remove contaminants are activated carbons sourced from different precursors like clay [151]. It showed tremendous results in the water treatment process, and its efficiency is based on its intrinsic properties [152]. To enhance the wastewater remediation process's efficiency, nanosorbents are used to eliminate contaminants that are difficult to remove during wastewater treatment.

Studies in previous reports showed polymer nanocomposites efficiency as adsorbents to remove contaminants such as heavy metals, pesticides, pharmaceuticals, perfluoroalkyl acids, etc. [153].

Polymer nanocomposites as filtration membranes: Designing and fabricating efficient filtration membranes are purposely done to exclude specific predetermined molecules or species like oils [154], dyes [155], solutes/salts [156], and heavy metals [157, 158]. Polymer nanocomposites were also employed to eliminate antimicrobial [159], flocculation/dewatering of sludge [160], removal of chlorinated byproducts [161], and natural organic matter [162]. To eliminate all these various sorbents, promising remediation capabilities are synthesized and utilized. Filtration membrane is widely used for water treatment due to its adaptable nature. It also has few inherent qualities like high sorption capacity, environmentally friendly, and cost-effective for wastewater treatment [163]. Meanwhile, the physical separation of large particles of pollutants is a distinctive characteristic of filtration membranes [164].

Polymer nanocomposites as monitoring and detection devices: Polymer nanocomposites are also used as monitoring and detecting devices based on pH sensitivity, affinities for both organic and inorganic ions, and responses to microorganisms [165]. Polymer nanocomposites can sense and detect, which is derived by intrinsic properties of nanomaterials and polymer. Polymer nanocomposites are utilized for the detection of contaminants such as (a) heavy metals, (b) trace organic and inorganic contaminants, (c) persistent organic pollutants, and (d) pathogens in aqueous solution [166]. Additionally, some polymer nanocomposites are used for monitoring (a) pH [167], (b) dissolved oxygen [168], and (c) chemical oxygen demand [169] of water systems.

Polymer nanocomposites as antimicrobial agents: Eliminating microbial contaminants *Escherichia coli*, *Staphylococcusaureus,* etc., from water is one of the most challenging tasks during water treatment operations. In several studies, nanomaterials are used for their anti-microbial properties [170]. In recent years, the field of disinfection has received enormous attention due to the challenges associated with other disinfection methods. Apart from the nanomaterials, specific polymeric matrices contribute to the antimicrobial activity of polymer nanocomposites [171]. This procedure is expected to receive more attention in future as it is a viable alternative in *the* water treatment process. There is a need to investigate this technique more to eliminate the challenges encountered during the application.

5. **Biomedical:** Polymer nanocomposites are extensively used to heal lost and damaged organs or tissues [172]. Tissue engineering and the drug delivery system are among the most important fields using polymer nanocomposites [173]. A report suggests that polymer–clay nanocomposites are quite efficient for delivering antimicrobial drugs [174]. The films composed of semi-synthetic cellulose derivative (carmellose-sodium) and chlorhexidine diacetate like mucoadhesive for oral infectious treatment. Polymer nanocomposites offer promising mucoadhesive, mechanical, and chemical properties [175]. Three different fields of medicine are prevention, diagnosis, and therapy. Nanoscale

liposomes or micelles are used through a topical vaccine delivery system in the case of prevention as it provides an effective and easy way to generate cell-mediated immune response [176]. To detect or diagnose biomolecular signals at a very low concentration and detect diseases at an early stage, nanocantilevers, nanotubes, and nanowires are used to increase the sensitivity of detection devices [177]. The introduction of nanotechnology has benefited molecular imaging, computed tomography, and magnetic resonance imaging technology. Nanotechnology provides 3D images of tissues and organs with more information and higher resolution [178]. Nanocomposites can replace Lead-based products to provide light-weight and flexible radiation shields for diagnostic radiology and nuclear medicine. The utilization of nanoparticles as a drug carrier crosses the blood–brain barrier. Nanoparticles in the field of therapy can be used to destroy cancer cells. Scaffolds based on tissue growth can be produced using soft tissue engineering materials like (a) nanofibers, (b) nanotubes, and (c) peptide-based self-assembled nanostructure. Nanostructured materials, nanocomposites, and nano-coatings are extensively used for scaffolds and implants for bone and cartilage replacement in orthopaedics and dentistry. Nanocomposites also benefit vascular stents by providing nanoscale biocompatible or drug-eluting coatings. Nanotechnologies already made its impact in the field of pacemakers and hearing aids implantable devices. It is further developed and equipped with a smaller size and increased power provided by nanoscale electronics. Silver nanocrystals type of antibacterial nanoparticles has already been used in protective clothing, medical textiles, and wound dressings. Nano-enabled products in the health care field commercially available are surgical blades with nanoscale diamond coatings, medical tools, surgical threads with gold nano-coatings, and suture needles composed of stainless steel nanoparticles.

6. **Chemicals:** Chemical sector is one of the many fields which are benefited from nanotechnologies. Replacement of micro-fillers by nanoparticles as fillers in paints and other coatings, improves their swelling, scratch, radiation, abrasion, heat, and environmental ageing resistance [179]. Reduction in the formation of cracks and voids can be achieved by incorporating nanoparticles in the solution during the evaporation phase of the traditional sol–gel coating. Nanofillers can lead to antibacterial, antistatic, flame retardant, and transparent UV protective coatings. Improved performance of polymer composites can be achieved by using nanofillers [180]. Nanofillers, when added to polymer matrices, provide unique performance such as resistance to heat distortion. The addition of nano clay allows the improvement in heat distortion temperature, which is not possible in any other method. Nanoparticles found suitable for these applications should comprise of carbon allotropes and polymers.
7. **Construction:** Recently, polymer nanocomposite is introduced to structures to improve existing construction materials [181]. Nanomaterials are found in almost every house or building, specifically in three types of products like concrete, coatings and paints, and insulation. The addition of PVA and montmorillonite in polymer nanocomposite when added to concrete is responsible for increasing cement composites' properties without affecting the compression

strength [182]. A new approach is used to incorporate nanoparticle adhesives for building and civil engineering applications for retrofitting structures. An investigation is focussed on the properties of nano clay modified epoxy adhesive to strengthen concrete members with CFRP [183]. Identical research is carried on the preparation of PU-clay nanocomposite [184]. Another important issue in construction is the coating of concrete walls with polymer paint prone to weather damage. Polymer nanocomposites proved to be better than neat polymers for this purpose as it can cover the pores and crevices present on the concrete and other surfaces. It helps in resisting pollution and environmental attacks such as chloride ions and water seepage. The application of polymer nanocomposites to concrete surface demonstrated improvement in moisture penetration resistance [185]. Nanoporous structures like aerogels can be made out of silica or carbon to provide 2 to 8 times more efficient thermal and acoustical insulation than traditional insulation materials. The addition of nano clay to polymers in building materials provides flame resistance. It is also considered to be used as spraying or painting nanosensors to monitor stress and the temperature or air quality on the surface of building or structure.

8. **Electronics:** The three main areas of concern in electronics applications are displays, memory, and integrated circuits [186]. Nanowires, CNTs, and graphene are used for displaying like (a) organic light-emitting diodes, (b) organic light-emitting transistors, (c) electrophoretic paper, and (d) field emission display. Recent research is focussed on producing devices that are easier to manufacture, consume less energy, thinner and lighter, and can be flexed without being damaged. The memory chips are designed to increase memory and reduce power consumption. Recent advancements include the formation of p-n junctions with the help of graphene, integrated circuits fabrication by CNTs, and nanowires to create transistors without p-n junctions.

6 Review Questions

(1) What is a carbon nanotube? Explain why they are not as prevalent as other forms of carbon.
(2) What is nanocomposite? Classify polymer-based nanocomposite.
(3) What is the difference between top-down and bottom-up methods for creating nanostructures?
(4) Describe the defects formed on the external layer of MWCNT structures and elucidate the importance of interlayer distance in overcoming above stated defects.
(5) List out the factors which make nanocellulose as the most demanding and suitable material to fabricate composite material.
(6) Which method is suitable for the fabrication of polymer nanocomposites out of melt compounding and solvent method? Justify the answer with practical reasons.

(7) Explicate some new techniques used for the manufacturing of CNT-polymer nanocomposites.
(8) State the purposes of adding nanomaterials in the fabrication of composite for the use of automobile and aerospace.
(9) Elucidate the use of nanocomposite in the various fields of the biomedical.
(10) Explain the role of interphase bonding between polymer and clay nanoparticles and its types in detail.

References

1. Thostenson, E.T., Li, C., Chou, T.W.: Nanocomposites in context. Compos. Sci. Technol. **65**(3–4), 491–516 (2005)
2. Thrower, P., Mason, T.W.: Materials in Today's World. McGraw-Hill, USA (2008)
3. https://commons.wikimedia.org/w/index.php?curid=65688187
4. Hussain, F., Hojjati, M., Okamoto, M., Gorga, R.E.: Polymer-matrix nanocomposites, processing, manufacturing, and application: an overview. J. Compos. Mater. **40**(17), 1511–1575 (2006)
5. Khezri, K., Mahdavi, H.: Polystyrene-silica aerogel nanocomposites by in situ simultaneous reverse and normal initiation technique for ATRP. Microporous Mesoporous Mater. **228**, 132–140 (2016)
6. Jordan, J., Jacob, K.I., Tannenbaum, R., Sharaf, M.A., Jasiuk, I.: Experimental trends in polymer nanocomposites—a review. Mater. Sci. Eng. A **393**(1–2), 1–11 (2005)
7. RTO Lecture Series.: EN-AVT-129. (May 2005)
8. Kojima, Y., Usuki, A., Kawasumi, M., Okada, A., Fukushima, Y., Kurauchi, T., Kamigaito, O.: Mechanical properties of nylon 6-clay hybrid. J. Mater. Res. **8**(5), 1185–1189 (1993)
9. Kojima, Y., Usuki, A., Kawasumi, M., Okada, A., Kurauchi, T., Kamigaito, O.: Sorption of water in nylon 6-clay hybrid. J. Appl. Polym. Sci. **49**(7), 1259–1264 (1993)
10. Sahoo, N.G., Rana, S., Cho, J.W., Li, L., Chan, S.H.: Polymer nanocomposites based on functionalized carbon nanotubes. Prog. Polym. Sci. **35**(7), 837–867 (2010)
11. Potts, J.R., Dreyer, D.R., Bielawski, C.W., Ruoff, R.S.: Graphene-based polymer nanocomposites. Polym. **52**(1), 5–25 (2011)
12. Schmidt, D., Shah, D., Giannelis, E.P.: New advances in polymer/layered silicate nanocomposites. Curr. Opin. Solid State Mater. Sci. **6**(3), 205–212 (2002)
13. Alexandre, M., Dubois, P.: Polymer-layered silicate nanocomposites: preparation, properties and uses of a new class of materials. Mater. Sci. Eng. R. Rep. **28**(1–2), 1–63 (2000)
14. https://www.marketsandmarkets.com/Market-Reports/polymer-nanocomposites-market-228956069.html
15. Chung, D.D. Composite Materials: Functional Materials for Modern Technologies. Springer Science & Business Media (2013)
16. Khan, W.S., Hamadneh, N.N., Khan, W.A.: Polymer nanocomposites—synthesis techniques, classification and properties. Science and Applications of Tailored Nanostructures, pp. 50–67. (2016)
17. Pandey, N., Shukla, S.K., Singh, N.B.: Water purification by polymer nanocomposites: an overview. Nanocomposites **3**(2), 47–66 (2017)
18. Olad, A.: Polymer/clay nanocomposites. In: Advances in Diverse Industrial Applications of Nanocomposites. IntechOpen, pp. 113–138. (2011)
19. Mittal, V. (ed.).: Spherical and Fibrous Filler Composites. Wiley (2016)
20. Akpan, E.I., Shen, X., Wetzel, B., Friedrich, K.: Design and synthesis of polymer nanocomposites. In: Polymer Composites with Functionalized Nanoparticles pp. 47–83. Elsevier (2019)

21. Bower, C.A.: Studies on the form and availability of organic soil phosphorous. IOWA Agric. Exp. Stat. Res. Bull. **28**, 362 (1949)
22. Esteves, A.C.C., Barros-Timmons, A., Trindade, T.: Nanocompósitos de matriz polimérica: estratégias de síntese de materiais híbridos. Quim. Nova **27**(5), 798–806 (2004)
23. Kumar, A.P., Depan, D., Tomer, N.S., Singh, R.P.: Nanoscale particles for polymer degradation and stabilization—trends and future perspectives. Prog. Polym. Sci. **34**(6), 479–515 (2009)
24. Valapa, R.B., Loganathan, S., Pugazhenthi, G., Thomas, S., Varghese, T.O.: An overview of polymer—clay nanocomposites. In: Clay-Polymer Nanocomposites, pp. 29–81. Elsevier (2017)
25. Raquez, J.M., Habibi, Y., Murariu, M., Dubois, P.: Polylactide (PLA)-based nanocomposites. Prog. Polym. Sci. **38**(10–11), 1504–1542 (2013)
26. Zaarei, D., Sarabi, A.A., Sharif, F., Kassiriha, S.M.: Structure, properties and corrosion resistivity of polymeric nanocomposite coatings based on layered silicates. J. Coat. Technol. Res. **5**(2), 241–249 (2008)
27. Dolez, P.I.: Nanomaterials definitions, classifications, and applications. In: Nanoengineering, pp. 3–40. Elsevier (2015)
28. Kroto, H.W., Heath, J.R., O'Brien, S.C., Curl, R.F., Smalley, R.E.: C60: buckminsterfullerene. Nature **318**(6042), 162–163 (1985)
29. Iijima, S., Ajayan, P.M., Ichihashi, T.: Growth model for carbon nanotubes. Phys. Rev. Lett. **69**(21), 3100 (1992)
30. Thostenson, E.T., Ren, Z., Chou, T.W.: Advances in the science and technology of carbon nanotubes and their composites: a review. Compos. Sci. Technol. **61**(13), 1899–1912 (2001)
31. Salvetat, J.P., Bonard, J.M., Thomson, N.H., Kulik, A.J., Forro, L., Benoit, W., Zuppiroli, L.: Mechanical properties of carbon nanotubes. Appl. Phys. A **69**(3), 255–260 (1999)
32. Ma, P.C., Siddiqui, N.A., Marom, G., Kim, J.K.: Dispersion and functionalization of carbon nanotubes for polymer-based nanocomposites: a review. Compos. A Appl. Sci. Manuf. **41**(10), 1345–1367 (2010)
33. Green, M.J., Behabtu, N., Pasquali, M., Adams, W.W.: Nanotubes as polymers. Polymer **50**(21), 4979–4997 (2009)
34. Yazid, M.N.A.W.M., Sidik, N.A.C., Mamat, R., Najafi, G.: A review of the impact of preparation on stability of carbon nanotube nanofluids. Int. Commun. Heat Mass Trans. **78**, 253–263 (2016)
35. Iijima, S.: Carbon nanotubes: past, present, and future. Phys. B **323**(1–4), 1–5 (2002)
36. Grady, B.P.: Carbon Nanotube-Polymer Composites: Manufacture, Properties, and Applications. Wiley (2011)
37. Yu, M.F., Lourie, O., Dyer, M.J., Moloni, K., Kelly, T.F., Ruoff, R.S.: Strength and breaking mechanism of multiwalled carbon nanotubes under tensile load. Science **287**(5453), 637–640 (2000)
38. Treacy, M.J., Ebbesen, T.W., Gibson, J.M.: Exceptionally high Young's modulus observed for individual carbon nanotubes. Nature **381**(6584), 678–680 (1996)
39. Zhou, H.W., Mishnaevsky, L., Jr., Yi, H.Y., Liu, Y.Q., Hu, X., Warrier, A., Dai, G.M.: Carbon fiber/carbon nanotube reinforced hierarchical composites: effect of CNT distribution on shearing strength. Compos. B Eng. **88**, 201–211 (2016)
40. Valentino, O., Sarno, M., Rainone, N.G., Nobile, M.R., Ciambelli, P., Neitzert, H.C., Simon, G.P.: Influence of the polymer structure and nanotube concentration on the conductivity and rheological properties of polyethylene/CNT composites. Phys. E. **40**(7), 2440–2445 (2008)
41. De Volder, M.F., Tawfick, S.H., Baughman, R.H., Hart, A.J.: Carbon nanotubes: present and future commercial applications. Science **339**(6119), 535–539 (2013)
42. https://www.transparencymarketresearch.com/carbon-nano-tubes-market.html
43. Deplancke, T., Lame, O., Barrau, S., Ravi, K., Dalmas, F.: Impact of carbon nanotube prelocalization on the ultra-low electrical percolation threshold and on the mechanical behavior of sintered UHMWPE-based nanocomposites. Polymer **111**, 204–213 (2017)
44. Wang, H., Xie, G., Fang, M., Ying, Z., Tong, Y., Zeng, Y.: Mechanical reinforcement of graphene/poly (vinyl chloride) composites prepared by combining the in-situ suspension polymerization and melt-mixing methods. Compos. B Eng. **113**, 278–284 (2017)

45. Alian, A.R., Dewapriya, M.A.N., Meguid, S.A.: Molecular dynamics study of the reinforcement effect of graphene in multilayered polymer nanocomposites. Mater. Des. **124**, 47–57 (2017)
46. Arash, B., Wang, Q., Varadan, V.K.: Mechanical properties of carbon nanotube/polymer composites. Sci. Rep. **4**, 6479 (2014)
47. Li, Y., Wang, S., Wang, Q.: A molecular dynamics simulation study on enhancement of mechanical and tribological properties of polymer composites by introduction of graphene. Carbon **111**, 538–545 (2017)
48. Saito, R. Dresselhaus, G., Dresselhaus, M.S.: Physical Properties of Carbon Nanotubes. London, Imperial College Press, (1998)
49. Smalley, R.E.: Carbon Nanotubes: Synthesis, Structure, Properties, and Applications, vol. 80. Springer Science & Business Media (2003)
50. Zhang, R., Zhang, Y., Zhang, Q., Xie, H., Qian, W., Wei, F.: Growth of half-meter long carbon nanotubes based on Schulz-Flory distribution. ACS Nano **7**(7), 6156–6161 (2013)
51. Jasti, R., Bhattacharjee, J., Neaton, J.B., Bertozzi, C.R.: Synthesis, characterization, and theory of [9]-,[12]-, and [18] cycloparaphenylene: carbon nanohoop structures. J. Am. Chem. Soc. **130**(52), 17646–17647 (2008)
52. Zhao, X., Liu, Y., Inoue, S., Suzuki, T., Jones, R.O., Ando, Y.: Smallest carbon nanotube is 3 Å in diameter. Phys. Rev. Lett. **92**(12), 125502 (2004)
53. Sugime, H., Esconjauregui, S., Yang, J., D'Arsié, L., Oliver, R.A., Bhardwaj, S., Cepek, C., Robertson, J.: Low temperature growth of ultra-high mass density carbon nanotube forests on conductive supports. Appl. Phys. Lett. **103**(7), 073116 (2013)
54. Hamada, N., Sawada, S.I., Oshiyama, A.: New one-dimensional conductors: graphitic microtubules. Phys. Rev. Lett. **68**(10), 1579 (1992)
55. Zhang, M., Li, J.: Carbon nanotube in different shapes. Mater. Today **12**(6), 12–18 (2009)
56. Hanemann, T., Szabó, D.V.: Polymer-nanoparticle composites: from synthesis to modern applications. Materials **3**(6), 3468–3517 (2010)
57. Dufresne, A.: Nanocellulose: a new ageless bionanomaterial. Mater. Today **16**(6), 220–227 (2013)
58. Moon, R.J., Martini, A., Nairn, J., Simonsen, J., Youngblood, J.: Cellulose nanomaterials review: structure, properties and nanocomposites. Chem. Soc. Rev. **40**(7), 3941–3994 (2011)
59. Fendler, J.H. (ed).: Nanoparticles and Nanostructured Films: Preparation, Characterization, and Applications. Wiley (2008)
60. Agwuncha, S.C., Anusionwu, C.G., Owonubi, S.J., Sadiku, E.R., Busuguma, U.A., Ibrahim, I.D.: Extraction of cellulose nanofibers and their eco/friendly polymer composites. In: Sustainable polymer composites and nanocomposites, pp. 37–64. Springer, Cham (2019)
61. Trache, D., Hussin, M.H., Haafiz, M.M., Thakur, V.K.: Recent progress in cellulose nanocrystals: sources and production. Nanoscale **9**(5), 1763–1786 (2017)
62. Phanthong, P., Reubroycharoen, P., Hao, X., Xu, G., Abudula, A., Guan, G.: Nanocellulose: extraction and application. Carbon Resour. Convers. **1**(1), 32–43 (2018)
63. Khalil, H.A., Bhat, A.H., Yusra, A.I.: Green composites from sustainable cellulose nanofibrils: a review. Carbohyd. Polym. **87**(2), 963–979 (2012)
64. Trache, D., Tarchoun, A.F., Derradji, M., Hamidon, T.S., Masruchin, N., Brosse, N., Hussin, M.H.: Nanocellulose: from fundamentals to advanced applications. Front. Chem. **8**, 392 (2020)
65. Ray, S.S.: A new possibility for microstructural investigation of clay-based polymer nanocomposite by focused ion beam tomography. Polymer **51**(17), 3966–3970 (2010)
66. Jiang, L., Lam, Y.C., Tam, K.C., Chua, T.H., Sim, G.W., Ang, L.S.: Strengthening acrylonitrile-butadiene-styrene (ABS) with nano-sized and micron-sized calcium carbonate. Polymer **46**(1), 243–252 (2005)
67. Tortora, M., Vittoria, V., Galli, G., Ritrovati, S., Chiellini, E.: Transport properties of modified montmorillonite-poly (e-caprolactone) nanocomposites. Macromol. Mater. Eng. **287**(4), 243–249 (2002)
68. Gorrasi, G., Tortora, M., Vittoria, V., Pollet, E., Lepoittevin, B., Alexandre, M., Dubois, P.: Vapor barrier properties of polycaprolactone montmorillonite nanocomposites: effect of clay dispersion. Polymer **44**(8), 2271–2279 (2003)

69. Mrlik, M., AlMaadeed, M.A.S.: Fillers in advanced nanocomposites for energy harvesting. In: Fillers and Reinforcements for Advanced Nanocomposites, pp. 401–424. Woodhead Publishing (2015)
70. Okada, A., Usuki, A.: The chemistry of polymer-clay hybrids. Mater. Sci. Eng. C **3**(2), 109–115 (1995)
71. Christopher, O.O., Lerner, M.: Nanocomposites and Intercalation Compound. Academic Press, San Diego, Encyclopedia of Physical Science and Technology (2001)
72. Becker, O., Varley, R.J., Simon, G.P.: Thermal stability and water uptake of high performance epoxy layered silicate nanocomposites. Eur. Polym. J. **40**(1), 187–195 (2004)
73. Wang, S., Hu, Y., Song, L., Wang, Z., Chen, Z., Fan, W.: Preparation and thermal properties of ABS/montmorillonite nanocomposite. Polym. Degrad. Stab. **77**(3), 423–426 (2002)
74. Vyazovkin, S., Dranca, I., Fan, X., Advincula, R.: Kinetics of the thermal and thermo-oxidative degradation of a polystyrene–clay nanocomposite. Macromol. Rapid Commun. **25**(3), 498–503 (2004)
75. Yuen, S.M., Ma, C.C.M., Chiang, C.L., Chang, J.A., Huang, S.W., Chen, S.C., Chuang, C.Y., Yang, C.C., Wei, M.H.: Silane-modified MWCNT/PMMA composites–Preparation, electrical resistivity, thermal conductivity and thermal stability. Compos. A Appl. Sci. Manuf. **38**(12), 2527–2535 (2007)
76. Guthy, C., Du, F., Brand, S., Winey, K.I., Fischer, J.E.: Thermal conductivity of single-walled carbon nanotube/PMMA nanocomposites. J. Heat Transfer **129**(8), 1096–1099 (2007)
77. Choi, E.S., Brooks, J.S., Eaton, D.L., Al-Haik, M.S., Hussaini, M.Y., Garmestani, H., Li, D., Dahmen, K.: Enhancement of thermal and electrical properties of carbon nanotube polymer composites by magnetic field processing. J. Appl. Phys. **94**(9), 6034–6039 (2003)
78. Du, F., Guthy, C., Kashiwagi, T., Fischer, J.E., Winey, K.I.: An infiltration method for preparing single-wall nanotube/epoxy composites with improved thermal conductivity. J. Polym. Sci., Part B: Polym. Phys. **44**(10), 1513–1519 (2006)
79. Kiliaris, P., Papaspyrides, C.D.: Polymer/layered silicate (clay) nanocomposites: an overview of flame retardancy. Prog. Polym. Sci. **35**(7), 902–958 (2010)
80. Levchik, S.V.: Introduction to flame retardancy and polymer flammability. In: Flame Retardant Polymer Nanocomposites, pp. 1–29. (2007)
81. Koo, J.H., Pilato, L.A.: Polymer nanostructured materials for high temperature applications. SAMPE J. **41**(2), 7–19 (2005)
82. Pavlidou, S., Papaspyrides, C.D.: A review on polymer–layered silicate nanocomposites. Prog. Polym. Sci. **33**(12), 1119–1198 (2008)
83. Yano, K., Usuki, A., Okada, A., Kurauchi, T., Kamigaito, O.: Synthesis and properties of polyimide–clay hybrid. J. Polym. Sci. Part A: Polym. Chem. **31**(10), 2493–2498 (1993)
84. Lange, J., Wyser, Y.: Recent innovations in barrier technologies for plastic packaging—a review. Packaging Technol. Sci: Int. J. **16**(4), 149–158 (2003)
85. Koh, H.C., Park, J.S., Jeong, M.A., Hwang, H.Y., Hong, Y.T., Ha, S.Y., Nam, S.Y.: Preparation and gas permeation properties of biodegradable polymer/layered silicate nanocomposite membranes. Desalination **233**(1–3), 201–209 (2008)
86. Ranjan S, Dasgupta N, Lichtfouse E. (eds).: Nanoscience in Food and Agriculture, 1st edn. Cham, Springer International Publishing (2016)
87. Adame, D., Beall, G.W.: Direct measurement of the constrained polymer region in polyamide/clay nanocomposites and the implications for gas diffusion. Appl. Clay Sci. **42**(3–4), 545–552 (2009)
88. Olad, A., Rashidzadeh, A.: Preparation and anticorrosive properties of PANI/Na-MMT and PANI/O-MMT nanocomposites. Prog. Org. Coat. **62**(3), 293–298 (2008)
89. Jeon, I.Y., Baek, J.B.: Nanocomposites derived from polymers and inorganic nanoparticles. Materials **3**(6), 3654–3674 (2010)
90. Ajayan, P.M., Schadler, L.S., Braun, P.V.: Nanocomposite Science and Technology. Wiley (2006)
91. Tanahashi, M.: Development of fabrication methods of filler/polymer nanocomposites: With focus on simple melt-compounding-based approach without surface modification of nanofillers. Materials **3**(3), 1593–1619 (2010)

92. Velasco, J.I., Ardanuy, M., Antunes, M.: Layered double hydroxides (LDHs) as functional fillers in polymer nanocomposites. In: Advances in Polymer Nanocomposites, pp. 91–130. Woodhead Publishing (2012)
93. Rehab, A., Salahuddin, N.: Nanocomposite materials based on polyurethane intercalated into montmorillonite clay. Mater. Sci. Eng. A **399**(1–2), 368–376 (2005)
94. Song, W., Zheng, Z., Tang, W., Wang, X.: A facile approach to covalently functionalized carbon nanotubes with biocompatible polymer. Polymer **48**(13), 3658–3663 (2007)
95. Hlavatý, V., Oya, A.: Intercalation of methacrylamide into sodium, calcium and alkylammonium exchanged montmorillonites. Appl. Clay Sci. **9**(3), 199–210 (1994)
96. Jannapu Reddy, R.: Preparation, characterization and properties of injection molded graphene nanocomposites. Doctoral Dissertation, Wichita State University (2010)
97. Gojny, F.H., Wichmann, M.H.G., Köpke, U., Fiedler, B., Schulte, K.: Carbon nanotube-reinforced epoxy-composites: enhanced stiffness and fracture toughness at low nanotube content. Compos. Sci. Technol. **64**(15), 2363–2371 (2004)
98. Moisala, A., Li, Q., Kinloch, I.A., Windle, A.H.: Thermal and electrical conductivity of single-and multi-walled carbon nanotube-epoxy composites. Compos. Sci. Technol. **66**(10), 1285–1288 (2006)
99. Ma, P.C., Kim, J.K., Tang, B.Z.: Effects of silane functionalization on the properties of carbon nanotube/epoxy nanocomposites. Compos. Sci. Technol. **67**(14), 2965–2972 (2007)
100. Lee, H.S., Choi, M.Y., Srinivasan, A., Baek, D.H., Seo, S.W.: Microphase structure and physical properties of polyurethane/organoclay nanocomposites. In: Abstracts of Papers of the American Chemical Society, vol. 228, pp. U466-U466. 1155 16th ST, NW, Washington, USA (Aug, 2004)
101. Vaia, R.A., Ishii, H., Giannelis, E.P.: Synthesis and properties of two-dimensional nanostructures by direct intercalation of polymer melts in layered silicates. Chem. Mater. **5**(12), 1694–1696 (1993)
102. Yang, F., Ou, Y., Yu, Z.: Polyamide 6/silica nanocomposites prepared by in situ polymerization. J. Appl. Polym. Sci. **69**(2), 355–361 (1998)
103. Caseri, W.R.: Nanocomposites of polymers and inorganic particles: preparation, structure and properties. Mater. Sci. Technol. **22**(7), 807–817 (2006)
104. Althues, H., Henle, J., Kaskel, S.: Functional inorganic nanofillers for transparent polymers. Chem. Soc. Rev. **36**(9), 1454–1465 (2007)
105. Omanovic-Miklicanin, E., Badnjevic, A., Kazlagic, A., Hajlovac, M.: Nanocomposites: a brief review. Heal. Technol. **10**, 51–59 (2020)
106. Philip, P., Jose, E.T., Chacko, J.K., Philip, K.C., Thomas, P.C.: Preparation and characterisation of surface roughened PMMA electrospun nanofibers from PEO-PMMA polymer blend nanofibers. Polym. Testing **74**, 257–265 (2019)
107. Pereao, O.K., Bode-Aluko, C., Ndayambaje, G., Fatoba, O., Petrik, L.F.: Electrospinning: polymer nanofibre adsorbent applications for metal ion removal. J. Polym. Environ. **25**(4), 1175–1189 (2017)
108. Wang, C., Fang, C.Y., Wang, C.Y.: Electrospun poly (butylene terephthalate) fibers: entanglement density effect on fiber diameter and fiber nucleating ability towards isotactic polypropylene. Polymer **72**, 21–29 (2015)
109. Raghavan, P., Lim, D.H., Ahn, J.H., Nah, C., Sherrington, D.C., Ryu, H.S., Ahn, H.J.: Electrospun polymer nanofibers: the booming cutting edge technology. React. Funct. Polym. **72**(12), 915–930 (2012)
110. Pereao, O., Bode-Aluko, C., Laatikainen, K., Nechaev, A., Petrik, L.: Morphology, modification and characterisation of electrospun polymer nanofiber adsorbent material used in metal ion removal. J. Polym. Environ. **27**, 1843–1860 (2019)
111. Putz, K.W., Compton, O.C., Palmeri, M.J., Nguyen, S.T., Brinson, L.C.: High-nanofiller-content graphene oxide–polymer nanocomposites via vacuum-assisted self-assembly. Adv. Func. Mater. **20**(19), 3322–3329 (2010)
112. Wang, D., Kou, R., Choi, D., Yang, Z., Nie, Z., Li, J., Saraf, L.V., Hu, D., Zhang, J., Graff, G.L., Liu, J., Pope, M.A., Aksay, I.A.: Ternary self-assembly of ordered metal oxide-graphene nanocomposites for electrochemical energy storage. ACS Nano **4**(3), 1587–1595 (2010)

113. Moniruzzaman, M., Winey, K.I.: Polymer nanocomposites containing carbon nanotubes. Macromolecules **39**(16), 5194–5205 (2006)
114. Ma, P.X., Zhang, R.: Synthetic nano-scale fibrous extracellular matrix. J. Biomed. Mater. Res.: Official J. Soc. Biomater. Jpn. Soc. Biomater. Aust. Soc. Biomater. **46**(1), 60–72 (1999)
115. Grossiord, N., Loos, J., Regev, O., Koning, C.E.: Toolbox for dispersing carbon nanotubes into polymers to get conductive nanocomposites. Chem. Mater. **18**(5), 1089–1099 (2006)
116. Razzaz, A., Ghorban, S., Hosayni, L., Irani, M., Aliabadi, M.: Chitosan nanofibers functionalized by TiO_2 nanoparticles for the removal of heavy metal ions. J. Taiwan Inst. Chem. Eng. **58**, 333–343 (2016)
117. Zhang, Q., Du, Q., Hua, M., Jiao, T., Gao, F., Pan, B.: Sorption enhancement of lead ions from water by surface charged polystyrene-supported nano-zirconium oxide composites. Environ. Sci. Technol. **47**(12), 6536–6544 (2013)
118. Xia, H., Wang, Q., Li, K., Hu, G.H.: Preparation of polypropylene/carbon nanotube composite powder with a solid-state mechanochemical pulverization process. J. Appl. Polym. Sci. **93**(1), 378–386 (2004)
119. Masuda, J.I., Torkelson, J.M.: Dispersion and major property enhancements in polymer/multiwall carbon nanotube nanocomposites via solid-state shear pulverization followed by melt mixing. Macromolecules **41**(16), 5974–5977 (2008)
120. Vigolo, B., Penicaud, A., Coulon, C., Sauder, C., Pailler, R., Journet, C., Bernier, P., Poulin, P.: Macroscopic fibers and ribbons of oriented carbon nanotubes. Science **290**(5495), 1331–1334 (2000)
121. Mamedov, A.A., Kotov, N.A., Prato, M., Guldi, D.M., Wicksted, J.P., Hirsch, A.: Molecular design of strong single-wall carbon nanotube/polyelectrolyte multilayer composites. Nat. Mater. **1**(3), 190–194 (2002)
122. Wardle, B.L., Saito, D.S., Garcia, E.J., Hart, A.J., de Villoria, R.G., Verploegen, E.A.: Fabrication and characterization of ultrahigh-volume-fraction aligned carbon nanotube—polymer composites. Adv. Mater. **20**(14), 2707–2714 (2008)
123. Hristozov, D., Malsch, I.: Hazards and risks of engineered nanoparticles for the environment and human health. Sustainability **1**(4), 1161–1194 (2009)
124. Hedmer, M., Kåredal, M., Gustavsson, P., Rissler, J.: Carbon nanotubes. Arbete och H€alsa. Occupational and Environmental Medicine at Sahlgrenska Academy, p. 252. University of Gothenburg (2013)
125. Meador, M.: A future needs and opportunities in nanotechnology for aerospace applications: a NASA perspective. In: National Institute of Aerospace Nanotechnology Workshop Hampton, (Feb, 2014) VA
126. Gorinevsky, D., Hyde, T.T.: Adaptive membrane for large lightweight space telescopes. In: Highly Innovative Space Telescope Concepts, vol. 4849, pp. 330–338. International Society for Optics and Photonics (Dec, 2002)
127. Joshi, M., Chatterjee, U.: Polymer nanocomposite: an advanced material for aerospace applications. In: Advanced Composite Materials for Aerospace Engineering, pp. 241–264. Woodhead Publishing (2016)
128. Siegel, R.W., Chang, S.K., Ash, B.J., Stone, J.A.P.M., Ajayan, P.M.: Mechanical behavior of polymer and ceramic matrix nanocomposites. Scripta Mater. **44**(8–9), 2061–2064 (2001)
129. Poulin, P., Vigolo, B., Launois, P.: Films and fibers of oriented single wall nanotubes. Carbon **40**(10), 1741–1749 (2002)
130. Zhu, J., Wilkie, C.A.: Thermal and fire studies on polystyrene—clay nanocomposites. Polym. Int. **49**(10), 1158–1163 (2000)
131. Zhu, J., Start, P., Kenneth, A.: Mauritz. Thermal stability and flame retardancy of PMMA-clay nanocomposites. Polym. Degrad. Stab. **77**, 253–258 (2002)
132. Anadão, P.: Polymer/clay Nanocomposites: Concepts, Researches, Applications and Trends for the Future, pp. 1–16. New Trends and Developments, Nanocomposites (2012)
133. Kawasumi, M.: The discovery of polymer-clay hybrids. J. Polym. Sci. Part A: Polym. Chem. **42**(4), 819–824 (2004)

134. Gul, S., Kausar, A., Muhammad, B., Jabeen, S.: Research progress on properties and applications of polymer/clay nanocomposite. Polym.-Plast. Technol. Eng. **55**(7), 684–703 (2016)
135. Mueller, N.C., van der Bruggen, B., Keuter, V., Luis, P., Melin, T., Pronk, W., Reisewitz, R., Rickerby, D., Rios, G.M., Wennekes, W., Nowack, B.: Nanofiltration and nanostructured membranes—should they be considered nanotechnology or not? J. Hazard. Mater. **211**, 275–280 (2012)
136. Pendergast, M.M., Ghosh, A.K., Hoek, E.M.V.: Separation performance and interfacial properties of nanocomposite reverse osmosis membranes. Desalination **308**, 180–185 (2013)
137. Humplik, T., Lee, J., O'hern, S.C., Fellman, B.A., Baig, M.A., Hassan, S.F., Atieh, M.A., Rahman, F., Laoui, T., Karnik, R., Wang, E.N.: Nanostructured materials for water desalination. Nanotechnology **22**(29), 292001 (2011)
138. Das, R., Ali, M.E., Abd Hamid, S.B., Ramakrishna, S., Chowdhury, Z.Z.: Carbon nanotube membranes for water purification: a bright future in water desalination. Desalination **336**, 97–109 (2014)
139. Zhang, L., Shi, G.Z., Qiu, S., Cheng, L.H., Chen, H.L.: Preparation of high-flux thin film nanocomposite reverse osmosis membranes by incorporating functionalized multi-walled carbon nanotubes. Desalin. Water Treat. **34**(1–3), 19–24 (2011)
140. Ho, W., Sirkar, K.: Membrane Handbook. Springer Science & Business Media (2012)
141. Liang, C.Y., Uchytil, P., Petrychkovych, R., Lai, Y.C., Friess, K., Sipek, M., Reddy, M.M., Suen, S.Y.: A comparison on gas separation between PES (polyethersulfone)/MMT (Na-montmorillonite) and PES/TiO2 mixed matrix membranes. Sep. Purif. Technol. **92**, 57–63 (2012)
142. Lua, A.C., Shen, Y.: Preparation and characterization of polyimide—silica composite membranes and their derived carbon–silica composite membranes for gas separation. Chem. Eng. J. **220**, 441–451 (2013)
143. Zornoza, B., Téllez, C., Coronas, J.: Mixed matrix membranes comprising glassy polymers and dispersed mesoporous silica spheres for gas separation. J. Membr. Sci. **368**(1–2), 100–109 (2011)
144. Zhao, Y., Jung, B.T., Ansaloni, L., Ho, W.W.: Multiwalled carbon nanotube mixed matrix membranes containing amines for high pressure CO2/H2 separation. J. Membr. Sci. **459**, 233–243 (2014)
145. Kim, H.W., Yoon, H.W., Yoon, S.M., Yoo, B.M., Ahn, B.K., Cho, Y.H., Shin, H.J., Yang, H., Paik, U., Kwon, S., Choi, J.Y., Park, H.B.: Selective gas transport through few-layered graphene and graphene oxide membranes. Science **342**(6154), 91–95 (2013)
146. Shen, J., Liu, G., Huang, K., Jin, W., Lee, K.R., Xu, N.: Membranes with fast and selective gas-transport channels of laminar graphene oxide for efficient CO_2 capture. Angew. Chem. **127**(2), 588–592 (2015)
147. Akharame, M.O., Oputu, O.U., Pereao, O., Fagbayigbo, B.O., Razanamahandry, L.C., Opeolu, B.O., Fatoki, O.S.: Nanostructured Polymer Composites for Water Remediation. In: Nanostructured Materials for Treating Aquatic Pollution, pp. 275–306. Springer, Cham (2019)
148. Rekos, K., Kampouraki, Z.C., Sarafidis, C., Samanidou, V., Deliyanni, E.: Graphene oxide based magnetic nanocomposites with polymers as effective bisphenol–a nanoadsorbents. Materials **12**(12), 1987 (2019)
149. He, T., Wang, L., Fabregat-Santiago, F., Liu, G., Li, Y., Wang, C., Guan, R.: Electron trapping induced electrostatic adsorption of cations: a general factor leading to photoactivity decay of nanostructured TiO_2. J. Mater. Chem. A **5**(14), 6455–6464 (2017)
150. Wang, H., Wang, Y.N., Sun, Y., Pan, X., Zhang, D., Tsang, Y.F.: Differences in Sb (V) and As (V) adsorption onto a poorly crystalline phyllomanganate (d-MnO_2): adsorption kinetics, isotherms, and mechanisms. Process Saf. Environ. Prot. **113**, 40–47 (2018)
151. Oves, M., Ansari, M.O., Khan, M.Z., Shahadat, M., Ismail, I.M.: Modern Age Waste Water Problems. Springer International Publishing (2020)

152. Ahmad, J., Deshmukh, K., Hägg, M.B.: Influence of TiO_2 on the chemical, mechanical, and gas separation properties of polyvinyl alcohol-titanium dioxide (PVA-TiO2) nanocomposite membranes. Int. J. Polym. Anal. Charact. **18**(4), 287–296 (2013)
153. Šupová, M., Martynková, G.S., Barabaszová, K.: Effect of nanofillers dispersion in polymer matrices: a review. Sci. Adv. Mater. **3**(1), 1–25 (2011)
154. Yan, L., Hong, S., Li, M.L., Li, Y.S.: Application of the Al_2O_3–PVDF nanocomposite tubular ultrafiltration (UF) membrane for oily wastewater treatment and its antifouling research. Sep. Purif. Technol. **66**(2), 347–352 (2009)
155. Liang, B., Zhang, P., Wang, J., Qu, J., Wang, L., Wang, X., Guan, C., Pan, K.: Membranes with selective laminar nanochannels of modified reduced graphene oxide for water purification. Carbon **103**, 94–100 (2016)
156. Yin, J., Zhu, G., Deng, B.: Graphene oxide (GO) enhanced polyamide (PA) thin-film nanocomposite (TFN) membrane for water purification. Desalination **379**, 93–101 (2016)
157. Abdullah, N., Gohari, R.J., Yusof, N., Ismail, A.F., Juhana, J., Lau, W.J., Matsuura, T.: Polysulfone/hydrous ferric oxide ultrafiltration mixed matrix membrane: preparation, characterization and its adsorptive removal of lead (II) from aqueous solution. Chem. Eng. J. **289**, 28–37 (2016)
158. Ghaemi, N.: A new approach to copper ion removal from water by polymeric nanocomposite membrane embedded with γ-alumina nanoparticles. Appl. Surf. Sci. **364**, 221–228 (2016)
159. Jo, Y.J., Choi, E.Y., Choi, N.W., Kim, C.K.: Antibacterial and hydrophilic characteristics of poly (ether sulfone) composite membranes containing zinc oxide nanoparticles grafted with hydrophilic polymers. Ind. Eng. Chem. Res. **55**(28), 7801–7809 (2016)
160. Huang, P., Ye, L.: In situ polymerization of cationic polyacrylamide/montmorillonite composites and its flocculation characteristics. J. Thermoplast. Compos. Mater. **29**(1), 58–73 (2016)
161. Xie, P., de Lannoy, C.F., Ma, J., Wang, Z., Wang, S., Li, J., Wiesner, M.R.: Improved chlorine tolerance of a polyvinyl pyrrolidone-polysulfone membrane enabled by carboxylated carbon nanotubes. Water Res. **104**, 497–506 (2016)
162. Lee, J., Ye, Y., Ward, A.J., Zhou, C., Chen, V., Minett, A.I., Lee, S., Liu, Z., Chae, S.R., Shi, J.: High flux and high selectivity carbon nanotube composite membranes for natural organic matter removal. Sep. Purif. Technol. **163**, 109–119 (2016)
163. Thomas, S., Mishra, R.K., Asiri, A.M. (eds.): Sustainable Polymer Composites and Nanocomposites. Springer (2019)
164. Akharame, M.O., Fatoki, O.S., Opeolu, B.O., Olorunfemi, D.I., Oputu, O.U.: Polymeric nanocomposites (PNCs) for wastewater remediation: an overview. Polym.-Plast. Technol. Eng. **57**(17), 1801–1827 (2018)
165. Palit, S.: Nanomaterials for Industrial Wastewater Treatment and Water Purification. Handbook of Ecomaterials, Springer, Cham (2017)
166. Goei, R., Dong, Z., Lim, T.T.: High-permeability pluronic-based TiO_2 hybrid photocatalytic membrane with hierarchical porosity: fabrication, characterizations and performances. Chem. Eng. J. **228**, 1030–1039 (2013)
167. Raoufi, N., Surre, F., Rajarajan, M., Sun, T., Grattan, K.T.: Optical sensor for pH monitoring using a layer-by-layer deposition technique emphasizing enhanced stability and re-usability. Sens. Actuators, B Chem. **195**, 692–701 (2014)
168. Hsu, L., Selvaganapathy, P.R., Brash, J., Fang, Q., Xu, C.Q., Deen, M.J., Chen, H.: Development of a low-cost hemin-based dissolved oxygen sensor with anti-biofouling coating for water monitoring. IEEE Sens. J. **14**(10), 3400–3407 (2014)
169. Gutiérrez-Capitán, M., Baldi, A., Gómez, R., García, V., Jimenez-Jorquera, C., Fernández-Sánchez, C.: Electrochemical nanocomposite-derived sensor for the analysis of chemical oxygen demand in urban wastewaters. Anal. Chem. **87**(4), 2152–2160 (2015)
170. Pelaez, M., Nolan, N.T., Pillai, S.C., Seery, M.K., Falaras, P., Kontos, A.G., Dunlop, P.S.M., Hamilton, J.W.J., Byrne, J.A., O'Shea, K., Entezari, M.H., Dionysiou, D.D.: A review on the visible light active titanium dioxide photocatalysts for environmental applications. Appl. Catal. B **125**, 331–349 (2012)

171. Yuan, Y., Liu, F., Xue, L., Wang, H., Pan, J., Cui, Y., Chen, H., Yuan, L.: Recyclable escherichia coli-specific-killing AuNP–polymer (ESKAP) nanocomposites. ACS Appl. Mater. Interfaces. **8**(18), 11309–11317 (2016)
172. Ma, P.X.: Scaffolds for tissue fabrication. Mater. Today **7**(5), 30–40 (2004)
173. Feldman, D.: Polymer nanocomposites in building, construction. J. Macromol Sci, Part A **51**(3), 203–209 (2014)
174. Carretero, M.I., Pozo, M.: Clay and non-clay minerals in the pharmaceutical industry: part I. Excipients and medical applications. Appl. Clay Sci. **46**(1):73–80 (2009)
175. Gajdziok, J., Holešová, S., Štembírek, J., Pazdziora, E., Landová, H., Doležel, P., Vetchý, D.: Carmellose Mucoadhesive Oral Films Containing Vermiculite/Chlorhexidine Nanocomposites as Innovative Biomaterials for Treatment of Oral Infections, p. 580146. BioMed Research International, Article ID (2015)
176. Saraceno, R., Chiricozzi, A., Gabellini, M., Chimenti, S.: Emerging applications of nanomedicine in dermatology. Skin Res. Technol. **19**(1), e13–e19 (2013)
177. Roszek, B., De Jong, W.H., Geertsma, R.E.: Nanotechnology in Medical Applications: State-of-the-Art in Materials and Devices. RIVM report 265001001/2005 (2005)
178. Meaney, J.F., Goyen, M.: Recent advances in contrast-enhanced magnetic resonance angiography. Eur. Radiol. **17:**B2–B6 (2007)
179. Mathiazhagan, A., Joseph, R.: Nanotechnology-a new prospective in organic coating-review. Int. J. Chem. Eng. Appl. **2**(4), 225–237 (2011)
180. Gacitua, W., Ballerini, A., Zhang, J.: Polymer nanocomposites: synthetic and natural fillers a review. Maderas. Ciencia Y Tecnología **7**(3), 159–178 (2005)
181. Majeed, K., Jawaid, M., Hassan, A.A.B.A.A., Bakar, A.A., Khalil, H.A., Salema, A.A., Inuwa, I.: Potential materials for food packaging from nanoclay/natural fibres filled hybrid composites. Mater. Des. **46**, 391–410 (2013)
182. Pourjavadi, A., Fakoorpoor, S.M., Hosseini, P., Khaloo, A.: Interactions between superabsorbent polymers and cement-based composites incorporating colloidal silica nanoparticles. Cement Concr. Compos. **37**, 196–204 (2013)
183. Al-Safy, R., Al-Mahaidi, R., Simon, G.P., Habsuda, J.: Experimental investigation on the thermal and mechanical properties of nanoclay-modified adhesives used for bonding CFRP to concrete substrates. Constr. Build. Mater. **28**(1), 769–778 (2012)
184. Amini, R.S., Tirri, T., Wilen, C.E.: Synthesis and characterization of polyurethane (PU)/clay nanocomposite adhesives. J. Appl. Polym. Sci. **129**, 1678–1685 (2013)
185. Scarfato, P., Di Maio, L., Fariello, M.L., Russo, P., Incarnato, L.: Preparation and evaluation of polymer/clay nanocomposite surface treatments for concrete durability enhancement. Cement Concr. Compos. **34**(3), 297–305 (2012)
186. Korkin, A., Rosei, F. (eds.): Nanoelectronics and Photonics: from Atoms to Materials, Devices, and Architectures. Springer Science & Business Media (2008)

Machining of Nano-Structured Polymer Composites

Bao Le, Islam Shyha, and Dehong Huo

Abstract Nanocomposites have been discovered and researched for over 60 years due to their advanced characteristics such as mechanical, thermal and electrical properties compared to other materials (i.e., metals, ceramics and alloys). Among the most functional nanomaterials, polymer nanocomposites have found many industrial applications, especially as structural materials. Although near-net-shape (NNS) manufacturing processes could be employed to fabricate these materials, higher qualities in terms of machine surface and dimensional accuracy, especially in complex features are still required since they are crucial requirements in modern manufacturing. Therefore, machining seems to be an inevitable process and have found huge potential to generate high-precision products. However, machining of polymer nanocomposites is more severe than that of other materials due to their anisotropic, heterogeneous structure and high mechanical properties (i.e., high abrasiveness, fracture toughness, tensile strength) of their reinforcing constituents. These factors could result in low machined surface quality, typical damages introduced into the machined surfaces and tool wear acceleration. Therefore, investigation on machining behaviours of these polymer nanocomposites is necessary to provide suitable cutting conditions. This chapter addresses these materials' machinability when using major machining processes, including conventional, non-conventional, and micromachining.

B. Le (✉)
Mechanical and Construction Engineering Department, Northumbria University, Newcastle upon Tyne NE1 8ST, UK
e-mail: bao.le@northumbria.ac.uk

I. Shyha
Mechanical Engineering and Design, School of Engineering and the Built Environment, Edinburgh Napier University, Edinburgh EH10 5DT, UK

D. Huo
Mechanical Engineering, School of Engineering, Newcastle University, Newcastle upon Tyne NE1 7RU, UK

I. Shyha and D. Huo (eds.), *Advances in Machining of Composite Materials*, Engineering Materials, https://doi.org/10.1007/978-3-030-71438-3_14

1 Introduction

Polymer nanocomposites have been applied widely due to their high properties per weight (specific properties) such as strength and stiffness compared to other materials (i.e., metals and their alloys). These characteristics provide enormous potential to manufacture light-weight products using these nanocomposites as structural materials. Conventional machining processes such as milling, turning, or drilling could be employed as a post-processing method to attain higher surface quality and dimensional accuracy. Applying these techniques to polymer nanocomposites shows high flexibility in choosing workpiece materials over other non-conventional methods (i.e., Electrical Discharge Machining (EDM), laser machining) maintaining comparable machining accuracy and productivity. However, the reinforcing materials mostly have higher strength, stiffness, fracture toughness (i.e., carbon nanotube (CNT), graphene) or hardness, abrasiveness (i.e., ceramic nano-fillers) over the matrix materials that make these materials hard to machine or low machinability. It leads to the machining behaviour of these polymer nanocomposites significantly depending on reinforcements' mechanical properties and matrix-filler interphase.

Consequently, critical machinability indicators, including surface roughness, tool wear and tool life have become the main concerns in machining polymer nanocomposites. This chapter will address both conventional and non-conventional machining processes of polymer nanocomposites (Fig. 1).

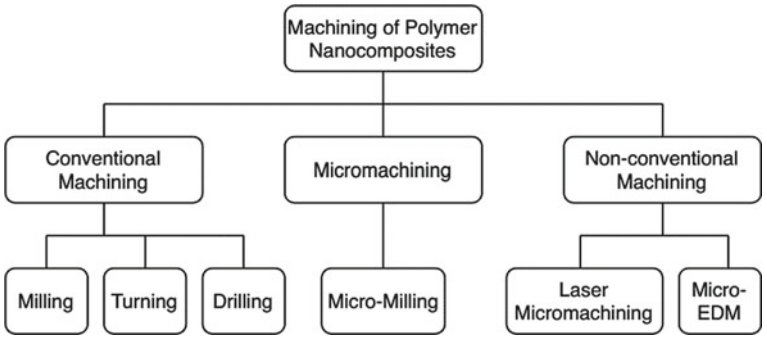

Fig. 1 Classification of machining of polymer nanocomposites

2 Machining of Polymer Nanocomposites

2.1 Polymer Nanocomposites as High-Performance Engineering Materials

The advancement of material science has observed metals and alloys' substitution by polymer composites, mostly fibre-reinforced based (FRP) as high-performance engineering materials. Carbon fibre reinforced polymers (CFRP), glass fibre reinforced polymers (GFRP), and aramid fibre reinforced polymers (AFRP) are the most common polymer composites that have been widely applied to manufacture primary structures in aerospace, marine or automotive industry. The demand for finding other lighter materials while providing comparable or even higher mechanical properties (i.e., stiffness, tensile strength, fatigue strength) than conventional metallic materials is the main reason for this replacement.

The near-net-shape methods (i.e., moulding, shaping) are mostly applied in the productions of FRPs. However, machining as a finishing process is still required if high dimensional accuracy and surface quality are concerned. Figure 2 shows an example of applying polymer composites machining in manufacturing aeroplane wing box structure (stringers and ribs). In this case, machining methods such as milling, or drilling are required to attain high dimensional accuracy (or low tolerance), and surface quality for assembly surfaces.

As the first polymer nanocomposites appeared in the past 50 years or so, these materials have been considered the successor of polymer composites in industrial applications. Polymer nanocomposites are considered as a branch of composite materials. The term "nanocomposite" indicates the size of filler in at least one dimension less than hundreds of nanometres. Similar to polymer composites with macro-sized fillers (hereafter called conventional composites), the most common filler form used in polymer nanocomposites is fibrous such as carbon nano-fibre (CNF), carbon

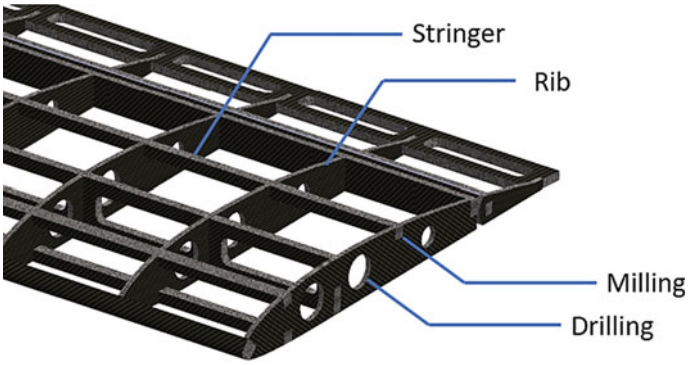

Fig. 2 An example of micromachining of polymer composites in manufacturing aircraft wing box structure

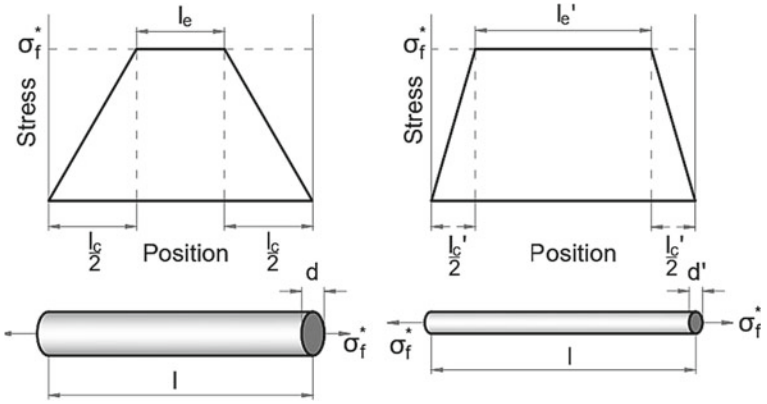

Fig. 3 Effect of fibre diameter on reinforcing efficiency of fibre

nanotube (CNT). Another sheet form like graphene is still considered as fibre. Due to the high mechanical reinforcing efficiency of the fibrous form (stiffness, strength) compared to particles. Fibre size reduction (diameter) can benefit the reinforcing efficiency of mechanical properties due to the aspect ratio (length/diameter). The strengthening efficiency of fibre can be identified based on the critical length:

$$l_c = \frac{\sigma.d}{2\tau} \tag{1}$$

where σ is the ultimate tensile strength of fibre, τ is the shear strength of the fibre-matrix bond, and d is the fibre diameter. For the same fibre length, reducing fibre diameter (d) can reduce the critical length, hence increasing the effective fibre length (l_e) (Fig. 3).

Additionally, the stiffness and strength of nano-fibres are much higher than their conventional counterparts. For example, single-walled carbon nanotubes (SWCNTs) have the stiffness five times higher than carbon fibres. It leads to a much better reinforcing efficiency of these nano-fibres. The rule of the mixture can theoretically estimate this efficiency:

$$E_c = E_m V_m + E_f V_f \tag{2}$$

E and *V* represent elastic modulus and volume fraction, respectively, whereas the subscript c, m, and f denote composite, matrix, and filler. Furthermore, the high filler-matrix bonding of polymer nanocomposites in the molecular level also contributes to these materials' advanced mechanical properties compared with conventional polymer nanocomposites.

However, these advanced properties also make enormous challenges for machining as they are hard to machine. The state-of-the-art machining of polymer nanocomposites has been observed a limited application despite nanocomposites'

high potential as structural materials in many applications (e.g., aircraft components, automobile industry and sporting goods) and research studies had to be undertaken to investigate this in more detail. It is mostly due to their high production cost. Within this chapter's scope, some typical processes of polymer nanocomposites will be discussed, including conventional and non-conventional techniques. In general, surface roughness and surface damage (or integrity) indicate the machinability of materials. For conventional machining, cutting force, tool wear (or damage) should also be considered.

2.2 Milling of Polymer Nanocomposites

Milling is considered as the most common process among conventional machining techniques due to its high feasibility and flexibility when dealing with complex geometries and various materials. Therefore, this machining process is considered feasibly applied for polymer nanocomposites (Fig. 4). The machined surface quality is the most crucial objective when applying the machining process (Fig. 5). The primary adaption is to investigate the surface roughness respond concerning the variations of machining parameters. Feed rate, depth of cut (DoC) and cutting speed are mostly chosen as significant variables like cutting metallic materials.

Additionally, filler content is also considered because of its effect on work-piece structure and mechanical properties. The contributions of these inputs to the machined surface roughness are identified by applying Analysis of Variance (ANOVA) [1] or Taguchi method [2]. Feed rate is the most dominant factor affecting the surface roughness following by cutting speed and DoC while filler content shows the unobvious influence. The variations of surface roughness when milling different polymer nanocomposites as a function of feed rate is shown in Fig. 6.

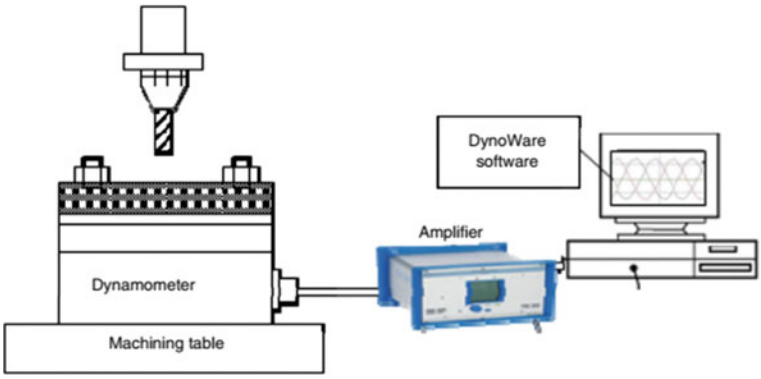

Fig. 4 A typical setup for milling of polymer nanocomposites. Open access from [3]

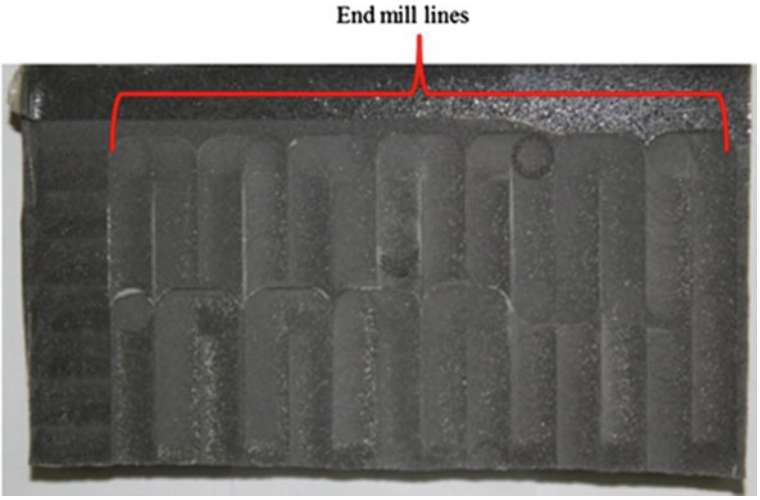

Fig. 5 An example of the machined surface of polymer nanocomposites using end-milling (open access from [2])

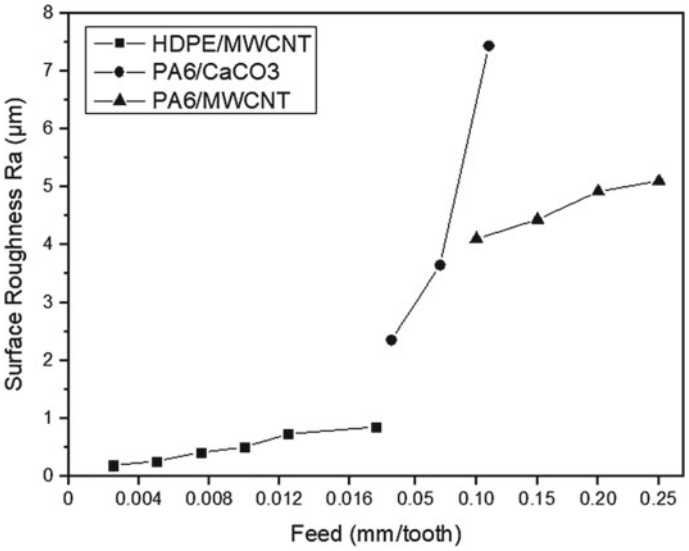

Fig. 6 Effect of feed rate on surface roughness when end-milling polymer nanocomposites (adapted from [4–6])

The behaviour of surface roughness variation when milling polymer nanocomposites is generally similar to metal cutting. The optimal surface quality can be obtained by cutting at low DoC and feed rate levels combined with high cutting speed. The small weight fraction of CNTs or graphene also contributes to surface quality improvement due to their lubricating nature [7]. Additionally, incorporating these nano-fillers into the matrix also plays a crucial role in improving polymer nanocomposites' thermal conductivity, consequently reducing the heat around the cutting area, hence reducing the roughness of the machined surface.

2.3 Drilling of Polymer Nanocomposites

As polymer nanocomposites' commercial applications are still limited due to their high production cost, the drilling applications (Fig. 7) mostly focus on hybrid polymer nanocomposites in which nano-fibres such as MWCNT, CNF are used as secondary reinforcing materials. Since the primary polymer composites are mostly CFRP or GFRP, the delamination is still the main challenge in this machining field. The small addition of nano-fibres (<1 wt.%) can reduce the drilling-induced delamination as they tend to bridge the crack between laminates (Fig. 8), hence improving internal laminate shear strength (ILSS) [8] and fracture toughness [9]. Figure 9 shows some reduction trends of delamination as a function of the nano-fibres addition. However, feed rate and cutting speed effect on these criteria are still dominant while cutting tool diameter shows unobvious influence [10]. In terms of cutting geometry, both twist and split point drills are suitable for this kind of machining (Fig. 10), but the

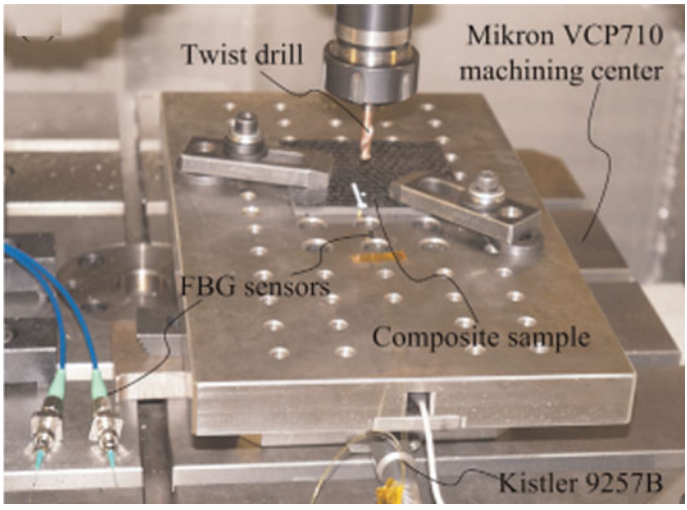

Fig. 7 A setup of drilling epoxy/carbon fibre/MWCNT nanocomposites. Copyright permission from [9]

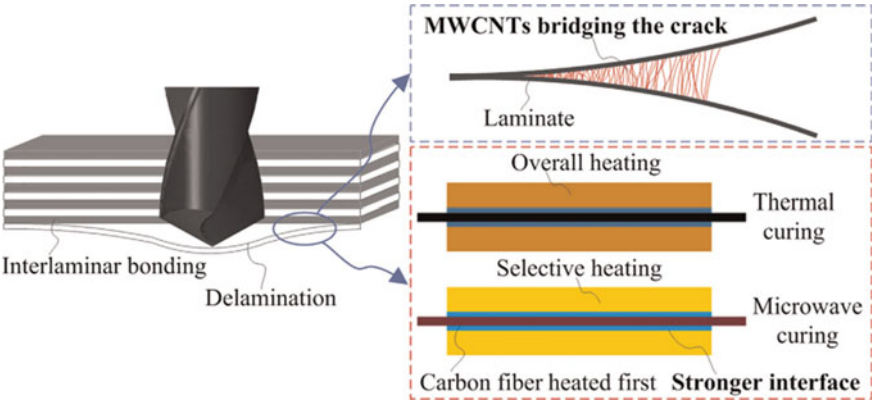

Fig. 8 The schematic represents the role of MWCNTs addition in reducing delamination by bridging the crack during drilling of epoxy/carbon fibre/MWCNT nanocomposites. Copyright from [9]

former type of drill seems to have better performance during the drilling process [11].

The reduction of delamination factor due to the presence of nano-fires consequently leads to better surface quality. Additionally, these hybrid nanocomposites' higher thermal conductivity can also contribute to less thermal damage on the machined surfaces than those without nano-fibres. In terms of machining parameters, feed rate and cutting speed are considered significant factors that affect the surface quality. The mechanism of surface roughness being affected by these variables is identical to drilling metallic materials. The cutting regime with low feed rates and high cutting speeds can generate low cutting forces and less built-up edge (BUE), hence improving the surface quality.

2.4 Turning of Polymer Nanocomposites

Surface roughness is the most critical objective when turning polymer nanocomposites, identical to other mechanical machining techniques (milling, drilling). This machining process shows similar surface roughness behaviour trends as a function of cutting parameters (cutting speed, feed rate, depth of cut) and filler loading. The high cutting forces due to the increase in the cross-sectional area at high feed rates lead to low surface quality. Therefore, the feed rate is considered the most influential factor in surface roughness when turning into polymer nanocomposites. However, the roles of MWCNTs in improving machined surface quality are not apparent although some of the nano-fillers such as MWCNTs [14] or $CaCO_3$ [15] nano-particles have been proved in reducing cutting forces due as lubricants. Figure 11 represents a typical setup for turning of epoxy/MWCNT nanocomposites.

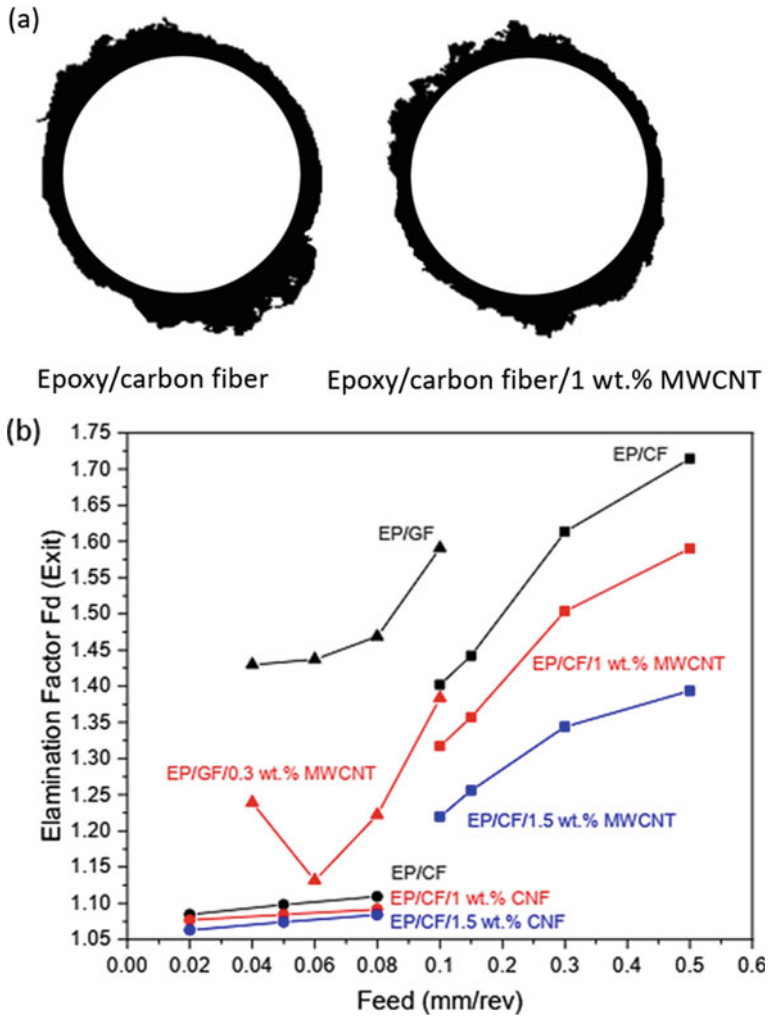

Fig. 9 Delamination in the drilling of polymer hybrid nanocomposites: **a** Computerised tomography depicts delamination from the drilling of epoxy/carbon fibre/MWCNT nanocomposites. Copyright permission from [9]); and **b** The reduction of delamination factor at the exit as a function nano-fibre content (adapted from [8, 12, 13])

3 Mechanical Micromachining of Polymer Nanocomposites

It is seen that the advancement of machining has aimed to improve two main features: (i) higher machining precision/lower tolerance and (ii) smaller feature size or miniaturization [16] which are critical requirements from modern manufacturing. The former refers to ultra-precision machining while the latter indicates mechanical micromachining. However, these two processes share some common

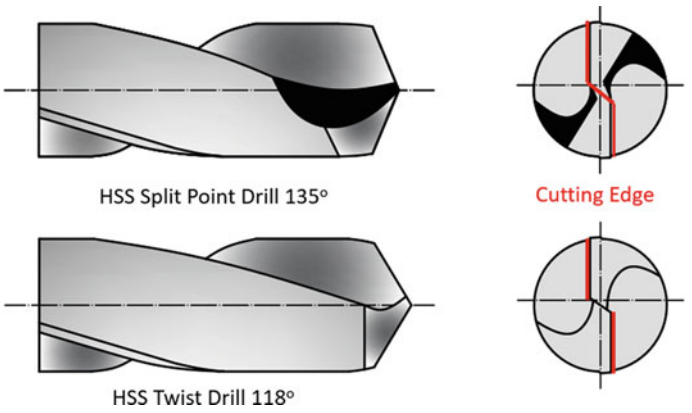

Fig. 10 Examples of tools used for drilling of polymer nanocomposites

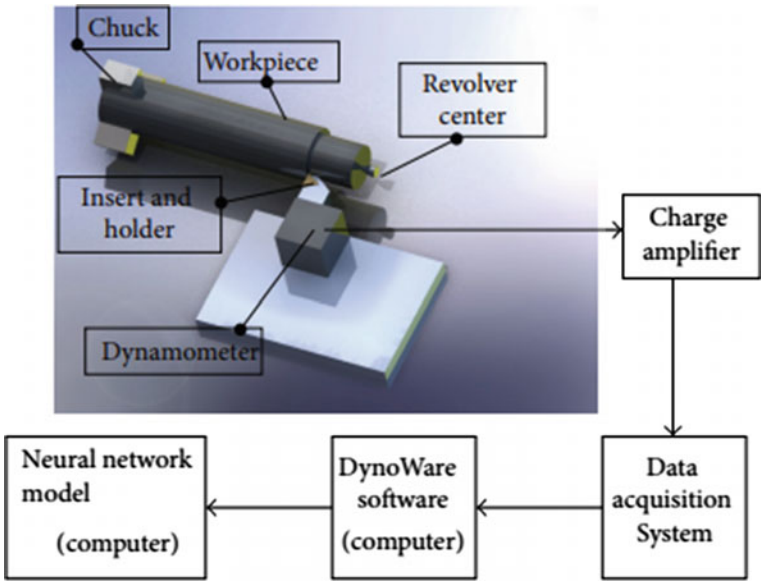

Fig. 11 A schematic represents the experimental setup of turning epoxy/MWCNT nanocomposites. Open access from [15]

characteristics such as uncut chip thickness (UCT), chip formation and specific cutting forces. Within the scope of this chapter, both terms will be referred to as micromachining. Some standard techniques, including micro-milling, micro-turning, and micro-drilling of polymer nanocomposites, are mentioned. In the context of

nanocomposites being commercially applied, the needs of employing micromachining techniques to generate high-quality products in terms of dimensional accuracy, surface quality with from polymer nanocomposites deem to be necessary (Fig. 12).

Micromachining generally exhibits the same material removal mechanism as conventional machining with the physical contact between the mechanical cutting tool and workpiece. However, the miniaturization of a machine tool to attain micro-ranges of UCT leads to some critical differences called 'size effects' between these two techniques. Therefore, it seems necessary to illuminate the fundamentals of mechanical micromachining and its distinct features compared to conventional methods (drilling, turning or milling) (Sect. 3.1). The subsequent studies on micromachining of polymer nanocomposites are discussed in the next Sects. (3.2 to 3.4). The main conclusions and limitations from micromachining polymer nanocomposites research are indicated as their critical importance in prospects.

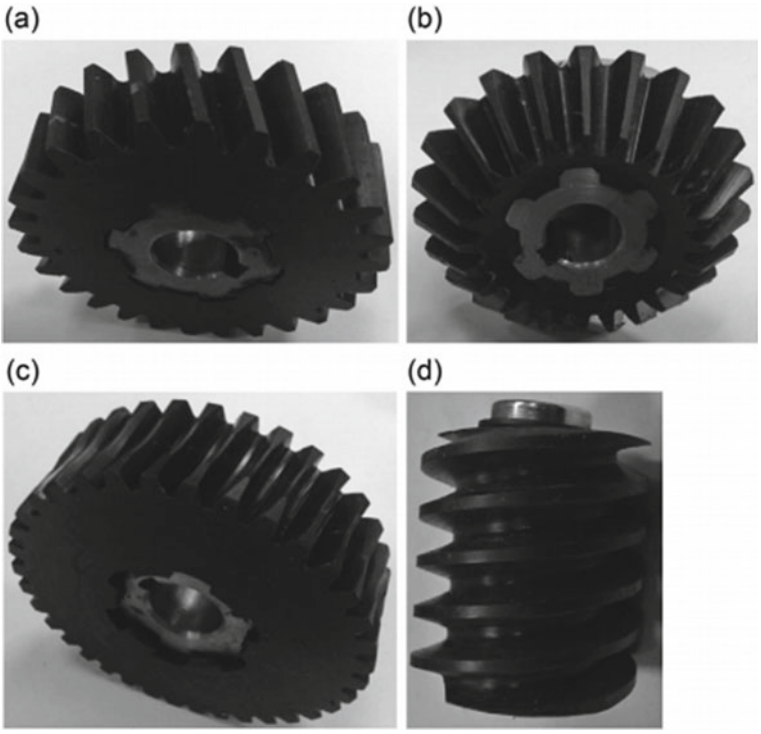

Fig. 12 Applications of micromachining of polymer nanocomposites: **a** a CNT/acetal helical gear, **b** a CNT/acetal bevel gear, **c** a CNT/acetal wheel gear, **d** a CNT/acetal worm gear. Copyright permission from [17]

3.1 Removal Mechanisms of Micromachining and Differences from Macro-Scale

In general, micromachining is considered a miniaturized version of conventional machining as they share the common kinematic cutting mechanism. However, some critical issues regarding the size effects appear when downscaling the UCT into comparable values with cutting edge radius or grain size. It leads to the dominant effects of workpiece microstructure and minimum uncut chip thickness (MUCT) which are usually neglected in macro-scale machining.

Microstructure Effect

In conventional machining at macro-scale, microstructure effect is mostly neglected as the material removal rate (MRR) is relatively high. Work-piece material, in this case, is assumed to be homogenous and isotropic. However, when the micro cutting-tool is employed in micromachining, the cutting edge radius approaches the grain size of material; hence this assumption is no longer valid. The required specific cutting force [18] or specific cutting energy [19] during the micromachining process, hence become higher due to the tool breaking individual grains bonding by atom forces (Fig. 13). It also leads to the cutting force variation as the tool passing between grain boundaries. The schematic representing these differences between micromachining and conventional machining in terms of microstructure effect is shown in Fig. 14. The grain boundary effects on cutting forces [20] or machined surface morphology

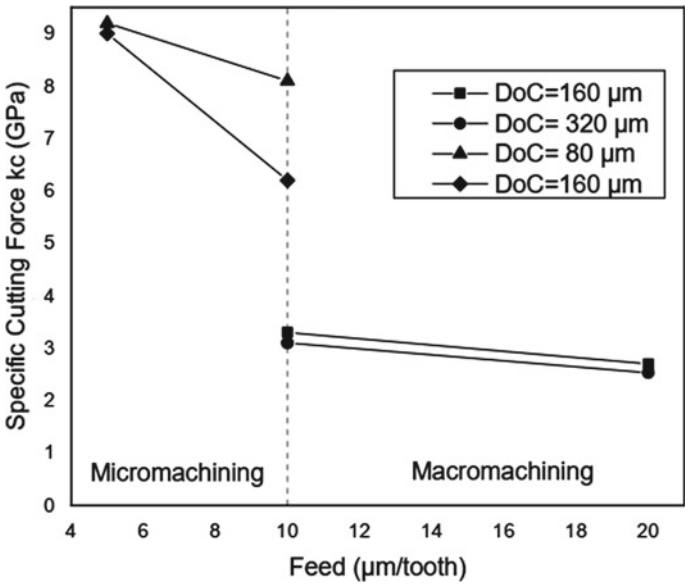

Fig. 13 Comparison of specific cutting force between micro and macro-milling of AISI 1045 Steel (adapted from [18])

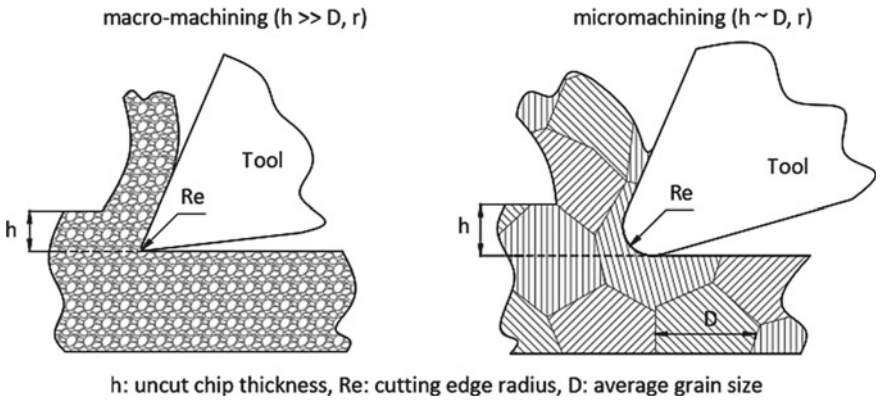

Fig. 14 Microstructure effect in micromachining resulting from the low ratio between UCT to cutting edge radius and grain size. adapted from [22]

[21] have also been investigated. Micromachining of single-phase materials and multiphase materials has been investigated to clarify the microstructure's effects on machining key indicators.

The different elastic recoveries [23], unbalance plastic strains [24], or the burr formations at the grain boundary [25] in these multiphase materials were claimed to be the main reasons for high cutting force variations as well as low surface quality (Fig. 15).

Minimum Uncut Chip Thickness (MUCT) and Cutting Edge Radius

Uncut chip thickness (UCT) and its correlation with cutting edge radius identify the fundamental distinction between macro and micro-machining. UCT is miniaturized in micro-machining; its values become comparable with cutting edge radius, leading to the difference in cutting mechanism from conventional machining. If these values are below a minimum uncut chip thickness (MUCT), there is no material being removed and subsequently, no chip formation.

It is observed from Fig. 16 that when UCT is much greater than MUCT and cutting edge radius in case of macro-machining, the cutting mechanism mostly occur as shearing. Due to the meagre ratio between cutting edge radius and UCT (r/h), the cutting tool is considered as ideally sharp, and the effect of cutting edge radius is ignored. However, when reducing UCT into micro-range in micro-machining. UCT, in this case, becomes comparable with cutting edge radius. The workpiece material is now both sheared and ploughed due to the considerable effect of cutting edge radius. A further reduction of UCT values below MUCT (hm) makes the material removal unfeasible, leading to the ploughing-dominant regime.

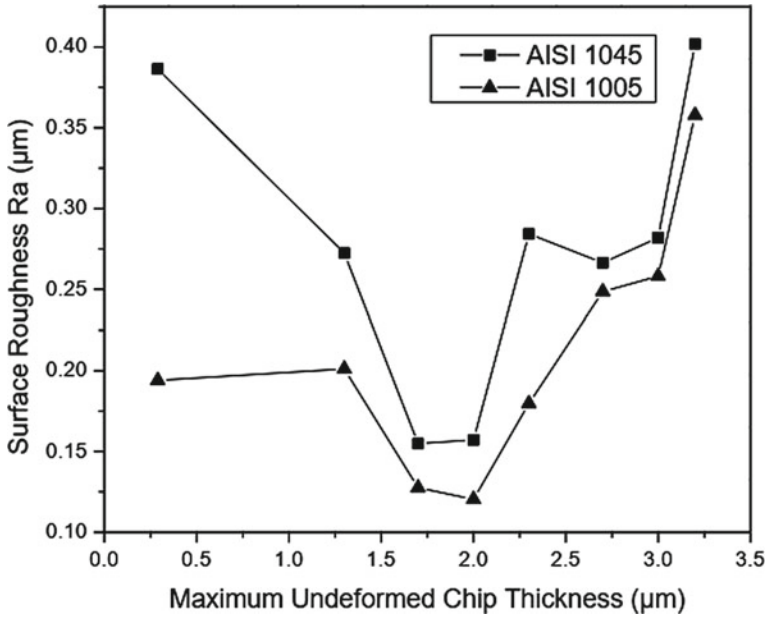

Fig. 15 Effect of microstructure on surface quality when micro-milling steel at a spindle speed of 30,000 rpm and DoC of 75 μm adapted from [23]

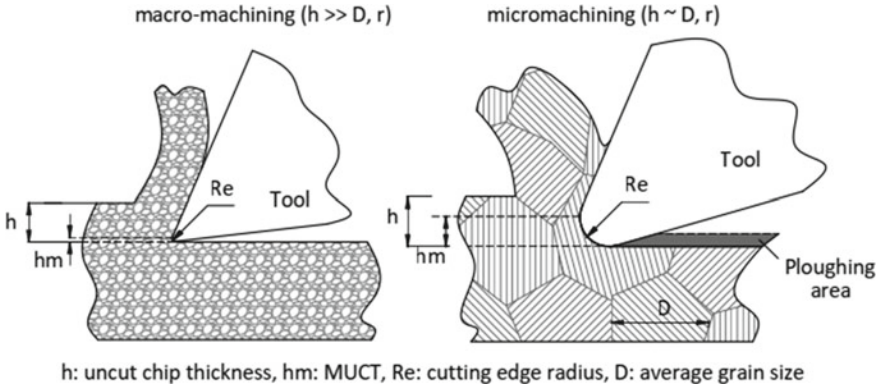

Fig. 16 Size effect affecting cutting mechanism as uncut chip thickness being reduced. adapted from [22]

3.2 Micromachining of Polymer Nanocomposites

Despite many polymer nanocomposites being commercially used, micromachining applications on these materials have only focused on carbon nanotube (CNT)-based

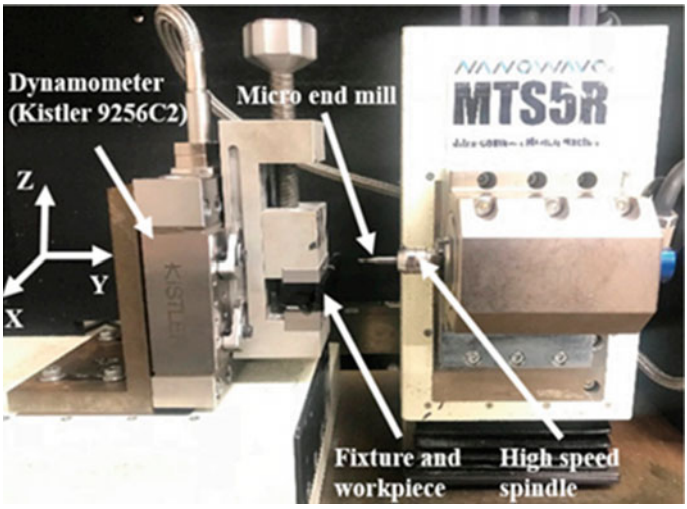

Fig. 17 Micro-milling of polyester/halloysite nano-clay nanocomposites using miniature machine tool (Open access from [26])

and graphene-based nanocomposites, using micro-milling. Figure 17 shows a typical setup for micro-milling of polymer nanocomposites using a miniature machine tool.

For that reason, this section of the chapter will discuss the micromachining behaviour of polymer nanocomposites reinforced by CNT and graphene. The main objectives include cutting forces, machined surface generation, chip formation and tool wear during micro-milling processes. The most important factors that affect these categories will be highlighted with the cutting mechanisms or models (if available) to explain nanocomposites' micromachining.

Micromachining of CNT-Based Nanocomposites

The incorporations of CNTs into polymer matrix mostly improve various characteristics such as mechanical, thermal, and electrical properties of polymer nanocomposites. However, within this section's scope, only thermomechanical properties will be analysed since they have shown significant influences on micromachining behaviour when micro-milling of polymer nanocomposites. CNTs play a positive role in dissipating heat generating from the cutting zone, reducing burr formation and improving the dimensional accuracy when micro-milling polymer nanocomposites (Fig. 18). Furthermore, the addition of CNTs into the polymer matrix is also the main reason for cutting forces and better-machined surface quality [27] (Fig. 19). It is due to incorporations of CNTs improved both mechanical and thermal properties of nanocomposites, hence leading to the dominance of strengthening effects and the subordination of thermal softening effects (especially at high feed rates) and consequently, cutting force increments during micro-milling process following by

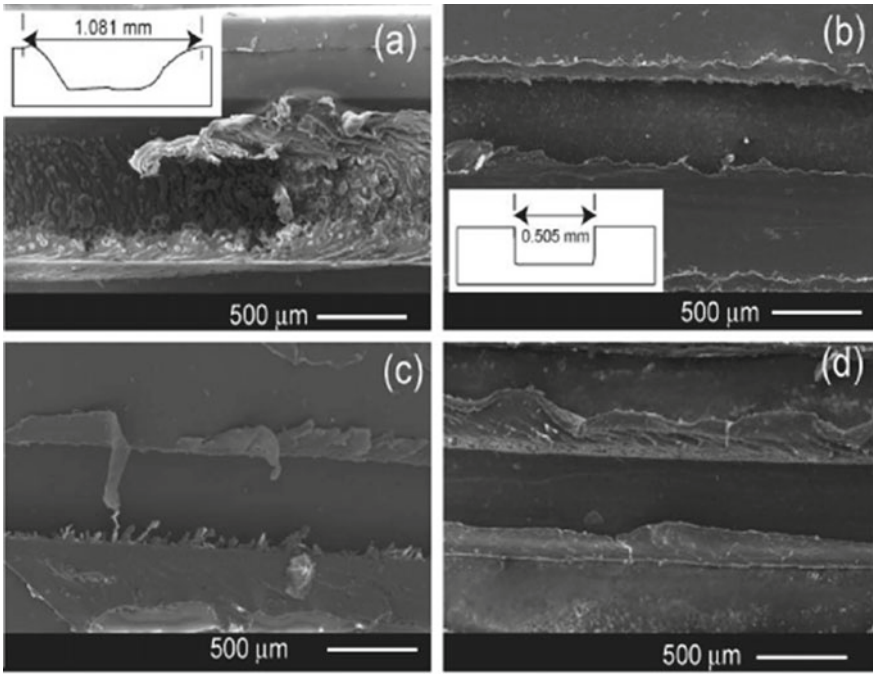

Fig. 18 SEM images of machined slots when micro-end milling of: **a** Plain PC, **b** PC/2 wt.% xGNP-M-5, **c** PC/2 wt.% xGNP-M-25, and **d** PC/1 wt.% xGNP-M-5/1 wt.% MWCNT nanocomposites (cutting speed of 80 m/min and FPT of 3 µm). Copyright permission from [27]

the reductions of surface roughness. These analyses are supported by the investigations on chip formation with discontinuous morphology compared to continuous chips in a micro-milling neat polymer.

A mechanistic micro-milling model [28] was applied to explain the mechanism of cutting force variations in the consideration the effects of CNT addition and fibre orientation when micro-milling of MWCNT reinforced polystyrene (PS) nanocomposites (PS/MWCNT) (Fig. 20). The radial force (dF_r) and tangential force (dF_t) acting on a small element of cutting edge with its height of dz can be obtained as follows:

$$dF_t = \begin{cases} (K_{tc}(\psi)h + K_{te}(\psi))dz & \text{when} \quad h \geq h_m \text{ (shearing)} \\ \left(K_{tp}(\psi)A_p + K_{te}(\psi)\right)dz & \text{when} \quad h < h_m \text{ (ploughing)} \end{cases}$$
$$dF_r = \begin{cases} (K_{rc}(\psi)h + K_{re}(\psi))dz & \text{when} \quad h \geq h_m \text{ (shearing)} \\ \left(K_{rp}(\psi)A_p + K_{re}(\psi)\right)dz & \text{when} \quad h < h_m \text{ (ploughing)} \end{cases} \tag{3}$$

K_{tc}, K_{rc}, K_{re} and K_{te} are the tangential and radial cutting and edge coefficients. K_{tp} and K_{rp} are ploughing constants. These coefficients are expressed as a function

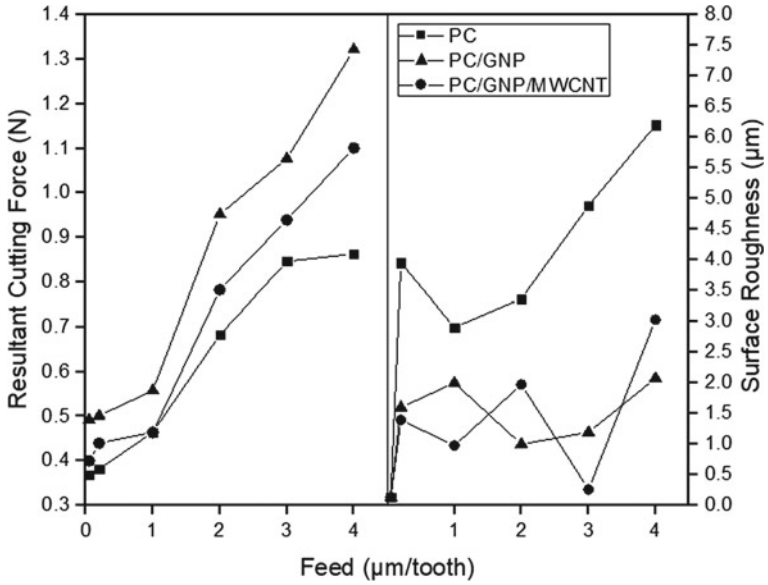

Fig. 19 The variations of surface roughness and cutting forces at various FPTs when micro-milling different polymer nanocomposites. Adapted from [27]

of CNT fibre orientation angle (Ψ). The cutting coefficients refer to shearing of the workpiece while the edge coefficients specify the friction between the cutting tool and workpiece. These coefficients can be obtained from experiments with different chip thicknesses/ feed rate and cutting force compensations [29] using the Kalman filter (KF) method [30]. They are identified via a nonlinear curve fitting as the following equation:

$$e = \sum_{i=1}^{n} \sum_{j=1}^{m} \left(F_{expi,j} - F_{theo}\right)^2 \tag{4}$$

where n is the level number of feed rates, m is the number of samples, F_{exp} is the experimental results regarding the cutting forces, and F_{theo} is their theoretical results. The UCT (h) can be obtained from the chip thickness model [31] in the consideration the effects of MUCT, elastic recovery, and tool vibration (Fig. 21) as follow:

$$h = \max\left(0, \left\| C_i^j F_i^j \right\| - \left\| C_i^j I_i^{j-1} \right\|\right) \tag{5}$$

The superscript (j) is the tooth path number, and the subscript (i) is the rotation angle. C, F represent the tool centre positions and cutting edge location, respectively, while I denotes the intersection between $C_i^j F_i^j$ and tool path j-1. In the case of UCT

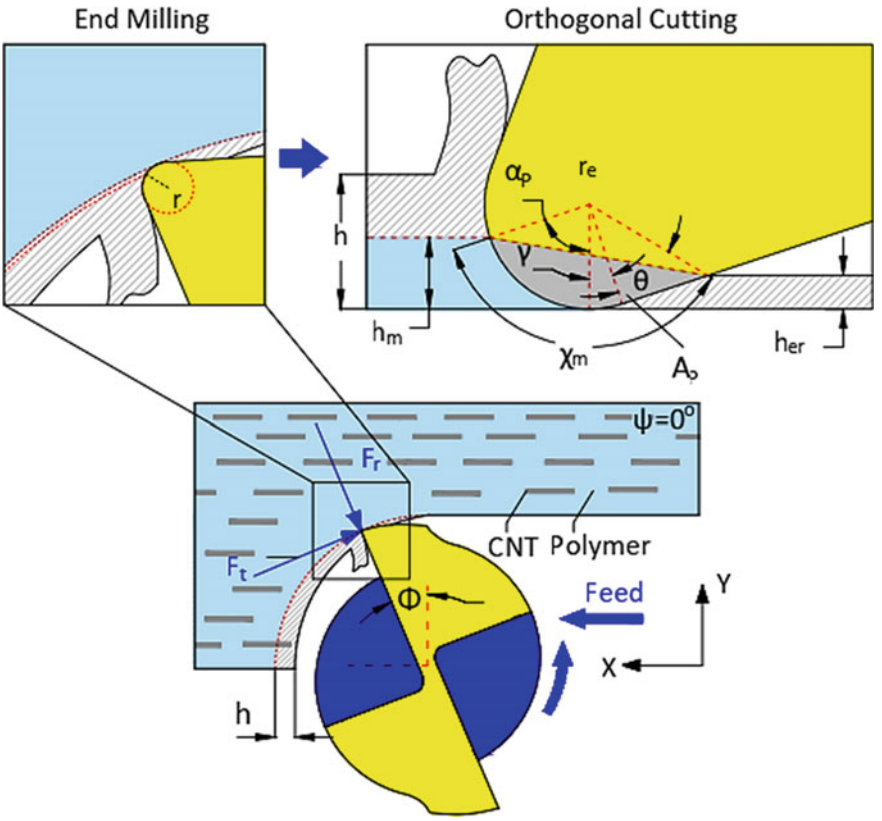

Fig. 20 Schematic representing the mechanistic model for micro-milling of Polymer/CNT nanocomposites. adapted from [28]

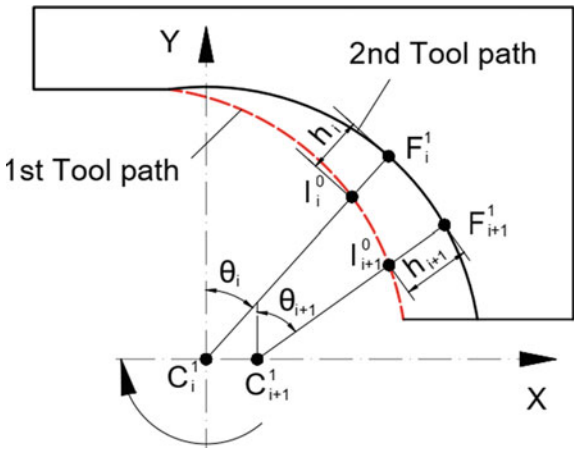

Fig. 21 Schematic representing chip thickness model in micro-milling

being infinitesimal compared to the micro-milling tool diameter, the variation of UCT is inconsiderable.

Therefore, it could be considered to be equivalent to feed rate by simplifying the 2D micro-milling to orthogonal cutting (top of Fig. 20). The ploughing area (A_P) can be identified as follow:

$$A_P \approx \frac{1}{2} r_e^2 (\alpha_P + \gamma) + \frac{1}{2} r_e (l_1 - l_2) \tag{6}$$

where

$$l_1 \approx \left(\frac{h_{er} - r_e(1 - \cos\gamma)}{\sin\gamma} \right)$$

$$l_2 \approx \sqrt{r_e^2 + l_1^2} \sin(\alpha_P + \gamma + \theta); \theta = \tan^{-1}\left(\frac{l_1}{r_e}\right)$$

The effective rake angle (α_P) is identified from:

$$\alpha_P = \cos^{-1}\left(1 - \frac{h}{r_e}\right) \tag{7}$$

The elastic recovery ratio (h_{er})can be obtained from the experimental data by applying scratching tests with a conical tool (apex angle of 90° and edge radius of 15 μm) [29]. The MUCT (h_m) is determined by the minimum energy method [32]. Its value is obtained when a transition from shearing to ploughing is recognized as the minimum cutting energy is attained. The MUCT can also be approximated from the following equation:

$$h_m = r_e(1 - \cos\chi_m) \quad \text{where} \quad \chi_m \approx \beta_s \tag{8}$$

The friction angle (β_s) is determined from the orthogonal cutting test using a cutting tool with 0° rake angle. This model exhibited high agreement with the experimental data regarding the cutting force variation in ploughing and shearing dominant regimes as a function of CNT content and CNT fibre orientation. A significant increase of cutting force and tool wear can be seen at a high CNT load due to high interaction between the cutting tool and CNT. This was confirmed by the high cutting coefficients when micro-milling at CNT based nanocomposites compared to other materials. Besides, small and debris chip formation can be observed from micro-milling at high CNT loading due to these materials' high brittleness.

The continuous and curly chip formations have been observed when micro-milling PC/CNT nanocomposites at every feed rate [33]. It is due to the presence of CNT as a lubricant, reducing the friction coefficient between tool rake face and workpiece, hence eliminating chip formation from being broken during the micro-cutting process. Additionally, better chip surface quality has been observed from micro-milling of PC/CNT nanocomposites compared to those of neat PC with adiabatic

shear bands on chip surfaces, indicating low thermal conductivity of these neat polymers. Subsequently, higher heat concentration in the cutting area led to the formation of built-up-edge (BUE) along tool rake face, resulting in low machined surface quality when micro-milling neat PC compared to that of micro-milling of PC/CNT nanocomposites.

There is a ductile-to-brittle transition of workpiece material property as CNT additional content reaching a certain threshold, for example, 5 wt.% [34], thereby reducing MUCT magnitudes micromachining brittle high-filler-content nanocomposites. Additionally, the presence of CNT exhibited significant influence on improving machined surface quality due to high thermomechanical properties of these nanocomposites that have been highlighted in the studies as mentioned earlier. On the other hand, cutting forces were significantly influenced by cutting speed regardless of the CNT loadings. Based on that, it could indicate that the incorporation of CNTs improves micro-machined surface quality. Simultaneously, its influences on cutting force and chip formation when micromachining CNT-based polymer nanocomposites are still unapparent with different experimental results and explanations.

In general, the reinforcements in terms of thermomechanical properties due to CNT addition, MUCT, cutting edge radius and microstructure effects have been addressed to explain micro-machining behaviours of CNT-based polymer nanocomposites. However, CNT content's roles, cutting speed or feed rate have been still minor controversy with different claims from relevant studies. It reconfirms the high complication of micromachining of polymer nanocomposites that requires further investigation in the future aspects.

Micromachining of Graphene-Based Nanocomposites

Like CNT-based polymer nanocomposites, the micromachining of graphene-based polymer nanocomposites showed better performance [35], in terms of low cutting force and high surface quality due to the addition of graphene compared to neat polymer (Fig. 22). These phenomena' explanations are similar to those of CNT additions in thermomechanical improvements, leading to strain hardening dominance/thermal-softening subordination and lubricating effect of graphene, resulting in less tool-chip fraction.

However, as graphene content increasing, the high specific area of graphene nanoplatelets (GNP) attributes to considerable GNP-tool interaction. It is associated with high interlocking between GNP and polymer matrix due to GNP's rough and wrinkled surfaces resulting in high cutting force when micro-milling polymer/GNP nanocomposites. Figure 23 shows different variations of cutting forces considering the effect of graphene addition.

In general, micro-milling of graphene-based polymer nanocomposites shows similar machinability behaviour to their CNT-based counterparts. It is possibly due to the similarities in terms of mechanical properties between graphene and CNT. The roles of graphene in micro-machining of these nanocomposites have been highlighted.

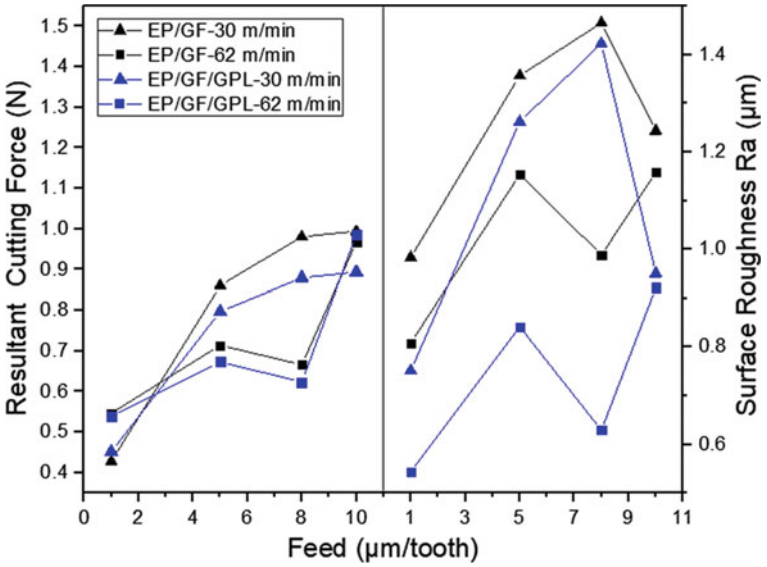

Fig. 22 Cutting force and surface roughness versus feed rate when micro-milling Epoxy/0.8 vol.% GF composites and Epoxy/0.8 vol.% GF/0.2 wt.% GPL hybrid nanocomposites. adapted from [36]

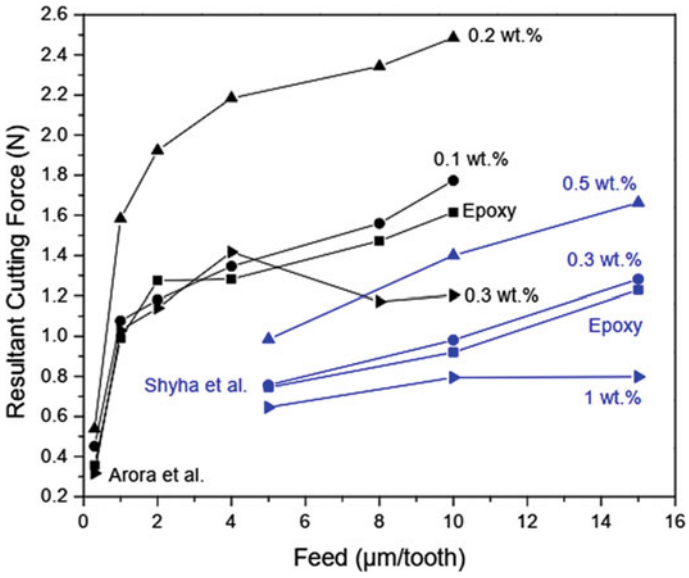

Fig. 23 Different trends of cutting forces as a function of graphene addition when micromachining graphene reinforced polymer nanocomposites. adapted from [22]

3.3 *Tool Wear in Micromachining of Polymer Nanocomposites*

Beside machined surface roughness, tool wear is also considered a vital machinability indicator in the manufacturing cost aspect. The tool wear study in micromachining of polymer nanocomposites primarily focuses on the effect of nano-filler addition such as graphene or CNTs. The most common variation of tool wear behaviour as a function of nano-fibres addition is being reduced in the beginning then accelerating at high filler contents. This trend can be explained based on various mechanism including (i) the improvement of the thermo-mechanical properties of polymer nanocomposites as a result of nano-fibre additions, (ii) the nature of nano-fibres, and (iii) the dominance of micro-structure effect in micromachining. First, the incorporation of CNTs or graphene improves mechanical properties and thermal conductivity of polymer nanocomposites. This thermo-mechanical improvement significantly affects the micro-cutting characteristics, including tool wear. As conduction materials, CNTs or graphene stimulate faster heat dissipation around the cutting area during the machining process, reducing the workpiece debris smearing on the clearance surfaces. Additionally, the strengthening effect of these nano-fibres also restricts polymer chains' relative sliding, hence reducing the elastic recovery exhibited on the clearance face. These effects minimize the rubbing between tool and clearance face, which consequently reduce the tool wear. Second, both CNTs and graphene are considered as lubricants [37, 38]. It leads to a decrease in the effective coefficient of friction between cutting tool and workpiece, contributing to tool wear reduction. However, the agglomeration tends to appear as high concentrations of nano-fibres being employed. In micromachining where microstructure effect becomes more influential (Sect. 3.1), this could lead to the tool being trapped by nano-fibre bundles, hence increases the tool wear. Figure 24 shows an example of tool wear when micro-milling of epoxy/graphene nanocomposites.

4 Non-Conventional Micromachining of Polymer Nanocomposites

While the mechanical micromachining has been applied to manufacture mechanical micro-components (i.e., micro-gears, micro-wheels), non-conventional micromachining of polymer nanocomposites exhibits high feasibility in micro-electronic productions, especially laser micromachining. This method could be employed to cut a wide range of different features from thin films, arrays to complex 3D structures in multifunctional capacitors [40]. Additionally, micro-electrical discharge machining (EDM) is also feasible for polymer nanocomposites with high conductive fillers (i.e., CNT, graphene). Similarly, this technique can also produce micro-features with

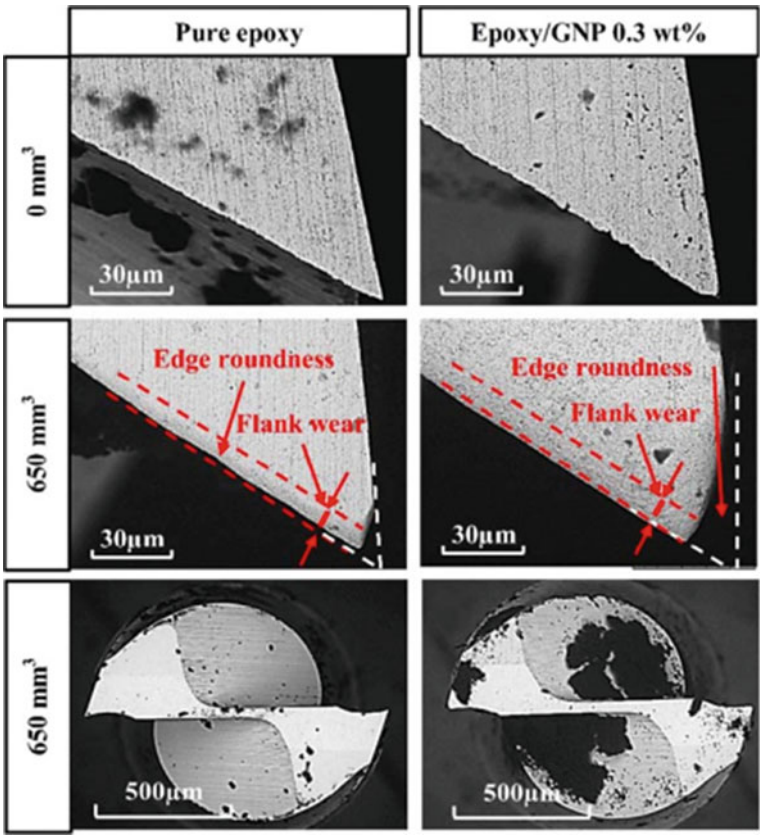

Fig. 24 SEM images of tool wear when micro-milling of epoxy/graphene nanocomposites and neat epoxy. open access from [39]

high complexity [41]. However, the high loading of reinforcement could lead to machined defects. Besides, the low material removal rate also makes it less efficient than mechanical micromachining.

5 Review Questions

(1) What are the main reason behind applying machining of polymer nanocomposites in the industry?
(2) What are the current reasons that make the commercial applications of machining of polymer nanocomposites limited?
(3) What are the main reasons that make the machining of polymer composites more complicated than metals or alloys?

(4) Discuss the general classification machining of polymer nanocomposites.
(5) Show the main objectives of machining of polymer nanocomposite
(6) Discuss the most applied techniques for machining of polymer nanocomposite
(7) What are micromachining and its differences from ultra-precision machining?
(8) Discuss the differences in terms of material removal mechanism between micromachining and macro-machining.
(9) What are the main reason behind applying the micromachining of polymer nanocomposites in the industry?
(10) What are the current reasons for the research limitations of machining of polymer nanocomposites?
(11) What are the most applied polymer nanocomposites in micromachining?
(12) What are the most common objectives for micromachining of polymer nanocomposite research?
(13) What are the main reasons that make micromachining of polymer nanocomposites complicated than conventional machining of other materials?
(14) Discuss mechanisms, equations, theories and models that can explain the micromachining of polymer nanocomposites.

References

1. Zinati, R.F., Razfar, M.: Experimental and modeling investigation of surface roughness in end-milling of polyamide 6/multi-walled carbon nano-tube composite. Int. J. Adv. Manuf. Technol. **75**, 979–989 (2014)
2. Pang, J., Ansari, M., Zaroog, O.S., Ali, M.H., Sapuan, S.: Taguchi design optimization of machining parameters on the CNC end milling process of halloysite nanotube with aluminium reinforced epoxy matrix (HNT/Al/Ep) hybrid composite. HBRC J. **10**, 138–144 (2014)
3. Kiliçkap, E., Yardimeden, A., Çelik, Y.H.: Investigation of experimental study of end milling of CFRP composite. Sci. Eng. Compos. Mater. **22**, 89–95 (2015)
4. Farshbaf Zinati, R., Razfar, M., Nazockdast, H.: Surface integrity investigation for milling PA 6/MWCNT. Mater. Manuf. Process. **30**, 1035–1041 (2015)
5. Zinati, R.F., Razfar, M.R.: An investigation of the machinability of PA 6/nano-$CaCO_3$ composite. Int. J. Adv. Manuf. Technol. **68**, 2489–2497 (2013)
6. Gong, Y., Baik, Y.-J., Li, C.P., Byon, C., Park, J.M., Ko, T.J.: Experimental and modeling investigation on machined surfaces of HDPE-MWCNT polymer nanocomposite. Int. J. Adv. Manuf. Technol. **88**, 879–885 (2017)
7. Rao, G.H.K., Ansari, M., Begum, S.: Effect of cutting parameters on the surface roughness of MWCNT reinforced epoxy composite using CNC end-milling process. Int. J. Sci. Res. **2**, 51–55 (2013)
8. Kumar, D., Singh, K.: Investigation of delamination and surface quality of machined holes in drilling of multiwalled carbon nanotube doped epoxy/carbon fiber reinforced polymer nanocomposite. Proc. Inst. Mech. Eng. Part L: J. Mater.: Design Appl. **233**, 647–663 (2019)
9. Li, N., Li, Y., Zhou, J., He, Y., Hao, X.: Drilling delamination and thermal damage of carbon nanotube/carbon fiber reinforced epoxy composites processed by microwave curing. Int. J. Mach. Tools Manuf. **97**, 11–17 (2015)
10. Karimi, Z.N., Heidary, H., Yousefi, J., Sadeghi, S., Minak, G.: Experimental investigation on delamination in nanocomposite drilling. FME Trans. **46**, 62–69 (2018)

11. Ponnuvel, S., Moorthy, T., Lokachari, S.: Investigation on the machinability characteristics of MWCNTs filled epoxy/glass fabric hybrid nanocomposite using various drill bits. In: Applied Mechanics and Materials, pp. 956–962 (2014)
12. Ponnuvel, S., Moorthy, T.: Investigation on the influence of multi walled carbon nanotubes on delamination in drilling epoxy/glass fabric polymeric nanocomposite. Proc. Eng. **51**, 735–744 (2013)
13. Rajakumar, I.P.T., Hariharan, P., Srikanth, I.: A study on monitoring the drilling of polymeric nanocomposite laminates using acoustic emission. J. Compos. Mater. **47**, 1773–1784 (2013)
14. Al-Khaldi, T., Mansour, E., Gaafer, A., Habib, S.: Machinability of EPOXY/MWCNTs NANOCOMPOSITES during turning operation. Journal Homepage: www.feng.bu.edu.eg **1,** 26–30 (2019)
15. Haghi, M., Farshbaf Zinati, R., Razfar, M.R.: Experimental and modeling study of the turning process of PA 6/nano calcium carbonate composite. J. Compos. **2013** (2013)
16. Rajurkar, K.: Nontraditional manufacturing processes. In: Handbook of Design, Manufacturing and Automation, pp. 211–241 (1994)
17. Yousef, S.: Polymer nanocomposite components: a case study on gears. In: Lightweight Composite Structures in Transport, pp. 385–420. Elsevier (2016)
18. De Oliveira, F.B., Rodrigues, A.R., Coelho, R.T., De Souza, A.F.: Size effect and minimum chip thickness in micromilling. Int. J. Mach. Tools Manuf. **89**, 39–54 (2015)
19. Vogler, M.P., DeVor, R.E., Kapoor, S.G.: Microstructure-level force prediction model for micro-milling of multi-phase materials. J. Manuf. Sci. Eng. **125**, 202–209 (2003)
20. Venkatachalam, S., Fergani, O., Li, X., Guo Yang, J., Chiang, K.-N., Liang, S.Y.: Microstructure effects on cutting forces and flow stress in ultra-precision machining of polycrystalline brittle materials. J. Manuf. Sci. Eng. **137** (2015)
21. Shimada, S., Ikawa, N., Tanaka, H., Uchikoshi, J.: Structure of micromachined surface simulated by molecular dynamics analysis. CIRP Ann. **43**, 51–54 (1994)
22. Le, B., Khaliq, J., Huo, D., Teng, X., Shyha, I.: A review on nanocomposites. Part 2: micromachining. J. Manuf. Sci. Eng. **142** (2020)
23. Mian, A.J., Driver, N., Mativenga, P.T.: A comparative study of material phase effects on micro-machinability of multiphase materials. Int. J. Adv. Manuf. Technol. **50**, 163–174 (2010)
24. Simoneau, A., Ng, E., Elbestawi, M.: Surface defects during microcutting. Int. J. Mach. Tools Manuf. **46**, 1378–1387 (2006)
25. Vogler, M.P., DeVor, R.E., Kapoor, S.G.: On the modeling and analysis of machining performance in micro-endmilling, Part I: surface generation. J. Manuf. Sci. Eng. **126**, 685–694 (2004)
26. Fu, G., Huo, D., Shyha, I., Pancholi, K., Saharudin, M.S.: Experimental investigation on micro milling of polyester/halloysite nano-clay nanocomposites. Nanomaterials **9**, 917 (2019)
27. Kumar, M.N., Mahmoodi, M., TabkhPaz, M., Park, S., Jin, X.: Characterization and micro end milling of graphene nano platelet and carbon nanotube filled nanocomposites. J. Mater. Process. Technol. **249**, 96–107 (2017)
28. Mahmoodi, M., Mostofa, M., Jun, M., Park, S.S.: Characterization and micromilling of flow induced aligned carbon nanotube nanocomposites. J. Micro Nano-Manuf. **1**, 011009 (2013)
29. Park, S., Malekian, M.: Mechanistic modeling and accurate measurement of micro end milling forces. CIRP Ann. **58**, 49–52 (2009)
30. Altintas, Y., Park, S.: Dynamic compensation of spindle-integrated force sensors. CIRP Ann. **53**, 305–308 (2004)
31. Jun, M.B., Liu, X., DeVor, R.E., Kapoor, S.G.: Investigation of the dynamics of microend milling—Part I: model development (2006)
32. Malekian, M., Mostofa, M., Park, S., Jun, M.: Modeling of minimum uncut chip thickness in micro machining of aluminum. J. Mater. Process. Technol. **212**, 553–559 (2012)
33. Samuel, J., DeVor, R.E., Kapoor, S.G., Hsia, K.J.: Experimental investigation of the machinability of polycarbonate reinforced with multiwalled carbon nanotubes. J. Manuf. Sci. Eng. **128**, 465–473 (2006)

34. Samuel, J., Dikshit, A., DeVor, R.E., Kapoor, S.G., Hsia, K.J.: Effect of carbon nanotube (CNT) loading on the thermomechanical properties and the machinability of CNT-reinforced polymer composites. J. Manuf. Sci. Eng. **131**, 031008 (2009)
35. Shyha, I., Fu, G.Y., Huo, D.H., Le, B., Inam, F., Saharudin, M.S., et al.: Micro-machining of nano-polymer composites reinforced with graphene and nano-clay fillers. In: Key Engineering Materials, pp. 197–205 (2018)
36. Chu, B., Samuel, J., Koratkar, N.: Micromilling responses of hierarchical graphene composites. J. Manuf. Sci. Eng. **137**, 011002 (2015)
37. Berman, D., Erdemir, A., Sumant, A.V.: Graphene: a new emerging lubricant. Mater. Today **17**, 31–42 (2014)
38. Cornelio, J.A.C., Cuervo, P.A., Hoyos-Palacio, L.M., Lara-Romero, J., Toro, A.: Tribological properties of carbon nanotubes as lubricant additive in oil and water for a wheel–rail system. J. Market. Res. **5**, 68–76 (2016)
39. Fu, G., Huo, D., Shyha, I., Pancholi, K., Alzahrani, B.: Experimental investigation on micro-machining of epoxy/graphene nano platelet nanocomposites. Int. J. Adv. Manuf. Technol. 1–15 (2020)
40. Das, R.N., Egitto, F.D., Antesberger, T.E., Marconi, F., Lin, H., Lauffer, J.M., et al.: Laser processing of 3-D structures for embedded and integrated components: an application of flexible and printable nanomaterials in microelectronics. In: 2008 58th Electronic Components and Technology Conference, pp. 444–451 (2008)
41. Wan, Y., Kim, D., Park, Y.-B., Joo, S.-K.: Micro electro discharge machining of poly-methylmethacrylate (PMMA)/multi-walled carbon nanotube (MWCNT) nanocomposites. Adv. Compos. Lett. **17**, 096369350801700401 (2008)

Green, Natural Fibre and Hybrid Composites

Mohamad Midani and Ahmed H. Hassanin

Abstract The use of composite materials has seen a surge in many applications such as aerospace, automotive, marine, and medical and sports equipment. The increasing demand for more sustainable and renewable materials has increased natural fibres' interest as a reinforcement for composite materials. Natural fibres are environmentally friendly, but they also have high specific properties due to their lightweight. This chapter provides an overview of natural fibre and hybrid composites, the types of fibre used, their extraction methods, properties, and microstructure. Moreover, a special section is dedicated to the conversion techniques from fibres to preforms, and the manufacturing methods from preforms to final composites. At the end of the chapter, there is a comprehensive list of all commercial applications of natural fibre composites compiled from JEC Composites Market news from 2011 to 2019, with a discussion on the prospects of adopting natural fibre composites in the industry.

1 Introduction

The twentieth century's advent brought a new generation of composite materials marked by their high strength to weight ratio, high specific stiffness, and outstanding corrosion resistance compared to most common metallic materials, such as steel and aluminium. Composites can form directional mechanical properties, low thermal expansion properties and high dimensional stability. This unique combination of outstanding mechanical, thermal and physical properties makes composites eligible to take over traditional materials in many applications, especially when weight saving

M. Midani
Department of Materials Engineering, German University, Cairo, Egypt

Wilson College of Textiles, NC State University, Raleigh, NC, USA

A. H. Hassanin (✉)
Department of Textiles Engineering, Alexandria University, Alexandria, Egypt
e-mail: ahassan@ncsu.edu

Materials Science and Engineering Department, Egypt-Japan University of Science and Technology (E-JUST), New Borg El-Arab City, Alexandria, Egypt

I. Shyha and D. Huo (eds.), *Advances in Machining of Composite Materials*,
Engineering Materials, https://doi.org/10.1007/978-3-030-71438-3_15

is needed. Composites are currently used in various applications such as aircraft, spacecraft, satellites, ships, wind turbine blades, automotive, chemical equipment, sporting goods and construction technology.

Most of the current commercial composites are made from petroleum-based synthetic polymers. This raises a sustainability concern, due to the reliance on the ever-depleting petroleum resource, concerns about environmental pollution, increased petroleum price, and disposal difficulty. Meanwhile, naturally based materials are abundant from agriculture, animal resources, and urban environments that accumulate to problematic levels. This raises a major challenge on maximizing the sustainable and profitable use of these natural resources as a raw material for high value-added products which require innovative and environmentally friendly solutions. Consequently, the utilization of natural-based materials (green resources), has gained considerable attention. Green composites are made up from natural fibres as reinforcements, such as wood pulp, kenaf, hemp, flax, jute, sisal, wool, silk…etc. and matrix. Matrix or resins could be synthetic or could be natural or green based. Using synthetic matrix with natural based materials as reinforcements or vice versa, this is called hybrid composites.

Natural fibres are fibres obtained from natural sources which could either be a protein or cellulosic fibres. Protein or animal fibres are mostly obtained from animals, while cellulosic fibres are obtained from plants. Cellulose natural fibres consist of three main organic constituents; cellulose, hemicellulose, and lignin.

Usually, cellulosic fibres are classified depending on the part of the plant from which they are extracted, for instance, fibres extracted from the stem are classified as bast fibres. In contrast, fibres extracted from the leaves are classified as leaf fibres, in addition to other parts of the plants, such as seed, fruit, stalk, or grass as shown in Fig. 1.

Natural fibres could be further classified into two types based on how they are found in nature. First, fibres that are present in fibre form. Second, fibres embedded in a natural matrix. The first type of fibres is used right away since the fibres are already found in fibre form, they don't need further extraction, they may only require washing, drying then cutting such as cotton and wool. However, the second type of fibres requires further processing through many extractions or separation processes. These processes could be chemical, biological, or mechanical. The extraction process is considered successful upon efficient extraction of the cellulose fibrils from the hemicellulose binding them and from within the lignin matrix in which they are embedded. Examples of these types of extracted fibres are flax, hemp, jute, sisal, etc.

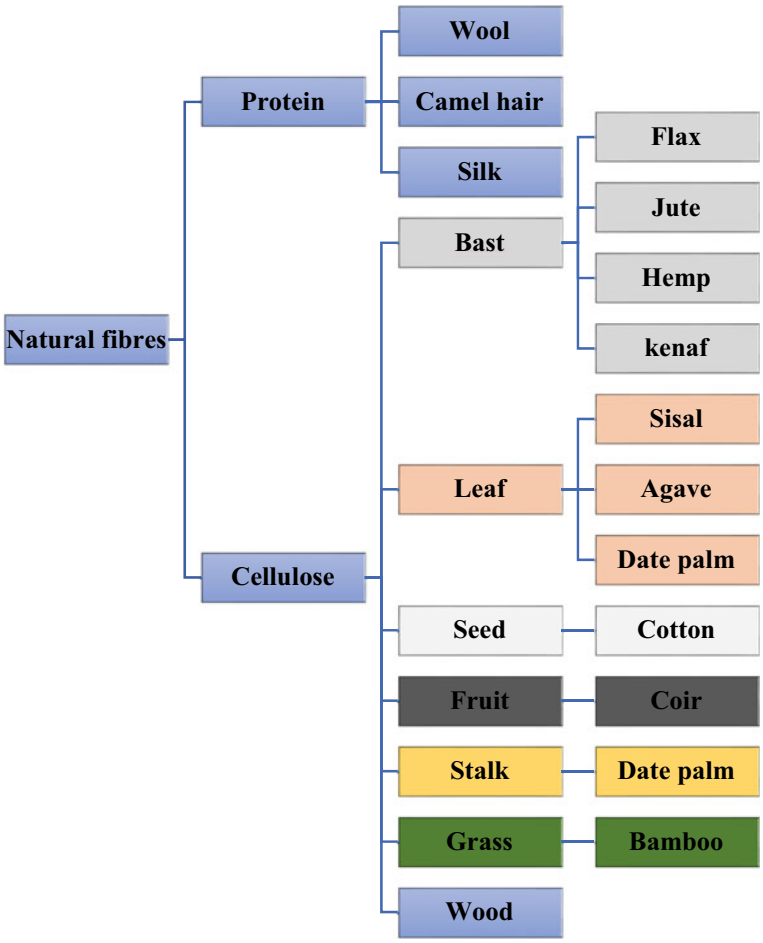

Fig. 1 Natural fibre classification [1]

2 Cellulosic Fibres

2.1 World Consumption of Cellulosic Fibres

Cellulosic fibres are the primary natural materials used in technical applications, especially composites, Table 1. shows the world consumption of natural cellulosic fibres by type in values and quantities. Cotton fibres are excluded as they mainly used for textile applications. As it can be noticed that Flax and Jute are the two most consumed natural fibres. Flax and Jute are used in many other applications rather than composites such as clothing, home textile and packaging materials.

Table 1 World consumption of vegetable fibres by fibre type in values and quantities

	$US million			10^3 tons		
	2010	2017	CAGR (%)	2010	2017	CAGR (%)
Flax	1641.00	1963.20	2.6	427.8	455	0.9
Jute and other bast	1056.90	1085.60	0.4	815.9	592.4	-4.5
Coconut	306.4	543.1	8.5	672.5	1080.10	7
Hemp	10.9	16.3	5.8	13.2	20	6.1
Sisal	5.8	8.2	5.1	5.7	4	-4.9
Other vegetables	77.9	93.6	2.7	31.6	0	–
Total	3100	3700	2.6	2000	2200	1.3

Table 2 Unit values of vegetable fibres in US$/Kg

	$US/ Kg*		
	2010	2017	CAGR (%)
Flax	3.8	4.3	1.7
Jute and other bast	1.3	1.8	5.1
Coconut	0.5	0.5	1.4
Hemp	0.8	0.8	−0.2
Sisal	1.0	2.0	10.4
Other vegetables	2.5	0.0	–

*Unit values (for each fibre) are average of fibre, yarn and fabric form

As it can be noticed from Table 2 that Flax prices are the highest among the other natural fibres. Jute comes after Flax from the price point of view. This can be attributed to using these fibres in other high added value applications such as clothing and home textiles, as mentioned earlier.

The Asia Pacific and Europe are the main regions consuming natural fibres, as indicated in Table 3. It is known that Asia Pacific countries are primary producers

Table 3 World consumption of vegetable fibres by region in values

	$US million		
	2010	2017	CAGR (%)
Asia Pacific	1244.4	1825.7	5.6
Europe	1110.6	1028.6	−1.1
Middle East	447.3	460.0	0.4
North America	228.0	299.3	4.0
Africa	162.3	168.3	0.5
South America	64.2	48.0	−4.1
World	**3270**	**3830**	**2.3**

for many natural cellulosic fibres such as Jute, Kenaf, Coir, Kapok…. etc. While in Europe are the primary producers of Flax fibres namely France, Belgium, Belarus and Ukraine.

2.2 The Microstrucssssture of Cellulosic Fibres

Cellulosic natural fibres, which are also called lignocellulosic fibres, consist of three major organic constituents, cellulose, hemicellulose, and lignin. Table 4 indicates the percentages of cellulose, Lignin and Hemicellulose of some standard natural cellulosic fibres. This structure is thought to be like a composite; where cellulose is surrounded by hemicellulose and embedded in lignin as a matrix, as shown in Fig. 2. Lignin is an amorphous organic polymer that consists of aromatic structures in addition to aliphatic chains. Lignin acts as a natural glue, and it binds the cellulose fibres together. Its weight fraction is 10–25% for non-woody plants and 20–30% for

Table 4 Cellulose, lignin and hemicellulose content of some standard natural cellulosic fibres (1, 2, 3, and 4)

Fibre	Cellulose (wt. %)	Hemicellulose (wt. %)	Lignin (wt. %)	Waxes (wt. %)
Cotton	82.7	5.7	0.7–1.6	0.6
Bagasse	55.2	16.8	25.3	–
Bamboo	26–43	30	21–31	–
Date palm fibre (midribs)	45.47	24.9	29.31	–
Flax	71	18.6–20.6	2.2	1.5
Kenaf	72	20.3	9	–
Jute	61–71	14–20	12–13	0.5
Hemp	68	15	10	0.8
Ramie	68.6–76.2	13–16	0.6–0.7	0.3
Sisal	67–78	10–14	8–11	2
Abaca	56–63	20–25	7–9	3
Coir	32–43	0.15–0.25	40–45	
Oil palm	65	—	29	–
Pineapple	81	—	12.7	–
Banana	64	20	5	–
Curaua	73.6	9.9	7.5	–
Wheat straw	38–45	15–31	12–20	–
Rice husk	35–45	19–25	20	–
Rice straw	41–57	33	8–19	8–38

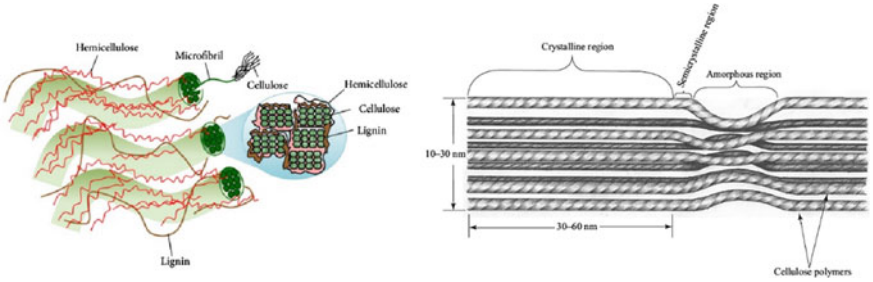

Fig. 2 The microstructure of natural cellulosic fibres and cellulose polymer chains showing cellulose crystalline and amorphous regions [1]

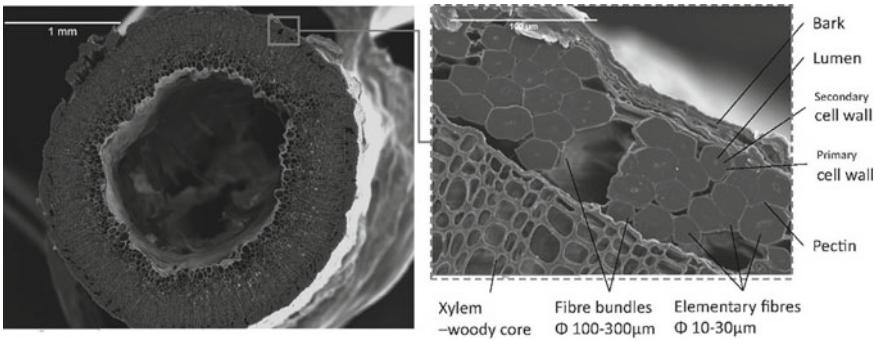

Fig. 3 SEM image of the cross-section of flax plant stem [3]

woody plants. The hemicellulose acts as the bridge between cellulose microfibrils and lignin.

Cellulosic fibres have both crystalline and amorphous regions. Crystalline regions are highly oriented and packed, unlike the amorphous regions, as shown in Fig. 2. Native cellulose initially found in plants is cellulose I, while after alkaline treatment it is converted to regenerated cellulose or cellulose II. Cellulose I is a crystalline material formed of parallel chains oriented in the same direction with amorphous regions between the crystalline regions as shown in Fig. 2. Native cellulosic or cellulose I fibres such as cotton, flax, jute, ramie…etc., have a high degree of crystallinity ranged from 65 to 70%. On the contrary, regenerated cellulose fibres or cellulose II have crystallinity ranged from 35 to 40% [2]. Figures 3 and 4 are showing the morphological structure and the cross-section of different cellulosic fibres.

2.3 Cellulosic Fibres Classification

As mentioned earlier in this chapter, cellulosic fibres are classified depend on the part of the plant from which they are extracted; for instance, fibres extracted from

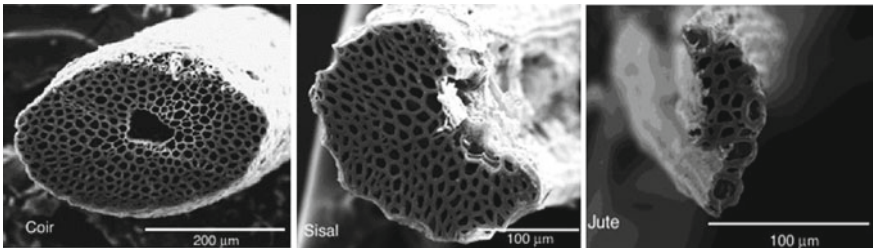

Fig. 4 SEM image Cross-section of different cellulosic fibres [4]

the stem are classified as bast fibres. In contrast, fibres extracted from the leaves are classified as leaf fibres.

1. ***Bast fibres***

Bast fibres are those obtained from the stems of different plants. Flax, Jute, Hemp, Ramie and Kenaf are the main plants used to supply bast fibres. Bast fibres, especially Flax, are long, fine and soft, so they are usually used for textile, sacks and cordage products. Bast fibre has a high cellulose content which can reach up to 70% as shown in Table 4. Bast sfibres crystallinity can be 80 to 90%, which lead to better mechanical properties [3, 4].

2. ***Leaf fibres***

Leaf fibres are extracted from leaves of flowering plants (monocotyledonous) that usually have parallel-veined leaves. The main plants supply the leaf fibres: sisal, abaca, pineapple, banana and Date palm leaves. Leaf fibre can have cellulose contents as high as 70% [3]. Longleaf fibre can be obtained in sisal and abaca plants, where the fibre can reach 1 to 4 m long [5]. These fibres are usually used for cordage as it is long and stiff.

3. ***Seed fibres***

Seed fibres are obtained from the seed of plants. Cotton is one of the most known and used fibres, which is obtained from seeds. Cotton fibre has a high cellulose content reach 85–91% with a crystallinity around 65%.

4. ***Fruit fibres***

Fruit fibres are usually obtained from the fruit of the plant. Coir fibre is the most widespread fruit fibres. It is obtained from the outer shell, or husk, of the coconut.

5. ***Stalk fibres***

Stalk fibres are extracted from the straw or stalk of different crops such as rice, wheat and barley. These fibres usually have a length of 0.5–2.5 mm and have low lignin, while the cellulose level is broadly similar to wood [4].

6. ***Grass fibres***

sAlso known as grass, canes or reeds fibres. Sugar cane (bagasse) and bamboo are examples of canes fibres. At the same time, Esparto Spanish grass or Halfa are examples of grasses fibres and reeds that are a common fibre source. These fibres are usually used to make different technical products such as ropes, sandals, baskets, mats and paper [4].

7. ***Wood fibres***

Wood fibre is mostly obtained from the wood tree. Wood fibre usually has a high lignin content and short length in millimetres to not be spun or woven. The main applications of wood fibres in wood composites are particle boards and MDF and paper making.

2.4 Cellulosic Fibres Extraction

The cellulosic part of the lignocellulosic material can be obtained by removing the non-cellulosic parts, lignin and hemicellulose. This process is called fibre extraction in which one has to get rid of the non-cellulosic materials and get the high crystalline part which is the cellulosic fibres. The reason is that the non-cellulose components, such as lignin and hemicellulose, do not contribute to the tensile loads, limiting the fibre's load-bearing capacity. Besides, noncellulosic materials accelerate biological, ultraviolet and thermal degradation [6].

Fibre extraction methods include different techniques. It could be biological, chemical and physical. The extraction techniques can be listed as shown in Fig. 5. Each method has its advantages and disadvantages in terms of the yield and quality of the extracted fibres. One technique could be chosen, or it could be a combination of more than one technique to achieve the maximum cellulose content.

2.5 Cellulosic Fibres Properties

Interest in natural fibre-based products is growing for many reasons such as low cost, lightweight, biodegradability and sustainability. The type of fibre selected for a certain application depends on its properties. Consequently, natural fibres characteristics such as mechanical, physical and chemical properties will be of great importance when the material is selected for any engineering or technical applications.

Although all-natural cellulosic fibres have the same three main constituents which are cellulose, hemicellulose and lignin, yet, they differ in the content percentages as it can be seen above in Table 4 which directly lead to a significant difference in the physical and mechanical properties such as density, fibre length, tensile strength and modulus.

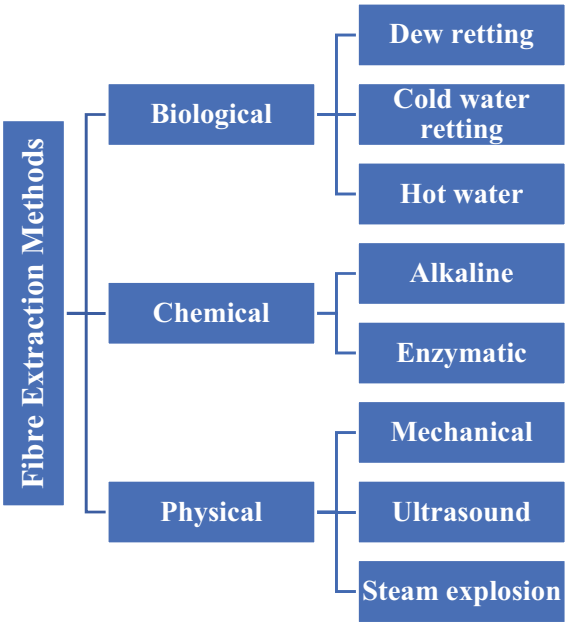

Fig. 5 Cellulosic fibre extraction methods [7]

It can be clearly noticed from Table 5 that flax, hemp, ramie and jute fibres have the highest mechanical properties (tensile strength and young modulus). Specific tensile strengths of flax, hemp, jute and ramie are very close to E-glass values, while the specific young modulus is equal to or greater sometimes than E-glass.

It is proven that achieving high mechanical properties in natural cellulosic fibres is related mainly to three critical factors: cellulose content, crystallinity, and microfibrils in fibre axes direction. These factors tend to be achieved in bast fibres such as flax, jute, hemp, kenaf and ramie. It should be noted that the properties of natural fibres suffer from high levels of variability, which is common in all-natural products.

Natural fibre properties can differ significantly depending on chemical composition and structure, which are related directly to the following factors:

- Fibre type
- Growing conditions
- Harvesting time
- Extraction technique
- Treatment
- Storage conditions.

Examples of such effects of factors mentioned above are the tensile strength reduction that has been noticed for flax fibres due to changing the extraction method from manually to mechanically. The drop was around 20% [8]. Tensile strength was reduced by 15% over 5 days after optimum harvest time in hemp fibres grown in New Zealand [9]. The tensile strength of hemp fibres grown in windy and dry conditions

Table 5 Natural sfibre properties compared to E-glass [17]

Fibre	Density (g/cm^3)	Length (mm)	Failure strain (%)	Tensile strength (MPa)	Young's Modulus (GPa)	Specific tensile strength (MPa/g cm^3)	Specific Young's modulus (GPa/g cm^3)
Ramie	1.5	900–1200	2.0–3.8	400–938	44–128	270–620	29–85
Flax	1.5	5–900	1.2–3.2	345–1830	27–80	230–1220	18–53
Hemp	1.5	5–55	1.6	550–1110	58–70	370–740	39–47
Jute	1.3–1.5	1.5–120	1.5–1.8	393–800	10–55	300–610	7.1–39
Harakeke	1.3	4–5	4.2–5.8	440–990	14–33	338–761	11–25
Sisal	1.3–1.5	900	2.0–2.5	507–855	9.4–28	362–610	6.7–20
Alfa	1.4	350	1.5–2.4	188–308	18–25	134–220	13–18
Cotton	1.5–1.6	10–60	3.0–10	287–800	5.5–13	190–530	3.7–8.4
Coir	1.2	20–150	15–30	131–220	4–6	110–180	3.3–5
Silk-	1.3	Continuous	15–60	100–1500	5–25	100–1500	4–20
Feather	0.9	10–30	6.9	100–203	3–10	112–226	3.3–11
Wool	1.3	38–152	13.2–35	50–315	2.3–5	38–242	1.8–3.8
E-glass	2.5	Continuous	2.5	2000–3000	70	800–1400	29

was lower than those grown under wind-free conditions [10]. The effect of fibre treatment showed significant influences on cellulosic fibres' physical and mechanical properties such as tensile strength, stiffness, crystallinity index, crystals size, degree of polymerization, and fibre surface properties [11–13]. Alkaline treatment or mercerization is one of the standard methods to treat natural fibre. During the mercerization process, lignin and hemicellulose are removed, which leads to:

- More fibrillation
- Less fibre diameter
- More surface roughness
- Increase surface area
- More reactive sites on the surface of fibre which leads to better fibre wetting.

Exceeding the optimum mercerization parameters, NaOH concentration, treatment duration, and treatment temperature will harm mechanical and physical properties. In many studies, it was proved that a transition from cellulose I (crystalline) to cellulose II (amorphous) would occur at severe alkaline treatment conditions. This transition will lead to a significant deterioration in mechanical properties [14–16].

3 Manufacturing Techniques of Natural Fibre and Hybrid Composites

Having known the fibres composition, types and characteristics, this part of the current chapter is devoted to illustrating the different manufacturing processes and techniques used to manufacture natural fibres and hybrid composites. Before we go forward to manufacturing techniques, it is necessary to go through a crucial issue: fibre architecture because many composites are firmly dependent on the arrangement and distribution of fibres inside the matrix. The fibre architecture definition encompasses many fibre parameters such as fibre diameter and length and the fibres' structural configuration [18].

3.1 Preform Manufacturing

Yarns used to prepare the composite preforms could be spun yarn or continues filaments, as shown in Fig. 6. Continuous filaments (CF) are mostly synthetic materials such as polypropylene, polyester and polyamide also CF could be regenerated cellulose such as rayon, modal, bamboo…etc. Continuous filaments are produced by melt spinning in case of thermoplastic polymers. On the other hand, wet or dry spinning is used to produce CF in thermoset polymers.

Spun yarns are produced by gathering together a bundle of staple fibres and then twist it to increase cohesion force between the staple fibres, consequently, form a

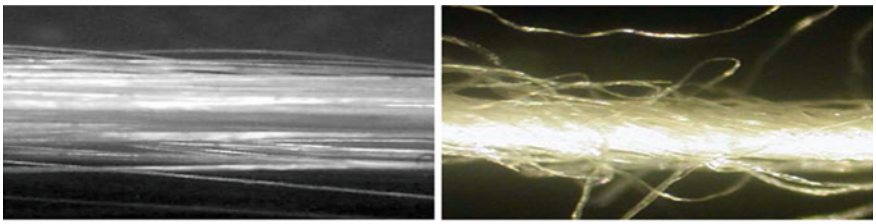

Fig. 6 Yarn types, **a** continuous filament yarn, and **b** spun yarn

yarn with enough mechanical properties for further processing. Ring spinning, open-end spinning, and air-jet spinning are the most used techniques to produce spun yarn from different staple fibres such as cotton, flax, jute, wool…etc.

Yarns either continuous filament or spun, can be assembled in different architectural forms as illustrated in Fig. 7. It could be stacks of unidirectional plies or produced using existing textile technologies such as weaving, knitting or braiding.

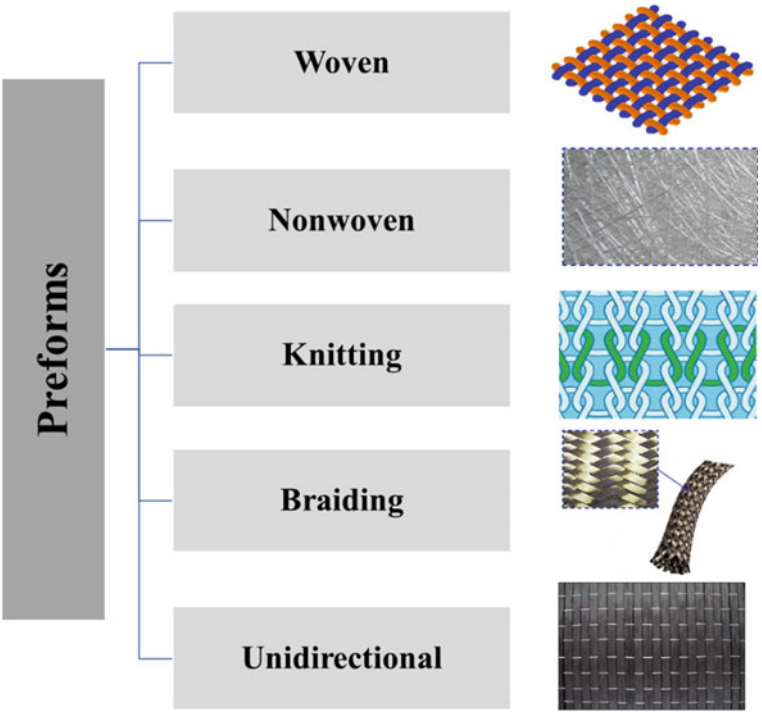

Fig. 7 Types of preforms

Woven fabric is composed of two constituents, warp yarns and weft yarns, usually the angle between the warp and weft direction is 90o. The most critical parameters of woven fabrics are related to fabric constructions.

Woven fabric construction parameters are:

- Dimeter of warp yarn or warp yarn count
- The diameter of weft yarn or weft yarn count
- Number of warp yarns per cm (warp density)
- Number of weft yarns per cm (weft density)
- The areal density of fabric gm/m^2
- Fabric structure.

In addition to the above parameter, fibre types of both warp and weft are of great importance. According to the above construction parameters and fibre material types, one can figure out the characteristics of woven fabric, which will be the preform for the composite structure.

Knitted fabrics are composed of interlaced loops. The horizontal row of loops is known as course, while the vertical row of loops is known as a wale. Knitted fabrics are formed with fewer stages than woven fabrics stages, making it much quicker, easier, and less costly. Knitting technology is classified into warp knitting, and weft knitting, usually weft knitted fabrics are not used in composites.

Knitted fabric construction parameters are:

- The diameter of yarn or yarn count
- Number of courses per cm
- Number of wales per cm
- Stitch length
- The areal density of fabric gm/m^2
- Fabric structure.

The braided fabric looks similar to woven fabric, but yarns are not orthogonal. Usually, the angle between yarns is between 20° and 160°. A braid is made by intertwining three or more yarns or strands with same or different materials. Braided fabric can be classified according to the shape, and it could be:

- Flat
- Tubular
- Solid.

Nonwoven fabric is neither woven nor knitted. These fabrics are made directly from fibre either short or continues filaments, that are consolidated with different methods. Consolidation method may be mechanical, or chemical or thermal. Properties and characterization of nonwoven fabric are firmly dependents on the fibre type and technology formation [19]. Unlike woven and knitted fabrics, nonwoven fabrics are engineered fabrics, and they are designed to perform a specific function. Moreover, the nonwoven fabrics are made through a one-step process from fibre to fabric, eliminating many steps, hence lowering the production cost to the extent that can make those fabrics cost-effective for even disposable applications.

3.2 Manufacturing Techniques

After constructing the preform that any technique from the ones mentioned above could be manufactured, the preform will go through the final stage or component production stage. The final properties of composite structure depend not only on the material type but also on how the composites are manufactured. Manufacturing green or natural fibre and hybrid composites can be manufactured using the conventional composite manufacturing processes such as hand layup, resin transfer moulding RTM, filaments winding and compression moulding. In this chapter, some selected techniques used in natural and hybrid composites will be reviewed.

Hand Layup

Resins or matrix materials are impregnated by hand into preforms that could be woven, knitted and nonwoven. This is usually carried out by rollers or brushes, using nip-roller type impregnators for pressing resin into the fabrics. Laminates are left to cure under standard atmospheric conditions or could be cured inside ovens or autoclaves. The main advantages of this method are simplicity and low tooling cost.

Pultrusion

Pultrusion is a composite manufacturing technique where continuous yarns are firstly entirely impregnated with the thermoset polymeric matrix then pulled through a heated die to form composites. The pultrusion process is accomplished by pull rather than push as in case of extrusion. The main advantage of the pultrusion process is the ability to form complex shapes such as I beam, C section, tubes and rods. The pultrusion process is a continuous production process.

Filament Winding

This process is mainly used for creating tubular components that are hollow and have a circular or oval cross-section, such as pipes and tanks. Yarns are passed through a resin bath then the impregnated yarns are wound onto a mandrel. Yarns orientations can be controlled by the traverse feeding mechanism, in conjunction with the mandrel's speed of rotation. Filament winding is mostly used for producing pipes especially for the petroleum industry and pressure vessels.

Resin Transfer Moulding (RTM)

In this process RTM, preforms are laid up in the form of single or multi stacks. These stacks of preforms are sometimes pre-pressed to the mould shape and held together using a binder. Then these preforms are stacked into the mould tool. The second mould tool is then clamped over the first mould. Resin is injected into the cavity mainly by pressure, and sometimes vacuum can also be applied to assist resin in being drawn into the fabrics. Once all the stack of preforms is wet out, the resin inlets are closed, and the laminate can be cured. This process can take place at either room temperature or elevated temperature. Generally, all thermoset resins such as unsaturated polyester, vinyl ester and epoxy can be used in this method.

Resin Infusion

Resin infusion or Vacuum Assisted Resin Transfer Moulding (VARTM) is a complicated manufacturing composite technique. Usually, it creates void-free or very low voids composites even in large or complicated moulds. In this process, the preform is laid into the mould in a dry form without any resin and then confined by a specific stack of bagging materials (such as peel ply, infusion mesh and bagging film) before being subjected to vacuum pressure using a vacuum pump. Once all the air has been removed or vacuumed from the bag, and the preform has been fully compressed, the resin is introduced to the preform through a pipe known as the spiral tube, then resin infuses through the preform under the vacuum pressure. After the resin has completely infused through the preform, the resin supply is closed, and the composite is left to cure under vacuum pressure.

Compression Moulding

There are two types of compression moulding, cold compression moulding and hot compression moulding. In this process, two matched metal moulds could be flat or shaped and used to fabricate composite products. In compression moulding, one plate is stationary while the other plate is movable. Preform and matrix are placed in between the two moulds then heat and pressure are applied as required for composite for a specific period. In the thermoplastic matrix, heat will be necessary to melt the matrix and flow through the preform. For thermoset matrix curing of the composite may take place either at room temperature or at some elevated temperature.

Many attempts have been tried to utilize the natural materials in the composite application using the techniques mentioned above and others. Sometimes just one technique has been used in the manufacturing process, and at other times a combination of more than one technique was used.

Mohareb et al. used VARTM to develop sandwich structure using lightweight and relatively thick core materials in particleboard panels from lignocellulosic resources attached to skin materials made of woven fabric to construct a high-performance structure for various technical applications [20]. In a similar work, Hassanin et al. used VARTM technique to develop high-performance particleboard from a mixture of wood particles and short glass fibres as hybrid core materials. In contrast, two layers of woven jute fabric were used as skin layers [21]. In the work of Hamouda et al. sandwich composites based on coir fibre nonwoven mats as core material and glass fibre is woven roving as the skin was manufactured by Vacuum Assisted Resin Transfer Moulding technique as well [22]. Sharkawi et al. have developed rebars for reinforcing light concrete to replace steel rebars. The RTM technique was implemented to produce natural yarns reinforced polyester bars with different fibre volume fractions [23].

4 Applications of Natural Fibre and Hybrid Composites

Applications of natural fibre composites (NFC) can be dated back to Ancient Egyptians who used to make bricks out of clay mud and straws, and this has been depicted on the tomb walls of Thebes showing Egyptian slaves mixing clay mud with straws and then drying the bricks in the sun [24]. Recently, the use of natural fibres as a reinforcement for polymer composites has gained a lot of attention, especially in the research community. There are numerous review articles published on the applications of NFC [25–28]. However, to date, the commercial use of NFC is limited to wood-plastic composites and automotive inner door panels [29]. Moreover, no single report or article has a statistic on the current NFC market, and most reports discuss the envisioned potential markets.

4.1 Barriers to the Diffusion of NFC

The world consumption of natural fibres that can be used as a reinforcement for composites is US$ 3.8 billion in 2017 with a CAGR of 2.3% from 2010 to 2017, as shown in Table 3. This is a strong indicator that the market is not growing as anticipated. This raises a valid concern; what's holding them back, what are the barriers to the adoption of NFC in the numerous applications of composite materials? To answer this question, one should refer to the diffusion of innovation theory developed by E. M. Rogers which explains how new ideas, technologies and products spread among participant in a certain social system [30].

i. Factors affecting the diffusion of innovation

Five main factors affect innovation diffusion: relative advantage, compatibility, complexity, trialability, and communicability.

In terms of comparative advantage, natural fibre reinforcements have many advantages over its inorganic counter-part glass fibres. They have low density, high specific properties, biodegradable, renewable resources, low carbon footprint, good thermal and acoustic insulation. Those relative advantages have to be emphasized when developing new products from NFC. This explains why the automotive industry is at the forefront of NFC adoption. These are all requirements for modern-day vehicles, especially with electric vehicles' growth and strict environmental regulation.

In terms of compatibility natural fibre reinforcements fall short, their hydrophilic nature makes them incompatible with the existing hydrophobic resin systems used in the industry. Moreover, their low thermal resistance limits their compatibility with thermoplastic matrices with high melting temperature. Furthermore, the high variability in their mechanical, chemical and physical properties and lack of standardization limit their compatibility with the quality standards set forth by specific industries such as the automotive and the aerospace. In addition, their coarse and hard nature makes them challenging to spin using existing spinning lines, and challenging

to convert into woven preforms, this explains why most natural fibre reinforcements are used in the nonwoven form. Moreover, their surface functional groups' incompatibility with the functional groups in existing resin systems results in poor fibre-matrix interfacial adhesion and very low load transfer efficiency. Finally, their low annual availability and seasonality make them incompatible with the large and consistent consumption of specific supply chains, such as the wind energy and construction industries. Such a low level of compatibility is the main reason preventing the diffusion of NFC and limiting their adoption.

In terms of complexity, the majority of the industry has the very low experience and knowledge on how to deal with natural fibre reinforcements, and there is a big gap between different value chain actors; upstream processors of fibres are low-tech, while downstream composite manufacturers are very high-tech. Hence, there is a compelling need to bridge this gap between the different value-chain actors and educate the farmers, fibre processors, and fabric makers on this new end-use of natural fibres, and meanwhile educate the composite manufacturers on this new type of reinforcement and how it has unique nature which is different from their synthetic counterparts.

In terms of trialability, natural fibre reinforcements are mostly grown in developing countries such as Bangladesh, India, Sri Lanka and Kenya. At the same time, composite manufacturers are primarily located in developed countries such as the United States, Western Europe, and Japan. This geographic barrier makes it difficult for composite manufacturers to try and experiment with natural fibre reinforcements easily. Moreover, the wide ban on planting hemp significantly limits its trialability. Flax is an exception in this context since it's mostly grown in France and Belgium, and the fact that there are many composite manufacturers located in those regions with easy and quick access to flax has significantly increased its trialability and made it the leading natural fibre reinforcements and the most widely used.

In terms of communicability, which means how easy is it for the user to see the benefits of using NFC? We will find that the most important benefits of using natural fibre reinforcements are intangible. They address a particular perceptual dimension related to protecting the environment, for instance, reduced carbon footprint, biodegradability, and renewability. Hence, their benefits cannot be easily and directly seen by the user. Other direct benefits can be easily perceived, such as their lightweight, high specific properties, good thermal insulation and vibration damping. The fact that their most important benefits cannot be easily seen by the user significantly limits their spread and adoption.

ii. The adopter groups

Another view of the diffusion of innovation theory is the adopter groups. The adopters of any new product or technology can be divided into two broad groups: the visionaries and the pragmatists [31]. The visionaries are those innovators and early adopters who are always excited about trying new things. Simultaneously, the pragmatists are the late adopters who are more resistant to changes and think hundred times before buying or trying a new product or technology. In this case, a value proposition that might attract the visionaries might never get acceptance by the pragmatists who

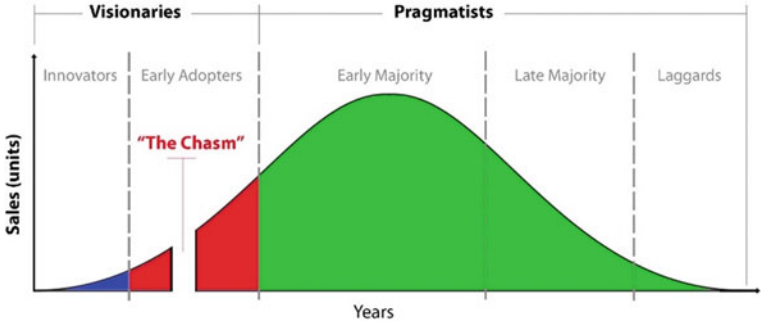

Fig. 8 Innovation adoption lifecycle

represent the mass market, and this is known as the chasm, as shown in Fig. 8. This clearly explains where the NFC is currently standing, and it's widely investigated and though after by researchers, hobbyists, entrepreneurs, and technology enthusiasts who represent the visionary group. Unfortunately, it's not getting that much acceptance by the industry and the end-markets who represent the pragmatist group. This is why most of the work done on NFC is part of a research program or coming out of a hobbyist garage. Their applications are mostly concentrated in sporting goods, musical instruments and small consumer products. NFC products should be developed from their early conception stages with the pragmatists in mind to cross this chasm and get a higher acceptance by the industry and the mass market. This is a big challenge because pragmatists look for fibres with competitive price, wide availability, and consistent properties. Unfortunately, this is not the case since most natural fibre reinforcements are expensive, and their annual availability is limited, and their properties suffer from high variability. The automotive industry is an exception in this context since the value proposition of the NFC, in this case, is fulfilling the strict environmental regulation imposed on such industry. Moreover, they can work closely with the tier 1 and 2 suppliers and control the entire chain from the farm to the final composite panels to ensure consistent quality, price and supply.

4.2 Commercial Applications of NFC

The commercial applications and indicators of industrial adoption of NFC have been compiled from JEC Composites International Market News (the world's leading composite industry magazine and exhibition) from 2011 to 2019, excluding wood-plastic composites [32]. Table 6 lists the commercial applications, indicating the product name, developer, announcement date, fibre type, and industry.

It's evident from Table 6 that NFC is widely used in sporting goods, including, surfboards, paddleboards and blades, skis, snowboards, bicycles, and skateboards. Figure 9 illustrates an example of NFC applications in sporting goods [33–37].

Table 6 Commercial applications of NFC compiled from JEC composites international market news 2011–2019 [32]

Application	Company/Institution	Date	Fibre	Industry
Domes for morris columns in Paris	JCDecaux and the city of Paris	Apr 2019	Flax	Outdoor advertising
Roof top tents	NaïtUp and Dehondt	Apr 2019	Flax	Sporting goods
Porsche 718 Cayman GT4 Clubsport body parts (driver and co-driver doors and the rear wing)	Porsche	Jan 2019	Flax and Hemp	Automotive
Mould tooling system	KS composites and composites evolution	Nov 2018	Carbon-flax hybrid	Industrial
Aerospace cabin interiors, cover panels and fuselage cladding panels, and onboard meals galleys	Assystem Technologies, Arkema, Cobratex, Specific Polymers, Cirimat, Compositadour, Lisa Aeronautics and Mécano ID	Nov 2018	Long bamboo strips	Aerospace
Volvo XC60 semi-structural automotive interior parts	Volvo Cars and Bcomp	Jun 2018	Flax (powerRibs)	Automotive
Longboard deck	ITA RWTH Aachen University and TU Clausthal	May 2018	Highly oriented natural fibre	Sporting goods
Savoy guitar	Blackbird and Ekoa linen	Dec 2017	Flax	Musical instruments
En V. fly-fishing rods	Edge rods and Lingrove	Dec 2017	Flax prepreg	Sporting goods
Electric GT racing car	Bcomp	Nov 2017	Flax (powerRibs)	Automotive
SeaBubble water taxi prototype	Décision and Carboman group	Jun 2017	Natural fibres	Marine
LINA car chassis	TU/Ecomotive	May 2017	Flax	Automotive
Pedestrian bridge	TU/e, TU Delft, NPSP composite, Avans Hogeschool and HZ University	Nov 2016	Hemp and Flax	Construction
Car parts (cup holder and fuse box)	Ford and Jose Cuervo	Jul 2016	Agave	Automotive
3D printed table	Oak Ridge National Laboratory	Jul 2016	Bamboo	Construction

(continued)

Table 6 (continued)

Application	Company/Institution	Date	Fibre	Industry
E-class of Mercedes-Benz roof frame	BASF and Mercedes-Benz	Apr 2016	Natural fibres	Automotive
CARBIO Hybrid automotive roof	Composites Evolution, SHD Composite Materials, KS Composites, Delta Motorsport, Jaguar Land Rover and Cranfield University	Oct 2015	Carbon-Flax hybrid	Automotive
AmpliTex SURF	Bcomp	Aug 2015	Flax	Sporting goods
Paddle board	BIC sports and Composites Evolution	Mar 2015	Flax	Sporting goods
Urban One Bamboo bicycle	Guapa Cycles and Composites Evolution	Feb 2015	Flax and bamboo	Sporting goods
Formula Student Electric car entire body	e-gnition team of the Technical University of Hamburg (TUHH)	Jan 2015	Flax	Automotive
Alpaca travel guitar	Alpaca Guitars	May 2014	Carbon-Flax hybrids	Musical Instruments
Volkswagen Golf seating, door panels, and front-end modules	FAURECIA and VW	Apr 2014	Flax	Automotive
Jaguar F-Type floor panel	EcoTechnilin and Jaguar	Dec 2013	Natural fibres	Automotive
Kayak paddle blade	VE Paddles and Bcomp	Dec 2013	Flax	Sporting goods
Speaker cone	Focal	Sept 2013	Flax	Musical instruments
Be.e electric scooter body	Van.Eko and Waarmakers	Aug 2013	Flax and Hemp	Automotive
BioMobile body, chassis and most structural parts	Haute Ecole du Paysage, d'Ingénièrie et d'Architecture de Genève	May 2013	Natural fibres	Automotive
ski Otwo	Stöckli and Bcomp	Jun 2013	Flax	Sporting goods
eco-kiteboard	FFC and Bcomp	Apr 2013	Flax	Sporting goods

(continued)

Table 6 (continued)

Application	Company/Institution	Date	Fibre	Industry
Wind turbine blade	University of Nottingham	Feb 2013	Flax	Energy
Packaging	VTT Technical Research Centre of Finland	Jan 2013	Peat	Industrial
Snowboard	Magine and Composites Evolution	Aug 2012	Flax	Sporting goods
Surfboard	Samsara and Composites Evolution	Jun 2012	Flax	Sporting goods
Monobloc chair	Werner Aisslinger and BASF	Jun 2011	Hemp and Kenaf	Construction

Moreover, the use of NFC in automotive is growing, especially in electric vehicles, racing and sports cars. Figure 10 illustrates examples of NFC applications in automotive [38–43].

Similarly, there is a growing interest in using NFC in interiors, building and construction, especially with the increasing trend for eco- and green buildings. Figure 11 illustrates examples of utilizing NFC in making chairs and pedestrian bridge [44, 45].

Finally, several attempts to develop musical instruments from NFC due to their special resonance and vibration damping. Figure 12 illustrates the applications of NFC in making guitars and speaker cones [46, 47].

5 Review Questions

(1) What are the main classes of natural fibres?
(2) Describe the microstructure of cellulosic fibres.
(3) What is the classification of cellulosic fibres?
(4) Discuss in details, the cellulosic fibre extraction methods.
(5) What are the main factors that affect natural fibre properties?
(6) What are the primary forms of composites preforming?
(7) Explain the available manufacturing methods to produce natural and hybrid fibre composites.
(8) What are the applications of natural fibre and hybrid composites?
(9) What are the reasons behind the fast-growing of natural fibres-based composites?
(10) Discuss in details the barriers to the diffusion if natural fibre composites.

Fig. 9 NFC applications in sporting goods, **a** Samsara surfboard, **b** Cobratex skateboard, **c** Magine snowboard, **d** Urban One bicycle and **e** ski Otwo (photos courtesy of JEC Composites) [33–37]

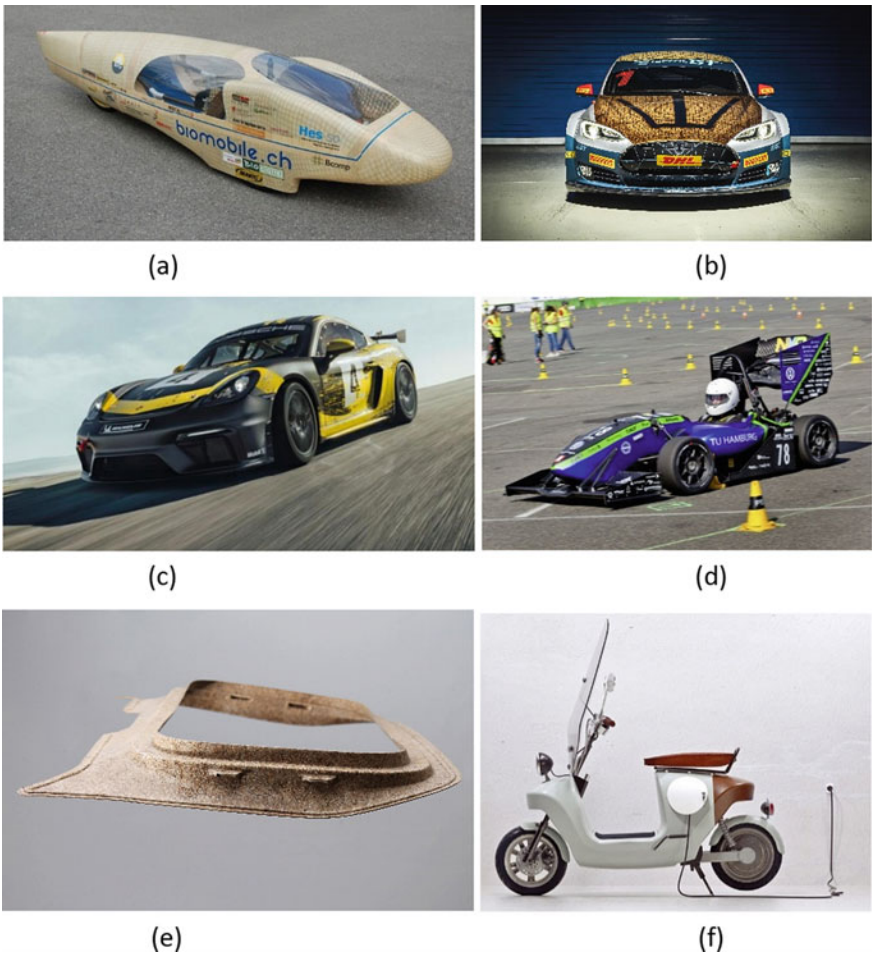

Fig. 10 NFC applications in automotive, **a** biomobile, **b** electric GT racing car, **c** Porsche 718 Cayman GT4 Clubsport **d** e-gnition Formula Student Electric car, **e** E-class of Mercedes-Benz roof frame, and **f** Be.e electric scooter (photos courtesy of JEC Composites) [38–43]

Fig. 11 NFC applications in building and construction, **a** Werner Aisslinger monobloc chair, and **b** AE + T pedestrian bridge (photos courtesy of JEC Composites) [44, 45]

Fig. 12 NFC applications in musical instruments, **a** Savoy guitar, and **b** Focal speaker cone (photos courtesy of JEC Composites) [46, 47]

References

1. Elseify, L.A., Midani, M., Shihata, L.A., El-Mously, H.: Review on cellulosic fibers extracted from date palms (Phoenix Dactylifera L.) and their applications. Cellulose **26**, 2209–2232 (2019)
2. Kalia, S., Kaith, B.S., Kaur, I.: Cellulose Fibers: Bio- and Nano-Polymer Composites Green Chemistry and Technology. Springer (2011)
3. Zeng, X., Mooney, S.J., Sturrock, C.J.: Assessing the effect of fiber extraction processes on the strength of flax fiber reinforcement. Composites: Part A **70**, 1–7 (2015)
4. Fidelis, M.E., Pereira, T.V., Gomes, O.F.M., Silva, F.A., Filho, R.D.: The effect of fiber morphology on the tensile strength of natural fibers. J. Mater. Res. Technol. **2**(2), 149–157 (2013)
5. Encyclopedia Britannica, https://www.britannica.com/science/leaf-fiber
6. Fan, M., Fu, F.: Advanced High Strength Natural Fibre Composites in Construction. Elsevier (2017)
7. Sood, M., Dwivedi, G.: Effect of fiber treatment on flexural properties of natural fiber reinforced composites: a review. Egypt. J. Pet. **27**, 775–783 (2018)
8. Ali, A., Hussain, T., Shaker, K., Nawab, Y., Jabbar, M., Militky, J., Baheti, V.: Hydrophobic treatment of natural fibers and their composites—a review. J. Ind. Text. **47**(8), 2153–2183 (2018)

9. Bos, H.L., Van Den Oever, M.J., Peters, O.C.: Tensile and compressive properties of flax fibres for natural fibre reinforced composites. J. Mater. Sci. **37**, 1683–1692 (2002)
10. Pickering, K.L., Beckermann, G.W., Alam, S.N., Foreman, N.J.: Optimising industrial hemp fibre for composites. Composites: Part A **38**, 461–468 (2007)
11. Thygesen, L.G., Asgharipour, M.R.: The effects of growth and storage conditions on dislocations in hemp fibres. J. Mater. Sci. **43**, 3670–3673 (2008)
12. Kalia, S., Kaith, B.S., Kaur, I.: Pretreatments of natural fibers and their application as reinforcing material in polymer composites—a review. Polym. Eng. Sci. **49**(7), 1253–1272 (2009)
13. Gassan, J., Bledzki, A.K.: Alkali treatment of jute fibers: relationship between structure and mechanical properties. J. Appl. Polymer Sci. **71**, 623–629 (1999)
14. Ray, D., Sarkar, B.K., Rana, A.K., Bose, N.R.: Effect of alkali treated jute fibres on composite properties. Bull. Mater. Sci. **24**(2), 129–135 (2001)
15. El Oudiani, A., Chaabouni, Y., Msahli, S., Sakli, F.: Crystal transition from cellulose I to cellulose II in NaOH treated Agave americana L. fibre. Carbohydr. Polyms. **86**, 1221–1229 (2011)
16. Hatakeyama, T.: Effect of bound water on structural change of regenerated cellulose. Makromol. Chem. **188**, 1875–1884 (1987)
17. Pickering, K.L., Efendy, M.G., Le, T.M.: A review of recent developments in natural fibre composites and their mechanical performance. Compos. Part A **83**, 98–112 (2016)
18. Hull, D., Clyne, T.W.: An Introduction to Composite Materials, 2 edn. Cambridge University Press, (1996)
19. Albrecht, W., Fuchs, H., Kittelmann, W.: Nonwoven Fabrics. WILEY-VCH, (2003)
20. Mohareb, A.S.O. Hassanin, A.H., Badr, A.A., Hassan, K.T.S., Farag, R.: Novel composite sandwich structure from green materials: mechanical, physical, and biological evaluation. J Appl Polym Sci **132**(28): 42253 (1:8) (2015)
21. Hassanin, A.H., Hamouda, T., Candan, Z., Kilic, A., Akbulut, T.: Developing high-performance hybrid green composites. Compos Part B **92**, 384–394 (2016)
22. Hamouda, T., Hassanin, A.H., Kilic, A., Candan, Z., Bodur, M.S.: Hybrid composites from coir fibers reinforced with woven glass fabrics: physical and mechanical evaluation. Polym Compos **38**(10), 2212–2220 (2015)
23. Sharkawi, A.M., Mehriz, A.M., Showaib, E.A., Hassanin, A.: Performance of sustainable natural yarn reinforced polymer bars for construction applications. Constr. Build. Mater. **158**, 359–368 (2018)
24. Elsayed, M.S.G.: Straw bale is future house building material. National Organization for Building Harmony, Egypt (2000)
25. Pandey, J.K., Ahn, S.H., Lee, C.S., Mohanty, A.K., Misra, M.: Recent advances in the application of natural fiber based composites. Macromol. Mater. Eng. **295**, 975–989 (2010)
26. Mohammed, L., Ansari, M.N.M., Pua, G., Jawaid, M., Islam, M.S.: A review on natural fiber reinforced polymer composite and its applications. Int. J. Polymer Sci. 1–15 (2015). Retrieved from https://doi.org/10.1155/2015/243947
27. Sanjay, M.R., Arpitha, G.R., Laxmana Naik, L., Gopalakrishna, K., Yogesha, B.: Applications of natural fibers and its composites: an overview. Nat. Resour. **7**: 108–114. (2016) https://doi.org/10.4236/nr.2016.73011
28. Pecas, P., Carvalho, H., Salman, H., Leite, M.: Natural fibre composites and their applications: a review (2018). https://doi.org/10.3390/jcs2040066
29. Puglia, D., Biagiotti, J., Kenny, J.M.: A review on natural fibre-based composites—Part II: application of natural reinforcements in composite materials for automotive industry. J. Nat. Fibres **1**(3) (2004)
30. Rogers, E.: Diffusion of Innovations, 5th edn. Simon and Schuster. ISBN 978-0-7432-5823-4, (2003)
31. Crawford, M., Di Benedetto, A.: New Products Management, 10th edn., McGraw-Hill International Edition. ISBN 978-0073404806
32. JEC Composites.: International Composites News: Natural Fiber (2019). Retrieved May/10, 2019, from https://www.jeccomposites.com/knowledge/international-composites-news?f%5B0%5D=field_product%3A29

33. JEC Composites.: Biotex Flax Fabric used to Create Eco-friendly Surfboard (2012). Retrieved May/10, 2019, from https://www.jeccomposites.com/knowledge/international-composites-news/biotex-flax-fabric-used-create-eco-friendly-surfboard
34. JEC Composites.: A Consortium to Develop Biosourced Composites Using Bamboo Fibres (2018). Retrieved May/10, 2019, from https://www.jeccomposites.com/knowledge/international-composites-news/consortium-develop-biosourced-composites-using-bamboo-fibres
35. JEC Composites.: Magine and CIC Showcase Biocomposite Snowboard (2012). Retrieved May/10, 2019, from https://www.jeccomposites.com/knowledge/international-composites-news/magine-and-cic-showcase-biocomposite-snowboard
36. JEC Composites.: A Bicycle Made with Bamboo and Flax Composite (2015). Retrieved May/10, 2019, from https://www.jeccomposites.com/knowledge/international-composites-news/bicycle-made-bamboo-and-flax-composite
37. JEC Composites.: Bcomp with Linen Incredible (2013). Retrieved May/10, 2019, from https://www.jeccomposites.com/knowledge/international-composites-news/bcomp-linen-incredible
38. JEC Composites.: Huntsman Bio-based Materials help to Take Sustainable Mobility to the Next Level (2013). Retrieved May/10, 2019, from https://www.jeccomposites.com/knowledge/international-composites-news/huntsman-bio-based-materials-help-take-sustainable-mobility
39. JEC Composites.: A Renewable Lightweight Composite Panels For The Electric GT Racing Car (2017). Retrieved May/10, 2019, from https://www.jeccomposites.com/knowledge/international-composites-news/renewable-lightweight-composite-panels-electric-gt-racing
40. JEC Composites.: Porsche 718 cayman GT4 Clubsport Featuring Natural-Fibre Body Parts (2019). Retrieved May/10, 2019, from https://www.jeccomposites.com/knowledge/international-composites-news/porsche-718-cayman-gt4-clubsport-featuring-natural-fibre
41. JEC Composites.: An Electric Race Car Made with Natural Fibres Fabrics (2015). Retrieved May/10, 2019, from https://www.jeccomposites.com/knowledge/international-composites-news/electric-race-car-made-natural-fibres-fabrics
42. JEC Composites.: First Automobile Roof Frame Made of Natural Fiber (2016). Retrieved May/10, 2019, from https://www.jeccomposites.com/knowledge/international-composites-news/first-automobile-roof-frame-made-natural-fiber
43. JEC Composites.: Van.eko Launches the World's First Bio-based Electric Scooter (2013). Retrieved May/10, 2019, from https://www.jeccomposites.com/knowledge/international-composites-news/vaneko-launches-worlds-first-bio-based-electric-scooter
44. JEC Composites.: First Natural Fiber Monobloc Chair. (2011). Retrieved May/10, 2019, from https://www.jeccomposites.com/knowledge/international-composites-news/first-natural-fiberfibre-monobloc-chair
45. JEC Composites.: A Biocomposite Bridge (2016). Retrieved May/10, 2019, from https://www.jeccomposites.com/knowledge/international-composites-news/biocomposite-bridge
46. JEC Composites.: Blackbird Introduces its Savoy Guitar (2017). Retrieved May/10, 2019, from https://www.jeccomposites.com/knowledge/international-composites-news/blackbird-introduces-its-savoy-guitar
47. JEC Composites. Focal introduces a speaker cone made of flax fibres composites (2013). Retrieved May/10, 2019, from https://www.jeccomposites.com/knowledge/international-composites-news/focal-introduces-speaker-cone-made-flax-fibres-composites
48. Thakur, V.K.: Lignocellulosic Polymer Composites: Processing, Characterization, and Properties. Scrivener Publishing LLC (2015)

Machining of Bio-composites

Mridusmita Roy Choudhury and Kishore Debnath

Abstract Due to growing environmental concerns, the engineers and researchers have shifted to using renewable resources to replace many non-renewable, conventional materials like metals and synthetic fibres. Natural fibre-reinforced polymer composites (bio-composites) are usually human-made materials that have gained huge attention in various fields of engineering applications. However, the difficulties in the secondary manufacturing of these composites due to the anisotropic and heterogeneous nature create a barrier in the large-scale production of bio-composites products. This chapter deals with various machining operations associated with natural fibre-reinforced composites. The challenges faced during the machining of natural fibre-reinforced composites have been summarised. Different ways of assisting the quality and improvement of the machined surface have been discussed.

1 Introduction

The popularity of polymer composites is increasing rapidly over the past decades due to their excellent properties and potentiality to replace many conventional materials. Reinforcing the polymer composites with natural fibre can resolve the problem associated with on-going environmental issues. Natural fibre-reinforced polymer composites are humanmade sustainable materials which are also called bio-composites. Bio-composites may be partially degradable or fully degradable based on the nature of the polymer matrix. Fully degradable bio-composites are called green composites. Green composites consist of biodegradable polymer derived from natural sources. The fabrication of bio-composites composites is not a complicated process. Scientists over the past years have developed many advanced processing technologies to obtain high-quality, reinforced composites.

Large scale production of simple and complex bio-composites products requires the assembly of many single composite parts. In this regard, some secondary manufacturing processes such as machining, joining, will be necessary. The machining

M. R. Choudhury · K. Debnath (✉)
Department of Mechanical Engineering, NIT Meghalaya, Shillong 793003, India

I. Shyha and D. Huo (eds.), *Advances in Machining of Composite Materials*,
Engineering Materials, https://doi.org/10.1007/978-3-030-71438-3_16

operations required to produce natural fibre-reinforced composites products include drilling, milling, turning, etc. Anisotropic and in-homogeneous natures of the natural fibre-reinforced composites act as barriers during machining operations and produce defects such as delamination, fibre pull-out, matrix burning, chipping, spalling, micro-cracks, and also, reduce the strength of the composite structure [1]. These defects may lead to stress concentration and immature failure of composites during their service life. These damages are the consequent result of the higher induced forces and temperature during machining. It is essential to study their machining behaviour to increase the applications of bio-composites in various fields. The most critical machining operation for the assembly of multiple components is hole making "drilling". Many researchers have extensively studied the drilling behaviour of bio-composites. However, research data related to milling and turning of bio-composites are relatively less. Bio-composites' machining behaviour is influenced by factors such as feed rate, spindle speed, tool geometry, depth of cut, machining conditions, fibre characteristics, etc. The high-quality machined surface of bio-composites with minimum damage can be obtained by selecting a proper parametric setting.

In this chapter, an attempt is made to provide details on machining bio-composites and addressing the challenges faced. The effect of varying machining process parameters on the quality of the machined surface has been discussed.

2 Bio-composites

Bio-composites are composed of natural fibre and polymer matrix. Natural fibre can replace many of the expansive synthetic fibres when the high elastic modulus is not an essential factor. Owing to the excellent properties, biodegradability, and inexpensive nature of natural fibres, they have been used as reinforcing materials over the past years. Natural fibre can be derived from plant, animal, and mineral-based sources as well. There are different shapes of the natural fibres in the polymer matrix, such as short and long fibre reinforcement, mat fibre reinforcement, flake reinforcement, and particulate reinforcement. The reinforcement element of the composites holds and binds together by the matrix material. The integrity, tolerance, and durability of composites laminate are determined by the matrix material. Many petrochemical-based polymer matrices are available in the market obtained from fossil fuels like coal and natural gas [2]. The petroleum-based polymer matrixes are of two types: thermoplastic polymer and thermosetting polymer. The thermoplastic polymer can quickly melt at its melting temperature and re-moulded in the required shape upon cooling. Thermosetting polymers are infusible and insoluble materials that can be cured with the help catalyst [3]. Due to the growing environmental concern, researchers have focused on developing a bio-sustainable polymer that can degrade to the environment called a biodegradable polymer. Natural fibre-reinforced composites may be fully biodegradable or partially-biodegradable depending upon the nature of the polymer matrix used.

The polymer matrix for the fabrication of bio-composites can be selected based on their thermal, mechanical, and application areas. Table 1 illustrates various polymers and their properties that have been used by manufacturers for the fabrication of bio-composites. The potentiality of poly(lactic) acid (PLA) polymer has been increased over the past decades due to its biodegradable nature. Figure 1 shows two bio-composites, such as bamboo/PLA and bagasse/PLA. Woven bamboo fibres have been used to fabricate the bamboo/PLA bio-composites in the compression moulding machine. The bagasse/PLA bio-composite has been manufactured using short bagasse fibre in an injection moulding machine. PLA based bio-composites have found their applications in packaging industries, automobile industries and making mobile phone and computer shells.

Table 1 Various polymer materials studied for the fabrication of bio-composites [4–6]

Polymer	Density, ρ (g/cm^3)	Tensile strength (MPa)	Origin	Remark
Epoxy	1.25	69	Petroleum-based thermoset	– High water resistance – Low curing shrinkage – Long working times ability – Non-biodegradable
Polyester	1.37	123	Petroleum-based thermoset	– Easy to use – Lowest cost – Non-biodegradable
Vinylester	1.05	76	Petroleum-based thermoset	– Very high chemical and environmental resistance – Non-biodegradable
Phenolic	1.35	6	Petroleum-based thermoset	– High fire resistance – Non-biodegradable
Glycix	1.61	–	Petroleum-based thermoset	– Biodegradable
Polyethylene	0.9–1.4	15	Petroleum-based thermoplastic	– Poor weathering resistance – Flammable – High thermal expansion – Non-biodegradable

(continued)

Table 1 (continued)

Polymer	Density, ρ (g/cm^3)	Tensile strength (MPa)	Origin	Remark
Polypropylene	0.9–1.24	33	Petroleum-based thermoplastic	– Difficult to process – Comparatively expensive – Limited availability – Non-biodegradable
Polystyrene	0.96–1.05	18.6–50.9	Petroleum-based thermoplastic	– Flammable – Low impact resistance – Brittle – Non-biodegradable
Polyvinyl chloride	1.38	69–25	Petroleum-based thermoplastic	– Poor resistance to UV – Poor resistance at low and high temperatures – Non-biodegradable
PLA	1.24	28	Natural thermoplastic	– Non-toxic – Poor impact strength – Low-cost – Biodegradable
PGA	1.53	14.03	Natural thermoplastic	– Biodegradable
PHA	–	4	Natural thermoplastic	– High molecular weight – Biodegradable
PLGA	1.30	20.7–42	Natural thermoplastic	– Biodegradable
PCL	1.11–1.14	8.5–19.6	Natural thermoplastic	– Biodegradable
PEA	1.09	25	Natural thermoplastic	– Biodegradable
Starch	1.3	62	Natural thermoplastic	– Biodegradable
PBS	1.23	25	Natural thermoplastic	– Biodegradable
PHB	1.25	28	Natural thermoplastic	– Biodegradable

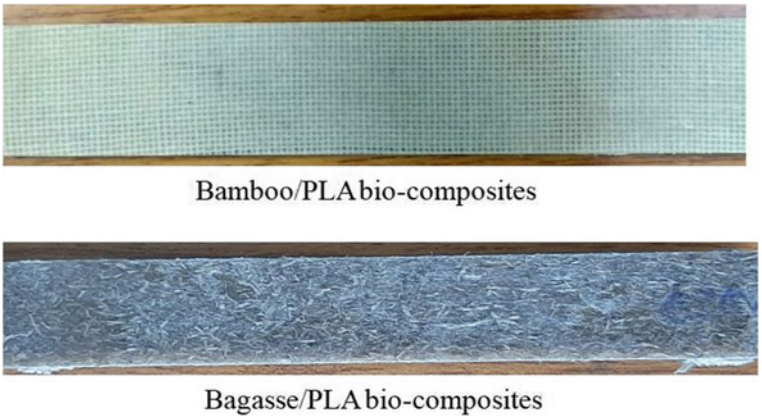

Fig. 1 PLA based bio-composites

3 Machining of Bio-composites

Various conventional and non-conventional techniques are used for machining of bio-composites to obtain the final shape. Amongst these techniques, drilling is the most commonly used machining operation in natural fibre-reinforced composites. Drilling operation is carried out to achieve a circular hole on the composite surface. The drilled hole may be pilot, through, or blind according to the purpose of applications. There are various drilling techniques available that can be employed to produce a hole, as illustrated in Fig. 2. Conventional drilling is the most common and widely used technique to make a hole in the composite parts [7]. The mechanical drilling operation typically produces holes required to facilitate the bolted and riveted joints. The details of different tools used for mechanical drilling of natural fibre-reinforced composites are presented in Table 2. The drilling tool's geometry plays a vital role

Fig. 2 Different drilling techniques for making a hole in bio-composites

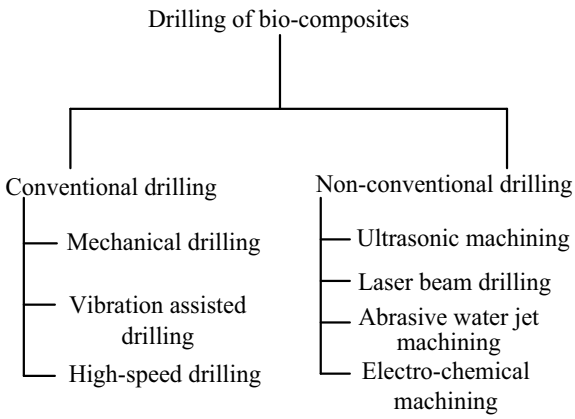

Table 2 Tool and tool material used for drilling of bio-composites [7, 8]

Cutting tools	Straight-flute drill, core drill, step-core drill, trepanning tool, 8-facet drill, Jo drill, 4-facet drill, tripod drill, parabolic drill, step drill, straight shank drill, brad and spur drill, candlestick drill, saw drill and dagger drill
Materials	High-speed steel (HSS), solid carbide, coated cemented carbides, uncoated cemented carbides and polycrystalline diamond

in determining the hole's quality by affecting the operation's forces. The traditional twist drill used for producing a hole in conventional materials is not suitable for polymeric bio-composites. The chisel edge of a drill bit contributes the maximum amount of induced force in the drilling operation. Therefore, the drilling tool's smaller point angle is suitable for making a hole in bio-composites [1, 8]. Small point angle in the drilling tool helps in making the chisel edge sharp. Vibration assisted drilling (VAD) is a different form of the mechanical drilling process. In VAD, vibration is established with a piezo-electric crystal oscillator either on tool or composites to establish distinct contact between them.

VAD is pulsed intermittent drilling and proved to be a potential drilling method for making a hole in fibre-reinforced composites [9, 10]. High-speed drilling is conducted in a high-speed machine, producing a high-quality hole on bio-composites [7]. High-speed drilling of bio-composites is much costly process as compared to the mechanical drilling and VAD process. Looking into the damage produced in bio-composites during conventional drilling, researchers have shifted their interest to the novel and non-conventional techniques such as ultrasonic machining, laser beam drilling, abrasive machining, and electrochemical machining. The non-conventional methods are beneficial while making macro-, micro-, and nano-holes in bio-composites. In ultrasonic machining, high-frequency mechanical vibration is produced with the help of a transducer. Laser beam drilling is a contact-less material removal process where pulsed laser energy is focused on the surface to be drilled. While in abrasive water jet machining, a high-pressure water jet is focused on the composite's surface to produce the required hole. Electro-chemical machining is an electrochemical process used to remove material from the composite materials.

Milling, turning, and grinding are the machining operations used to obtain the final shape, tolerance, and assemble of various smaller composites parts. Milling and turning operations are needed for getting a finished and accurate dimension of the fabricated natural fibre-reinforced composites product. The non-homogeneous and non-isotropic internal structure of the natural fibre of bio-composites makes the machining task very difficult to perform by inducing different surface defects. Hence, assessing the caused damage related to the machining of natural fibre-reinforced composites and the failure mechanism analysis will help select optimal parametric settings to composite manufacturing industries. This will also lead to the large-scale production of composites part by improving their machine-ability.

4 Challenges During Machining of Bio-composites

Defect-free and high-quality machining is crucial for manufacturing bio-composites products since the induced damage may lead to premature failure when applied to practical field [11]. Defects in the machined surface during machining of bio-composites have become the challenges for the manufactures to overcome. This can be eliminated by directly observing and controlling the induced damages (delamination, surface roughness, burr formation, micro-cracks, fibre burning, etc.) or indirectly monitoring the induced machining forces and temperature. The damages that occur during the machining of bio-composites are discussed below.

4.1 Delamination

Delamination is the most commonly visible defect in the machining of bio-composites. Delamination generally occurs when the layers of composites laminate get separated from each other (Fig. 3). This type of defect may occur at the time of entry and exit of the drill bit during bio-composites drilling. The delamination at the entry of the drill is called peel-up delamination. Peel-up delamination is the result of the twisting moment produced by the induced torque during machining. The second type of delamination called push-out delamination occurs at the exit of the drill bit. The induced thrust force is the cause of push-out delamination in the composite laminates [12]. As the drill bit starts to penetrate the composite laminate, the top-most layer of the laminate gets abraded and moves upward by the action of cutting edge. As the tool progresses with the downward feed, the abraded layer gets spiralled along with the drill bit's flute, resulting in the separation of one layer of the laminate from the other. As the tool's cutting edge reaches the lower-most layer of the composites laminate, it pushes the lower layer by the compressive thrust force's action. Due to this action, the lower layers of composites' interlaminar bond decrease in strength and finally drawn away.

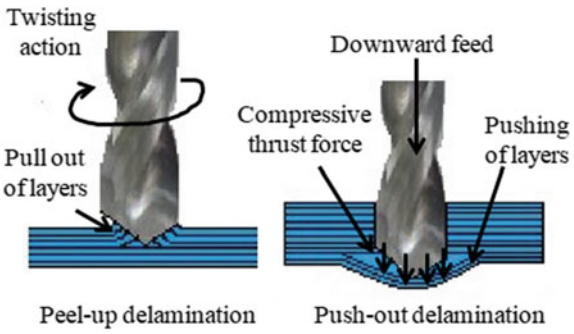

Fig. 3 Delamination mechanism

The occurrence of delamination defect is considered very dangerous as it results in the low quality of the machine surface. The overall reduction in strength of the composite also occurs due to the presence of this defect. Manufacturers should minimise delamination defects during machining to reduce the rejection rate of composite parts in the inspection unit. Due to the risk of delamination, researchers have focused on developing various techniques to measure and quantify this defect. Some of the techniques and methods of measuring and quantifying delamination are visual methods, image processing, acoustic emission, scanning acoustic microscopy, ultrasonic C-scan, radiography, computerized X-ray tomography, and shadow moire laser interferometer [13]. Delamination in the composite parts can be quantified by different non-dimensional parameters, such as delamination factor (F_d), delamination size, damage ratio and shape's circularity [14]. Equations established to estimate the delamination factor, delamination size, damage ratio, and shape's circularity are given in the Eqs. (1–4) [15].

$$\text{Delamination factor } (D_f) = \frac{\text{Overall area (nominal area and delaminated area)}}{\text{Nominal area}} = \frac{A_{\text{nominal}} + A_{\text{delaminated}}}{A_{\text{nominal}}} \tag{1}$$

$$\text{Delamination size} = \frac{D_{\text{maximum}} - D}{2} \tag{2}$$

$$\text{Damage ratio} = \frac{D_{\text{maximum}}}{A_{\text{avgerage}}} \tag{3}$$

$$\text{Shape's circularity} = 4\Pi \frac{A_e}{P_e^2} \tag{4}$$

Terms used in the above equations can be understood by Fig. 4. which shows delamination produced during drilling of nettle/epoxy bio-composites. The nominal area ($A_{nominal}$), delaminated area ($A_{delamination}$), maximum diameter ($D_{maximum}$), nominal diameter ($D_{nominal}$), equivalent area (A_e), and equivalent perimeter (P_e) of the delaminated drilled hole is illustrated in the figure.

Delamination is also associated with the milling operation of bio-composites. Assessment of delamination produced in milling operation is also essential to obtain a high-quality damage-free milled surface. Delamination induced in milling operation is quantified by the delamination factor given by Eq. (5) [16]. It is the ratio of the width of maximum damage (W_{max}) to the nominal width of the cut (W). Delamination occurred during milling operation performed in bamboo/PLA green composites shown in Fig. 5. The maximum damage (W_{max}) and the nominal width of the cut (W) are identified in the figure.

$$\text{Delamination factor } (F_d) = \frac{W_{\max}}{W} \tag{5}$$

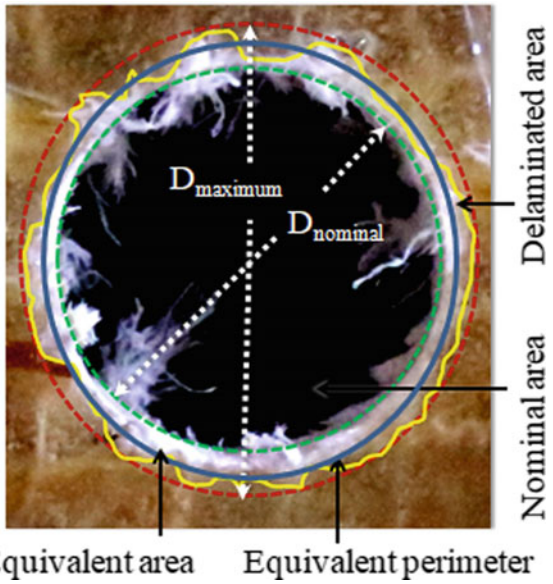

Fig. 4 Measurement of delamination factor

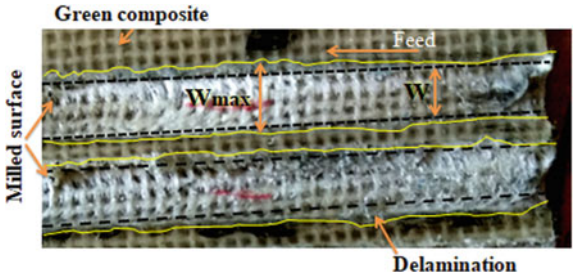

Fig. 5 Delamination in milling surface

The SEM image of delamination produced during milling of kenaf fibre reinforced bio-composites is shown in Fig. 6 [17].

4.2 Surface Roughness

Surface irregularities and error in the hole's size are called geometric defects that occur during bio-composites machining. The accurate size of the hole, coupled with a smooth machined surface is essential to obtain a close tolerance of the composite components' dimensions. The surface roughness of a machined surface, and the drilled hole's accuracy significantly affect the composite's components' integral structure. The factors such as precision fits, fatigue loads, fastener holes, and aesthetic requirements depend upon the composite laminate's geometric accuracy. The surface

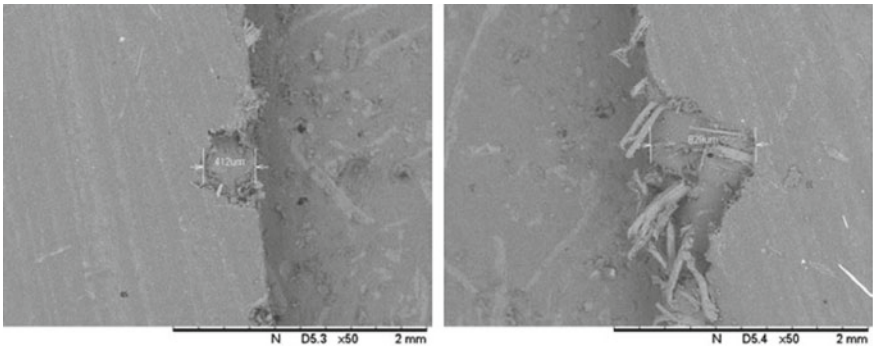

Fig. 6 SEM image showing delamination during milling of kenaf fibre reinforced bio-composites [17]

of bio-composites during machining becomes rough, mainly because of two reasons. The first reason is the presence of un-sheared fibre extremities on the surface after the machining. These extremities kept leaned in the feed's direction on the machined surface, which causes a roughened surface. The presence of fibre extremities on the surface after machining is shown in Fig. 7a. Secondly, due to the interface break down of fibres during machining. The low adhesion among the elementary fibres of the composites allows breaking down their interface bonding quickly in the presence of shearing force. The breaking of interface bonding of the elementary fibres due to shear is called interface break. The interface break phenomenon is shown in Fig. 7b. The surface roughness of a machined surface of a bio-composite can be analysed basically by three methods: centreline average (CLA) method, root mean square (RSM) method, and ten-point height method. The irregularities on a surface can be denoted by picks and valleys concerning the vertical deviations.

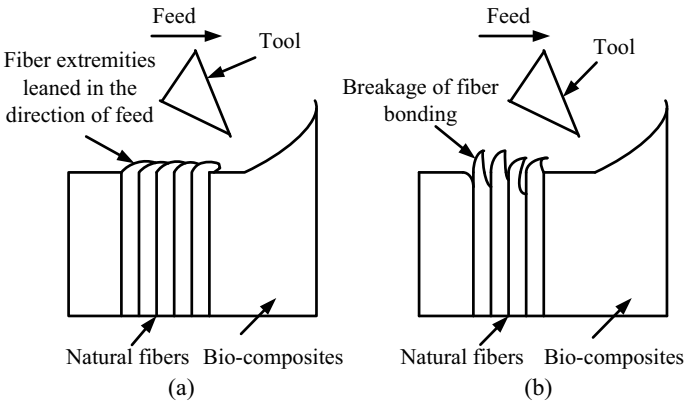

Fig. 7 Surface roughness due to **a** fibre extremities leaned in the direction feed and **b** interface break between the fibres

In CLA method, surface roughness (R) is measured by taking the arithmetic mean of the vertical deviations from the nominal surface. The arithmetic sign of the deviations is neglected in this method. In the RSM method, surface roughness is measured by taking the square root of the arithmetic mean of the square of the vertical deviations from the mean line. Mathematical equations used for calculating surface roughness by CLA and RSM methods are given in Eqs. (6)–(7). The ten-point height method is the easiest way to calculate the surface roughness of a machined surface. In this method, five values of the highest peaks and lowest valleys are considered. These values are measured from a line drawn parallel to the mean line. To calculate the surface roughness arithmetic difference between the average of five peak values and five valley values are obtained. The mathematical equation of the ten-point height method is given in Eq. 8.

$$\mathrm{R(CLA\ \ method)} = \frac{Y_1 + Y_2 + Y_3 + Y_4 \ldots + Y_n}{n} = \frac{A_1 + A_2 + A_3 + A_4 \ldots + A_n}{n} \tag{6}$$

$$\mathrm{R(RSM\ method)} = \sqrt{\frac{Y_1^2 + Y_2^2 + \ldots + Y_n^2}{n}} \tag{7}$$

$$\mathrm{R(ten\text{-}point\ height\ method)} = \frac{1}{5}[(R_1 + R_2 + R_3 + R_4 + R_5) - (R_6 + R_7 + R_8 + R_9 + R_{10})] \tag{8}$$

Nowadays, various instruments are available that can be used to measure the surface roughness of the machined surface. These instruments are easy to use and provide accurate results digitally in a few seconds. Some of such instruments are stylus probe instrument, profilometer, Tomlinson surface meter and Taylor-Hobson Talysurf. A stylus probe surface roughness tester (Surtronic S-128, Make: Taylor Hobson) has been used to measure a drilled hole's surface roughness during drilling of nettle/epoxy bio-composites [15]. The surface roughness was measured in six diverse zones of hole surface separated by 0°–180°. The surface roughness is measured in microns (μm), and the arithmetic average height (Ra) was considered throughout the analysis, as shown in Fig. 8. The surface characteristic of the milling surface of bamboo/PLA has been analysed by measuring the surface roughness using Taylor Hobson, Surtronic S-128 at a cut-off length of 0.25 mm as shown in Fig. 9.

The surface roughness profile of three different bio-composites (bamboo/polypropylene, miscanthus/polypropylene and sisal/polypropylene) before and after milling process is shown in Fig. 10 [18] Peaks represent the exceed fibre extremities occur due to imperfect fibre shearing. Valleys represent the detached fibre result from a breakage at the fibre–fibre interface. The roughness profile of the milled surface of sisal and miscanthus fibre bio-composites is more irregular than the bamboo fibre reinforced bio-composites. Figure 11 shows the SEM image of bio-composites before and after profile milling of different bio-composites [18]. Different morphological behaviour is observed based on the

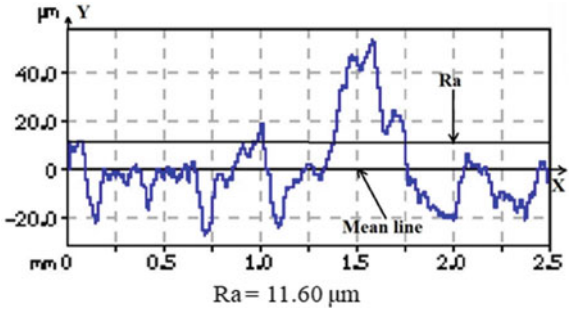

Fig. 8 Surface roughness graph obtained during drilling of nettle/epoxy bio-composites using an 8-facet drill bit

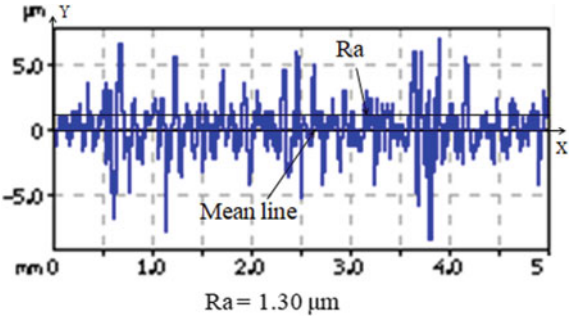

Fig. 9 Surface roughness graph obtained during milling of bamboo/PLA bio-composites using end mill cutter

different cutting signature of the reinforced natural fibres. The surface morphology of bamboo/polypropylene bio-composites appears to be smooth compared to the other two bio-composites. In another study, the morphology of a drilled hole made on sisal/epoxy and sisal/PP bio-composites at low feed and spindle speed using parabolic drill bit is compared, and more damage is found in the hole produced on sisal/epoxy than the sisal/PP bio-composites [19]. This because of the lower glass transition temperature of PP compared to epoxy.

Moreover, due to thermoplastic softening characteristic of PP, the formation of recast layer occurs. This recast layer helps in preventing moisture absorption when reinforced with natural fibres. Fibre pull-out (an overhanging bunch of uncut fibres at the exit of the hole), bending of fibres protruding out of the hole sidewall, fibre de-bonding hole sidewall is observed during drilling of sisal/epoxy bio-composites. Smearing of thermoplastic polymers, protrusion of clustered fibres, buckling of fibres and de-bonding are observed during drilling of sisal/PP bio-composites [19].

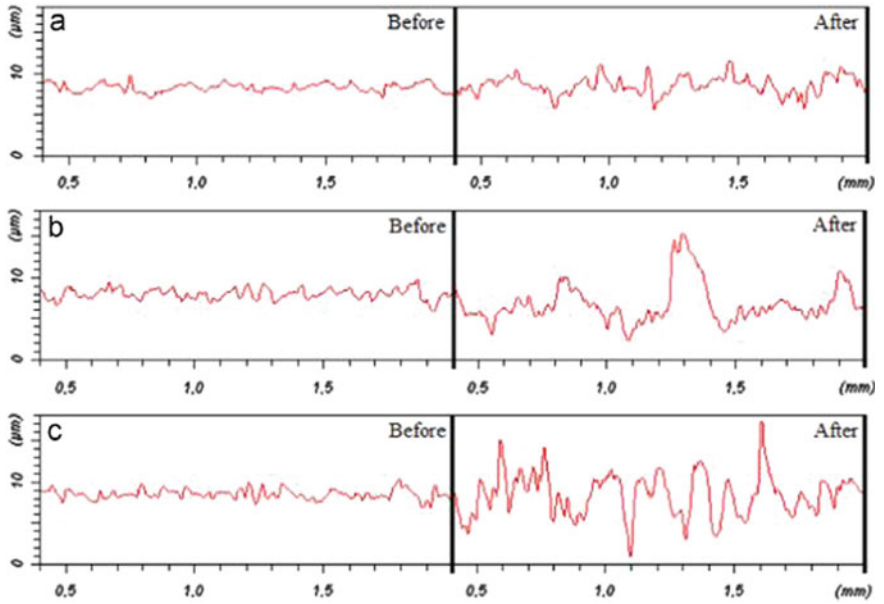

Fig. 10 Surface roughness pattern before and after profile milling of **a** bamboo/polypropylene, **b** miscanthus/polypropylene, and **c** sisal/polypropylene [18]

4.3 Other Machining Defects

In addition to the difficulties mentioned in the above sections, some other difficulties such as the formation of micro-cracks, matrix burning, fibre bulking, chipping and spalling are also related to machining bio-composites [20, 21]. These defects are also important to be considered form a design point of view as this can reduce the overall strength of the composite laminate.

Micro-cracks in the composite laminates originate when exposed to tensile and fatigue loading, different temperature conditions, and thermo-cycling. The inter-laminar crack, ply crack, and transverse crack are the micro-cracks class at the interface. The developed micro-cracks in composite progress in the traverse direction and the composite's thickness significantly affect the composite's mechanical and thermal properties. The properties like effective moduli, Poisson ratios, and thermal expansion coefficients of the composite are mostly affected by the presence of micro-cracks [22]. Micro-cracks act as a stimulating agent for other kinds of defects such as delamination, fibre braking, fibre spalling, and fibre chipping. The buckling of fibres occurs due to too much moisture present in the composite material's reinforced fibres. Fibre buckling weakens the adhesive bonding between the fibre and matrix material. This may lead to interlaminar de-bonding in the presence of machining forces. Another problem associated with the machining of bio-composites is the formation

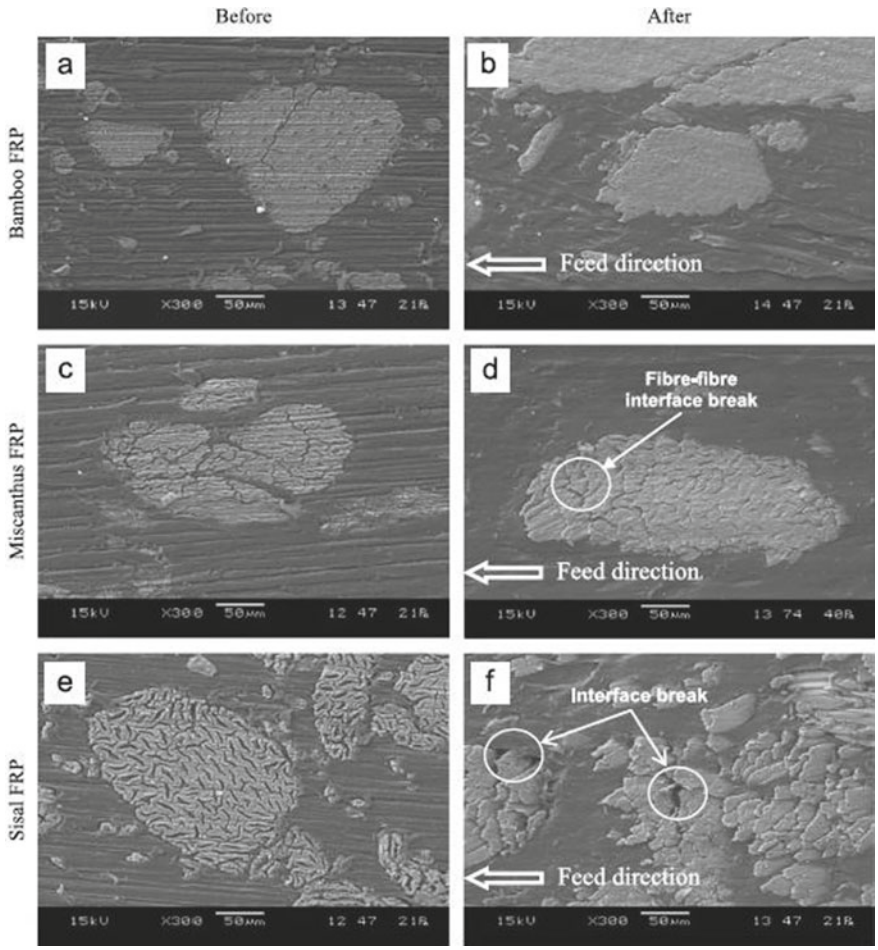

Fig. 11 SEM image of surface morphology of bio-composites before and after profile milling process [18]

of burrs. Burrs are the undesirable projection coming out form the composites material and act as a barrier during assembly operations [23, 24]. Figure 12 shows the formation of burrs during milling of bagasse/PLA green composites. The chips that get partially deformed during machining tend to bend in the direction of feed and results in the formation of burrs.

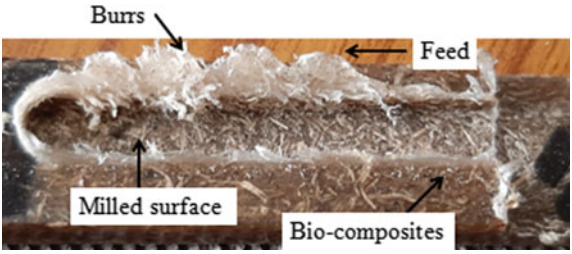

Fig. 12 Formation of burrs during milling of bio-composites

4.4 Machining Induced Forces

The damages produced during machining of bio-composites result from higher machining forces induced during the operations [8]. Damage previously present in the machined surface becomes severe in the presence of higher induced forces. The thrust force and torque are the indirect assessment of damage produced during drilling. High forces induced during machining may lead to tool wear or tool blunting. This is due to the high friction between the natural fibre and the tool's cutting edge [8]. Keeping the induced forces to minimum value the damages associated with bio-composites machining can also be controlled. Therefore, it is crucial to monitor the induced forces during machining of bio-composites. In a drilling operation, mainly two forces are essential to study: thrust force and torque. Force exerted on the composites in the axial direction by the drill bit is called thrust force. The tangential force generated during drilling is called cutting force or torque. The induced forces during drilling are highly depended upon the process parameters. The mathematical model for induced thrust (F_{thrust}) and torque (F_{torque}) obtained during drilling of coir/polyester in relation to the process parameters such as spindle speed (s), feed rate (f), and drill bit diameter (d) is given in the Eqs. (9)–(10) [25].

$$F_{\text{thrust}} = 16.6 + 8.8\,\text{d} + 0.0120\,\text{s} + 8.3\,\text{f} - 0.00425\,\text{ds} + 0.0767\,\text{sf} - 28.3\,\text{fd} \tag{9}$$

$$F_{\text{torque}} = 2.93 - 0.257\,\text{d} + 0.000542\,\text{s} - 1.1\,\text{f} + 0.000045\,\text{ds} + 0.000700\,\text{sf} + 1.45\,\text{fd} \tag{10}$$

In milling operation mainly three orthogonal components of forces such as F_x (force in the x-direction), F_y (force in the y-direction), and F_z (force in the z-direction) are important to determine. The resultant of these three forces, i.e., F_w is generally used to study the milling behaviour of bio-composites. The resultant force (F_w) is calculated using Eq. (11) [26].

$$F_w = \sqrt{F_x^2 + F_y^2 + F_z^2} \tag{11}$$

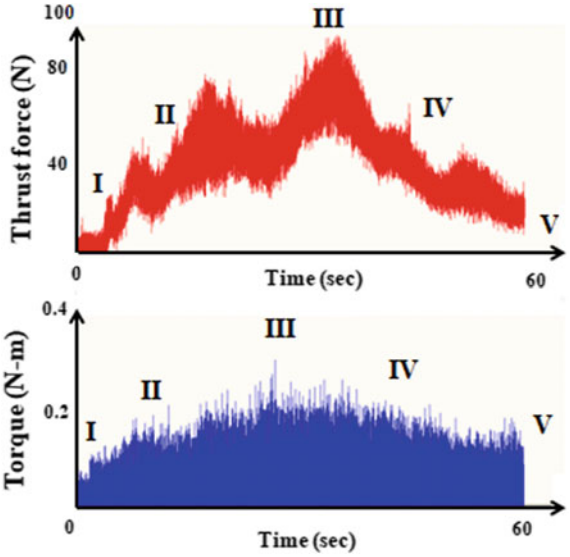

Fig. 13 Induced forces captured by a dynamometer during drilling of nettle/epoxy bio-composites. (feed: 8 mm/min; spindle speed: 710 RPM; drill bit: step drill)

The induced forces can be measured with the help of dynamometer. A dynamometer is connected with a multi-channel charge amplifier and data acquisition system to monitor the induced forces. The composite to be machined has to be mounted on the dynamometer with the help of fixture. Force signal captured during drilling of nettle/epoxy bio-composites with a dynamometer attached to the multi-channel charge amplifier (Make: Kistler, Type: 5070 A) and data acquisition card (Make: Kistler, Type: 5697A1) is shown in Fig. 13. Signals of both thrust force and torque are shown in the figure for drilling time of 60 s. The signals can be divided into five different zones based on different drilling stages, namely zone-I, zone-II, zone-III, zone-IV, and zone-V [19].

Zone-I with the smaller value of thrust forces corresponds to the drilling stage when the drill bit's chisel edge just touches the composite material. As the drill bit indented and the thickness of composites thrust force suddenly rises as denoted by zone-II. After that cutting stage of drilling comes into play when the thrust force reaches its highest value, denoted by zone-III. The cutting stage remains until the drill bit removes the bottom layer of the composites. As the drill bit's cutting tip exits the last layer of the composite, the thrust force starts decreasing, and this stage is denoted by zone-IV in the figure. In this stage, only the reaming of the hole occurs. At the zone V, the thrust force becomes significantly less as there is no contact between the drill bit and the composite laminate. The torque signals differ from the thrust force signal as visible in the figure. Unlike the thrust force signal, the fluctuation of the torque signal is less. However, the torque also attends its maximum value during the cutting stage is denoted by zone-III.

4.5 Machining Induced Temperature

During machining of the bio-composites, the temperature is generated at the tool and composites' interface due to the frictional force. The induced temperature during machining of bio-composites has a tremendous effect on the tool wear rate, stability of tool, machine-ability of the composites, and material removal rate. The induced temperature within the matrix polymer's glass transition temperature has no adverse effect on the machined surface quality. The temperature within the matrix polymer's glass transition temperature helps ease machining by softening the polymer [8]. However, higher induced temperature leads to thermal damage to the machined surface. The polymer begins to degrade at a temperature more than the melting temperature of the polymer. Fibre burning, tool wear, decreased tool hardness and cutting performance and high surface roughness are the main issues associated with higher induced temperature. Thermal damages can lead to complete failure of the composite during its service life. To prevent the damage associated with higher induced temperature, it is essential to monitor the generated temperature during machining operations. Scientists and engineers have developed many temperature measuring techniques over the past decades to monitor the induced temperature. Some of the temperature measuring techniques are natural or dynamic thermocouple, artificial or embedded thermocouple, special thermometer with optical fibre, radiation technologies (infrared pyrometer, infrared thermography, etc.). The artificial thermocouple is very much useful in measuring temperature during the drilling operation. In this technique, the thermocouple inserted in more than one place near the machining zone. Radiation technologies used for measuring the machining temperature are contact-less devices. Temperature measurement by a thermal image camera (Make: Testo, Model: 885–2 SET) using radiation technology to capture thermographs during milling of bamboo/PLA green composites is shown in Fig. 14. The recorded thermographs can be further analysed by data Capture Program installed in a computer. Figure 15 represents the induced drilling temperature for different drill bits at different drilling stage during making a hole in nettle/epoxy bio-composites [15]. The induced temperature increases as the drill bit progress and reaches the lower laminate of the bio-composites. It can be seen that drilling temperature at the top ply is minimum for 8-facet drill bit. The 8-facet drill bit is multifaceted. The additional clearance faces of 8-facet drill allow ease removal of chips during drilling. Thus, induced heat during the process is carried away by the escaped chips. In step drill bits, the friction between the drill bit and the laminate is more due to two cutting lips (primary and secondary cutting lips). Due to high friction, the induced temperature is more when the step drill is used for making a hole in bio-composites.

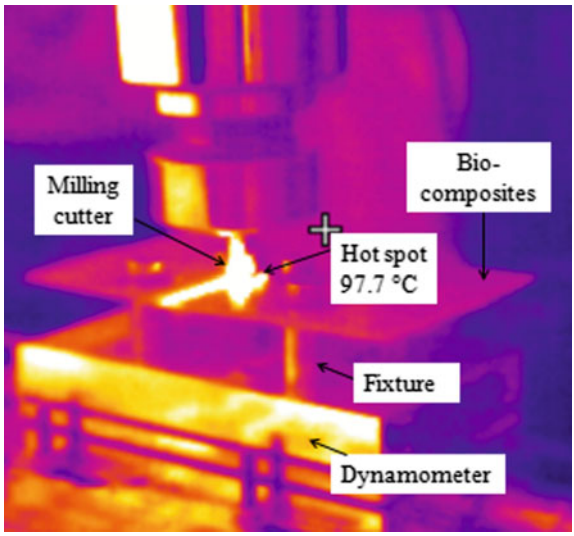

Fig. 14 Thermal image obtained during milling of bio-composites

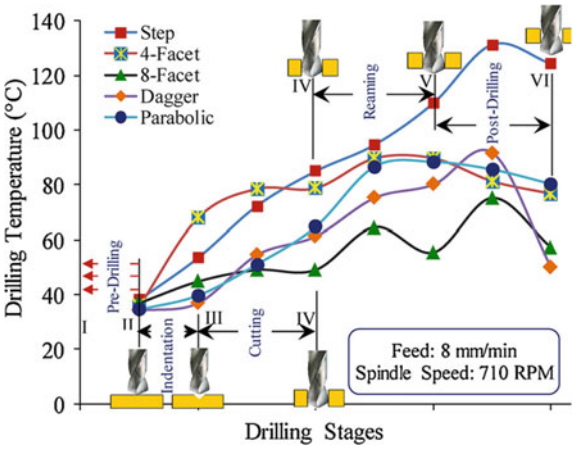

Fig. 15 Drilling temperature variations at the top ply of nettle/epoxy bio-composites with different drill bits at different drilling operation stages [15]

5 Research to Study Machining Behaviour of Bio-composites

Researchers have given a significant emphasis to minimise the damage produced during machining of bio-composites by parametric study and optimization of machining process parameters. Many research works have been published to study the machining behaviour of the bio-composites. Various machining operations such as drilling, milling, turning, grinding, abrasive water jet cutting, and laser beam machining of bio-composites are presented in Tables 3, 4 and 5, giving the basic idea of different machining process parameters and response chosen to study the machining behaviour of different bio-composites.

Table 3 Literature reviews on drilling of bio-composites

Process parameters	Drilling			
	Composites	Response	Process	References
– Feed rate – Spindle speed – Drill geometry	Sisal/polypropylene	– Chip characteristic – Thrust force – Torque – Morphology	Parametric study by experimental analysis	[19]
– Feed rate – Spindle speed – Drill geometry	Sisal/PLA Grewia optiva/PLA	– Thrust force – Torque – Delamination	Response surface methodology	[27]
– Feed rate – Spindle speed – Drill geometry	Nettle/polypropylene	– Thrust force – Torque	Response surface methodology	[20]
– Feed rate – Spindle speed – Drill geometry	Sisal/epoxy Nettle/epoxy	– Thrust force – Torque – Microstructure analysis – Hole edge quality	Parametric study by experimental analysis	[28]
– Feed rate – Spindle speed – Drill geometry	Nettle/epoxy	– Thrust force – Torque – Temperature – Delamination – Surface roughness	Parametric study by full factorial experimental analysis	[15]
– Feed rate – Spindle speed – Drill geometry	Bamboo/PLA	– Thrust force – Torque	Taguchi's optimization technique	[1]
– Feed rate – Spindle speed – Drill geometry	Sisal/polypropylene	– Thrust force – Torque	Response surface methodology	[29]
– Fibre orientation – Hole size – Coupling agent	Flax yarn/polypropylene	– Tensile properties	Parametric study by experimental analysis	[30]
– Feed rate – Spindle speed	Banana/epoxy	– Delamination – Quality of hole	Parametric study by experimental analysis	[31]
– Feed rate – Spindle speed – Drill diameter	Coir/polyester	– Thrust force – Torque – Tool wear	Taguchi's optimization technique	[25]

(continued)

Table 3 (continued)

Process parameters	Drilling			
	Composites	Response	Process	References
– Feed rate – Spindle speed – Drill diameter	Coir/polyester	– Thrust force – Torque – Tool wear	Nelder–Mead and genetic algorithm optimization method	[32]
– Drill diameter	Coir/polyester	– Thrust force – Torque – Tool wear	Statistical modelling	[33]
– Feed rate – Spindle speed – Drill diameter	Coir/polyester	– Thrust force – Torque – Tool wear	Response surface methodology	[34]
– Fibre treatment	Roselle/sisal/polyester (hybrid composite)	– Hole profile analysis	Parametric study by experimental analysis	[35]
– Feed rate – Spindle speed – Drill diameter	Roselle/sisal/polyester (hybrid composite)	– Thrust force – Torque	Response surface methodology and artificial neural network	[36]
– Feed rate – Spindle speed – Drill diameter – Fibre Fibre treatment – Fibre orientation	Coir/polyester	– Thrust force – Torque – Delamination	Parametric study by factorial design of experiment	[37]
– Feed rate – Spindle speed – Drill diameter	Basalt/sisal/epoxy	– Thrust force – Delamination	Taguchi's optimization technique	[38]
– Feed rate – Spindle speed – Drill diameter	Bamboo/polyester	– Delamination	Taguchi's optimization technique and regression analysis	[39]
– Feed rate – Spindle speed – Drill diameter	Sisal/epoxy Banana/epoxy Roselle/epoxy	– Thrust force – Torque – Delamination	Regression model	[40]

(continued)

Table 3 (continued)

Process parameters	Drilling			
	Composites	Response	Process	References
– Feed rate – Spindle speed – Drill geometry	Rice husk/polyester	– Delamination	Parametric study by experimental analysis	[41]
– Feed rate – Spindle speed	Hemp/polyester	– Delamination – Tensile strength	Taguchi's optimization technique	[42]
– Feed rate – Spindle speed – Drill diameter	Sisal/epoxy Banana/epoxy Roselle/epoxy	– Thrust force – Torque	Regression model and SEM analysis	[43]
– Feed rate – Machining time	Hemp/vinyl ester	– Cutting forces – Cutting energy – Hole dimension – Hole circularity – Temperature	Comparative experimental analysis of conventional drilling and ultrasonically assisted machining	[44]
– Feed rate – Spindle speed – Reinforcement weight percentage	Banyan tree sawdust/polypropylene	– Surface roughness – Hole diameter	Experimental analysis in CNC drilling	[45]
– Feed rate – Spindle speed	Wood-plastic			
– Feed rate – Spindle speed – Reinforcement weight percentage	Banana fibre/polypropylene			

6 Effect of Process Parameters on Machining Quality

The quality of the bio-composites' machined surface depends on process parameters such as feed rate, speed, depth of cut, fibre orientation in the composite laminate, machining conditions, and tool geometries. To select the optimum process parameters to obtain a high-quality machined surface, it is essential to study their responses. Based on the different machining operations of bio-composites presented in Tables 3, 4 and 5 in Sect. 5, a mapping of responses such as induced force, temperature, delamination, surface roughness, and tool wear with the process parameters such as feed rate, spindle speed, tool diameter, depth of cut, drill bit geometry, milling cutter tool material, and fibre orientation has been carried out. Figure 16 represents the mapping

Table 4 Literature reviews on milling of bio-composites

Process parameters	Milling			
	Composites	Response	Process	References
– Speed – Feed rate – Depth of cut	Kenaf/epoxy	– Surface roughness – Delamination factor	Full factorial design of experiments and response surface methodology	[17]
– Speed – Feed rate	Hemp/epoxy Jute/epoxy Banana/epoxy	– Surface roughness – Delamination factor	Taguchi's optimization technique	[16]
– Speed – Feed rate – Depth of cut	Jute/polyester	– Thrust force – Torque	Taguchi's optimization technique and fuzzy model	[46]
– Speed – Feed rate – Depth of cut	Kenaf/polyester	Surface roughness	Taguchi's optimization technique	[47]
– Cutting speed – Feed rate – Fibre orientation – Tool geometry	Jute/epoxy	– Cutting force – Delamination factor – Surface roughness	Parametric study by experimental analysis	[48]
– Cutting speed – Feed rate – Fibre orientation – Depth of cut	Jute/polyester	– Forces – Surface roughness – Material removal rate	Taguchi's optimization technique and grey relational analysis	[49]
– Speed – Feed rate – Depth of cut	Jute/polyester	– Thrust force – Torque	Taguchi's optimization technique and fuzzy rule	[50]
– Tool geometry – Depth of cut	Wood-based materials	– Wearing of the PCD edges of cutters	Experimental analysis of micro–milling	[51]
– Spindle speed – Feed rate – Depth of cut	Kenaf/epoxy	– Surface roughness	Full factorial design of experiments and response surface methodology	[52]

(continued)

Table 4 (continued)

Process parameters	Milling			
	Composites	Response	Process	References
– Spindle speed – Feed rate – Depth of cut	Bamboo/ polypropylene Sisal/ polypropylene Miscanthus/ polypropylene	– Tribological behaviour – Surface analysis	Parametric study by experimental analysis	[18]
– Feed rate – Spindle speed – Reinforcement weight percentage	Banyan tree sawdust/polypropylene	– Surface roughness – Slot width – Average thickness value of chips – SEM analysis	Experimental analysis of CNC milling	[45]
– Feed rate – Spindle speed	Wood-plastic			
– Feed rate – Spindle speed – Reinforcement weight percentage	Banana fibre/polypropylene			

with different colour coding. Blue colour represents lower value, orange colour represents medium value, and red colure represents the higher value of response in the mapping. The effect of process parameters on the responses can be understood from the mapping. During drilling of coir/polyester bio-composites the minimum value of induced forces and tool wear is noticed at 0.3 mm/rev feed rate, 600 rpm spindle speed and 6 mm drill diameter [25].

6.1 Effect of Feed

The feed rate is a vital process parameter in the machining of bio-composites. It helps in determining the overall quality of the machining surface [1, 15, 20]. A damage free machining surface in bio-composites can be obtained by selecting the optimum feed rate setting. The indirect assessment of evaluating the machining quality through induced forces increases with an increase in the feed rate [60]. When the feed rate increases, the machining tool is subjected to a higher thickness or cross-sectional area of the uncut or un-deformed material. The chip thickness also tends to increase with an increase in feed rate. Hence, the damages resulting from the higher induced forces also increases with an increase in feed rate [61]. A lower feed rate during machining is recommended for bio-composite to obtain a damage-free surface. At lower feed rate interaction of tool with the composite laminate is more. The rubbing of fibre with the tool results in temperature generation [15]. The induced temperature within the glass transition temperature results in easy machining of the composites by

Table 5 Literature reviews on turning, grinding, abrasive water jet cutting, and laser beam machining of bio-composites

Process parameters	Turning			
	Composites	Response	Process	References
– Cutting speed – Feed rate – Composite formulation	Banyan tree sawdust/polypropylene	– Turning roughness – Turning dimension	Parametric study by experimental analysis in CNC turning	[45]
– Cutting speed – Feed rate – Fibre weight percentage	Banana fibre/polypropylene	– Turning roughness – Turning dimension		
– Cutting speed – Feed rate	Wood-plastic	– Turning roughness – Turning dimension		
– Feed rate	Wood-plastic	– Surface roughness	Parametric study by experimental analysis	[53]
– Feed rate – Spindle speed – Depth of cut	Wood-plastic	– Surface roughness	Parametric study by experimental analysis	[54]
– Traverse speed of cutting head – Size of abrasive particles	Wood-plastic	– Surface topography	Experimental analysis in water jet and abrasive water jet turning	[55]
– Tool nose radius – Positive geometry of tool – Spindle speed – Feed rate	Wood-plastic	– Material sharing – Surface roughness	Parametric study by experimental analysis	[56]
– Feed rate – Spindle speed – Depth of cut	Wood-plastic	– Material removal rate – Surface roughness	Parametric study by experimental analysis	[57]
Grinding				
– Rotational speed – Feed rate – Composite formulation	Banyan tree sawdust/polypropylene	– Surface roughness – Grinding dimension	Parametric study by experimental analysis in CNC turning	[45]

(continued)

Table 5 (continued)

Process parameters	Turning			
	Composites	Response	Process	References
– Rotational speed – Feed rate	Wood-plastic	– Surface roughness – Grinding dimension		
Abrasive water jet cutting				
– Traverse speed – Water pressure – Coupling agent – Reinforcement weight percentage	Banyan tree sawdust/ polypropylene	– Kerf taper angle – Surface roughness	Parametric study by experimental analysis	[45]
– Traverse speed – Water pressure – Reinforcement weight percentage	Banana fibre/polypropylene	– Kerf taper angle – Kerf width – Surface roughness		
– Traverse speed – Water pressure	Wood-plastic	– Kerf taper angle – Kerf width		
– Pumping system pressure – Standoff distance – Nozzle speed	Wood dust/ epoxy	– Surface roughness – Delamination – Process time	Response surface methodology	[58]
– Hydraulic pressure – Traverse speed – Standoff distance	Banana/epoxy	– Surface roughness – Kerf taper ratio	Full factorial design of experiments	[59]
Laser beam machining				
– Laser power – Cutting Speed – Reinforcement weight percentage – Coupling agent	Banyan tree sawdust/ polypropylene	– Kerf taper angle – Kerf width – Surface roughness	Parametric study by experimental analysis	[45]
– Laser power – Cutting speed – Fibre weight percentage – Etching speed – Frequency – Pulse duration	Banana fibre–fibre/polypropylene	– Width – Length – Kerf taper angle – Kerf width – Surface roughness		

(continued)

Table 5 (continued)

Process parameters	Turning			
	Composites	Response	Process	References
– Laser power – Etching speed – Hatching angle – Pulse duration – Frequency	Wood-plastic	– SEM analysis – Micro-hardness – Surface roughness		

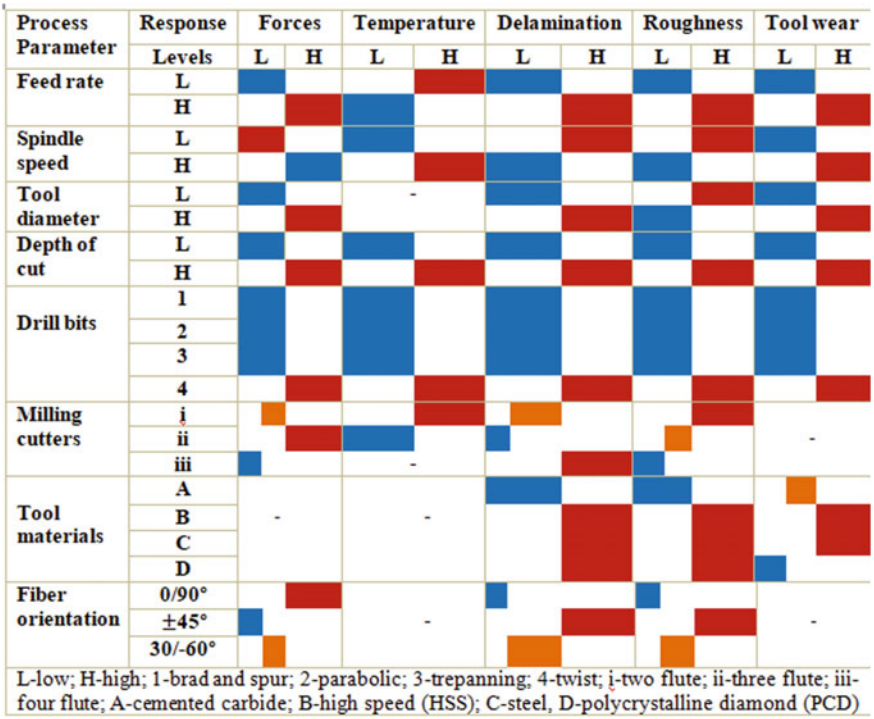

Fig. 16 Mapping of responses with the process parameters during machining of bio-composites

softening the polymer. The effect of feed rate on the induced thrust force and torque during drilling of nettle/epoxy bio-composites using different drill bit is shown in Figs. 17 and 18, respectively [15]. The induced forces increase with the increase in feed rate. The minimum forces are obtained when the dagger drill bit is used for making holes.

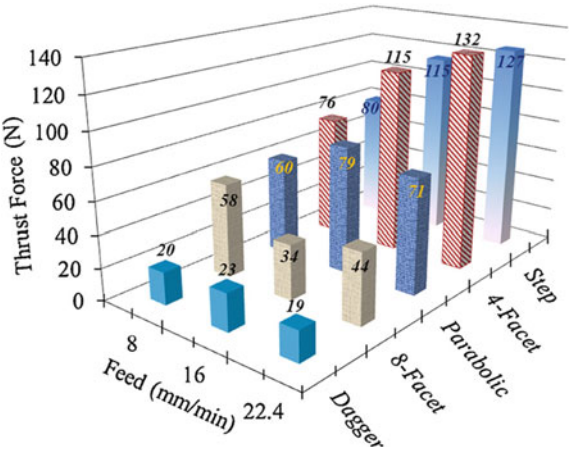

Fig. 17 Effect of feed rate on thrust force during drilling of nettle/epoxy bio-composites [15]

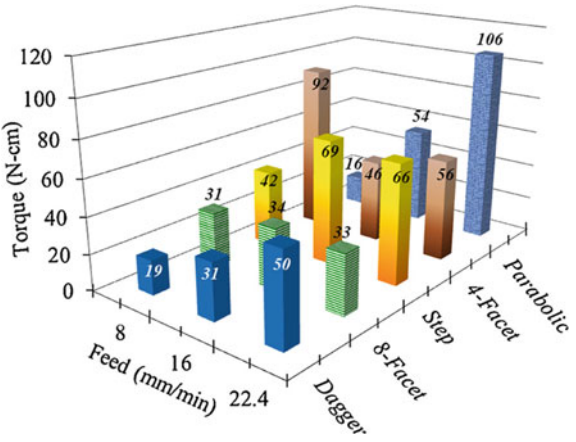

Fig. 18 Effect of feed rate on torque during drilling of nettle/epoxy bio-composites [15]

6.2 *Effect of Spindle Speed*

Spindle speed is the least significant parameter contributing to the machining induced damage [29, 40]. However, some other researchers have found the speed as the most significant parameter related to the induced damages [21, 31]. Higher spindle speed is recommended for producing lower induced force and damages during machining of bio-composites. This is because of the lower resistance to cut due softening of the polymer due to induced temperature. However, the produced chips follow a ductile mode or continuous pattern at low spindle speed—formation of continuous chip results in a crack-free machined surface [22]. To obtain damage—and the crack-free machined surface, it is essential to evaluate the optimum setting of spindle speed. The effect of spindle speed on induced thrust and torque during drilling of bamboo/PLA bio-composites for different drill geometries are shown in Figs. 19 and 20 [1]. It can

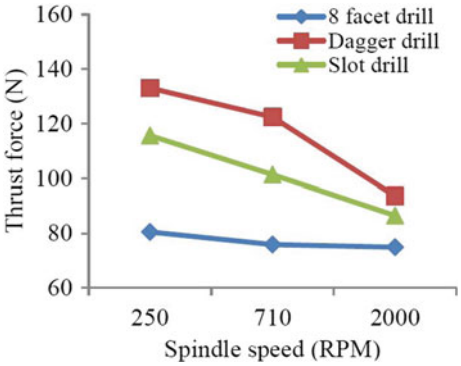

Fig. 19 Effect of spindle speed on thrust force during drilling of bamboo/PLA bio-composites [1]

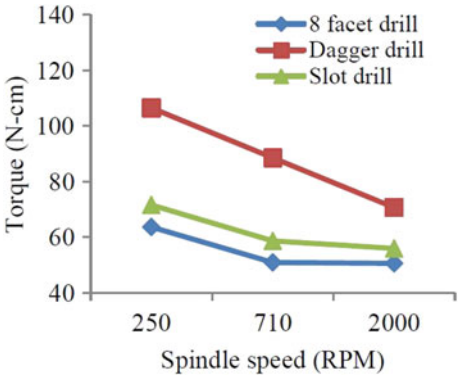

Fig. 20 Effect of spindle speed on torque during drilling of bamboo/PLA bio-composites [1]

be seen that with the increase in spindle speed, the induced thrust force and torque decrease for all drill geometries.

6.3 Effect of Depth of Cut

Another process parameter mainly related to milling operation is the depth of cut, with an increase in depth of cut induced forces and damages in the machine surface increases [17, 46]. More loads are imparted on the tool at a higher depth of cut as the tool is exposed to the laminate's more uncut thickness. The optimum value of depth of cut to obtain a minimum value of output response (forces, surface roughness, and delamination) during milling operation of bio-composites is summarised in Table 6. The machined surface quality also depends upon the size, geometry, and material of the cutting tool.

Table 6 The optimum depth of cut value in minimising the response during milling operation of bio-composites

Machining operation	Bio-composites	Response value	Selected values of depth of cut (mm)	Optimum values of depth of cut (mm)	References
Milling	Kenaf/epoxy	Surface roughness	1–2	1	[47]
Milling	Kenaf/epoxy	Surface roughness, delamination factor	1, 2, and 3	2	[17]
Milling	Jute/isophthalic polyester	Thrust force	1, 1.5, and 2	1.5	[50]
Milling	Jute/isophthalic polyester	Torque	1, 1.5, and 2	1	[50]
Milling	Jute/polyester	Force, surface roughness, MRR	2, 4, 5, 6, and 8	4	[49]
Milling	Kenaf/epoxy	Surface roughness	1, 1.5, and 2	2	[52]

6.4 Effect of Cutting Tool

The quality of the machined surface deteriorates as the size of the cutting tool increases. This is because of the increase in the cross-sectional area of the chip's uncut thickness, due to the increase in the area load on the cutting tool increases, which results in higher cutting forces. The smaller diameter of cutter is recommended during bio-composites machining unless any constraint related to design [36, 37]. The geometry of the drill can drastically affect the induced forces. In the case of drilling operations, induced force depends upon the indentation effect as the chisel edge alone can induce 50% of the axial thrust. A blunt chisel edge of the drill bit depends upon the cutting forces. This is why obtaining a poor machined surface while using four facets or twist drills to make holes in bio-composites. This defect can be eliminated by correcting and strengthening the tool lip. However, many advances in drill bit design have been reported by many designers to improve the quality of hole in bio-composites as presented in Table 2 [27, 29, 39, 62]. In milling operations, multi flutes cutter produces high quality machined surface compared to the two flutes cutter. More cutting edges in the multi flutes cutter allow higher feed rate as a tiny volume of materials is removed by each flute. More is the number of flutes lesser will be the induced forces and damages during machining [48]. A comparative analysis of surface roughness produced by different drill geometries, such as 4-facet, 8-facet, parabolic, step and dagger drill bit during drilling of nettle/epoxy bio-composites is shown in Fig. 21 [15]. Minimum surface roughness is found to be produced by 8-facet drill bit. Peel-up and push-out delamination produced by different drill bits

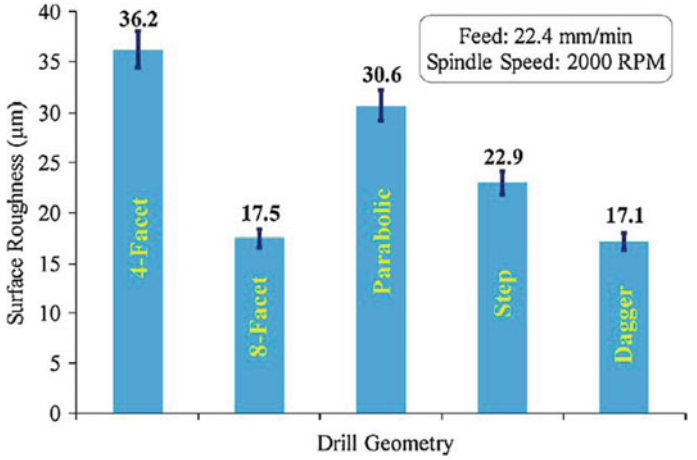

Fig. 21 Comparisons of Ra values with different drill bits [15]

can be observed in Fig. 22. Induced temperature and delamination are found to be less during making hole with 8-facet drill bit. During drilling of sisal/epoxy bio-composites minimum induced thrust force are observed for the parabolic drill bit [19]. The maximum thrust value is observed when holes are produced using the step drill. The piercing of bio-composites' constituents is dominating compared to cutting fibres and matrix when step drill is used for making holes in bio-composites [19]. When Jo, twist, and parabolic drill bits are compared, the parabolic drill bit is found

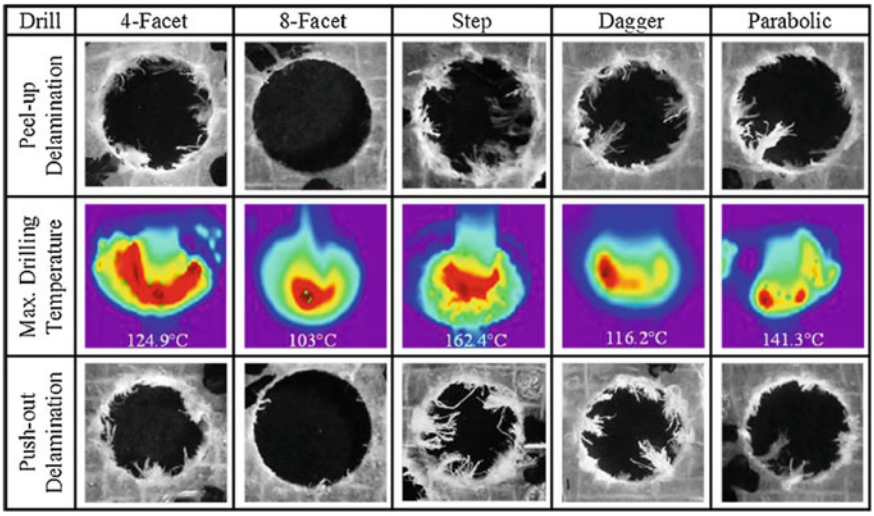

Fig. 22 Damage produced at a feed of 22.4 mm/min and a spindle speed of 2000 RPM during drilling of nettle/epoxy bio-composites [15]

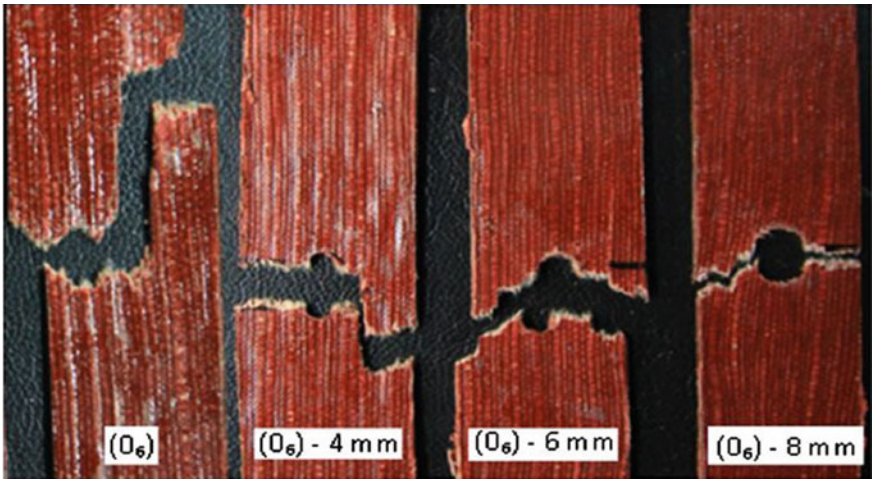

Fig. 23 Failed flax/polypropylene bio-composite samples under tensile loading for different open hole size [30]

to induce minimum torque during drilling of sisal/epoxy bio-composites [19]. The size of the tool used for machining has a significant effect on the machining quality of bio-composites. The strength of flax/PP bio-composite is decreased under tensile loading as the size of the open hole increased [30]. This is due to the increased in stress concentration due to the increased in open hole size. Failed test specimens under different open hole size are shown in Fig. 23 The laminate splitting is found to be decreased as the size of the open hole increases.

6.5 Effect of Nature of Reinforced Fibres

The characteristic of fibres used as the reinforcement in bio-composites also plays an important role in determining the machined surface quality. Types of natural fibre, fibre dimensions, fibre treatment, fibre orientation angle and fibre content in the composites are important factors to consider while dealing with the damage produced during machining [33, 35, 37, 43, 63, 64]. Chemically treated fibre is more resistant to the machining forces and can resist the damage-prone during machining [35]. When roselle/polyester and sisal/polyester bio-composite specimens with 30 wt% fibre content are treated for 8 h provide better dimensional accuracy during machining in comparison to the other fibre content (5, 10, and 20%) and time for treatment (2, 4, and 6 h) [35]. During milling of jute/epoxy bio-composites, the delamination and surface roughness is found to be less for the specimens having 0°/90° fibre orientation angle and maximum for ±45° [48]. Failed flax/polypropylene bio-composite samples (untreated and maleican-hydride grafted polypropylene (MAPP) treated) under tensile loading for different laminate lay-up are shown in Fig. 24 [30].

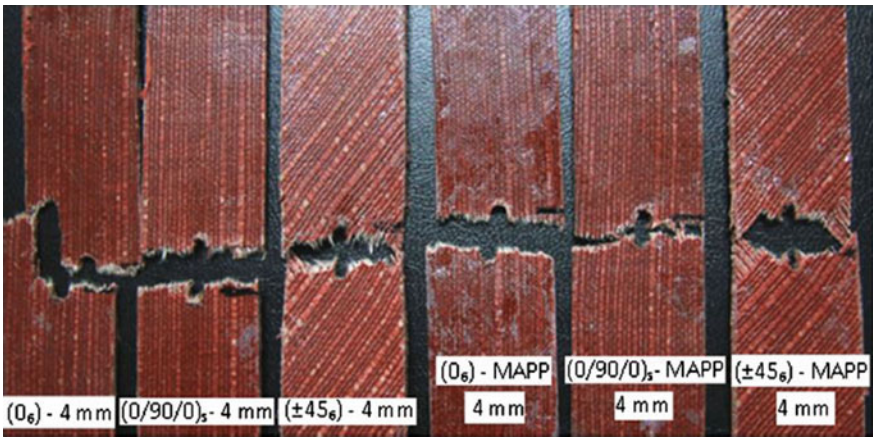

Fig. 24 Failed untreated and MAPP treated flax/polypropylene bio-composite samples under tensile loading for different laminate lay-up (4 mm hole size) [30]

Strength retention by MAPP treated samples is found to be more than the untreated samples. The stress transfer mechanism in MAPP treated samples is more due to the strong interfacial adhesion between fibre and matrix. Thus, tensile fracture and matrix crack can be noticed for the MAPP treated samples. Untreated flax/PP bio-composites failed mostly due to splitting and inter-ply delamination. The SEM image shown in Fig. 25 shows more adhesion between the fibre and matrix for the MAPP treated flax/pp bio-composites than untreated flax/pp bio-composites [30].

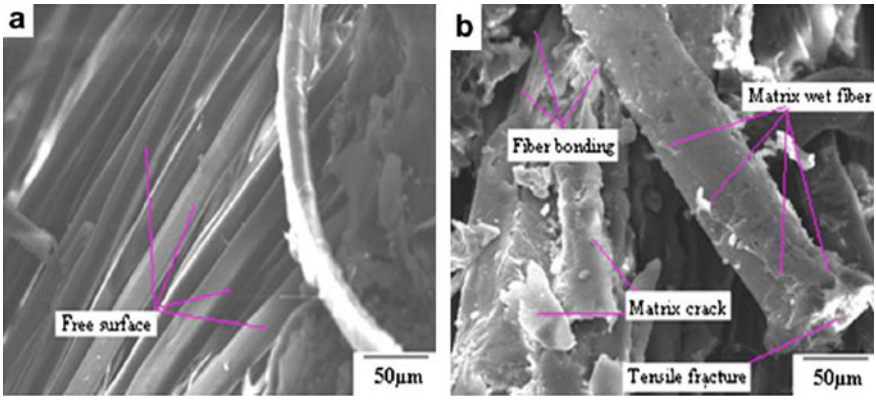

Fig. 25 SEM image of tensile damaged flax/polypropylene bio-composite **a** axial—untreated sample, and **b** axial—MAPP treated (4 mm hole size sample) [30]

7 Conclusions

Natural fibre-reinforced bio-composites are sustainable materials that fit today's environmental conditions. Researchers have carried out many attempts in the development and performance improvement of bio-composites over the past years. The study of bio-composites' machining behaviour has gained importance as the manufacturer sifted to use the raw materials from conventional and synthetic petroleum-based to bio-based. Among the many machining operations required for bio-composites production, holes made by drilling and excess materials removal by milling operations are expected. However, many challenges in terms of machined surface damage during machining cause due to heterogeneous and anisotropic nature of bio-composites. Challenges faced during the machining of bio-composites have a direct effect of different process parameters. The machined surface's quality can be determined by direct assessment via observing the induced damages (delamination, surface roughness, matrix cracking, matrix degradation, fibre burning, burr formation, etc.). In the indirect assessment, determining a quality characteristic of the machined surface is carried out by monitoring the induced forces, temperature, and tool wear. Innovation and development of many techniques and instruments help the manufacturers quantify the machined surface's quality characteristic. The machined surface quality is significantly affected by the process parameters like spindle speed, feed rate, depth of cut, tool material, tool geometry, tool size, fibre orientation in the composite laminate, and nature and geometry the tool. With the implementation of various experimental and optimisation techniques to study the machining behaviour of bio-composites, researchers have found that parametric setting at higher spindle speed, lower feed rate, smaller tool size, multi-faceted cutting tool, cemented carbide tool material, lower depth of cut, and $\pm 45^\circ$ fibre orientation can significantly improve the machining quality and minimising surface damage. Shifting of the conventional way of machining bio-composites to the non-conventional way of machining such as abrasive jet machining, ultrasonically assisted machining, and laser machining has the scope of improving the quality machined surface of bio-composites.

8 Review Questions

(1) What is bio-composite?
(2) How can the use of bio-composites help in addressing environmental issues?
(3) Write some of the applications pf bio-composites?
(4) What are the different classifications of polymer?
(5) Name some biodegradable polymer.
(6) Discuss why machining operations are required for bio-composites?
(7) What are the different machining operations available for bio-composites?
(8) Is the machining process of bio-composites being same as that of conventional materials?

(9) What are the difficulties arising during machining of bio-composites?
(10) What are measures used for the assessment of the defect arises during machining of bio-composites?
(11) How to measure the induced forces during machining of bio-composites?
(12) How the induced forces during machining impacts ate machining quality of bio-composites?
(13) How to measure the induced temperature during machining of bio-composites?
(14) How the induced temperature during machining impacts ate machining quality of bio-composites?
(15) How the process parameters during machining of bio-composites affect the quality of the machined surface?

References

1. Choudhury, M.R., Debnath, K.: Experimental analysis of tensile and compressive failure load in single-lap bolted joint of green composites. Compos. Struct. **225**, 111180 (2019)
2. Bajpai, P.K., Singh, I., Madaan, J.: Development and characterization of PLA-based green composites: a review. J. Thermoplast. Compos. Mater. **27**(1), 52–81 (2014)
3. Faruk, O., Bledzki, A.K., Fink, H.P., Sain, M.: Biocomposites reinforced with natural fibers: 2000–2010. Prog. Polym. Sci. **37**(11), 1552–1596 (2012)
4. Sinha, R.: Outlines of Polymer Technology: Manufacture of Polymers. Prentice Hall of India Private Limited, India, New Delhi (2004)
5. Gholampour, A., Ozbakkaloglu, T.: A review of natural fiber composites: properties, modification and processing techniques, characterization, applications. J. Mater. Sci. **55**, 829–892 (2020)
6. Potluri, R.: Natural Fiber-Based Hybrid Bio-composites: Processing, Characterization, and Applications, in Green Composites, p. 146. Spinger, Singapore (2019)
7. Lotfi, A., Li, H., Dao, D.V., Prusty, G.: Natural fiber–reinforced composites: a review on material, manufacturing, and machinability. J. Thermoplast. Compos. Mater. (2019) https://doi.org/10.1177/0892705719844546
8. Debnath, K., Choudhury, M.R., Srivatsan, T.S.: Secondary Manufacturing Techniques for Polymer Matrix Composites, in Primary and Secondary Manufacturing of Polymer Matrix Composites, pp. 155–172. CRC Press, USA (2017)
9. Sadek, A., Attia, M.H., Meshreki, M., Shi, B.: Characterization and optimization of vibration-assisted drilling of fibre reinforced epoxy laminates. CIRP Ann.—Manuf. Technol. **62**(1), 91–94 (2013)
10. Arul, S., Vijayaraghavan, L., Malhotra, S.K., Krishnamurthy, R.: The effect of vibratory drilling on hole quality in polymeric composites. Int. J. Mach. Tools Manuf. **46**(3–4), 252–259 (2006)
11. Aldahdooh, M., Bunnori, N.M., Johari, M.M., Jamrah, A., Alnuaimi, A.: Retrofitting of damaged reinforced concrete beams with a new green cementitious composites material. Compos. Struct. **142**, 27–34 (2016)
12. Park, S.H., Kim, D.J., Ryu, G.S., Koh, K.T.: Tensile behavior of ultra high performance hybrid fiber reinforced concrete. Cement Concr. Compos. **34**(2), 172–184 (2012)
13. Toledo Filho, R.D., Koenders, E.A.B., Formagini, S., Fairbairn, E.M.R.: Performance assessment of ultra high performance fiber reinforced cementitious composites in view of sustainability. Mater. Des. **36**(0):880–888 (2012)
14. Davim, J.P.: Machining Composites Materials. Wiley, Hoboken, New jersey (2013)

15. Choudhury, M.R., Srinivas, M.S., Debnath, K.: Experimental investigations on drilling of lignocellulosic fiber reinforced composite laminates. J. Manuf. Process. **34**, 51–61 (2018)
16. Babu, G.D., Babu, K.S., Gowd, B.U.: Effect of machining parameters on milled natural fiber-reinforced plastic composites. Int. J. Advan. Mech. Eng. **1**, 1–12 (2013)
17. Azmi, H., Haron, C.H.C., Ghani, J.A., Suhaily, M., Yuzairi, A.R.: Machinability study on milling kenaf fiber reinforced plastic composite materials using design of experiments. IOP Conf. Series: Mater. Sci. Eng. **344**, 012027 (2018)
18. Chegdani, F., Mezghani, S., El Mansori, M., Mkaddem, A.: Fiber type effect on tribological behavior when cutting natural fiber reinforced plastics. Wear **332**, 772–779 (2015)
19. Debnath, K., Singh, I., Dvivedi, A.: Drilling characteristics of sisal fiber-reinforced epoxy and polypropylene composites. Mater. Manuf. Process. **29**(11–12), 1401–1409 (2014)
20. Debnath, K., Singh, I., Dvivedi, A.: On the analysis of force during secondary processing of natural fiber-reinforced composite laminates. Polym. Compos. **38**(1), 164–174 (2017)
21. Babu, G.D., Babu, K.S., Gowd, B.U.: Effects of drilling parameters on delamination of hemp fiber reinforced composites. Int. J. Mech. Prod. Eng. Res. Dev. **2**, 1–8 (2012)
22. Nairn, J.A.: Matrix microcracking in composites. Polym. Matrix Compos. **2**, 403–432 (2000)
23. Hocheng, H., Puw, H.Y., Huang, Y.: Preliminary study on milling of unidirectional carbon fibre-reinforced plastics. Compos. Manuf. **4**(2), 103–108 (1993)
24. Dornfeld, D., Min, S.: A Review of Burr Formation in Machining, pp. 3–11. Control and Removal, Springer, Berlin, Heidelberg, In Burrs-Analysis (2010)
25. Jayabal, S., Natarajan, U.: Drilling analysis of coir-fibre reinforced polyester composites. Bull. Mater. Sci. **34**(7), 1563–1567 (2011)
26. Sorrentino, L., Turchetta, S.: Cutting forces in milling of carbon fibre reinforced plastics. Int. J. Manuf. Eng. (2014) https://doi.org/10.1155/2014/439634
27. Bajpai, P.K., Debnath, K., Singh, I.: Hole making in natural fiber-reinforced polylactic acid laminates: an experimental investigation. J. Thermoplast. Compos. Mater. **30**(1), 30–46 (2017)
28. Debnath, K., Sisodia, M., Kumar, A., Singh, I.: Damage-free hole making in fiber-reinforced composites: an innovative tool design approach. Mater. Manuf. Process. **31**(10), 1400–1408 (2016)
29. Bajpai, P.K., Singh, I.: Drilling behaviour of sisal fibre reinforced polypropylene composite laminates. J. Reinf. Plast. Compos. **32**(20), 1569–1576 (2013)
30. Gobi Kannan, T., Wu, C.M., Cheng, K.B.: Influence of laminate lay-up, hole size and coupling agent on the open hole tensile properties of flax yarn reinforced polypropylene laminates. Compos. Part B: Eng. **57:**80–88 (2014)
31. Venkateshwaran, N., Elaya Perumal, A.: Hole quality evaluation of natural fiber composite using image analysis technique. J. Reinforced Plast. Compos. **32**(16):1188–1197 (2013)
32. Jayabal, S., Natarajan, U.: Optimization of thrust force, torque, and tool wear in drilling of coir fiber-reinforced composites using nelder-mead and genetic algorithm methods. Int. J. Adv. Manuf. Technol. **51**, 371–381 (2010)
33. Jayabal, S., Velumani, S., Navaneethakrishnan, P., Palanikumar, K.: Mechanical and machinability behaviors of woven coir fiber-reinforced polyester composite. Fibers Polym. **14**(9), 1505–1514 (2013)
34. Jayabal, S., Natarajan, U.: Modelling and optimisation of thrust force, torque and tool wear in drilling of coir fibre reinforced composites using response surface method. Int. J. Mach. Mach. Mater. **9**(1–2), 149–172 (2011)
35. Athijayamani, A., Thiruchitrambalam, M., Natarajan, U., Pazhanivel, B.: Influence of alkali-treated fibres on the mechanical properties and machinability of roselle and sisal fibre hybrid polyester composite. Polym. Compos. **31**(4), 723–731 (2010)
36. Athijayamani, A., Natarajan, U., Thiruchitrambalam, M.: Prediction and comparison of thrust force and torque in drilling of natural fibre hybrid composite using regression and artificial neural network modelling. Int. J. Mach. Mach. Mater. **8**(1–2), 131–145 (2010)
37. Balaji, N.S., Jayabal, S., Kalyana Sundaram, S., Rajamuneeswaran, S., Suresh, P.: Delamination analysis in drilling of coir-polyester composites using design of experiments. Advan. Mater. Res. **984:**185–193 (2014)

38. Sakthivel, M., Vijayakumar, S., Prasad, N.K.: Drilling analysis on basalt/sisal reinforced polymer composites using ANOVA and regression model. Appl. Math. Sci. **9**(66), 3285–3290 (2015)
39. Abilash, N., Sivapragash, M.: Optimizing the delamination failure in bamboo fiber reinforced polyester composite. J. King Saud Univ.-Eng. Sci. **28**(1), 92–102 (2016)
40. Chandramohan, D., Marimuthu, K.: Thrust force and torque in drilling the natural fiber reinforced polymer composite materials and evaluation of delamination factor for bone graft substitutes-a work of fiction approach. Int. J. Eng. Sci. Technol. **2**, 6437–6451 (2010)
41. Azuan, S.A., Juraidi, J.M., Muhamad, W.M.W.: Evaluation of delamination in drilling rice husk reinforced polyester composites. Appl. Mech. Mater. **232**, 106–110 (2012)
42. Babu, G.D., Babu, K.S., Gowd, B.: Optimization of machining parameters in drilling hemp fiber reinforced composites to maximize the tensile strength using design experiments. Indian J. Eng. Mater. Sci. **20**, 385–390 (2013)
43. Chandramohan, D., Marimuthu, K.: Drilling of natural fiber particle reinforced polymer composite material. Int. J. Advan. Eng. Res. Study **1**, 134–145 (2011)
44. Wang, D., Onawumi, P.Y., Ismail, S.O., Dhakal, H.N., Popov, I., Silberschmidt, V.V., Roy, A.: Machinability of natural-fibre-reinforced polymer composites: conventional vs ultrasonically-assisted machining. Compos. A Appl. Sci. Manuf. **119**, 188–195 (2019)
45. Ramesha, N.: PhD Thesis "Studies on Advanced Machining Characteristics of Green Plastic Composites". University of Mysore, Department of Polymer Science, (2017)
46. Balasubramanian, K., Sultan, M.T.H., Cardona, F., Rajeswari, N.: Machining analysis of natural fibre reinforced composites using fuzzy logic. IOP Conf. Series: Mater. Sci. Eng. **15**, 012051 (2016)
47. Bin Harun, A., Bin Che Haron, C.H., Binti, J., Ghani, A., Binti Mokhtar, S., Ting, S.T.: Study the effect of milling parameters on surface roughness during milling kenaf fibre reinforced plastic. Advan. Environ. Biol. **9**:46–53 (2015)
48. Çelik, Y.H., Kilickap, E., Kilickap, A.İ: An experimental study on milling of natural fiber (jute)-reinforced polymer composites. J. Compos. Mater. **53**, 3127–3137 (2019)
49. Sankar, B.R., Umamaheswarrao, P., Srinivasulu, V., Chowdari, G.K.: Optimization of milling process on jute polyester composite using Taguchi based grey relational analysis coupled with principle component analysis. Mater. Today: Proc. **2**, 2522–2531 (2015)
50. Vinayagamoorthy, R., Rajeswari, N.: Analysis of cutting forces during milling of natural fibered composites using fuzzy logic. Int. J. Compos. Mater. Manuf. **2**, 15–21 (2012)
51. Miklaszewski, S., Zurek, M., Beer, P., Sokolowska, A.: Micromechanism of polycrystalline cemented diamond tool wear during milling of wood-based materials. Diam. Relat. Mater. **9**, 1125–1128 (2000)
52. Azmi, H., Haron, C.H.C., Ghani, J.A., Suhaily, M., Sanuddin, A.B., Song, J.H.: Study on machinability effect of surface roughness in milling kenaf fiber reinforced plastic composite (unidirectional) using response surface methodology. ARPN J. Eng. Appl. Sci. **11**, 4761–4766 (2016)
53. Somsakova, Z., Zajac, J., Michalik, P., Kasina, M.: Machining of wood plastic composite (pilot experiment). Materiale Plastice **49**(1), 55–57 (2012)
54. Zajac, J., Hutyrová, Z., Orlovský, I.: Investigation of surface roughness after turning of one kind of the bio-material with thermoplastic matrix and natural fibers. Advan. Mater. Res. **941**, 275–279 (2014)
55. Hutyrová, Z., Ščučka, J., Hloch, S., Hlaváček, P., Zeleňák, M.: Turning of wood plastic composites by water jet and abrasive water jet. Int. J. Advan. Manuf. Technol. **84**, 1615–1623 (2016)
56. Hutyrová, Z., Zajac, J., Mital, D., Harničárová, M., Valíček, J.: Evaluation of share material after turning of wood plastic composite. In: Solar Energy and Building International Conference, IEEE Explorer, pp. 1–5. Sousse, Tunisia (2015)
57. Hutyrová, Z., Harničarová, M., Zajac, J., Valíček, J., Mihok, J.: Experimental study of surface roughness of wood plastic composites after turning. Advan. Mater. Res. **856**, 108–112 (2014)

58. Bhowmik, S., Ray, A.: Prediction and optimization of process parameters of green composites in AWJM process using response surface methodology. Int. J. Advan. Manuf. Technol. **87**(5–8), 1359–1370 (2016)
59. Patel, J.K., Shaikh, A.A.: An experimental investigation of AWJ parameters on banana fiber reinforced composite. Int. J. Eng. Res. Technol. **3**(12), 608–613 (2014)
60. Mizobuchi, A., Takagi, H., Sato, T., Hino, J.: Drilling machinability of resin-less "green" composites reinforced by bamboo fiber. WIT Trans. Built Environ. **9**, 185–194 (2008)
61. Hutyrová, Z., Zajac, J., Michalik, P., Mita, D., Duplák, J., Gajdoš, S.: Study of surface roughness of machined polymer composite material Int. J. Polym. Sci. (2015) https://doi.org/10.1155/2015/303517
62. Jayabal, S., Natarajan, U., Sekar, U.: Regression modeling and optimization of machinability behaviour of glass-coir-polyester hybrid composite using factorial design methodology. Int. J. Advan. Manuf. Technol. **55**, 263–273 (2011)
63. Sridharan, V., Muthukrishnan, N.: Optimization of machinability of polyester/modified jute fabric composite using grey relational analysis (GRA). Procedia Eng. **64**, 1003–1012 (2013)
64. Babu, D., Babu, K.S., Gowd, B.U.M.: Drilling uni-directional fiber-reinforced plastics manufactured by hand lay-up influence of fibers. Am. J. Mater. Sci. Technol. **1**(1), 1–10 (2012)

Grinding and Abrasive Machining of Composite Materials

Mark J. Jackson and Martin J. Toward

Abstract The grinding or abrasive machining of composite materials is a complex system that relies on the use of hard materials such as alumina and diamond to achieve precisely machined functional surfaces. This chapter focuses on the grinding of polymer matrix composites (PMCs), metal matrix composites (MMCs), and ceramic matrix composites (CMCs) and explains how abrasive grain and bonding characteristics affect the grindability of fibrous materials surrounded by a binder. The chapter reviews the current literature surrounding the specification of abrasive products in use for shaping PMCs, MMCs and CMCs and provides an insight into the future specifications of abrasive grains and bonded products for grinding increasingly complex composite materials.

1 Introduction

Polymer-matrix composites (PMCs) are materials composed of a variety of short or continuous fibers bonded together to an organic polymer matrix. PMCs transfer loads between fibers through the matrix using an appropriate agent that provides stress paths within the composite structure. Some of the advantages of using PMCs include high stiffness and high strength along the direction of aligned fibers. PMCs are divided into two categories, reinforced and advanced composites. Reinforced plastic composite materials typically consist of polyester resins reinforced with low-stiffness glass fibers. Advanced composites consist of fiber and matrix combinations that have much higher strength and stiffness. The PMC is designed so that the mechanical loads that are being applied to the material are supported by the reinforcing agents. The function of the matrix is to bond the fibers together and to transfer loads between them. PMCs contain ~60% reinforcing fiber by volume. The fibers that are commonly

M. J. Jackson (✉)
School of Integrated Studies, College of Technology and Aviation, Kansas State University, Salina, KS 67401, USA
e-mail: mjjackson@ksu.edu

M. J. Toward
Department of Engineering, University of Liverpool, Liverpool L69 3BX, UK

I. Shyha and D. Huo (eds.), *Advances in Machining of Composite Materials*, Engineering Materials, https://doi.org/10.1007/978-3-030-71438-3_17

found and used within PMCs include fiberglass, graphite and aramid. Fiberglass has a relatively low stiffness and at the same time exhibits a high tensile strength compared to other fibers. The reinforcing fibers focus their mechanical properties along their lengths rather than their widths and are arranged and oriented in different forms and directions to provide different physical properties and advantages based on their application. The properties of the matrix determine the resistance of the PMC to processes that includes impact damage, water absorption, chemical attack, and high-temperature creep. This PMC matrix is weak and easily ground away using conventional abrasive cutting tools composed of aluminum oxide or silicon carbide abrasive grains bonded together in a tight matrix usually vitrified with a large number of open pores.

Metal Matrix Composites (MMCs) are made by dispersing a reinforcing material into a metal matrix. The reinforced surface can be coated to prevent a chemical reaction with the matrix. Carbon fibers are commonly used in an aluminium matrix to synthesize composites having low density and high strength. However, carbon reacts with aluminum to create a brittle compound (Al_4C_3) on the surface of the fiber. The matrix is the monolithic material into which the reinforcement is embedded and is continuous. This means that there is a path through the matrix to any point in the material, unlike two separate materials that are sandwiched together. In structural applications, the matrix is usually a lighter metal such as aluminum, magnesium, or titanium, and provides a compliant support for the reinforcement. In high-temperature applications, cobalt and cobalt–nickel alloy matrices are common. The reinforcement material is embedded into a matrix and does not always reinforce the compound, but is used to change physical properties such as wear resistance, friction coefficient, and thermal properties. The reinforcement can be continuous, or discontinuous. Discontinuous MMCs can be isotropic, and can be worked with standard metalworking techniques, such as machining with polycrystalline diamond tools (PCD) or grinding with bonded diamond tools. Continuous reinforcement uses monofilament fibers such as carbon fiber or silicon carbide that are embedded into the matrix. Discontinuous reinforcement uses whiskers or very short fibers, or particles. The most common reinforcing materials are alumina and silicon carbide fibers. Again, resin bonded diamond tools are usually used to grind MMCs.

Ceramic matrix composites (CMCs) are a sub-group of composite materials as well as being a sub-group of monolithic ceramics (MC). They consist of ceramic fibers embedded in a ceramic matrix. The matrix and fibers consist of a ceramic material. The use of long length multi-strand fibers increases cracking resistance, elongation and thermal shock resistance. The most common reinforcement is the continuous-length ceramic fiber that has an elastic modulus that is higher than that of the matrix. The role of the fiber increases the energy expended during crack propagation and bridges cracks without fracturing providing the composite with a high ultimate tensile strength (UTS). Ceramic fiber reinforcements increase the composite's resistance to crack propagation and allow CMCs to avoid brittle failure. This behavior is different from the behavior of ceramic fibers in polymer matrix composites (PMCs) and metal matrix composites (MMCs), where the fibers typically fracture prior to the matrix owing to the higher strain capabilities of those matrices.

Carbon (C), silicon carbide (SiC), alumina (Al_2O_3) and mullite (Al_2O_3–SiO_2) fibers are commonly used in CMCs. The matrix materials are usually the same materials as the fibers used for reinforcement. CMCs include a combination of type of fiber/type of matrix such as carbon-fiber-reinforced carbon (C/C), or C/SiC for carbon-fiber-reinforced silicon carbide. Commercially available CMCs are C/C, C/SiC, SiC/SiC and Al_2O_3/Al_2O_3. Owing to the higher toughness of CMCs, diamond cutting and grinding wheels are predominantly used to shape parts made from CMCs.

The characteristic of abrasive grains and their placement in an appropriate bonding agent has a significant effect on the quality of ground components made from composite materials. The next sections describe the importance of such characteristics.

2 Characteristics of Grinding Grains and Grinding Tools for Composite Materials

2.1 Shape

The shape of an abrasive grain impacts the grain strength, grinding performance, and packing characteristics that affects grinding wheel formulation and manufacture. Shape will affect the *r* term in the undeformed chip thickness (t') equation:

$$t' = \left\{[Vw/(Vs.C.r)].(d/De)^{1/2}\right\}^{1/2} \quad (1)$$

where r is the ratio of undeformed chip width-to-chip depth (~5–20 depending on grain size), V_w is the workpiece speed, V_s is the grinding wheel speed, C is the average grain density, d is depth of cut and D_e is the equivalent diameter. This equation controls grinding power, finish and force per grain. Shape and size are interlinked especially for particles of indeterminate shape, i.e. an imperfect sphere, cube, etc. For synthetic diamond particles, there exists an infinite combination of particle shapes derived from the transition between octahedral and cubic shapes. Crystal imperfections and polycrystalline particles further add to the wide variety of diamond shapes. Recent developments in engineered ceramic abrasives have led to the manufacture of extruded seeded gel alumina grains that increase the size of porosity creating the conditions for making large open porosity grinding wheels. These grains allow large depths of cut to be taken and also allow coolant to flood the contact zone. Their aspect ratios vary from 4:1 to 8:1 and are very effective when grinding PMCs (Fig. 1).

A blocky rounded grain shape will be far stronger than an angular, sharp-cornered grain. Quantifying blocky and angular shapes and defining the characteristics key to the performance of shape have been the sources of study both for grinding performance and batch-to-batch quality control during grinding wheel manufacture. A

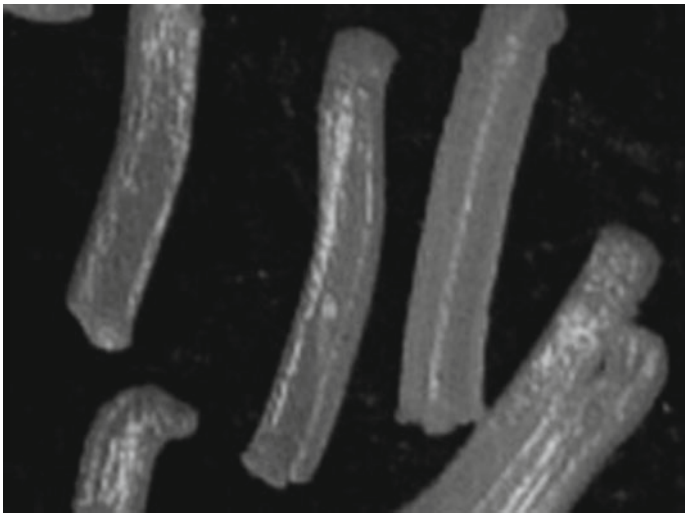

Fig. 1 Extruded seeded gel abrasive grains with high aspect ratio. (Courtesy of Philip Varghese of Norton-Saint Gobain)

variety of parameters describing the shape of particle projections, classified according to the feature of the measurement, are described by Jackson and Hitchiner [1].

Two key diametric dimensions are the major and minor diameters, d_a and d_b [1], which provide a fundamental measure of particle size (Fig. 2). Although size is an

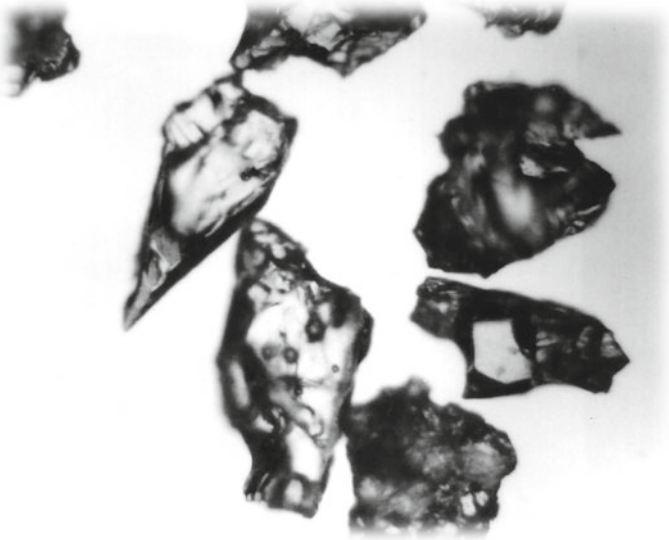

Fig. 2 A collection of defined shape abrasive grains

important feature, it is grain shape that governs the grain's abrasiveness. Algebraic combinations of linear dimensions provide measures of shape.

The calculated values from abrasive grain projections include:

(a) **Aspect ratio**, the ratio of the major-to-minor diameter d_a/d_b. A useful parameter to describe grain elongation and packing characteristics;
(b) **Projection area**, the area enclosed by the boundary of its projection. It is an indirect measure of size and bulk of the particle. It is an important component of the calculation of grain convexity; and
(c) **Convexity**, is a characteristic that strongly relates to the strength of the grain and its abrasive potential. A grain is convex if an idealized elastic membrane stretched across its projection leaves no space between itself and the grain's surface. The degree of convexity correlates with lower mechanical integrity but higher abrasive aggressiveness with the grain being, on average, less blocky. Convexity also correlates to the characteristic of grain irregularity. Convexity C as a parameter is defined as,

$$C = \left(A_f + A_p\right)/A_p. \tag{2}$$

where, A_p is the the projected area of the grain, A_f is the fill area between the grain projection and the idealized elastic membrane stretched across the projection [1].

(d) Grain '**sharpness**' is a parameter that has been developed specifically for the characterization of abrasive grains based on chip formation modeling where the rate of cutting is governed by the degree of penetration into the workpiece (Fig. 3).

The functional relationship between the two orthogonal areas, Ω and Λ, is known as the groove function and is shown in reference [1]. The function embodies the abrasive characteristics of an agglomeration of particles presented in a grinding wheel or on a coated abrasive product.

2.2 Abrasive Wear

Abrasive wear tends to occur progressively caused by interactions of the abrasive grain with the workpiece. These interactions are both physical and chemical, and are complex in nature. They can involve mechanical fracture (abrasion) and plastic deformation. Heat from friction and chip formation can lead to localized diffusion, chemical degradation and decomposition of the grain, and melting. The clean surfaces exposed by the creation of a chip are highly reactive and can drive chemical reactions that would normally occur at much higher temperatures. Even the presence of oxygen in the atmosphere has a profound effect by neutralizing the clean surface of the metal chip. Grinding in a vacuum will generally lead to high levels of loading from metal-to-metal contact and grain-to-metal adhesion.

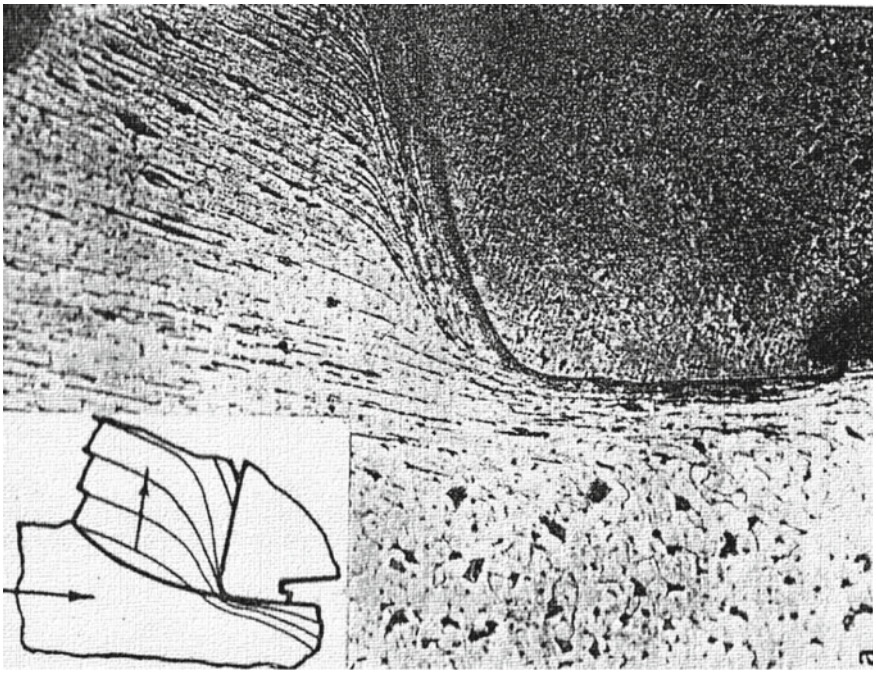

Fig. 3 Physical projection of the abrasive grain into workpiece showing penetration depth in relation to the abrasive grain

Hardness is the key factor in controlling abrasive wear characterized by mechanical micro-fracture and plastic deformation. In general a grain has to be at least 20% harder than the workpiece to be suitable as an abrasive. Temperature plays an important factor as localized temperatures can easily exceed several hundred centigrade and hardness of abrasives such as alumina decreases with temperature. The impact of hardness and other abrasive wear controlling factors can be seen by the comparison of typical G-Ratio values for the major abrasive type diamond and cubic boron nitride (cBN), alumina and silicon carbide grinding various industrial workpieces. When grinding polymer matrix composites (PMCs) with alumina the wear is essentially mechanical for each abrasive type especially at low wheel speeds where heat generation is minimal. The effect in this case of hardness is apparent. Diamond with its superior hardness provides a G-Ratio of typically 100 times greater than the second hardest abrasive, cBN, at slightly over half the hardness. Similarly, the G-Ratio for cBN is about 100 times higher than for silicon carbide with a similar proportional reduction in hardness. Alumina abrasive, with a hardness approaching that of the workpiece, gives a very poor G-Ratio and is in effect non-functional as an abrasive for MMCs and CMCs.

2.3 Abrasive Grain Fracture Toughness

Hardness provides a measure for the tendency of grain to wear by abrasive wear on the atomic scale, fracture toughness (or the inverse term known as friability) provides a measure for the loss of abrasive due to breakdown by fracturing or splintering of the grain typically at the micrometer level (micro-fracture) or macro and/or mesoscale (macro-fracture). The degree of fracture is in large degree dependent on grain properties such as crystal size and morphology, impurities, inclusions and pre-existing cracks, and shape. It is also dependent on the level and nature of the forces applied to the grain during grinding and from factors in the grinding environment such as rapid cooling from lubricant. Abrasive wear leads to the creation of wear flats that dramatically increases the force exerted on the grain and in turn leads to increased levels of fracture (Fig. 4).

Fracture toughness, particularly in diamond grains, is most commonly evaluated by a vibrating impact test. A grain sample of a known particle size distribution is placed in a tube with steel ball bearings and shaken with a fixed amplitude and frequency for a given length of time. The grain particle size distribution is then re-measured to assess the level of breakdown. The grain is either measured as received to give a Toughness Index (TI) value; or after processing at high temperatures, typical of those seen in wheel manufacturing process or use, to give a Thermal Toughness Index (TTI) value.

The high temperature processing can occur either in vacuum, or in the manufacturing atmosphere, or even after mixing with wheel bond that is dissolved with hydrofluoric acid subsequent to heat treatment. In general the TTI will be less than

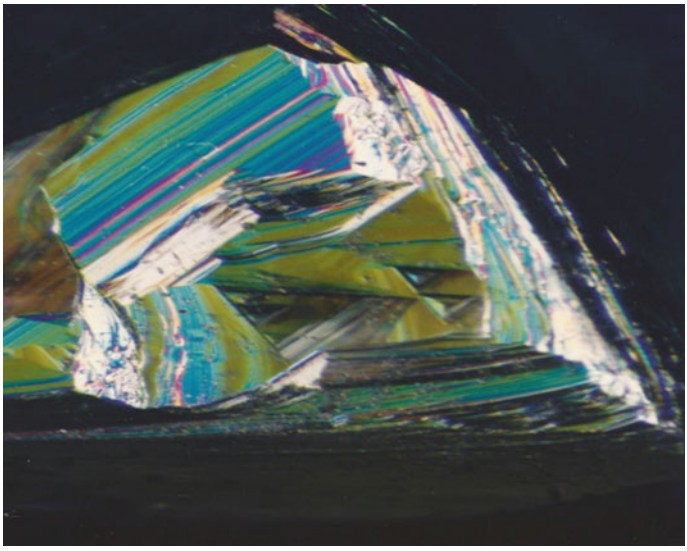

Fig. 4 Diamond grain showing wear flat and edge fracture

the TI as temperature causes the expansion of inclusions, reactions with the atmosphere, and infiltration of surface flaws with the bond. Where the grain has previously been through a significant degree of crush processing, especially for fused alumina grain, high temperature calcining can actually increase the TTI by annealing existing cracks. Crushing strength measurements are also made on single grains.

Methods of evaluating grain strength from fly cutting measurements using single grains have been developed. Evaluated grain strengths in terms of the onset of fracture for a given grain shape. Ten primary edge models for the morphology of fractured grains are typically used to characterize the fractured grains [1]. The probability of survival of an abrasive grain is given by the equation:

$$P_t = 1 - e^{-\gamma t} \tag{3}$$

where, γ is the fracture coefficient. Values for γ and primary fracture modes are shown in reference [1]. The technique distinguishes between alumina and SiC abrasive grains, showing the friable nature of the latter, as well as more subtle differences between various grades within a grain family. Grain toughness must be matched to both the wheel bond characteristics and the grinding conditions. Ideally the grain should fracture creating the loss of relatively fine particles typically at the micron or sub-micron level; a process termed micro-fracturing. The remaining portion of the grain should remain sharp and able to cut. If the grain is too tough relative to the bond holding it, or the grinding force per grain is extremely high, the grain is lost without doing any useful work. If the bond is strong enough to hold the grain but grinding forces per grain, and/or the grain crystallite size are large, then fracture is often caused by coarse loss of grain by macro-fracturing without the full amount of possible useful work being obtained.

If the abrasive grain is much weaker than the bond and/or prone to high abrasive wear due to mechanical, heat or chemical wear, then glazing occurs resulting in the creation of wear flats, high grinding forces and increased interface temperatures. Higher forces will lead to more fracture. The ideal stable state for wheel wear is a limited amount of abrasive wear controlled by micro-fracture. The maximum amount of wear flat area is set by the start of thermal damage. For ferrous materials this limit is about 1–2% of the wheel surface when using alumina or SiC abrasives, and about 4–5% when using cBN or diamond abrasives due to their higher thermal diffusivity or ability to remove heat from the grinding zone.

Fracture behavior is also important in terms of the abrasive grain's reaction to impact during dressing [1]. The application of micro-truing to grain structure is not limited to cBN and diamond. A growing awareness of the benefits of controlling fracture at the micro-level has led to the development of new family of engineered alumina abrasive grain structures. A description of conventional abrasives and bonding used used for those abrasive grains can be found in reference [1].

2.4 Medium Hardness Abrasive Grains

Properties of abrasive grains depend on the fusion process and its chemistry, but also on the comminution process. The cast ingot is initially split and sorted. Comminution is produced by passing the material through roll crushers. These processes create major fractures resulting in a grain that is sharp, flawed and anisotropic. Subsequent processing in steel- or rubber-lined ball mills reduces grain size by rounding the grain's edges to produce angular, or blocky, forms.

Fused aluminum oxide (brown): α-alumina containing 2–4% titanium dioxide that increases abrasive grain toughness. The most widely used abrasive in wheels to grind high-tensile-strength materials, and for rough grinding, deburring and snagging, low-alloy metals, ferrous materials. Brown, fused alumina is a tough, sharp but blocky abrasive. Depending on the processing regime, the grain is typically about 50% single crystal and can be provided in high, medium and low density configurations based on shape and packing characteristics. The grain may also be calcined after sizing to toughen it by annealing cracks generated in the crushing process. The material is sometimes termed blue fired (BFA) as the grain changes color due to surface oxidation of impurities. Specialty coatings such as silane (for resin-bonded wheels to resist coolant interactions) or red iron oxide (for resin- and rubber-bonded wheels to increase surface area) may also be applied to improve performance.

Low titanium dioxide content fused aluminum oxide: has 1–2% TiO_2 content, and is used in bonded or coated applications that require an abrasive that is slightly tougher than white aluminum oxide. Reducing TiO_2 content deteriorates the abrasive's toughness, but increases its friability. Light BFA is commonly used in depressed center wheels, cut-off wheels, and for surface and cylindrical grinding of heat sensitive metals and alloys, where fast cutting is required at lower temperatures.

Fused alumina (white): is standard multi-crystalline white, fused alumina (WFA) with sodium β-alumina contamination and is the most friable grain in the fused alumina family. It is considerably harder than BFA (Fig. 5a).

Single crystal fused alumina (white): is single crystal grain that has been produced in deep pour fusion pots and separated from any sodium β-alumina contamination. This is the hardest and most brittle of the alumina family of grains used most commonly for grinding tool and high alloy steels that are very sensitive to heat.

Pink alumina: is WFA to which less than 0.5% chromium oxide has been added during the fusion process to produce a grain that is slightly tougher than regular WFA. It is used for grinding unhardened high alloy steels (Fig. 5b).

Ruby alumina: is WFA to which 3% chromium oxide has been added to provide additional toughness over pink alumina (Fig. 5c). Used for grinding highly alloyed steels.

It can be inferred there is a steady increase in toughness but reduction in hardness in the following order: Single crystal WFA → WFA → pink WFA → ruby WFA → light BFA → BFA → Blue fire BFA. In general the wheel maker will blend various grain types and sizes to combine the properties of each. In addition to chromium, other metal oxide additions have been investigated including vanadium and beryllium.

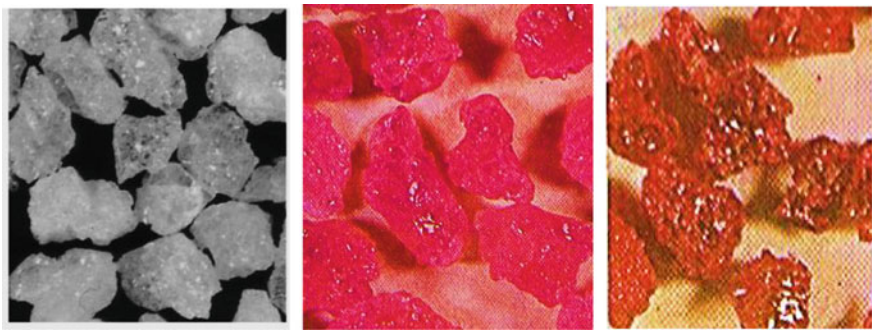

Fig. 5 Fused alumina: (a) white alumina; (b) pink alumina, and (c) ruby alumina (courtesy of Mike Hitchiner, Norton-Saint Gobain)

Sintered Alumina: is a family of grains developed in the 1950s produced from *unfused* alumina. Several processes exist based on both raw bauxite and Bayer processed alumina. The most common is to use a feed material of raw bauxite milled to <5 μm. The mix with binder is first extruded to produce rods which are cut into short cylinders, or cones, in the green state. They are then fired in rotary kilns at (1350–1500 °C) using natural impurities in the bauxite as sintering agents. The resulting grain is extremely tough especially at the relatively large sizes the technology allowed to be produced (8–20#) and the material found great success, until the advent of alumina–zirconia grain, in billet conditioning and other rough grinding operations. It is still used as a blend component with alumina–zirconia especially for the grinding of stainless steels (Fig. 6).

Engineered abrasive grains have microstructures that have been produced with controlled crystal sizes from the sub-micron to micron level by processes other than simple fusion and comminution. These include seeded-gel/sintering and agglomeration techniques. The result is a family of grain types that micro-fracture at controlled micron, or sub-micron, levels and have the ability to be trued, enhancing wheel life and process control compared with fused aluminum oxide grains.

Ceramic seeded-gel based abrasives—The development and commercial success of first sintered and extruded alumina family of grains followed by the development of rapidly chilled, fused alumina–zirconia grains had a major impact on the research programs of abrasive manufacturer regarding the importance controlling grain size. Furthermore, for alumina grains it was known that reducing the crystal size from the macro scale, common in fused material, to microscale grains (or ideally <0.5 micron sized crystalline grains) significantly enhanced grain properties such as hardness (Fig. 7).

Rather than using traditional fusing or sintering processes with the associated limitations on cooling and crystallization rates, it was possible to consolidate microstructures by sintering well dispersed sub-micron pre-cursors by the seeded gel route. This allowed the consolidation of α-alumina into a homogeneous and fully densified grain

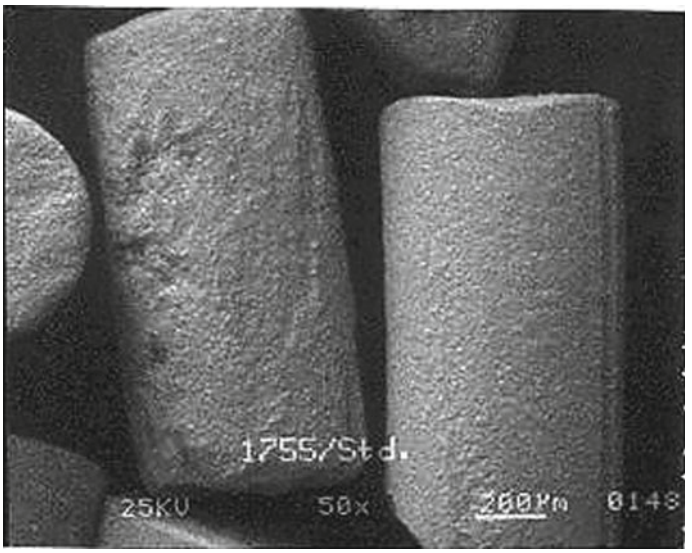

Fig. 6 Example of sintered extruded alumina grain (courtesy of Mike Hitchiner, Norton-Saint Gobain)

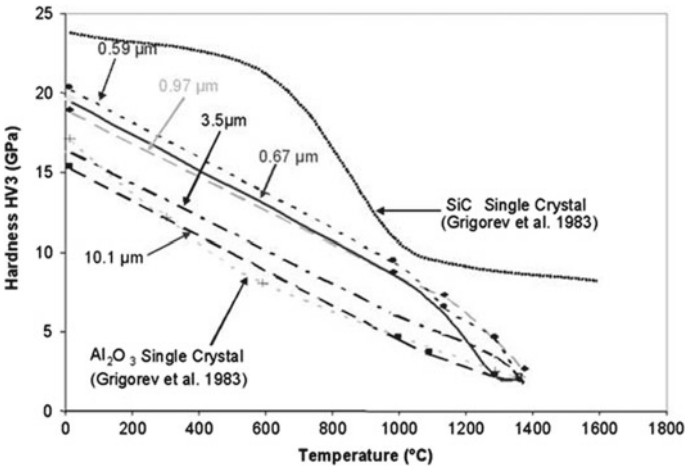

Fig. 7 Effect of crystal size and temperature on hardness of alumina grains (courtesy of Mike Hitchiner, Norton-Saint Gobain)

structure. The starting point of this new process is the manufacture of Boehmite, γ-aluminum oxide hydroxide (γ-AlO (OH)), from a modified version of the Ziegler process originally developed for the production of linear alcohols. The material is

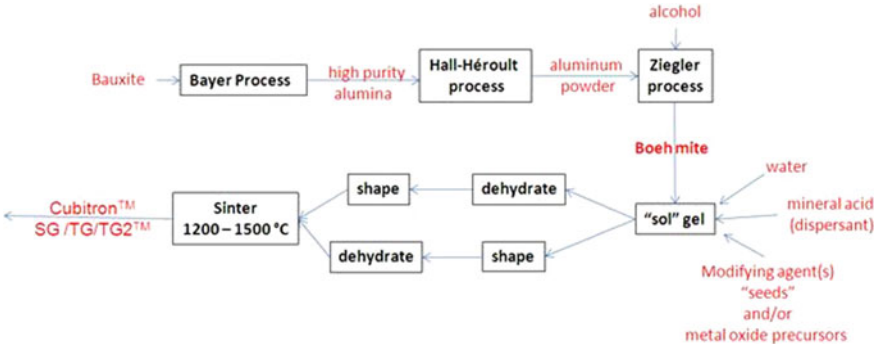

Fig. 8 Manufacturing route for production of "Ceramic" alumina grain (courtesy of Mike Hitchiner, Norton-Saint Gobain)

produced as a sub-micron powder which, mixed with water and a suitable acid dispersant, forms an agglomerate-free seeded-gel of aluminum hydrate ($Al_2O_3.H2O$) with a grain size ~100 nm. The seeded-gel is then dehydrated, shaped and sintered (Fig. 8).

Firing seeded-gel from Boehmite at 1400–1500 °C produces a large amount of porosity and relatively large grains of up >1 μm in size. This is due to high activation energy to convert from a transitional τ- to α-alumina phase resulting in infrequent nucleation with rapidly uncontrollable growth rates. Attempting to control growth rates with lower temperatures, e.g., 1200 °C, leads to larger crystals with higher porosity.

There are two routes that have been developed to reduce the activation energy and control crystal size and densification. The first is the creation of a bi- or multi-composite structure through the use of modifying agents, the second is the controlled creation of a single α-alumina structure through the use of seeding agents (Fig. 9).

Magnesium oxide (MgO) forms a bi-composite structure of α-alumina plus a spinel structure of magnesium aluminate ~25% by volume as shown in Fig. 9b. A fine acicular spinel structure within a relatively coarse α-alumina phase is apparent. This particular grain was used primarily used for low force coated abrasive applications. Multi-phase systems using various modifying agents including zirconia, manganese oxide, chromium oxide, nickel oxide and numerous rare earth oxides were developed over a period of time. One particularly effective material contains magnesia together with yttria and other rare earth oxides such as lanthana and neodymia to produce a dense and hard abrasive grain. In Fig. 9c, the microstructure shows a fine α-alumina phase with a sub-micron magnetoplumbite-type structure of needles and plates formed from adding modifiers to α-alumina. The structures created by the modifiers are believed to provide high strength and novel micro-fracturing properties.

The alternative route to control crystallization rates is by seeding the seeded gel with nano-sized (<100 nm) α-alumina particles, or other materials with a crystallographic match to α-alumina such as α-ferric oxide or various titanates. Additions of 1–5% of seeding agent creates a heterogeneous nucleation condition by increasing the number of nucleation sites from $10^{11}/cm^3$ to $10^{14}/cm^3$, and an average crystal

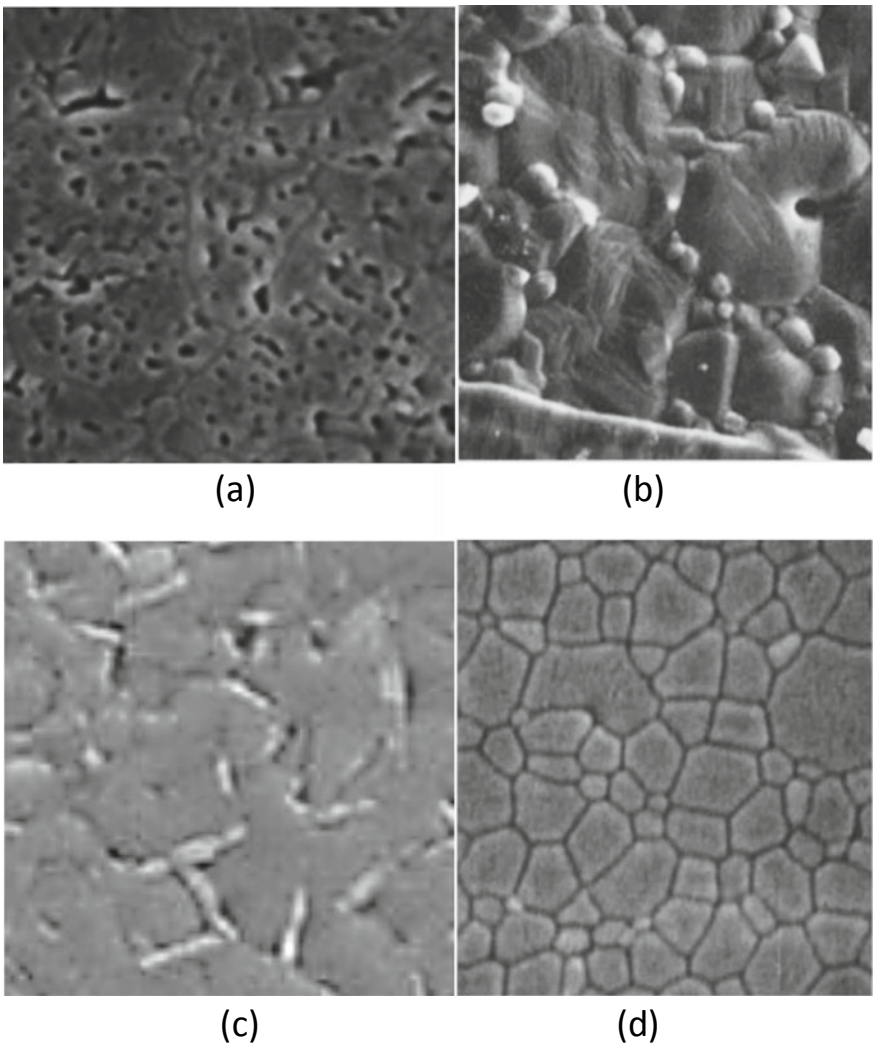

Fig. 9 **a** Sintered alumina microstructure from Boehmite with no modifying agent (image size: 3 μm × 3 μm); **b** Sintered alumina microstructure from Boehmite, with MgO modifying agent (image size: 3 μm × 3 μm); **c** Sintered alumina microstructure from Boehmite plus magnesia, yttria, lanthana and neodymia modifying agents (image size: 1.5 μm × 1.5 μm); and **d** Sintered alumina microstructure from Boehmite with seeding agent (image size: 1.5 μm × 1.5 μm) (courtesy of Mike Hitchiner, Norton-Saint Gobain)

size of about 400 nm (Fig. 9d). This type of grain is sold commercially under the name Norton SG™. One limitation of such a small crystal size is surface reactivity with vitrified bonds when making grinding wheels. Bonds had to be developed to be fired at <1000 °C rather than the 1200 °C of older bonds used for fused alumina abrasives. It is apparent that single-phase seeded microstructures are smaller than the multi-phase microstructures and would be expected to be harder and tougher than fused abrasives. It would also be expected to give longer life but require higher forces to micro-fracture when used as abrasive grain, or should be used at a lower concentration in a blended abrasive product. Further performance optimization can be obtained by bond formulation and grain shape. Seeded-gel manufacturing allows a much greater control of grain shape. Standard crushing and milling methods can produce a typically strong blocky or a weak angular shape. The angularity can be further increased by careful processing of soft, dried pre-sintered material (Fig. 10a–c). The grains are also weak but extremely successful if orientated correctly on a coated application with relatively low grinding forces.

Extruded rectangular prisms with extraordinary aspect ratios and having the appearance of smooth, surface defect free needles are shown in Fig. 10. Norton uses TG™ grains with an aspect ratio of 4–5, and TG2™ with an aspect ratio of 8 in their products (Fig. 10d). These grains maintain a high toughness but they also have a very low packing density. Typical blocky grains may pack to ~50% by volume; an extruded grain with an aspect ratio of 8 has a packing density closer to 30%. This provides for a very high level of permeability and excellent coolant access in the grinding wheel. Owing to the toughness, shape and ability to provide coolant, the stock removal capabilities can be enhanced to produce burn free surfaces on materials such as PMCs.

The most recent variant on the SG-type alumina abrasive is a grain called Norton Quantum™ (NQ™) which maintains the sub-micron crystallite size and associated hardness of the SG abrasive family of grains but has controlled levels of inclusions to promote micro-fracture the lower force levels (Fig. 11). This also allows the grain to be micro-trued with dress depths in the 5–15 μm range to generate sharp, fractured but durable cutting edges. Figure 11 shows the comparison between traditional seeded-gel abrasive grains (Norton SG™) and the submicron crystallite sized abrasive grains (Norton NQ™).

Agglomerated grains—The fusion process creates grains with crystallites comparable in size to the grain, i.e. 50–200 μm, while the seeded gel process creates crystallite sizes in 0.2–5 μm range. The latest edition to the engineered grain family is to produce agglomerated grains made by fusion, comminution, agglomeration, sintering, and re-communtion. The resulting grain has a controlled crystallite size that bridges the gap between SG™ and fused alumina. Since the size, shape and chemistry of the crystallites are controlled by the initial comminution process the possible variations in resulting grain grinding properties are enormous. Furthermore, the options for blending of SG™, NQ™ and Vortex™ grains in the same wheel offers an extraordinary range of complimentary grain properties.

As an example, it has been found that agglomerated grains pack to give a naturally high level of porosity in the resulting grinding wheel (Fig. 12). In addition to

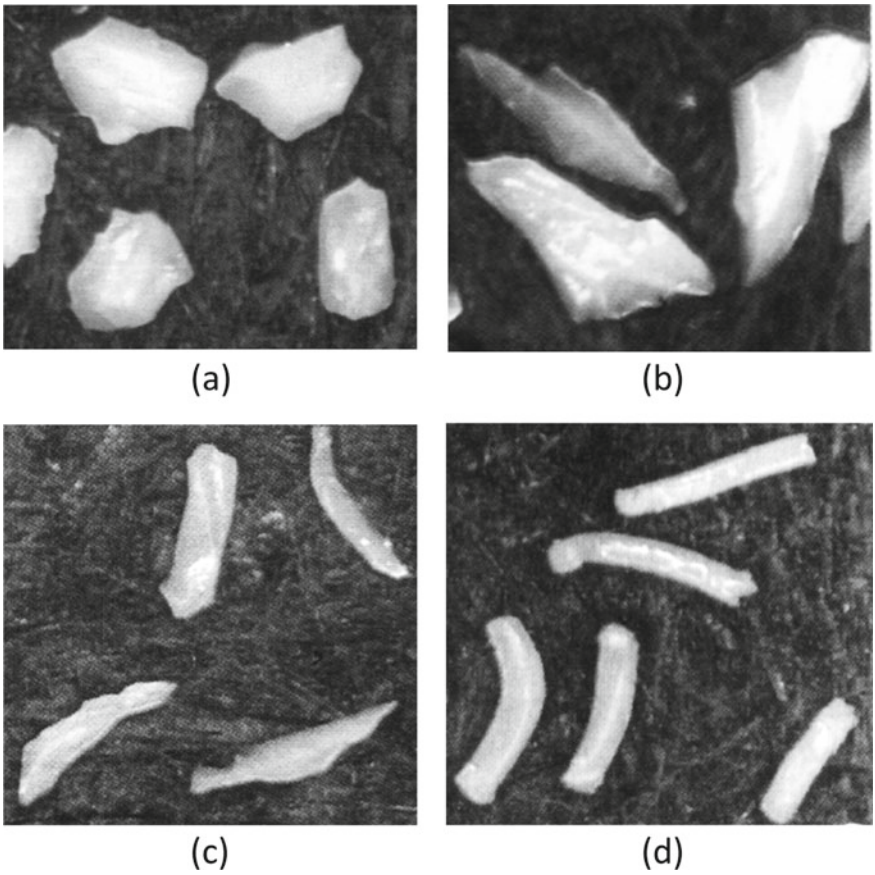

Fig. 10 **a** Tough blocky ceramic grain produced by milling; **b** Friable angular grain produced by crushing; **c** Weak extreme angular grain produced by crushing in green state; and **d** Extruded TG2^{TM} ceramic grain (courtesy of Mike Hitchiner, Norton-Saint Gobain)

the creation of very sharp crushed crystallites in the initial comminution process combined with controlled strength, the agglomeration binder allows controlled crystals to break out to minimize the effects of wear flats, resulting in a very low temperature grinding zone on heat sensitive materials such as PMCs.

Conventional abrasives can be applied to the grinding of polymer matrix composites (PMCs) and applications of bonded abrasive products to the grinding of PMCs are described further in this chapter.

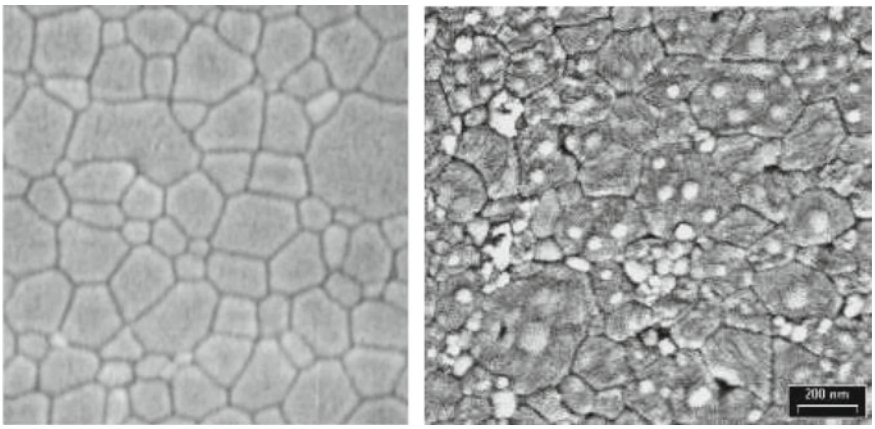

Fig. 11 **a** micro-structure of Norton SG^{TM} seeded-gel alumina grain and **b** micro-structure of Norton Quantum^{TM} NQ grain (courtesy of Mike Hitchiner, Norton-Saint Gobain)

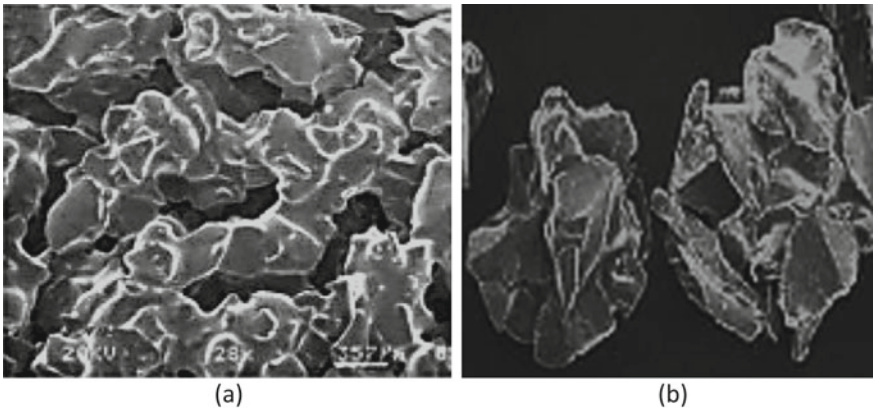

Fig. 12 Norton Vortex ™ agglomerated aluminum oxide grain **a** magnified image of open pores between grains and **b** Macro image showing agglomerated abrasive grains (courtesy of Mike Hitchiner, Norton-Saint Gobain)

2.5 High Hardness Abrasive Grains

Natural diamond, generally of a color, shape or inclusion level unpopular for the jewelry business, remains the standard for single point dressing tools and stones in rotary dressing form rolls. Crushed natural diamond is used in grinding wheels particularly in plated single layer products requiring abrasive grains with extreme sharpness and good convexity (Fig. 13).

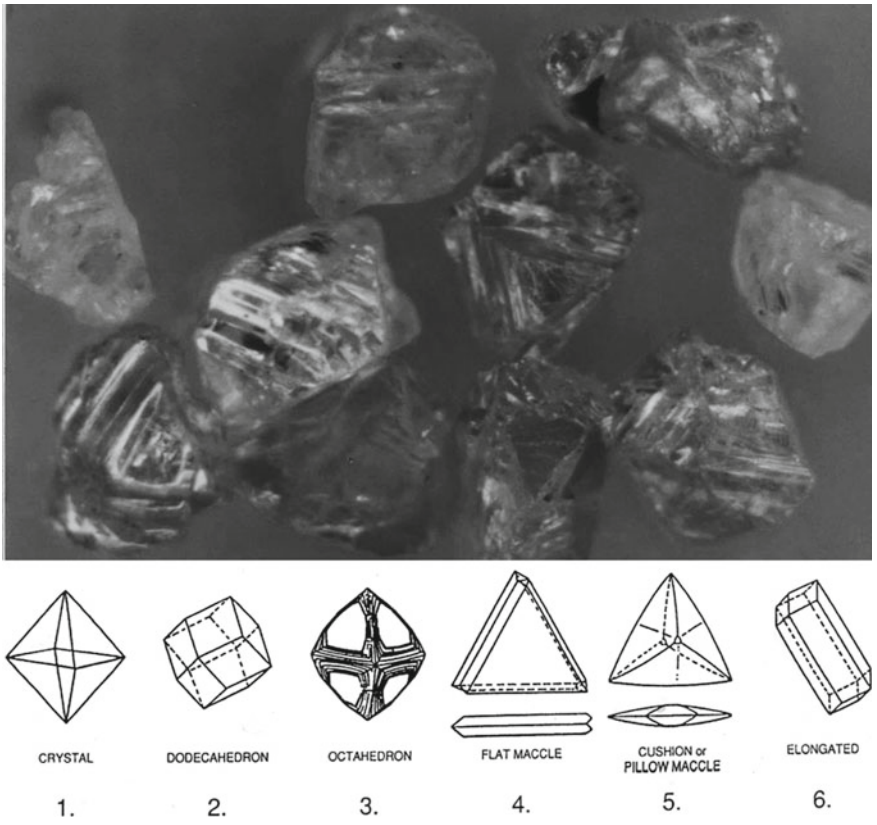

Fig. 13 Collection of natural diamonds of varying sharpness and convexity and their associated forms of habit

Natural diamond is formed at depths of 150–200m below the earth's surface under extreme temperature and pressure in the mantle. It may then be carried up in molten kimberlite and lamproite rocks where it is found at the earth's surface within alluvial deposits produced from erosion most commonly within old formations known as cratons. Large diamonds of the size used in dressing tools are believed to form and remain over great period of time in the mantle, but microdiamonds (<0.5 mm) are believed to form in kimberlite and lamproitic magma.

Some fields may contain predominantly micro-diamonds that were uneconomic due to the lack of traditional gem quality material. Furthermore, most of the major diamond deposits are in politically unstable areas of the world especially South and central Africa, although mines in Australia and Canada have recently become active while Russia has produced large quantities of both gem and industrial diamonds for many decades.

Synthetic diamond is created by the application of extreme high temperature and pressure to graphite precursors. The stable form of carbon at room temperature and pressure is graphite with its familiar layered hexagonal lattice structure. Although bonding within the lattice is sp^3 covalent, bonding between layers is Van de Waals bonding, resulting in low frictional resistance. Diamond, which is meta-stable at room temperature and pressure, has a cubic arrangement of atoms with sp^3 covalent bonding with each carbon atom bonded to 4 others. The direct conversion of graphite to diamond requires temperatures of 2500 K and pressures of >100 kbar. Diamonds produced by this route are termed high pressure, high temperature (HPHT). The severity of the growth conditions can be reduced significantly by the use of a metal solvent such as nickel or cobalt. Graphite has a higher solubility in these solvents than diamond; therefore at the high process temperatures and pressures the graphite dissolves in the molten solvent and diamond then precipitates out. The higher the temperatures, the faster is the precipitation rate and the greater the number of nucleation sites.

The earliest diamonds were grown fast at high temperatures and had weak, angular shapes with a mosaic structure. Also, the principal crystallographic planes of diamond are the cubic (100) plane, dodecahedron (011) plane and octahedron (111) plane. The relative rates of growth on these planes are governed by the temperature and pressure conditions and the metal solvent present. In general at low temperatures the primary growth plane is cubic, while at the highest temperatures is it octahedron.

Careful control of the growth conditions allows the shape to be engineered to specific applications. The blockiest and strongest form of diamond is the intermediate cubo-octahedral used in the strongest metal bonds for cutting or grinding composite materials (Fig. 14).

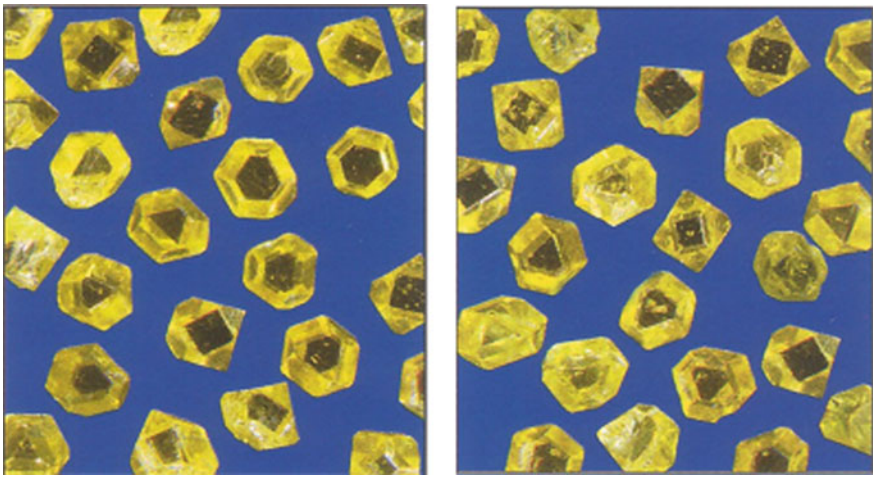

Fig. 14 Cubo-octahedral synthetic diamonds

High temperature and pressures are generated by three main press designs: the belt press, the cubic anvil press and the split-sphere (BARS) press. The belt press as developed for the first diamond synthesis consists of an upper and lower anvil applying pressure to a cylindrical inner cell or bombe. The pressure is confined radially by a steel belt. Belt presses with substantial bombe volumes have been developed in recent years for the growth of large single crystals. The bombe is doped with a seed crystal and a temperature gradient is created within such that diamonds are gradually and steadily deposited over a prolonged period of time. The resulting diamond crystal is then cut along specific crystallographic directions to produce needles and blocks suitable for diamond dressing tools. Owing to the superior hardness associated with diamond, MMCs and CMCs are typically ground with diamond embedded in resin, vitrified or a tough, or brittle, metal bond.

2.6 Grinding Products for Composite Materials

Abrasive grains are mixed with bonding agents in order to make products for grinding composite materials. A variety of products can be used with composite materials such as grinding wheels, coated abrasives, microfinishing tape, and diamond tools for correcting the truth of wheels. A selection of products is shown in Fig. 15. The products produced are optimized for use on composite materials and contain a careful selection of grain, bond and fillers to achieve the requirements specified by the user of those products.

A careful blend of both passive and active fillers are added to bonding systems based on the type of composite ground and the environment in which they are ground. For PMCs, conventional abrasives with both vitrified and resin bonds are typically used, while for MMCs and CMCs, diamond abrasive grains in resin, vitrified and metal bonds are used depending on the power developed by the machine tool, the specific metal removal rates and other operational factors associated with cross feed, linear feed, depths of cut and coolant application in order to minimize the melting of the matrix of the composite material and subsequent fiber pull-out.

3 Grinding of Composite Materials

The grinding of composite materials is becoming a significant part of industrial and academic research in recent years, especially with the advent of highly sophisticated aircraft components made with MMCs and CMCs. The following section describes some recent activities reported in the scientific literature [2–26].

Fig. 15 A selection of abrasive products commonly used for the processing of composite materials (courtesy of Mike Hitchiner, Norton-Saint Gobain)

3.1 Polymer Matrix Composites (PMCs)

El Wakil [2] describes the grinding of PMCs as being more difficult and complicated than the grinding of metals. He states that the direction of fiber ply is critical in achieving the right result and that conventional polymer matrices tend to melt if the grinding zone becomes too hot. A minimum bonding matrix of 30% by volume is required to prevent fibers from being pulled out due to the rotation of the grinding wheel. El Wakil suggests using a softer aluminum oxide grinding wheel such as WA46I8V, i.e., 46 grain size, I-hardness, 8-structure, vitrified bond. When compared to a harder wheel, the softer wheel gave better surface finish results and did not burn the polymer matrix [2]. Wang et al. [3] also ground PMCs and found that lower grinding forces are generated with high abrasive grain size and a lower concentration of abrasive. However, the opposite effect was noted for lower grain size and higher grain concentrations. Surface roughness was significantly improved using the latter specification [3]. From the research studies published so far, PMCs appear to be produce the best results when vitrified alumina grinding wheels are used at low cutting speeds.

3.2 Metal Matrix Composites (MMCs)

For the processing of Al/SiC/Graphite MMCs, electrical discharge abrasive grinding techniques are known to be very effective in producing good surface finishes [4]. A high metal removal rate and high wheel speed (~1300 rpm) are known to produce the best results [4–6]. Resin-bonded diamond wheels appear to be better at producing good surface finishes at high wheel speeds and depths of cut [6]. The resin bonded wheels were compared to electroplated wheels and it was found that electroplated grinding wheels tended to wear quickly probably due to the reduced amount of clearance between abrasive grains and the body of the wheel. The use of modelling techniques for the analysis of grinding MMCs was conducted by Di Ilio et al. [7] focusing on the relationship between cutting parameters and grindability. They concluded that the sliding component of grinding energy was negligible and that the normal and tangential components of grinding force were linear. They also showed that workpiece roughness decreased as the hardness of the MMC increased [7].

Wheel speed is slightly affected by metal removal rate [8, 9], whereas the removal rate is influenced strongly by electrolyte concentration and the magnitude of current in electrical discharge grinding of MMCs with peripheral wheels [10–12] and slotted grinding wheels [13]. In studies focusing on the mechanical properties of ground MMCs [14] and MMCs reinforced with alumina and SiC particles [14], resin-bonded diamond wheels produced no subsurface damage to the composite compared to vitrified SiC grinding wheels that produced significant amount of subsurface damage. It is expected that grinding with resin-bonded diamond wheels improves the fatigue life of ground MMCs compared to using conventional abrasives in a stiff bonding matrix [14]. A brief synthesis of the literature tends to suggest that resin-bonded diamond grinding wheels are best suited to grinding MMCs at reasonably high cutting speeds.

3.3 Ceramic Matrix Composites (CMCs)

Ceramic matrix composites are a new form of composite materials with enhanced properties owing to their hybrid construction. Their processing is described very well in a paper by Singh et al. [15] through methods such as solid state processing, seeded gel formation, laser synthesis, processing using the Pechini method, melt synthesis, co-precipitation and hydrothermal synthesis. New developments include spray and plasma drying, ball milling and mixing and final sintering of CMCs [15, 16]. C/SiC CMCs have been noted to fail by fibers being extruded from their matrix rather than being pulled out of the matrix [16]. This is thought to be caused by the direction in which grinding takes place rather than on operational parameters such as grinding wheel speed or metal removal rate. The authors also found that surface finish was dependent on fiber characteristics rather than the undeformed chip thickness [16]. Singh and Rao [17] found that improvements in grinding CMCs were achieved by

cryogenically cooling the surface of the CMC to form brittle grinding conditions. Subsurface damage was also minimized according to their experimental study.

Wang and Lin [18] studied the grindability of CMCs using electron microscopy techniques. They discovered that the normal and tangential force components act differently to the grinding of metals and is a function of fiber orientation and direction. They also stated that the machine tool used needs to be stiff, powerful and have dynamic performance characteristics that produce a very good surface finish on CMCs. They also stated that wheel durability is also an issue that needs to be addressed in order to make the grinding of CMCs economically viable [18]. Tawakoli and Azarhoushang [19, 20] studied the use of a segmented wheel for grinding CMCs. They noticed that rubbing and plowing regimes were reduced due to intermittent cutting which improved surface finish and grinding force magnitude. An increase in grinding ratio was also observed [19]. A special ultrasonic-assisted grinding method was developed that improved G-ratio even further and reduced tangential and normal forces [20]. Surface waviness of ground CMCs was investigated by Cao et al. [21] to understand how waviness is affected by grinding.

Their studies implied that the work would further enhance the understanding of assembling, sealing and the lubricity of CMCs. Polymer concrete structures were the focus for Shamray et alia's [22] work associated with grindability. The purpose of the study was focused on finding ways to accurately grind polymer concrete structures and to use them for vibration dampening applications such as machine tools. They concluded that grinding forces are substantially less with polymer concrete compared to steel structures [22].

The development of CMCs in large part is due to increased use of these materials in the aerospace industry [23, 24]. Pratt and Whitney in the USA recently published their growth plan for geared turbofans and described the requirements for the development of new materials. As a result of the growth plan, engineers at Norton-Saint Gobain have already started characterizing the grinding characteristics of these materials [25].

Further studies on the grinding of CMCs for aerospace applications were published by Hitchiner et al. [25] and compared the grindability of other materials of interest such as γ-titanium aluminide [26]. Their studies showed that CMCs have better grindability than monolithic ceramics (MC) using standard resin-bonded diamond grinding wheels. The relationships between specific grinding energy, G-ratio and specific material removal rates are shown in Figs. 16 and 17 [26].

4 Conclusion

The expected growth in the use of composite materials can only be matched by the ability to process these materials in an economically feasible manner. As the complexity and difficulty in machining these materials become more prevalent due to the development of MMCs and CMCs and their hybrids, the more likely grinding will become the standard route for processing. The current published knowledge is

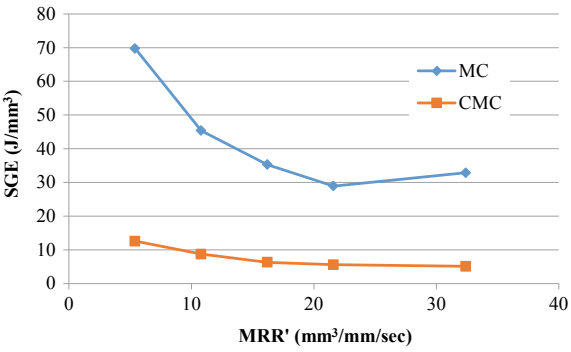

Fig. 16 Specific grinding energy (SGE) versus specific material removal rate (MRR') when grinding CMCs and monolithic ceramics (MC). (Courtesy of Philip Varghese of Norton-Saint Gobain)

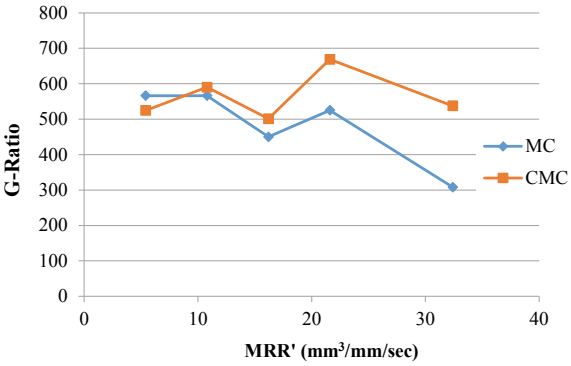

Fig. 17 Grinding ratio (G-ratio) versus specific material removal rate (MRR') when grinding CMCs and monolithic ceramics (MC). (Courtesy of Philip Varghese of Norton-Saint Gobain)

limited at this time but can be expected to grow as demand for these materials grows ever larger. It is expected that the material presented in this chapter will stimulate further investigations into the grindability of advanced composite materials. It is speculated that the effects of abrasive grain behavior and that of the bonding agent will further ignite the development of new abrasive products to grind composite materials and their hybrids. Indeed, fundamental understanding of tribological interactions between grain, bonding agent and workpiece material has already started and will further allow grinding to be transformed into a science rather than a practical art.

5 Review Questions

(1) Describe the differences between PMCs, MMCs and CMCs.
(2) Explain the mechanism of composite failure in CMCs and why they are different to the failure mechanisms exhibited in PMCs and MMCs?
(3) What are the essential characteristics of the undeformed chip thickness equation? What is r and how is the grain's aspect ratio defined?

(4) What effect does grain shape have on the magnitude of the undeformed chip thickness?
(5) If r is equal to 10, what is the size of the undeformed chip thickness compared to a value of 20?
(6) What is the concept of convexity applied to an abrasive grain?
(7) Describe the mechanisms of abrasive fracture.
(8) What is grain toughness and how would you define grain strength?
(9) Describe the differences between conventional abrasive grains.
(10) What are engineered abrasive grains and how does the microstructure of those grains significantly improve grinding performance of PMCs?
(11) How are MMCs and CMCs ground and what type of abrasive is used for those materials?
(12) Describe the mechanisms of fiber pull-out for PMCs and explain how failure mechanisms differ for CMCs compared to MMCs.
(13) What are monlithic ceramics and how do they compare with CMCs?
(14) Which is easier to grind, MCs or CMCs? Explain your answer in terms of grinding characteristics and the formulation of the grinding wheel used to grind these materials.
(15) Agglomerated abrasive grains offer a great deal of advantages in terms of improved grindability for composite materials. Justify this statement in terms of abrasive grain and grinding wheel formulation.

Acknowledgements The authors would like to thank Dr. Mike Hitchiner, Dr. Philip Varghese and Patrick Redington of Norton-Saint Gobain for information regarding the grinding of composite materials.

References

1. Jackson, M.J., Hitchiner, M.P.: High Performance Grinding and Advanced Cutting Tools, Springer Series in Applied Sciences and Technology (www.springer.com/series/8884), vol. 1. pp. 1–100. ISBN 978-1-4614-3115-2. (2013) https://doi.org/10.1007/9781-4614-3116-9
2. El Wakil, S.D.: Grinding processes for polymer matrix materials. In: 'Machining Technoology for Composite Materials, pp. 65–74. Woodhead Publishing, UK, (2011)
3. Wang, H., et al.: Surface grinding of carbon-fiber reinforced plastic composites: effect of tool variables. Advan. Mech. Eng. **8**(9), 1–14 (2016)
4. Yadav, R.N., Yadava, V.: Influence of input machining parameters of slotted electrical discharge abrasive grinding of Al/SiC/Gr MMC. Mater. Manuf. Process. **28**, 1361–1369 (2013)
5. Kwak, J., Kim, Y.: Mechanical properties and grinding performance on aluminium-based MMCs. J. Mater. Process. Technol. **201**, 596–600 (2008)
6. Anand Ronal, B., et al.: Studies on the influence of grinding wheel bond material on the grindability of MMCs. Mater. Design **30**, 679–686 (2009)
7. Di Llio, A., Paoletti, A., D'Addona, D.: Characterization and modelling of the grinding process of MMCs. CIRP Ann.—Manuf. Technol. **58**:291–294 (2009)
8. Shristastava, P.K., Dubey, A.K.: Experimental modelling and optimization of electric discharge diamond face grinding of MMCs. Int. J. Advan. Manuf. Technol. **69**, 2471–2480 (2013)

9. Yadav, R.S., Yadava, V.: Experimental investigation of electrical discharge diamond peripheral surface grinding of hybrid MMCs. J. Manuf. Process. **27**, 241–251 (2017)
10. Liu, J., Yue, T., Guo, Z.: Grinding aided electrochemical discharge machining of particulate reinforced MMCs. Int. J. Advan. Manuf. Technol. **68**, 2349–2357 (2013)
11. Shanawa, A.M., et al.: Grinding of aluminium silicon carbide MMCs by electrolytic in-process dressing grinding. Int. J. Advan. Manuf. Technol. **57**, 143–150 (2011)
12. Yadav, R.S., Yadava, V.: Performance study of electrical discharge diamond face surface grinding on hybrid MMCs. J. Mech. Sci. Technol. **31**(1), 317–325 (2017)
13. Yadav, R.N., Yadava, V.: Multiobjective optimization od slotted electrical discharge abrasive grinding of MMCs using artificial neural network and non-dominated sorting generic algorithm. Proc. Inst. Mech. Engrs. J. Eng. Manuf. Part B **227**(10):1442–1452 (2013)
14. Zong, Z.W.: Grinding of aluminium based MMCs reinforced with alumina and SiC particles. Int. J. Advan. Manuf. Technol. **21**, 79–83 (2003)
15. Singh, N., et al.: Ceramic matrix composites: processing techniques and recent advancements. J. Mater. Environ. Sci. **8**(5), 1654–1660 (2017)
16. Du, J., et al.: New observations of the fiber orientations effect on machinability in grinding C/SiC CMCs. Ceram. Int. **44**:13916–13928 (2018)
17. Singh, V., Ghosh, S., Venkateswara Rao, P.: Grindability Improvement of Composite Ceramic with Cryogenic Coolant. Proceeding world congress on engineering, vol. 2, pp. 1–5. London, UK, (2010)
18. Wang, Y.G., Lin, B.: Research on the grinding force and surface morphology of fiber-reinforced CMCs. Advan. Mater. Des. Mech. **569**, 131–135 (2012)
19. Tawakoli, T., Azarhoushang, B.: Intermittent grinding of CMCs utilizing a segmented wheel. Int. J. Mach. Tools Manuf. **51**, 112–119 (2011)
20. Azarhoushang, B., Tawakoli, T.: Development of a novel ultrasonic unit for grinding CMCs. Int. J. Adv. Manuf. Technol. **57**, 945–955 (2011)
21. Cao, X., et al.: A study on grinding surface waviness of woven CMCs. Appl. Surf. Sci. **279**, 503–512 (2013)
22. Shamray, S., et al.: High efficiency, high speed grinding of a composite wheel consisting of polymer concrete and steel structures. Procedia CIRP **46**, 607–610 (2016)
23. Boyer, R.R., Cotton, J.D., Mohaghegh, M., Schafrik, R.E.: Materials considerations for aerospace applications. MRS Bull. **40**(12), 1055–1066 (2015)
24. Anon.: Pratt & Whitney's Geared Turbofan Growth Plan, Aviation Week & Space Technology. (2013). https://aviationweek.com/awin/pratt-whitney-s-geared-turbofan-growth-plan
25. Hitchiner, M., Besse, J., Varghese, K.P.: Grinding Innovation in a Growing Defense Market, MFG4. The Future Conference, pp. 1–9. Hartford, Connecticut, USA (2012)
26. Bright, R., Biro, A., Hitchiner, M.: Grinding of γ-titanium aluminide with superabrasives, Intertech Conference, pp. 1–8. Indianapolis, Indiana, USA, (2015)

Cutting Tools for Machining Composites

Rangasamy Prakash and Vijayan Krishnaraj

Abstract The machining of composite components finds lot of challenges due to the abrasive nature of the fibres used. The problems such as delamination, fibre pull-out and resin degradation which may be encountered during machining of workpiece and deciding its quality characteristics. Also, the tool wear is a major concern which has to be considered in controlling tooling cost and impact final product cost. Therefore, it is necessary to appropriately select the suitable cutting tool which is expected to cause minimum damages to workpieces. This chapter discusses the cutting tools used when machining (mainly drilling and milling) polymer matrix composites (PMC). The chapter will also discuss cutting conditions, cutting tool materials, cutting tool geometry and coatings. The machinability characteristics due to the effect of cutting parameters and tool materials/geometries during drilling various composite materials will be compared. High speed edge trimming of carbon fibre reinforced polymer (CFRP) materials using fluted and router tools is also discussed to determine the effect of tool geometry and tool coating materials on surface roughness of machined surfaces and the tool wear. This chapter also discusses the cutting tools for machining of metal matrix composites (MMC) and ceramic matrix composites (CMC).

1 Introduction

Composite materials find extensive applications in aerospace, naval, space, and automotive industries due to their unique characteristics such as strength to weight ratio and stiffness to weight ratio, etc., Machining is an essential post processing required to produce components to their final dimensional requirements and to make them assembly ready.

R. Prakash (✉)
Department of Mechanical Engineering, PSG College of Technology, Coimbatore, Tamilnadu, India
e-mail: rpr.mech@psgtech.ac.in

V. Krishnaraj
Department of Production Engineering, PSG College of Technology, Coimbatore, Tamilnadu, India

I. Shyha and D. Huo (eds.), *Advances in Machining of Composite Materials*, Engineering Materials, https://doi.org/10.1007/978-3-030-71438-3_18

The machining of composites faces a lot of challenges not only with respect to work parts and also in cutting tools used. The cutting tool for machining composites decides the various process criteria such as material removal rate, surface quality and tool wear. Therefore, the selection of cutting tools rests on the nature of matrix and also on the reinforcement materials of composites. Hence, it is necessary to select the cutting tool of right material, right geometry to extend the tool life in order to improve the part quality and to minimize cost of machining involved.

The main aspect of machinability is to discuss in detail the force, torque, tool life, and surface finish. Though there are a number of interrelated factors which affect the machinability of the material, the most important factors are the cutting parameters, the properties of the work and tool materials, geometry of the cutting tool, clamping of work and the type of machine tool.

Therefore, in this chapter cutting tool requirements for different types of composites are discussed.

2 Classification of Cutting Tools

The cutting tool for machining composite is selected based on the following criteria:

i. Type and percentage of matrix used
ii. Type and percentage of reinforcement used
iii. Cutting conditions
iv. Surface finish
v. Material removal rate
vi. Tool life
vii. Tool cost.

The cutting tools used for machining of composites are classified based on tool geometry and tool material as follows:

i. **Based on tool geometry**:

- Single point cutting tool
- Drill tool
- End mill
  - Straight fluted
  - Helical fluted
    - Single helix
    - Double helix
  - Router
    - Trapezoidal shape tooth
    - Pyramidal shape tooth

- Diamond grit grinding wheel

ii. **Based on tool material**:

(i) Solid tools

- High speed steel (HSS)
- Tungsten Carbide (WC)
- Polycrystalline diamond (PCD)
- Cubic boron nitride (CBN)
- Polycrystalline boron nitride (PCBN)
- Diamond

(ii) Coated tools

- TiN, TiAlN, TiCN and Al_2O_3 coated
- Diamond like carbon (DLC) coated
- PVD—Diamond coated over carbide substrate
- CVD—Diamond coated over carbide substrate

3 Tool Requirements for Machining Polymer Matrix Composites

3.1 Introduction

Even though the fiber-reinforced composite components are produced to near net shape through various moulding methods, it is important to perform machining in order to produce components to their final dimensional requirements and to make them assembly ready. In these composite structures, cut-outs and holes are to be produced in large numbers. For example, in an aircraft fuselage structure, millions of holes are required for joining purposes. Drilling and milling of such materials is a challenging task to manufacturing engineers because of differential machining properties.

The cutting parameters in drilling are the spindle speed, and feed rate and in milling are the spindle speed, feed and depth of cut. The tool parameter involves the tool material and tool geometry. Though the machining technique on PMC material is similar to that of metals, the fiber proportion and their orientation in PMC (fibers in continuous or chopped strands, fibers in unidirectional or bi-directional) play an important role in deciding the machinability of the material.

Drilling and milling are the two most common machining processes involved. Certain applications of composite materials, such as in aircraft structures or in machine elements, require accurate surfaces for bearing mounting or adhesive joints. Hence machining processes such as edge trimming have to be done at the edges to ensure the desired surface quality and dimensional stability of the composite components. Hence, manufacturing composite parts for various applications involves a

sequence of processes such as moulding, machining and joining. These composite parts need to be manufactured without any damages or defects in order to meet the functional and assembly requirements.

3.2 Cutting Tools for Drilling of Polymer Matrix Composites

3.2.1 Introduction

Polymer matrix composite materials are increasingly used in high performance applications because of superior strength to weight ratio and stiffness to weight ratio. Cut-outs and holes exist in most of the composite structures. Due to their laminated constructions several types of damages like matrix cracking and thermal alterations, fiber pullout and fuzzing, are introduced during drilling in addition to geometrical defects similar to those found in metal drilling. About 60% of the rejections are due to the defects in the holes. These defects would create reduction in structural stiffness, leading to variation in the dynamic performance of the whole structure. Many of these problems are due to the use of non-optimal cutting tool designs, rapid tool wear, and machining conditions (Konig et al. [1]; Komanduri et al. [2]). Bhatnagar et al. [3] have modelled the mechanism of chip formation of UD-CFRP and showed that cutting forces are dependent on the fiber angle as well as the direction of cutting.

According to the Polymer technology (Lubin [4]) series data the cutting speeds from 77.36 to 154.72 m/mm, point angle 60–120°, helix angle 10–50°, clearance angle 9–20° can be selected for drilling PMC material. Apart from the drill diameter and feed employed, the torque and thrust force in drilling are mainly influenced by work material, drill geometry, drill wear and related features. The total drill torque is only slightly affected by the chisel edge length. By thinning the web, it is possible to reduce the axial thrust by 30 to 35%. Both thrust and torque rise sharply if the drill is allowed to dull too much. Figure 1 shows the thrust force and torque acting on a standard twist drill (Arshinov and Alekseev [5]).

In PMC, delamination near the entry and exit portion of the hole, fiber pull out, excessive tool wear are the main problems during drilling. In drilling, the drill always exerts a compressive thrust force on the work piece. The laminate under the drill thus tends to be drawn away from the interlaminar bond around the hole. As the drill approaches the end, the uncut thickness becomes smaller and the resistance to deformation decreases. At some point the loading exceeds the interlaminar bond strength and delamination occurs. This happens before the laminate is completely penetrated by the drill as shown in Fig. 2a. The chisel edge of the drill will first abrade the laminate initially. It, then by moving forward, tends to pull the abraded material away along the flute. The material spirals up before it is machined completely as shown in Fig. 2b.

This action introduces a peeling force upwards to separate the upper laminate from the uncut portion held by the downward acting thrust force. The cutting force acting in the peripheral direction is the driving force for delamination. It generates a peeling

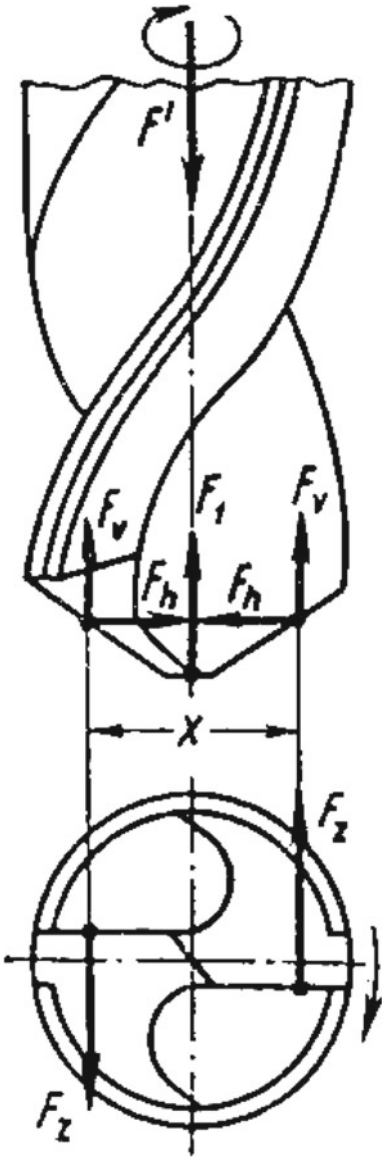

Fig. 1 Forces acting on a drill (Arshinov [5])

force in the axial direction through the slope of the drill flute and is a function of tool geometry and friction between the tool and workpiece. Delamination caused by peel-up becomes progressively more difficult as drilling proceeds, since the thickness resisting the lamina bending becomes greater.

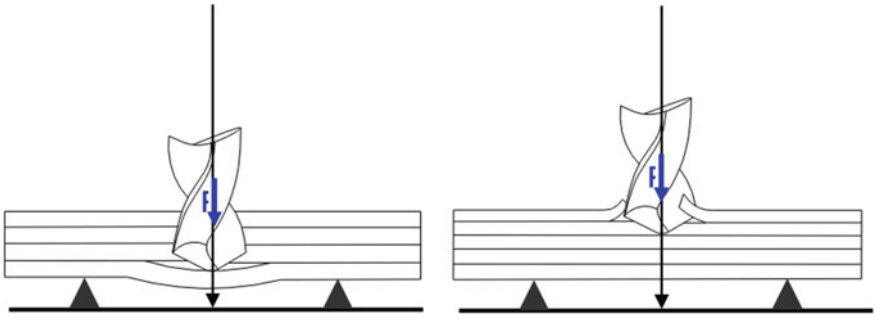

(a) Push – Out at Exit (b) Peel – Up at Entrance

Fig. 2 Drill bit showing delamination at exit and at entrance (Zitoune [6])

3.2.2 Effect of Tool Material

In general, the desirable properties for a cutting tool material are, small grain size to be able to produce a sharp cutting edge, high hot hardness to provide excellent abrasive wear resistance, good toughness to maintain a sharp cutting edge without chipping or deformation under a cutting force's dynamic action, good thermal conductivity to remove heat from cutting zone, and thermal stability to maintain integrity at cutting temperatures and low chemical affinity to the workpiece material. The degree to which each of these properties is needed depends on the workpiece material. The micro constituents in the work material reduce the tool life. In case of fiber reinforced composite materials, the fiber size, shape, position (orientation) and proportion influence the cutting forces and tool life.

As high speed steel is less resistant to wear, its tool life is less when used on fibers like glass and graphite which are highly abrasive in nature. Sakuma et al. [7] drilled holes using four drill materials and investigated drill wear pattern, thermal conductivity of tool material, flank wear width and cutting forces and reported that K01 grade carbide drill has the highest wear resistance when compared to HSS, P10 grade carbide and ultra-fine grain drills. It is found that when cutting speed is increased, the rate of wear on the nose in every tool material starts to increase remarkably at a certain speed. Davim and Reis [8] investigated drilling of CFRP using HSS, cemented carbide (K10) helical flute and cemented carbide four flute drills and concluded that helical flute carbide drill is better because of the hot hardness when compared to HSS drill and positive rake angle when compared to four flute cemented carbide drills. The various types of wear were classified into four groups which may depend upon the cutting speed, feed rate, and geometry of contact, coolant, tool material and work material. The types of wear include adhesive, abrasive, fatigue, and corrosive wear. One of the best methods to improve the productivity or tool life of a drill is to add a coating or surface treatment. Coatings and surface treatments build a barrier between the drill and the workpiece but coatings do not seem to have influence while drilling of PMC materials. Ramulu, et al. [9] have showed that better quality

holes can be achieved while drilling Graphite/Bismaleimide composites using PCD four-faceted drill.

Table 1 gives the typical tool materials used for drilling and its critical machining parameters. For drilling PMC, carbide drill of grade K10 or K20 and PCD is found suitable. While drilling with carbide drills, thrust force was found to be smaller than that of HSS drills, whereas the thrust force of the polycrystalline diamond drill was one third of that of the HSS drill. The PCD drills produced the highest quality holes and suffered the least amount of wear, but the number of literature related to the life or economy seems to be less. Apart from tool materials, tool geometry has direct influence on forces, and quality of drilled holes.

Quality of the holes drilled in PMC has been investigated using Tool maker's microscope, enhanced radiography, computerized tomography (CT), ultrasonic C scan, digital analysis. Ravishankar et al. [10] showed that, it is possible to evaluate the drilling induced damages in composites through AE signal characterization. A simple and cost effective technique to evaluate delamination in drilling composite laminates using digital scanning has been proposed by Khashaba [11]. Seif et al. [12] used Shadow Moiré laser based imaging technique for dark composite parts where visual inspection is difficult. Zitoune et al. [13] have studied further delamination

Table 1 Typical tool materials and critical drilling parameters on composites

Cutting parameters		Machinability characteristics						
Work material	Cutting tool	Vc m/min	f (mm/r)	F_z N	Tq Nm	Wear mm	No holes	Ra (μm)
CFRP Vf 0.62	WC One shot drill, Φ6.35 mm	60	0.048	60	0.2	0.07	32	
GFRP Vf 0.4	Tipped WC Φ6 mm	18.85	0.02	30	–	–	50	–
	TiN HSS Φ6 mm	18.85	0.02	35	–	–	30	–
	HSS Φ6 mm	18.85	0.02	40	–	–	30	–
GF/Polyester	Carbide tipped Φ6 mm	47	0.1	74	–	0.13–0.21	30	–
Gr/Bi	HSS Φ6.35 mm	54	0.028	150	–	0.45	18	5.24
	PCD Φ6.35 mm	54	0.028	50	–	–	40	1.13
KFRP Vf0.55	HSS Candle stick drill	30	0.1	410	–	–	250>	2–3

Vc = Cutting speed m/min, f = Feed rate mm/rev, Fz = Thrust N, Tq = Torque Nm, Ra = Surface roughness (Ra in μm)

at entry and exit while drilling of long fiber composite, and reported that there is influence of manufacturing processes of the composite plate materials and concluded that the delamination of the laminates manufactured in oven is larger compared to the one of the drilled plates manufactured in autoclave. While drilling T700-M21 (3rd generation resin) in comparison with T2H-EH2 (2nd generation resin) presented enhanced machining conditions i.e. better surface finish and minimal defect at hole exit (Zitoune et al. [6]) because of the presence of thermoplastic nodulus.

Khashaba [11] showed that by increasing the cutting speed in drilling cross-winding, woven and chopped composites reduced the push-out delamination as a result of decreasing the thrust force. The depth of the affected zone and the severity of the damage decreases with an increase in cutting speed. At lower feed rates, delamination occurred at the sub-laminate, whereas at higher feed rates it occurred at the early stage of the drilling. The relationship between spindle speed and feed rate are important in terms tool life and quality of hole. The effect of spindle speed on hole quality and cutting force is less when compared to feed rate. Increasing cutting speed resulted in lower thrust force and torque due to the high temperatures produced which softens the matrix. Ramkumar [14] showed that maintaining critical thrust below 70 N improves the quality of the hole, and proposed to use a cutting speed of 12 m/min, feed rate of 0.04 mm/rev with workpiece vibration. A spindle speed of 1000 rpm (5 m/min) and a feed rate of 0.02 mm/rev is reported to be better in case of drilling glass fiber reinforced plastic (Arul et al. [15]). For high volume fraction glass fiber reinforced plastics, Velayudham [16] suggested to use a cutting speed of 80 m/min, feed rate of 0.1 mm/rev and maintain thrust force during drilling below 100 N. Spindle speed of 490 rpm (10 m/min), and feed rate of 0.02 mm/rev is reported to be the critical process parameters for glass fiber reinforced plastics (Zitoune [6]). Table 2 presents preferred cutting speeds and feeds for various combinations.

The variations in the preferred process parameters (Table 3) are based on manufacturing process, volume fraction of the composite, tool material and geometry. In general high spindle speed and low feed rate is preferable for drilling polymer matrix composites (Enemuoh [17]). The data available in the Tables 1, 2 and 3 were collected from various literatures.

But at very high speeds, tool wear is a major problem; still there is a gap in the literature in the fields of optimum parameters at high spindle speed, drill life and economy of using high spindle speed. It is presumed that there is a critical thrust force beyond which delamination is initiated.

Table 2 Typical tool geometries and critical drilling parameters on composites

Cutting parameters		Machinability characteristics				
Work material	Tool geometry	Vc (m/min)	Feed (mm/rev)	Thrust (N)	Torque (Nm)	Df
KFPR Vf 0.36	Candle stick drill HSS Φ 10	30	0.01	430	–	–
CFRP	Special drill Φ10 Carbide K20	18	0.05	120	0.3	–
GFRP Vf 0.4	Trepanning tool HSS Φ 10	50	0.2	40	0.5	–
CFRP	Φ 6.35 Point angle of 75° to 160°	45–65	0.03–0.04	40	–	–
CFRP Vf 0.55	Helical flute Φ 5 Carbide K10	16	0.04	–	–	1.042
CFRP Vf 0.55	Brad & Spur Φ 5 Carbide K10	30	0.05	–	–	1.01
GFRP Vf 0.65	Brad & Spur Φ 5 Carbide K10	55	0.05	6.27	–	1.024
CFRP Vf 0.55	Candle stick Saw drill	31	0.02	–	–	1.30
CFRP Vf 0.55	Twist drill Step drill Saw drill Candle stick Core drill	28–31	0.007 0.049 0.0051 0.069 0.0047	35 29.8 28.6 25.1 42.6	–	–
CFRP Vf 0.55	Step core drill	1200 rpm	0.006	–	–	–
GFRP Vf 0.4	Φ 6, 3 flute solid carbide	12	0.04	20	–	–
UD GFRP Vf 0.56	Φ 6 HSS 90° point angle	28	0.075	60	–	1.03

Vc = Cutting speed m/min, f = Feed rate mm/rev, Fz = Thrust N, Tq = Torque Nm, Df: Delamination factor

3.3 Cutting Tools for Milling (Edge Trimming) of CFRP Composites

3.3.1 Introduction

Unlike in the case of metals, the machining of Fiber-Reinforced Composites (FRPs) is characterized by uncontrolled fracture and the machining forces oscillate due to the subsequent constituents. Owing to the inhomogeneous and anisotropic material properties, machining of CFRP comes along with certain difficulties such as fiber pull-out, delamination and decomposition of matrix material, which results in a degradation of the surface quality and the material properties. The different material

Table 3 Critical drilling parameters on composites

Cutting parameters		Machinability characteristics			
Work material	Tool geometry	Speed (m/min)	Feed (mm/rev)	Thrust N	DF
GFRP Vf 0.4	HSS Φ6 mm	12	0.04	30	–
GFRP Vf 0.4	Tipped WC Φ6 mm	18.5	0.02	30	1.005
GFRP Vf 0.63	Tripod, Carbide K10, Φ6.5 mm	80	0.1	50	1.02
GFRP Vf 0.66	Tipped carbide K10, Φ6.5 mm Point angle 85°	80	0.08	50	–
GFRP Vf 0.63	Coated carbide	19	0.08	–	–
GFRP Vf 0.65	Carbide K20 Φ6 mm	10	0.02	–	–

Fz = Thrust N, Df: Delamination factor

properties of the constituent phases and the different failure modes drastically reduce the tool life. Hence, specially designed tools are required for machining of FRPs.

Machinability is mainly influenced by the mechanical properties of the CFRP which is determined by the type of fiber, the matrix material, the fiber volume content, the fiber orientation and the manufacturing process. For the application of composite materials, such as in the case of aircraft structures or in machine elements, some accurate surfaces for bearing mounting or adhesive joints are required. Hence it is important to carry out proper machining such as edge trimming in order to ensure surface quality and dimensional stability at the edges of parts.

Peripheral milling is normally known as 'edge trimming' because the tool diameter is small and the axial engagement encompasses the entire thickness of the workpiece. Figure 3 presents the schematic diagram of edge trimming operation and the direction of the cutting forces induced.

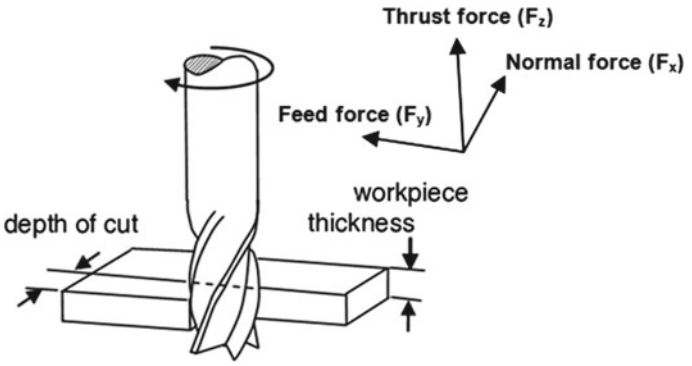

Fig. 3 Edge trimming

3.3.2 Fluted and Router Cutting Tools for High Speed Edge Trimming of CFRP Composites

Materials and Methods

This section presents the effect of various cutting conditions and different types of the cutting tools such as helical flute, and router type tools during edge trimming of quasi-isotropic CFRP laminate. The effect of cutting tool geometries and cutting parameters on cutting forces, the surface quality of the trimmed edges of CFRP laminates is studied. The modern cutting tools (router tools) selected for machining CFRP, have complex geometries in cutting edges and surfaces. Hence, the traditional method of direct tool wear evaluation is both difficult and inadequate. Taking this into consideration, an acoustic emission (AE) sensing has been employed for online monitoring of the performance of router tools to determine the relationship between AE signal and the length of machining.

The quasi-isotropic CFRP as shown in Fig. 4 is made using unidirectional prepregs supplied by Hexcel Composite Company, referenced under HEXPLY UD T700 268 M21 34% (T700-M21). The quasi-isotropic CFRP laminate has the stacking sequence of $[90°/-45°/0°/+45°]_{2s}$. CFRP laminates are compacted using a vacuum pump and then cured in an autoclave. The nominal fibre volume fraction is found to be 0.59.

As the CFRP materials are highly abrasive in nature, it is necessary that cutting tools incorporate a unique tool geometry that can effectively respond to these requirements.

Two varieties of router tools with different geometries and one helical fluted tool made up of tungsten carbide of grade of K600 (ultra-fine grain cemented carbide) are considered to investigate the performance on edge trimming. The teeth on the router tool are shaped by two intersecting flutes, right angle and left angle. The right angle flutes were inclined at 15 degrees. The intersection of these flutes creates cutting teeth of trapezoidal and pyramidal shapes.

Figure 5a–c shows the three tools of Ø6 mm made up of tungsten carbide namely router type—trapezoidal tooth (Tool T1), router type—pyramidal tooth (Tool T2) and four fluted helical end mill (Tool T3).

Table 4 shows the detailed specification of three different tools for edge trimming of CFRP material.

Fig. 4 Quasi-isotropic CFRP laminate (Prakash [18])

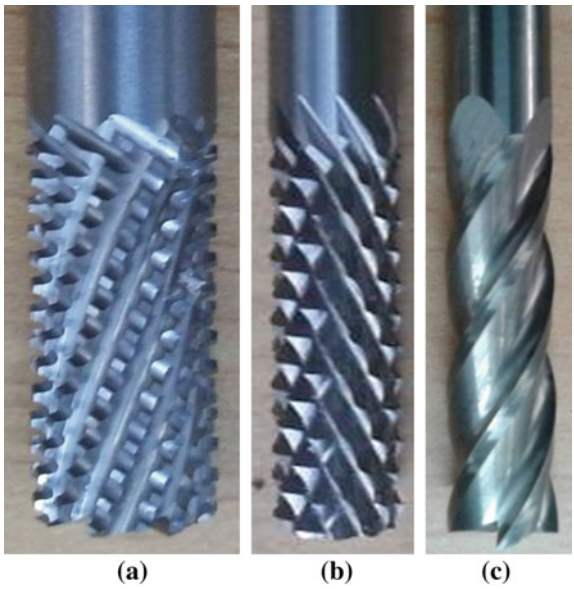

Fig. 5 **a** Tool T1 **b** Tool T2 **c** Tool T3

Table 4 Cutting tools and their specification (Prakash [18])

Tool	Specification	Tool image	Tooth shape	Tooth profile
Tool T1	Pitch = 3.42 mm No. of flutes-12 Tooth shape-trapezoidal	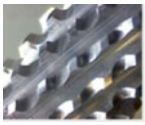	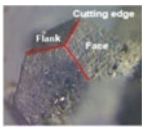	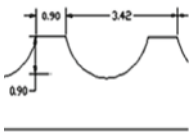
Tool T2	Pitch = 2.42 mm No. of flutes-12 Tooth shape-pyramidal	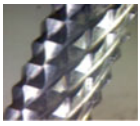	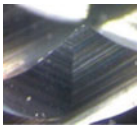	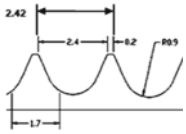
Tool T3	Helix angle 30° No. of flutes-4 Tooth shape- helical flute			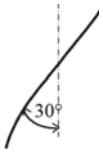

Figure 6 shows the schematic representation of set up used for edge trimming and the online measurement of cutting forces, cutting tool temperatures, and tool wear.

Table 5 presents the different machining parameters at different levels selected provided with, the axial depth of cut of 4.16 mm, the radial depth of cut of 0.5 mm,

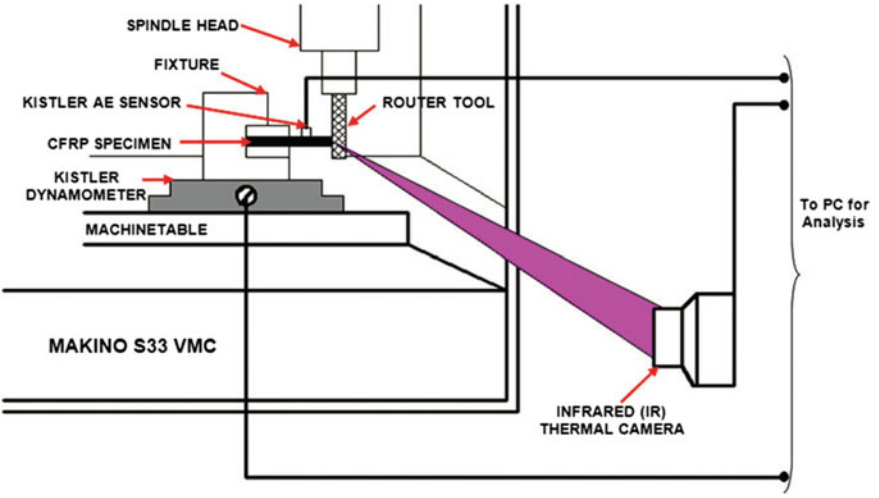

Fig. 6 Schematic diagram of experimental setup for edge trimming (Prakash [19])

Table 5 Machining parameters (Prakash [18])

S.No.	Cutting parameters	Levels
1	Spindle speed (rpm)	3000, 6000, 9000
2	Feed (mm/rev)	0.1, 0.15, 0.2
3	Radial depth of cut (mm)	0.5

and the cutting configuration of up milling with dry condition for all the cutting trials during edge trimming operations.

Effect of tool geometries and cutting parameters

Cutting Forces

The cutting force is one of the important process criteria for considering the surface damage of workpieces and failures in the cutting tool. The resultant cutting force R(N) is calculated using the Eq. (1) from the three forces, feed force F_y (cutting force acting along the direction of the feed), normal force F_x (cutting force acting perpendicular to the feed) and thrust force F_z (cutting force acting along the axis of the cutting tool) generated during the edge trimming process.

$$R(N) = \sqrt{(Fx)^2 + (Fy)^2 + (Fz)^2} \tag{1}$$

Figure 7a–c are the force graphs representing the machining behaviour of three different tools at the machining conditions of spindle speed 3000 rpm, feed rate 0.1 mm/rev and radial depth of cut 0.5 mm. From these force graphs it is observed that the lowest magnitude and fluctuations of feed force (F_y) generated while using

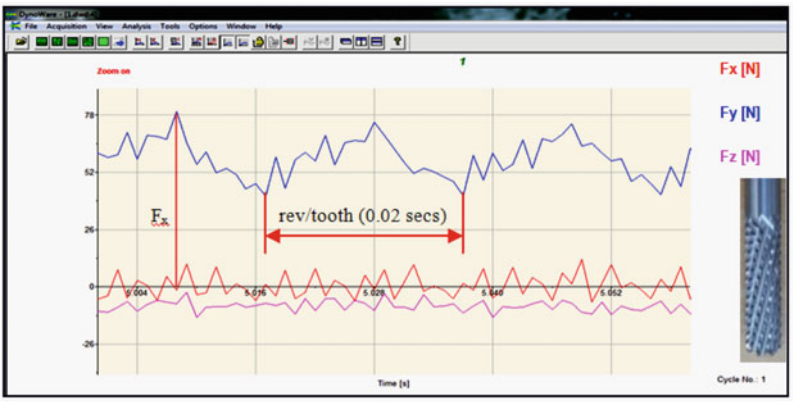

(a)

(b)

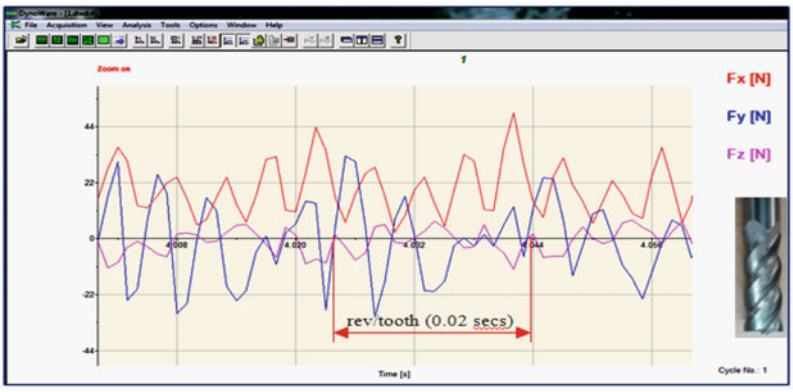

(c)

Fig. 7 Cutting forces graphs at 3000 rpm; 0.1 mm/rev and WOC = 0.5 mm observed for **a** Tool T1; **b** Tool T2, and **c** Tool T3

trapezoidal tooth router tool (T1) when compared to other tools. Whereas the normal force (F_x) and the thrust force (F_z) induced in this case are very low in magnitude, though the fluctuations are high. Therefore the geometry of trapezoidal tooth of this kind of router (T1) performs well in chip removal with lesser damages or defects. However, in the case of pyramidal tooth router tool (T2), the normal force induced with high magnitude and fluctuations results in more damages in the workpiece.

The resultant cutting force increases with an increase in spindle speed as well as feed for all the three kinds of tools. It is also inferred that tool T1 generated lower cutting force when compared to other two tools because of the trapezoidal shape of the cutting teeth. Tool T2 has generated comparatively higher cutting forces because of the pyramidal shape with smaller cutting edge and clearance face, when compared to trapezoidal cutting edge. Also tool T2 induced greater ploughing action and improper shearing of fibers resulting in increased fiber protrusion on the edges of the plies of the CFRP laminate.

The mean percentage of increase in cutting force with tool T2 when compared to tool T1 at all three spindle speeds as 56.7% and mean percentage of increase in cutting force with tool T3 when compared to tool T1 at all three spindle speeds as 58.66%. When machining with tool T1, the minimum force measured was 15.21 N at a spindle speed of 3000 rpm and feed of 0.1 mm/rev. When machining with helical fluted tool T3, the maximum force measured was 59.26 N at a spindle speed of 9000 rpm and feed of 0.2 mm/rev. The reason for these highest forces in tool T3 is that the tool cuts the largest chip per tooth (three times as large as the other tools T1 and T2 which have the 12 number of flutes which is 3 times more when compared to tool T1 with 4 flutes).

Surface Roughness

Tool T1 gives a moderate surface roughness due to the trapezoidal shape of cutting teeth when compared to tools T2 and T3. The mean percentage decrease in surface roughness value with tool T1, when compared to T2, is 32.87%. The surface roughness obtained using tool T3 at all spindle speeds is less because of tool T3 has helical flutes. The mean percentage decrease in surface roughness value with tool T3, when compared to T2 is 57.89%. However, the scooping action of these flutes while machining results in lowering the roughness in the edges of the machined workpieces. Tool T2 gives the higher surface roughness value at all spindle speeds due to the presence of a sharp cutting edge of pyramid shaped tooth profile.

Delamination

Delamination is one of the important measure of surface quality of the trimmed edges of the CFRP laminates. It is observed that there is no delamination occurred while using tool T1 and tool T2. Since the axial force developed was small, the delamination of top plies was controlled to a very minimum level. This is due to unique geometry of cutting tooth with more number of flutes on router tools T1 and T2. A significant delamination value was measured while using tool T3 because the tool tends to develop a high axial force which in turn separates or disintegrates the extreme top plies of CFRP laminate. Yet another reason for delamination with the

helical fluted tool is that the chip per tooth is three times higher than the other tools, as the number flutes in the helical flute tool is one-third of the number of flutes in both the router tools. Further, the chip is not broken into small segments because of the continuous cutting edge in the helical flute tool. These continuous chips make the impact of the cutting edge on the laminate to cause severe delamination.

Acoustic Emission (AE) Signal Measurement

Crack propagation is one of the macroscopic sources of AE. Cracks and other discontinuities in a work material concentrate on stresses. Crack jumps are accompanied by a rapid release of potential energy, a small part of which is released in the form of stress waves. Materials produce acoustic emissions when they are stressed beyond their normal design ranges to final failure. During plastic deformation, dislocations move through the material's crystal lattice structure producing low-amplitude AE signals, which can be measured only over short distances under laboratory conditions. AE waves generated are related to failure propagated such as deformation or damages during cutting. Therefore, AE waves caused by cutting action between the cutting tool and the workpiece is considered as part of the performance of the cutting tool. AE Out (Filter) mean value increases as the wear in the tool increases during continuous machining. The magnitude of the AE signal is considered as the measure of performance of the tool. Higher the AE signal, the poorer is the performance of the tool.

The AE signals were recorded on edge trimming under the cutting conditions of high spindle speed of 9000 rpm and high feed of 0.2 mm/rev for 1 m length of machining of CFRP laminate.

From the Fig. 8, it is observed that AE Out (Filter) value increases with an increase in the length of machining for all the three types of tools. In other words, tool performance decreases as the length of machining progresses. AE signal level is the function of machining performance. Since the router tool T1 has the lowest chip thickness/tooth and better tool geometry when compared to tool T2 & T3, it results in

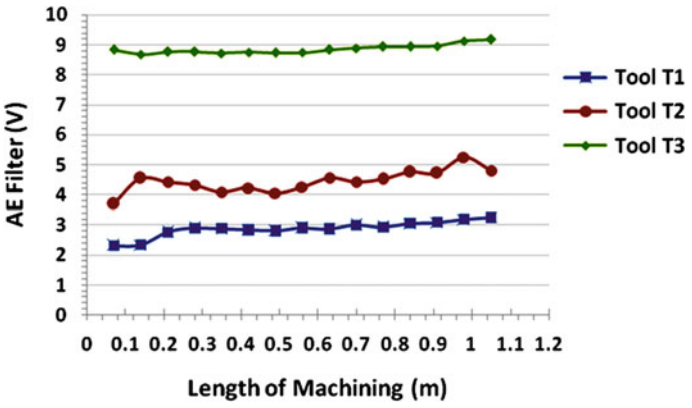

Fig. 8 AE Out (filter) values Vs Length of machining for different tools (Prakash [18])

Table 6 Consolidated results (Prakash [18])

Tool	Output Responses			
	Cutting Force	Surface Roughness	Delamination	Cutting Efficiency
Tool T1	Low	Moderate	Low	High
Tool T2	Moderate	High	Low	Moderate
Tool T3	High	Low	High	Low

lowest signal values of AE out filter values (in Volts). Therefore, tool T1 is considered to provide better cutting efficiency when compared to tools T2 and T3. The flute tool has the highest AE out filter, values which in turn indicate the poor cutting efficiency while trimming of CFRP laminate.

Table 6 depicts the output responses such as cutting force, surface roughness, and delamination for the three different tools used for edge trimming of CFRP laminate. From the analysis, it is inferred that tool T1 generates low cutting force, offers no delamination with a moderate surface roughness, and also provides high cutting efficiency, while the tool T3 generates a higher cutting force, increased delamination with a good surface finish. Tool T2 seems to provide a moderate cutting force, with a high surface roughness and low delamination.

Summary

- It was found that the trapezoidal tooth router (T1) generated lower cutting force and moderate surface roughness with no delamination while machining of CFRP materials. The performance of the tool was also found to be the superior among the three tools, as the cutting tooth of trapezoidal shape with more cutting area creates lower surface damages in the trimmed edges.
- It was observed that the machined edges of CFRP specimens have no delamination as both the router tools (T1 and T2) have discontinuous cutting edges unlike in the case of continuous edge in the helical flute tool.
- The pyramidal tooth router (T2) generated higher surface roughness when compared to the other two types of tools. The cutting tooth has a small flat edged pyramid form creates more indentations on the workpiece surface. This, in turn, results in increasing the surface roughness.
- The helical flute end mill (T3) generated higher cutting forces and more delamination when compared to router tools (T1 and T2). The continuous flutes with higher helical angle cause the pulling action of the extreme top and bottom plies of the laminate, which results in delamination.

Fig. 9 Cutting Tools (Router type) (Prakash [19])

3.3.3 Coated Router Tools for High Speed Edge Trimming of CFRP Composites

Introduction

This chapter presents the investigations on effect of coatings on surface quality of trimmed edges and tool wear, during high-speed edge trimming of CFRP materials. Two different coated router tools (trapezoidal tooth type) namely titanium aluminium nitride (TiAlN) coated and diamond like carbon (DLC) coated routers were used for studying the effect of coatings during high-speed edge trimming operation. The experimental study gives the effect of machining parameters (cutting speed and feed) and coating materials, on cutting force, cutting temperatures, which significantly influence surface roughness of the workpiece and tool wear.

Materials and Methods

Hardness of the tool material and coefficient of friction between tool/work interface play a major role in attaining the desired surface quality of the work and longer tool life. Figure 9 shows the cutting tools selected for conducting this study. Two different coatings, namely titanium aluminium nitride (TiAlN) and diamond like carbon (DLC) coatings were selected for achieving quality trimmed edge surfaces and extended tool life due to their excellent tribological properties.

These coatings are thin, chemically inert and also have a low surface roughness. The standard thickness of the coatings is 4 μm and it was deposited on tungsten carbide router tools using the PVD magnetron sputtering technique. Table 7 shows the specification and the properties of three different router tools used in the experiment.

Table 8 shows the machining parameters considered with their different levels to conduct edge trimming operation using uncoated and coated router tools while keeping the radial depth of cut of 0.5 mm as constant and the axial depth of cut is equal to the laminate thickness of 4.16 mm.

Effect of coatings and cutting parameters

Cutting Force

In edge trimming, more than one cutting edge is engaged in cutting at the same time which presents difficulty to the process with respect to fibre orientation, chip size, and cutting forces. The cutting forces generated have a direct relationship between

Table 7 Specification and properties of router tools (Prakash [19])

Tools used	Uncoated router tool	TiAlN coated router tool	DLC coated router tool
Specification	Material–Tungsten Carbide, Diameter = 6 mm, Pitch = 3.42 mm, No. of flutes (right-handed) = 12, Tooth shape—Trapezoidal		
Vickers Hardness	2500 HV	3500 HV	3000 HV
Coefficient of friction	0.6	0.5	0.1–0.2
Thermal conductivity W/m°K	88	4.63	100–150

Table 8 Machining parameters (Prakash [19])

Cutting Parameters	Levels
Cutting speed (m/min)	226, 283, 339
Feed rate (mm/rev)	0.1, 0.15, 0.2
Radial depth of cut (mm)	0.5

the thickness of the chip produced while trimming. Therefore, the lesser the chip thickness, lower the cutting forces. As the chip thickness is also the function of feed value from the Eq. (2), a smaller feed will result in smaller chip thickness, thus reducing the cutting force generated.

$$\text{Maximum chip thickness } a_{\max} = \frac{v_f \sin\phi}{TN} \tag{2}$$

(Source: Jamal Sheikh-Ahmad [20])

Where, v_f—feed speed, T—Number of cutting edges, N—Spindle speed, and ϕ—Total engagement angle.

The resultant cutting force is the function of cutting speed and feed. It is further observed that the resultant cutting forces systematically increases with an increase in feed for all three cutters. This is due to the geometrical increase in chip thickness as a result of increasing the feed. However, the behaviour with cutting speed is not always consistent.

In case of uncoated and TiAlN coated tool, for most feeds, the resultant force tend to increase with an increase in cutting speed and decreases with a further increase in cutting speed. Since the chip thickness does not change with the increase of cutting speed, this force behaviour might be a result of the dynamic response of the cutter/spindle at this particular cutting speed. In the case of DLC coated tool, the resultant force does not change significantly with cutting speed as the expected and the resultant forces are comparatively lower than those obtained for the other

tools. This could be attributed to the properties of low coefficient of friction and high thermal conductivity.

Cutting Temperature

The rise in temperature is an inevitable factor regarding high-speed machining processes. Hence it is necessary to monitor the cutting temperatures in edge trimming of CFRP laminate under high-speed conditions. The cutting temperature generated during machining is also the function of cutting speed and feed. It is observed that the cutting temperature does not change significantly with process parameters for the uncoated tool and the DLC coated tool. However, the behaviour of the cutting temperatures for the TiAlN coated tool is similar to that of the resultant force. Furthermore, the cutting temperatures for the uncoated and DLC coated tools are lower than those for the TiAlN coated tool. The cutting tool temperature is generally lower for cutting tools with a high thermal conductivity. It is observed that the cutting temperatures for all the cutting conditions fall below the glass transition temperature ($T_g = 187°C$) of CFRP material, which ensures the absence of thermal damage.

The maximum temperature is attained at the intermediate cutting speed of 283 m/min and low feed of 0.1 mm/rev with TiAlN-coated router due to the reason of high heat accumulation at the machining zone (i.e. shear zone where exact shearing of material takes place). Further, heat dissipation is comparatively slower due to its poor thermal conductivity. DLC coated routers, generates less temperature when compared to TiAlN coated routers. This is because of the DLC coating which has very low coefficient of friction and excellent thermal conductivity when compared to TiAlN coating.

Surface Roughness

Surface roughness (Ra) value increases with an increase in feed, as deduced from the equation for ideal surface roughness. However, the behaviour of surface roughness with speed is similar to that of the cutting forces. An increase in feed per tooth (resulting from increasing the feed rate) causes an increase in surface roughness as well. This may be attributed to the heat generated as a result of higher friction. An increase in feed rate causes a sharp rise in feed force, which in turn causes higher friction. Surface roughness tends to decrease with an increase in cutting speed. Among all the factors, the feed rate is the most influential one in determining surface roughness.

As the cutting speed increases, the Ra value increases initially and then decreases. Surface roughness is the highest at the intermediate level of cutting speed (i.e. at 283 m/min) and at all feeds the cutting forces generated were higher as the frictional resistance developed to cut the material is high, thereby the temperature generated at this condition is also showing with higher values. At this stage of higher temperature, the resin gets softened and facilitates further machining with less cutting force. These reasons will also be considered for the result of higher surface roughness at this intermediate condition. While a low surface roughness value is obtained at 339 m/min and 0.1 mm/rev while using DLC coated tool, a high surface roughness value is obtained at 283 m/min and 0.2 mm/rev while using the TiAlN coated tool. DLC

coated tools provide better surface quality with minimum damages when compared to the other tools at high cutting speed conditions. Since the surface roughness is the measure of cutting force and the cutting temperature generated, the surface roughness observed in the trimmed edges of CFRP work materials using DLC coated router is lower which is because of its unique composition and structure with its salient characteristics of low coefficient of friction and excellent thermal conductivity, and wear resistance and non-sticking characteristics.

Tool Wear

Since tool wear leads to undesirable consequences such as increased cutting forces, cutting temperatures, and degradation of surface finish, therefore, it is extremely desirable to control the same. Abrasion is the primary wear mechanism when trimming CFRPs. Therefore, a great deal of resistance to abrasive wear and high fracture toughness are essential for cutting tools during trimming. Thermal conductivity is an important property because most of the heat generated during cutting has to be dissipated through the cutting tool. The fine-grained cemented carbides with coatings such as TiAlN and diamond like carbon (DLC) tend to meet these requirements.

Tool wear occurs both on the face and flank, but depending upon the machining conditions, one of these types of wear may predominate. Figure 10a, b presents the wear of the uncoated tool occurred as rounding of the cutting edge at tooth corner. Flank wear is measured as the width of the wear land on the clearance side as shown

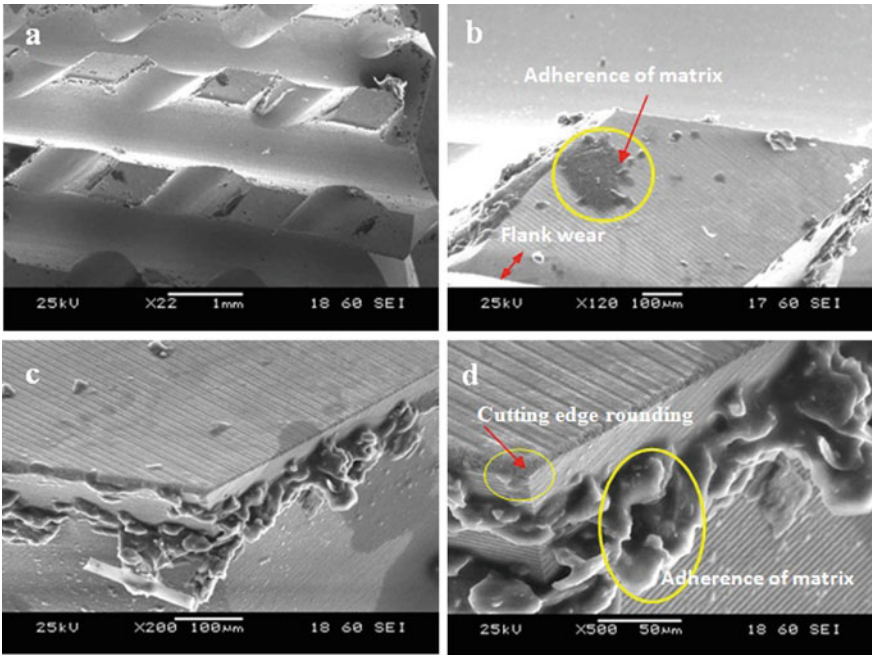

Fig. 10 **a–d** SEM Images of uncoated router tool (after machining) (Prakash [19])

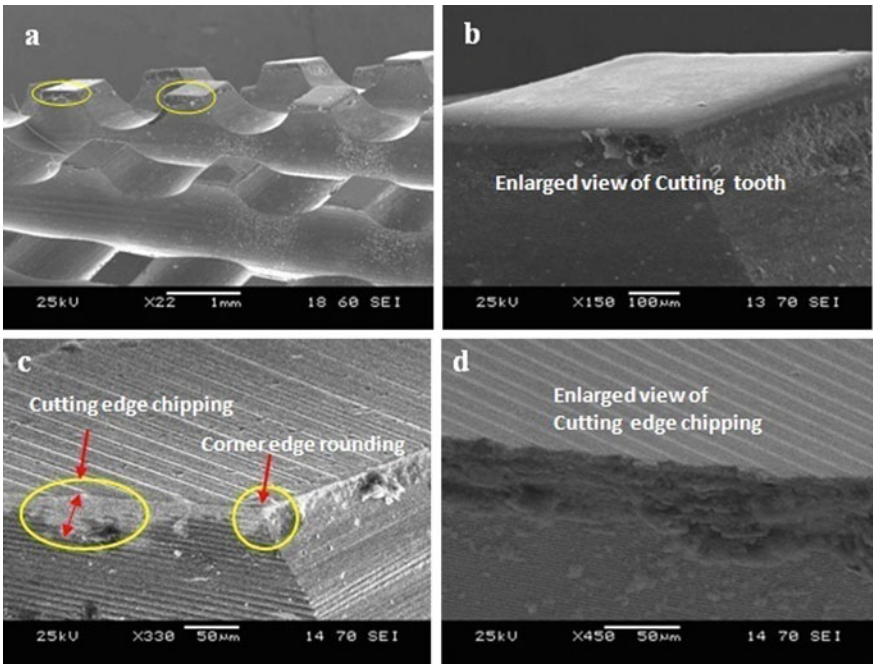

Fig. 11 **a–d** SEM Images of TiAlN coated router tool (after machining) (Prakash [19])

in Fig. 10b. Figure 10c, d shows the damage at the corners (Cutting edge rounding (CER)) and the adherence of matrix at the tool faces (Ali Faraz et al. [21]).

The wear of the TiAlN coated tool seems to occur due to chipping of the coating and rounding of the uncovered substrate, as shown in Fig. 11a, b. Figure 11c, d shows the CER and the cutting edge chipping.

Wear of the DLC coated tool was also found to be uniform rounding of the edge and corner of the tooth, as shown in Fig. 12a, b. Figure 12c, d shows the CER at the DLC coated tool. The wear of DLC cutter was relatively smaller than that of the TiAlN coated and uncoated tools. The main reasons could be its very low coefficient of friction, and hardness of the DLC coated router. SEM images also show matrix adhering to the surface of the tool due to high cutting temperatures.

Figure 13 shows the effect of direct tool wear (measured using tool makers microscope) on length of machining for uncoated and coated router tools at the machining conditions of intermediate cutting speed 283 m/min and a feed 0.2 mm/rev. From the comparison of among three tools, it reveals that the DLC coated routers seem to perform better well with lesser tool wear and fewer surface damages on the trimmed edges.

Tool Wear Monitoring Using AE

The crest factor (C) is defined either by Eq. (3) and is a monitoring index that gives an idea of how much of impact occurring in a time waveform.

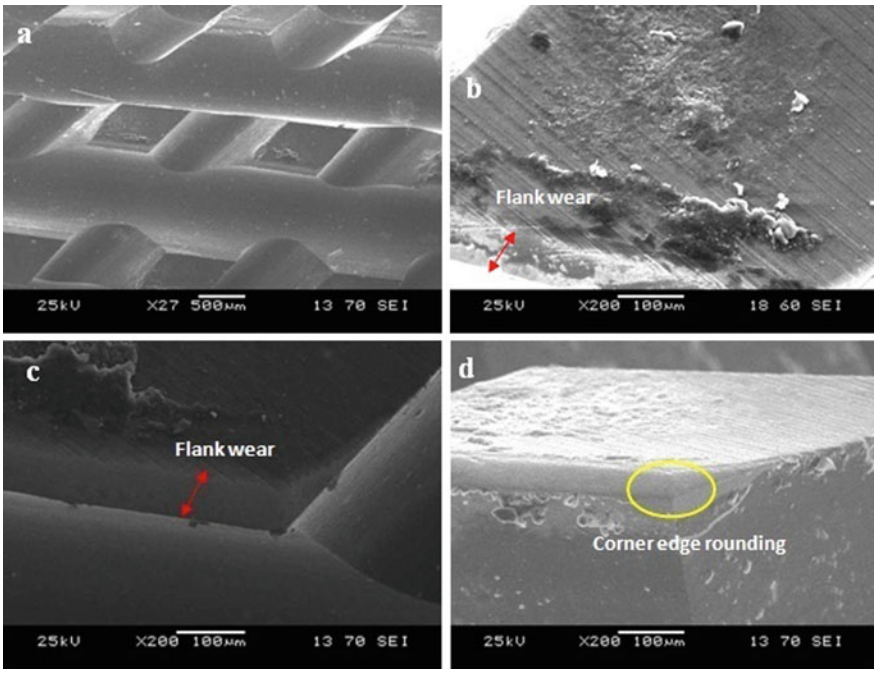

Fig. 12 **a–d** SEM Images of DLC coated router tool (after machining) (Prakash [19])

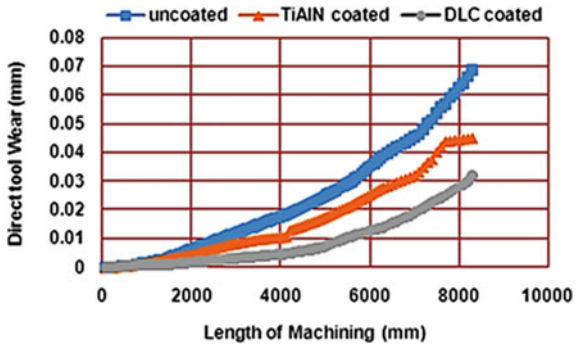

Fig. 13 Comparison of direct tool wear for the three tools (Prakash [19])

$$Crest\,factor(C) = \frac{Peak\ amplitude\ of\ a\ waveform}{RMS} \tag{3}$$

The crest factor is trended over time to see if the amount of impacting increases or stays the same.

Acoustic emission online tool condition monitoring and evaluation of tool wear is performed at the cutting speed of 283 m/min and a feed of 0.2 mm/rev. The variation

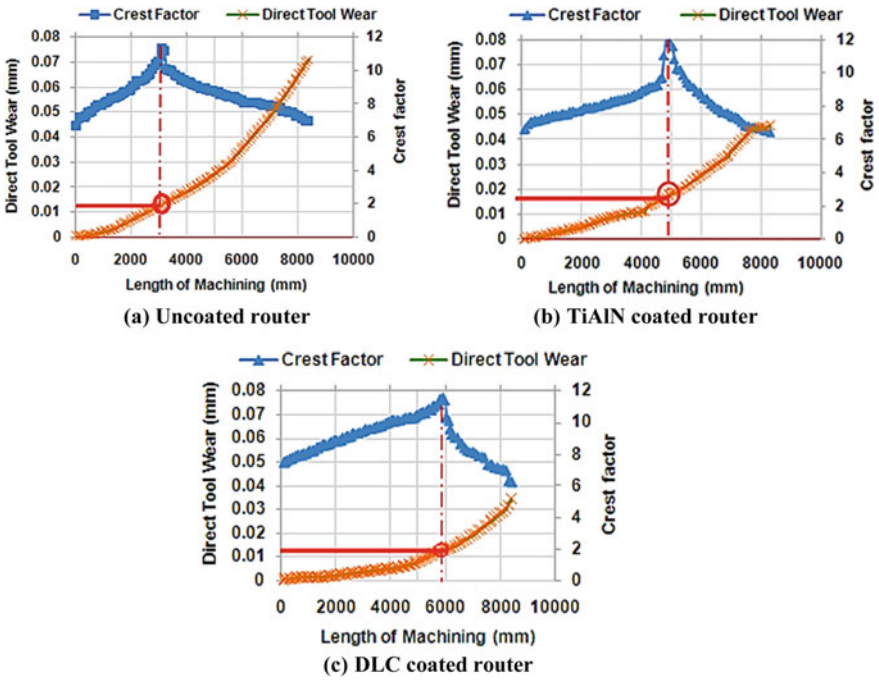

Fig. 14 **a–c** Tool wear monitoring for the three tools (Prakash [19])

in the AE signal crest factor and direct tool wear with the length of machining are presented in Fig. 14a–c.

It is understood that the value of the crest factor increases rapidly up to a certain length of machining, and then decreases rapidly with a further increase in cutting length. This decrease is possibly due to the rubbing of worn router flank with work material, resulting into low energy release. Further, a decrease in monitoring index beyond a certain value of wear could be due to dampening of the AE signals by the thermal influence associated with worn cutting edges in rubbing mode at higher tool wear condition. Corresponding to change in the trend of the monitoring index is a sudden increase in tool wear, which clearly indicates a threshold for limiting the usable router condition for trimming of CFRP composite (Velayudham [22]). Thus, from the graph, a control monitoring strategy can be determined at the point where the change in the curve of crest factor indicating that thereafter, the tool could be considered as a worn tool. Thus, the life of the three tools regarding machining length before regrinding/recoating can also be predicted. The tool life in terms of total machining length (in mm) for the three tools was determined from the graphs for all the three tools.

Table 9 shows the comparison of tool life for all tools and the DLC coated router tool provides a high total machining length with fewer surface damages on CFRP trimmed edges.

Table 9 Tool life (total machining length) for the three tools (Prakash [19])

Tool	Tool life in terms of total machining length in mm
Uncoated router tool	3150
TiAlN Coated router tool	4830
DLC Coated router tool	5880

Summary

- High-speed edge trimming with a low coefficient of friction DLC-coated router tool generated cutting tool temperature well below the glass transition temperature. Also, it was observed that there were no defects due to thermal degradation of resins with DLC-coated router tool.
- DLC-coated router tool trimmed the edges with a good surface finish of lower surface roughness value is achieved due to its better surface characteristics when compared to other two types of router tools.
- While considering the performance of the tool, the DLC-coated router tool performs well for the highest machining length of around 5.9 m which is about 46% increase in length of machining when compared to the value of uncoated router with relatively fewer surface damages. This significant increase in length of machining causes significant reduction in tooling cost which is an essential requirement in industry perception.
- Although TiAlN-coated router tool produced less tool wear and higher tool performance than uncoated router tool, TiAlN-coated router tool generated higher cutting forces at certain conditions when compared to uncoated tools because of the coating thickness which may reduce the cutting edge sharpness (i.e. increase the edge radius).
- Online tool condition monitoring using AE approach is found to be an appropriate technique for measuring the performance of cutting tools having high complex geometry such as router tools for machining polymer composites.

4 Cutting Tools for Machining Metal Matrix Composites

4.1 Introduction

Metal matrix composites (MMCs) offer high strength-to-weight ratio, high stiffness and better damage resistance over a wide range of operating conditions, making them an attractive option in replacing conventional materials for many engineering applications. Typically the metal matrix materials of MMCs are aluminum alloys, titanium alloys, copper alloys and magnesium alloys, while the reinforcement materials are silicon carbide, aluminium oxide, boron carbide, graphite etc. in the form of fibres, whiskers and particles [23].

MMCs are shown to cause excessive tool wear, which in turn induces such damage phenomena as fiber pullout, particle fracture, delamination and debonding at the fibre or particle and matrix interface. The parameters that are the major contributors to the machinability of these composites are the reinforcement type and orientation, tool type and geometry and the machining parameters. Although MMCs are generally processed near-net shape, subsequent machining operations are inevitable. On machining of MMCs it is obvious that the reinforcement material, type of reinforcement (particle or whisker), volume fraction of the reinforcement, and matrix properties as well as the distribution of these particles in the matrix are the factors that affect the overall machinability of these composites.

Machining Al/SiC composites is one of the major problems which resist its widespread engineering applications. Previous studies have shown that the tool wear is excessive, and the surface finish is poor when carbide tools are used. The SiC particles are much harder than the WC tool material that leads to a high wear rate by abrasion. The cutting edge is rapidly worn, and that results to poor surface finish. In addition, due to friction, high temperature and pressure, the Al/SiC composite work-material adheres to the cutting edge to form a built-up-edge (BUE) which also has a negative effect on surface finish [24].

This chapter deals with the cutting tool requirements for machining metal matrix composites. The tool materials normally available are ranging from high-speed steel to poly crystalline diamond including diamond coated tools. Improper tooling not only escalate the component cost, also induce subsurface damage of a MMC component. The hardness of matrix is the most significant characteristics which affects the machinability of MMC. Higher the matrix hardness shortens the tool life. The reinforcement hardness is also a dominant factor for tool wear. The coarser reinforcements and higher volume fractions largely influenced the tool performance and required cutting tools with high hardness.

4.2 Cutting Tools

The most commonly used tool material is polycrystalline diamond (PCD) [25], although cubic boron nitride (CBN), alumina, silicon nitride and tungsten carbide (WC) tooling are used as cutting materials. Cutting speed, feed and depth of cut in machining of particulate MMCs have a similar effect on tool life and surface finish to that of machining metals although some differences are noticeable due to the ceramic particles. The ceramic- reinforced particles tend to dislodge from the matrix and roll in front of the cutting tool, thereby plowing through the machined surface and generating grooves on it [26].

Hung et al. [27] reported that the cubic boron nitride (CBN) and poly-crystalline diamond (PCD) tools are better than a tungsten carbide (WC) tool in terms of wear resistance. The PCD tools can be used for the finishing operations resulting with minimum sub-surface damages, while a WC tool could be used economically for a roughing operation. The parameter, grain size of the cutting tool influences a major

role in deciding the tool life. The tool life of the large grain sized PCD tools are higher as they are not chipped off even at higher cutting conditions. The tool life can also be improved better by diamond coating of carbide tools with complex geometry. The PCD tools can be used effectively to machine MMCs in turning, milling, facing, drilling, boring, reaming, threading, tapping, and grinding.

The less expensive diamond-coated tools offer as a promising alternative to solid diamond tool, if adequate adhesion of the coating is guaranteed. PCD diamond tools are the most preferred, while carbide tools are preferred over ceramic tools [24]. While machining of these composites with carbide tooling, low-cutting speeds and high-feed rates are utilized to minimize tool wear. At higher cutting speeds, the carbide tool is subjected to catastrophic failure.

Tomac and Tonnessen [28] investigated the machinability of Al-SiC MMCs using PCD, chemical vapor deposition (CVD), and coated tungsten carbide tools and revealed that abrasive wear is the main mode of tool failure. The PCD tools had over 30 times higher tool life than carbides they used under similar cutting conditions. In addition, the CVD tools were better than other less hard cutting tools except PCD. While comparing the performance of chemical vapor deposition (CVD) coatings of TiN, TiCN and Al_2O_3, the inserts with TiN coating performed the best in maximizing the tool life. Tonshoff and Winkler [29] reported that the TiN coatings have shorter life and the PCD-coated tools showed good performance before the deterioration of the coating film. Compared to coated of PCD tools, PCD-tipped tools showed better results. To minimize the surface roughness and sub-surface damage PCD tools are preferred since the wear rate associated with them is the lowest among available tool materials. Although PCD tools are used for machining Al/SiC composites, the high cost associated with them limits their use [30].

Since abrasion is the primary source of tool wear at different feed rates, the recommendations are to use high feed rates and depths of cut during roughing operations. Several researchers have also indicated that polycrystalline diamond (PCD) tools are the only tool material that is capable of providing a useful tool life during the machining of particulate light metal MMCs. PCD is sufficiently harder than most of the ceramic reinforcements and has no chemical tendency to react with the workpiece material. Furthermore, PCD tools contain larger grain structures that withstand more abrasion wear by micro-cutting compared to tools with a smaller grain structure. El-Gallab and Sklad [31], studied the performance of PCD tools during turning MMCs. Grooves on the tool face along the chip flow direction were observed. The grooves on the rake face filled with smeared work material and formed a built-up edge, which seemed to be beneficial since it protected the tool rake from further abrasion.

Coelho et al. [32] continued their attempts by developing PCD tipped drill bits to drill MMC and presented a comparison among the results of different drill tests including the PCD drill bits and other tools such as HSS, diamond coated HSS, WC and TiN coated carbide tools. PCD-tipped drill bits perform the best under different cutting conditions among all the drill materials.

Varadarajan et al. [33] studied that polycrystalline boron nitride (PCBN) tools outperformed coated carbides in terms of tool wear and surface finish. Ding et al.

[34] studied the machinability characteristics with various PCBN and PCD tools. Compared to PCBN tools, the improved tool life was found when using PCD tools.

Diamond tools seem to be the best tool to machine Al/SiC MMCs with acceptable tool life [35]. Diamond is harder than SiC and does not have chemical tendency to react with work material. For cutting tools, diamond is mainly used in two forms: either brazed PCD or chemical vapor deposition (CVD). PCD tools consist of a thin layer of fine diamond particles sintered together and brazed onto a cemented carbide substrate. CVD diamond is a more recent super hard tool material; it consists of pure diamond coating over a carbide substrate. Compared to PCD, CVD diamond is harder, exhibits a lower-friction coefficient, higher abrasion resistance, higher-thermal conductivity and better chemical and thermal stability. Other drawbacks associated to PCD tools are the presence of cobalt binder, which limits the cutting speed and also costs higher [36]. The high thermal conductivity of CVD diamond tool allows heat dissipation and leads to a more uniform and a reduced level temperature distribution avoiding tool failure and limiting adhesive wear [37].

5 Cutting Tools for Machining Ceramic Matrix Composites

Advanced ceramic materials have been used increasing use in industrial applications because of their superior thermal, chemical, and wear-resistance characteristics of ceramics as compared to those of traditional materials. However, a primary obstacle to the use of ceramics for many applications is the high cost of machining these hard materials.

Diamond-cutting tools specifically, diamond-grit grinding wheels are needed in machining ceramics because of the high hardness of the materials. The high price of diamond grinding wheels the expense associated with using diamond materials and the costs of wheel conditioning (e.g., trueing and dressing) makes machining of ceramics difficult. Of all machining processes, grinding is unmatched for the most precision operations. The current requirement is that they should not only machine these ceramic materials but also produce a workpiece with precise dimensions and surface quality.

In the last three decades, an enormous interest in advanced ceramic materials has emerged. However, due to the high cost of ceramic machining, the use of ceramic components is not as enormous as the interest. Currently, diamond grinding accounts for more than 80% of the total ceramic machining [38] and remaining techniques for machining include ultrasonic machining (USM), electrical discharge machining (EDM), abrasive water jet machining (AWJ), laser machining (LM), laser-assisted machining (LAM), plasma-assisted machining, single-point machining, electron-beam and ion-beam machining, microwave machining, and combined machining. Some researchers (Ives et al. [39]) demonstrated that a ductile regime takes place on a localized scale when the grit penetration is limited to a small size, and in this ductile manner there is a decrease in the subsurface damage. But this ductile regime grinding requires low and precise feeds, very small grit depths, and extremely low

material removal rate. The single point turning operation for ceramic machining was also studied in laboratory. Kiso et al. [40] reported that turning with sintered polycrystalline diamond tool is a promising machining process for ZrO2, but not for Si3N4 because of short tool life. Researchers investigated that, in single-point turning, there is a critical-depth parameter which defines the transition from brittle to ductile behaviour in the machined workpiece surface, and in this ductile manner the sub-surface damage can be reduced [41–45].

6 Review Questions

(1) What are the important factors influencing machinability? And also discuss the significance of cutting tool parameters on machinability of Polymer matrix composites.
(2) List out the various damages introduced during machining of FRP. Also list the reasons for them.
(3) Discuss (i) the forces induced on a standard twist drill and (ii) the effect of forces to cause delamination during drilling of FRP.
(4) What are the important properties of tool material? And also discuss the effect of drill tool material on tool wear and quality of drilled holes.
(5) Describe the effect of typical tool materials and critical drilling parameters on PMC composites.
(6) Describe the effect of typical tool geometries and critical drilling parameters on PMC composites.
(7) Describe the effect of critical drilling parameters on machinability of PMC composites.
(8) What is edge trimming process? And discuss the various forces induced during this machining process.
(9) Discuss the various tool geometries of cutting tools used for edge trimming.
(10) Discuss the effect of tool geometries and cutting parameters on cutting forces, surface roughness and delamination caused during edge trimming operation.
(11) Describe the importance of online condition monitoring of cutting tool using acoustic emission technique.
(12) Discuss the effect of coatings (TiAlN and DLC) and cutting parameters on cutting forces, cutting temperature and surface roughness and tool wear caused during edge trimming operation.
(13) What is the crest factor in acoustic emission technique? And also discuss the significance of crest factor in determining the tool life in length of machining.
(14) Discuss the various tool requirements for machining metal matrix composites.
(15) What does ductile regime mean? And list the various machining processes used for machining ceramic matrix composites.

References

1. Konig, W., Cronjager, L., Spur, G., Tonshoff, H.K.: Machining of new materials. Ann. CIRP. **39**(2), 673–680 (1990)
2. Komanduri, R.: Machining of fiber-reinforced composites. Mech. Eng. **114**, 58–64 (1993)
3. Bhatnagar, N., Ramakrishnan, N., Naik, N.K., Komanduri, R.: On the machining of fiber reinforced plastic composite laminates. Int. J. Mach. Tools Manufact. **35**(5), 701–716 (1995)
4. Lubin, G.: Hand book of fiber glass and advanced plastic composites, Polym. Technol. Ser. (1969)
5. Arshinov, V., Alekseev, G.: Metal cutting theory and cutting tool design. MIR Publishers, Moscow (1976)
6. Zitoune, R., Collombet, F., Hernaiz Lopez, G.: Experimental and analytical study of the influence of HexFit® glass fiber composite manufacturing process on delamination during drilling. Int. J. Mach. Mach. Mater. **3**(3–4), 326–342 (2008)
7. Sakuma, K., Yakoo, Y., Seto, M.: Study on drilling of reinforced plastics (GFRP & CFRP)-Relation between tool material and wear behavior. Bull. JSME **27**(228), 1237–1244 (1984)
8. Davim, J.P., Reis, P.: Study of delamination in drilling carbon fiber reinforced plastics (CFPR) using design experiments. Comp. Str. **59**, 481–487 (2003)
9. Ramulu, M., Young, P., Kao, H.: Drilling of Graphite/Bismaleimide composite material. J. Matl. Engg. Perf. **8**(3), 330–338 (1999)
10. Ravishankar, S.R., Murthy, C.R.L.: Characteristics of AE signals obtained during drilling composite laminates. NDT&E Int. **33**, 341–348 (2000)
11. Khashaba, U.A.: Delamination in drilling GFR thermoset composites'. Comp. Struct. **63**(3), 313–327 (2004)
12. Seif, M.A., Khashaba, U.A., Rojas-Oviedo, R.: Measuring delamination in carbon/epoxy composites using a shadow moire laser based imaging technique. Comp. Str. **79**, 113–118 (2007)
13. Zitoune, R., Collombet, F.: Influence of machining quality on composite part manufacturing. In: Davim, J. P. (ed.) Drilling of Composite Materials, Series: Materials and Manufacturing Technology (2009)
14. Ramkumar, J., Aravindan, S., Malhotra, S.K., Krishnamurthy, R.: An enhancement of the machining performance of GFRP by oscillatory assisted drilling. Int. J. Ad. Manuf. Tech. **23**, 240–244 (2004)
15. Arul, S., Vijayaraghavan, L., Malhotra, S.K., Krishnamurthy, R.: Influence of tool material on dynamics of drilling of GFRP composites. Int. Jl. Adv Manuf Tech. **29**, 655–662 (2006)
16. Velayudham, A., Krishnamurthy, R.: Effect of point geometry and their influence on thrust and delamination in drilling of polymeric composites. Jl. of Mat. Proc. Tech. **185**, 204–209 (2007)
17. Enemuoh, U.E., Sherif, E.L., Gizawy, A., Okafor, C.A.: An approach for development of damage free drilling of carbon fiber reinforced thermosets. Intl. J. Machine Tools and Mfr. **41**, 1795–1814 (2001)
18. Prakash, R., Krishnaraj, V., Zitoune, R., Sheikh-Ahmad, J.: High-speed edge trimming of CFRP and online monitoring of performance of router tools using acoustic emission. Materials **9**(10), 798 (2016)
19. Prakash, R., Krishnaraj, V., Sheikh-Ahmad, J.: High-speed edge trimming of carbon fiber-reinforced polymer composites using coated router tools. J. Compos. Mater. **53**(28–30), 4189–4202 (2019)
20. Sheikh-Ahmad, Jamal: Machining of Polymer Composites. Springer Publications, New York (2009)
21. Faraz, Ali., Biermann, Dirk, Weinert, Klaus: Cutting edge rounding; an innovative tool wear criterion in drilling CFRP composite laminates. Mach. Tools Manuf. **49**, 1185–1190 (2009)
22. Velayudham, A., Krishnamurthy, R., Soundarapandian, T.: Acoustic emission based drill condition monitoring during drilling of glass/phenolic polymeric composite using wavelet packet transform. Mater. Sci. Eng., A **412**, 141–145 (2005)

23. Paulo Davim, J.: Machining of Metal Matrix composites, Springer Publications, 2011
24. Manna, A., Bhattacharayya, B.: A study on machinability of Al/SiC metal-matrix composites. J. Mater. Process. Technol. **140**, 711–716 (2003)
25. Weinert, K., König, W.: A consideration of tool wear mechanism when machining Metal Matrix Composites (MMC). Ann. CIRP **42**(1), 95–98 (1993)
26. El-Gallab, M., Sklad, M.: Machining of Al/SiC particulate metal matrix composites. Part II: Workpiece surface integrity, J Mater Process Tech **83**(1–3), 277–285 (1998)
27. Hung, N.P., Venkatesh, V.C., Loh, N.L.: Cutting tools for metal matrix composites, Key Engineering Materials, Trans Tech Publications, Switzerland, 138–140, 289–326 (1998)
28. Tomac, N., Tannessen, K., Rasch, F.O.: Machinability of particulate aluminium matrix composites. Ann. CIRP **41**(1), 55–58 (1992)
29. Tonshoff, H.K., Winkler, J.: The influence of tool coatings in machining of magnesium. Surf. Coat. Tech. **94–95**, 610 (1997)
30. Ding, X., Liew, W.Y.H., Liu, X.D.: Evaluation of machining performance of MMC with PCBN and PCD tools. Wear **259**(7–12), 1225–1234 (2005)
31. El-Gallab, M., Sklad, M.: Machining of Al/SiC particulate metal-matrix composites.Part I: tool performance. J. Mater. Process. Tech. **83**(1–3), 151–158 (1998)
32. Coelho, R.T., Aspinwall, D.K., Wise, M.L.H.: Drilling and reaming aluminium-based Metal Matrix Composites (MMC) using PCD tooling. Trans NAMRI/SME (1994)
33. Varadarajan, Y.S., Vijayaraghavan, L., Krishnamurthy, R.: The machinability characteristics of aluminosilicate fiber reinforced Al alloy composite. Mater. Manuf. Process. **17**, 811–824 (2002)
34. Ding, X., Liew, W.Y.H., Liu, D.: Evaluation of machining performance of MMC with PCBN and PCD tools. Wear **259**(7–12), 1225 (2005)
35. Chambers, A.R.: The machinability of light alloy MMCs. Compos. Part A **27A**, 143–147 (1996)
36. Cappelli, E., Pinzari, F., Ascarelli, P., Righini, G.: Diamond nucleation and growth on different cutting tool materials: influence of substrate pre-treatments. Diamond Relat Mater **5**, 292–296 (1996)
37. Durante, S., Rutteli, G., Rabezzana, F.: Aluminium based MMC machining with diamond coated cutting tools. Surf. Coat. Technol. **94–95**, 632–640 (1997)
38. Allor, R.L., Jahanmir, S.: Current problems and future directions for ceramic machining. Am. Ceram. Soc. Bull. **75**(7), 40–43 (1996)
39. Ives, I.K., Evans, C.J., Jahanmir, S., Polvani, R.S., Strakna, T.J., Mcglauflin, M.L.: Effect of ductile-regime grinding on the strength of hot-isostatically-pressed silicon nitride. NIST Spec. Publ. **847**, 341–352 (1993)
40. Kiso, H., Taguchi, T., Fukuhara, M., Kimura, T.: Machining of advanced ceramics by turning with sintered polycrystalline diamond tool. Bull. Jpn. Soc. Precis. Eng. **21**(2), 142–143 (1987)
41. Strenkowski, J.S., Hiatt, G.D.: Technique for predicting the ductile regime in single point diamond turning of brittle materials. Am. Soc. Mech. Eng. Prod. Eng. Div. (Publication) PED. Fundam. Issues Mach. **43**, 67–80 (1990)
42. Blackley, W.S., Scattergood, R.O.: Ductile-regime machining model for diamond turning of brittle materials. Precis. Eng. **13**(2), 95–103 (1991)
43. Zhao, Y., Dong, S., Li, Z., Wang, H.: Diamond turning model in brittle-ductile transition of brittle materials. WeixiJiagongJishu/Micro Fabrication Technol. **4**, 70–76 (1998)
44. Beltrao, P.A., Gee, A.E., Corbett, J., Whatmore, R.W., Goat, C.A., Impey, S.A.: Single point diamond turning of ferroelectric materials. Ferroelectrics **228**(1–4), 229–239 (1999)
45. Ajjarapu, S.K., Fesperman, R.R., Patten, J.A., Cherukuri, H.P.: Experimental and numerical investigation of ductile regime machining of silicon nitride. AIP Conf. Proc. **712**, 1377–1383 (2004)

Health and Safety Considerations in Machining of Composites

Mamidala Ramulu and Mohammad Sayem Bin Abdullah

Abstract Machining of composite creates dust particles that can enter the human respiratory system and reach the bloodstream. Several toxicology studies depict the harmful effect of composite dust on animals. This chapter briefly reviews the detrimental impacts of composite dust, exposure limit of dust, and methods to collect and control dust generation. The relationship of machining parameters to dust formation is discussed based on the limited existing literature. A safe dust collection and real-time dust analysis system based on the isokinetic sampling technique is illustrated in this chapter.

1 Introduction

The advantages of composite materials, such as high specific strength, low thermal expansion, superior corrosion resistance, and flexibility in design, have led to their extensive application in aerospace, marine, automobile, and sports industries [1]. The applications of composite materials require subsequent machining processes (trimming, milling, drilling, etc.) to provide net shape of designed parts and part assembly. However, the machining of fiber-reinforced composite (i.e., CFRP, GFRP) creates dust. The dust generation during FRP machining poses health and environmental hazards. The morphology and concentration of these dust particles determine the severity of potential health and environmental hazard. Although some toxicological studies have depicted the potential health hazard associated with composite machining, only a few efforts have been given on understanding the dust generation in composite machining and its possible remedies. This chapter briefly reviews the dust generation in composite machining, discusses dust formation in relation to machining parameters, and describes methods of dust collection and analysis.

M. Ramulu (✉) · M. S. B. Abdullah
Department of Mechanical Engineering, University of Washington, Seattle, WA 98195, USA
e-mail: ramulum@uw.edu

M. S. B. Abdullah
e-mail: sayemab@uw.edu

I. Shyha and D. Huo (eds.), *Advances in Machining of Composite Materials*,
Engineering Materials, https://doi.org/10.1007/978-3-030-71438-3_19

2 Dust Generation in Composite Machining and Health Issues

Dust generated during machining of composites can adversely affect human health. Exposure to the skin, inhalation, ingestion of broken fibers, and fine particles may lead to health complications. A few toxicology studies conducted on rabbits and rats confirm adverse effects on the lungs in the presence of composite dust [2–7].

Rats exposed to chopped carbon fibers for 16 weeks (30 h/week) showed a slight decrease in body weight and experienced a slower respiratory rate during the first four weeks [2]. However, no consistent effect on lung function was reported. The size (20–60 μm) and diameter (7 μm) of the examined fibers (20 mg/m^3) did not cause any other systematic toxicity except the variable respiratory rate. In another study, Pitch based CFRP aerosol (diameter: 1–2 μm, concentration: 47 or 106 mg/m^3) caused transient inflammatory responses in the lungs of rats when exposed [3]. However, carbon fiber induced inflammatory effects reversed within ten days after exposure.

In a series of studies on machining various composites [4–7], fiber-epoxy dust caused a definitive histopathologic response in the rat lung after an intratracheal dose. While composite dust at the tool face ranged from 7 to 11 μm in width, a fair amount of particles ranged from 0.8 to 2 μm with a small fraction of less than 0.2 μm [4]. The histopathologic response and dust particle size indicate the possibility of composite dust to be fibro-genic in humans [5]. Both the PAN (polyacrylonitrile) and pitch based graphite/epoxy may cause biologic effects in the human lung as the dust affects rat's lung. Cured composite dust may pose a greater threat than nuisance dust [6]. Bourcier [7] recommended developing local exhaust systems to effectively remove dust and establish the relationship between total and respirable dust loadings for various composite processing operations. Another potential health hazard associated with composite machining is skin exposure. Skin exposure to carbon fiber and glass fiber has been reported to cause dermatitis, rashes, skin, and nose irritation [8–10]. However, the skin may become desensitized if exposed continuously [8]. However, rashes developed in human skin due to carbon fiber dust exposure may disappear after a few months of removal from the exposure [9]. Unlike carbon and glass fiber, few fibers, i.e. Kevlar, showed no potential for skin sensitization and harmful skin irritation except mild skin irritation by mechanical abrasion [8, 10].

3 Exposure Limit and Distribution of Dust Particles

Dust particles generated in composite machining are of different sizes and concentrations. Kwan [11] determined the aerodynamic size distribution of dust from machining (milling, drilling, and grinding) of CFRP. Most of the particles from machining operations have an aerodynamic diameter between 5 and 10 μm. These are non-respirable and deposited in the nasopharynx region. Additionally, dust particles larger than 10 μm aerodynamic diameter can trap in the nasal cavity. On the

other hand, particles of 2–5 μm in aerodynamic diameter could reach the trachea and the terminal bronchi. Whereas particles less than 2 μm in aerodynamic diameter can reach the alveoli and particles less than 1 μm may easily enter the blood stream via ciliary interchange [10].

Several agencies have set exposure limits regarding dust size and concentration to reduce the risk of composite dust inhalation. Occupational Safety & Health Administration (OSHA) defines respirable dust as those dust particles that are small enough to penetrate the nose and upper respiratory system and deep into the lungs. National Institute for Occupational Safety and Health (NIOSH) considers fibers with less than 3.5 μm diameters small enough to be respirable [12]. The Mine Health and Safety Administration (MHSA) considers dust of less than 5 μm of aerodynamic diameter as respirable [13]. According to MHSA, 25% and 90% of total dust are respirable if their aerodynamic diameters are respectively equal or less than 5 μm and 2 μm. In terms of mass concentration, the OSHA limit for respirable and total dust at the source are respectively 5 mg/m^3 and 15 mg/m^3 [13]. Miller [13, 14], Iyer [10], Haddad et al. [15] Nguyen-Dinh et al. [16] reported dust particles of less than 1.5 μm in size and higher dust concentration than OSHA limit. Table 1 presents a survey of dust particle distribution from recent composite machining experiments.

4 Dust in Relation to Machining Processes and Parameters

The amount of dust created during machining is dependent on the nature of the machining process [4–6, 11], speed, feed [10, 15, 16], tool geometry [16–18], cutting tool material [15, 16, 18], fiber orientation, and work-piece [13, 19]. The drilling operation produces lower concentrations of dust than milling or routing, while higher than grinding and sanding [4, 7, 11]. According to a CFRP machining study by Kwan

Table 1 Dust size and concentration reported in CFRP machining

Process	Speed, feed, depth of cut, materials	Size and/or concentration
Haddad et al. (2014) [15] Nguyen Dinh et al. (2020) [16]	Speed: 150, 250, 350, 700, 1400 m/min; Feed rate: 125, 250, 500, 1000, 1500 mm/min; DOC: 2 mm Speed: 150, 250 m/min; Feed: 500, 1000, 1500 mm/min; DOC: 2, 3 mm Work-piece: CFRP	As low as 0.25 μm Large quantity < 1.5 microns Concentration > 5 mg/m^3 (OHSA limit) Concentration ~ OHSA Limit at Speed: 150 m/min, Feed Speed: 1500 mm/min (for burr tool)
Miller (2014) [13] Iyer (2016) [10]	Spindle Speed: 1000, 3000, 6000 RPM m/min; Feed rate: 127, 381, 635 mm/min; DOC: 2.54, 3.81, 6.35 mm Work-piece: CFRP, HExMC	Aerodynamic diameter: as low as 0.12 μm [13], 0.19 μm [10] (CFRP) Large quantity < 1 microns Total dust: 50 mg/m^3 > limit Respirable dust: 30 mg/m^3 > limit

[11], 9.3% dust in drilling and 28.7% dust in milling can potentially reach the trachea and the terminal bronchi. Meanwhile, 2.5% of drilling dust and 20% of milling dust have aerodynamic diameter less than 2 μm, which can reach alveoli. The weight percentage of the non-respirable dust are ranged from 51% in milling and 88% in drilling.

Both speed and feed also influence the size and amount of dust. In CFRP trimming, multiple studies reported the presence of dust less than theoretical chip thickness [15, 16]. Dust particles count in CFRP trimming increases with increasing cutting speed; however, it decreases with increasing feed [10, 16]. For a constant feed and depth of cut combination, higher spindle speed creates more contact with the work-piece, which eventually produces more dust. The dust increases 2–8 times in high-speed cutting. In contrast, higher feed produces a lower count of smaller dust due to coarse cut. However,the feed rate comparatively appears to have less effect on the amount of dust particles [13, 15]. An increase in depth of cut increases dust particle counts due to higher contact with the work-piece [10]. Overall, the combination of higher feed speed, lower cutting speed, and lower depth of cut generates chips in the form of fiber-matrix chunk and reduces the count of harmful particles in machining processes [10, 16].

The tool geometry, tool material, and cutting edge geometry also influence dust generation in composite machining due to differences in chip formation mechanism [15–17, 19]. A 4-flute diamond-coated tool generated more dust than the tungsten carbide burr tool and diamond coated burr tool in CFRP trimming [15]. The effect of coating on dust generation is minimal [15]. Nguyen-Dinh et al. [16] studied the effects of helix angle, grooves of cutting edge, and tool wear on harmful composite particles. The presence of helix on the cutting tool decreases dust generation at different conditions as a straight flute tool poses higher radial force [16]. The higher radial force causes tool vibration. The tool vibration combined with engaged straight cutting edge obstructs the evacuation of larger fiber–matrix chips and disintegrate them into smaller dust. Meanwhile, the presence of grooves on the cutting edge reduces the dust dispersion due to dust adherence in the cavity. Tool wear also reduces the amount of dust as it alters the chip formation. Worn cutting edges create larger and heavier chips that may fall on the machining table. Klocke et al. reported more aerosol dust for PCD tools than carbide tools during milling of composite [18]. The PCD tool also produces better surface finish as it produces smaller chips, thus creates more dust. Hence, the dust concentration can be shifted towards coarser from fine dusts by changing tool material and tool geometry. However, the effect on surface integrity still needs to be validated.

The dust formation is influenced by fiber orientation and work-piece material as well. The size of the chips also varies depending on fiber orientation [19]. Miller [13] reported the highest and the lowest mass concentration of dust respectively for 0° and 90° fiber. At least 50% of the particles have an aerodynamic diameter less than 0.12 μm, 0.31 μm, 0.21 μm, and 0.35 μm respectively for milled 0°, 45°, 90°, 135° fibers. Long fibers of diameter less than 1 μm have been identified for 0°, 90° fibers. The dust generation also depends on work-piece material. Iyer reported a larger count of particles capable of reaching alveoli for milling CFRP than milling

HexMC material [10]. In conclusion, the optimization of process parameters may reduce composite dust while sacrificing the least roughness.

5 Dust Collection and Characterization Techniques

For effective dust removal from the machining environment, few scholars and NIOSH recommended developing a local exhaust system in dry machining of composite or flood coolant as an alternative to reduce dust levels [4, 7, 11]. However, very few studies have shown the efforts to develop and demonstrate a safe method to investigate and characterize dust particles emitted in composite machining. The few studies on CFRP machining induced dust collection includes Miller [13, 14] and Iyer [10] on milling and trimming, and Hagino et al. [17] on drilling. Miller developed a fully functional dust collection (Fig. 1) for milling of CFRP, where they utilized an isokinetic sampling tower with real-time instrumentation. A dust enclosure made of flexible box and membrane surrounds the work-piece and tool holder. A blower and HEPA filer are installed on one side of the dust enclosure. A vacuum and an isokinetic sampling tower are installed on the other side. During the machining process, the active blower takes composite chips into a flexible anti-static conductive vacuum hose, attached to the tool holder. The other vacuum pulls the chips and dust through an isokinetic sampling tower. The isokinetic sampling tower consists of real-time instrumentations- isokinetic nozzle, cascade impactor, pump, and pressure gauge. The impactor separates particles larger than a certain aerodynamic size due to substantial inertial difference. Eventually, the smaller particles pass through the impactor.

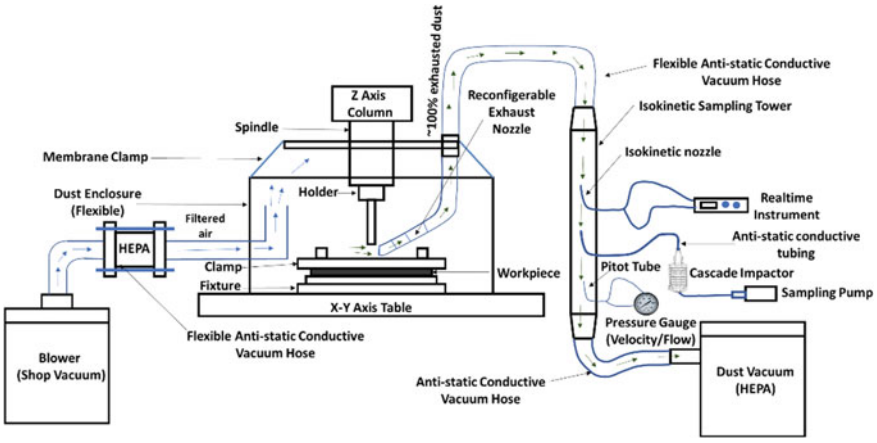

Fig. 1 Dust collection and analysis based on isokinetic smapling for composite machining [13]

The impactor is disassembled and cleaned thoroughly before each dust collection. A Teflon membrane installed at stage-10 of the impactor collects the particles for SEM/toxicology analysis. The air velocity in the isokinetic ducts is measured using a combination of pitot tubes and magnehelics. Rotameters ensure controlled airflow to the cascade impactors and real-time sampling instruments. An Ultrafine Particle Counter (UPC) measures the real-time concentrations of ultrafine particles (0.02–1 μm) up to 500,000 particles/cm^3. Particles ranging from 0.3 to 20 μm are characterized in real-time by Optical and Condensational Particle Counters (OPCs). An aerosol monitor, gravimetrically calibrated according to NIST traceable (SAE) fine dust standard, measures real-time mass concentrations of dust up 400 mg/m^3. A microdust detector, Microdust Pro, detects airborne dust up to 2500 mg/m^3. It is placed in the sampling tower using a nozzle.

The GRIMM 1.109 Portable Aerosol Spectrometer is used for particle analysis, which can measure 0.25 μm to 32 μm sized particles. Particles are collected on a PTFE filter both for gravimetric calibration and further analysis. Scattered light photometry inside an optical measuring cell detects each particle in the aerosol individually. The scattered light impulse of each particle is counted based on the intensity of the scattered light signal attributed to particle size. The aerosol spectrometer collects the particle size distribution of solid aerosol particles in many size classes. Real-time data is captured using the GRIMM 1178 LabVIEW software. Detail of all the instruments is available in the following studies, Miller [13, 14] and Iyer [10].

This dust collection technique is validated through rigorous experimentation and received a patent. This technique provides a controlled environment for dust collection and analysis. Hence, isokinetic sampling could be used to analyze dust particles generated from machining operations in a safe and self-contained environment. Miller [13] reported consistent patterns among the dust and cutting conditions. Short test cuts followed by this real-time instrumentation technique is an effective method to analyze dust particles and evaluate cutting conditions for extensive experimentation. The author recommended developing a rating system to describe and quantify the dust produced from dry cutting for material, tool, and cutting condition combinations.

Hagino et al. [17] developed an inside suction technique to collect dust in CFRP drilling. They designed hollow-type drill bits that have holes in the center. The suction line was extended up to the drill bits and the tool holder. Both the drill bit and tool holder were kept inside the suction line. The dust collector could collect 50% to 75% of chips through the suction line during the drilling process. Denkena et al. conducted a numerical [20] and an experimental [21] study on an energy-efficient dust collection for milling CFRP. In their system, an exhaust hood was coupled with a dust sensor and a force sensor cutting tool. Local dust extraction systems may require less energy for suction purposes than the central extraction system, which also improves the dust collection rate. The extraction starts when the dust sensor reading exceeds the regulatory limit during the cutting processes. However, none of the studies discussed controlled dust collection and analysis techniques.

6 Hazard Mitigation Approaches

Hazard mitigation requires both engineering controls and workplace administrative controls to eliminate and minimize exposure to dust and fumes [22, 23]. Engineering controls include proper interventions to remove hazards (dust and fumes) from the machining/working environment, ensuring controlled ventilation, air cleaning, and maintenance of the equipment. On tool extraction system, i.e., dust and fume collector is an effective engineering control. However, the extraction system may vary in design depending on the machining process. Respiratory protection may not be necessary if the extraction system works perfectly. The average dust concentration should be monitored and kept below the permissible exposure limit, 15 mg/m^3. The machining parameters and cutting tools should be optimized to produce a minimal amount of dust while maintaining considerable roughness.

Administrative controls consist of policies, requirements, and practices to promote safety in the workplace. Administrative controls are intended to minimize exposure to hazards. Administrative control includes- authorised training of workers, rotation of workers, proper review and handling of Material Safety Data Sheet (MSDS), restrictive access to hazardous materials, using appropriate signs and safety instructions, ensuring personal and industrial hygiene practice. Administrative control is dependent on the knowledge and work practice of users. It is an additional tool for a better workplace once the engineering control is established.

Additionally, personal protective equipment (PPE), i.e. gloves, goggles, and protective clothing, ear protection, must be used if engineering controls are too expensive or impractical. PPEs are selected according to health authority regulations. Dust particles from composite machining are also harmful to the machine and relevant equipment. Therefore, protocols are needed to maintain the machine and other equipment.

7 Summary

Machining of composite generates dust particles capable of reaching different parts of the human respiratory system. The dust particles of less than 5 μm in aerodynamic diameter are repairable, while particles less than 2–3 μm can reach the alveoli and subsequently into the bloodstream. Toxicology studies show the adverse effect of respirable composite dust on experimental animals. Dust generated from composite (i.e. CFRP) machining often goes beyond the exposure limit and may affect human health. Thus, dust produced in composite machining requires monitoring and proper control through a fully functional dust collection technique. A few methods of dust collection techniques have been briefly presented in this chapter. Isokinetic sampling technique can be a useful tool to analyze dust particles in real-time and evaluate a cutting process before extensive experimentation. Dust size and concentration are

strongly related to process parameters, such as speed, feed, depth of cut, tool geometry, tool material, and fiber orientation. An optimum selection of process parameters can lead to controllable dust size and concentration in composite machining. However, the balance between dust reduction and higher roughness requires further scientific investigations. Additional investigations are needed to develop a rating system to quantify the dust from composite machining for a specific material, tool, and cutting conditions.

8 Review Questions

(1) What is the dust exposure limit in terms of size and concentration?
(2) How does process parameters affect dust generation?
(3) What is an isokinetic sampling system?
(4) How does isokinetic sampling work?
(5) What are the future research scopes related to health and safety considerations when machining composites?

References

1. Che, D., Saxena, I., Han, P., Guo, P., Ehmann, K.F.: Machining of carbon fiber reinforced plastics/polymers: a literature review. J. Manuf. Sci. Eng. **136**, (2014). https://doi.org/10.1115/1.4026526
2. Owen, P., Glaister, J., Ballantyne, B., Clary, J.: Subchronic inhalation toxicology of carbon fibers. J. Occup. Med. Off. Publ. Ind. Med. Assoc. **28**, 373–376 (1986)
3. Warheit, D.B., Kellar, K.A., Hartsky, M.A.: Pulmonary cellular effects in rats following aerosol exposures to ultrafine Kevlar aramid fibrils: Evidence for biodegradability of inhaled fibrils. Toxicol. Appl. Pharmacol. **116**, 225–239 (1992). https://doi.org/10.1016/0041-008X(92)90302-9
4. Boatman, E.S., Covert, D., Kalman, D., Luchtel, D., Omenn, G.S.: Physical, morphological, and chemical studies of dusts derived from the machining of composite-epoxy materials. Environ. Res. **45**, 242–255 (1988). https://doi.org/10.1016/S0013-9351(88)80050-1
5. Luchtel, D.L., Martin, T.R., Boatman, E.S.: Response of the rat lung to respirable fractions of composite fiber-epoxy dusts. Environ. Res. **448**, 57–69 (1989). https://doi.org/10.1016/S0013-9351(89)80085-4
6. Martin, T.R., Meyer, S.W., Luchtel, D.R.: An evaluation of the toxicity of carbon fiber composites for lung cells in vitro and in vivo. Environ. Res. **49**, 246–261 (1989). https://doi.org/10.1016/S0013-9351(89)80070-2
7. Bourcier, D.R.: Exposure evaluation of composite materials with emphasis on cured composite dust. Ph.D. Thesis. University of Washington (1989)
8. Ramulu, M., Kramlich, J.: Machining of fiber reinforced composites: review of environmental and health effects. Int. J. Environ. Conscious. Des. Manuf. **11**, 19 (2003)
9. Eedy, D.J.: Carbon-Fibre-Induced Airborne Irritant Contact Dermatitis. Contact Dermatitis **35**, 362–363 (1996)
10. Iyer, A.K.: Characterization of composite dust generated during milling of uni-directional and random fiber composites. MS Thesis. University of Washington (2015)

11. Kwan, J.K.: Health hazard evaluation of the postcuring phase of graphite composite operations at the Lawrence Livermore National Laboratory, Livermore. California, United States (1990)
12. Burr, G.A.: Health hazard evaluation (1994) Report No. 89-0001, NIOSH, HETA 1989-0001-2436,General Electric Corporation, Evendale, OH
13. Miller, J.L.: Investigation of machinability and dust emissions in edge trimming of laminated carbon fiber composites. Ph.D. Thesis. University of Washington (2014)
14. Miller, J.l.: Methods and systems for particle collection and analysis. US Patent 9726578 B2 (2017)
15. Haddad, M., Zitoune, R., Eyma, F., Castanie, B.: Study of the surface defects and dust generated during trimming of CFRP: influence of tool geometry, machining parameters and cutting speed range. Compos. Part. Appl. Sci. Manuf. **66**, 142–154 (2014). https://doi.org/10.1016/j.compositesa.2014.07.005
16. Nguyen-Dinh, N., Hejjaji, A., Zitoune, R., Bouvet, C., Salem, M.: New tool for reduction of harmful particulate dispersion and to improve machining quality when trimming carbon/epoxy composites. Compos. Part. Appl. Sci. Manuf. **131**, (2020). https://doi.org/10.1016/j.compositesa.2020.105806
17. Hagino, M., Inoue, T., Mizoguchi, M., Aoki, W., Matsumoto, F.: Department of mechanical engineering, national institute of technology, et al. Dust collection validity and effect of hole shape accuracy of CFRP with developed hollow-type drill and dust collector. Int. J. Autom. Technol. 10:324–33 (2016). https://doi.org/10.20965/ijat.2016.p0324
18. Klocke, F., Koenig, W., Dietz, C.: Environmental effects and safety in machining fibrous composites. Mach. Ceram. Compos. 1st edn. CRC Press, pp 411–25 (1999)
19. Arola, D., Ramulu, M., Wang, D.H.: Chip formation in orthogonal trimming of graphite/epoxy composite. Compos. Part. Appl. Sci. Manuf. **27**, 121–133 (1996). https://doi.org/10.1016/1359-835X(95)00013-R
20. Denkena, B., Dittrich, M.-A., Rahner, B.-H.: Smart and energy-efficient dust suction concept for milling of fibre-reinforced plastics. Prod. Eng. **11**, 723–729 (2017). https://doi.org/10.1007/s11740-017-0776-x
21. Denkena, B., Bergmann, B., Rahner, B.-H.: Energy-efficient control of dust extraction for the machining of fibre-reinforced plastics. Proc. CIRP **78**, 49–54 (2018). https://doi.org/10.1016/j.procir.2018.08.178
22. Asmatulu, E., Alonayni, A., Alamir, M.: Safety concerns in composite manufacturing and machining. In: Naguib, H.E. (ed.). Behav. Mech. Multifunct. Mater. Compos. XII, Denver, United States: SPIE, p. 68 (2018) https://doi.org/10.1117/12.2296707
23. Ahmad, J.: Health and safety aspects in machining FRPs. In: Ahmad, J. (ed.). Mach. Polym. Compos., Springer, Boston, MA, US, pp. 293–307 (2009). https://doi.org/10.1007/978-0-387-68619-6_7

Recycling of Composite Materials

Norshah Aizat Shuaib, Al Amin Mohamed Sultan, Sikiru Oluwarotimi Ismail, Abdullah Abdul Samat, Nur'ain Wahidah Ya Omar, Azwan Iskandar Azmi, and Paul Tarisai Mativenga

Abstract Usage of composite material is rising across various sectors such as automotive, wind energy and aerospace. Compared to metal matrix composites (MMCs) and ceramic matrix composites (CMCs), thermoset based polymer matrix composites (PMCs) dominate the market. The heterogeneous nature of composite materials and cross-linked nature of the thermoset matrix make recycling to be difficult. Research and development in recycling such material is required. In this chapter, composite recycling techniques are explained and reviewed from the aspect of energy consumption and mechanical properties of the recyclate. Possible reuse applications are suggested. This chapter highlights the concept of composite material sustainability and circular economy.

N. A. Shuaib (✉) · A. A. Samat · N. W. Y. Omar · A. I. Azmi
Faculty of Mechanical Engineering Technology, Universiti Malaysia Perlis, Pauh Putra Campus, 02600 Arau, Perlis, Malaysia
e-mail: norshahaizat@unimap.edu.my

A. A. M. Sultan
Faculty of Manufacturing Engineering, Universiti Teknikal Malaysia Melaka, Hang Tuah Jaya, 76100 Melaka, Malaysia

S. O. Ismail
Centre for Engineering Research, Department of Engineering, School of Physics, Engineering and Computer Science, University of Hertfordshire, AL10 9AB England, UK

A. A. Samat
Centre of Excellence for Unmanned Aerial Systems, Universiti Malaysia Perlis, 01000 Kangar, Perlis, Malaysia

P. T. Mativenga
School of Mechanical, Aerospace and Civil Engineering, The University of Manchester, Manchester, England M13 9PL, United Kingdom

I. Shyha and D. Huo (eds.), *Advances in Machining of Composite Materials*, Engineering Materials, https://doi.org/10.1007/978-3-030-71438-3_20

1 Introduction

A composite material can be defined as a combination of matrix and reinforcement, resulting in a material with superior properties. The reinforcement mainly used to increase strength and stiffness. The matrix sustains the reinforcement in the designed orientation. Three composite types—polymer-matrix composite (PMC), metal-matrix composite (MMC), and ceramic-matrix composite (CMC)—are in demand of various sectors. Composites could also be classified based on reinforcement such as particulate composites, fibre-reinforced composites, and structural composites. Of these, thermoset composites like carbon fibre reinforced polymers (CFRPs) and glass fibre reinforced polymers (GFRPs) dominated the markets [1]. In the UK, the composite market is well segmented where three main players dominate 81%: aerospace (36%), wind energy (33%), and automotive (12%). Both marine and industrial have 7% respectively, sports (2%), and others (3%). [1, 2].

Composite materials are rapidly gaining popularity and usage due to their combined lightweight, stiffness, and strength features. Although it is difficult to find absolute statistics on the total global composite production, the composites market projected to grow from £55 billion in 2016 to £87.47 billion by 2022 [3]. The first large-scale commercial applications of composite materials began in the military sector during World War II and in the late 1940s and early 1950s. Since then, global use of composite materials has proliferated from 158,800 tonnes in 1960 to 6.1 million tonnes in 2004, representing a 3,800% growth in the last 45 years [4].

Between all types of composite material, PMCs dominate the market with thermoset based products account for more than two-thirds [1]. On account of this, most recycling technologies focused on the recovery of PMCs compared to MMCs and CMCs. It is estimated that around five to 10 million tonnes of GFRP are produced globally every year with the demand for CFRP forecasted at approximately 157,000 tonnes annually. The high demand leads to the issue of scrap waste during production [5]. The MMCs and CMCs have a lower need in terms of volume compared to PMCs. This situation leads to the limited availability of the MMCs and CMCs composites scrap for recycling [1]. Apart from manufacturing waste, end of life waste becomes significant to the product end of service stage.

The heterogeneous nature of composite causes recycling of material to be highly challenging. As opposed to thermoplastic polymers, the thermoset polymers have difficulties in recycling due to its cross-linked nature. This is the reason research and development in recycling technologies focus on the recovery of thermoset based products.

The condition of rising composite waste is difficult due to the limited availability of waste processing centres. Recycling technology is still relatively new and progressing with recyclates hardly finding application in the market. Individual businesses that assume responsibility for their waste, often confronted with the issues of economics scale and transportation costs. Based on literature, most studies within the area of composite recycling focused on reuse applications and the strength of recycled fibre only. The aspect of environmental impact is rarely considered.

This chapter explains the availability of composite recycling methods from the aspect of process details, energy demand, and recyclate mechanical properties. The focus is on PMCs, particularly on GFRP and CFRP as these composites dominate the current market in terms of volume. Limited studies on PMCs and MMCs reviewed in this chapter. The strength of recyclate and new composite product also being discussed and compared between the different methods. Possible reuse applications thus suggested. This chapter seeks to simultaneously analyses composite recycling initiatives from the aspect of feasibility, environmental, and economic aspects. The study will be a vital decision-making tool regarding composite material sustainability in the future.

2 Composite Waste

The increasing demand for composites has balanced effects on the generated wastes, both nationally and internationally. Halliwell [6] pointed out that only 0.08% of composite waste collected in Europe; a situation indicative of issues with a collection scheme may not be well-designed or is affected by challenges in the waste post-treatment. There are two types of waste mainly associated with product output: manufacturing waste [7, 8] and end-of-life waste [6, 9]. CFRP represents about 40% of the UK composite production by value but corresponds to only 2% of the volume since the vast majority is GFRP [7, 10]. Numerous research has recently been conducted on CFRP recycling due to the cost differentials compared to virgin carbon fibres as well as the value of CFRP being ten times higher than GFRP [10].

The price for virgin GFRP and CFRP is in the range of £15.30–21.60 and £23.50–26.10 per kg, respectively [11]. The Boeing company estimates the cost of manufacturing virgin CFRP to be in the range of £22 to £44 per kg, while the price range of the recycled version is only £12–18 per kg [12]. Although there is a price difference, these are still within the current market range in the UK. The ELG Carbon Fibre Ltd compared prices between virgin and recycled CFRP materials and found the former to be £15/kg, and the latter at £9/kg. Based on this capability, 2,000 tonnes of CFRP waste are recycled every year at the cost of £0.60/kg, pricing deduced from the electricity and gas costs involved [8]. The limited capacity has prevented many manufacturers from sending their composite waste to this centre.

By 2030, the GFRP waste projected to reach an estimated 170,000 tonnes per annum [7]. Aerospace and wind energy are the main composite sectors in the country. The UK aerospace industry is the second largest in the world and supplies; 17% of the global market and 75% of aircraft components [13]. Composite waste within the aerospace sector, therefore would be significant with the use of composites, especially in the mainframe of aircraft steadily increasing over the years [14–16]. For example, the composite portion utilized in the Boeing-777 is 10% of the total weight of the mainframe. This composite usage increases to 22% for the Airbus A380 and up to 50% for the Boeing 787 Dreamliner.

It stated that 6,000 to 8,000 commercial planes expected to reach their end-of-life by 2030 globally [17]. Based on recent data, a total of 1,229 commercial aeroplanes and 1,102 military aircraft are currently operational in the UK [18, 19]. The maximum zero-fuel-weight for A380 is 369 tons; by taking 22% of composite percentage (as a medium composite use in Airbus A380), the composite weight per aircraft would be about 81.18 tonnes. Thus, the total estimated composite end-of-life from aircraft alone can reach to 190,000 tonnes.

For wind turbines, waste from rotor blades projected to reach 225,000 tons by 2034 [20]. In 2015 alone, there were more than 6,037 operational wind turbines in 729 individual projects in the UK [21]. Since 23,597 wind turbines deployed from 2005 to 2012 [22], the situation alerted the stakeholders to be ready for dealing with a massive amount of composite waste in the near future. Landfills are the standard disposal route for composite waste, while legislative pressure has prompted for a more environmentally sound solution to be found and practised. Some of the legislation and policies associated with composite-based products are discussed in the following sub-section.

3 Drivers for Composite Recycling

3.1 Legislation and Policies

A significant and growing body of literature has agreed on environmental legislation as the influential factor to recycling enhancements [1, 23]. About 95% of these legislations derived from the European Union [9]. The end-of-life legislation and policies that are most relevant to composite waste discussed in this section [9, 24].

3.1.1 The Landfill Directive (1999/31/EC)

The UK government is considering restrictions on the landfilling of biodegradable and recyclable wastes, including landfill bans [25]. Stringent technical requirements for waste and landfills have introduced to prevent or reduce the negative impact of waste [9]. The Landfill Directive stipulates that materials with high organic content such as composite (i.e. wind turbine blades with an organic content of 30%) are to find alternative end-of-life routes.

3.1.2 UK Landfill Tax and Operator's Gate Fee

UK Landfill Tax and Operator Gate Fee, a payable charge for the disposal of waste at landfills, associated with the landfill directive. These measures aimed as the disincentives for landfill disposal of waste and to encourage the utilization and practice of environmentally sound routes such as recycling, composting, and recovery.

Two rates of landfill tax—a standard rate and a lower rate for inert materials—are implemented with the most composite waste falling under the standard rate of taxation. Records indicate a sharp steady increase in disposal costs in the UK. Rates were climbing from £7 per tonne in 1996 to £72 per tonne in 2013, £80 in 2014, and £82.60 in 2015 [26]. The total landfill disposal cost, coupled with the Landfill Operator Gate Fee (£20/tonne) is currently at approximately £100 per tonne [7]. The total composite waste landfilling cost in 2015 was almost £304 million; a significant cost driver for developing alternative waste management routes [27].

3.1.3 End-of-Life Vehicles Directives (ELV) (2000/53/EC)

UK required to divert at least 95% (by weight) of ELV from the landfills under Regulations 2003, 2005, and 2010, including recycling at least 85% and energy recovery at an additional 10%. This circumstance has represented a noteworthy driver towards improving recycling performance in the automotive composite sector. A recycling route must be available if composites are significantly substituting metals in this area [7, 28].

3.1.4 The Framework Directive on Waste (2008/0241 (COD))

The EU Waste Framework Directive (WFD 2008/98/EC), a backbone for the resource efficiency management efforts [29] has transposed into the UK law as the "Waste (England and Wales) Regulations 2011", the "Waste (Scotland) Regulations 2012", and the "Waste Regulations (Northern Ireland) 2011" [30]. These regulations legally enshrine the waste hierarchy, such as prevention, reuse, recycling, and finally the least preferred disposal method of energetic valorization (energy recovery) through incineration and landfill. The waste management hierarchy illustrates in Fig. 1.

3.2 Embodied Energy and Cost of Virgin Materials Production

Virgin or original fibre has high embodied energy. Carbon fibre and glass fibre has a range of embodied energy from 183 to 704 MJ/kg and 13–45 MJ/kg [31, 32],

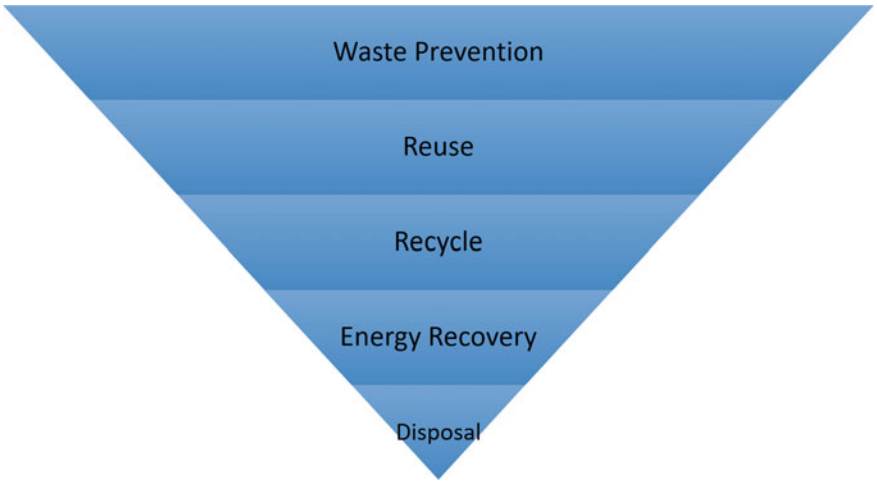

Fig. 1 Waste management hierarchy

respectively. The replacement of virgin fibre with the recycled precursor, especially in short fibre or filler application can avoid usage of energy for virgin fibre production.

Replacing virgin fibre with recycled fibre can have a monetary advantage of around £403 per tonne [33]. Although there are changes of properties during the recycling process, the use of recycled fibre is still financially attractive.

High monetary value and embodied energy of carbon fibre are one of the reasons why most studies and industries are interested in recovering carbon fibre compared to glass fibre.

4 Challenges in Composite Recycling

There are various obstacles discussed in the literature, such as the difficulty to separate homogeneous particles from the composite without damaging their properties. The applicability of reclaimed materials in mainstream production is a crucial question yet to be fully answered [1, 34]. Numerous studies have attempted to explain other obstacles in composite recycling, such as the low value of recyclates [7, 35] and variations in the feedstock [36]. All of these mentioned issues are related to the physical research of composite recycling with many efforts in place or progress to develop better recycling processes and the enhancement of recyclate quality. However, there has been limited research attempted on the non-physical challenges of composite recycling; for example, an issue acknowledged in the literature is the insufficient amount of composite scrap collection for recycling operation [20] and logistics management issues [1]. These factors are also related to high capital, operating costs, and little

supply chain pressure [7]. Research on these non-physical aspects should be as critical as the physical attributes due to each factor being interlinked and accountable during the implementation stage.

Since the technical and non-technical challenges are interlinked, it is crucial to examine both to arrive at a comprehensive solution. As could be seen, the logistic and scrap amount are often among the overlooked factors that may drive future recycling performance, especially once the recycling technology barrier has disappeared [37]. For efficient implementation of recycling activities, hundreds of tonnes of composite waste expected every week [20]. Some composite wastes and proper methods of collection related study started to take place, and more study area still needs to be identified to make this a reality [38–40]. Hence, more research opportunities are available in the area of composites product take-back, composites reverse-supply chain, composites collection schemes, and also composites recycling.

5 Composite Recycling Methods

Composite recycling methods can be classified into four main categories, namely combustion or energy recovery, mechanical, thermal, and chemical recycling technologies. Other methods, such as high voltage fragmentation, biotechnological, and electrochemical, are rarely investigated.

5.1 Composite Recycling Process Chain

The chain of composite recycling process explained in Fig. 2. Pre-processes such as dismantling and size reduction, are required for easy transportation and storage. Classification and treatment are essential to post recycling stages to improve recyclate quality for remanufacturing purposes.

Manufacturing waste and scrap do not need to undergo dismantling and downsizing steps. For the end of life of composite waste such as aeroplane structure and wind turbine blade, foreign materials need to be separated first from the fibre reinforced composite part. Metal inserts and fasteners can be separated using magnetic fields. The separation process is time-consuming and requires a human workforce, as materials sometimes mixed chemically or glued together, which makes physical separation without affecting the recyclate quality to be almost impossible. Size reduction is essential to reduce large composite waste into a smaller size to fit into a recycling machine, reactor, or chamber.

During the recycling stage, reinforcement components of a composite (fibre or filler) can be separated from the matrix part. However, the challenge is to maintain the quality and mechanical properties of the fibre for reuse stage in the new composite product. The recyclate is typically in the form of fibre recovered with residual resin and filler. Therefore, classification usually used to separate the fibrous structure and

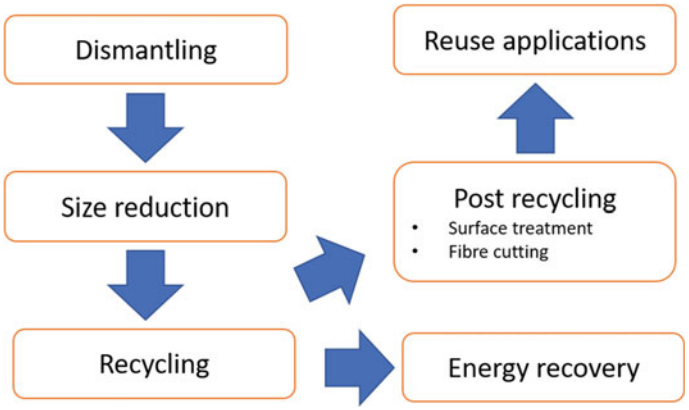

Fig. 2 Composite recycling process chain

powder rich fraction. Chopping stage may require for the fibrous fraction to obtain desired fibre length.

In thermal and chemical recycling processes, the organic part of fibre reinforced composites still recovered; but the quality degraded. The use of recovered matrix is still under development as compared to the use of recovered fibre. The recovered can form into non-woven mats for prepreg and sheet moulding compound applications. Chemical treatment of recycled fibre surface recommended for enhancing interfacial bonding between the fibre surface and virgin thermoplastic matrix in new composite products. The treatment is to ensure good mechanical properties of the product compared to its original counterparts.

5.2 Combustion

Combustion or incineration aims to recover energy from the organic part of the composite waste. During the process, the heat used to break the bond of thermoset and thermoplastic matrices. The combusted polymer is the source of energy. The matrix has high calorific value and can convert to other types of energy, such as mechanical or electrical energy. The value depends on the type of composite. For example, oil and solid condensable product from pyrolysis process of glass fibre reinforced the thermoset polyester. It found to have around 27–33 MJ/kg of gross calorific value [41]. The high temperature from the incineration can be used as a source of heat energy for the steam boiler, then used to spin a steam turbine for electricity generation. However, the conversion efficiency from heat to electrical energy is only about 35% [42].

Material recovery is rare since the leftover after the process is in the form of ash residue that consists of incombustible fibre and fillers. The fibre and fillers are

not comparable to their virgin precursor. Nevertheless, the solid inorganic residue is possible to be as source material for cement production [43]. Another drawback is that certain types of filler absorb energy during incineration as the filler requires high temperature to decompose [44]. For instance, alumina trihydrate absorbs energy during incineration. Hence, yield calorific value from the process can be reduced by 3.3% [45]. Apart from that, the leftover residues need to dispose of in the landfill. The landfilling may lead to other environmental issues and additional cost.

GFRP waste burned in a cement kiln. The glass fibre and mineral fillers are raw materials for cement production, while the matrix part can be combusted for the energy source of the kiln. It highlighted that the organic part of the waste could replace usage of fossil fuel and reduce carbon footprint by around 16% [46]. Besides, composite waste combusted with coal can minimize sulphur emission in a fluidized bed process [47].

The choice of composite waste to be incinerated depends on its percentage of organic proportion in the material composition. For sheet moulding compound (SMC), the ratio of resin is only around 35% by weight which makes the SMC waste not suitable to be combusted. Disposal via incineration is not preferable for fibre with high monetary value as the recovered fibre and filler are not reusable. This explains why the combustion process is preferred only for GFRP and not CFRP. Nonetheless, using heat to process composite waste for resin decomposition at a temperature can recover fibre with minimal quality degradation.

5.3 Mechanical Recycling

Mechanical recycling is a process of reducing composite waste into forms of fibrous and filler fractions. The fractions can be reused as reinforcement in new composite products. Removal of foreign objects is vital in mechanical recycling to avoid damage of cutter in a mechanical recycling machine.

Mechanical composite recycling usually loosely referred to grinding although it can be confused with the abrasive grinding process using a wheel. Wittmann machines use the concept of milling utilizing the hammer, and IIT m-series machine crushes glass fibre composites between rollers and grinding ring to produce powder fractions. In terms of fibre length distribution, the uniform distribution could acquire when recycling using cutting mills. For long retained fibre, hammer mills could be used despite a faster rate of wear in cutting blades. Impact method in reducing the size of sheet moulding compound is desirable to retain long fibre length [48].

Composite waste typically comes in a bulk form, especially the end of life waste. Size reduction via cutting and shredding process is vital to ensure the waste can fit into a mechanical recycling machine. The smaller size of waste can facilitate transportation of the material from the collection centre to the recycling facility. As a result of size reduction, coarse material obtained from the waste with the size of 50 mm to 100 mm. The next stage is a further size reduction of the material using grinding or milling technique into a length of 50 μm to 10 mm. Typically, a milling

or grinder machine consists of a screen with different aperture size. The aperture can be used as a guide to predict the maximum length of recyclates.

According to literature and industrial practices, mechanical recycling is widely practised to transform GFRP waste into reusable recyclates. Shuaib and Mativenga [49] compared two granulator technologies of Wittmann MAS1 granulator (Fig. 3) and Eco-Wolf grinder Model GM-2411-50 in terms of energy demand and recyclate quality. Based on the physical appearance of recyclate from both technologies, the recyclate from Wittmann and Eco-Wolf machines mainly consists of flake and fibrous structure, respectively. Laboratory unit of Retsch SM2000 cutting mill used to recycle shredding leftovers from a pultrusion company [50]. The milled waste is in the form of fine and coarse material. AEG Co mini granulator used for grinding and sifting

Fig. 3 Wittmann MAS1 granulator

process [51]. The granulator has two grinding disks where one disk is rotating, and the other is fixing. The grinding process cut the composite into 10 cm × 10 cm pieces. After a classification step, only the fibrous fraction used for analysis and mechanical tests.

Mechanical recyclates consist of flake, fibrous, and powder components with various sizes lower than aperture size of the machine. Size classification via sieving is necessary to separate the obtained recycle material for reuse applications. A 'zig-zag' classifier was used by controlling airflow to separate recyclates based on their density and particulate size [52]. Recycling processes at industrial scales used various separation technique, such as the combination of air classifier, screens and cyclone.

Recyclates in flake form is generally not reusable in thermoplastic-based composites. Such recyclate may reprocess for further size reduction. Compared to other recycling methods, resin elimination on recyclate surface for mechanical recyclate is relatively low. During the recycling, resin from a part of the fibres not entirely removed. Residual resin is still in a presence on fibre surface, therefore preventing interfacial bonding to be formed within the new matrix. Post-treatment of recovered fibrous fractions is needed to obtain clean fibre, thus ensuring good interfacial bonding with new matrix in reuse applications. Powder rich fraction can be used as a filler in cementitious products to replace the sand or fine aggregates. Mechanical recycling is not desirable to recycle high-value fibre, such as carbon fibre as it is challenging to retain the long fibre. Fibres are far off from their original forms with a significant size reduction. Given the price of carbon fibre is around ten times higher than glass fibre, the mechanical approach is not preferable to process composite with high monetary value.

In the recycling of metal matrix composite using the mechanical approach, the ball milling process is used for downsizing of SiC particles reinforced aluminium turning chips [53]. The process transformed the waste into a powdered form. The powder combined with molten aluminium to create a new, hybrid composite. Apart from that, the compression process utilized in separation of metal matrix and the creation of a condensed composite [54].

5.4 Thermal Recycling

5.4.1 Fluidized Bed

In fluidized bed recycling, materials fed through a hopper and placed on silica sand bed [55]. Heat which comes from a fluidized air passed over the bed with velocities ranges between 0.4 m/s to 1.0 m/s. Typical operating temperatures are around 450 °C to 550 °C. The heat causes degradation of resin and other organic constituents of composite materials and contaminants. The recovered fibre and filler transported into a cyclone and rotating sieve for separation. The burnt gases channelled through an exhaust for energy recovery. Past studies show potential in recovering glass fibres from thermoset composites [55, 56]. The temperature of 450 °C is an acceptable

limit with minimal 50% of strength reduction. An advantage of this method is its high tolerance for mixed and contaminated materials [10].

5.4.2 Conventional and Microwave Pyrolysis

In pyrolysis processes, GFRP and CFRP waste heated at 300–800 °C in an inert atmosphere that results in the polymeric resin volatilized, while the fibres and fillers are recovered [1]. The temperature needs to be controlled within an optimum range to maintain the fibre strength. By-products of the process in forms of liquid and gases can supply energy or feedstock for other chemical processes.

The ELG Carbon Fibre Ltd in England is one such example of a UK recycling company practising their patented thermal recycling method [57]. The recycled fibre is sold in milled, chopped, and pelletized forms [8]. Other companies with this approach are Carbon Conversions in the USA, Karborek in Italy, CFK Valley Stade Recycling GmbH and Hadeg Recycling Ltd in Germany, and Recycle Industry Co Ltd (Japan) [58].

Microwave pyrolysis uses microwave radiation as a source of heating. The rapid heating process reduces processing time, hence reducing the possibility of fibre strength degradation. The radiation heats the material from the inner and not from the surface as in the conventional heating process. The diffuse nature of electromagnetic radiation is capable of heating waste uniformly [59].

5.5 Chemical Recycling

A solvent such as acid, alcohol, or water is essential in the chemical recycling method to break the chemical bond of the organic part of fibre reinforced composite materials [34]. During the process, the matrix depolymerized into monomers. Polymeric resin decomposed into solvent while the inorganic part (fibre and filler) recovered for reuse applications in new composite products. The process can retain long fibre with excellent strength. The process has less thermal exposure at a lower temperature compared to most thermal recycling methods. Compared to mechanical recycling, the chemical approach has less fibre movement and agitation. Still, this method is not yet commercially viable and mostly conducted in a laboratory-scale setup.

The processes classified according to temperature and pressure states of the solvent used, namely sub, near, and supercritical. In terms of the critical state of the solvent, the supercritical fluid is preferable as the solvent that has less impact on the environment and human health [60]. The state and type of solvent are essential parameters in controlling effect on fibre strength.

Past studies have carried out analyzes on the hydrolysis process using water on glass fibre [61, 62] and carbon fibre composites [63–66]. Some studies used subcritical and supercritical alcohol in recycling carbon fibre reinforced epoxy waste [66–68]. While other studies focused on recovering the fibre, a study successfully formed unsaturated polyester resin from a yield of a supercritical alcohol process [69].

For metal matrix composite, the matrix separated from the reinforcement by adding a flux [54]. The addition can change interface energy between the two constituents.

5.6 Other Recycling Methods

Several recycling methods, such as high voltage fragmentation (HVF), biotechnological, and electrochemical, are relatively new and only available at a pilot or laboratory-scale. With low recycling capacity and high cost, these methods mainly focus on CFRP waste with the primary aim to maintain fibre surface quality and fibre length.

Despite relatively new compared to other mature recycling technologies, HVF recycling shows potential for the industrial-scale process with high retention of fibre strength and low energy consumption [70, 71]. HVF method uses the electrodynamic principle to disintegrate material into smaller parts. Generated high voltage electrical pulse passes through the material repetitively. The principle initially used to break rocks in mining applications in the early 1960s [72]. The pulse creates a plasma channel that moves through the material, particularly along with the weakened material interfaces. As a result, tensile stresses developed in the material, which causes internal fracture and material disintegration. Given that fibre reinforced composite is a multi-component material which consists of boundaries between fibre, matrix, and filler, the shockwave generated by the electrical pulses in the HVF process can utilized for material fragmentation.

Past studies compared mechanical and HVF method by recycling GFRP waste [71, 73]. SELFRAG laboratory equipment used to recycle chopped strand glass fibre reinforced with unsaturated polyester with fibre fraction by volume around 30% [73]. The study compared fibre characteristic and process energy demand between HVF and mechanical recycling processes. Potential of HVF over mechanical recycling is highlighted, and the study recommended for upscaling of the current laboratory-scale machine. Another study recycled sheet moulding compound waste by characterizing residual resin content and fibre length distribution [71]. It suggested that the current HVF system has low recycling throughput because the machine is not yet optimized to recycle composite waste. In Cleansky Project, demonstrator setup is created with a recycling rate of 5.65 kg per hour with energy consumption of only 1.2 kWh (or 0.33 MJ) per kg for CFRP waste [70]. The setup has achieved the technology readiness level (TRL) 6 and found to be economical. Besides the potential in HVF, it remarked that using high voltage electrical treatment in separating resin from the

fibre in unidirectional CFRP laminate can lead to a weight loss of the composite and resin elimination [74].

Researchers at Hohenstein Institute in Germany uses a microbiological system to degrade polymer part of composites via biochemical approach [75]. Minimal fibre damage reported, and the fibre is suitable to be used in new products. The method has low material throughput and currently being used only to recycle CFRP waste.

The electrochemical method also utilized to degrade matrix in composite waste and recover fibre with a clean surface. A study experimented by immersing CFRP waste in a different solution of NaCl and different applied current [76]. The concentration of the solution or electrolyte needs to be controlled since higher concentration can cause severe fibre damage. Despite high retention of fibre strength at 80%, the recycling throughput was low and currently only available at a laboratory-scale. The process requires 21 days to break down a matrix of 2 grams CFRP waste. Another study developed a method named electrically driven heterocatalytic decomposition (EHD) method, which used the electrochemical principle at room temperature and atmospheric pressure [77]. Fibre strength retention discovered being excellent (90% compared to virgin fibre); improvement of 27% can be observed through fibre interfacial shear strength. Other advantages of EHD method is non-toxicity nature and no size requirement of the waste. There is no presence of other environmental issues compared to the other methods, such as dust in mechanical recycling, by-product gases (pyrolysis), and solvent (solvolysis). A study by Kamavaram et al. [78] investigated the potential of using electrolysis in ionic liquids to recycle aluminium based metal matrix composites. It explained that the high purity of aluminium (more than 98%) could recovered; however, this depends on the concentration of the liquid and applied voltage.

6 Environmental Impact of Composite Recycling Processes

Environmental impact of composite recycling processes can be assessed by considering resource consumption. Effect of manufacturing processes mostly dominated by electrical energy consumption which usually expressed in terms of kilowatt-hour (kWh) or megajoule (MJ). The power source is the main contributor to the overall energy footprint of the process or product. Apart from minimizing the cost of electricity, reducing energy in the composite recycling process is vital to ensure less collateral damage [58]. Concerning material embodied energy, CFRP recycling is more favourable than GFRP as the production of carbon fibre is ten times more energy-intensive as compared to the production of glass fibre [32].

Figure 4 shows electricity energy demand for composite recycling processes found in scientific literature and industrial report. Differences in energy demand may attribute to several factors such as recycling rate, reactor efficiency, and type of waste.

Comparing the pyrolysis methods, heating using microwave radiation has an advantage of low energy demand compared to the conventional heating. Selective and

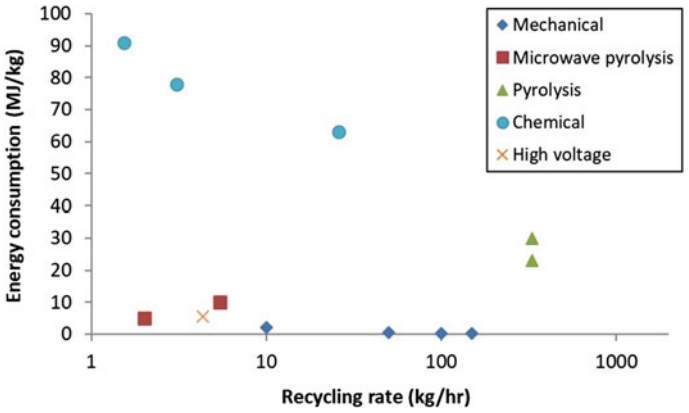

Fig. 4 Relationship between energy consumption and processing rate for different composite recycling methods

bulk heating by microwave radiation leads to a more insufficient residence time of the sample in the reactor, therefore reducing the energy demand [79]. For the mechanical process, the range of energy demand is not influenced by the type of material. This is because energy requirement in mechanical recycling machine mainly dominated by its basic power to run the machine in comparison with the actual energy used for cutting (tip energy). Energy demand reported for pyrolysis process does not consider energy recovered from combustion liquid and gaseous by-product. The recovery estimated to be around 33 MJ to 36 MJ [41, 80], but the value depends on the type of the decomposed polymer.

Generally, the energy demand of recycling processes is lower than the embodied energy of virgin material. Recovery of the material for reuse applications can give environmental benefits as the use of virgin material can be avoided. For instance, recycling of aluminium metal matrix composites using electrolysis process used energy between 11 MJ/kg and 24 MJ/kg [78] of aluminium. The range is notably lower than the embodied energy of pure aluminium, which is in the range of 196 MJ/kg to 257 MJ/kg [32].

It noted that resource consumption depends on the nature of each recycling method. Each method has a mix of energy sources. Mechanical recycling depends only on electrical energy usage. Thermal and chemical recycling processes typically involve resource in the form of material usage. For pyrolysis method, continuous nitrogen flow is a must to ensure inert atmosphere and extract gaseous by-products out from the reactor. Chemical recycling requires the use of a solvent, such as acid nitric and alcohols. On the other hand, natural gas is an input for the fluidized bed process alongside the use of electricity for cyclone, air heater, draught fan, and afterburner. Based on the literature, the use of energy for auxiliary units is sometimes not mentioned. The energy requirement for auxiliary units may not be significant for a laboratory-scale process. For industrial-scale process, the resources used by the auxiliary units are substantial and unneglected.

Other than that, the process by-products can be a significant contributor to environmental impact; for example, a mixed solution and waste-water from chemical and high voltage fragmentation process, respectively. In the thermal recycling process, liquid and gaseous by-product would be an environmental concern if they unused for energy recovery. Heat loss is highlighted in an energy flow analysis of the fluidized bed process [81]. The aspect of environmental credentials is rarely considered in the literature as most of the studies focused on mechanical properties of recovered fibre and reuse applications. This circumstance is where life cycle assessment (LCA) plays an important role to assess the environmental impact of recycling processes holistically.

7 Quality of Recycled Fibre and New Composite Product

The main objective of composite recycling is to ensure composite recyclate can be reused in potential applications. From the literature, most studies focused on recovering glass fibre or carbon fibre from the composite waste. Recovery of the matrix is challenging and not feasible as the polymer structure broken during the recycling process. Typically, the matrix or organic part combusted for energy recovery of used as a chemical feedstock.

Quality of recyclate is determined by the comparison of physical and mechanical properties of single fibre between recycled and virgin counterpart [82]. The aim is to recover fibre with properties comparable to the virgin fibre. This is important to ensure the commercial viability of the recycled fibre. Single fibre properties commonly discovered in the literature are tensile strength and tensile modulus.

Table 1 demonstrates the single fibre tensile strength discovered in the literature. The ratio of strength between recycled and original fibre is highly influenced by processing parameters and type of material. Glass fibre is more sensitive towards heating temperature and residence time in the reactor. This situation explains why recovered glass fibre has poorer fibre strength retention in comparison with carbon

Table 1 Recycled fibre tensile strength compared to virgin counterpart

Process	Ratio of tensile strength of recycled fibre to virgin fibre	Sources
Chemical	0.47–0.99	[61–64, 66, 83–85]
Electrochemical	0.80	[76]
Fluidised bed	0.54–0.74	[55, 86]
High voltage fragmentation (HVF)	0.88	[71]
Mechanical	0.80–0.82	[52, 71]
Microwave pyrolysis	0.79	[87]
Pyrolysis	0.17–0.96	[88–92]

fibre in thermal recycling. For pyrolysis process, the ratio is 17–67% for glass fibre [88–90] and 80–96% for carbon fibre [87, 91, 92].

High operating temperatures of 400–600 °C can significantly degrade the strength of glass fibre. A study treated glass fibre in a temperature range of 150–650 °C for two hours [93]. The study found that the strength reduction occurred around 150–250 °C, which is below the processing temperature used in most thermal recycling methods. The damage on the fibre also influenced by the residence time in the thermal reactor. Because of this, it is desirable to use rapid heating technique, such as microwave heating to process glass fibre based composite waste to minimize degradation of recycled fibre strength. In terms of elasticity, exposure to heat below 650 °C did not significantly change the modulus of glass fibre [93–95].

Figure 5 compares the mechanical performance of a new composite product made from recovered fibre for each recycling method. For thermal recycling processes, recycled products reported having an inferior performance compared to the virgin counterpart. This condition is attributable to fibre sizing degradation during the recycling process, hence leads to poor interfacial bonding between the recovered fibre and new polymer as a binder. Besides, resin elimination may not be 100%, and there is residual resin on the fibre surface. Coupling agents can be used to enhance bonding. For mechanical recyclates from glass fibre waste, silane was added in resin to improve adhesion with recycled fibre or filler [50, 96, 97].

More reuse applications found in a mechanical process than the other recycling methods. It is because mechanical recycling is available at industrial scale to recycle GFRP waste [98]. Moreover, the method has a high recycling rate with minimum energy consumption. It expected that chemical, microwave pyrolysis, and fluidized bed processes have fewer remanufactured products as most of the studies only used small or laboratory-scale processes.

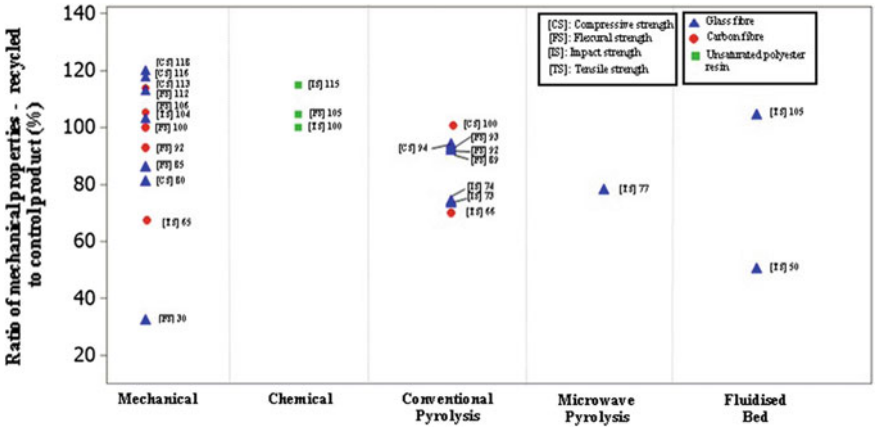

Fig. 5 Comparison of mechanical properties between recycled and control products adapted from Shuaib and Mativenga [79]

8 Application of Composite Recyclate

Material costs may reduce by nearly 45 and 50% with recycled production and end-of-life (EoL) glass and carbon fibre wastes, respectively [99]. Therefore, several end products have manufactured through composite recyclates from retired composite products. These end products include, among others, but limited to the ladders, table tennis bats, house doors, and laser pointer case [82]. In other words, there are many potential applications for ground FRP composite recyclates, as investigated and reported. For instance, a desirable natec pedal crank has fabricated with recycled carbon FRP composites [100].

Furthermore, composite recyclates sometimes applied as reinforcements: fillers, particulates, and short/chopped fibres for manufacturing of some improved structural and non-structural composite components [99]. The properties and applications of the newly recycled composite materials depend on the nature of recyclates and recycling methods. For simplicity, numerous applications of composite recyclates in different manufacturing industries subsequently classified and elucidated.

8.1 Automobile Sector

With the leading and increasing application of composites in automobiles [101], automobile industries have taken a healthy initiative and developed the most vital interest to add more recyclable components in automotive structures. For examples, a mixture of polymer materials/recyclates have identified to produce a few automobiles separating functional units, including dashboards and bumpers. New bumpers have developed from either recycled polycarbonate (PC) or polybutylene terephthalate (PBT) bumper. Beyond that, recycled thermoplastic olefin bumpers have produced other automobile parts, such as bumper fascias, air dams, splash shields, as well as air claddings after preferably reinforced with recyclate/fibre.

In addition, brackets that accommodate car radio antennae, small under-the-hood-parts and splash shields have manufactured, using recycled acrylonitrile butadiene styrene (ABS) and polyester or PC alloys. Also, power-train applications, air conditioning evaporative housings, fender liners, as well as vents have produced from recycled polypropylene (PP). In contrast, polyethylene terephthalate (PET) has been recycled and used in headliners and car engine covers [101, 102]. An iStream hybrid structural FRP composite chassis has developed. It was simple, has low-cost steel tubular members and 14 composite ipanels, compared with conventional stamped steel chassis with typically 100 s of stamped metal panels [103]. Each rCF ipanel cost nearly €30, while traditional woven fabric prepreg cost €300/panel. Now, is it possible to manufacture a car from 100% recycled materials in the future: 2030 or 2050 [1]?

8.2 Aerospace Industry

The Aircraft Fleet Recycling Association (AFRA) (formed by Boeing and 10 other aerospace companies), Airbus Process for Advanced Management of End-of-Life Aircraft (PAMELA), Materials Innovation Technology (MIT), and Recycled Carbon fibre Limited (RCF) have committed for more than a decade in improving the management of retired aircraft. By 2029, 10–15 million pounds of CF recyclate estimated to be generated by the aerospace industry from manufacturing and EoL aircrafts [1].

8.3 Wind Energy

Wind energy is one of the global and increasing renewable energy supply. It is produced by wind turbines, with 40% of total blade mass. Nearly all turbine blades made from glass fibre/epoxy composites, with a glass-epoxy ratio of 60%. Both manufacturing and EoL turbine blade of the average lifetime of two decades generate a vast amount of composite wastes, the estimated quantity is more than 1 million tonnes over the next two decades [104]. Due to the fact that the key turbine parts made up of thermosetting composite materials, recycling, and disposal of new and EoL scrap is a growing global challenge. Unfortunately, there are no commercial operations to embark on recycling of the new and EoL wind turbine composite materials.

8.4 Electrical and Electronics Industry

Milled recycled carbon fibres (rCFs) used to manufacture conductive materials that provide electrical conductivity and antistatic behaviours in polymeric composites and coatings. For example, epoxy antistatic floor coatings and integrated circuit trays [103].

8.5 Other Applications

Other possible applications for composite recyclate described in this section. Typically, the use of recyclate is to improve strength and reduce cost by avoiding the use of virgin material.

- *Subsea buoyancy*—Milled rCF applied in deep-sea oil and gas exploration [103]. They have the largest volume market for milled CFs.
- *Manufacturing (Additive/3D printing and net-shape)*—Milled rCFs utilized to produce filaments for 3D printing or additive manufacturing (AM) processes

[103]. For instance, these materials may use to fabricate prototyping objects, drones, and cars. The first 3D-printed car from Local Motors contained 20 and 80% of rCF and ABS plastic [103], respectively. Additionally, chopped rCF used in net-shape manufacturing of parts, through the application of preforming for resin transfer moulding or stamp forming process.

- *Building/construction company*—Pulverished waste FRP composite products converted to artificial woods experimentally [105]. The woods can be nailed, drilled, notched and sawn, showing their similar properties when compared with natural woods. Also, ground glass reinforced polyester (GRP) has used diversely: GRP/plastic lumber with a bolted tenon joint to solid wood and GRP/wood flake blend particleboard [106].
- *Compounding*—The mechanical properties (essentially stiffness) of some injection moulded milled rCF polymeric compounds. It might be chopped, or pellet rCF applied in sheet and bulk moulding compounds (S/BMC), especially in applications of long fibres that are not suitable for complex geometry, small product, and exact requirements of surface quality.

Finally, further improvement in the development of more economical processing, optimization techniques, the performance of recycled composites, as well as the general acceptance of recycled composite products by educating the markets is required. The purpose is to increase applications of the composite recyclates, as there are no end-users for the recycled materials [1]. In addition, formulation of models for predicting the quantity of recyclates, recycled material value, and effect of the variance of processing parameters on recyclate quality, cost and environmental impact are recommended for future works, probably towards vision 2030, 2050 and beyond. Importantly, in addition to the cost reduction, the mechanical properties of the rCF reinforced products increase.

9 Conclusions

Rising of demand for the composite material, particularly on the fibre reinforced type comes together with manufacturing and end of life waste problem. The heterogeneity and cross-linked nature of thermoset polymer lead to a challenging task for the recovery of material during recycling stage. Legislation and the high value of fibre are drivers for composite users to recycle their waste.

This chapter reviewed the studies on composite recycling methods. Most recycling technologies developed to recover polymer-based composites on account of its high demand, and waste volume, thus raises the urgency for recycling. Mature recycling process, such as mechanical and pyrolysis, operated at an industrial scale and commercially available. Recycling methods, such as microwave pyrolysis, high voltage fragmentation, and others are relatively new and only conducted at a pilot or laboratory setup. In terms of environmental impact, the process energy demand

for recycling is far lower compared to the embodied energy of the original fibre. The processing rate positively drives the energy demand.

Recovered fibre and new composite product made from the recyclate have comparable performance with virgin counterparts. Potential applications in the automotive, aerospace and renewable energy sector suggested in this chapter. The commercial viability of composite recycling only is realized if virgin fibre can be substituted by recycled fibre in both active and passive applications. Recycling of fibre reinforced composite waste is essential to avoid loss of valuable materials. Recyclate can return into the market using the concept of circular economy via closed-loop or cross-sector applications.

10 Review Questions

(1) Define the term composite material.
(2) Explain the motivation to recycle composite material from energy and financial perspectives.
(3) Explain the difference between the price of CFRP and GFRP.
(4) Discuss technical and non-technical challenges in recycling composite material.
(5) Describe the steps in a composite recycling process chain.
(6) Compare procedure of mechanical and pyrolysis recycling methods.
(7) What is the difference between conventional and microwave pyrolysis?
(8) Compare resource consumption in mechanical, pyrolysis, and chemical recycling methods.
(9) In thermal recycling processes, explain reasons for glass fibre strength reduction.
(10) Describe three applications of composite recyclate.

Acknowledgements The author would like to acknowledge the support from the Fundamental Research Grant Scheme (FRGS) under grant numbers of FRGS/1/2018/TK03/UNIMAP/02/15 and RACER/2019/FKP-COSSID/F00411 from the Ministry of Education Malaysia as well as funding by the UK Engineering and Physical Sciences Research Council (EPSRC), under grant EP/K026348/1, Efficient X-sector use of HeterogeneoUs MatErials in Manufacturing (EXHUME). Also, thank you to Universiti Malaysia Perlis, Universiti Teknikal Malaysia Melaka, University of Hertfordshire and University of Manchester for the kind support.

References

1. Yang, Y., Boom, R., Irion, B., van Heerden, D.-J., Kuiper, P., de Wit, H.: Recycling of composite materials. Chem. Eng. Process.: Process Intensification **51**, 53–68 (2012)
2. Ccf. Composites Sector Increasing M & A Update: Spring 2013 (2013)

3. Marketsandmarkets. Composites Market worth 115.43 Billion USD by 2022 (2017)
4. Mazumdar, S.: Composites growth realizing its global potential. Composites World. 7 (2005)
5. Shuaib, N.A., Mativenga, P.T., Kazie, J., Job, S.: Resource efficiency and composite waste in UK supply chain. Procedia CIRP. **29**, 662–667 (2015)
6. Halliwell, S.: End of life options for composite waste recycle, reuse or dispose? National Composites Network Best Practice Guide (2006)
7. Bains M, Stokes E. Developing a Resource Efficiency Action Plan For the Composite Sector: Scoping Study. 2013
8. ELGCF. Converting composite waste into high quality reusable carbon fibre (2015)
9. Cherrington, R., Goodship, V., Meredith, J., Wood, B.M., Coles, S.R., Vuillaume, A., et al.: Producer responsibility: defining the incentive for recycling composite wind turbine blades in Europe. Energy Policy **47**, 13–21 (2012)
10. Job, S.: Composite recycling: summary of recent research and development (2010)
11. Granta Design Limited. CES EduPack software (2015)
12. Asmatulu, E., Overcash, M., Twomey, J.: Recycling of aircraft: state of the art in 2011. J. Ind. Eng. **2013**, 1–8 (2013)
13. Smith, F., Shakspeare, P.: UK composites 2013: a study into the status, opportunities and direction for the UK composite industry (2013)
14. Agp. Lifting off—implementing the strategic vision for UK Aerospace (2013)
15. Hale, J.: Boeing 787 from the Ground Up 06. Boeing. 9 (2006)
16. Osborne, J.: The UK composites industry—turning ideas into investments. Reinforced plastics. 3 (2013)
17. McConnell, V.P.: Launching the carbon fibre recycling industry. Reinf. Plast. **54**(2), 33–37 (2010)
18. Eurostat. Commercial Aircraft Fleet by Type of Aircraft. 2014
19. Think, D.: UK Armed forces aircraft numbers. pp. 8–10 (2012)
20. Larsen, K.: Recycling wind. Reinf. Plast. **53**(1), 20–25 (2009)
21. Ukwed. UK Wind energy database—operational figures at a glance (2015)
22. Renewable UK. Small and medium wind UK market report (2013)
23. Howarth, J., Sada, S.R.M., Mativenga, P.T.: Energy intensity and environmental analysis of mechanical recycling of carbon fibre composite. J. Cleaner Prod. **81**, 46–50 (2014)
24. Stewart, R.: Management, pp. 39–61. Elsevier, Recycling and Reuse of Waste Composites (2010)
25. Eunomia, R.: Consulting. Landfill Bans: feasibility research. Waste and Resources Action Programme (2012 Nov)
26. Rybicka, J., Tiwari, A., Leeke, G.A.: Technology readiness level assessment of composites recycling technologies. Journal of Cleaner Production. 2016;112, Part 1:1001-12
27. UK Government. 2013 UK greenhouse gas emissions, provisional figures and 2012 UK greenhouse gas emissions, final figures by fuel type and end-user. National Statistics: Department of Energy & Climate Change (2014)
28. Bains, M., Carruthers, J.: Composite material resource efficiency action plan December 2013 (2013)
29. Dwivedy, M.: Modeling and assessment of e-waste management issues in India: generation, flows and extended producer responsibility: Birla Institute of Technology and Science (2013)
30. Defra: Environmental management guidance: waste legislation and regulations (2014)
31. Duflou, J.R., Deng, Y., Van Acker, K., Dewulf, W.: Do fiber-reinforced polymer composites provide environmentally benign alternatives? A life-cycle-assessment-based study. MRS Bull. **37**(04), 374–382 (2012)
32. Song, Y.S., Youn, J.R., Gutowski, T.G.: Life cycle energy analysis of fiber-reinforced composites. Compos. Part A: Appl. Sci. Manuf. **40**(8), 1257–1265 (2009)
33. Bains, M., Stokes, E.: Developing a resource efficiency action plan for the composites sector. URS & Netcomposites (2013)
34. Oliveux, G., Dandy, L.O., Leeke, G.A.: Current status of recycling of fibre reinforced polymers: review of technologies, reuse and resulting properties. Prog. Mater Sci. **72**, 61–99 (2015)

35. Witik, R.A., Teuscher, R., Michaud, V., Ludwig, C., Månson, J.-A.E.: Carbon fibre reinforced composite waste: an environmental assessment of recycling, energy recovery and landfilling. Compos. Part A **49**, 89–99 (2013)
36. Lettieri, P., Yassin, L., Simons, S.J.R.: Management, recycling and reuse of waste composites, Elsevier, pp. 152–91 (2010)
37. Srivastava, S.K.: Green supply-chain management: a state-of-the-art literature review. Int J. Manage. Rev. **9**(1), 53–80 (2007)
38. Mativenga, P.T., Agwa-Ejon, J., Mbohwa, C., Sultan, A.A.M., Shuaib, N.A.: Circular economy ownership models: a view from South Africa industry. Procedia Manuf. **8**, 284–291 (2017)
39. Sultan, A.A., Lou, E., Mativenga, P.T.: What should be recycled: an integrated model for product recycling desirability. J. Cleaner Prod. **154**, 51–60 (2017)
40. Sultan, A.A.M., Tarisai, P., Lou, E.: Managing Supply chain complexity: foresight for wind turbine composite waste. Procedia CIRP. **69**(May), 938–943 (2018)
41. Cunliffe, A.M., Williams, P.T.: Characterisation of products from the recycling of glass fibre reinforced polyester waste by pyrolysis. Fuel **82**(18), 2223–2230 (2003)
42. Karuppannan Gopalraj, S., Kärki, T.: A review on the recycling of waste carbon fibre/glass fibre-reinforced composites: fibre recovery, properties and life-cycle analysis. SN Appl. Sci. **2**(3), 433 (2020)
43. Vijay, N., Rajkumara, V., Bhattacharjee, P.: Assessment of composite waste disposal in aerospace industries. Procedia Environ. Sci. **35**, 563–570 (2016)
44. Wang, P.H., Zimmermann, N.: Composite recycling techniques: a literature review. Juniper Online J. Mater. Sci. **6**(1) (2020)
45. Pickering, S.J.: Recycling technologies for thermoset composite materials—current status. Compos. A Appl. Sci. Manuf. **37**(8), 1206–1215 (2006)
46. EuCIA. Composites recycling made easy: European Composites Industry Association; 2013 [Available from: http://www.avk-tv.de/files/20130212_recycling_made_easy.pdf
47. Fenwick NJ, Pickering SJ. Using waste material to reduce emissions—combustion of glass reinforced plastic with coal in a fluidised bed. Conference on Engineering Profit From Waste IV; 9–11 November London 1994. p. 157-66
48. Derosa, R., Telfeyan, E., Gaustad, G., Mayes, S.: Strength and microscopic investigation of unsaturated polyester BMC reinforced with SMC-recyclate. J. Thermoplast. Compos. Mater. **18**(4), 333–349 (2005)
49. Shuaib, N.A., Mativenga, P.T.: Effect of Process Parameters on Mechanical Recycling of Glass Fibre Thermoset Composites. Procedia CIRP. **48**, 134–139 (2016)
50. Meira Castro, A.C., Ribeiro, M.C.S., Santos, J., Meixedo, J.P., Silva, F.J.G., Fiúza, A., et al.: Sustainable waste recycling solution for the glass fibre reinforced polymer composite materials industry. Constr. Build. Mater. **45**, 87–94 (2013)
51. Kouparitsas, C.E., Kartalis, C.N., Varelidis, P.C., Tsenoglou, C.J., Papaspyrides, C.D.: Recycling of the fibrous fraction of reinforced thermoset composites. Polym. Compos. **23**(4), 682–689 (2002)
52. Palmer J. Mechanical recycling of automotive composites for use as reinforcement in thermoset composites [Phd]: University of Exeter 2009
53. Tan, X., Zhang, B., Liu, K., Yan, X., Han, J., Liu, X., et al.: Microstructure and mechanical property of the 2024Al matrix hybrid composite reinforced with recycled SiCp/2024Al composite particles. J. Alloy. Compd. **815**, (2020)
54. Nishida, Y.: Recycling of Metal Matrix Composites. Adv. Eng. Mater. **3**(5), 315–317 (2001)
55. Pickering, S.J., Kelly, R.M., Kennerley, J.R., Rudd, C.D., Fenwick, N.J.: A fluidised-bed process for the recovery of glass fibres from scrap thermoset composites. Composites Science and Technology. **60**(4), 509–523 (2000)
56. Kennerley, J.R., Kelly, R.M., Fenwick, N.J., Pickering, S.J., Rudd, C.D.: The characterisation and reuse of glass fibres recycled from scrap composites by the action of a fluidised bed process. Compos. A Appl. Sci. Manuf. **29**(7), 839–845 (1998)
57. Black S. Composite recycling is gaining traction. Composite world. 2017:1–5

58. Job S, Leeke G, Mativenga PT, Oniveux G, Pickering S, Shuaib NA. Composites Recycling: Where are we now? 2016
59. Lam, S.S., Chase, H.A.: A review on waste to energy processes Using microwave pyrolysis. Energies. **5**(10), 4209–4232 (2012)
60. Morin, C., Loppinet-Serani, A., Cansell, F., Aymonier, C.: Near- and supercritical solvolysis of carbon fibre reinforced polymers (CFRPs) for recycling carbon fibers as a valuable resource: State of the art. J. Supercrit. Fluids **66**, 232–240 (2012)
61. Oliveux, G., Bailleul, J.-L., Salle, E.L.G.L.: Chemical recycling of glass fibre reinforced composites using subcritical water. Compos. A Appl. Sci. Manuf. **43**(11), 1809–1818 (2012)
62. Kao CC, Ghita OR, Evans KE, Oliveux G. Mechanical characterisation of glass fibres recycled from thermosetting composites using water-based solvolysis process 18th International Conference on Composite Materials; 21 – 26 August 2011; Jeju Island2011
63. Liu, Y., Shan, G., Meng, L.: Recycling of carbon fibre reinforced composites using water in subcritical conditions. Mater. Sci. Eng., A **520**(1–2), 179–183 (2009)
64. Okajima, I., Hiramatsu, M., Sako, T.: Recycling of carbon fiber reinforced plastics using subcritical water Advanced Materials Research. **222**, 243–246 (2011)
65. Bai, Y., Wang, Z., Feng, L.: Chemical recycling of carbon fibers reinforced epoxy resin composites in oxygen in supercritical water. Mater. Des. **31**(2), 999–1002 (2010)
66. Piñero-Hernanz, R., García-Serna, J., Dodds, C., Hyde, J., Poliakoff, M., Cocero, M.J., et al.: Chemical recycling of carbon fibre composites using alcohols under subcritical and supercritical conditions. J. Supercrit. Fluids **46**(1), 83–92 (2008)
67. Hyde, J.R., Lester, E., Kingman, S., Pickering, S., Wong, K.H.: Supercritical propanol, a possible route to composite carbon fibre recovery: A viability study. Compos. A Appl. Sci. Manuf. **37**(11), 2171–2175 (2006)
68. Jiang, G., Pickering, S.J., Lester, E.H., Turner, T.A., Wong, K.H., Warrior, N.A.: Characterisation of carbon fibres recycled from carbon fibre/epoxy resin composites using supercritical n-propanol. Composites Science and Technology. **69**(2), 192–198 (2009)
69. Yamada, K., Tomonaga, F., Kamimura, A.: Improved preparation of recycled polymers in chemical recycling of fiber-reinforced plastics and molding of test product using recycled polymers. J Mater Cycles Waste Manag. **12**(3), 271–274 (2010)
70. Weh A. Final report summary—SELFRAG CFRP (High voltage pulse fragmentation technology to recycle fibre-reinforced composites). SELFRAG AG; 2015
71. Rouholamin D, Shyng YT, Savage L, Ghita OR. A comparative study into mechanical performance of glass fibre recovered through mechanical grinding and high voltage pulse power fragmentation. 16th European Conference on Composite Materials; Seville2014
72. Bluhm, H., Frey, W., Giese, H., Hoppe, P., Schultheiss, C., Strassner, R.: Application of pulsed HV discharges to material fragmentation and recycling. Dielectrics and Electrical Insulation, IEEE Transactions on. **7**(5), 625–636 (2000)
73. Mativenga PT, Shuaib NA, Howarth J, Pestalozzi F, Woidasky J. High voltage fragmentation and mechanical recycling of glass fibre thermoset composite. CIRP Annals—Manufacturing Technology. 2016
74. Oshima, K., Matsuda, S., Hosaka, M., Satokawa, S.: Rapid removal of resin from a unidirectional carbon fiber reinforced plastic laminate by a high-voltage electrical treatment. Sep. Purif. Technol. **231**, (2020)
75. Hohenstein Institute. Biotechnology innovation helps with recycling carbon fibres (press information) Bönnigheim, Germany 2015 [Available from: http://www.hohenstein.de/media/pdf/635-EN_06_Recycling_Carbonfasern_2015_101440.pdf
76. Sun, H., Guo, G., Memon, S.A., Xu, W., Zhang, Q., Zhu, J.-H., et al.: Recycling of carbon fibers from carbon fiber reinforced polymer using electrochemical method. Compos. A Appl. Sci. Manuf. **78**, 10–17 (2015)
77. Zhu J-H, Chen P-y, Su M-n, Pei C, Xing F. Recycling of carbon fibre reinforced plastics by electrically driven heterogeneous catalytic degradation of epoxy resin. Green Chemistry. 2019;21(7):1635–47

78. Kamavaram, V., Mantha, D., Reddy, R.G.: Recycling of aluminum metal matrix composite using ionic liquids: Effect of process variables on current efficiency and deposit characteristics. Electrochim. Acta **50**(16), 3286–3295 (2005)
79. Shuaib NA, Mativenga PT, editors. Energy Intensity and Quality of Recyclate in Composite Recycling. ASME 2015 International Manufacturing Science and Engineering Conference; 2015 June 8–12, 2015; Charlotte, North Carolina
80. Åkesson D, Foltynowicz Z, Christéen J, Skrifvars M. Products obtained from decomposition of glass fiber-reinforced composites using microwave pyrolysis. Polimery. 2013;58
81. Meng, F., McKechnie, J., Turner, T.A., Pickering, S.J.: Energy and environmental assessment and reuse of fluidised bed recycled carbon fibres. Compos. A Appl. Sci. Manuf. **100**, 206–214 (2017)
82. Asmatulu E, Twomey J, Overcash M. Recycling of fiber-reinforced composites and direct structural composite recycling concept. Journal of Composite Materials. 2013
83. Okajima, I., Hiramatsu, M., Shimamura, Y., Awaya, T., Sako, T.: Chemical recycling of carbon fiber reinforced plastic using supercritical methanol. J. Supercrit. Fluids **91**, 68–76 (2014)
84. Liu, Y., Meng, L., Huang, Y., Du, J.: Recycling of carbon/epoxy composites. J. Appl. Polym. Sci. **94**(5), 1912–1916 (2004)
85. Shyng YT, Ghita OR. Fragmentation Analysis Of Glass Fibres Recovered From Hydrolysis Processes. 19th International Conference on Composite Materials; Montreal2013
86. Yip, H.L.H., Pickering, S.J., Rudd, C.D.: Characterisation of carbon fibres recycled from scrap composites using fluidised bed process. Plast., Rubber Compos. **31**(6), 278–282 (2002)
87. Lester, E., Kingman, S., Wong, K.H., Rudd, C., Pickering, S., Hilal, N.: Microwave heating as a means for carbon fibre recovery from polymer composites: a technical feasibility study. Mater. Res. Bull. **39**(10), 1549–1556 (2004)
88. Criado, M., García-Díaz, I., Bastidas, J.M., Alguacil, F.J., López, F.A., Monticelli, C.: Effect of recycled glass fiber on the corrosion behavior of reinforced mortar. Constr. Build. Mater. **64**, 261–269 (2014)
89. Cunliffe, A.M., Jones, N., Williams, P.T.: Pyrolysis of composite plastic waste. Environ. Technol. **24**(5), 653–663 (2003)
90. Williams, P.T., Cunliffe, A., Jones, N.: Recovery of value-added products from the pyrolytic recycling of glass-fibre-reinforced composite plastic waste. J. Energy Inst. **78**(2), 51–61 (2005)
91. Onwudili, J.A., Insura, N., Williams, P.T.: Autoclave pyrolysis of carbon reinforced composite plastic waste for carbon fibre and chemicals recovery. J. Energy Inst. **86**(4), 227–232 (2013)
92. Meyer, L.O., Schulte, K., Grove-Nielsen, E.: CFRP-recycling following a pyrolysis route: Process optimization and potentials. J. Compos. Mater. **43**(9), 1121–1132 (2009)
93. Feih, S., Boiocchi, E., Mathys, G., Mathys, Z., Gibson, A.G., Mouritz, A.P.: Mechanical properties of thermally-treated and recycled glass fibres. Compos. B Eng. **42**(3), 350–358 (2011)
94. Feih, S., Manatpon, K., Mathys, Z., Gibson, A.G., Mouritz, A.P.: Strength degradation of glass fibers at high temperatures. J. Mater. Sci. **44**(2), 392–400 (2009)
95. Thomason, J.L., Yang, L., Meier, R.: The properties of glass fibres after conditioning at composite recycling temperatures. Compos. A Appl. Sci. Manuf. **61**, 201–208 (2014)
96. Ribeiro MCS, Meira-Castro AC, Silva FG, Santos J, Meixedo JP, Fiúza A, et al. Re-use assessment of thermoset composite wastes as aggregate and filler replacement for concrete-polymer composite materials: A case study regarding GFRP pultrusion wastes. Resources, Conservation and Recycling. 2013(0)
97. Meira Castro, A.C., Carvalho, J.P., Ribeiro, M.C.S., Meixedo, J.P., Silva, F.J.G., Fiúza, A., et al.: An integrated recycling approach for GFRP pultrusion wastes: recycling and reuse assessment into new composite materials using Fuzzy Boolean Nets. J. Clean. Prod. **66**, 420–430 (2014)
98. Palmer, J., Ghita, O.R., Savage, L., Evans, K.E.: Successful closed-loop recycling of thermoset composites. Compos. A Appl. Sci. Manuf. **40**(4), 490–498 (2009)
99. Hagnell, M.K., Åkermo, M.: The economic and mechanical potential of closed loop material usage and recycling of fibre-reinforced composite materials. J. Clean. Prod. **223**, 957–968 (2019)

100. Perry, N., Bernard, A., Laroche, F., Pompidou, S.: Improving design for recycling—Application to composites. CIRP Ann. **61**(1), 151–154 (2012)
101. Hodzic, A.: Re-use, recycling and degradation of composites. In: Baillie, C. (ed.) Green composites: Polymer composites and the environment, pp. 252–268. Woodhead Publishing Limited, Cambridge, United Kingdom (2000)
102. Sherman, L.M.: Compounders take the lead in post-use bumper recycling. Plastics Technology. **3**, 27–29 (1996)
103. Gehr M. Recycled carbon fibre: A new approach to cost effective lightweighting 2020 [Available from: https://www.igcv.fraunhofer.de/content/dam/igcv/de/docs/Travelling_Conference_Unterlagen/03_Recycled%20Carbon%20Fibre_Gehr_ELGCF.pdf
104. Papadakis, N.: Designing composite wind turbine blades disposal recycling and reuse. In: Goodship, V. (ed.) Management, Recycling and Reuse of Waste Composites, pp. 443–457. Woodhead Publishing Limited and CRC Press, Cambridge, United Kingdom (2010)
105. Demura K, Ohama Y, Satoh T, editors. Properties of artificial woods using FRP powder, Disposal and recycling of organic and polymeric construction materials. Proceedings of the International Rilem Workshop; 1995 26–28 March 1995; Tokyo, Japan
106. Conroy, A., Halliwell, S., Reynolds, T.: Composite recycling in the construction industry. Compos. A Appl. Sci. Manuf. **37**(8), 1216–1222 (2006)